Program and Abstracts

14th International Conference

on Modulated Semiconductor Structures

Schedule

Sunday July 19th	16:00	18:00	Registration (at Registration desk in 3F entrance hall)
	17:00	19:00	Welcome Reception (Sponsored by Nippon Cryogenic Ltd.)

Session Timetable

	7/20 (Mon)	7/21 (Tue)	7/22 (Wed)	7/23 (Thu)	7/24 (Fri)
9:00		Session M2 Terahertz dynamics and devices	Session M5 Spintronics I	Session M6 Spintronics II	Session M9 Nanophotonics
10:00	Opening				
	Plenary 1	Coffee	Coffee	Coffee	Coffee
11:00		Session M3 Physics and devices for quantum information processing	Plenary 3	Session M7 Nanostructure growth	Pleanry 5
	Pleanry 2				
12:00	Photo		Plenary 4		Plenary 6
					Closing
13:00	Lunch	Lunch	Free afternoon or optional excursion	Lunch	
14:00	Session M1 Transport in nanostructures	Session M4 Optical properties of quantum dots		Session M8 Novel materials and physics	
15:00					
16:00	Poster Session Mo-mP	Poster Session Tu-mP		Poster Session Th-mP	
17:00					
		Special Session for Solar Cells 18:00-20:00	18:30 Banquet at “Kachoen”		

Monday July 20th

Opening Ceremony (Main Hall) 10:00 – 10:30

Session Plenary 1,2 (Main Hall) 10:30 – 12:00

PL1 (2) 10:30 – 11:15 **David D. Awschalom** (*Center for Spintronics and Quantum Computation, University of California, Santa Barbara, CA 93106 USA*)
Manipulating single spins and coherence in semiconductors

PL2 (4) 11:15 – 12:00 **Yoshihisa Yamamoto**[1,2] ([1]*E. L. Ginzton Laboratory, Stanford University, CA, USA,* [2]*National Institute of Informatics, Tokyo, Japan*)
Bose-Einstein condensation and superfluidity of exciton-polaritons

12:00 – 12:15 **Conference Photo**

12:15 – 14:00 **Lunch Break**

Session M1 (International Conference Room) 14:00 – 16:00

Transport in nanostructures

M1a (6) 14:00 – 14:30 **H. Klauk** (Invited) (*Max Planck Institute for Solid State Research, Stuttgart, Germany*)
Field-Effect Transistors Based on Carbon Nanotubes and ZnO Nanowires with Organic/Inorganic Hybrid Gate Dielectrics

M1b (7) 14:30 – 14:45 **Carlo Colombo**[1], **Dance Spirkoska**[2], **Tonko Garma**[1,2], **Martin Heiss**[1,2], **Fabien Vialla**[1], **Joseph Dufouleur**[2], **Gerhard Abstreiter**[2], **A. Fontcuberta i Morral**[1,2] ([1]*LMSC, Ecole Polytechnique Federale de Lausanne, Lausanne, Switzerland,* [2]*Walter Schottky Institut, TU Muenchen, Garching, Germany*)
Doping of catalyst-free MBE grown GaAs nanowires, transport properties and related devices

M1c (8) 14:45 – 15:00 **O. Makarovsky**[1], **O. Thomas**[1], **A.G. Balanov**[1], **A. Patanè**[1], **L. Eaves**[1], **R. P. Campion**[1], **C. T. Foxon**[1], **E. E. Vdovin**[1], **D.K. Maude**[2] ([1]*School of Physics and Astronomy, The University of Nottingham, Nottingham, UK NG7 2RD, UK,* [2]*Grenoble High Magnetic Field Laboratory, CNRS, F-38042 Grenoble, France*)
A quantum analogue of the STM multiple-tip effect revealed by wavefunction imaging of quantum dots

M1d (9) 15:00 – 15:15 **C. Payette**[1,2], **S. Amaha**[3], **T. Hatano**[3], **K. Ono**[4], **J. A. Gupta**[1], **G. C. Aers**[1], **D. G. Austing**[1,2], **S. V. Nair**[5], **S. Tarucha**[3,6] ([1]*Institute for Microstructural Sciences M50, NRC, Ottawa, Ontario K1A 0R6, Canada,* [2]*Department of Physics, McGill University, Montreal, Quebec H3A 2T8, Canada,* [3]*Quantum Spin Information Project, ICORP, JST, Atsugi, Kanagawa 243-0198, Japan,* [4]*RIKEN , Wako, Saitama 351-0198, Japan,* [5]*Center for Advanced Nanotechnology, University of Toronto , Toronto, Ontario M5S 3E3, Canada,* [6]*Department of Applied Physics, University of Tokyo, Tokyo 113-0033, Japan*)
Gate adjustable coherent three and four level mixing in a vertical quantum dot molecule

M1e (10) 15:15 – 15:30 **G. Shinkai[1,2], T. Hayashi[1], T. Ota[1], K. Muraki[1], T. Fujisawa[2]** ([1]*NTT Basic Research Laboratories, 3-1 Morinosato-Wakamiya, Atsugi, 243-0198, Japan,* [2]*Reseach Center for Low-Temperature Physics, Tokyo Institute of Technology, 2-12-1 Ookayama, Meguro, 152-8551, Japan*)

Bidirectional current drag effect utilizing cotunneling of two-electrons in coupled double quantum dots

M1f (11) 15:30 – 15:45 **Markus Schlapps[1], Stefan Geissler[1], Teresa Lermer[1], Janusz Sadowski[2], Werner Wegscheider[1], Dieter Weiss[1]** ([1]*Department of Applied Physics, University of Regensburg, Universitätsstr. 31, 93040 Regensburg, Germany,* [2]*Max-Lab, Lund University, Sweden, Ole Römers väg 1, SE-223 63 Lund, Sweden*)

Coulomb blockade transport across lateral (Ga,Mn)As nanoconstrictions

M1g (12) 15:45 – 16:00 **T. Kodera[1], K. Ono[2], N. Kumagai[1], T. Nakaoka[1], S. Tarucha[1,3,4], Y. Arakawa[1,5,6]** ([1]*Institute for Nano Quantum Information Electronics, the University of Tokyo, 4-6-1, Komaba, Meguro-ku, Tokyo 153-8505, Japan,* [2]*RIKEN, 2-1, Hirosawa, Wako-shi, Saitama 351-0198, Japan,* [3]*School of Engineering, the University of Tokyo, 7-3-1, Hongo, Bunkyo-ku, Tokyo 113-0033, Japan,* [4]*ICORP-JST, 3-1, Morinosato Wakamiya, Atsugi-shi, Kanagawa 243-0198, Japan,* [5]*Institute of Industrial Science, the University of Tokyo, 4-6-1 Komaba, Meguro-ku, Tokyo 153-8505,* [6]*Research Center for Advanced Science and Technology, the University of Tokyo, 4-6-1 Komaba, Meguro-ku, Tokyo 153-8505*)

Resonant tunneling in a vertical pillar structure including a self-assembled quantum dot coupled with a quantum well

Poster Session Mo-mP (Meeting Room 501, 502) 16:00–18:00

Mo-mP2 (14) **M. Grydlik, M. Brehm, H.Groiss, T. Fromherz, F. Schäffler, G. Bauer** (*Institute of Semiconductor and Solid State Physics, University of Linz, Altenbergerstrasse 69 4040 Linz, Austria*)

Inverted Ge islands in 111 faceted Si pits - a novel approach towards islands with higher aspect ratio

Mo-mP3 (15) **T. Yang, Y. L. Cao, H. M. Ji, W. Q. Ma, P. F. Xu, Y. X. Gu** (*Institute of Semiconductors, Chinese Academy of Sciences, P. O. Box 912, Beijing 100083, China*)

Comparative study of p-doped and undoped 1.3-μm InAs/GaAs quantum-dot lasers

Mo-mP4 (16) **T. Ito, T. Ito, T. Akiyama, K. Nakamura** (*Department of Physics Engineering, Mie University, 1577 Kurima-Machiya, Tsu, Mie , Japan*)

Ab initio-based approach to structural modulation of AlN on 4H-SiC(11-20) during MBE growth

Mo-mP5 (17) **T. Nishiwaki, M. Yamaguchi, N. Sawaki** (*Department. of Electrical Engineering and Computer Science, Nagoya University, C3-1(631), Furo-cho, Chikusa-ku, Nagoya 464-8603, Japan*)

Growth of AlGaAs/GaAs (11n)A facets by selective MBE

Mo-mP6 (18) **M. Brehm[1], M. Grydlik[1], G. Vastola[2], M. J. Beck[3], H. Lichtenberger[1], T. Fromherz[1], F. Montalenti[2], F. Schaffler[1], L. Miglio[2], G. Bauer[1]** ([1]*Institut of Semiconductor Physics, University of Linz, Austria, Altenbergerstrasse 65, A-4040 Linz, Austria , Austria,* [2]*L-NESS and Materials Science Department, University of Milano-Bicocca, I-20125 Milano, Italy,* [3]*Department of Physics and Astronomy, Vanderbilt University,, Nashville, Tennessee 37235, USA*)

Morphological evolution at the early stages of Ge island formation on Si(001) revisited: the key role of the wetting layer

Mo-mP7 (19) **T. Yamashita, T. Akiyama, K. Nakamura, T. Ito** (*Department of Physics Engineering, Mie University, 1577 Kurima-Machiya, Tsu, Mie 514-8507, Japan*)

Theoretical investigation on the structural stability of GaAs nanowires with two different types of facets

Mo-mP8 (20) **T. Mano, T. Kuroda, B. Mcskimming, A. Ohtake, K. Mitsuishi, T. Noda, K. Sakoda** (*National Institute for Materials Science, 1-2-1 Sengen, Tsukuba, Ibaraki 305-0047, Japan*)

Self-assembly of symmetric, unstrained GaAs quantum dots without wetting layer by droplet epitaxy

Mo-mP9 (21) **T. Toujyou[1], T. Noda[2], T. Teraoka[1], T. Konishi[1], S.Tsukamoto[1]** ([1]*Anan National college of Technology, 265 Aoki Minobayashi Anan, Tokushima 7740017, Japan,* [2]*National Institute for Materials Science, 1-2-1 Sengen Tsukuba, Ibaraki 3050047, Japan*)

$insitu$ STM observation of nano-structures generated near InAs quantum dots on GaAs(001) surface

Mo-mP10 (22) **A.Bonanni[1], A.Navarro-Quezada[1], T.Li[1], B.Faina[1], R.Lechner[1], G.Bauer[1], M.Rovezzi[2], F.D'Acapito[2], W.Stefanowicz[3], M.Kiecana[3], M.Sawicki[3], T.Dietl[3]** ([1]*Institut für Halbleiter und Festkörperphysik, Johannes Kepler University, Altenbergerstr. 69, Linz - Austria,* [2]*Italian Collaborating Research Group ESRF, Grenoble - France,* [3]*Institute of Physics, Polish Academy of Sciences, Warsaw - Poland*)

Controlling the aggregation of magnetic cations in GaN

Mo-mP11 (23) **R. J. Young, L. O. Mereni, V. Dimastrodonato, S. B. Healy, E. P. O'Reilly, E. Pelucchi** (*Tyndall National Institute, University College Cork, Cork , Ireland*)

Highly uniform site-controlled quantum dots with record spectral purity

Mo-mP12 (24) **A. Ishii[1], Hiroki Asano[1], Mami Yokoyama[1], Shiro Tsukamoto[2]** ([1]*Dept.Applied Mathematics and Physics, Tottori University, 4-101 Koyama-Minami, Tottori-City, Tottori 680-8552, Japan,* [2]*Center for Collaborative Research, Anan National College of Technology, Anan, Tokushima 774-0017, Japan*)

Structure determination of Pd-catalyst supported on S-terminated GaAs (001) using DFT calculation

Mo-mP13 (25) **Mami Yokoyama[1], Shiro Tsukamoto[2], Akira Ishii[1]** ([1]*Department of Applied Mathematics and Physics, Tottori University, 4-101 Koyama-Minami, Tottori 680-8552, Japan ,* [2]*Center for Collaborative Research, Anan National College of Technology, Anan, Tokushima 774-0017, Japan*)

Structure determination of Pd-catalyst supported on S-terminated GaN (0001) using DFT calculation

Mo-mP22 (34) **N. Kumagai[1], S. Ohkouchi[1,2], S. Nakagawa[1,4], M. Nomura[1], Y. Ota[1,4], M. Shirane[1,2], Y. Igarashi[1,2], S. Yorozu[1,2], S. Iwamoto[1,3,4], Y. Arakawa[1,3,4]** (*[1]INQIE, Univ. of Tokyo, 4-6-1 Komaba, Meguro-ku, Tokyo 1538505, Japan, [2]NEC, 34 Miyukigaoka, Tsukuba 3058501, Japan, [3]IIS, Univ. of Tokyo, 4-6-1 Komaba, Meguro-ku, Tokyo 1538505, Japan, [4]RCAST, Univ. of Tokyo, 4-6-1 Komaba, Meguro-ku, Tokyo 1538505, Japan*)

Suppression of indefinite peaks in InAs/ GaAs quantum dot spectrum by low temperature Indium-flush method

Mo-mP23 (35) **T. Shindo, R. Kaji, S. Adachi, S. Muto** (*Department of Applied Physics, Hokkaido University, N13 W8, Kitaku, Sapporo 060-8628, Japan*)

Polarization conversion of excitonic photoluminescence under zero and nonzero magnetic field in a single InAlAs quantum dot

Mo-mP24 (36) **A. Laucht, N. Hauke, J. M. Villas-Boas, F. Hofbauer, M. Kaniber, G. Böhm, J. J. Finley** (*Walter Schottky Institut, Technische Universität München, Am Coulombwall 3, 85748 Garching , Germany*)

Experimentally probing dephasing of zero dimensional exciton-polaritons

Mo-mP25 (37) **D. Lucot, G. Faini, J.C. Harmand, D. G Mailly, G. Patriarche** (*CNRS - Laboratoire de Photonique et de Nanostructures, route de Nozay, Marcoussis 91460, France*)

Growth and electrical characterizations of semiconducting nanowires

Mo-mP26 (38) **K. Akahane, N. Yamamoto** (*National Institute of Information and Communications Technology, 4-2-1, Nukui-Kitamachi, Koganei, Tokyo 1848795, Japan*)

Formation of InAs quantum dots at ultra-high growth rates

Mo-mP27 (39) **S. Hiratsuka[1], Y. Mizoguchi[1], S. Takeda[1], S. Saravanan[2], N. Ohtani[1]** (*[1]Department of Electronics, Doshisha University, 3-1 Tatara-Miyakodani, Kyotanabe-shi, Kyoto 610-0321, Japan, [2]ATR Wave Engineering Laboratories, Keihanna Science City, Kyoto, Japan*)

Photoluminescence properties of annealed and non-annealed InAs quantum dots

Mo-mP28 (40) **D. Sarkar[1], H. P. van der Meulen[1], J. M. Calleja[1], J. M. Meyer[2], R. J. Haug[2], K. Pierz[3]** (*[1]Departamento de Física de Materiales, Universidad Autónoma de Madrid, E-28049 Madrid, Spain, , [2]Institut für Festkörperphysik, Leibniz Universität Hannover, D-30167 Hannover, Germany, [3]Physikalisch-Technische Bundesanstalt Braunschweig, D-38116 Braunschweig, Germany,*)

Magneto-photoluminescence spectroscopy of single InAs/AlAs quantum dots

Mo-mP29 (41) **K. Shibata[1], M. Jung[1], K. M. Cha[1], M. Sotome[1], K. Hirakawa[1,2]** (*[1]IIS and INQIE, University of Tokyo, 4-6-1 Komaba, Meguro-ku, Tokyo 153-8505, Japan, [2]CREST-JST, 4-1-8 Honcho, Kawaguchi, Saitama 332-0012, Japan*)

Control of tunnel coupling strength between InAs quantum dots and nanogap metallic electrodes through In-Ga intermixing

Mo-mP30 (42) **W.Q. Ma[1], X.J. Yang[1], M. Chong[1], T. Yang[1], L.H. Chen[1], J. Shao[2], X. Lü[2], W. Lu[2], C.Y. Song[3], H.C. Liu[1]** (*[1]Institute of Semiconductors, Chinese Academy of Sciences, Qinghua East Road A35, P.O. Box 912, Beijing 100083 100083, P. R. China, [2] Shanghai Institute for Technical Physics, Chinese Academy of Sciences, Shanghai 200083, P. R. China, [3] Institute for Microstructural Sciences, National Research Council, Ottawa, Canada K1A 0R6*)

Two-color quantum dot infrared photodetector using Fowler-Nordheim tunneling

Mo-mP31 (43) **J. H. Paek, T. Nishiwaki, M. Yamaguchi, N. Sawaki** (*Department of Electronics, Nagoya University, Furo-cho 3C-1, Chikusa-ku, Nagoya*)

MBE-VLS growth of a catalyst-free GaAs/AlGaAs core-multishell nanowire on (111) silicon substrate

Mo-mP32 (44) **A. K. Nowak[1], E. Gallardo[1], D. Sarkar[1], D. Sanvitto[1], H. P. van der Meulen[1], J. M. Calleja[1], J. M. Ripalda[2], L. González[2], Y. González[2]** ([1]*Departamento de Física de Materiales, Universidad Autónoma de Madrid, E-28049 Madrid, Spain, ,* [2]*Instituto de Microelectrónica de Madrid, Centro Nacional de Microelectrónica, Consejo Superior de Investigaciones Científicas, Isaac Newton 8, PTM Tres Cantos, E-28760 Madrid, Spain,*)

Temperature dependent single photon emission in InP/GaInP quantum dots

Mo-mP33 (45) **E. Gallardo[1], L.J. Martínez[2], A.K. Nowak[1], D. Sarkar[1], D. Sanvitto[1], H.P. van der Meulen[1], J.M Calleja[1], I. Prieto[2], A.R. Alija[2], D. Granados[2], A.G. Taboada[2], J.M. García[2], P.A. Postigo[2]** ([1]*Departamento de Física de Materiales, Universidad Autónoma de Madrid, E-28049 Madrid, Spain, Dpto. de Física de Materiales (C-IV), Facultad de Ciencias, C/ Francisco Tomás y Valiente, n 7, Ctra. Colmenar Viejo, Km. 15, 28049 Cantoblanco, MADRID, SPAIN 28049, Spain,* [2]*Instituto de Microelectrónica de Madrid, Centro Nacional de Microelectrónica, Consejo Superior de Investigaciones Científicas, Isaac Newton 8, PTM Tres Cantos, E-28760 Madrid, Spain, Instituto de Microelectrónica de Madrid, Isaac Newton 8, PTM Tres Cantos, E-28760 Madrid, Spain*)

Quantum correlation spectroscopy of single quantum rings embedded in photonic crystal microcavities

Mo-mP34 (46) **M. Mehta[1], D. Reuter[2], A. Melnikov[2], A. D. Wieck[2], S. Michaelis de Vasconcellos[1], T. Baumgarten[1], A. Zrenner[1], C. Meier[1]** ([1]*Experimental Physics, University of Paderborn, Warburger Strasse 100, Paderborn 33098, Germany,* [2]*Applied Solid State Physics, Ruhr University , Bochum, Germany*)

Intentionally positioned self-assembled InAs quantum dots in an electroluminescent p-i-n junction diode

Mo-mP35 (47) **L. Xu[1], K.Ozasa[2], H.Kakoi[1], Y.H.Liang[1], Y.Arai[1], W.Araki[1]** ([1]*School of Science and Engineering, Saitama University, 255 Shimo-Ohkubo, Sakuraku, Saitama 338-0825, Japan,* [2]*RIKEN, 2-1 Hirosawa, Wako, Saitama 351-0198, Japan*)

Γ-X crossover in InGaAs/GaAs quantum dots due to the indentation of a flat cylindrical nanoprobe

Mo-mP36 (48) **K.Y. Chuang, C.Y. Chen, T.E. Tzeng, David J.Y. Feng, T. Lay** (*Department of Photonics, National Sun Yat-Sen University, Kaohsiung 804, TAIWAN*)

Modulation-doping effect on the optical characteristics of vertically coupled InGaAs quantum dots

Mo-mP37 (49) **E. Cruz-Hernandez[1], J. Hernandez-Rosas[2], J.S. Rojas-Ramirez[2], R. Contreras-Guerrero[2], R. Mendez-Camacho[3], C. Mejia-Garcia[3], V.H. Mendez-Garcia[4], M. Lopez-Lopez[2]** ([1]*Graduate School of Science and Engineering, Ehime University, 3 Bukyo-cho, Matsuyama, Ehime 790-8577, Japan,* [2]*Physics Department, CINVESTAV-IPN, Mexico DF, 07000, Mexico,* [3]*Superior School of Physics and Mathematics-IPN, Mexico DF, 07000, Mexico,* [4]*Optical Communications Research Institute, UASLP, San Luis Potosi, 78210, Mexico*)

Optical transitions in AlGaAs/GaAs quantum wires on GaAs(631) substrates studied by photoreflectance spectroscopy

Mo-mP38 (50) **T.E. Tzeng, K.Y. Chuang, C.Y. Chang, David J.Y. Feng, T. Lay** (*Department of Photonics, National Sun Yat-Sen University, Kaohsiung, Taiwan 804, TAIWAN*)

Photovoltaic response in multi-stack $In_xGa_{1-x}As$ quantum dots

Mo-mP39 (51) **E.Y. Lin, C.Y. Chen, S.L. Chen, T.E. Tzeng, David J.Y. Feng, T. Lay** (*Department of Photonics, National Sun Yat-Sen University, Kaohsiung, Taiwan 804, TAIWAN*)

Modulation spectroscopy on metamorphic InAs quantum dots

Mo-mP40 (52) **Y. Saeki[1], Y. Nakazato[1], S. Izumi[1], T. Nukui[1], A. Tackeuchi[1], J. H. Jung[2], J. H. You[2], T. W. Kim[2], Y-H. Kim[3]** ([1]*Department of Applied Physics, Waseda University, 3-4-1 Okubo, Shinjuku-ku, Tokyo 169-8555, Japan,* [2]*Division of Electronic and Computer Engineering, Hanyang University, Seoul 133-791, Korea,* [3]*Division of Materials Science and Engineering, Hanyang University, Seoul 133-791, Korea*)

Time-Resolved Photoluminescence Study of ZnO Nanocrystals Embedded in a Hybrid Polymer Composite Layer

Mo-mP41 (53) **Y. Shoji[1,3], R. Oshima[1], A. Takata[2], A. Uedono[3], Y. Okada[1,2]** ([1]*Research Center for Advanced Scienceand Technology (RCAST), The University of Tokyo, c/o Okada lab. 505 CCR, 4-6-1 Komaba, Meguro-ku153-8904, Tokyo, Japan,* [2]*Graduate School of Engineering, The University of Tokyo, c/o Okada lab. 505 CCR, 4-6-1 Komaba, Meguro-ku 153-8904, Tokyo, Japan,* [3]*Institute of Applied Physics, University of Tsukuba, 1-1-1 Tennodai, Tsukuba 305-8973, Ibaraki, Japan*)

The effect of spacer layer thickness on vertical alignment of InGaAs/GaNAs quantum dots grown on GaAs(311)B substrate

Mo-mP42 (54) **A. Takata[1], R. Oshima[2], Y. Shoji[2,3], Y. Okada[1,2]** ([1]*School of Engineering, The University of Tokyo, 4-6-1 Komaba, Meguro-ku, Tokyo 1538904, Japan,* [2]*Research Center for Advanced Science and Technology, The University of Tokyo, 4-6-1 Komaba, Meguro-ku, Tokyo 1538904, Japan,* [3]*Institute of Applied Physics, University of Tsukuba, 1-1-1 Tennodai, Tsukuba, Ibaraki 3058973, Japan*)

Growth of multi-stacked InAs/GaNAs quantum dots grown with As_2 source in atomic hydrogen-assisted molecular beam epitaxy

Mo-mP43 (55) **B. Bansal[1,2], S. Godefroo[2], M. Hayne[3], G. Medeiros-Ribeiro[4], V. Moshchalkov[2]** ([1]*IMM, High Field Magnet Laboratory, University of Nijmegen, Toernooiveld 7, 6525 ED Nijmegen, The Netherlands,* [2]*INPAC-Institute for Nanoscale Physics and Chemistry, KU Leuven, Celestijnenlaan 200D, Leuven B-3001, Belgium,* [3]*Department of Physics, Lancaster University, Lancaster LA1 4YB, UK,* [4]*Laboratório Nacional de Luz Síncrotron, P.O. Box 6192, 13084-971 Campinas-SP, Brazil*)

Excitons and biexcitons in type-II InP/GaAs quantum dots

Mo-mP44 (56) **M. Royo Valls, J.I. Climente, J.L. Movilla, F. Rajadell, J. Planelles** (*Departament de Química Física i Analítica, Universitat Jaume I, Av./ de Vicent Sos Baynat, Castelló 12071, Spain*)

Electron-hole complexes in semiconductor nanorods

Mo-mP45 (57) **D. Salloch[1], U. Wieser[1], U. Kunze[1], T. Hackbarth[2]** ([1]*Werkstoffe und Nanoelektronik, Ruhr-Universitaet Bochum, Bochum 44780, Germany,* [2]*DaimlerChrysler Forschungszentrum Ulm, Wilhelm-Runge-Straße 11, D-89081 Ulm, Germany*)

Efficient injection-type ballistic rectification in Si/SiGe cross junctions

Mo-mP46 (58) **B. Marquardt[1], M. Geller[1], A. Lorke[1], D. Reuter[2], A. Wieck[2]** (*[1]Experimental Physics, University Duisburg-Essen, Lotharstraße 1, Duisburg, Germany, [2]Department of Applied Physics, Ruhr-University, Universitätsstraße 150, Bochum, Germany*)

A two-dimensional electron gas as a sensitive detector to observe the charge carrier dynamics of self-assembled QDs

Mo-mP47 (59) **J. I. Climente[1], M.F. Doty[2], M. Korkusinski[3], M. Scheibner[4], A.S. Bracker[4], D. Gammon[4], P. Hawrylak[3]** (*[1]Department of Physical and Analytical Chemistry, Universitat Jaume I, Castellon, Spain, [2]Department of Materials Science, University of Delaware, Newark, USA, [3]Institute of Microstructural Sciences, National Research Council, Ottawa, Canada, [4]Naval Research Labs, Washington, USA*)

Holes in double quantum dots: effects of the spin-orbit interaction

Mo-mP48 (60) **A. Babinski[1], A.Golnik[1], T.Tite[1], P.Kossacki[1], J.Gaj[1], S.Raymond[2], Z.Wasilewski[1,2]** (*[1]Institute of Experimental Physics, University of Warsaw, Hoza 69 00-681 Warszawa, POLAND, [2]Institute for Microstructural Sciences, NRC, Ottawa, CANADA*)

Optical anisotropy of a triexciton in a quantum dot

Mo-mP49 (61) **W. Lu, I. Kamiya** (*Toyota Technological Institute, 2-12-1 Hisakata Tempaku, Nagoya, Japan 4688511, Japan*)

Temperature dependence of electronic energy transfer in PbS quantum dot films

Mo-mP50 (62) **R. Oshima[1], A. Takata[2], Y. Shoji[1,3], Y. Okada[1,2]** (*[1]Research Center for Advanced Science and Technology, The University of Tokyo, 4-6-1 Komaba, Meguro-ku, Tokyo 153-8904, Japan, [2]Graduate School of Engineering, The University of Tokyo, 4-6-1 Komaba, Meguro-ku, Tokyo 153-8904, Japan, [3]Institute of Applied Physics, University of Tsukuba, 1-1-1 Tennodai, Tsukuba, Ibaraki 305-8573, Japan*)

InAs/GaNAs strain-compensated quantum dots stacked over 50 layers for use in high-efficiency solar cell

Mo-mP51 (63) **T. Kawazu[1], T. Mano[1], T. Noda[1], H. Sakaki[1,2]** (*[1]National Institute for Materials Science, 1-2-1 Sengen, Tsukuba, Ibaraki, Japan, [2]Toyota Technological Institute, 2-12-1 Hisakata, Tempaku-ku, Nagoya, Japan*)

Thermal annealing of GaSb quantum dots in GaAs formed by droplet epitaxy

Mo-mP52 (64) **K. Umeno, R. Noma, Y. Furukawa, S. Mitsuyoshi, H. Okada, A. Wakahara, H. Yonezu** (*Department of Electrical and Electronic Engineering, Toyohashi University of Technology, 1-1, Hibarigaoka, Tempaku-cho, Toyohashi, Aichi 441-8580, Japan*)

Growth and luminescence characterization of self-assembled InGaAsN/GaPN quantum dots for photonics applications on Si

Mo-mP53 (65) **T. Kamimura[1,2,3], K. Matsumoto[1,3,4]** (*[1]National Institute of Advanced Industrial Science and Technology, 1-1-1 Umezono, Tsukuba, Ibaraki 3058568, Japan, [2]the Japan Society for the Promotion of Science, 5-3-1 kojimachi, chiyodaku, Tokyo, 1028471, Japan, [3]CREST-JST, 4-1-8 Honcho, Kawaguvhi, Saitama, 332-0012, Japan, [4]ISIR, Osaka University, 8-1 Mihogaoka, Ibaraki, Osaka, 567-0047, Japan*)

Channel length dependence of Single-walled carbon nanotube multi-functional quantum transistor characteristics

Mo-mP54 (66) **T. Kitada, A. Mukaijo, T. Takahashi, T. Mukai, K. Morita, T. Isu** (*Center for Frontier Research of Engineering, Institute of Technology and Science, The University of Tokushima, 2-1 Minami-josanjima-cho, Tokushima 770-8506, Japan*)

Doping effect on photocarrier lifetime in InAs quantum dots with strain-relaxed InGaAs barriers grown by molecular beam epitaxy

Mo-mP55 (67) **T. Endoh** (*Center for Interdisciplinary Research, TOHOKU UNIVERSITY, Aramaki aza Aoba 6-3, Aoba-ku, Sendai 980-8578, Japan*)

High Performance Multi-Nano-Pillar Vertical MOSFET Scaling from 50nm to 15nm Node

Mo-mP56 (68) **L. Gence[1], V. Callegari[2], A. Dinescu[3], S. Melinte[1], S. Demoustier-Champagne[2]** ([1]*UCL-Ecole Polytechnique de Louvain - Laboratoire de Microélectronique DICE, 1, Rue Archimède, Louvain-la-Neuve 1348 , Belgium,* [2]*UCL- Ecole Polytechnique de Louvain - Laboratoire de chimie et de physique des hauts polymères, 1, Place croix du sud, Louvain-la-Neuve 1348 , Belgium,* [3]*National Institute for RandD in Microtechnologies IMT, 126A, Erou Iancu Nicolae street, 077190, Bucharest, ROMANIA*)

Hybrid polymer nanowire based electronic devices: correlated characterization

Mo-mP57 (69) **Dong Uk Lee[1], E. Kim[1], Goon-Ho Park[2], Won-Ju Cho[2]** ([1]*Department of Physics, Hanyang University, 17 Haengdang-dong, Seongdong-gu, Seoul 133-791, Korea,* [2]*Department of Electronic Materials Engineering, Kwangwoon University, Seoul 139-701, Korea*)

Electrical characterization of multilayered SiC nano-particles for application as tunnel barrier engineered non-volatile memory

Mo-mP58 (70) **D. Kammerlander[1,2], G. Ferrari[1,3], F. Troiani[1], G. Goldoni[1,2]** ([1]*CNR-INFM Research Center for nanoStructures and bioSystems at Surfaces (S3), Via Campi 213/A, Modena 41100, Italy,* [2]*Dipartimento di Fisica, Univ. di Modena e Reggio Emilia, Via Campi 213/A, Modena 41100, Italy,* [3]*CNISM Research Unit of Modena, 41100 Modena, Italy*)

Optical signatures of neutral and charged excitons in inorganic semiconducting nanotubes

Mo-mP59 (71) **K. Morita, T. Takahashi, T. Kanbara, S. Yano, T. Mukai, T. Kitada, T. Isu** (*Center for Frontier Research of Engineering, Institute of Technology and Science, The University of Tokushima, 2-1 Minami-jyosanjima-cho, Tokushima, 770-8506, Japan*)

Large optical Kerr signal of GaAs/AlAs multilayer cavity with InAs quantum dots embedded in strain-relaxed barriers

Mo-mP60 (72) **T. Sogawa[1], H. Sanada[1], H. Gotoh[1], H. Yamaguchi[1], S. Miyashita[2], P. V. Santos[3]** ([1]*NTT Basic Research Laboratories, NTT Corporation, 3-1 Morinosato Wakamiya, Atsugi-shi, Kanagawa 243-0198, Japan,* [2]*NTT Advanced Technology Corporation, 3-1 Morinosato Wakamiya, Atsugi-shi, Kanagawa 243-0198, Japan,* [3]*Paul Drude Institute, Hausvogteiplatz 5-7,10117 Berlin, Germany*)

Polarization anisotropy of dynamic quantum wires formed by surface acoustic waves

Mo-mP61 (73) **J. Renard, H. Mariette, E. Monroy, B. Gayral** (*CEA-CNRS "Nanophysique et semiconducteur" group, CEA-Grenoble, INAC/SP2M, 17 rue des Martyrs, 38054 Grenoble, France*)

Suppression of non-radiative recombination up to room temperature in long-lived GaN/AlN quantum dots

Mo-mP62 (74) **H. Wang[1], Liming Jiang[1], Huiting Wu[1], Qian Gong[2], Songlin Feng[2]** ([1]*College of Physics and Engineering, Qufu Normal University, , [2]Key laboratory of wireless sensor network and communication, Shanghai Institute of Micro-system and Information Technology,*)

Hydrogenic impurity states in zinc-blende InGaN/GaN cylindrical quantum-well wires

Mo-mP63 (75) **J.I.Climente[1,2], A. Bertoni[2], G. Goldoni[2,3]** ([1]*Departament de Química Física i Analítica, Universitat Jaume I, Castello, Spain, [2]CNR-INFM research center for nanoStructures and bioSystems at Surfaces, Via Campi 213/a, Modena, Italy, [3]Department of Physics, Univ. of Modena and Reggio E., Via Campi 213/a, Modena , italy*)

Photoluminescence of trions in quantum dots: the dominant role of valence band correlations

Mo-mP64 (76) **T. Okuhata[1], T. Sakka[1], S. Taguchi[1], A. A. Yamaguchi[2], T. Honda[1]** ([1]*Department of Electrical Engineering and Electronics, Graduate School of Engineering, Kogakuin University, 2665-1 Nakano-machi, Hachiohji, Tokyo 1920015, Japan, [2]Research Laboratory for Integrated Technological System, Kanazawa Institute of Technology, 1-2-3 Atago, Minato-ku, Tokyo, 1050002, Japan*)

Surface recombination processes of GaN crystallites

Mo-mP65 (77) **R. B. Chen[1], C. Chang[2], M. F. Lin[3]** ([1]*Center of General Studies, National Kaohsiung Marine University, Center of General Studies, National Kaohsiung Marine University, Kaohsiung, Taiwan, [2]Center of General Education, Tainan University of Technology, Center of General Education, Tainan University of Technology, Tainan, Taiwan, [3]Department of Physics, National Cheng Kung University , Department of Physics, National Cheng Kung University, Tainan, Taiwan*)

Electric-field-tunable electronic properties of graphene quantum dots

Mo-mP66 (78) **K. B. Hong[1], M. K. Kuo[1], T. R. Lin[2]** ([1] *Institute of Applied Mechanics, National Taiwan University, 1, Sec. 4, Roosevelt Road, Taipei 10672, TAIWAN, [2]Department of Mechanical and Mechatronic Engineering, National Taiwan Ocean University, 2, Beining Road, Keelung 20224, TAIWAN*)

Strain fields and transition energies for single and vertically stacked InAs/GaAs semiconductor quantum dots

Mo-mP67 (79) **EE Vdovin[1,2], O Makarovsky[1], L. Eaves[1], Yu.N. Khanin[2], A. Patane[1]** ([1]*University of Nottingham, School of Physics and Astronomy , United Kingdom, [2]Institute of Microelectronics Technology RAS, 142432 Chernogolovka, Russia*)

Sensitive detection of photoexcited carriers by resonant tunnelling through a single quantum dot

Mo-mP69 (80) **K. Fukui, I. Kamiya** (*Toyota Technological Institute, 2-12-1 Hisakata, Tempaku, Nagoya 468-8511, Japan*)

Luminescence from InAs/GaAs surface related states

Mo-mP70 (81) **Y. Kitauchi[1], K. Tomioka[1,2], Y. Kobayashi[1], S. Hara[1,2], T. Fukui[1,2], J. Motohisa[1]** ([1]*Graduate School of Information Science and Technology, Hokkaido University, North 14 West 9 Sapporo 060-0814, Japan, [2]Research Center for Integrated Quantum Electronics, Hokkaido University, North 13 West 8, Sapporo 060-8628, Japan*)

Structural transition of InP nanowires in selective-area metalorganic vapor phase epitaxy

Mo-mP71 (82) **M. J. Korkusinski, M. Zielinski, E. Kadantsev, P. Hawrylak** (*Institute of Microstructural Sciences, National Research Council of Canada, 1200 Montreal Rd, Bldg M50, Office 105, Ottawa K1A0R6, Canada*)

Atomistic theory of electronic and optical properties of self-assembled quantum dots

Mo-mP72 (83) **M. Mamizuka[1], O. Kojima[1], T. Kita[1], O. Wada[1], K. Akahane[2]** ([1]*Department of Electrical and Electronics, Graduate School of Engineering, Kobe University, Rokkodai 1-1, Nada, Kobe , Japan,* [2]*National Institute of Information and Communications Technology, 4-2-1 Nukui-kitamachi, Koganei, Tokyo, Japan*)

Resonant enhancement of excitonic photoluminescence via biexciton process in stacked InAs quantum dots

Mo-mP73 (84) **Yasuaki Masumoto[1], Ken Goto[1], Bipul Pal[1], Michio Ikezawa[1], Premila Mohan[2], Junichi Motohisa[2], Takashi Fukui[2]** ([1]*Institute of Physics, University of Tsukuba, 1-1-1 Tennoudai, Tsukuba, Ibaraki 3058571, Japan,* [2]*Research Center for Integrated Quantum Electronics, Hokkaido University, Sapporo 060-8628, Japan*)

Spectral diffusion of type-II excitons in InP/InAs/InP core-multishell nanowires

Mo-mP75 (85) **E. Storace[1], J. Weis[1], K. von Klitzing[1], S. De Franceschi[2,3], F. Jabeen[3], S. Rubini[3], F. Capotondi[3], F. Martelli[3]** ([1] *Max-Planck-Institut fanduumlr Festkandoumlrperforschung, Heisenbergstrasse 1 , Germany,* [2]*CEA, INAC/SPSMS/LaTEQS, 17 Rue des Martyrs, 38054 Grenoble, France,* [3]*Laboratorio Nazionale TASC-INFM-CNR, Area Science Park, S.S. 14, km. 163.5, I-34012 Trieste, Italy*)

Magnetotransport in MBE-grown III-V nanowires

Mo-mP76 (86) **M. Panfilova, S. Michaelis de Vasconcellos, A. Pawlis, K. Lischka, A. Zrenner** (*University of Paderborn, Warburger Str. 100, 33098 Paderborn, Germany*)

Photocurrent-spectroscopy of CdSe quantum dot photodiodes

Mo-mP77 (87) **C.-H. Lee[1], J. Yoo[1], Y.-J. Doh[1], G.-C. Yi[2]** ([1]*Department Materials Science and Engineering, POSTECH, Pohang, Gyeongbuk 790-784, Republic of Korea,* [2]*National Creative Research Initiative Center for Semiconductor Nanorods, Department of Physics and Astronomy, Seoul National University, Seoul 151-747, Korea*)

ZnO/$Mg_{0.2}Zn_{0.8}O$ Coaxial Nanorod Heterostructures for High Performance Electronic Nanodevice Applications

Mo-mP78 (88) **G. Granger, S. A. Studenikin, A. S. Sachrajda, A. Kam, P. J. Poole, G. C. Aers, R. L. Williams** (*Institute for Microstructural Sciences, National Research Council of Canada, 1200 Montreal Rd, Building M-50, Ottawa, K1A 0R6, Canada*)

Electron transport in gated InGaAs/InP and InAsP/InP quantum well ridge structures fabricated by nanotemplate technology

Mo-mP79 (89) **G. Zhang, K. Tateno, S. Suzuki, H. Gotoh, H. Nakano** (*NTT Basic Research Laboratories, 3-1 Morinosato-Wakamiya, Atsugi, Kanagawa 243-0198, Japan*)

Evidence of different doping modes in tapered VLS nanowires by studying axial distribution of carrier concentration in Si-doped InAs nanowires

Mo-mP80 (90) **C. Nishimura[1], G. Imamura[1], M. Fujii[1], T. Kawashima[2], T. Saitoh[2], S. Hayashi[1]** ([1]*Department of Electrical and Electronic Engineering, Kobe University, Rokkodai, Nada, Kobe 657-8501, Japan,* [2]*Panasonic Corporation, 3-1-1 Yagumo-Nakamachi, Moriguchi, Osaka 570-8501, Japan*)
Boron and Germanium Distribution in Individual Boron-doped $Si_{1-x}Ge_x$ Alloy Nanowires Grown by a Vapor Liquid Solid process

Mo-mP81 (91) **M. Hassan Abdellatif, O. S. Kopylov, Jin Dong Song, Won Jun Choi, Nam Ki Cho, Jung Il Lee** (*KIST, Korea institute of sience and technology, KIST International RandD Academy, Nano-Science Research Division, 39-1, San wolgok-dong, Sungbuk-ku, Seoul, Korea 136-791*)
Critical Exciton Temperature in InAs/GaAs quantum dot sample by infrared time resolved spectroscopy

Mo-mP82 (92) **M. Csontos[1], Y. Komijani[1], T. Ihn[1], K. Ensslin[1], D. Reuter[2], A. D. Wieck[2]** ([1]*Solid State Physics Laboratory, ETH Zürich, Schafmattstrasse 16, Zürich 8093, Switzerland,* [2]*Angewandte Festkörperphysik, Ruhr-Universität Bochum, 44780 Bochum, Germany*)
Observation of excited states in a p-type GaAs quantum dot

Tuesday July 21st

Session M2 (International Conference Room) 9:00 – 10:30

Terahertz dynamics and devices

M2a (94) 9:00 – 9:30 **R. Huber[1], A. A. Anappara[1], A. Sell[1], G. Günter[1], G. Biasiol[2], L. Sorba[2], S. De Liberato[3], C. Ciuti[3], A. Tredicucci[2], A. Leitenstorfer[1]** (Invited) ([1]*Department of Physics and Center for Applied Photonics, University of Konstanz, Germany,* [2]*Laboratorio NEST CNR-INFM and Scuola Normale Superiore, Pisa; Laboratorio Nazionale TASC CNR-INFM, Trieste, Italy,* [3]*Laboratoire Matériaux et Phénomènes Quantiques, Université Paris Diderot - Paris 7 and CNRS, Paris; Laboratoire Pierre Aigrain, Ecole Normale Superieure, Paris, France*)
Non-adiabatic control of intersubband cavity polaritons

M2b (97) 9:30 – 9:45 **T. Unuma[1,2], Y. Ino[3], M. Kuwata-Gonokami[3], K. Hirakawa[1]** ([1]*Institute of Industrial Science and INQIE, University of Tokyo, 4-6-1 Komaba, Meguro-ku, Tokyo 153-8505, Japan,* [2]*Department of Applied Physics, Nagoya University, Furo-cho, Chikusa-ku, Nagoya 464-8603, Japan,* [3]*Department of Applied Physics and INQIE, University of Tokyo, 7-3-1 Hongo, Bunkyo-ku, Tokyo 113-8656, Japan*)
Breakdown of the semiclassical miniband picture for transient electron transport in GaAs-based superlattices

M2c (98) 9:45 – 10:00 **A. Wade[1], D. Smirnov[1], S. Kumar[2], B.S. Williams[3], Q. Hu[2], J.L. Reno[4]** ([1]*National High Magnetic Field Laboratory, Tallahassee, Florida 32310, USA,* [2]*Massachusetts Institute of Technology, Cambridge, Massachusetts 02139, USA,* [3]*University of California at Los Angeles, Los Angeles, California 90095, USA,* [4]*Sandia National Laboratories, Albuquerque, New Mexico 87185-0601*)
Magnetic field assisted sub-THz quantum cascade lasers

M2d (99) 10:00 – 10:15 **T. T. Lin, K. Ohtani, H. Ohno** (*Laboratory for Nanoelectronics and Spintronics, Research Institute of Electrical Communication, Tohoku University, 2-1-1 Katahira, Aoba-ku, Sendai, Miyagi 980-8577, Japan*)

Fabrication and operation of a metal-metal waveguide GaAs terahertz quantum cascade laser

M2e (100) 10:15 – 10:30 **E. Mujagi'c**[1], **S. Schartner**[1], **M. Nobile**[1], **H. Detz**[1], **A. M. Andrews**[1], **P. Klang**[1], **W. Schrenk**[1], **C. Deutsch**[2], **K. Unterrainer**[2], **M. P. Semtsiv**[3], **W. T. Masselink**[3], **G. Strasser**[1,4] ([1]*Institute for Solid State Electronics, Vienna University of Technology, Floragasse 7, Vienna 1040, Austria,* [2]*Photonics Institute, Vienna University of Technology, Gußhausstr. 25-29, Vienna 1040, Austria,* [3]*Department of Physics, Humboldt University Berlin, Newtonstrasse 15, Berlin 12489, Germany,* [4]*Department of Electrical Engineering and Physics, State University of New York, 332 Bonner Hall, NY, Buffalo, 14260-1920, USA*)

Tailored beams in quantum cascade ring lasers

10:30 – 11:00 **Coffee Break**

Session M3 (International Conference Room) 11:00 – 12:30

Physics and devices for quantum information processing

M3a (102) 11:00 – 11:30 **R. J. Warburton**[1], **Daniel Brunner**[1], **Brian D. Gerardot**[1], **Paul A. Dalgarno**[1], **Nick G. Stoltz**[2], **Pierre M. Petroff**[2] (Invited) ([1]*School of Engineering and Physical Sciences, Heriot-Watt University, Edinburgh EH14 4AS, UK,* [2]*Materials Department, University of California, Santa Barbara, California 93106, USA*)

Coherent Hole Spin in a Semiconductor Quantum Dot

M3b (103) 11:30 – 11:45 **A. J Bennett**[1], **R. M. Stevenson**[1], **A. J. Hudson**[1,2], **R. J. Young**[1], **C. A. Nicoll**[2], **D. A. Ritchie**[2], **A. J. Shields**[1] ([1]*Toshiba Research Europe Limited, 260 Science Park, Milton Road, Cambridge CB58QE, UK,* [2]*Cavendish Laboratory, Cambridge University, JJ Thomson Avenue, Cambridge, CB3 0HE, U K.*)

Phase and coherence of entangled photon pairs from a single quantum dot

M3c (104) 11:45 – 12:00 **E. Stock**[1], **A. Lochmann**[1], **J. A. Töfflinger**[1], **W. Unrau**[1], **A. Toropv**[2], **A. Bakarov**[2], **A. Kalagin**[2], **V. Haisler**[2], **D.Bimberg**[1] ([1]*Institut für Festkörperphysik, Technische Universität Berlin, Germany , Hardenbergstr. 36, Berlin 10623, Germany,* [2]*Institute of Semiconductor Physics, Novosibirsk, Russia*)

Microcavity quantum dot single photon source electrically driven at 1 GHz

M3d (105) 12:00 – 12:15 **S. Michaelis de Vasconcellos**[1], **S. Gordon**[1], **M. Bichler**[2], **D. Reuter**[3], **A. Wieck**[3], **A. Zrenner**[1] (*[1]Department of Physics, University of Paderborn, Warburger Str. 100, 33098 Paderborn, Germany, [2]Walter-Schottky-Institute, TU Munich, Am Coulombwall, 85748 Garching b. München, Germany, [3]Applied Solid State Physics, Ruhr-University of Bochum, Universitätsstraße 150, 44780 Bochum, Germany*)

Demonstration of an optoelectronic quantum phase gate

M3e (106) 12:15 – 12:30 **T. Nakaoka**[1,2,3], **K. Watanabe**[1], **N. Kumagai**[1], **Y. Arakawa**[1,3] (*[1]Institute for Nano Quantum Information Electronics, the University of Tokyo , 4-6-1 Komaba, Meguro-ku, Tokyo 153-8505 Japan, [2]PRESTO, Japan Science and Technology Agency, 4-1-8 Honcho Kawaguchi, Saitama 332-0012, Japan, [3] Institute of Industrial Science, the University of Tokyo, 4-6-1 Komaba, Meguro-ku, Tokyo 153-8505 Japan*)

Lateral single electron transport in capped self-assembled quantum dots

12:30 – 14:00 **Lunch Break**

Session M4 (International Conference Room) 14:00 – 16:00

Optical properties of quantum dots

M4a (108) 14:00 – 14:15 **S. Ates**[1], **S. M. Ulrich**[1], **S. Reitzenstein**[2], **A. Löffler**[2], **A. Forchel**[2], **P. Michler**[1] (*[1]Institut für Halbleiteroptik und Funktionelle Grenzflächen, Universität Stuttgart, Allmandring 3, 70569 Stuttgart, Germany, [2]Technische Physik, Universität Würzburg, Am Hubland, 97074 Würzburg, Germany*)

Two-photon interference from the resonance fluorescence of a single quantum dot in a microcavity

M4b (109) 14:15 – 14:30 **T. Kuroda**[1], **T. Mano**[1], **T. Belhadj**[1,2], **M. Abbarchi**[1,3], **C. Mastrandrea**[3], **M. Gurioli**[3], **B. Urbaszek**[2], **T. Amand**[2], **X. Marie**[2], **N. Ikeda**[1], **Y. Sugimoto**[1], **K. Asakawa**[1], **K. Sakoda**[1] (*[1]Quantum Dot Research Center, National Institute for Materials Science, 1 Namiki, Tsukuba 305-0044, Japan, [2]Université de Toulouse, LPCNO, INSA-CNRS-UPS, 135 avenue de Rangueil, 31077 Toulouse Cedex 4, France, [3]Dipartimento di Fisica, CNISM, Università di Firenze, and LENS, Via Sansone 1, I-50019, Sesto Fiorentino, Italy*)

Quantum statistics of correlated two photons with biexciton-exciton cascades: saturation effect

M4c (110) 14:30 – 14:45 **T. Grange**[1], **E. A. Zibik**[2], **B. A. Carpenter**[2], **N. E. Porter**[2], **R. Ferreira**[1], **G. Bastard**[1], **D. Stehr**[3], **S. Winnerl**[3], **M. Helm**[3], **H. Y. Liu**[4], **M. S. Skolnick**[2], **L. R. Wilson**[2] (*[1]Laboratoire Pierre Aigrain, Ecole Normale Supérieure, CNRS, Paris, France, , [2]Department of Physics and Astronomy, University of Sheffield, UK, , [3]Institute of Ion Beam Physics and Material Research, Dresden, Germany, , [4]EPSRC National Centre for III-V Technologies, Sheffield, UK*)

Carrier relaxation in quantum dots: strong energy dependence in the terahertz domain

M4d (111) 14:45 – 15:00 **C. Hermannstädter[1], G. J. Beirne[1,4], M. Witzany[1], L. Wang[2], A. Rastelli[3], W.-M. Schulz[1], M. Jetter[1], O. G. Schmidt[3], P. Michler[1]** ([1]*Institut für Halbleiteroptik und Funktionelle Grenzflächen, Universität Stuttgart, Allmandring 3, 70569 Stuttgart, Germany,* [2]*Max-Planck-Institut für Festkörperforschung, Heisenbergstr. 1, 70569 Stuttgart, Germany,* [3]*Institut für Integrative Nanowissenschaften, IFW Dresden, Helmholtzstr. 20, 01069 Dresden, Germany,* [4]*Cavendish Laboratories, University of Cambridge, J. J. Thomson Ave., Cambridge, CB3 0HE, UK*)

Time-Resolved Optical Studies of the Charge Carrier Dynamics in Lateral InGaAs Quantum Dot Molecules

M4e (112) 15:00 – 15:15 **H. Sanada, T. Sogawa, H. Gotoh, Y. Tokura, H. Yamaguchi, H. Nakano, H. Kamada** (*NTT Basic Research Laboratories, 3-1, Morinosato-Wakamiya, Atsugi, Kanagawa 243-0198, Japan*)

Excited-state spectroscopy of charged quantum dots in magnetic field

M4f (113) 15:15 – 15:30 **J. van Bree[1], N. A. J. M. Kleemans[1], P. J. van Veldhoven[1], R. Nötzel[1], A. Yu. Silov[1], C. Pryor[2], M. E. Flatté[2], P. M. Koenraad[1]** ([1]*Photonics and Semiconductor Nanophysics, Eindhoven University of Technology, Den Dolech 2, Eindhoven 5600 MB , The Netherlands,* [2]*Department of Physics and Astronomy and Optical Science and Technology Center, University of Iowa, Iowa City, Iowa 52242, USA*)

Size-dependent exciton g-factor in self-assembled InAs/InP quantum dots

M4g (114) 15:30 – 15:45 **Y. Harada, O. Kojima, T. Kita, O. Wada** (*Department of Electrical and Electronics Engineering, Graduate School of Engineering, Kobe University, Rokkodai 1-1, Nada, Kobe 6578501, Japan*)

Magnetic-field control of exciton fine structure splitting in nitrogen δ-doped GaAs

M4h (115) 15:45 – 16:00 **S. Kriechbaumer[1], G. Springholz[1], T. Schwarzl[1], A. Hochreiner[1], W. Heiss[1], E. Kaufmann[1], M. Simma[1], H. Groiss[1], F. Schäffler[1], T. Wojtowicz[2], K. Koike[3], H. Harada[3], Y. Yano[3]** ([1]*Insitut fuer Halbleiter- und Festkoerperphysik, Johannes Kepler University, Altenbergerstr. 69, A-4040 Linz, Austria,* [2]*Institute of Physic, Polish Academy of Sciences, Lotnikov 32/46, 02-668 Warzawa, Poland,* [3]*Osaka Institute of Technology, Asahi-ku Ohmiya, Osaka 535-8585, Japan*)

Widely tunable intense MIR photoluminescence mission from epitaxial Pb(Sr)Te quantum dots embedded in CdTe

Poster Session Tu-mP (Meeting Room 501, 502) 16:00–18:00

Tu-mP2 (117) **T. Inoue[1], N. Yasuoka[1,2], O. Kojima[1], T. Kita[1], O. Wada[1]** ([1]*Department of Electrical and Electronics Engineering, Kobe University, 1-1 Rokkodai, Nada, Kobe, Hyogo 657-8501, Japan,* [2]*Fujitsu Laboratories Ltd., 10-1 Morinosato-Wakamiya, Atsugi, Kanagawa, 243-0197, Japan*)

Polarization controlled emission from stacked InAs quantum dots

Tu-mP3 (118) **J. Y. Lim[1,2], J. D. Song[1], W. J. Choi[1], J. I. Lee[1], S. H. Han[1], H. S. Yang[2], J. S. Kim[3]** ([1]*Nano Science Research Division, Korea Institute of Science and Technology, 39-1 Hawolgok dong, Sungbuk gu, Seoul 136-791, Korea,* [2]*Department of Physics, Chung-ang University, Seoul, Korea,* [3]*Department of Physics, Yeungnam University, Gyeongsan, Korea*)

Structural properties of GaP anti-quantum dots on the GaAs grown by droplet epitaxy

Tu-mP4 (119) **S. Roddaro[1], P. Caroff[2], G. Biasiol[3], F. Rossi[4], C. Bocchi[4], K. Nilsson[2], L. Fröberg[2], J.B. Wagner[2], L. Samuelson[2], L.-E. Wenersson[2], L. Sorba[1,3]** ([1]*NEST CNR-INFM and Scuola Normale Superiore, P.za S.Silvestro 12, 56127 Pisa, Italy,* [2]*Solid State Physics and the Nanometer Structure Consortium, P.O. Box 118, Lund, Sweden,* [3]*TASC CNR-INFM Laboratory, Area Science Park 34012 Trieste, Italy,* [4]*Istituto CNR-IMEM, Parco Area delle Scienze 43100 Parma, Italy*)

Controlled growth of InAs nanowires on engineered substrates

Tu-mP5 (120) **T. Fukushima[1], M. Ito[1], Y. Hijikata[1], H. Yaguchi[1], S. Yoshida[1], M. Okano[2], M. Yoshita[2], H. Akiyama[2], S. Kuboya[3], R. Katayama[3], K. Onabe[3]** ([1]*Graduate School of Science and Engineering, Saitama University, 255 Shimo-Okubo, Sakura-ku, Saitama 338-8570, Japan,* [2]*ISSP, The University of Tokyo, 5-1-5 Kashiwanoha, Kashiwa-shi, Chiba 277-8581 Japan,* [3]*Department of Advanced Materials Science, The University of Tokyo , 5-1-5 Kashiwanoha, Kashiwa-shi, Chiba 277-8583 Japan*)

Photoluminescence from single isoelectronic traps in nitrogen delta-doped GaAs grown on GaAs(111)A

Tu-mP6 (121) **N. Cho, S. J. Park, J. D. Song, W. J. Choi, J. I. Lee** (*Nano Device Research Division, KIST, Hawolgok-Dong, Sungbuk-Gu, Seoul , Korea*)

Growth of low density InGaAs quantum dots using MEMBE

Tu-mP7 (122) **G. Ferrari[1,2], G. Cuoghi[3], A. Bertoni[1], G. Goldoni[1,3], E. Molinari[1,3]** ([1]*S3 CNR-INFM National Research Center, Via Campi 213/A, Modena 41100, Italy,* [2]*CNISM Research Unit of Modena, Via Campi 213/A, 41100 Modena, Italy,* [3]*Department of Physics, University of Modena and Reggio Emilia, Via Campi 213/A, 41100 Modena, Italy*)

Edge localization, Landau levels and Aharonov-Bohm oscillations in core multi-shell nanowires

Tu-mP9 (123) **A.A. Vasilchenko** (*Kuban State Technological University, Russia, Krasnodar, Moskovskaya, 2*)

Oscillations of electron density in the quantum dot with large number of electrons in high magnetic field

Tu-mP10 (124) **A. Schramm[1,2], S. Schulz[2], T. Zander[2], Ch. Heyn[2], W. Hansen[2]** ([1]*Optoelectronics Research Centre, Tampere University of Technology, Korkeakoulunkatu 3, 33720 Tampere, Finland,* [2]*Institute of Applied Physics, University of Hamburg, Jungiusstrasse 11C, 20355 Hamburg, Germany*)

Strong competition between thermal and tunneling emission processes in self-assembled quantum dots

Tu-mP11 (125) **A. Schramm, V. Polojärvi, A. Tukiainen, A. Aho, M. Pessa** (*Optoelectronics Research Centre, Tampere University of Technology, Korkeakoulunkatu 3, 33720 Tampere, Finland*)

Dislocation-induced electron and hole levels in InAs quantum-dot Schottky diodes

Tu-mP12 (126) **M. Jung[1], W. Song[1], J. S. Lee[1], N. Kim[1], B.-C. Woo[1], J. Kim[1], K. Hirakawa[2]** ([1]*Korea Research Institute of Standards and Science, Daejeon 305600, Korea,* [2]*IIS and INQIE, University of Tokyo, Tokyo, Japan*)

Nanogap formation of indium oxide core/shell heterostructure nanowires

Tu-mP13 (127) **H. Kumano[1,2], H. Nakajima[1], H. Sasakura[1], I. Suemune[1,2]** ([1]*Research Institute for Electronic Science, Hokkaido University, Kita-21, Nishi-10, kita-ku, Sapporo 001-0021, Japan,* [2]*Japan Science and Technology Corporation (CREST), Kawaguchi, 332-0012, Japan*)

Two-mode photon interference in a quantum-dot single photon emitter

Tu-mP14 (128) **S. Lee[1], T. Yoo[1], M. Dobrowolska[2], J. K. Furdyna[2]** ([1]*Korea University, 5Ga Anamdong, Sungbukgu, Seoul 136-701, R. of Korea,* [2]*University of Notre Dame, Notre Dame IN 46556 USA*)

Polarization phenomena in the asymmetric double layers of self-assembled quantum dots

Tu-mP15 (129) **I.Ulfat[1,2,3], J. Adell[1,2], J. Sadowski[1,2], L.Iver[1], J. Kanski[1]** ([1]*Chalmers University of Technology22100, MAX-lab, Ole Romers Vag 1, Box-118, SE-22100 Lund , Sweden,* [2]*MAX-lab, Lund University, SE-22100 Lund, Sweden,* [3]*Department of Physics, University of Karachi, Karachio75270, Pakistan*)

(GaMn)As Nanowires- A Synchrotron-based Investigation

Tu-mP16 (130) **C.-Y. Jin[1], O. Kojima[2], T. Kita[2], O. Wada[1,2], M. Hopkinson[3], K. Akahane[4]** ([1]*Division of Frontier Research and Technology, CREATE, Kobe University, Kobe, Japan, Division of Frontier Research and Technology, CREATE, Kobe University, 1-1 Rokkodai, Nada, Kobe 657-8501, Japan 657-8501, Japan,* [2]*Department of Electrical and Electronic Engineering, Graduate School of Engineering, Kobe University, Kobe, Japan,* [3]*Department of Electronic and Electrical Engineering, EPSRC National Center for III-V Technologies, University of Sheffield, Sheffield, UK,* [4]*National Institute of Information and Communications Technology, Tokyo, Japan*)

All-optical switching using InAs/GaAs quantum dots within a vertical cavity structure

Tu-mP17 (131) **M. Kujiraoka[1,2], J. Ishi-Hayase[1,3,4], K. Akahane[1], N. Yamamoto[1], K. Ema[2], M. Sasaki[1]** ([1]*National Institute of Information and Communications Technology, 4-2-1, Nukui-Kitamachi, Koganei, Tokyo 1848795, Japan,* [2]*Department of Physics, Sophia University, 7-1 Kioi-cho, Chiyoda-ku, Tokyo 1028554, Japan,* [3]*The University of Electro-Communications, 1-5-1 Chofugaoka, Chofu, Tokyo 1828585, Japan,* [4]*PRESTO, Japan Science and Technology Agency (JST), 4-1-8 Honcho, Kawaguchi, Saitama 3320012, Japan*)

Control of ensemble effect on Rabi oscillations in quantum dots

Tu-mP18 (132) **M. Mongillo[1], G. Katsaros[1], P. Spathis[1], C. Mouchet[2], P. Gentile[3], E. Rouviere[2], S. de Franceschi[1]** ([1]*CEA, INAC/SPSMS/LaTEQS, 17 rue des Martyrs, F38054 Grenoble, France,* [2]*CEA, DRT/LCH, 17 rue des Martyrs, F38054 Grenoble, France,* [3]*CEA, INAC/SiNAPS, 17 rue des Martyrs, F38054 Grenoble, France*)

Silicon nanowires, functionality at the nanoscale

Tu-mP19 (133) **T. Saito, T. Nakaoka, Y. Arakawa** (*Institute for Nano Quantum Information Electronics, The University of Tokyo, 4-6-1 Komaba, Meguro-ku, Tokyo 153-8505, Japan*)

Magnetic field dependence of exciton fine structures in InAs/GaAs quantum dots: exchange vs. Zeeman splittings

Tu-mP20 (134) **S. Kim**[1], **B. Y. Yu**[2], **J. Lee**[1], **G. Ghibaudo**[3] ([1]*Korea Institute of Science and Technology(KIST), Nano Device Research Center, Korea Institute of Science and Technology, 39-1 Hawolkok, Seongbuk, Seoul, Republic of Korea,* [2]*Korea Institute of Science and Technology(KIST), Advanced Metal Research Center, Korea Institute of Science and Technology, 39-1 Hawolkok Seongbuk, Seoul, Republic of Korea ,* [3]*IMEP-MINATEC, INPG-CNRS, IMEP-MINATEC, INPG-CNRS, 3 rue Parvis Louis Neel, BP257, 38016 Grenoble, France*)

Effect of Oxygen on the Low-Frequency Noise in ZnO Nanowire Devices

Tu-mP21 (135) **K. Shimoda**[1], **T. Yasui**[1], **Y. Kuroki**[2], **M. Takata**[2] ([1]*Department of Mechanical Enginerring, Nagaoka University of Technology, 1603-1 Kamitomioka, Nagaoka, Niigata 9402111, Japan,* [2]*Department of Electrical Enginerring, Nagaoka University of Technology, 1603-1 Kamitomioka, Nagaoka, Niigata 9402111, Japan*)

Characterization of $Zn_{1-x}Cr_xO$ nano crystals grown by catalytic ECH processes

Tu-mP22 (136) **M. Muraguchi**[1], **T. Endoh**[1], **Y. Takada**[2], **Y. Sakurai**[2], **S. Nomura**[2], **K. Shiraishi**[2], **M. Ikeda**[3], **K. Makihara**[3], **S. Miyazaki**[3], **Y. Shigeta**[4] ([1]*Center for Interdisciplinary Research, Tohoku University, Sendai, Japan,* [2]*Graduate School of Pure and Applied Science, University of Tsukuba, Tsukuba, Japan,* [3]*Graduate School of Advanced Sciences of Matter, Hiroshima University, Hiroshima, Japan,* [4]*Graduate School of Life Science, University of Hyogo, Hyogo, Japan*)

Importance of Electronic State of Two-Dimensional Electron Gas for Electron Injection Process in Nano-Electronic Devices

Tu-mP23 (137) **Wei-Ting Hsu**[1], **Yu-An Liao**[1], **Shu-Kai Lu**[1], **Shun-Jen Cheng**[1], **Pei-Chin Chiu**[2], **Jen-Inn Chyi**[2], **W. Chang**[1] ([1]*Department of Electrophysics, National Chiao Tung University, 1001 University Road, Hsinchu 300, TAIWAN,* [2]*Department of Electrical Engineering, National Central University, Chung-li, 320 Taiwan*)

Tailoring of the Wave Function Overlaps and the Carrier Lifetimes in InAs/$GaAs_{1-x}Sb_x$ Type-II Quantum Dots

Tu-mP24 (138) **H. Y. Chao, J. H. Cheng, J. Y. Lu, S. H. You, Y. H. Chang, C.L.Cheng, Y. F.Chen, C. T. Wu** (*Department of Physics, National Taiwan University, No. 1, Sec. 4, Roosevelt Road, Taipei, 10617 Taiwan(R.O.C.)*)

Growth and characterization of ZnO/ZnTe core-shell nanowire and its device applications

Tu-mP25 (139) **I. Kanazawa** (*Department of Physics, Tokyo Gakugei University, Nukuikitamachi 4-1-1, Koganeishi, Tokyo 184-8501, Japan 184-8501, Japan*)

Anomalouly induced-charge on a domain wall of a semiconductor-dot atom

Tu-mP26 (140) **L .Worschech, B. Brandenstein-Köth, S. Lang, S. Höfling, A. Forchel** (*Technische Physik, Wuerzburg University, Am Hubland, 97074 Wuerzburg, Germany*)

Magnetic-field asymmetry of nonlinear mesoscopic transport in channels coupled to a single metallic gate

Tu-mP27 (141) **S. Shimomura**[1], **T. Fujita**[2], **S. Imadu**[1], **T. Kitada**[3] (*[1]Dept. of Electrical and Electronics Eng. and Computer Sci., Graduate School of Science and Engineering, Ehime University, 3, Bunkyo-Cho, Matsuyama, Ehime 790-8577, Japan, [2]Graduate School of Engineering Science, Osaka University, 1-3 Machikaneyama, Toyonaka, Osaka 560-8531, Japan, [3]Institute of Socio Technoscience, the University of Tokushima Graduate School, 2-1 Minamijyousanjima-cho,Tokushima 770-8506,Japan*)

Anisotropic modal gain spectra of GaAs self-assembled quantum-wire laser structures on (775)B GaAs substrates

Tu-mP28 (142) **Y. Mizoguchi**[1], **S. Hiratsuka**[1], **S. Takeda**[1], **S. Saravanan**[2], **M. Hosoda**[3], **N. Ohtani**[1] (*[1]Department of Electronics, Doshisha University, 1-3, Tatara-Miyakodani, Kyotanabe-shi, Kyoto 610-0321, Japan, [2]ATR Wave Engineering Laboratories, 2-2-2, Hikaridai, Keihanna Science City, Kyoto 619-0288, Japan, [3]Department of Applied Physics, Osaka City University, 3-3-138, Sugimoto, Sumiyoshi-ku, Osaka 558-8585, Japan*)

Influence of the number of turns and the distortion of the shape on the optical properties of semiconductor microtubes.

Tu-mP29 (143) **K. A. Piegdon, C. Meier, M. Urbanski, A. Hoischen, H.-S. Kitzerow, S. Declair, J. Foerstner, T. Meier** (*Center for Optics and Photonics Paderborn (CeOPP), Department of Physics and Department of Chemistry, University of Paderborn, Warburger Str. 100, 33098 Paderborn, Germany*)

Self-assembled Quantum Dots in a liquid-crystal-tunable microdisk resonator

Tu-mP30 (144) **D. N Krizhanovskii**[1], **D.M.Whittaker**[1], **E.Cerda**[2], **R.A.Bradley**[1], **A.P.D.Love**[1], **K.Guda**[1], **P.Santos**[2], **M.S.Skolnick**[1], **J.S.Roberts**[1] (*[1]Sheffield University, Department of Physics and Astronomy, Hicks building, Sheffield S37RH, UK, [2]Paul-Drude-Institut für Festkörperelektronik, Berlin, Germany, [3]3EPSRC National Centre for the III-V Technologies, University of Sheffield, Sheffield, UK, S37RH*)

Spontaneous formation and imprinting of vortices in the microcavity optical parametric oscillator

Tu-mP31 (145) **S. N. Ghosh**[1], **B. B. Buckley**[2], **N. Samarth**[3], **D.D. Awschalom**[2], **S. Ghosh**[1] (*[1]School of Natural Sciences, University of California, Merced , Merced CA 95340, USA, [2]Department of Physics, University of California, Santa Barbara, Santa Barbara, CA 93106, USA, [3]Materials Research Institute, Penn State University, University Park, Pennsylvania 16802, USA*)

Study of Optical Bistability and Bimodal Lasing in Coupled Microdisks

Tu-mP32 (146) **B. Gayral, J.-M. Gérard** (*CEA-Grenoble, INAC/SP2M, 17 rue des Martyrs, Grenoble 38054, France*)

High Purcell factor microcavity containing quantum dots : how to measure the Q-factor?

Tu-mP33 (147) **S. Reitzenstein, C. Kistner, T. Heindel, A. Rahmi-Iman, C. Schneider, S. Hofling, A. Forchel** (*Technische Physik, University of Würzburg, Am Hubland, Würzburg 97074, Germany*)

Cavity Quantum Electrodynamics in Electrically Contacted Quantum Dot-Micropillar Cavities

Tu-mP34 (148) **X.-L. Wang[1], S. Furue[1], M. Ogura[1], V. Voliotis[2], M. Ravaro[2], A. Enderlin[2], R. Grousson[2]** ([1]*Nanotechnology Research Institute, National Institute of Advanced Industrial Science and Technology (AIST) , 1-1-1 Umezono, Tskuba Central 2, Tsukuba 305-8568, Japan,* [2]*Institut des Nanosciences de Paris, CNRS UMR 7588, Université Pierre et Marie Curie, Campus Boucicaut, 140 rue de Lourmel, 75015 Paris, France*)

Highly efficient extraction of spontaneous emission through coupling of evanescent waves

Tu-mP35 (149) **K. Tanabe, M. Nomura, D. Guimard, S. Iwamoto, Y. Arakawa** (*Institute for Nano Quantum Information Electronics, Research Center for Advanced Science and Technology, and Institute of Industrial Science, University of Tokyo, 4-6-1 Komaba, Meguro-ku, Tokyo 153-8505, Japan*)

Fabrication and optical characterization of photonic crystal nanocavities with InAs quantum dots bonded on silicon substrates

Tu-mP36 (150) **A. Matyas[1,2], C. Jirauschek[1,2], P. Lugli[1], T. Kubis[3]** ([1]*Emmy Noether Group "Modeling of Quantum Cascade Devices", TU München, Arcisstr. 21, Munich D-80333, Germany,* [2]*Institute for Nanoelectronics, TU München, Arcisstr. 21, Munich D-80333, Germany,* [3]*Walter Schottky Institute, TU München, Am Coulombwall 3, Garching D-85748, Germany*)

Comparison between semiclassical and quantum carrier transport analysis of THz quantum cascade lasers

Tu-mP37 (151) **Y. Kamiyama, A. Tomioka, T. Anzai, K. Iwamoto** (*Graduate School of Engineering, Osaka Electro-Communication University, 18-8 Hatucho, Neyagawa, Osaka 572-8530, Japan*)

Discrete or Continuous Energy Tuning of Amplified Spontaneous Emissions from Conductive Polymer Films

Tu-mP38 (152) **M. De Zoysa, T. Asano, S. Noda** (*Department of Electronic Science and Engineering, Kyoto University, Noda Laboratory, Department of Electronic Science and Engineering Kyoto University Nishikyo-ku, Kyoto 615-8510, JAPAN*)

Control of thermal radiation using intersubband transitions in quantum wells

Tu-mP39 (153) **J. Y. Lu, H. Y. Chou, J. C. Wu, S. Y. Wei, Y. H. Chang** (*Department of Physics, National Taiwan University, No. 1, Sec. 4, Roosevelt Road, Taipei 10617 , Taiwan(R.O.C)*)

Tuneable surface plasmon modes in core (dielectric)-shell (metal) nanocylinder pair

Tu-mP40 (154) **Y. Inose[1], T. Ohtsuki[1,2,3], H. Kunugita[1,2,3], K. Ema[1,2,3], M. Sakai[1,2,3], A. Kikuchi[1,2,3], K. Kishino[1,2,3]** ([1]*Department of Engineering and Applied Sciences, Sophia University, 7-1 Kioi-cho, Chiyoda-ku, Tokyo 102-8554, Japan,* [2]*Sophia Nanotechnology Research Center, Sophia University, 7-1 Kioi-cho, Chiyoda-ku, Tokyo 102-8554, Japan,* [3]*CREST, Japan Science and Technology Agency, 4-1-8 Honcho, Kawaguchi-shi, Saitama-ken 332-0012, Japan*)

Anderson localization of light in random configuration of dielectric circular cylinders

Tu-mP41 (155) **S. Nakayama[1,3], S Ishida[2], S. Iwamoto[1,2,3], D. Bordel[3], E. Augendre[4], L. Clavelier[4], Y. Arakawa[1,2,3]** (*[1]RCAST, the University of Tokyo, 4-6-1 Komaba, Meguro-ku, JAPAN 153-8505, JAPAN, [2]IIS, the Univ. of Tokyo, 4-6-1 Komaba, Meguro-ku, Tokyo, JAPAN, [3]INQIE, the Univ. of Tokyo, 4-6-1 Komaba, Meguro-ku, JAPAN 153-8505, JAPAN, [4]CEA LETI Minatec, F38054, Frenoble, FRANCE*)

Enhancement of photoluminescence from germanium by utilizing air-bridge type photonic crystal slab

Tu-mP42 (156) **Makoto Takada[1], Yasuhiro Idutsu[1,2], Daimotsu Kato[1], Sotaro Ida[1], Saki Ito[1], Hiroyasu Sato[1], Jae-Hoon Huh[1,3], Hirotaka Sasakura[1,2], Hidekazu Kumano[1,2], I. Suemune[1,2]** (*[1]Research Institute for Electronic Science, Hokkaido University, Sapporo, Japan, [2]CREST, Japan Science and Technology Agency, Tokyo, Japan, [3]GCOE, Hokkaido University, Sapporo, Japan*)

Drastic enhancement of luminescence of InAs quantum dots embedded in niobium metal

Tu-mP43 (157) **M. Broell, S. Schwaiger, D. Heitmann, S. Mendach** (*Institute of Applied Physics, University of Hamburg, Jungiusstrasse 11C, 20355 Hamburg, Germany*)

Rolled-up metal/semiconductor microtubes as hyperlenses working in the visible

Tu-mP44 (158) **S. Furukawa[1], R. Kaji[1], S. Adachi[1], S. Muto[1], H. Sasakura[2]** (*[1]Department of Applied Physics, Hokkaido University, N13 W8, Kitaku, Sapporo 060-8628, Japan, [2]Research Institute for Electronic Science, Hokkaido University, N21 W10, Kitaku, Sapporo 001-0021, Japan*)

Direct observation of nuclear spin pumping dynamics in a single InAlAs quantum dot

Tu-mP45 (159) **K. Tomoda, Y. Nakano, S. Adachi, S. Muto** (*Department of Applied Physics, Hokkaido University, N13, W8, Kitaku, Sapporo 060-8628, Japan*)

Transient grating studies of phase and spin coherences of excitons in GaAs single quantum wells

Tu-mP46 (160) **M. Murata, T. Tsuchiya** (*Hokkaido University, Graduate School of Engineering, Sapporo 060-8628, Japan*)

Controllable Dresselhaus field in microscopically inversion symmetric quantum wells

Tu-mP47 (161) **X. J. Wang[1], Y. Puttisong[1], I. A. Buyanova[1], H. Carrére[1,2], F. Zhao[2], A. Balocchi[2], X. Marie[2], C. W. Tu[3], W. M. Chen[1]** (*[1]Linköping University, Department of Physics, Chemistry and Biology, 58183 Linköping, Sweden, [2]Université de Toulouse, LPCNO: INSA, UPS, CNRS, 135 avenue de Rangueil, 31077 Toulouse cedex, France, [3]University of California, Department of Electrical and Computer Engineering, La Jolla, CA92093, USA*)

Efficient room temperature spin filter based on GaNAs quantum wells

Tu-mP48 (162) **Q. Zhang[1], X.Q. Wang[1], X. W. He[1], C. M. Yin[1], B. Shen[1], Y. Ishitani[2], A.Yoshikawa[2]** (*[1]State Key Laboratory of Artificial Microstructure and Mesoscopic Physics, School of Physics, Peking University, Chengfu Road 209, Haidian District, Beijing 100871, China, [2] Department of Electronics and Mechanical Engineering, Chiba University, 1-33 Yayoi-cho, Inage-ku, Chiba 263-8522, Japan*)

A method for detecting polarity of wurtzite semiconductor

Tu-mP49 (163) **C. Simserides**[1], **A. Lipińska**[2], **A. Majhofer**[3], **K. N. Trohidou**[1], **T. Dietl**[2,4] (*[1]Institute of Materials Science, NCSR Demokritos , Athens, Greece, [2]Institute of Physics, Polish Academy of Science, Warszawa, Poland, [3]Institute of Experimental Physics, University of Warsaw , Warszawa, Poland, [4]Institute of Theoretical Physics, University of Warsaw , Warszawa, Poland*)

Influence of antiferromagnetic interactions and of alloy disorder on the ferromagnetic properties of p-(Cd,Mn)Te quantum wells

Tu-mP50 (164) **J. Beyer**[1], **I. A. Buyanova**[1], **S. Suraprapapicha**[2], **C. W. Tu**[2], **W. M. Chen**[1] (*[1]Department of Physics, Chemistry and Biology, Linköping university, Linköping, Sweden, [2]Department of Electrical and Computer Engineering, University of California at San Diego, La Jolla, USA*)

Optical spin injection in novel InAs quantum dots structures

Tu-mP51 (165) **M. Goryca**[1,2], **T. Kazimierczuk**[1], **M. Nawrocki**[1], **A. Golnik**[1], **J. A. Gaj**[1], **P. Wojnar**[3], **G. Karczewski**[3], **P. Kossacki**[1,2] (*[1]Institute of Experimental Physics, University of Warsaw, ul. Hoza 69, 00-681 Warszawa, Poland, [2]Grenoble High Magnetic Field Laboratory, CNRS, BP 166, F-38042 Grenoble Cedex 09, France , [3]Institute of Physics, Polish Academy of Sciences, al. Lotnikow 32/46, 02-668 Warszawa, Poland*)

Optical manipulation of a single Mn spin in a CdTe quantum dot

Tu-mP52 (166) **M. Larsson, H. A. Nilsson, H. Q. Xu** (*Division of Solid State Physics, Lund University, Box 118, S-221 00 Lund , Sweden*)

g-factors and exchange energy of few-electron single and double quantum dots defined in an InGaAs/InP heterostructure

Tu-mP53 (167) **J. Ogawa**[1], **M. Kohda**[1,2], **F. Matsukura**[3], **Y. Ohno**[3], **H. Ohno**[3], **J. Nitta**[1] (*[1]Department of Materials Science, Tohoku University, 6-6-02, Aramaki-aza Aoba, Aobaku, Sendai, Miyagi 9808579, Japan, [2]PRESTO, Japan Science and Technology Agency, 4-1-8, Honcho, Kawaguchi, Saitama 3320012, Japan, [3]Laboratory for Nanoelectronics and Spintronics, Research Institute of Electrical Communication, Tohoku University, 2-1-1, Katahira, Aobaku, Sendai, Miyagi 9808577, Japan*)

Width and temperature dependences of lithographically induced magnetic anisotropy in (Ga,Mn)As wires

Tu-mP54 (168) **Tetsuya Horii, Yuta Inoue, Jun Okabayashi, Junji Yoshino** (*Daprtment of Physics, Tokyo Institute of Technology, 2-12-1, Ookayama, Meguro-ku, Tokyo 1528551, Japan*)

Layer thickness dependence of magnetic anisotropy in (Ga,Mn)As

Tu-mP55 (169) **T. Matsuura**[1], **N. Monta**[2], **T. Koga**[1,2] (*[1]Creative Research Initiative Sousei, Hokkaido University, Kita21 Nishi10, Kita-ku, Sapporo 001-0021, Japan, [2]Graduate School of Information Science and Technology, Hokkaido University , Kita14, Nishi9, Kita-ku, Sapporo, 060-0814, Japan*)

Magnetic control of Rashba splittings in symmetric InAs quantum wells

Tu-mP56 (170) **W. Koehl, C. Poblenz, M. H. Wong, U. Mishra, J. Speck, D. D. Awschalom** (*Center for Spintronics and Quantum Computation, University of California, Santa Barbara California 93106 USA*)

Current-Induced Spin Polarization in Gallium Nitride

Tu-mP57 (171) **Yu Nishitani, Masaki Endo, Fumihiro Matsukura, Hideo Ohno** (*Laboratory for Nanoelectronics and Spintronics, Research Institute of Electrical Communication, Tohoku University, Katahira 2-1-1, Aoba-ku, Sendai, Miyagi 980-8577, Japan*)

Magnetic anisotropy in a ferromagnetic (Ga,Mn)Sb thin film

Tu-mP58 (172) **H. Nosho[1], T. Asami[1], T. Okamoto[1], T. Umi[1], S. L. Lu[2], Z. C. Niu[3], A. Tackeuchi[1]** ([1]*Department of Applied Physics, Waseda University, 3-4-1, Okubo, Shinjuku-ku, Tokyo 169-8555, Japan,* [2]*Suzhou Institute of Nano-tech and Nano-bionics, Chinese Academy of Sciences, Dushu Lake Higher Education Town, Ruoshui Road 398, Suzhou Industrial Park, Suzhou, 215125, China,* [3]*State Key Laboratory for Superlattice and Microstructure, Institute of Semiconductors, Chinese Academy of Sciences, No.A35, QingHua East Road, Haidian District, Beijing,100083, China*)

Spin relaxation in high In content InGaAs/GaAs quantum wells

Tu-mP59 (173) **Yasuaki Masumoto, Keisuke Kawana, Shinichi Tomimoto** (*Institute of Physics, University of Tsukuba, 1-1-1 Tennoudai, Tsukuba, Ibaraki 3058571, Japan*)

Coherent spin precession of electrons and excitons in charge tunable InP quantum dots

Tu-mP60 (174) **F. Matsukura[1,2], M. Sawicki[1,3], D. Chiba[2,1], A. Korbecka[4], Y. Nishitani[1], J. A. Majewski[4], T. Dietl[3,4,2], H. Ohno[1,2]** ([1]*Laboratory for Nanoelectronics and Spintronics, Research Institute of Electrical Communication, Tohoku University, Sendai, Japan,* [2]*Semiconductor Spintronics Project, Exploratory Research for Advanced Technology, Japan Science and Technology Agency, Tokyo, Japan,* [3]*Institute of Physics, Polish Academy of Sciences, Warszawa, Poland,* [4]*Institute of Theoretical Physics, University of Warsaw, Warszawa, Poland*)

SQUID magnetometry of the effect of electric-field on magnetization of (Ga,Mn)As

Tu-mP61 (175) **Y. Guo[1,2], F. Matsukura[2,1], K. Ohtani[2], H. Ohno[2,1]** ([1]*Semiconductor Spintronics Project, Exploratory Research for Advanced Technology, Japan Science and Technology Agency, Tokyo, Japan,* [2]*Laboratory for Nanoelectronics and Spintronics, Research Institute of Electrical Communication, Tohoku University, Sendai, Japan*)

Epitaxy and characterization of Co doped ZnO on ZnO substrate

Tu-mP62 (176) **T. Takahashi, S. Matsuzaka, Y. Ohno, H. Ohno** (*Research Institute of Electrical Communication, Tohoku University, 2-1-1 Katahira, Aoba-ku, Sendai, Miyagi*)

Optical detection of zero-field spin precession of high mobility two dimensional electron gas in a gated GaAs/AlGaAs quantum well

Tu-mP63 (177) **N. T. Bagraev[1], O.N. Guimbitskaya[2], L. E. Klyachkin[1], A. M. Malyarenko[1], A. I. Ryskin[3], A. S. Shcheulin[3], I. A. Shelykh[2]** ([1]*Ioffe Physical-Technical Institute of RAS, Politekhnicheskaya 26 , St.Petersburg, Russia,* [2]*Polytechnical University, St. Petersburg, 195251, Russia,* [3]*St.Petersburg University of Information Technologies, Mechanics and Optics, St. Petersburg, Russia*)

Spin transistor and spin Hall effects in CdF_2 nanostructures

Tu-mP64 (178) **M. Csontos[1], Y. Komijani[1], T. Ihn[1], K. Ensslin[1], D. Reuter[2], A. D. Wieck[2]** ([1]*Solid State Physics Laboratory, ETH Zürich, Schafmattstrasse 16, Zürich 8093, Switzerland,* [2]*Angewandte Festkörperphysik, Ruhr-Universität Bochum, 44780 Bochum, Germany*)

0.7 feature in p-type quantum point contacts tuned by combined in-plane and top gates

Tu-mP65 (179) **G. D. Fuchs[1], C. D. Weis[2], D. M. Toyli[1], T. Schenkel[2], D. D. Awschalom[1]** ([1]*Center for Spintronics and Quantum Computation, University of California, Santa Barbara, CA 93106, USA,* [2]*Lawrence Berkeley National Lab, Berkeley, CA 94720, USA*)

Excited-state spectroscopy of single spins in diamond

Tu-mP66 (180) **S. Matsuzaka**[1], **Y. Ohno**[1], **H. Ohno**[1,2] ([1]*Research Institute of Electrical Communication, Tohoku University, 2-1-1, Katahira, Aoba-ku, Sendai, Miyagi 9808577, Japan,* [2]*Exploratory Research for Advanced Technology, Japan Science and Technology Agency, Japan*)

Detection of local electron and nuclear spin dynamics by time-resolved Kerr microscopy

Tu-mP67 (181) **D. Chiba**[1,2,3], **M. Endo**[2], **Y. Nishitani**[2], **F. Matsukura**[2,1], **H. Ohno**[2,1] ([1]*Semiconductor Spintronics Project, ERATO, Japan Science and Technology Agency, Sanban-cho 5, Chiyouda-ku, Tokyo, Japan,* [2]*Laboratory for Nanoelectronics and Spintronics, RIEC, Tohoku University, Katahira 2-1-1, Aoba-ku, Sendai, Miyagi, Japan,* [3]*Institute for Chemical Research, Gokasho, Uji, Kyoto, Japan*)

Electric-field control of the anomalous Hall effect in (Ga,Mn)As thin films

Tu-mP68 (182) **T. Fukumura**[1,2], **T. Yamasaki**[1], **Y. Yamada**[1], **K. Ueno**[3], **M. Nakano**[1], **T. Makino**[3], **M. Kawasaki**[3,1,4] ([1]*Institute for Materials Science, Tohoku University, Sendai 980-8577, Japan,* [2]*PRESTO, Japan Science and Technology Agency, Saitama 332-0012, Japan,* [3]*WPI Advanced Institute for Materials Research, Tohoku University, Sendai 980-8577, Japan,* [4]*CREST, Japan Science and Technology Agency, Tokyo 102-0075, Japan*)

Room temperature ferromagnetic semiconductor Co-doped TiO_2 films grown on glass by sputtering method

Tu-mP69 (183) **D. Bougeard**[1], **J. M. LeBeau**[2], **D. Saxey**[3], **S. Ahlers**[1], **N. Sircar**[1], **V. Lang**[1], **A. Cerezo**[3], **G. Abstreiter**[1], **S. Stemmer**[2] ([1]*Walter Schottky Institut, Technische Universitaet Muenchen, Am Coulombwall 3 85748, Germany,* [2]*Materials Department, University of California, Santa Barbara, Santa Barbara, CA 93106-5050, USA,* [3]*Department of Materials, University of Oxford, Parks Road, Oxford OX1 3PH, UK*)

String-like self-assembly in $Ge_{1-x}Mn_x$

Tu-mP70 (184) **J. D. Song**[1], **J. K. Hong**[2], **S. J. Joo**[1,2], **S. H. Shin**[1], **S. H. Han**[1], **K. H. Shin**[1] ([1]*Korea Institute of Science and Technology, Nano Science Research Division, Korea institute of Science and Technology, Seoul 136-791, Korea,* [2]*Korea University, Department of Display Semiconductor, Korea University, Chungnam 339-700, Korea*)

InSb-based switching device operating at room temperature using magnetic controlled avalanche process for the application to magnetologic devices

Tu-mP71 (185) **D. M. Gvozdi'c**[1], **N. Čukari'c**[1], **U. Ekenberg**[2] ([1]*Faculty of Electrical Engineering, University of Belgrade, Bulevar Kralja Aleksandra 73b, Beograd 11120, Serbia,* [2]*School of Information and Communication Technology, Royal Institute of Technology, Isafjordsgatan 28, Electrum 213, SE-164 40, Kista, Sweden*)

Comparison between spin splitting obtained with an 8x8 matrix and various 2x2 matrices

Tu-mP72 (186) **S. Souma, M. Ogawa** (*Deparatment of Electrical and Electronics Engineering, Kobe University, Kobe Japan*)

Effect of interface structure on current spin-polarization in narrow gap semiconductor heterostructures

Tu-mP73 (187) **T. Kaizu**[1], **N. Kakuda**[2], **M. Takahasi**[3], **S. Fujikawa**[3], **K. Yamaguchi**[2] ([1]*Quantum Dot Research Center, National Institute for Materials Science, 3-13 Sakura, Tsukuba, Ibaraki 3050003, Japan,* [2]*Department of Electronic Engineering, The University of Electro-Communications, 1-5-1 Chofugaoka, Chofu, Tokyo 1828585, Japan,* [3]*Synchrotron Radiation Research Center, Japan Atomic Energy Agency, 1-1-1 Koto, Sayo-cho, Sayo-gun, Hyogo 6795148,Japan*)

Real-time X-ray diffraction measurements during Sb-mediated SK growth and annealing of InAs quantum dots

Tu-mP74 (188) **M. Ahmad Kamarudin**[1], **Q. D. Zhuang**[1], **T. N. Nuytten**[2], **V. V. Moshchalkov**[2], **M. Hayne**[1] ([1]*Department of Physics, Lancaster University, Lancaster, United Kingdom,* [2]*INPAC-Institute for Nanoscale Physics and Chemistry, Pulsed Field Group, K. U. Leuven, Leuven, Belgium*)

Influence of growth and capping layer temperatures on the properties of GaSb/GaAs quantum dots

Wednesday July 22nd

Session M5 (International Conference Room) 9:00 – 10:30 Spintronics I

M5a (191) 9:00 – 9:30 **T. Jungwirth**[1,2] (Invited) ([1]*Institute of Physics ASCR, v.v.i., Cukrovarnick´ a 10, 162 53 Praha 6, Czech Republic,* [2]*School of Physics and Astronomy, University of Nottingham, Nottingham NG7 2RD, United Kingdom*)

Spin-orbit coupling induced magneto-resistance effects in ferromagnetic semiconductor structures

M5b (192) 9:30 – 9:45 **A. Werpachowska**[1], **T. Dietl**[1,2] ([1]*Institute of Physics, Polish Academy of Sciences, Warsaw , Poland,* [2]*Institute of Theoretical Physics, University of Warsaw, Warsaw , Poland*)

Effect of inversion asymmetry on anomalous Hall effect in ferromagnetic (Ga,Mn)As

M5c (193) 9:45 – 10:00 **L. Rokhinson**[1], **A. Chernyshov**[1], **M. Overby**[1], **Y. Lyanda-Geller**[1], **X. Liu**[2], **J.K. Furdyna**[2] ([1]*Purdue University, Department of Physics and Birck Nanotechnology Center, Purdue University, West Lafayette, IN 47907 USA,* [2]*University of Notre Dame, Department of Physics, University of Notre Dame, Notre Dame, IN 46556 USA*)

Electric control of magnetization via control of carriers' spectrum anisotropy

M5d (194) 10:00 – 10:15 **P. Olbrich**[1], **S.A. Tarasenko**[2], **V.V. Bel'kov**[2], **Ch. Brinsteiner**[1], **W. Eder**[1], **D.R. Yakovlev**[2,3], **V. Kolkovsky**[4], **W. Zaleszczyk**[4], **G. Karczewski**[4], **T. Wojtowicz**[4], **D. Weiss**[1], **S.D. Ganichev**[1] ([1]*Terahertz Center, University of Regensburg, 93040 Regensburg, Germany,* [2]*A.F. Ioffe Physico-Technical Institute, Russian Academy of Sciences, 194021 St. Petersburg, Russia,* [3]*Experimental Physics 2, TU Dortmund University, 44221 Dortmund, Germany,* [4]*Institute of Physics, Polish Academy of Sciences, 02-668 Warsaw, Poland*)

Spin currents in diluted magnetic semiconductors induced by THz radiation

M5e (195) 10:15 – 10:30 **M. Harada, T. Uemura, Y. Imai, K. Matsuda, M. Yamamoto** (*Division of Electronics for Informatics, Hokkaido University, North14 West9,Kitaku,Sapporo 0600814, Japan*)

Tunneling anisotropic magneto-resistance in an epitaxial Co_2MnSi/n-GaAs junction

10:30 – 11:00 **Coffee Break**

Session Plenary 3,4 (Main Hall) 11:00 – 12:30

PL3 (197) 11:00 – 11:45 **Andre Geim** (*Centre for Mesoscience & Nanotechnology, University of Manchester, Oxford Road, Manchester M13 9PL, UK*)

Outlook over graphene flatland

PL4 (198) 11:45 – 12:30 **Leaven M.K. Vandersypen** (*Kavli Institute of Nanoscience, Delft University of Technology, Delft, the Netherlands*)

Coherence and control of single electron spins in quantum dots

12:30 – **Optional Excursion**

18:30- Banquet at "Kachoen"

"Kachoen" places in front of "Port Island Minami (South)" station, which is two stops from Shimin-hiroba on Port Liner.

Thursday July 23rd

Session M6 (International Conference Room) 9:00 – 11:15 **Spintronics II**

M6a (200) 9:00 – 9:30 **P. N. Hai**[1]**, S. Ohya**[1,2]**, S.E. Barnes**[3]**, S. Makeawa**[4,5]**, M. Tanaka**[1,2] (Invited) ([1]*Department of Electrical Engineering and Information Systems, University of Tokyo, Japan, ,* [2]*Japan Science and Technology Agency, ,* [3]*Physics Department, University of Miami, USA, ,* [4]*Institute for Materials Research, Tohoku University, Japan, ,* [5]*CREST, Japan Science and Technology Agency,*)

Electromotive force and magnetoresistance (100,000%) in magnetic tunnel junctions with zinc-blende MnAs nanomagnets

M6b (201) 9:30 – 9:45 **V. Jovanov, D. Heiss, F. Klotz, D. Rudolph, M. Bichler, M. S. Brandt, G. Abstreiter, J. J. Finley** (*Walter Schottky Institut, TU München, Am Coulombwall 3, 85748 Garching, Germany*)

All optical spin storage and readout in a single quantum dot

M6c (202) 9:45 – 10:00 **M. Ciorga, A. Einwanger, U. Wurstbauer, D. Schuh, W. Wegscheider, D. Weiss** (*Institute for Experimentall and Applied Physics, University of Regensburg, Universitaetsstrasse 31 D-93040 , Germany*)

All-electrical spin injection and detection scheme in an all-semiconductor lateral device

M6d (203) 10:00 – 10:15 **S. Lazic, P.V. Santos, R. Hey** (*Paul Drude Institute , Hausvogteiplatz 5-7 10117, Germany*)

Exciton transport by moving strain dots in GaAs quantum wells

M6e (204) 10:15 – 10:30 **K. Morita[1,2], H. Sanada[2], S. Matuzaka[2], Y. Ohno[2], H. Ohno[2,1]** ([1]*Semiconductor Spintronics Project, Exploratory Research for Advanced Technology, Japan Science and Technology Agency, 2-1-1 Katahira, Aoba-ku, Sendai 980-8577, Japan,* [2]*AgencyLaboratory for Nanoelectronics and Spintronics, Research Institute of Electrical Communication, Tohoku University, 2-1-1 Katahira, Aoba-ku, Sendai 980-8577, Japan,* [3]*Center for Frontier Research of Engineering, Institute of Technology and Science, The University of Tokushima, 2-1 Minami-jyosanjima-cho, Tokushima 770-8506, Japan*)

Two-color pump-probe measurements of intersubband excitonic interactions in GaAs/AlGaAs quantum wells

10:30 – 11:00 **Coffee Break**

Session M7 (International Conference Room) 11:00 – 12:30 Nanostructure growth

M7a (206) 11:00 – 11:30 **K. Kishino[1,2,3], H. Sekiguchi[1,3], A. Kikuchi[1,2,3]** (Invited) ([1]*Department of Engineering and Applied Sciences, Sophia University, 7-1 Kioi-cho, Chiyoda-ku, Tokyo 102-8554, Japan,* [2]*Sophia Nanotechnology Research Center, Sophia University, 7-1 Kioi-cho, Chiyoda-ku, Tokyo 102-8554, Japan,* [3]*CREST, Japan Science and Technology Agency, Kawaguchi, Saitama 330-0012, Japan*)

Growth and applications of GaN-based nanocolumns emitting from blue to red

M7b (208) 11:30 – 11:45 **B. Kim, Tomoyuki Tanikawa, Yoshio Honda, Masahito Yamaguchi, Nobuhiko Sawaki** (*Department of Electronics and Akasaki Research Center, Nagoya University, Furo-cho 3C-1, Chikusa-ku, Nagoya, Aichi 4648603, Japan*)

Fabrication of InGaN/GaN stripe structure on (111)Si and stimulated emission properties under photo-excitation

M7c (209) 11:45 – 12:00 **D. Spirkoska**[1], **M. Heigoldt**[1], **J. Arbiol**[2,3], **J. R. Morante**[3], **G. Abstreiter**[1], **A. Fontcuberta i Morral**[4] (*[1]Technische Universität München, Walter Schottky Institut, Am Coulombwall 3 85748 Garching, Germany, [2]TEM-MAT, Serveis Cientificotecnics, Universitat de Barcelona, C/ Lluis Sole i Sabaris 1-3, E-08028 Barcelona, CAT, Spain, [3]EME/CeRMAE/IN2UB, Departament d'Electronica, Universitat de Barcelona, C/ Marti i Franques 1, E-08028 Barcelona, CAT, Spain, [4]Laboratoire des materiaux Semiconducteurs, Instiut de Materiaux, Ecole Polytechnique Federale de Lausanne, 1015, Lausanne, Switzerland*)

Adding functionality to GaAs nanowires: from prismatic heterostructures to band gap engineering with only one material

M7d (210) 12:00 – 12:15 **M. Grydlik, M. Brehm, N. Hrauda, T. Fromherz, J. Stangl, F. Schäffler, G. Bauer** (*Institute of Semiconductor and Solid State Physics, University of Linz , Altenbergerstrasse 69 4040 Linz, Austria*)

Ordered SiGe islands on Si (001) for spectrally narrow photoluminescence

M7e (211) 12:15 – 12:30 **P. Jedrasik**[1], **U. Södervall**[1], **C.A. Dutu**[2], **D.A. Serban**[2], **P. Guillet**[3], **A. Vlad**[2], **C.-A. Fustin**[3], **J.F. Gohy**[3], **S. Melinte**[3] (*[1]MC2, Chalmers University of Technology, Göteborg, 41296, Sweden, [2]Unité CMAT, Université catholique de Louvain, Louvain-la-Neuve, 1348, Belgium, [3]Unité DICE, Université catholique de Louvain, Louvain-la-Neuve, 1348, Belgium*)

Ordered semiconducting functional polymer nano-architectures with three-dimensional structural control

12:30 – 14:00 **Lunch Break**

Session M8 (International Conference Room) 14:00 – 16:00 Novel materials and physics

M8a (213) 14:00 – 14:30 **M. Kawasaki**[1,2] (Invited) (*[1]WPI Advanced Institute for Materials Research (AIMR), Tohoku University, Japan, [2]CREST, Japan Science and Technology Agency (JST), Tokyo, Japan*)

ZnO/MgZnO heterostructures for optoelectronic devices

M8b (215) 14:30 – 15:00 **A. F. Morpurgo** (Invited) (*DPMC and Gap, University of Geneva, 24 quai Ernest-Ansermet, CH1211 Geneva, Switzerlands*)

New two-dimensional electronic systems at the surface of organic crystals

M8c (216) 15:00 – 15:15 **S. Moriyama**[1], **D. Tsuya**[1], **E. Watanabe**[1], **S. Uji**[1], **M. Shimizu**[2], **T. Mori**[2], **T. Yamaguchi**[2], **K. Ishibashi**[2] (*[1]International Center for Materials Nanoarchitectonics, National Institute for Materials Science, 1-1 Namiki, Tsukuba, Ibaraki 3050044, Japan, [2]Advanced Science Institute, RIKEN, 2-1 Hirosawa, Wako, Saitama 351-0198, Japan*)

Double quantum-dot devices in triple-layer graphene

M8d (217) 15:15 – 15:30 **A. Umeno**[1,2]**, K. Yoshida**[1,2]**, S. Sakata**[1,2]**, K. Hirakawa**[1,2] ([1]*Institute of Industrial Science and INQIE, Univ. of Tokyo, 4-6-1 Komaba, Meguro-ku Tokyo, 153-8505 Japan,* [2]*CREST-JST, 4-1-8 Honcho, Kawaguchi, Saitama 332-0012, Japan*)

Elementary process of electromigraion at gold nanojunctions

M8e (218) 15:30 – 15:45 **Q. P. Unterreithmeier, T. Faust, E. M. Weig, J. P. Kotthaus** (*Fakultät für Physik and Center for NanoScience (CeNS), Ludwig-Maximilians-Universität, München, Geschwister-Scholl-Platz 1, München 80539, Germany*)

Novel Transduction Schemes for Nanoelectromechanical Systems

M8f (219) 15:45 – 16:00 **I. Mahboob, C. Froitier, H. Yamaguchi** (*NTT Basic Research Labs., 3-1, Morinosato Wakamiya Atsugi-shi, Kanagawa 243-0198 , Japan*)

Manipulating the dynamical potential well of a parametric resonator

Poster Session Th-mP (Meeting Room 501, 502) 16:00–18:00

Th-mP1 (221) **L. He[1], M. Gong[1], C-F. Li[1], G-C. Guo[1], A. Zunger[2]** (*[1]Key Laboratory of Quantum Information, University of Science and Technology of China, 96 Jinzhai Road, Hefei, Anhui, P. R. China 230026, China, [2]National Renewable Energy Laboratory, Golden, Colorado, 410012,USA*)

Highly-reduced Fine-structure splitting in InAs/InP quantum dots

Th-mP2 (222) **A. J Bennett[1], R. B. Patel[1,2], C. A. Nicoll[2], D. A. Ritchie[2], A. J. Shields[1]** (*[1]Toshiba Research Europe Limited, 260 Science Park, Milton Road, Cambridge CB58QE, UK, [2]Cavendish Laboratory, Cambridge University, JJ Thomson Avenue, Cambridge, CB3 0HE, U K.*)

Interference of photons from a weak laser and a quantum dot

Th-mP3 (223) **Masayuki Shirane[1,2], Yuichi Igarashi[1,2], Yasutomo Ota[2,3], Masahiro Nomura[2], Naoto Kumagai[2], Shunsuke Ohkouchi[1,2], Akihiro Kirihara[1,2], Satomi Ishida[2], Satoshi Iwamoto[2,3], Shinichi Yorozu[1,2], Yasuhiko Arakawa[2,3]** (*[1]Nano Electronics Research Laboratories, NEC Corporation, 34 Miyukigaoka, Tsukuba, Ibaraki 3058501, JAPAN, [2]Institute for Nano Quantum Information Electronics, the University of Tokyo, 4-6-1 Komaba, Meguro-ku, Tokyo 153-8505, JAPAN, [3]Research Center for Advanced Science and Technology, the University of Tokyo, 4-6-1 Komaba, Meguro-ku, Tokyo 153-8904, JAPAN*)

Photon correlation spectroscopy of a single quantum dot within a photonic bandgap

Th-mP4 (224) **Y. Chen[1,2], N.Regnault[1], R. Ferreira[1], Bang - Fen Zhu[2], G.A. Bastard[1]** (*[1]LPA-ENS, 24 rue Lhomond F75005 Paris (France), [2]Department of Physics, Tsinghua University, Beijing (China)*)

Electron-phonon interaction in Quantum Cascade Lasers subjected to a strong magnetic field

Th-mP5 (225) **O. D. D. Couto, Jr.[1], S. Lazic[1], F. Iikawa[2], J. Stotz[3], R. Hey[1], P. V. Santos[1]** (*[1]Paul Drude Institute , Hausvogteiplatz 5-7 10117, Germany, [2]Institute of Physics, University of Campinas, Campinas-SP, Brazil, [3]Department of Physics, Engineering and Astronomy, Queens University, Kingston, ON, Canada*)

Evidence for photon anti-bunching in acoustically pumped dots

Th-mP7 (226) **O. Kojima[1], S. Watanabe[1], T. Kita[1], O. Wada[1], T. Isu[2]** (*[1]Department of Electrical and Electronics Engineering, Graduate School of Engineering, Kobe University, 1-1 Rokkodai, Nada, Kobe 6578501, Japan, [2]Department of Nano-Technology, Institute of Technology and Science, The University of Tokushima, 2-1 Minamijosanjima-cho, Tokushima 7708506, Japan*)

Spatial coherence effect on transient response of confined excitons in GaAs thin films

Th-mP8 (227) **S. Wiedmann[1], N.C. Mamani[2], G.M. Gusev[2], A.K. Bakarov[2], J. Claude PORTAL[1,3]** (*[1]LNCMI-CNRS / INSA, 135,avenue de rangueil TOULOUSE 31077 CEDEX 4, FRANCE , [2]Instituto de Física da Universidade de São Paulo, São Paulo, SP, Brazil, [3]Institut Universitaire de France, 103, bd Saint-Michel 75005 Paris*)

Magnetoresistance oscillations in triple quantum wells under microwave irradiation

Th-mP9 (228) **Y. Yonezawa**[1], **R. Hiraike**[1], **K. Miura**[2], **Y. Iguchi**[2], **Y. Kawamura**[1] ([1]*Frontier Science Innovation Center, Osaka Prefecture University, Osaka, Japan,* [2]*Transmission Devices RandD Laboratories, Sumitomo Electric Industries, Ltd, Osaka, Japan*)

Growth and characterization of strain-compensated InGaAs/GaAsSb type II multiple quantum wells on InP Substrate

Th-mP10 (229) **K. Koike, R. Kawaguchi, M. Yano** (*Nanomaterials Microdevices Research Center, Osaka Institute of Technology, 5-16-1 Omiya, Asahi-ku, Osaka 535-8585, Japan*)

Midinfrared photoluminescence from SnTe/PbTe/CdTe double quantum wells grown by molecular beam epitaxy

Th-mP11 (230) **H. Jeon**[1], **Seung Joo Lee**[1], **Seoung-Hwan Park**[2], **Tae Won Kang**[1], **Doyeol Ahn**[3], **G. Ihm**[4] ([1]*Dongguk University, 26, 3ga, Pil-dong, Chung-gu, Seoul 100-715, Korea,* [2]*Department of Electronics Engineering, Catholic University of Daegu, Kyeongbuk 712-702, Korea ,* [3]*Institute of Quantum Information Processing and Systems, University of Seoul, Seoul 130-743, Korea,* [4]*Department of Physics, Chungnam National University, Daejeon 305-764, Korea*)

Enhancement of optical gain in Li:CdZnO/ZnMgO quantum well lasers

Th-mP12 (231) **T. Hasegawa**[1], **S. Okamoto**[2], **M. Nakayama**[2] ([1]*Department of Material Science, University of Hyogo, 3-2-1 Koto, Kamigori, Ako-gun, Hyogo 6781297, Japan,* [2]*Department of Applied physics, Osaka City University, 3-3-138 Sugimoto, Sumiyoshi-ku, Osaka 5588585, Japan*)

Upconversion of photoluminescence due to subband resonances in a GaAs/AlAs multiple quantum well structure

Th-mP13 (232) **O. A. Shegai, V. I. Mashanov, A. I. Nikiforov, V. V. Ulyanov, O. P. Pchelyakov** (*Institute of Semiconductor Physics, pr.Lavrentieva 13, Novosibirsk 630090, Russia*)

Photoconductivity of Si/Ge/Si structures with 1.5 and 2ML of Ge layer

Th-mP14 (233) **K. Fujiwara**[1], **A. Satake**[1], **N. Takata**[1], **U. Jahn**[2], **E. Luna**[2], **H. T. Grahn**[2] ([1]*Dept of Electrical Engineering and Electronics, Kyushu Institute of Technology, Tobata, Kitakyushu 804-8550, Japan,* [2]*Paul Drude Institute for Solid State Electronics, Hausvogteiplatz 5-7, 10117 Berlin, Germany*)

Anti-Stokes and Stokes photoluminescence in non-uniform GaAs-based quantum wells

Th-mP15 (234) **Y. Sakasegawa, T. Ihara, K. Hirakawa** (*Institute of Industrial Science and Institute for Nano Quantum Information Electronics, University of Tokyo,, 4-6-1 Komaba, Meguro-ku, Tokyo 153-8505, Japan 1538505, Japan*)

Terahertz emission from semiconductor superlattices with photonic crystal structures

Th-mP16 (235) **K. Furuya**[1], **O. Numakami**[2], **T. Sugaya**[1], **N. Yagi**[2], **K. Komori**[1], **M. Mori**[1], **Y. Okano**[2], **M. Asada**[3] ([1]*Photonics Reserach Institute, National Institute of Advanced Industrial Science and Technology (AIST), AIST Tsukuba Central 2, 1-1-1 UMEZONO, TSUKUBA, IBARAKI 3058568, Japan,* [2]*Faculty of Knowledge Engineering, Tokyo City University, 1-28-1, TAMAZUTSUMI, SETAGAYA-KU, TOKYO 1588557, Japan,* [3]*Interdisciplinary Graduate School of Science and Engineering, Tokyo Institute of Technology, 2-12-1, S9-3 O-OKAYAMA, MEGURO-KU, TOKYO 1528552, Japan*)

Analysis of antenna integrated NDR-DCT oscillator for variable oscillation frequency in THz band

Th-mP17 (236) **M. P Mikhailova**[1], **K.D. Moiseev**[1], **E.V. Ivanov**[1], **Yu.P. Yakovlev**[1], **E.Hulicius**[2,2], **A. Hospodkova**[2,1], **J. Pangrac**[2,1], **K. Melichar**[2,1], **T. Šimeček**[2,1] (*[1]Ioffe Physical-Technical Institute RAS, 26, Politekhnichekaya street, St Petersburg 194021, Russia, [2]Institute of Physics AS CR, v.v.i., Prague, Czech Pepublic, 1600. Prague, Cukrovarnicka 10*)

Positive and negative electroluminescence in the type II heterostructures with a deep AlSb/InAsSb/AlSb quantum well

Th-mP18 (237) **R. Kido, A. Satake, K. Fujiwara** (*Dept of Electrical Engineering and Electronics, Kyushu Institute of Technology, Tobata, Kitakyushu 804-8550, Japan*)

Photoluminescence dynamics due to exciton and free carrier transport in GaAs/AlAs superlattices

Th-mP19 (238) **L. Schrottke, M. Giehler, R. Hey, H. T. Grahn** (*Paul Drude Institute for Solid State Electronics, Hausvogteiplatz 5-7, 10117 Berlin , Germany*)

Simulation of the interplay between stimulated emission and carrier distribution in quantum-cascade lasers

Th-mP20 (239) **A. Satake, T. Tanigawa, Y. Tanaka, K. Fujiwara** (*Kyushu Institute of Technology, Tobata, Kitakyushu 804-8550, Japan*)

Thermal escape process of photogenerated carriers from GaAs single-quantum-well contained in GaAs/AlAs superlattices

Th-mP21 (240) **K. S. Chang**[1], **Y. M. Song**[2], **Y. T. Lee**[2], **S. C. Yang**[1], **G. H. Kim**[1] (*[1]Korea Basic Science Institute, 52 Eoeun-dong, Yuseong-gu, Daejeon 305-333, Republic of Korea, [2]Gwangju Institute of Science and Technology, 1 Oryong-dong, Buk-gu, Gwangju 500-712, Republic of Korea*)

Circular and anamorphic microlens array fabricated by selective oxidation of chirped short-period superlattice of GaAs/AlGaAs

Th-mP22 (241) **M. Nakayama**[1], **T. Hirao**[1], **T. Hasegawa**[2] (*[1]Department of Applied Physics, Osaka City University, 3-3-138 Sugimoto, Sumiyoshi-ku, Osaka 558-8585, Japan, [2]Department of Material Science, University of Hyogo, 3-2-1 Koto, Kamigori-cho, Ako-gun, Hyogo 678-1297, Japan*)

Photoluminescence properties of exciton-exciton scattering in GaAs/AlAs multiple quantum wells

Th-mP23 (242) **M. Motyka**[1], **G. Sek**[1], **K. Ryczko**[1], **F. Janiak**[1], **J. Misiewicz**[1], **S. Belahsene**[2], **G. Boissier**[2], **Y. Rouillard**[2] (*[1]Institute of Physics, Wroclaw University of Technology, Wroclaw, Poland, Wybrzeze Wyspianskiego 27, 50-370 Wroclaw, Poland, [2]Institut d 'Electronique du Sud, Université Montpellier 2-CNRS, Montpellier, France, Place Eugene Bataillon, 34095 Montpellier Cedex 5, France*)

Modulation spectroscopy determined band gap discontinuities in GaInAsSb/Al(In)GaASb quantum wells

Th-mP24 (243) **M. Motyka**[1], **G. Sek**[1], **K. Ryczko**[1], **J. Misiewicz**[1], **T. Lehnhardt**[2], **S. Höfling**[2], **A. Forchel**[2] (*[1]Institute of Physics, Wroclaw University of Technology, Wroclaw, Poland, Wybrzeze Wyspianskiego 27, 50-370 Wroclaw, Poland, [2]Department of Applied Physics, University of Würzburg, Würzburg, Germany, Technische Physik Am Hubland, 97074 Würzburg, Germany*)

Optical properties of GaSb-based type II quantum wells emitting in the mid-infrared range

Th-mP25 (244) **T. Noda[1], H. Sakaki[1,2]** ([1]*National Institute for Materials Science, 1-2-1 Sengen, Tsukuba, Ibaraki , Japan,* [2]*Toyota Technological Institute, 201201 Hisakata, Tempaku-ku, Nagoya 468-8511, Japan*)

Anisotropic effective mass and hole transport in p-type (311)A thin GaAs quantum wells

Th-mP26 (245) **D. A. Kozlov, Z. D. Kvon, A. E. Plotnikov** (*Institute of Semiconductor Physics, Siberian Branch of the Russian Academy of Sciences (SB RAS), Novosibirsk, pr. Lavrentyeva 13, 630090, Russia*)

Semiclassical and quantum transport in the 2D electron gas in a hard-wall antidot lattice

Th-mP27 (246) **S.Y. Kim[1,2], S.H. Shin[1], J. D. Song[1], I. K. Han[1], T. W. Kim[2], Y. D. Jho[3]** ([1]*Korea Institute of Science and Technology, Nano Science Research Division, Korea institute of Science and Technology, Seoul 136-791, Korea,* [2]*Hanyang University, Department of Electronic computer communication, Hanyang University, Seoul 133-791 , Korea,* [3]*Gwangju Inst. of Sci. and Tech, Dep. of Info. and Comm., Gwangju Inst. of Sci. and Tech., Gwangju 500-712*)

Structural and electrical properties of InAs grown on $AlAs_{0.32}Sb_{0.68}$ metamorphic buffer layer/GaAs and its application to THz emission

Th-mP28 (247) **Y. Guo, T. C. Zhang, Z. X. Mei, C. Z. Gu, X. L. Du** (*Institute of Physics, Chinese Academy of Sciences, Zhong Guan Cun Nan San Jie Ba Hao,Beijing, China 100190, P.R.China*)

Double Heterojunction of n-ZnO/insulator-MgO/p-Si for Visible-Blind UV Detector

Th-mP29 (248) **P. Rauter[1], T. Fromherz[1], N.Q. Vinh[2], B.N. Murdin[3], G. Mussler[4], D. Grützmacher[4], G. Bauer[1]** ([1]*Institute of Semiconductor and Solid State Physics, University of Linz, Altenbergerstr. 69, 4040 Linz , Austria,* [2]*FOM Institute for Plasma Physics Rijnhuizen, Postbus 1207, NL-3430 BE Nieuwegein, The Netherlands,* [3]*Advanced Technology Institute, University of Surrey, Guildford, Surrey, GU2 7XH, United Kingdom,* [4]*Institut für Bio- und Nanosysteme, Forschungszentrum J D-52425 Jülich, Germany*)

Bias-induced relaxation-time manipulation in SiGe quantum well structures

Th-mP30 (249) **M. Nobile[1], S. Schartner[1], E. Mujagic[1], H. Detz[1], A. M. Andrews[1], P. Klang[1], W. Schrenk[1], G. Strasser[1,2]** ([1]*Center for Micro- und Nanostructures, Vienna University of Technology, Floragasse 7, 1040 Vienna, Austria,* [2]*University at Buffalo, The State University of New York, 332 Bonner Hall, Buffalo, NY 14260, USA*)

Intersubband absorption in InGaAs/GaAsSb multi quantum wells

Th-mP31 (250) **S. Gozu, T. Mozume, H. Ishikawa** (*National Institute of Advanced Industrial Science and Technology(AIST), 1-1-1, Umezono, Tsukuba 205-8568, Japan*)

Refractive index of high-carrier-doped InGaAs/AlAsSb coupled double quantum wells

Th-mP32 (251) **Y. Takada[1], M. Muraguchi[2], T. Endoh[2], S. Nomura[1], K. Shiraishi[1]** ([1]*Graduate School of Pure and Applied Sciences, University of Tsukuba, Tsukuba, Japan,* [2]*Center of Interdisciplinary Research, Tohoku University, Sendai, Japan.*)

Proposal of a new physical model for Ohmic contacts

Th-mP33 (252) **W. Susaki, T. Igawa, T. Inada, A. Tomioka** (*Osaka Electro-Communication University, 18-8 Hatucho, Neyagawa, Osaka 572-8530, Japan*)

Determination of Band Offsets in a $Ga_{0.5}In_{0.5}P/GaAs_{0.9}P_{0.1}$ Single Quantum Well by Photoreflectance with a Semiconductor Laser

Th-mP34 (253) **N. Ishimure, T. Akiyama, K. Nakamura, and T. Ito** (*Department of Physics Engineering, Mie University, Mie, Japan*)

Theoretical investigation for the strain effect on surface structure of InAs(111)A

Th-mP35 (254) **D. C. Heo[1], J. D. Song[1], I. K. Han[1], J. I. Lee[1], J. M. Kim[2], Y. T. Lee[2]** ([1]*Korea Institute of Science and Technology, Nano Science Research Division, Korea institute of Science and Technology, Seoul 136-791, Korea,* [2]*Gwangju Inst. of Sci. and Tech., Dep. of Info. and Comm., Gwangju Inst. of Sci. and Tech., Gwangju 500-712, Korea*)

Optical properties of fully digital-alloyed 1.3 μ m MQW and its application to laser diodes

Th-mP36 (255) **N. K. Cho[1,2], K. W. Kim[1], S. P. Ryu[1], J. D. Song[1], W. J. Choi[1], J. I. Lee[1], H. S. Jeon[2]** ([1]*Korea Institute of Science and Technology, Nano Device Research Center, KIST, Seoul 136-791, Korea ,* [2]*Seoul National University, School of Physics, Seoul National University, Seoul 151-747, Korea*)

Digital-alloy AlGaAs/GaAs distributed Bragg reflector for the application to 1.3 μ m surface emitting laser diodes

Th-mP37 (256) **Y. Yasutake, J. Igarashi, Y. Terada, N. Tana-ami, S. Fukatsu** (*Graduate School of Arts and Sciences, University of Tokyo, 3-8-1 Komaba, Meguro, Tokyo 1538902, Japan*)

Room temperature electroluminescence from 311 rod-like defects in InSb-quantum-dot-embedded-Si heterostructure

Th-mP38 (257) **K. Kurata, M. Murata, K. Kashiwabara, N. Ohtani** (*Department of Electronics, Doshisha University, 1-3 Tatara-Miyakodani, Kyotanabe-shi, Kyoto, 610-0321, Japan*)

Effect of a thin hole-blocking layer on carrier transport and luminescent properties in organic light-emitting diodes

Th-mP39 (258) **K. Nakajima, K. Bando, N. Ohtani** (*Department of Electronics, Doshisha University, 1-3, Tatara-Miyakodani, Kyotanabe-shi, Kyoto 610-0321, Japan*)

Improvement of dark current in organic near-infrared photodiodes by mixing a polymer in the active region

Th-mP40 (259) **K. Kajimoto, K. Uno, I. Tanaka** (*Department of Materials Science and Chemistry, 930 Sakaedani, Wakayama 6408510, Japan*)

Memory effect of pentacene field-effect transistors with embedded monolayer of semiconductor colloidal nano-dots

Th-mP41 (260) **L. Turyanska[1], U. Elfurawi[1], T. D. Bradshaw[1], M. Li[2], S. Mann[2], N. R. Thomas[1], A. Patane[1]** ([1]*School of Physics and Astronomy and Centre for Biomolecular Sciences, The University of Nottingham, Nottingham NG7 2RD, UK,* [2]*Centre for Organized Matter Chemistry, School of Chemistry, University of Bristol, Bristol BS8 1TS, UK*)

Hybrid nanocomposites based on colloidal PbS quantum dots

Th-mP42 (261) **G. J. Matt[1], T. Fromherz[1], M. Bednorz[1], S. Zamiry[2], C. Lungenschmied[3], C. J. Brabec[3], G. Bauer[1]** (*[1]Institute for Semiconductor and Solid State Physics, Johannes Kepler University, Austria, [2]Christian Doppler Laboratory for Surface Optics, Johannes Kepler University, Austria, [3]Konarka Austria, Austria*)

Sensing near to mid infrared light with an organic/inorganic hybrid heterojunction

Th-mP43 (262) **Won Tae Kim, Joo Hyung You, Jae Hun Jung, Tae Whan Kim*** (*National Research Laboratory for Nano Quantum Electronics, Division of Electronics and Computer Engineering, Hanyang University, Engineering center annex 509-1, Haengdang-dong, Seongdong-gu, Seoul*)

Carrier transport mechanisms of nonvolatile memory devices fabricated utilizing multi-walled carbon nanotubes embedded in a poly-4-vinyl-phenol layer

Th-mP44 (263) **T. Kawase, S. Komura, K. Miyazaki, D. Kim, M. Nakayama** (*Department of Applied Physics, Graduate School of Engineering, Osaka City University, 3-3-138 Sugimoto, Sumiyoshi-ku, Osaka 5588585, Japan*)

Characteristics of exciton polaritons in a ZnO Microcavity

Th-mP45 (264) **H. Okamoto[1], T. Kamada[1,2], K. Onomitsu[1], I. Mahboob[1], H. Yamaguchi[1,2]** (*[1]NTT Basic Research Laboratories, Atsugi, Kanagawa 243-0198, Japan, [2]Department of Physics, Tohoku University, Sendai, Miyagi 980-8578, Japan*)

Tunable coupling of mechanical vibration in GaAs microresonators

Th-mP46 (265) **A. S. Samardak[1,4], A. Nogaret[1], N. B. Janson[2], A. Balanov[3], I. Farrer[5], D. A. Ritchie[5]** (*[1]Department of Physics, University of Bath, Bath, BA2 7AY, UK, [2]Department of Mathematics, University of Loughborough, Loughborough, LE11 3TU, UK, [3]Department of Physics, University of Loughborough, Loughborough, LE11 3TU, UK, [4]Department of Electronics, Far Eastern National University, Vladivostok, 690950, Russia, [5]Cavendish Laboratory, University of Cambridge, Cambridge, CB2 1TN, UK*)

Noise induced phenomena in multi-thread excitable semiconductor 'neuron'

Th-mP47 (266) **F. Yamada, T. Shirasaka, K. Fukui, I. Kamiya** (*Toyota Technological Institute, 2-12-1 Hisakata, Tenpaku-ku Nagoya, Aichi 468-8511, Japan*)

Surface State Control of III-V Semiconductors using Molecular Modification

Th-mP48 (267) **Cesar E.P. Villegas, M. R.S. Tavares** (*CCNH, Universidade Federal do ABC, R. Santa Adélia 166, Sto André, 09210170, Brazil*)

Effects of mass induced anisotropy on Dirac-Fermions in graphene-based double quantum wires

Th-mP49 (268) **Nojoon Myoung[1], G. Ihm[1], S.J. Lee[2]** (*[1]Department of Physics, Chungnam National University, Gung Dong 220 Daejeon 305-764, Korea, [2]QSRC, Dongguk University, Seoul 100-715, Korea*)

Transport in zigzag graphene nanoribbons modulated by magnetic barriers

Th-mP50 (269) **K. Ogata, H. Dobashi, K. Koike, S. Sasa, M. Inoue, M. Yano** (*Osaka Institute of Technology, Asahi-ku, Osaka, JAPAN*)

Selective area growth of ZnO nanorods and enzyme immobilization toward the fabrication of glucose sensors

Th-mP51 (270) **Takaaki Tatani**[1,2]**, Hiroki Asano**[1,2]**, A. Ishii**[1,2] (*[1]Department of Applied Mathematics and Physics, Tottori University, Koyama, Tottori 680-8552, Japan, [2]JST-CREST , 5 Sanbancho, Chiyoda-ku, Tokyo 102-0075, Japan*)

Computational study for growth of GaN on graphite as 3D growth on 2D material

Th-mP52 (271) **S. Tsai, J.H. Ho, Y.H. Chiu, M.F. Lin** (*Department of physics, National Cheng Kung University , Physics Department, National Cheng Kung University 1 Ta-Hsueh Road Tainan 70101, Taiwan*)

Band structures of Bernal graphenes modulated by electric fields

Th-mP53 (272) **Y.H. Liu, J.Y. Wu, M.F. Lin** (*Department of Physics, National Cheng Kung University, No.1, Ta-Hsueh Road, Tainan City 701, Taiwan (R.O.C.)*)

The effects of the modulated magnetic field on the Landu levels of monolayer graphene ribbon

Th-mP54 (273) **N. T. Bagraev**[1]**, W. Gehlhoff**[2]**, L. E. Klyachkin**[1]**, A. A. Kudryavtsev**[1]**, A. M. Malyarenko**[1]**, V. V. Romanov**[1]**, I. A. Shelykh**[1] (*[1]Ioffe Physical-Technical Institute of RAS, Politekhnicheskaya 26 , St.Petersburg, Russia, [2]Institut fuer Festkoerperphysik, Technische Universitaet Berlin, D-10623 Berlin, Germany, [3]Polytechnical University, St. Petersburg, 195251, Russia*)

Proximity effects in S-Si-QW-S sandwich nanostructures

Th-mP55 (274) **J. Park, H. Smith, L. Grazulis, K. Eyink, W. C. Mitchel** (*Air Force Research Laboratory, Materials and Manufacturing Directorate, AFRL/RXPS, Wright -Patterson Air Force Base, Ohio, 45433*)

X-ray photoelectron spectroscopy study of interface structure of epitaxial graphene on 4H-SiC(0001)

Th-mP56 (275) **T. Lüdtke**[1]**, P. Mirovski**[1]**, R. Hüther**[1]**, Leonid Govor**[2]**, G. H. Bauer**[2]**, J. Parisi**[2]**, R. J. Haug**[1] (*[1]Abteilung Nanostrukturen, Institut für Festkörperphysik, Universität Hannover, Appelstr. 2, Hannover , Germany, [2]Institut für Physik, Universität Oldenburg, Carl-von-Ossietzky-Straße 9-11, Oldenburg*)

Charge transport through chains of nanoparticles

Th-mP57 (276) **Q. P. Unterreithmeier, T. Faust, J. P. Kotthaus** (*Fakultät für Physik and Center for NanoScience (CeNS), Ludwig-Maximilians-Universität, Geschwister-Scholl-Platz 1, München 80539, Germany*)

Nonlinear Switching Dynamics in Nanoelectromechanical Systems

Th-mP58 (277) **Y. H. Chiu**[1]**, Y. Y. Liao**[2]**, M. F. Lin**[1] (*[1]Department of Physics, National Cheng Kung University, Department of Physics, National Cheng Kung University, Tainan 70101, Taiwan 70101, Taiwan, [2]Department of Applied Physics, National University of Kaohsiung, Department of Applied Physics, National University of Kaohsiung, Kaohsiung 81148, Taiwan*)

Optical absorption spectra of monolayer graphene in spatially modulated electric potentials

Th-mP59 (278) **S. Kim**[1]**, B.-Y. Yu**[2]**, J. Lee**[1]**, S.-I. Lim**[1]**, I. Han**[1]**, G. Ghibaudo**[3] (*[1]Korea Institute of Science and Technology(KIST), Nano Device Research Center, Korea Institute of Science and Technology, 39-1 Hawolkok, Seongbuk, Seoul , Republic of Korea, [2]Korea Institute of Science and Technology(KIST), Advanced Metal Research Center, Korea Institute of Science and Technology, 39-1 Hawolkok Seongbuk, Seoul, Republic of Korea , [3]IMEP-MINATEC, INPG-CNRS, IMEP-MINATEC, INPG-CNRS, 3 rue Parvis Louis Neel, BP257, 38016 Grenoble, France*)

Low-frequency noise in GaAs Solar Cell with Multi-Quantum Well

Th-mP60 (279) **K. Konishi, K. Yoh** (*Research Center for Integrated Quantum Electronics, Hokkaido University, Sapporo, 060-8628 Japan*)

Transport characteristics of a single layer graphene grown on semi-insulating 4H silicon carbide

Th-mP61 (280) **K. Lee[1,2], Y. Lin[2], Y. Chen[2], Y. Huang[1,2]** ([1]*Graduate Institute of Electro-Optical Engineering, National Taiwan University of Science and Technology, No. 43, Sec. 4, Keelung Rd., Taipei 106, Taiwan,* [2]*Deaprtment of Electronic Engineering, National Taiwan University of Science and Technology, No. 43, Sec. 4, Keelung Rd., Taipei 106, Taiwan*)

Characterization of supercapacitor of variable content of nitrogen doping in carbon nanotubes with ruthenium dioxide

Th-mP62 (281) **T. Suzuki[1,2], Y. Yokomizo[2]** ([1]*Tokyo Metropolitan College of Industrial Technology, 8-17-1 Minami-senju, Arakawa-ku, Tokyo 116-0003, Japan,* [2]*Tokyo Metropolitan College of Aeronautical Engineering, 8-17-1 Minami-senju, Arakawa-ku, Tokyo 116-0003, Japan*)

Electronic states of atomic monolayers of various materials: Possibility of energy gap engineering

Th-mP63 (282) **S. Mátéfi-Tempfli[1], M. Mátéfi-Tempfli[1], S. Melinte[2], A. Vlad[2]** ([1]*Unité PCPM, Université catholique de Louvain, Place du Levant 3 B-1348, Belgium,* [2]*Unité DICE, Université catholique de Louvain, Place du Levant 3 B-1348, Belgium*)

Statistics and single element processing in nanoporous templates

Th-mP64 (283) **Hongwu Zhang[1], Nao Terasaki[1], Hiroshi Yamada[1], Chao-Nan Xu[1,2]** ([1]*National Institute of Advanced Industrial Science and Technology (AIST),kyushu center, Kyushu, Shuku807-1, Tosu, Saga, 841-0052,JAPAN,* [2]*CREST, Japan Science and Technology Corporation, Honcho 4, Kawaguchi, Saitama 32-0012, JAPAN*)

Detection of Stress distribution using Ca2MgSi2O7:Eu,Dy micro-particles

Th-mP65 (284) **K. I. Lin[1], J. T. Tsai[1], J. S. Hwang[1], M. C. Chen[2]** ([1]*Department of Physics, National Cheng Kung University, No.1, University Road, Tainan City 701 , Taiwan,* [2]*Institute of Nuclear Energy Research, No. 1000, Wenhua Rd., Longtan, Taoyuan 325, Taiwan*)

Polarity determination of InN by terahertz radiation

Th-mP66 (285) **I. Tanaka[1], Y. Tada[1], S. Nakatani[1], K. Uno[1], I. Kamiya[2], H. Sakaki[2]** ([1]*Wakayama University, 930 Sakaedani, Wakayama 640-8510, Japan,* [2]*Toyota Technological Institute, 2-12-1 Hisakata, Tempaku, Nagoya 468-8511, Japan*)

Resonant tunneling of electrons through single self-assembled InAs quantum dot studied by conductive atomic force microscopy

Th-mP67 (286) **J. T. Tsai[1], K. I. Lin[1], Y.T. Lu[1], J. S. Hwang[1], S. Gwo[2], M. C. Chen[3], G. C. Chi[3]** ([1]*Department of physics, National Cheng Kung University, No.1, University Road, Tainan City 701, Taiwan,* [2]*Department of Physics, National Tsing-Hua University, 101, Section 2, Kuang-Fu Road, Hsinchu 30013, Taiwan ,* [3]*Institute of Optical Science, National Central University, No.300, Jhongda Rd., Jhongli City, Taoyuan County 32001, Taiwan*)

Characterization of photoelastic effects on the optical properties of strained InN films

Th-mP68 (287) **K. Yoshida**[1], **A. Umeno**[1], **S. Sakata**[1], **K. Hirakawa**[1,2] ([1]*IIS, University of Tokyo, 4-6-1 Komaba, Meguro-ku, Tokyo 1538505, Japan,* [2]*CREST-JST, 4-1-8 Honcho, Kawaguchi, Saitama 332-0012, Japan*)

Electromigration-induced breakage mechanism of Ni nanowires

Th-mP69 (288) **H. Iwase**[1], **H. Choi**[1], **S. Yamada**[1], **M.Tanaka**[2], **I. Kimpara**[3] ([1]*Center for Nano Materials and Technology, Japan Advanced Institute of Sci. and Tech., 1-1, Asahidai, Nomi, Ishikawa 923-1292, Japan,* [2]*Department of Aeronautics, College of Engineering, Kanazawa Institute of Technology, 7-1, Ougigaoka, Nonoichi-machi, Ishikawa-gun, Ishikawa 921-8501, Japan,* [3]*Vice-president, Kanazawa Institute of Technology, 7-1, Ougigaoka, Nonoichi-machi, Ishikawa-gun, Ishikawa 921-8501, Japan*)

Study of rolled micro cantilever-like structures based on MBE-grown strained semiconductor layers

Th-mP70 (289) **P. Rauter**[1], **T. Fromherz**[1], **S. Winnerl**[2], **M. Zier**[2], **A. Kolitsch**[2], **M. Helm**[2], **G. Bauer**[1] ([1]*Institute of Semiconductor and Solid State Physics, University of Linz, Altenbergerstr. 69, 4040 Linz , Austria,* [2]*Institute of Ion Beam Physics and Materials Research, Forschunsgzentrum Dresden-Rossendorf, P.O. Box 510119, 01314 Dresden, Germany*)

Terahertz Si:B blocked-impurity-band detectors by ion implantation

Th-mP71 (290) **S. J. Jiao, P. D. Batista, K. Biermann, R. Hey, and P. V. Santos** (*Paul-Drude-Institut für Festkörperelektronik, Hausvogteiplatz 5-7, berlin 10117, Germany*)

Efficient photon detectors using surface acoustic waves

Th-mP72 (291) **K. Ohmori**[1], **Y. Ohkura**[2], **K. Shiraishi**[3], **K. Yamada**[1] ([1]*Waseda University, Bldg 120-5, 513 Waseda Tsurumaki-cho, Shinjuku-ku, Tokyo 162-0041, Japan,* [2]*Semiconductor Leading Edge Technologies (Selete), 16-1 Onogawa, Tsukuba, Ibaraki 305-8569, Japan,* [3]*University of Tsukuba, 1-1-1 Tennoudai, Tsukuba, Ibaraki 305-8573, Japan*)

Effect of carrier transport on threshold voltage variability in Si MOSFET

Th-mP73 (292) **T. Nuytten**[1], **M. Hayne**[2], **H. Y. Liu**[3], **M. Hopkinson**[3], **V. V. Moshchalkov**[1] ([1]*INPAC-Institute for Nanoscale Physics and Chemistry, Pulsed Fields Group, K.U.Leuven, Celestijnenlaan 200D, B-3001 Leuven 3001, Belgium,* [2]*Department of Physics, Lancaster University, Lancaster LA1 4YB, United Kingdom,* [3]*Department of Electronic and Electrical Engineering, University of Sheffield, Sheffield S1 3JD, United Kingdom*)

Band properties of $Ga_{1-x}In_xN_yAs_{1-y}$ multiple quantum wells studied by magneto-photoluminescence

Friday July 24th

Session M9 (International Conference Room) 9:00 – 10:30 Nanophotonics

M9a (294) 9:00 – 9:30 **S. J. Boyle[1], A. J. Ramsay[1], A. P. Heberle[2,3], M. Hopkinson[4], A. M. Fox[1], M. S. Skolnick[1]** (Invited) (*[1]Department of Physics and Astronomy, University of Sheffield, Sheffield, S3 7RH, UK, [2]Department of Physics and Astronomy, University of Pittsburgh, Pittsburgh, Pennsylvania 15260, USA, [3]Sullivan Park, RandD Center, Corning Incorporated, Corning, NY, 14831, USA, [4]EPSRC National Centre for III-V Technologies, University of Sheffield, Sheffield, S1 3JD, UK*)

Picosecond coherent control of dressed states in a single quantum dot

M9b (295) 9:30 – 9:45 **Ch. Strelow, C. M. Schultz, H. Rehberg, A. Stemmann, H. Welsch, Ch. Heyn, D. Heitmann, T. Kipp** (*Institute of Applied Physics, University of Hamburg, Jungiusstr. 11, 20355 Hamburg , Germany*)

Tailoring optical modes in semiconductor microtube bottle resonators

M9c (296) 9:45 – 10:00 **M. Nomura[1], N. Kumagai[1], S. Iwamoto[1,2,3], Y. Ota[2], Y. Arakawa[1,2,2]** (*[1]Institute for Nano Quantum Information Electronics, University of Tokyo, 4-6-1, Komaba, Meguro-ku, Tokyo 153-8505, Japan, [2]Research Center for Advanced Science and Technology, University of Tokyo, 4-6-1, Komaba, Meguro-ku, Tokyo 153-8505, Japan, [3]Institute of Industrical Science, University of Tokyo, 4-6-1, Komaba, Meguro-ku, Tokyo 153-8505, Japan*)

Observation of unique photon statistics of single artificial atom laser

M9d (297) 10:00 – 10:15 **D. Sanvitto[1], L. Vina[1], A. Lemaitre[2], J Bloch[2], E. Karimi[3,4], B. Piccirillo[3], L. Marrucci[3,4]** (*[1]Dept.. Fisica de Materiales. Universidad Autonoma, Campus de Cantoblanco. Madrid E28049, Spain, [2]LPN/CNRS, Route de Nozay, 91460, Marcoussis, France, [3]Dip. Scienze Fisiche, Universita' di Napoli, 80126 Napoli, Italy, [4]CNR-INFM Coherentia, Compl. Univ. di Monte S.Angelo, 80126 Napoli, Italy*)

Pulsed injection of vortices in a polariton condensate

M9e (298) 10:15 – 10:30 **E. A. Cerda-Méndez[1], D. Krizhanovskii[2], K. Biermann[1], K. Guda[2], R. Bradley[2], P. V. Santos[1], R. Hey[1], M. S. Skolnick[2]** (*[1]Paul-Drude-Institut, Hausvogteiplatz 5-7, Berlin 10117, Germany, [2]Department of Physics and Astronomy, University of Sheffield, Sheffield S3 7RH, United Kingdom*)

Dynamic control of polariton condensates using surface acoustic waves

10:30 – 11:00 **Coffee Break**

Session Plenary 5,6 (Main Hall) 11:00 – 12:30

PL5 (300) 11:00 – 11:45 **Susumu Noda** (*Department of Electronic Science and Engineering, Kyoto University, Kyoto 615-8510, Japan*)

Manipulation of Photons by Photonic Crystals

PL6 (302) 11:45 – 12:30 **Moty Heiblum** (*Braun Center for Sub Micron Research, Dept. of Condensed Matter Physics, Weizmann Institute of Science, Rehovot 76100, Israel*)

Physics observed through shot noise measurements

12:30 – 13:00 **Closing**

July 20 (Monday)

10:30 – 12:00

Plenary Session 1, 2

Main Hall

EP2DS-MSS Joint session

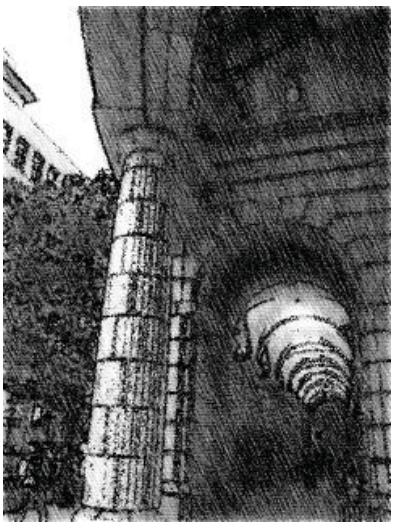

Kobe Daimaru Department Store

Manipulating single spins and coherence in semiconductors

David D. Awschalom

Center for Spintronics and Quantum Computation, University of California, Santa Barbara, CA 93106 USA

Keywords: spintronics, quantum information, quantum dots, diamond

Over eighty years since luminaries such as Pauli and Dirac developed the theory of electron spin, contemporary information technology still relies largely on classical electronics: the charge of electrons for computation and ferromagnets for permanent storage. With the advent of "semiconductor spintronics" and the discovery of long-lived spin coherence in solid state materials, new scientific and technological opportunities have emerged for quantum computing by combining elements of standard electronics with spin-dependent interactions between electrons, nuclei, electric and magnetic fields.

Research at the frontiers of this field includes both optical and electrical schemes to generate, manipulate, and transport coherent spin states in crystalline films and nanometer-scale structures. Moreover, the coupling of spins and photons in the solid state offers natural avenues for integrating quantum computing and communication. While many of these fundamental issues have been addressed using spin ensembles, we discuss recent developments aimed at controlling single spin states using a combination of optical and electrical techniques in a variety of semiconductor systems. The last few years have witnessed extraordinary progress in the ability to create and address single electron, nuclear, and magnetic ion spins by exploiting advances in highly sensitive experimental probes and sophisticated materials synthesis techniques [1].

A semiconductor quantum dot offers an ideal platform for isolating and probing a single electron spin. By placing an electrically-gated quantum dot into an integrated optical cavity, the spin in the quantum dot may be initialized, controlled, and read-out using both optical and electronic means. The non-destructive detection and dynamical observation of single electron spins in these quantum dots is demonstrated using a magneto-optical Kerr rotation measurement [2]. This technique provides a means to directly probe a spin off-resonance, thus minimally disturbing the system. By extension into the time domain, it allows for the direct observation of the coherent evolution of a single electron spin state (figure 1) [3]. The measurements reveal information about the relevant spin decoherence mechanisms, while also providing a sensitive probe of the local nuclear spin environment.

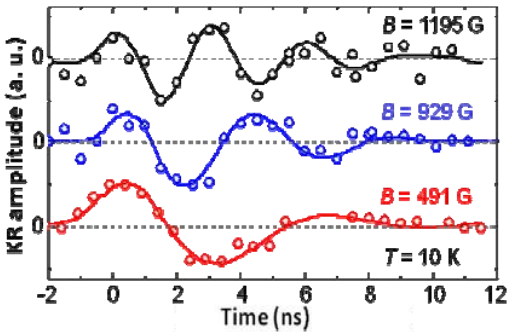

Figure 1. Time-resolved single electron spin precession within an electrically-gated quantum dot at different magnetic fields.

Within the limits of decoherence, practical quantum information processing schemes require fast single-qubit operations. For spin-based qubits, this involves performing arbitrary coherent rotations of the spin state on timescales much faster than the spin coherence time. A scheme for gigahertz all-optical

control of the spin state allows for ultrafast manipulation of a state through arbitrary angles [4]. These results represent progress toward the control and coupling of single spins and photons for quantum information processing as well as quantum non-demolition measurements of a single spin.

While these advanced materials provide exciting new avenues for quantum information processing primarily at low temperatures, spin qubits that operate at room temperature have appeared in the most unexpected of places: diamond – a material that has had a prominent place in the non-scientific world for generations. The electron spins of individual nitrogen-vacancy color centers can be imaged, initialized and manipulated at room temperature with coherence times sufficiently long that quantum error correction may be within reach [5]. There remain significant challenges, however, both in understanding the physics of these defects as well as the development of technologies based on their quantum properties.

Using magneto-optical imaging, photon antibunching, and pulsed electron spin resonance techniques, we describe gigahertz coherent control of isolated single spins (Figure 2) as well as their coupling to nearby nitrogen dopants [6]. The mechanisms of decoherence are explored with measurements probing the fundamental coherent dynamics of a central spin coupled to an adjustable bath of spins. The interactions can be continuously tuned with an applied magnetic field, allowing access to regimes with surprisingly different behavior [7], yielding insights into the loss of coherence for future quantum information processing systems. Combining these elements with precise implanting techniques [8], knowledge of the spin structure of the orbital excited state [9], and the fabrication of diamond microcavities [10] paves the way towards future spin-based quantum devices.

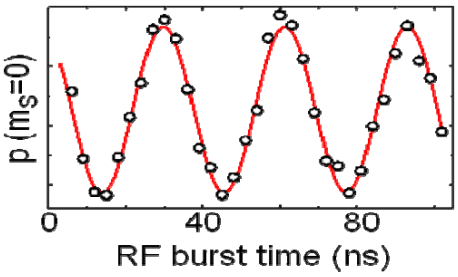

Figure 2. Electrically-driven single spin Rabi oscillations at GHz frequencies under ambient conditions.

References

1. R. Hanson and D. D. Awschalom, Nature **453**, 1043 (2008).
2. J. Berezovsky, M.H. Mikkelsen, O. Gywat, N.G. Stoltz, L.A. Coldren, D.D. Awschalom, Science **314**, 1916 (2006).
3. M. H. Mikkelsen, J. Berezovsky, N.G. Stoltz, L.A. Coldren, D.D. Awschalom, Nature Physics **3**, 770 (2007).
4. J. Berezovsky, M.H. Mikkelsen, N.G. Stoltz, L.A. Coldren, D.D. Awschalom, Science **320**, 349 (2008).
5. D.D. Awschalom, R.J. Epstein, R. Hanson, Scientific American **297**, 84 (2007).
6. R. Hanson, F.M. Mendoza, R.J. Epstein, D.D. Awschalom, Phys. Rev. Lett. **97**, 087601 (2006).
7. R. Hanson, V.V. Dobrovitski, A.E. Feiguin, O. Gywat, D.D. Awschalom *et al.*, Science **320**, 352 (2008).
8. C. D. Weis *et al.*, J. Vac. Sci. Tech. B **26**, 2596 (2008).
9. G. D. Fuchs, V. V. Dobrovitski, R. Hanson, A. Batra, C. D. Weis, T. Schenkel, D. D. Awschalom, *Phys. Rev. Lett*. **101**, 117601 (2008).
10. C.F. Wang *et al.*, Appl. Phys. Lett. **91**, 201112 (2007).

P12
M1
MoP
M2
M3
M4
TuP
M5
P34
M6
M7
M8
ThP
M9
P56

Bose-Einstein condensation and superfluidity of exciton-polaritons

Yoshihisa Yamamoto

E. L. Ginzton Laboratory, Stanford University, CA, USA

National Institute of Informatics, Tokyo, Japan

Keywords: exciton-polariton, Bose-Einstein condensation, superfuidity, microcavity

Particle-particle interaction and peculiar excitation spectra are keys for understanding BEC and superfluidity physics. A quantum field-theoretical formulation for a weakly interacting Bose condensed system was developed by Bogoliubov in 1947, which predicted the phonon-like excitation spectrum in the low-momentum regime. Exciton-polaritons in a semiconductor microcavity, which are elementary excitations created by strong coupling between quantum-well excitons and microcavity photons, were proposed as a new BEC candidate in solid-state systems [1]. Recent experiments with exciton-polaritons have demonstrated several standard but convincing signatures for supporting the polariton condensation, such as the polariton-bunching effect at above the condensation threshold [2], spontaneous spin polarization [3], formation of the long range spatial coherence [4], quantum degeneracy at thermal equilibrium conditions [5] and dynamical condensation in excited p-orbital states [6]. The particle-particle interaction, the Bogoliubov excitation spectrum and the quantized vortices are at the heart of BEC and superfluidity physics, but have only been studied theoretically for exciton-polaritons until very recently. In this talk, we also report the recent observation of interaction effects on the exciton-polariton condensate, such as the linear excitation spectra [7] and the vortex-antivortex pairs [8].

Reference

1. Atac Imamoglu et al., Phys. Rev. A **53**, 4250-4253 (1996).
2. H. Deng et al., Science **298**, 199-202 (2002).
3. H. Deng et al., PNAS **100**, 15318-15323 (2003).
4. H. Deng et al., Phys. Rev. Lett. **99,** 126403 (2007).
5. H. Deng et al., Phys. Rev. Lett. **97**, 146402 (2006).
6. C.W. Lai et al., Nature **450**, 529 (2007).
7. S. Utsunomiya et al., Nature Physics **4**, 700-705 (2008).
8. G. Roumpos et al., submitted for publication.

July 20 (Monday)

14:00 – 16:00

Session M1

Transport in nanostructures

International Conference Room

MSS-EP2DS Parallel session

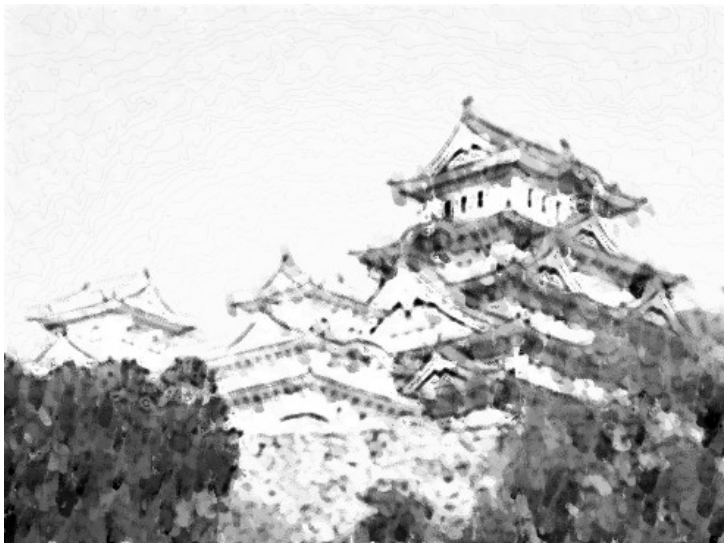

Himeji Castle

Field-Effect Transistors Based on Carbon Nanotubes and ZnO Nanowires with Organic/Inorganic Hybrid Gate Dielectrics

H. Klauk

Max Planck Institute for Solid State Research, Stuttgart, Germany

Keywords: nanowire transistors, carbon nanotube transistors

Nanoscale field-effect transistors (FETs) based on semiconducting carbon nanotubes or inorganic nanowires hold great promise for high-density logic circuits and memory arrays [1,2], and to replace thin-film transistors (TFTs) in active-matrix flat-panel displays where the larger transconductance, smaller capacitance, and smaller footprint of nanoscale FETs compared with hydrogenated amorphous silicon (a-Si:H) and organic TFTs may provide faster pixel charging and larger aperture ratio [3].

The synthesis of carbon nanotubes and crystalline nanowires often requires high temperatures that are incompatible with a variety of substrates, but the nanotubes and nanowires can usually be synthesized on a temperature-compatible growth substrate (e.g., silicon or metal) and then be transferred to the target substrate for FET assembly. If the temperature during FET manufacturing is below ~150 °C, high-performance nanotube or nanowire FETs can thus be implemented on polymeric substrates for flexible circuits or displays.

To take full advantage of the small size and excellent charge transport properties of nanotubes and nanowires, we have prepared FETs and circuits based on individual semiconducting carbon nanotubes as well as FETs and circuits based on single-crystalline ZnO nanowires, both with metal gates and source/drain contacts and a thin, hybrid organic/inorganic gate dielectric prepared at a temperature of less than 100 °C.

References

1. Z. Chen, J. Appenzeller, Y. M. Lin, J. Sippel-Oakley, A. G. Rinzler, J. Tang, S. J. Wind, P. M. Solomon, and P. Avouris, Science **311**, 1735 (2006).
2. A. Javey, S. W. Nam, R. S. Friedman, H. Yan, and C. M. Lieber, Nano Lett. **7**, 773 (2007).
3. S. Ju, J. Li, J. Liu, P. C. Chen, Y. G. Ha, F. Ishikawa, H. Chang, C. Zhou, A. Facchetti, D. B. Jones, and T. J. Marks, Nano Lett., **8**, 997 (2008).

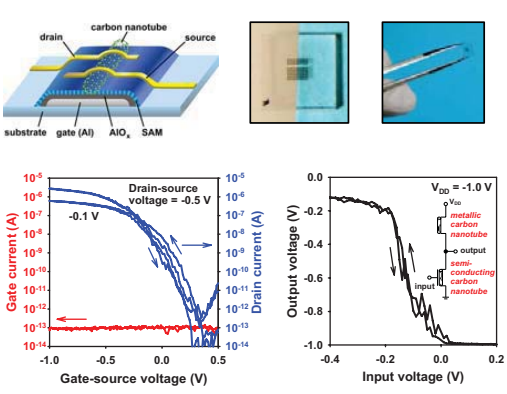

Fig. 1. Carbon nanotube field-effect transistors and circuits manufactured on a glass substrate.

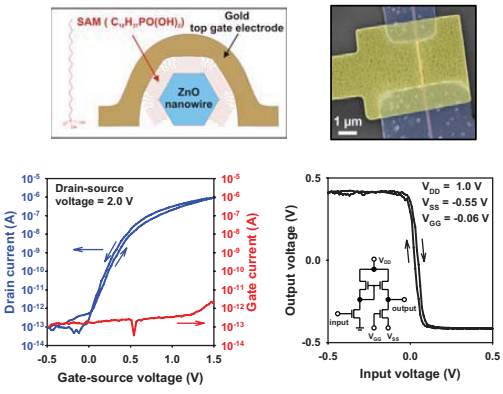

Fig. 2. ZnO nanowire field-effect transistors and circuits.

Doping of catalyst-free MBE grown GaAs nanowires, transport properties and related devices

C. Colombo*, D. Spirkoska**, T. Garma*,**, M. Heiß*,**, F. Vialla**, J. Dufouleur**, G. Abstreiter** and A. Fontcuberta i Morral*

* *LMSC, Ecole Polytechnique Federale de Lausanne, Lausanne, Switzerland*

** *Walter Schottky Institut, Technische Universität München, München, Germany*

Keywords: semiconductor nanowires, electronic transport, doping, solar cells

Semiconductor nanowires are filamentary crystals with a large aspect ratio and the diameter in the order of the nanometer range. Their study is a rapidly expanding field, due to the expectations that nanoscale objects and their associated phenomena offer to basic and applied science. Up to now, the synthesis of nanowires is mainly based on the vapour-liquid-solid and vapour-solid-solid mechanism. Common in both mechanisms is that a metal nanoparticle gathers and decomposes catalytically the precursor molecules. Supersaturation of the metal droplet follows and leads to the precipitation of a solid phase underneath the droplet in the form of a nanowire. Typically, gold is used as a catalyst. The use of such an extrinsic catalytic metal is in general not desired and some effort has been directed into finding alternatives. Recently, we have been able to synthesize III-V nanowires without the use of an external catalyst by MBE. The optical properties of the nanowires have shown to be excellent, due to the good crystal quality and purity.

For studies of the electronic transport phenomena in nanowires as well as for the fabrication of useful devices, controlled doping is an important issue. In this paper, we present our latest results in the investigation of doping of catalyst-free MBE grown GaAs nanowires, as well as the growth model that accounts for the results. We also present the electronic transport characterization of the nanowires. The magnetotransport properties from room temperature down to 300 mK will be presented and the transport mechanisms discussed. Finally, we present how coaxial p-i-n junctions can be realized for the fabrication of nanowire solar cells. The efficiency measurements are also presented. This work opens the route for the use of semiconductor nanowires in functional nanodevices.

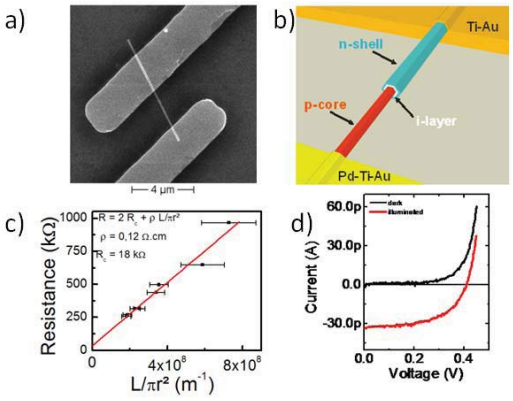

Fig.1 (a) Scanning electron micrograph of a contacted GaAs based nanowire (b) Schematic representation of a contacted coaxial p-i-n nanowire junction, (c) Measurement of the resistivity of a doped nanowire (d) Current-voltage characteristics in the dark and under illumination of a p-i-n junction working as a solar cell.

References

1. A. Fontcuberta i Morral et al., *Appl. Phys. Lett.* 92, 063112-3 (2008).
2. C. Colombo et al. *Phys. Rev. B*, 77, 155326 (2008).
3. A. Fontcuberta i Morral et al., *Small* 4, 899 (2008).

P12
M1
MoP
M2
M3
M4
TuP
M5
P34
M6
M7
M8
ThP
M9
P56

A quantum analogue of the STM multiple-tip effect revealed by wavefunction imaging of quantum dots

O. Makarovsky*, O. Thomas*, A. G. Balanov*, A. Patanè*, L. Eaves*, R. P. Campion*, C. T. Foxon*, E. E. Vdovin*, D.K. Maude**

*School of Physics & Astronomy, University of Nottingham, Nottingham NG7 2RD, UK
**Grenoble High Magnetic Field Laboratory, CNRS, F-38042 Grenoble, France

Keywords: quantum dots, magneto-tunnelling spectroscopy, GaMnAs, wavefunction

Recently, we reported a method of creating electrostatically-induced quantum dots (QDs) by diffusing ionised Mn interstitial donors (Mn_i) out of ferromagnetic GaMnAs into the vicinity of a GaAs quantum well (QW). Magnetotunnelling spectroscopy (MTS) of the tunnel current through a single dot revealed the spatial form of the ground and excited state electronic wavefunctions and a rich Fock-Darwin-like spectrum of energy levels with orbital angular momentum from 0 up to 11 [1]. Amongst the large ensemble of almost circular QDs produced by this technique, we also find a small number of elongated dots in which the orbital angular momentum is quenched – Fig. 1(a). MTS images of two elongated QD excited states are shown in Fig. 1(b). The spatial distribution of the Mn_i ions which form these elongated dots also influences the quantisation of the emitter states from which the conduction electrons tunnel into the dots. This gives rise to a MT spectrum which is a remarkable analogy to "multiple tip effect" in scanning tunnelling microscopy (STM) – Fig. 1(c). For example, the two resonances at 1.169V and 1.173V in Fig.1(c) are convolutions of the matrix elements between the ground state of the QD and the ground and first excited states of confined electrons in the emitter, respectively. On the 1.169V resonance, note how the two-lobed orbitals of the 2p-like emitter excited state acts in a similar way to an STM with a double-tip. When this effect is taken into account, we can extract high quality images of the ground and excited states of the elongated dots.

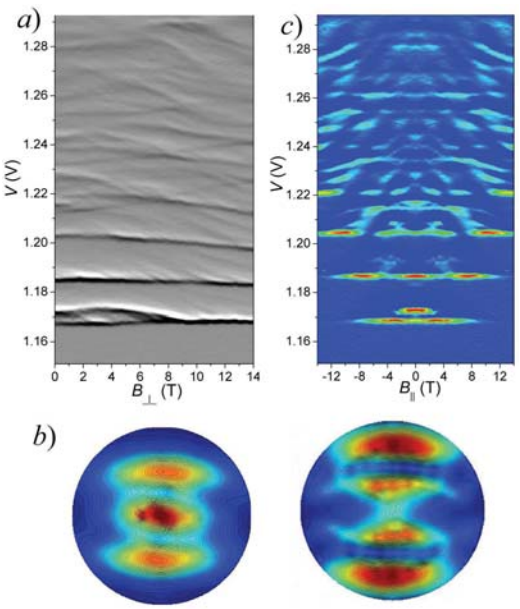

Fig.1 a) and c) plots of the differential tunnel conductance verses magnetic field B, applied perpendicular and parallel to the QD plane, respectively. b) Probability density images of two electronic bound states of an elongated QD obtained from the dependence of the conductance on $B_{||}$ at the 1.187V and 1.204V resonances.

References

[1] O. Makarovsky et al., *Phys. Rev. Lett.* **101**, 226807 (2008).

Gate adjustable coherent three and four level mixing in a vertical quantum dot molecule

C. Payette[1,2], S. Amaha[3], T. Hatano[3], K. Ono[4], J. A. Gupta[1], G. C. Aers[1], D. G. Austing[1,2], S. V. Nair[5] and S. Tarucha[3,6]

[1]*Institute for Microstructural Sciences M50, NRC, Ottawa, Ontario K1A 0R6, Canada*

[2]*Department of Physics, McGill University, Montreal, Quebec H3A 2T8, Canada*

[3]*Quantum Spin Information Project, ICORP, JST, Atsugi, Kanagawa 243-0198, Japan*

[4]*RIKEN, Wako, Saitama 351-0198, Japan*

[5]*Center for Advanced Nanotechnology, University of Toronto, Toronto, Ontario M5S 3E3, Canada*

[6]*Department of Applied Physics, University of Tokyo, Tokyo 113-0033, Japan*

Keywords: Coupled quantum dots, Magneto-tunnelling spectroscopy, Energy level mixing

By performing magneto-tunnelling spectroscopy, we can probe the single-particle energy spectra of the constituent quantum dots in a weakly coupled vertical quantum dot molecule made from a GaAs-AlGaAs-InGaAs structure [1,2]. The measured spectra are well reproduced by ideal elliptical parabolic energy spectra *except* where two or more energy levels approach each other. At the level crossings we nearly always observe pronounced anti-crossing behaviour. We attribute this to coherent mixing induced by anharmonicity and anisotropy in the probed dot's confinement potential. Recently, we measured and successfully modelled three-level mixing leading to resonant current suppression ("dark" state formation) in a device with a single gate wrapped around the mesa [2]. The couplings between each pair of approaching (basis) levels in the presence of a non-ideal confinement potential were characterized by coupling coefficients; however, these could not be experimentally altered in-situ.

Here, we describe new measurements demonstrating the modulation of coherent mixing in a device which has four gates (G_1-G_4- see Fig. 1 micrograph) surrounding the mesa rather than one. By application of different voltages to these gates we can perturb the probed dot's effective confinement potential and hence alter the coupling coefficients at the level crossings. This strongly influences both their energy dispersion as well as the branch current strengths.

Figure 1 shows a three level anti-crossing that can be altered by changing how the various gate voltages are swept. Specifically, we can gradually alter the nature of the anti-crossing from having one dominant coupling (A) to three dominant couplings (B) [2]. Figure 2 shows a four level anti-crossing which we can also probe and systematically alter in our device. Furthermore, we extend our simple model from Ref. 2 to characterize the gate adjustable coherent mixing.

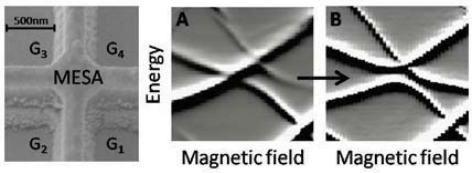

Fig.1 Micrograph of mesa with four gates and alteration of a three-level anti-crossing by application of different gate voltages.

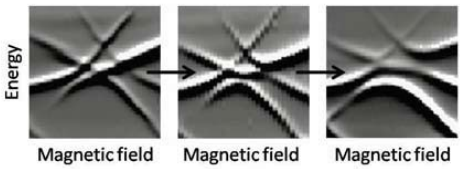

Fig.2 Evolution of a four-level anti-crossing.

References

1. K. Ono et al, Physica B **314**, 450 (2002).
2. C. Payette et al, Phys. Rev. Lett. **102**, 026808 (2009)

Bidirectional current drag effect utilizing cotunneling of two-electrons in coupled double quantum dots

G. Shinkai*,**, T. Hayashi*, T. Ota*, K. Muraki* and T. Fujisawa**

** NTT Basic Research Laboratories, NTT Corporation, 3-1 Morinosato-Wakamiya, Atsugi, 243-0198, Japan.*

*** Reseach Center for Low-Temperature Physics, Tokyo Institute of Technology, 2-12-1 Ookayama, Meguro, 152-8551, Japan.*

Keywords: current drag, double quantum dot, single-electron device

Various functional devices have been demonstrated by controlling single electrons in quantum dots (QDs). Coupled arrays of QDs provide current mirror devices or drag effect, in which current in the first array drags the electron in the second array. Here, we describe novel bidirectional drag effect, in which the polarity of the drag current can be switched by choosing two cotunneling processes. Namely, forward tunneling in the first double quatum dot (DQD) is accompanied by forward tunneling in the second DQD, or by backward tunneling. We observed reasonable drag effect for both processes, which encourages optimizing the device for complete mirror functions.

The coupled DQD device (DQD1 and DQD2) is identical to that used for qubit measurements [1], and its equivalent circuit is shown in Fig. 1(a). Large bias (V_{SD1} = 700 μV) is applied for DQD1 for driving the current in the forward direction, and effectively zero bias (V_{SD2} ~ 10 μeV) is applied to allow dragging in either directions. The elastic cotunneling processes take place at specific conditions illustrated in Fig. 2(a) and (b). When the energy offset of discrete levels in DQD1, ε_1, is made equal to that in DQD2, ε_2, as shown in Fig. 2(a) inset, forward tunneling in DQD1 is accompanied by backward tunneling in DQD2. This negatively correlated cotunnling is observed as a positive peak in I_1 and negative peak in I_2 as shown in Fig. 2(a). In contrast, when the energy configuration is made at $\varepsilon_2 = -\varepsilon_1$ as in Fig. 2(b) inset, positively correlated cotunneling is expected and actually observed as positive peaks in I_1 and I_2 as shown in Fig. 2(b). The drag current in I_2 reaches 50% of driving current in I_1 (evaluated as a peak height neglecting the background current) without special optimization. Some strategies for optimization will be given.

The work was partially supported by SCOPE, KAKENHI(19204033), and G-COE at TokyoTech.

References

1. G. Shinkai et al., Appl. Phys. Lett. 90, 103116 (2007); G. Shinkai et al., submitted.

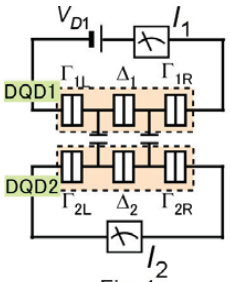

Fig. 1

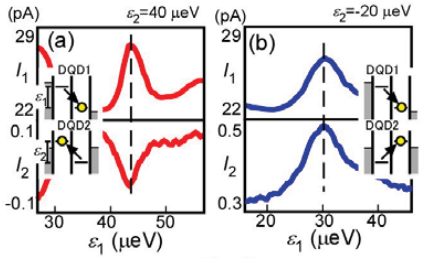

Fig. 2

Fig. 1 Schematic circuit and equivalent circuit of coupled DQD device.

Fig. 2 Negatively (a) and positively (b) correlated cotunneling. Insets show schematic energy diagrams. Currents I_1 and I_2 simultaneously measured as a function of ε_1 at ε_2=40 μeV (a) and -20 μeV (b).

Coulomb blockade transport across lateral (Ga,Mn)As nanoconstrictions

M. Schlapps*, S. Geissler*, T. Lermer*, J. Sadowski**, W. Wegscheider* and D. Weiss*
*Department of Applied Physics, University of Regensburg, Germany
** Max-Lab, Lund University, Sweden

Keywords: GaMnAs, constriction, Coulomb blockade, SET

Narrow constrictions in metallic (Ga,Mn)As films display large magnetoresistance effects [1-6]. Explanations of these large effects involve the formation of a tunneling barrier in the vicinity of the constriction due to carrier depletion [1, 2]. A pronounced dependence of the resistance on the in-plane magnetic field direction was ascribed to the tunneling anisotropic magnetoresistance (TAMR) [2] and, more recently, to a magnetization dependent metal-insulator transition (MIT) [4, 5]. On the other hand, experiments on a narrow (Ga,Mn)As channel revealed a Coulomb blockade anisotropic magnetoresistance effect (CBAMR), where the angular dependence of the resistance was ascribed to chemical potential anisotropies [6]. Hence the microscopic origin of the huge magnetoresistance effects is still under discussion. Here we revisit the problem of transport across a (Ga,Mn)As nanoconstriction. An electron micrograph of the device is shown in FIG. 1a). Based on measurements of the resistances' bias voltage and temperature dependence down to millikelvin temperatures at different in-plane magnetic field angles we compare the models currently used. We show that the MR can be connected to a distinct magnetization alignment in the constriction providing a plausible explanation for the observed spin-valve like behavior during a magnetic field sweep by means of the magnetization configurations in the device. At temperatures below $T \sim 30$ K the resistance increases continuously with decreasing temperature, both for the high resistance and low resistance state, thus indicating that the huge MR effects, that vanish above ~ 30 K, are only existent in the insulating regime. Therefore a picture involving a magnetization driven MIT is at odds with our experiment. Rather the device acts as a single electron transistor by using additional side-gates. We experimentally prove that Coulomb-blockade plays a decisive role in describing the MR effects. Furthermore we show that modeling the constriction as a granular metal, i.e. as conducting nanoscale

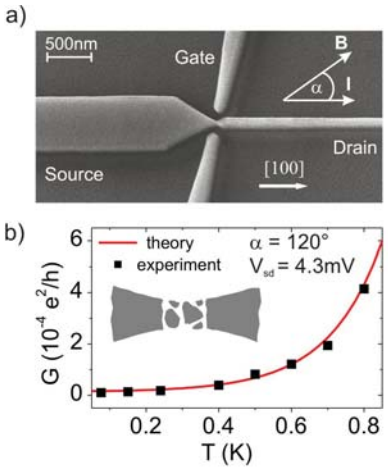

Figure 1: a) Electron micrograph of a typical sample with additional side gates. b) The temperature dependence of the conductance G can be described with a model for a granular metal system.

islands, separated by potential barriers [7], describes not only the temperature and bias dependence of the conductance quantitatively correct (see FIG. 1b)) but also allows to estimate the number of participating islands.

References

[1] C. Ruester et al. , PRL **91**, 216602 (2003).

[2] A. D. Giddings et al. , PRL **94**, 127202 (2005).

[3] M. Schlapps et al. , phys. stat. sol. (a) **203**, No. 14, 3597 (2006).

[4] M. Ciorga et al. , New J. Phys. **9**, 351 (2007).

[5] K. Pappert et al. , Nature Physics **3**, 573 (2007).

[6] J. Wunderlich et al. , PRL **97**, 077201 (2006).

[7] B. Abeles et al. , Advances in Physics **24**, 407 (1975).

Resonant tunneling in a vertical pillar structure including a self-assembled quantum dot coupled with a quantum well

T. Kodera[1], K. Ono[2], N. Kumagai[1], T. Nakaoka[1], S. Tarucha[1,3], and Y. Arakawa[1,4]

[1] *Institute for Nano Quantum Information Electronics, the Univ. of Tokyo, Meguro-ku, Japan*

[2] *RIKEN, Wako-shi, Japan,* [3] *ICORP-JST, Atsugi-shi, Japan,*

[4] *Institute of Industrial Science, RCAST, the Univ. of Tokyo, Meguro-ku, Japan*

Keywords: double quantum dots, self-assembled quantum dots,

Research toward quantum information conversion between electron states and photon states has attracted interests intensely, but so far there have been few reports on it [1]. The object of our research is to understand physics of optoelectronic nanostructure devices and to develop related techniques for future fusion devices of the quantum information processing and quantum optical communication.

In this work, we fabricate and characterize a vertical double quantum dot (QD) structure which has self-assembled InAs QDs and an InGaAs quantum well (QW). Self-assembled InAs QDs have a good optical controllability and response, while vertical QDs have good transport properties in a sense that electronic state and spin state can be identified well [2]. Therefore, combining and coupling these two types of QDs will provide a way to realize such a device that can convert information between photon states and electron states.

Figure 1(a) shows a cross sectional scanning electron microscope (SEM) image of the similar sample we used in our experiments. The sample growth is performed by molecular beam epitaxy (MBE) on a semi-insulating GaAs substrate. Triple barrier structure (TBS) is sandwiched by graded n-doped layers. The TBS consists of three GaAs barriers, a 12-nm-thick $In_{0.05}Ga_{0.95}As$ QW, and a self-assembled InAs QD layer. The QD and QW are in a weak coupling regime because of the center barrier thickness of 9 nm.

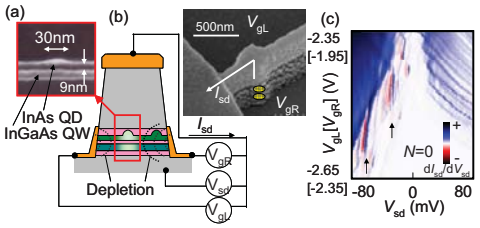

Fig.1 (a) Cross sectional SEM image of the sample. (b) Schematic picture and SEM image of the device. Measurement setups are also shown. (c) Measured dI_{sd}/dV_{sd} plot in the plane of V_g and V_{sd}.

Using the sample, we have realized a vertically coupled double QD by fabricating a vertical pillar structure with two gate electrodes as shown in Fig. 1(b). From the QD-sheet density of ~5×10^9 cm^{-2}, there are expected to be on average 1 or 2 QDs in the pillar whose diameter is ~400 nm. We measure the vertical current I_{sd} thorough both an InAs QD and an InGaAs QD by tuning the potential shape and the position of the InGaAs QD in the QW plane with gate voltages V_{gL} and V_{gR} applied independently.

Figure 1(c) shows the Coulomb diamond (CD) plot or differential conductance in the plane of source drain voltage (V_{sd}) and gate voltages (V_{gL} and V_{gR}) measured at 1.5 K. We have succeeded in observing peculiar characteristics of the double QD in series, such as vertical lines parallel to the V_g axis (indicated by arrows) corresponding to inter-dot resonances [3]. The controllability of the inter-dot level detuning is a key of future application to optoelectronic nanodevices. We have estimated the charging energy as ~20 meV from the CD. The large CD is a direct consequence of the strong confinement of self-assembled InAs QDs.

References

1. H. Kosaka *et al*, Phys. Rev. Lett. **100**, 096602 (2008)
2. T. Ota, *et al.*, Phys. Rev. Lett. **93**, 066801 (2004).
3. K. Ono *et al.* Physica B **314**, 450 (2002).

July 20 (Monday)

16:00 – 18:00

Poster Session Mo-mP

Meeting Room 501, 502

MSS-EP2DS Parallel session

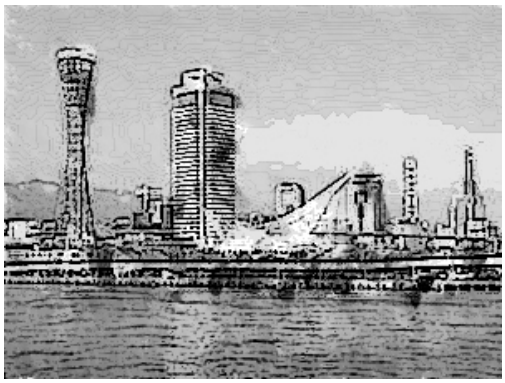

"Meriken" park and Kobe port tower

Inverted Ge islands in {111} faceted Si pits - a novel approach towards islands with higher aspect ratio

M. Grydlik*, M. Brehm, H.Groiss, T. Fromherz, F. Schäffler, G. Bauer

** Institute of Semiconductor and Solid State Physics, University of Linz, A-4040 Austria*

Keywords: SiGe, MBE growth, patterned Si(001) substrates, structural and optical properties

A detailed study of the so far unexplored Ge island nucleation on Si(001) substrates patterned with {111} faceted pyramidal pits, grown by solid source molecular beam epitaxy is reported. The Si(001) substrates were pit-patterned by e-beam lithography with periods of 350 nm and 400 nm. Hereafter {111} faceting of the pits is achieved by the anisotropic wet etchant tetramethylammoniumhydroxid (TMAH) that has substantially higher etch rates in the <100> directions as compared to the <111> directions**.** Due to the self-limiting of the etch process, an extremely uniform pit pattern is achieved. For the 45 nm thick Si buffer layer growth the substrate temperature was ramped from 450 °C to 550 °C. We demonstrate that these are the conditions in which the pit shape is preserved. After the buffer layer growth Ge was deposited at various growth temperatures T_g between 550°C and 700°C. For T_g = 550°C, Ge fills the pits in the form of truncated inverted {111} pyramids with a (001) oriented top surface with typical widths of 50 nm and heights of 20 nm. The islands obtained in such a growth mode are highly uniform in shape. As shown by transmission electron microscopy, high aspect ratios typically around 0.4 can be obtained. This value is larger than the one of islands grown on planar and pit-patterned substrates reported so far. Thus, with these islands the realization of true zero dimensional carrier confinement is feasible. Photoluminescence of the islands shows an emission band as high as 0.97 eV due to strong carrier confinement. For higher T_g (625°C and 700 °C) above the base of the inverted Ge pyramid, facets typical for domes and barns are formed at the sidewalls of the residual pits, which effectively reduce their inclination angles. Further Ge deposition finally results in a smoothening of the pits and in approaching of the {1 1 10} / {105} pit faceting, present typically for growth on plasma etched shallow pits. In this situation, we observe nucleation of upright domes on the bottom of nearly planarized pits.

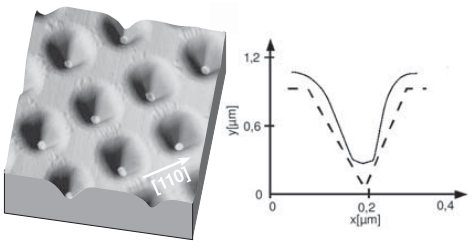

Fig.1 Three dimensional AFM image (1x1)µm^2. 4.8 ML of Ge grown at 550°C on pre-patterned Si (001) substrate. The Ge fills the pits and inverted islands with an aspect ratio of 0.4 are obtained. The solid line on the right side shows a cross-sectional line scan through a pit. The dotted line represents the original {111} pit wall facets.

Comparative study of p-doped and undoped 1.3-μm InAs/GaAs quantum-dot lasers

T. Yang, Y. L. Cao, H. M. Ji, W. Q. Ma, P. F. Xu and Y. X. Gu

Institute of Semiconductors, Chinese Academy of Sciences (CAS), P. O. Box 912, Beijing 100083, PRC

Keywords: quantum dot, p-doping, lasers, characteristic temperature

Much effort has been devoted to develop 1.3-μm InAs/GaAs self-assembled quantum dot (QD) lasers due to their potential uses in future metro/access network systems. In particular, it has been recently demonstrated that introducing p-doing in the QD lasers can significantly improve the temperature stability of the lasers, making it possible to fabricate uncooled directly-modulated 1.3-μm 10 Gb/s QD lasers for the uses [1]. In this paper, we present a comparative study on the characteristics of the p-doped and undoped 1.3-μm InAs/GaAs self-assembled QD lasers.

The QD lasers with and without p-doping in the active regions were grown on Si-doped GaAs substrates by MBE. The active regions of the lasers consists of five-staked layers of InAs QDs that were capped by 4-nm-thick $In_{0.17}Ga_{0.83}As$ strain-reducing layers and then separated by 40-nm-thick GaAs spacer layers. The active regions were sandwiched between n-type and p-type 1.4-μm-thick $Al_{0.4}Ga_{0.6}As$ cladding layers. The only difference between the two types of lasers with and without p-doping was whether the GaAs barrier layers in the active regions contain 5-nm-thick p-doing layers with Be (5×10^{17} cm^{-3}) or not. Broad area and ridge waveguide lasers were fabricated by standard lithography and wet etching to investigate the material and device characteristics of the QD lasers with and without p-doping. Lasers of various cavity lengths were obtained by cleaving.

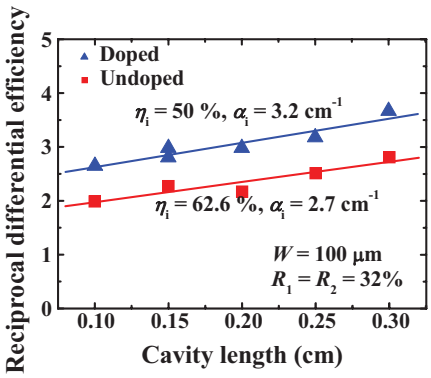

Fig.1 Reciprocal differential quantum efficiency vs. cavity length for the two types of broad-area lasers with and without p-doing, measured at RT.

Figure 1 shows the reciprocal differential quantum efficiency ($1/\eta_d$) as a function of cavity length (L) for the two types of broad-area QD lasers, measured at room temperature in a pulse mode (30 μs, 100 Hz). The squares and triangles respectively indicate experimental data derived from the two types of lasers. The red and blue lines are linearly fitted to the experimental data by the relation: $\eta_d = \eta_i/(1+ \alpha_i L/\ln(1/R))$, where η_i is internal quantum efficiency, α_i is internal loss, and R is power reflectivity of as-cleaved faces (R = 0.32). From the fitting, we obtained η_i of 62.6% and α_i of 2.7cm^{-1} for the undoped lasers, while they are 50% and 3.2 cm^{-1} for the p-type doped lasers, respectively. This implies that introducing the p-type doping in the active regions can cause increased internal loss and lowered internal quantum efficiency, resulting in increased threshold current density although it can significantly improve the temperature stability of the QD lasers [1]. Further results and discuss will be presented at the meeting.

This work was financially supported by "One-Hundred Talents Program" of CAS, the National High Technology Research and Development Program of China (Grant No. 2006AA03Z401), and the National Science Foundation of China (Grant No. 60876033).

References

1. K. Otsubo *et al.*, Jpn. J. Appl. Phys. **43**, L1124 (2004).

Ab initio-based approach to structural modulation of AlN on 4H-SiC(11 $\bar{2}$0) during MBE growth

Tomonori Ito, Takumi Ito, Toru Akiyama, and Kohji Nakamura

* *Department of Physics Engineering, Mie University, Tsu, Japan*

Keywords: Structural stability, AlN/SiC, MBE growth, *Ab inito* calculations

The growth of AlN with nonpolar orientation is of great interest and importance for potential applications in polarization-free light-emitting devices. It has been known, however, that the quality of AlN layers with polar (0001) orientations. Thus, improving the crystalline quality of nonpolar films remains a challenging issue. Horita et al. have successfully fabricated high quality of nonpolar AlN films on 4H-SiC(11 $\bar{2}$0) substrate using plasma assisted molecular beam epitaxy (MBE). Furthermore, they found that the crystal structure of AlN is modulated from 4H to 2H and vice versa by changing III/V ratio [1]. Despite these new findings, details of hetero epitaxial growth processes of AlN on the 4H-SiC (11 $\bar{2}$ 0) are still unclear. In order to clarify them, we theoretically investigate the elemental growth processes of AlN on the 4H-SiC(11 $\bar{2}$ 0) including adsorption-desorption behavior using our ab intio-based approach [2].

Our calculated migration potentials for one Al or one N adatom on the 4H-SiC(11 $\bar{2}$0) surface imply that the stable adsorption site for Al is close to the lattice site of 4H structure. This is because the Al adatom with smaller number of valence electrons favors the interatomic bonds with two C surface atoms having two electrons in their dangling bonds by occupying the lattice sites near 4H structure. On the other hand, N stays at the interstitial site located above top C atom, since the N adatom with larger number of valence electrons can form extra interatomic bonds with surface Si atoms without electrons in their dangling bonds. Furthermore, surface phase diagram calculations clarify that the Al adatom can reside in all the lattice sites on the surface without desorption while N can stay only at the most stable site under the conventional growth condition with temperature ~1200 K.

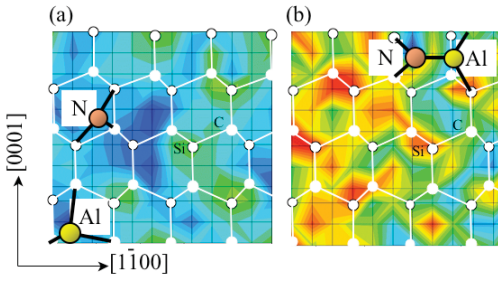

Fig.1 Calculated energy contour map of Al and N atoms on the 4H-SiC(11 $\bar{2}$0) surface after (a) N and (b) Al adsorptions, respectively.

Figure 1 shows the calculated energy contour map of Al and N atoms on the 4H-SiC(11 $\bar{2}$0) surface after (a) N and (b) Al adsorptions, respectively. This figure shows the distinctive atomic arrangements of Al and N atoms simultaneously located on the surface. After N adsorption, Al adatom independently occupies the 4H-like lattice site similar to that for one Al on the surface (Fig. 1(a)), while N adatom forms the dimer structure with pre-adsorbed Al (Fig. 1(b)). Furthermore, it is clear that Al adatom can easily diffuse across the surface to favor the 4H lattice sites even after N adsorption. On the other hand, N adatom is immobile to form the dimer structure with pre-adsorbed Al different from the 4H atomic arrangements on the surface. These findings are consistent with experimental results where the 4H-AlN appears under Al-rich condition, whereas N-rich conditions provide the 2H-AlN on the 4H-SiC(11 $\bar{2}$0) surface.

References

1. M. Horita, J. Suda, and T. Kimoto, phys. stat. sol C., **3**, 1503 (2006).
2. Y. Kangawa, T. Ito, Y. S. Hiraoka, A. Taguchi, K. Shirashi, and T. Ohachi, Surf. Sci. **507-510**, 285 (2002).

Growth of AlGaAs/GaAs (11n)A facets by selective MBE

T. Nishiwaki, M. Yamaguchi, and N. Sawaki

Department of Electronics, Nagoya University,Furo-cho 3C-1, Chikusaku, Nagoya 464-8603, Japan

Keywords: GaAs, Selective MBE, facet structure, inter-surface diffusion

Selective epitaxial growth of nano-wires/dots on a patterned substrate has attracted attention in the formation of quantum structures. Recently, we achieved a one-dimensionally aligned AlInAs quantum dot (QD) array in a narrow V-groove made of AlGaAs/GaAs facets [1]. The formation of AlInAs QDs was strongly influenced by the shape of the V-groove. Exact control of the V-groove structure will be essential to achieve the precise control of the dot formation. During the MBE growth on a rectangular stripe, the cross-sectional shape of the stripe is changed drastically depending on the growth conditions and/or stripe geometry. Figure 1(a) shows the schematic evolution of a [1-10] stripe, which is determined by surface diffusion of Ga adatoms on facets.

In this paper, we perform the modelling of the V-groove growth to analyze the migration of Ga adatoms between facets, on the basis of a diffusion equation;

$$\frac{dn(x,t)}{dt} = G\cos\theta - \frac{n(x,t)}{\tau(\theta)} + D(\theta)\frac{d^2}{dx^2}n(x,t) \quad ,$$

where $n(x,t)$ is the density of adatoms, G is the incident net flux, θ is the angle of the facet to (001) face. $\tau(\theta)$ and D are lifetime and diffusion coefficient of adatoms, respectively, to be determined empirically with experimental growth rates and diffusion lengths. For simplicity, we assume a constant D independent of facets and the characteristic behaviour is represented by the lifetime $\tau(\theta)$.

We found that the evolution of the cross sectional shape is well described by the numerical model as shown in Fig.1(b). Figure 2 shows the numerical adatom density n and the lateral flux on typical stages (facet structures). Figure 2(a) is for an initial stage on a rectangular stripe, and 2(b) is that with a narrow V-groove on the top. Attention should be focused on the direction of diffusion around the {111}A facet, which is changed during the growth. We found that sign change depends on the relative width and lifetime of adjacent facets. The formation of {115}A facet on the top is initiated by the ridge growth on the (001) top face, which has been induced by the short lifetime on the (001) face as compared to that on the {114}A side facets. The deviation of the numerical results from the experimental one is obvious on the (001) bottom face. The last fact suggests the presence of an additional potential barrier for the inter-surface migration across the boundary between (001) bottom face and {111}A facet [2].

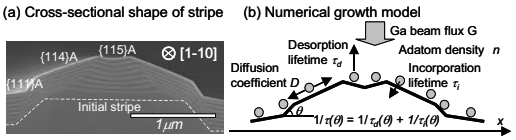

Fig.1 The cross-sectional shape of [1-10] stripe (a), and the numerical growth model (b).

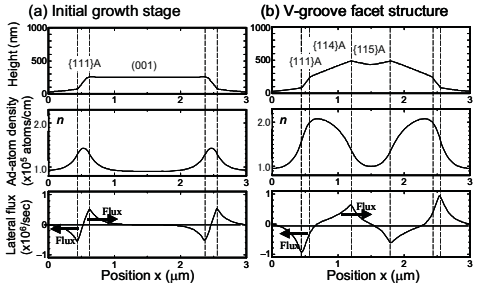

Fig.2 The cross-sectional shapes of facet structure (top panels), the adatom density (middle) and the lateral flux distribution (bottom) on facets. The plus sign of the lateral flux means that the diffusion occurs from left to right.

References

[1] T. Nishiwaki, M. Yamaguchi, and N. Sawaki: Semicond. Sci. Technol. **23** 105016 (2008).
[2] T. Ito, K. Shiraishi, H. Kageshima, and Y. Suzuki: Jpn. J. Appl. Phys. **37** L488 (1998).

Morphological evolution at the early stages of Ge island formation on Si(001) revisited: the key role of the wetting layer

M. Brehm*, M. Grydlik*, G. Vastola**, M. J. Beck***, H. Lichtenberger*, T. Fromherz*, F. Montalenti**, F. Schäffler*, L. Miglio**, and G. Bauer*

* *Institute of Semiconductor Physics, Johannes Kepler University, Linz, Austria*

** *L-NESS and Materials Science Department, University of Milano-Bicocca, I-20125 Milano, Italy*

*** *Department of Physics and Astronomy, Vanderbilt University, Nashville, Tennessee 37235, USA*

Keywords: SiGe islands, Stranski-Krastanow growth mode, island morphology.

So far the well established sequence of appearance of SiGe islands grown in the Stranski-Krastanow growth mode on planar Si(001) substrates with increasing Ge deposition, i.e. pre-pyramids (or mounds), pyramids, domes, barns and superdomes, was straightforwardly understood in terms of increasing aspect ratio, providing a larger volumetric strain relaxation. In this work we present clear experimental evidence for the formation of domes prior to pyramids at elevated growth temperatures (T_G > 675°C) and for an "overcritical" behaviour of the wetting layer (WL) (i.e. domes appear at the expenses of a WL thinning). Such findings are obtained from systematic investigations of atomic force microscopy (AFM) and photo-luminescence (PL) on samples grown by molecular beam epitaxy. By implementing a shallow Ge gradient [1] over 4" wafers we achieved an extremely high deposition resolution of 0.025 monolayers (ML). At T_G = 700°C and a Ge growth rate of 0.05 Å/s we observe dome formation at Θ = 4.2 ML, while pyramids appear later, i.e. at Θ > 4.38 ML. The dome formation is initiated by a Ge transfer of 1 ML from the WL to the islands, as determined from the abrupt shift of the WL PL by 60 meV at the onset of the island PL. At T_G = 625°C the common island formation sequence is observed, namely pre-pyramids and small pyramids forming already at about 2 ML followed by the nucleation of domes at 4.9 ML. In order to understand whether the domes are actually stable prior to pyramids, accurate density functional theory calculations of surface energies and finite element method simulations of the elastic energies were performed, taking particular care in determining the total energy variations in the first few MLs of the WL. By a morphological phase diagram we both confirmed the early stability of the Ge-rich domes and the depletion of the WL at their onset, also addressing the appearance first of pyramids at 625°C to be a kinetic effect, leading to metastable islands. An experimental proof for this prediction is obtained from extensive annealing experiments. After annealing at 700°C pyramids grown with Θ < 3.2 ML at 625°C form back to a completely flat WL, while for Θ > 3.2 ML domes are formed. Thus, we conclude that the critical WL thickness (t_c) for stable island nucleation is about 3.2 ML. At the same t_c domes are formed if we anneal an overcritical WL grown at 700°C. By our systematic AFM and PL experiments with 0.025 ML Ge coverage resolution and our consistent theoretical description we reveal up to now unobserved steps in the morphologically evolution of SiGe islands.

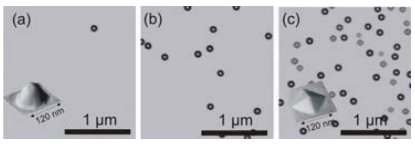

Fig.1 AFM surface inclination images of Ge islands grown on planar Si(001) substrates at 700°C with (a) 4.2 ML (b) 4.35 ML (c) 4.5 ML of Ge deposited. We stress the observation of rounded based domes at ~4.2 ML prior to the one of square based pyramids at 4.4 ML. The insets in (a) and (c) shows 3D AFM images of typical domes and pyramids.

References

1. M. Brehm et al., Appl. Phys. Lett. **93**, 121901 (2008).

Theoretical investigation on the structural stability of GaAs nanowires with two different types of facets

Tomoki Yamashita, Toru Akiyama, Kohji Nakamura and Tomonori Ito
Department of Physics Engineering, Mie University, Tsu, Japan

Keywords: Nanowire, Structural stability, wurtzite structure, zinc blende

Semiconductor nanowires (NWs) are expected to play a key role in future nanotechnology due to their potential application as building blocks in electronics and optoelectronics. In particular, NWs consisting of group III-V materials (III-V NWs) have attracted much attention because of their specific electronic and optical properties. It has been reported that III-V NWs along the [111] direction have two different types of facets. NWs with $\{111\}$ / $\{1\bar{1}00\}$ (in the zinc blende (ZB) structure / in the wurtzite (W) structure) facets are usually fabricated by the vapor-liquid-solid (VLS) mechanism and tend to have the W structure [1, 2]. On the other hand, NWs with $\{1\bar{1}0\}$ / $\{11\bar{2}0\}$ facets are generally grown by the selective area (SA) growth and tend to have various structures which depends on semiconductor materials [3–5]. For example, GaAs NWs grown by the SA growth has $\{1\bar{1}0\}$ / $\{11\bar{2}0\}$ facets and exhibit has the ZB structure including the W structure as stacking fault [3]. However, tapered NWs, which have both two types of facets, have been recently fabricated by the VLS mechanism [6]. The tapered region near the seed particle for NW growth has $\{1\bar{1}00\}$ facets and tends to have the W structure, while the NW base far from the seed particle has $\{1\bar{1}0\}$ / $\{11\bar{2}0\}$ facets with the ZB structure including several W segments. In spite of these findings, it is still unclear that the relationship between the orientation of NW facets and the structural stability from theoretical view point. In this study, we evaluate NW cohesive energy and surface energy of $\{111\}$ / $\{1\bar{1}00\}$ and $\{1\bar{1}0\}$ / $\{11\bar{2}0\}$ using our empirical interatomic potential calculations and first-principles calculations, respectively. Based on the calculated energies, we clarify the structural stability of GaAs NWs with $\{111\}$ / $\{1\bar{1}00\}$ facets and $\{1\bar{1}0\}$ / $\{11\bar{2}0\}$ facets.

Our calculated results show that for NWs with $\{111\}$ / $\{1\bar{1}00\}$ facets the W structure is more stable than the ZB structure over entire diameter range. This is because the surface energy of $\{1\bar{1}00\}$ exhibiting in the W structure is much lower than that of $\{111\}$ in the ZB structure by $\sim$800 meV/atom. Thus, the stability of NW facets is a very important factor determining the structure of NWs with $\{111\}$ / $\{1\bar{1}00\}$ facets. The preference of the W structure compared to the ZB structure is consistent with the experimental results for NW formation with $\{1\bar{1}00\}$ [6]. In contrast, the most stable structure in NWs with $\{1\bar{1}0\}$ / $\{11\bar{2}0\}$ facets depends on the NW diameters. The NWs consisting of $\{11\bar{2}0\}$ facets (the W structure) are favorable for diameters less than 29 nm, whereas those consisting of $\{1\bar{1}0\}$ facets (the ZB structure) are stabilized for diameters larger than 29 nm. Although $\{11\bar{2}0\}$ surface is more stable than $\{1\bar{1}0\}$ surface, the surface energy difference is relatively small ($\sim$60 meV/atom), resulting in the stabilization of the ZB structure for large diameters in which the contribution of NWs facets on the stability is negligible. However, the energy difference (5 meV/atom) between the ZB and the W structures for large diameters ($\sim$100 nm) still smaller than that in bulk GaAs (8 meV/atom). Therefore, the W structure can be incorporated in the ZB structure with large interval along the [111] direction, qualitatively consistent with experiments for NW formation with $\{1\bar{1}0\}$ / $\{11\bar{2}0\}$ facets.

References

[1] J. Johansson *et al.*, Nature Maters. **5**, 574 (2006).

[2] R. E. Algra *et al.*, Nature **456**, 369 (2008).

[3] J. Motohisa, J. Noborisaka, J. Takeda, M. Inari and T. Fukui, J. Cryst. Growth **272**, 180 (2004).

[4] P. Mohan, J. Motohisa and T. Fukui, Nanotech. **16**, 2903 (2005).

[5] K. Tomioka, J. Motohisa, S. Hara and T. Fukui, Jpn. J. Appl. Phys. **46**, 1102 (2007).

[6] M. C. Plante and R. R. LaPierre, J. Cryst. Growth **310**, 356 (2004).

Self-assembly of symmetric, unstrained GaAs quantum dots without wetting layer by droplet epitaxy

T. Mano, T. Kuroda, B. Mcskimming, A. Ohtake, K. Mitsuishi, T. Noda, and K. Sakoda

Quantum Dot Research Center, National Institute for Materials Science, Tsukuba, Japan

Keywords: Quantum dot, Molecular beam epitaxy, Droplet epitaxy,

Application of the self-assembled quantum dots (SA-QDs) to the single or entangled photon emitters is recently gathering great interest. In order to realize the high quality emitters, two issues are pointed out recently; (1) wetting layers (WL) cause the background emission, which degrades the fidelity of single photon emission, (2) asymmetry (strain and/or geometry) of the QDs causes fine structure splitting (FSS) [1]. In the case of InAs QDs on GaAs (100) by Stranski-Krastanov (S-K) mode, however, these two issues might be hardly overcome since they are intrinsically inevitable to form strained QDs. As an alternative method, droplet epitaxy (DE) is a powerful technique that does not require strain for SA-QD formation. In the previous studies, DE has been performed mainly for the formation of GaAs/AlGaAs QDs on (100) substrates. However, these issues still remained [2] due to the surface anisotropy and As-rich *c(4×4)* reconstruction. In this paper, we demonstrate DE on GaAs (111)A to solve them.

The sample was grown on GaAs (111)A in a molecular beam epitaxy system. After the growth of GaAs and AlGaAs layer, Ga droplets were formed by a supply of 0.09 ML of Ga (0.009ML/s) at 475°C without As_4 flux. Then, the samples were cooling down to 200°C and crystallized into GaAs by a supply of As_4 flux (2×10^{-6} Torr beam equivalent pressure). After crystallization, we annealed the sample at 400°C followed by the growth of AlGaAs capping layer. Finally, rapid thermal annealing process was carried out.

Fig. 1(a) shows an atomic force microscope (AFM) image of GaAs QDs before capping. The density, average base size and height are 7×10^{8} /cm^2, 45 nm, and 5 nm, respectively. Since we supplied less than 1 ML Ga to form QDs, two-dimensional WL should not form, which is advantageous effect of Ga-rich *(2×2)* reconstruction on (111)A surface [3]. The absence of WL was also confirmed by cross-sectional scanning transmission electron microscopy. In the AFM image, we cannot observe geometrical asymmetry of the QDs. We attribute this high symmetry to the three-hold symmetry of (111)A surface [3]. To check the FSS, we measured linear polarization dependence of photoluminescence (PL) emission from single QD. Fig. 1(b) and (c) shows micro-PL spectrum of single QD and its peak energy plotted against the polarization angle. The peak energy change is less than the resolution of around 20 μeV. This value is much smaller than those of strained QDs grown by S-K mode and unstrained QDs grown on GaAs (100) grown by DE [1,2]. Hence, these QDs grown on (111)A are promising for single or entangled photon emitters.

References

1. M. Bayer et al., Phys. Rev. B 59, R5300 (1999).
2. M. Abbarchi et al., Appl. Phys. Lett. 93, 162101 (2008).
3. K. W. Haberern and M. D. Pashley, Phys. Rev. B 3226.

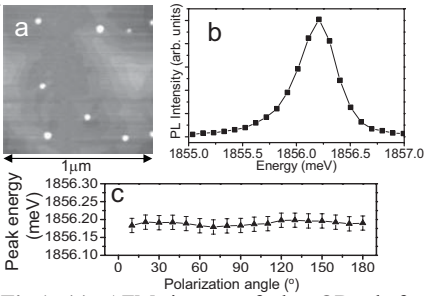

Fig.1 (a) AFM image of the QDs before capping. (b) Micro-PL spectrum from single QDs at 5 K. (c) Peak energy plotted against polarization angle.

in situ STM observation of nano-structures generated near InAs quantum dots on GaAs(001) surface

T. Toujyou*, T. Noda**, T. Teraoka*, T. Konishi*, and S.Tsukamoto*

* *Anan National college of Technology, Tokushima, Japan*

** *National Institute for Materials Science, Ibaraki, Japan*

Keywords: Quantum Dot, Scanning Tunnelling Microscope, Molecular Beam Epitaxy, *in situ* Observation

To examine features of the surface during growth, it is possible to perform true dynamic imaging by using a system in which the scanning tunneling microscopy (STM) is placed inside the molecular beam epitaxy (MBE) growth chamber, the so-called "STMBE system" [1]. We have already exhibited the use of this in situ STM-MBE system for InAs-GaAs(001) heteroepitaxial growth and the fundamental processes governing QD formation [2,3]. However, detailed microscopic mechanism of forming the InAs quantum dots (QDs) is still not fully understood yet.

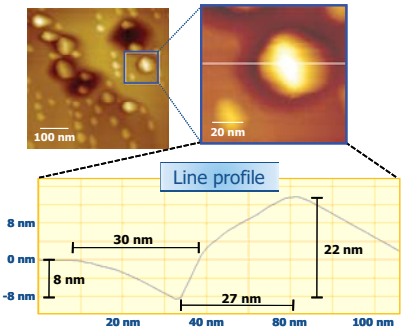

Fig1 STM image of QDs and its line profile

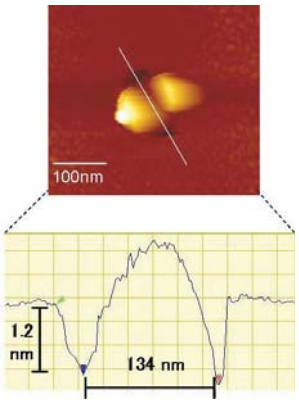

Fig.2 STM image of In droplets and its line profile

In this work we report in situ STM observations of the growth of InAs wetting layer (WL) and QDs, especially, we focused on ditch structures appeared near InAs QDs.

An experimental procedure is as follows. After removing oxides at 580°C under As_4 flux of $1.5x10^{-4}$Pa, GaAs buffer layer was grown 500nm at 560 °C. Next, InAs QDs were grown at 500 °C under In, As_4 fluxes, $8.6x10^{-5}$Pa and $1.5x10^{-4}$Pa, respectively, and InAs growth rate was 0.00289ML/s. STM measurement parameters were tip bias of -0.5V, tunneling current of 0.2nA, and scan speed of 200nm/s. The continuous STM image of 500nm x 500nm is shown in Fig.1. By observing the STM image in Fig.1, we confirmed that the ditch was generated around QDs. The line profile in Fig.1 shows clearly the ditch generated near QD edge. We speculate the formation process of the ditch as follows. In the initial state of the ditch generation, WL peels off by one atom layer. Surface reconstruction of these steps shows In rich (4x2) in its edges and (2x3) and/or (1x3) in the middle of the steps. It was found that GaAs peeling off was started when the dot width was over 40nm. Then these Ga atoms from the ditch mixed with InAs, and QDs grew up hugely. To confirm these exchange phenomena of In/Ga, we generated In droplets on GaAs at 150 °C and observed its at 200 °C, confirmed the presence of an etching effect and the ditch structures clearly as shown in Fig.2.

References

1. S. Tsukamoto and N. Koguchi, J.Cryst.Growth 201/202, 118 (1999); 209, 258 (2000).
2. S. Tsukamoto, T. Honma, G.R.Bell, A.Ishii, and Y.Arakawa, Small 2 (2006) 386-389.
3. T. Honma, S. Tsukamoto, and Y. Arakawa, Jpn.J.Appl.Phys. 45 (2006) L777-L779.

Controlling the aggregation of magnetic cations in GaN

A. Bonanni*, A. Navarro-Quezada*, T. Li*, B. Faina*, R. Lechner*, G. Bauer*, M. Rovezzi**, F. D'Acapito**, W. Stefanowicz***, M. Kiecana***, M. Sawicki***, and T. Dietl***

* *Institut für Halbleiter- und Festkörperphysik, Johannes Kepler University, Linz, Austria*

** *Italian Collaborating Research Group, BM08 "GILDA" - ESRF, Grenoble, France*

*** *Institute of Physics, Polish Academy of Sciences, Warsaw, Poland*

Keywords: growth of modulated structures, nanoscale characterization, ferromagnetic semiconductors

There is growing amount of evidence that owing to a significant contribution of *d* orbitals to the bonding, semiconductors alloyed with transition metals may allow to fabricate in a self-organized fashion nanocomposite semiconductor/ferromagnetic metal systems with a controllable size, shape, and motive of the buried ferromagnetic regions. Recent theoretical and experimental studies indicate that such modulated semiconductors may exhibit novel and hitherto unexplored functionalities in spintronics, but also in photonics and thermoelectrics.

We have carried out detailed studies of MOVPE-grown (Ga,Fe)N [1-5], either undoped or co-doped with Si or Mg, combining magnetic (SQUID [1,3,4] and EPR [1]), magnetooptical [2,3], and XANES [5] investigations with a comprehensive structural and chemical characterization by SIMS, TEM, EDS [1,2,4], synchrotron-XRD [4], and EXAFS [5]. Our finding demonstrate that the Fe ions are distributed in the nitride matrix in a way giving rise either to a diluted random alloy [1-5] or to ferromagnetic FeN_x nanocrystals that aggregate by precipitation [1,2,4,5] or to spinodal decomposition into (Ga,Fe)N regions more or less rich in the magnetic component [2,4]. Since this aggregation correlates with the ferromagnetic response and no spontaneous magnetization is observed in the films without Fe, we take our results as a strong support of the notion [6] that the high-T_C ferromagnetism discovered in a number of magnetically doped oxides and semiconductors results from a non-uniform distribution of the magnetic component.

Interestingly, we find that the aggregation of the Fe cations exhibits a strong dependence on the Ga flow rate and growth temperature, allowing – when appropriately mastered – a control of the solubility limit of the transition metal ions in GaN. Moreover, the formation of the Fe-rich nanocrystals and, hence, the ferromagnetic response of (Ga,Fe)N can be affected by doping with donors (Si) and acceptors (Mg). Our findings guide us to the far-reaching conclusion that the attractive force between magnetic cations can be adjusted by varying their charge state [4-6]. Finally, by elaborating novel protocols for depositing magnetic and shallow impurities in a δ-like fashion we start to take control over the magnetic nanocrystal shapes (dots *vs*. nanocolumns), and we foresee significant consequences for possible functionalities of these systems.

References

1. A. Bonanni, M. Kiecana, C. Simbrunner, Tian Li, M. Sawicki, M. Wegscheider, M. Quast, H. Przybylinska, A. Navarro-Quezada, R. Jakieła, A. Wolos, W. Jantsch, and T. Dietl, *Phys. Rev. B* **75**, 125210 (2007).

2. M. Wegscheider, Tian Li, A. Navarro-Quezada, B. Faina, A. Bonanni, W. Pacuski, R. Jakieła, and T. Dietl, *J. Phys.: Condens. Matter* **20**, 454222 (2008).

3. W. Pacuski, P. Kossacki, D. Ferrand, A. Golnik, J. Cibert, M. Wegscheider, A. Navarro-Quezada, A. Bonanni, M. Kiecana, M. Sawicki, T. Dietl, *Phys. Rev. Lett.* **100**, 037204 (2008).

4. A. Bonanni, A. Navarro-Quezada, Tian Li, M. Wegscheider, R.T. Lechner, G. Bauer, Z. Matej, V. Holy, M. Rovezzi, F. D'Acapito, M. Kiecana, M. Sawicki, and T. Dietl, *Phys. Rev. Lett.* **101**, 135502 (2008).

5. M. Rovezzi, F, D'Acapito, A. Navarro-Quezada, B. Faina, T. Li, A. Bonanni, F. Filippone, A. Amore Bonapasta, T. Dietl, *arXiv:0902.4614*

6. see, e.g., A. Bonanni, Topical Review, *Semicond. Sci. and Technol.* **22**, 41 (2007).

Highly uniform site-controlled quantum dots with record spectral purity

R.J. Young, L.O. Mereni, V. Dimastrodonato, S.B. Healy, E.P. O'Reilly, E. Pelucchi

Tyndall National Institute, University College Cork, Cork, Ireland

Keywords: MOVPE, quantum dot, site-controlled, spectral purity

The use of semiconductor Quantum Dots (QDs) as a light source in the nascent fields of quantum information processing and quantum key distribution has, so far, been limited by a demanding list of requirements. Applications requiring individual dots with specific properties, such as entangled photon production [1], have been limited to proof-of-principle demonstrations as traditional dot fabrication techniques lack the control of their placement and the consistency in exciton-confinement required to provide homogeneous optical properties. Recent work has shown that site-controlled dots grown on (111)B GaAs substrates, pre-patterned with tetrahedral pyramidal recesses [2], may provide an answer to these demands.

We will present a novel site-controlled QD system based on MOVPE growth in pyramidal recesses which demonstrates both an excellent degree of uniformity and high spectral purity. Unintentional impurity incorporation in the growth of site-controlled quantum dots usually leads to poor optical properties characterised by linewidths that are much broader than those measured from self-assembled systems. Our dot system, which employs an AlGaAs cladding layer surrounding GaAs barriers and an $In_xGa_{1-x}As$ quantum dot (illustrated in Fig. 1a) is grown by MOVPE at high temperature to reduce impurity incorporation. Optical studies at low temperature of a large number of quantum dots reveals a distribution of the neutral exciton's emission energy with a standard deviation of just 1.2meV (Fig. 1b) and linewidths as low as 18μeV. The former is comparable to the best values reported in other site-controlled systems and the latter is significantly better than the typical linewidths measured from the emission of self-organised dots grown in ultra-high vacuum MBE systems. An additional advantage of this system is the ease at which its emission energy can be tuned; varying the indium concentration in the quantum dot from x=0.15 to 0.45 results in an energy shift in the emission of ~100meV.

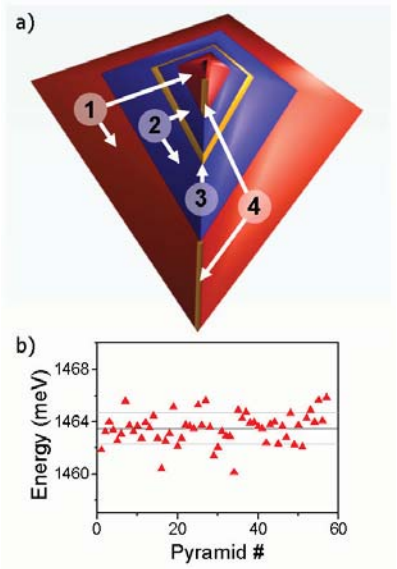

Fig.1 a) The sample layer structure; 1 – $Al_{0.55}Ga_{0.45}As$, 2 – GaAs, 3 – $In_xGa_{1-x}As$, 4 – vertical quantum wire. b) Emission energy of a large number of dots (grey bars span 2 s.d.'s).

We use an 8-band **k.p** method [3] to model the dot's active region, which we treat as a truncated inverted pyramid. We use this bandstructure to interpret the optical properties for different growth thicknesses and indium concentration of the samples.

We believe the excellent optical properties of this dot system along with its reproducibility will open new avenues of quantum information research.

References

1. R. Young et al., Phys. Rev. Lett. **102**, 030406 (2009)
2. E. Pelucchi et al., NanoLetters **7**, 1282 (2007)
3. A.D. Andreev et al., J. Appl. Phys. **86**, 297 (1999)

Structure determination of Pd-catalyst supported on S-terminated GaAs (001) using DFT calculation

A. Ishii*, H. Asano*, M. Yokoyama*, and S. Tsukamoto**

* *Department of Applied Mathematics and Physics, Tottori University, Tottori, Japan*

** *Center for Collaborative Research, Anan National College of Technology, Tokushima, Japan*

Keywords: Catalyst, GaAs, Pd, DFT

Transition metal catalyzed reactions have played an important role in synthetic and process chemistry. The homogeneous catalyst surely causes effective reaction, however, a lot of efforts and energy are required for reusing the catalyst. From this viewpoint, development of the easily treatable heterogeneous catalyst is strongly desired for reducing the waste of expensive rare metal. Although the polymer supported catalyst has been developed, it cannot tolerate under severe conditions such as high temperature and it is restricted to use in organic solvents. Recently, palladium acetate ($Pd(OAc)_2$) molecules immobilized on the S-terminated GaAs(001) has high catalytic activity and stability for Heck reaction [1]. For this catalytic activity, the bond of Ga-S [2] is considered to play an important role in chemical reaction.

For developing more effective catalysts, it is very important to know its detail structures. Therefore, in this paper, we try to determine the atomic structure of this catalyst, Pd on the S-terminated GaAs(001), by DFT calculations using VASP [3]. For the calculation, we used two type slab models of 2x1 supercell; S adsorbed on As-terminated GaAs(001)-(2x1) surface and S adsorbed on Ga-terminated GaAs(001)-(2x1) surface. For the S adsorbed on the Ga-terminated GaAs(001), we emulate GaAs(001)-(2x6)-S using the similar way as in a reference [4]. In the actual experimental situation, most of all topmost As atoms are considered to be desorbed, so that the Ga-terminated case seems to be the real model. For both case, the binding energies and the migration energies for Pd and S on GaAs(001) surface are very similar. We show the most stable structure for the Ga-terminated surface in Fig.1. According to the calculation, the adsorption energy for Pd is stronger for the co-adsorption of S than that for the adsorption of Pd alone. Moreover, the electronic wave function of Pd coupled strongly with the substrate.

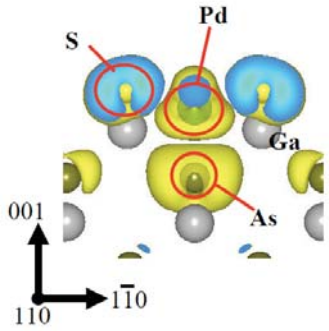

Fig.1 A most stable structure for Pd and S adsorbed on the Ga-terminated GaAs(001)-(2x1) surface. The electronic density is also shown.

This research was supported by Japan Science and Technology Agency (JST).

References

[1] M.Arisawa, M.Hamada, I.Takamiya, M.Shimoda, S.Tsukamoto, Y.Arakawa, A.Nishida, Adv.Synth.Catal. 348, 1063 (2006).

[2] S.Tsukamoto and N.Koguchi, Appl.Phys.Lett. 65, 2199 (1994).

[3] G.Kresse and J.Hafner, Phys.Rev.B 47, RC558 (1993).

[4] S.Tsukamoto, T.Ohno, and N.Koguchi, J.Cryst. Growth 175/176, 1303 (1997).

Structure determination of Pd-catalyst supported on S-terminated GaN (0001) using DFT calculation

M. Yokoyama*, S. Tsukamoto**, and A. Ishii*

* *Department of Applied Mathematics and Physics, Tottori University, Tottori, Japan*

** *Center for Collaborative Research, Anan National College of Technology, Tokushima, Japan*

Keywords: Catalyst, GaN, Pd, DFT

Transition metal catalyzed reactions have played an important role in synthetic and process chemistry. The homogeneous catalyst surely causes effective reaction, however, a lot of efforts and energy are required for reusing the catalyst. From this viewpoint, development of the easily treatable heterogeneous catalyst is strongly desired for reducing the waste of expensive rare metal. Although the polymer supported catalyst has been developed, it cannot tolerate under severe conditions such as high temperature and it is restricted to use in organic solvents. On the other hand, palladium acetate ($Pd(OAc)_2$) molecules immobilized on the S-terminated GaAs(001) has high catalytic activity and stability for Heck reaction [1]. However, the GaAs substrates including toxic As, it is not suitable for mass productions. To solve this problem, a new type catalyst was reported recentry [2], which transition metals were supported on the S-terminated GaN(0001).

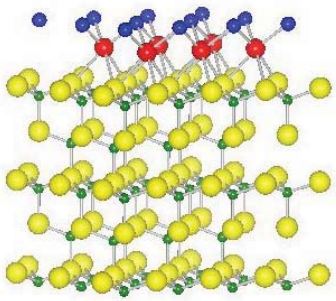

Fig.1 A structure of Pd on the S-terminated GaN(0001) determined by DFT calculation. Pd atoms (Red) are located between a GaN(0001) (Yellow) surface and an adsorbed S (Bule) layer.

For developing more effective catalysts, it is very important to know its detail structures. Therefore, in this paper, we try to determine the atomic structure of this catalyst, Pd on the S-terminated GaN(0001), by DFT calculations with plane wave expansion and pseudopotential methods using VASP [3]. For the calculation, we used 1x1 slab model supercell. A calculated atomic structrue of Pd atoms on the S-terminated GaN(0001) surface is shown in Fig.1, indicating that the stable position of Pd atom was between S and Ga atoms of the S-terminated GaN(0001). The binding energy of Pd on GaN(0001) was stronger than that of S. It means that the S adatom is easier to be desorbed from the GaN(0001) substrate than Pd during catalysis reaction.

This research was supported by Japan Science and Technology Agency (JST).

References

[1] M. Arisawa, M. Hamada, I. Takamiya, M. Shimoda, S. Tsukamoto, Y. Arakawa and A. Nishida, Adv. Synth. Catal. 348, 1063 (2006).

[2] N. Nishiwaki, T. Konishi, and S. Tsukamoto, "*Development of Practically Usable & Green Chemical Catalyst Supported on S-terminated GaN (0001)*", 36th Conference on the Physics and Chemistry of Semiconductor Interfaces (PCSI-36), Jan.11-15, 2009, Santa Barbara, California, USA.

[3] G. Kresse and J. Hafner, Phys. Rev. B 47, RC558 (1993).

Growth of InAs/GaAs quantum dots on germanium-on-insulator substrate by MOCVD for Silicon photonics

D. Bordel[1,2], M. Rajesh[1], D. Guimard[1], M. Nishioka[1], E. Augendre[3], L. Clavelier[3] and Y. Arakawa[1,2]

[1]Institute for Nano Quantum Information Electronics (INQIE), [2] LIMMS/CNRS-IIS, The University of Tokyo, IIS, 4-6-1 Komaba, Meguro-ku, Tokyo 153-8505, Japan

[3]CEA-LETI-Minatec, F38054 Grenoble, France

Keywords: Quantum dots, Laser, GeOI

New materials and architectures should be found in order to overcome the Si bottleneck. Because of the better transport properties of germanium, and the "on-insulator" advantages, germanium-on-insulator (GeOI) is considered as a future platform for CMOS components. Recently, MOSFET fabrication was reported on GeOI substrate [1]. Additionally, since GaAs is almost lattice-matched to Ge, GeOI becomes also an attractive platform for the integration of CMOS and GaAs-based optoelectronic devices. However, no optical source emitter has been reported on GeOI substrate yet.

Here, we report the growth of self-assembled InAs quantum dots (QDs) on GeOI substrate, grown by antimony-mediated metal organic chemical vapour deposition (MOCVD). InAs/Sb:GaAs QDs have allowed the realization of ground-state lasing at 1.3 μm with high modal gain by MOCVD [2].

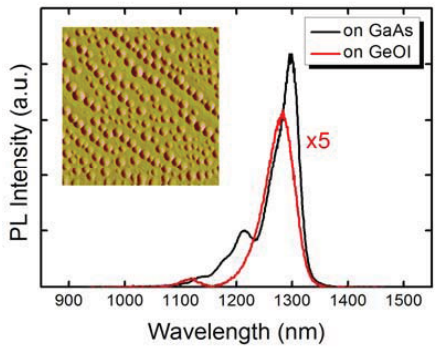

Fig.1 RT PL spectra of InAs/Sb:GaAs QD samples grown on GeOI and GaAs substrate. The inset shows the 1 × 1 μm^2 AFM image of the corresponding QDs on GeOI.

The GeOI substrates consist of a Ge (6 degree off-cut) thin layer, transfered by wafer bonding on silicon substrate (Smart-cut technology, LETI/Soitec). The QDs were grown on a 500 nm-thick GaAs buffer layer, with a nucleation layer grown at low temperature in order to minimize the antiphase domain formation. These QDs yield a density of 3 × 10^{10} cm^{-2} and emission in the 1.3 μm band at room temperature. The PL intensity of the InAs/Sb:GaAs grown on GeOI is ~5 times lower compared to that of high-emission efficiency reference InAs/Sb:GaAs, grown on conventional GaAs substrate. However, the PL intensity is ~5 times higher than that of QDs grown on silicon substrate, and recently reported by our group [3]. This finding suggests the better suitability of GeOI compared to bare silicon substrates for the growth of high-structural quality GaAs layers, and subsequent QD layers. These results are a first step towards the fabrication of QD lasers on GeOI substrate in the telecommunication band of 1.3 μm.

References

1. C. Le Royer *et al.*, Solid State Electron. 52, 1285 (2008).
2. D. Guimard *et al.*, Appl. Phys. Lett. 90, 241 (2007).
3. L. Lin *et al.*, Appl. Phys. Lett. 92, 263105 (2008).

Fine control of super low-density InAs quantum dots by intermittent growth using MBE

S. Sekiguchi, P. Patchakapat and K. Yamaguchi

Department of Electronic Engineering, The University of Electro-Communications,
1-5-1 Chofugaoka,Chofu,Tokyo 182-8585,Japan

Keywords: quantum dot, molecular beam epitaxy, InAs, intermittent growth.

Recent progress in growth technique of semiconductor quantum dots (QDs) allows various challenging applications. In particular, high-density QDs have been demonstrated by some unique techniques. However, control of low-density QDs has not been developed yet. The low-density control is one of important techniques for quantum information processing and communication devices based on the single QD structure. In conventional Stranski-Krastanov (SK) growth, abrupt transition of 2D-3D growth mode is not desirable for control of low-density QDs. Recently, we have been trying to fabricate super low-density InAs QDs by intermittent supplying and annealing method [1]. In this conference, we present a fine control method of super low-density InAs QDs (10^7 cm^{-2}) by intermittent growth (IMG) technique using molecular beam epitaxy (MBE) and reflection high-energy electron-beam diffraction (RHEED) equipments.

In this study, the InAs was grown on the GaAs(001) layer at 500℃ by MBE. Following the InAs growth of 1.0-1.5 monolayer (ML), the indium flux was intermittently supplied under As ambience. IMG of 0.3-ML InAs was repeated until RHEED observation of first initial 3D islanding. For After each IMG of 0.3-ML InAs, the sample was annealed for 2 (or 3) min.the InAs growth rate of 0.027 ML/s, initial 3D islands were formed at approximately 8 cycle number of IMG. At the initial 3D islanding, RHEED intensity of (004) diffraction beam increases slightly during the In supply and then is maintained during the annealing, as shown in Fig. 1. Figure 2 shows an atomic force microscopy (AFM) image of super low-density InAs QDs (5×10^7 cm^{-2}) grown by IMG with total cycle number of 10. Figure 3 shows QD density as a function of cycle number in IMG after initial 3D islanding. QD density monotonically increases with increasing the cycle number. It is found that one cycle IMG provides super low-density InAs-QDs with 1-2.5 $\times$ 10^7 cm^{-2}. Therefore, QD density can be controlled precisely by IMG cycle number after the initial 3D islanding. The presented IMG method is promising way for control super low-density QDs.

References

1. P. Patchakapat et al, ISCS 2007 TuC P7.

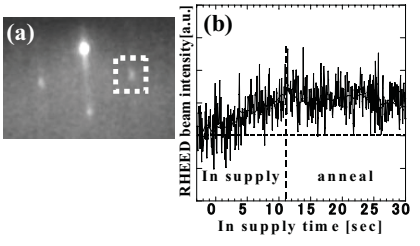

Fig.1 RHEED pattern(a), RHEED intensity of (004) diffraction beam as a function of In supplying and annealing time (b).

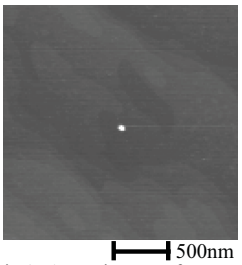

Fig.2 AFM image of super low-density InAs QDs grown by IMG.

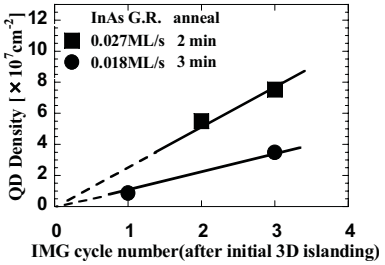

Fig.3 QD density vs. IMG cycle number after initial 3D islanding.

Parametric growth of InAlSb meta-morphic buffer layers on GaAs for the application to InSb-based electronic devices

S. H. Shin*,**, J. D. Song*, S. Y. Kim*, H. J. Kim*, J. Y. Chang*, S. H. Han*, T.G, Kim**

* *Nano Science Research Division, Korea institute of Science and Technology, Seoul 136-79, Korea*

** *School of Electrical Engineering, Korea University, Seoul 136-701, Korea*

Keywords: InSb, 2DEG, meta-morphic, GaAs

It has been one of main issues in the commercial and military electronic circuit applications to reduce power consumption and to increase operating speed. In fact, these two issues are in the relation of trade-off with conventional semiconductor materials, and achieving two targets at once had been considered as something beyond ability before 2DEGs using Sb-based semiconductor was introduced [1]. Especially, In(Ga)Sb 2DEGs are the most promising in the view of mobility and low-power consumption (up to ~ 40,000 cm^2/Vs @ 300K;see the section 2.9 of ref [1]) The striking characteristic of this In(Ga)Sb 2DEGs is the possibility to fabricate high-speed p-typed hole-driven 2DEGs [2]. This implies that we can imagine something CMOS-like low-power logic devices with III-V semiconductors with high-speed. As a result, this 2DEG structure has been chosen as one of candidates for next-Si [3].

To achieve high-quality InSb 2DEGs, the first hurdle to jump is the manipulation of strain between InSb and the wafers, because lattice constant of InSb is ~0.65 nm and those of conventional wafers such as GaAs and InP are ~0.56 and ~0.59 nm. Consequently, meta-morphic technology should be introduced during growth of buffers to overcome lattice mismatch and to produce flat surfaces for InSb 2DEGs on conventional wafers such as GaAs.

In this presentation, we report the parametrical approaches to grow flat $In_{0.64}Al_{0.36}Sb$ surface on GaAs, because $In_{0.64}Al_{0.36}Sb$ will be used as buffer and barriers for the 2DEGs. Using RMS roughness measured by AFM, we optimized growth temperature of the InAlSb buffer layers. Various modifications of InAlSb buffer layers were introduced. Finally, we succeeded in growing ~100 nm-thick InSb layers capped by $In_{0.64}Al_{0.36}Sb$ and grown on InAlSb meta-morphic buffer/GaAs wafer. This shows the mobility of ~ 40,000 cm^2/Vs at room-temperature. InSb-2DEG like structure was also grown on meta-morphic buffer/GaAs wafer, although the mobility of this structure is relatively low as ~ 13,000 cm^2/Vs at room-temperature. These results are good to fabricate InSb-based FET devices, however, there are many rooms to be enhanced.

Details of relationship between structural and electrical properties of these structures will be discussed in the presentation. This work is supported by KIST institutional research project of SPINTRONICS.

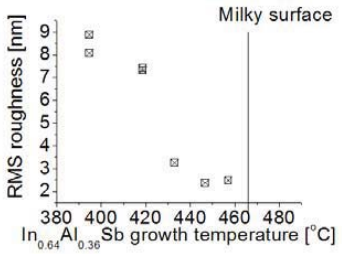

Fig.1 Effect of growth temperature of $In_{0.64}Al_{0.36}Sb$ on the RMS roughness

References

1. B. R. Bennett, et al., Solid-State Electronics **49**, 1875 (2005).

2. J. B. Boos, et al., IEICE Trans. Electron. **E91-C**, 1050 (2008).

3. R. F. Service, Science **323**, 1000 (2009).

Dislocation-filtering AlInSb interlayers for InSb quantum wells

T. D. Mishima, M. Edrisooriya and M. B. Santos
Homer L. Dodge Department of Physics and Astronomy, and
Center for Semiconductor Physics in Nanostructures
University of Oklahoma, Norman, OK, USA

Keywords: Dislocations, InSb, Quantum wells, Transmission electron microscopy

Among all the binary III-V semiconductors, InSb has the highest electron mobility and the narrowest band-gap. Magnetic-field sensors [1,2] and light-emitting diodes [3] are representatives of the devices based on InSb quantum wells (QWs) that exploit these material properties. Recent research on InSb QW field-effect transistors has attracted attention because of an improved switching speed and power consumption that outperforms transistors made of other semiconductors [4]. GaAs (001) and Si (001) substrates are usually used for InSb QW-based devices. However, such InSb QWs tend to suffer from a high density of structural defects, since GaAs and Si have large lattice mismatches of 14.6% and 19.3%, respectively, with respect to InSb [4,5]. For both types of InSb QWs, AlInSb is usually the material of choice for buffer and barrier layers [1-5]. Therefore, defect filtering in AlInSb layers is of great importance.

In this study, we report further investigations on AlInSb interlayers that are effective in reducing the density of threading dislocations (TDs) in InSb QWs [5]. Samples with a total of 1.5 µm of AlInSb were grown on on-axis GaAs (001) substrates by molecular beam epitaxy. The AlInSb layer consists of, in the order of growth, two periods of a 0.3µm-thick $Al_{0.1}In_{0.9}Sb$ parent layer and a 0.2µm-thick $Al_xIn_{1-x}Sb$ interlayer [5], followed by a 0.5µm-thick $Al_{0.1}In_{0.9}Sb$ parent layer. Four types of buffer layer structures, which differ in Al content from x = 0.15 to 0.3 with an increment of 0.05, were prepared.

Fig. 1(a) depicts a cross-sectional transmission electron microscopy (TEM) image of a sample with an Al content difference of 15% between the parent layers and interlayers, $\Delta x = (x–0.1)\times100\%$. TDs appear as line contrasts under the bright field image condition with g = 220 that was used to capture the image. It is clear that many TDs are bent at the interfaces between the parent layers and interlayers, leading to a decrease in TD density in the upper layers. Fig. 1(b) shows TD densities around the topmost surfaces of samples grown with different Δx, analyzed by plan-view TEM. At Δx = 15%, the minimum TD density of 4.4×10^8 /cm^2 was obtained, one of the lowest values reported for AlInSb layers [5]. In addition to further discussion of the data, we will report TEM techniques that were developed to evaluate structural defects in zinc-blende structures. This work was supported by the NSF under Grants Nos. DMR-0520550 and DMR-0808086.

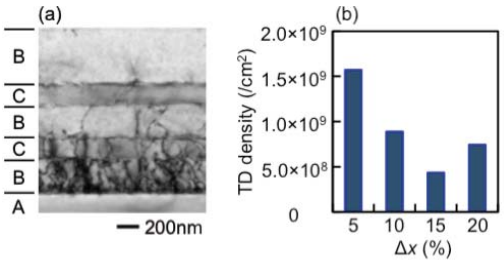

Fig.1 a) Cross-sectional TEM image of a sample with Al content difference of Δx = 15%. The constituent layers are A: GaAs (001) substrate, B: $Al_{0.10}In_{0.90}Sb$ parent layer, and C: $Al_{0.25}In_{0.75}Sb$ interlayer. b) TD densities around the topmost surfaces of the samples with different Δx.

References

1. A. Oral *et al.*, IEEE Trans. Magn. **38**, 2438 (2002).
2. S.A. Solin *et al.*, Appl. Phys. Lett. **80**, 4012 (2002).
3. B.I. Mirza *et al.*, Appl. Phys. Lett. **89**, 131110 (2006).
4. S. Datta *et al.*, Proc. IEEE IEDM (2005) 763.
5. T.D. Mishima *et al.*, Appl. Phys. Lett. **88**, 191908 (2006): Appl. Phys. Lett. **91**, 062106 (2007).

Photoluminescence properties of Er-doped β–$FeSi_2$ grown by ion beam synthesis methods

Y. Terai, T. Tsuji, K. Noda, and Y. Fujiwara

Division of Materials and Manufacturing Engineering, Graduate School of Engineering, Osaka University, Osaka, Japan

Keywords: Rare-earth doped semiconductor, iron disilicide

Semiconducting β-$FeSi_2$ has attracted much interest as silicon-based optoelectronics materials. β-$FeSi_2$ shows photoluminescence (PL) at 1.54 μm, which is a wavelength for fiber optics communications. For the application, advanced techniques for intense emission of β-$FeSi_2$ are necessary. The impurity-doping which acts as luminescent centers is considered to be effective to improve the PL intensity, but there are few reports on the luminescent centers in β-$FeSi_2$. In this study, we have fabricated Er-doped β-$FeSi_2$ (β-$FeSi_2$:Er) and investigated the 1.54 μm-PL originating from Er^{3+}.

β-$FeSi_2$:Er samples were prepared by an ion beam synthesis (IBS) methods. After the implantation of $^{56}Fe^+$ (100keV, 5×10^{16} cm^{-2}) into Si(100) substrates, $^{166}Er^+$ (200keV, 1×10^{16} cm^{-2}) was implanted into the substrates. After the implantations, the substrates were annealed at 600-800ºC for 0.5-8 h by a rapid thermal annealing in order to form β–$FeSi_2$ and remove implantation damages. For the comparison, undoped β-$FeSi_2$ and Er-doped Si (Si:Er) samples were prepared by IBS methods.

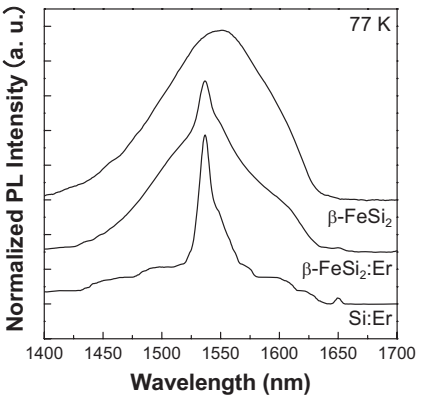

Fig.1 PL spectra from Er-doped β-$FeSi_2$, Er-doped Si and undoped β-$FeSi_2$.

Figure 1 shows PL spectra from β-$FeSi_2$:Er, Si:Er and undoped β-$FeSi_2$ at 77 K. The Si:Er shows a sharp PL at 1.54 μm due to $^4I_{13/2}$–$^4I_{15/2}$ transition of Er^{3+}. In contrast, undoped β–$FeSi_2$ shows a broad PL originating from interband transition in β–$FeSi_2$. In β-$FeSi_2$:Er, a characteristic PL in which both PLs were superimposed was observed. The result revealed that the interband transition of β–$FeSi_2$ and the 4f shell transition of Er^{3+} took place simultaneously. In order to investigate an energy transfer from β–$FeSi_2$ to Er^{3+}, we have measured a lifetime (τ) of Er^{3+} emission and an Er^{3+} optical excitation cross section (σ) which represents an efficiency of the energy-transfer from semiconductor host to Er^{3+} at 77 K. β-$FeSi_2$:Er and Si:Er showed almost the same σ of $\sigma = 9\times10^{-16}$ cm^2 (β-$FeSi_2$:Er) and $\sigma = 1\times10^{-15}$ cm^2 (Si:Er), respectively. The large value of σ indicates that the multiphonon-assisted energy transfer [1] between Er 4f shell and semiconductor host is accomplished in β-$FeSi_2$:Er as well as Si:Er. In the lifetime of Er^{3+} emissions, β-$FeSi_2$:Er showed the faster lifetime ($\tau = 0.98$ ms) than Si:Er ($\tau = 1.2$ ms), The fast lifetime suggests an efficient energy transfer in β-$FeSi_2$:Er. Detailed energy transfer model in β-$FeSi_2$:Er will be discussed based on the temperature dependence of PL intensity and lifetime.

References

1. A. Taguchi, K. Takahei and Y. Horikoshi, J. Appl. Phys. **76**, 7288 (1994).

Luminescence properties of Eu-doped ZnO films grown by sputtering-assisted metalorganic chemical vapor deposition

Y. Terai, K. Yamaoka, K. Yoshida, A. Yoshida and Y. Fujiwara

Division of Materials and Manufacturing Engineering, Graduate School of Engineering, Osaka University, Osaka, Japan

Keywords: Rare-earth doped semiconductor, ZnO, MOCVD

ZnO thin films with wide band-gap (~3.37 eV) have a potential as a host material for rare-earth (RE) doped semiconductor to obtain visible luminescence. The RE-doped ZnO is a candidate for an active layer in electroluminescence devices. Recently, we have developed a sputtering-assisted metalorganic chemical vapor deposition (MOCVD) system for the growth of RE-doped ZnO [1]. In the system, RE atoms could be easily doped by the RF sputtering of RE-oxide targets during the MOCVD growth of ZnO. In this study, we have grown Eu-doped ZnO (ZnO:Eu) thin films by the sputtering-assisted MOCVD because Eu^{3+} is the prospective dopant for red luminescence near 610 nm due to the intra-4f shell transition of $^5D_0$–^7F_J (J = 0–3) in Eu^{3+}.

In the growth of ZnO:Eu, ZnO host was grown by MOCVD using diethylzinc (DEZ) and O_2 at 760 °C. Eu ions were doped by RF magnetron sputtering of Eu_2O_3 target set up in the upper part of *c*-plane sapphire substrates. The Eu concentration was controlled by RF power (0-40 W) in the range of 0-5%. The film thickness was 750 nm.

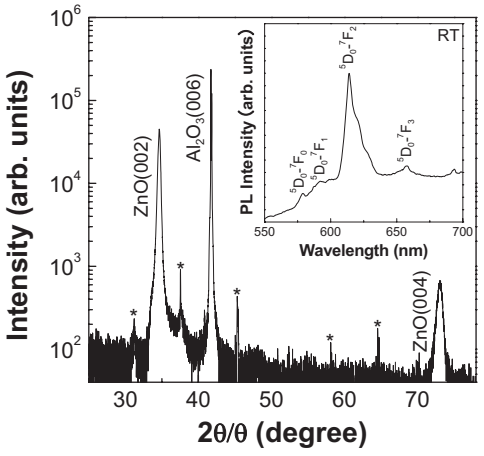

Fig.1 XRD pattern of Eu-doped ZnO. The inset shows room-temperature PL spectra from Eu-doped ZnO.

Figure 1 shows XRD pattern of the ZnO:Eu (Eu~1%) film. The film showed only ZnO (002) and (004) peaks. The *c*-axis oriented wurtzite structure was confirmed in ZnO:Eu films up to Eu~5%. In the dependence of ZnO(002) peak on Eu concentration, the peak position of ZnO(002) shifted to lower diffraction angle with increase of Eu concentration, indicating that Eu atoms substitute Zn sites. The inset of Fig. 1 shows photoluminescence (PL) spectra of ZnO:Eu (Eu~1%) under the 266 nm (4.66 eV)-excitation above the band-gap energy of ZnO at room temperature. In the PL spectra, two characteristic emissions were observed. The broad emission ranging 550-700 nm was assigned to defect-related luminescence such as Zn vacancies (V_{Zn}) or oxygen interstitials (O_i) in ZnO. On the other hand, the sharp emission at 610 nm originated from $^5D_0$–$^7F_2$ transition of Eu^{3+}. The sharp emission was observed only when the excitation energy was larger than the band-gap energy of ZnO. In time-resolved PL measurements under the 266 nm-excitation at 80 K, the 610 nm-emission showed a long decay time of ~300 μs. These results revealed that an energy transfer from ZnO host to Eu^{3+} is accomplished in ZnO:Eu.

References

1. K. Yamaoka, Y. Terai, T. Yamaguchi, and Y. Fujiwara, Phys. Status Solidi (c), **5**, 3125 (2008).

Fabrication of Metal/Quantum-Dot/Semiconductor (MDS) structure on silicon substrate

Naokatsu Yamamoto and Kouichi Akahane

* National Institute of Information and Communications Technology

4-2-1 Nukui-Kitamachi, Koganei, Tokyo 184-8795, Japan

Keywords: Quantum dot, Silicon photonics, Light emitting device, and Metal oxide semiconductor

Photonic devices on a silicon substrate have been investigated attractively in a worldwide as a silicon-photonics technology. Novel materials and device structures have also proposed to achieve the light-emitters on silicon substrate [1]. In this paper, we propose a simple structure of a metal/quantum dot /semiconductor (MDS) structure on silicon substrate, which will be used in the silicon photonics technology.

We have focused on the fabrication of a compound semiconductor quantum dot (QD) on Si for creating novel attractive devices [2]. InGaSb QDs were formed on the n-type Si (001) surface at 400 ˚C by solid source molecular beam epitaxy. The Si surface was prepared by a chemically etching of a hydroflolide acid solution and a thermal-cleaning process at approx. 950 ˚C before the QDs formation. Figure 1 shows an atomic-force microscope image of a 1.5 mono-layer (ML) InGaSb QD structure on Si surface. A dot-density and an average height were estimated with a 2.5 x 10^{10} /cm^2 and 8.8 nm, respectively. A formation mechanism of the QD structure may be based on a Volmer-Weber (VM) mode, since a drastically transition from streaky to spotty RHEED patterns was observed under the sub-ML growth. After the growing the QD structure, a 250 nm thick gold-film was deposited on to the QDs surface

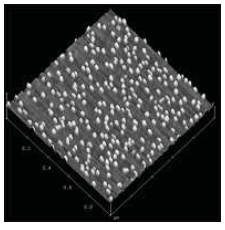

Figure 1 Atomic force microscope image of Sb-based QD on Silicon. (1μm^2)

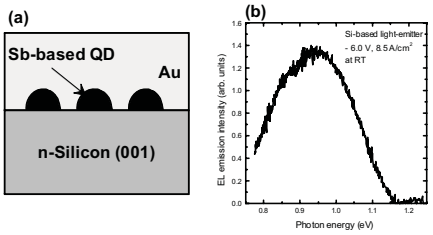

Figure 2 (a) MDS structure on Si substrate and (b) infrared light emission form MDS structure.

to fabricate a MDS structure shown in Fig. 2(a).

It is found that an infrared light emission is observed from this MDS structure under a current injection. Figure 2(b) shows an electroluminescence spectrum from the MDS structure applied – 6.0 V (the metal-side is as positive.) and 8.5 A/cm^2 at RT. We successfully demonstrated the infrared emission around 0.95 eV (1.3 μm) as the optical-communication waveband. The EL spectrum has a wideband emission characteristic as 270 meV (FWHM). It is considered that the simple MDS structure can be used for the light emitter fabricated on Si wafer. This emission may be caused from a type-II interface between the Sb-based QDs and Si surface. However, a more detailed study of the emission mechanism is needed to clarify an origin of emissions.

We believe that this MDS structure as a simple and CMOS compatible structure will enable us to achieve the attractive optoelectronic devices for the communication between a chip-to-fiber, chip-to-chip, and gate-to-gate on the Si substrate.

[1] M. Jo et.al. Physica E **21** (2004) 354

[2] N. Yamamoto et.al. Jpn. J. Appl. Phys. **46** (2007) 2401

A hierarchical investigation of ultra-large-scale and *ab initio* electronic structure calculations – Silicon cleavage process and resultant stepped surface –

T. Hoshi*,**, M. Tanikawa* and A. Ishii*,**
*Department of Applied Mathematics and Physics, Tottori University, Tottori, Japan
** Core Research for Evolutional Science and Technology, Japan Science and Technology Agency, Saitama, Japan

Keywords: order- theory, *ab initio* calculation, stepped Si (111)-2 × 1 surface, bias-dependent STM image

Hierarchical investigation was realized by ultra-large-scale and *ab initio* electronic structure theories and was applied to cleavage process of silicon and resultant stepped surface with predicted bias-dependent STM images.

The large-scale calculation methods were constructed with $10^3 - 10^7$ atoms. In several methods, the computational time is 'order- ' or linearly proportional to system size. Application studies were carried out with tight-binding form Hamiltonians. [1-4] Now the program code has the name of 'ELSES' (=Extra-Large-Scale Electronic Structure calculation). See the web pages [5] for the complete reference list. High-accuracy calculations of smaller systems were carried out by the standard *ab initio* molecular dynamics simulation with density functional theory and plane-wave bases.

This paper focuses on cleavage process of silicon crystal and the predicted step structure that appears on the cleaved surface. (i) Direct simulation of cleavage process was realized by large-scale calculation with the generalized-Wannier-states theory (Fig. 1 (a)). [1] As results, a stepped (111)-2 × 1 surface is predicted, which is not yet confirmed experimentally. (ii) Large-scale calculation method of the Green's function [2] was applied to the resultant stepped surface and a bias-dependent STM image was concluded. (iii) A selected region near the step edge of the stepped surface was investigated by the *ab initio* calculation (Fig. 1 (b)). which gives two (meta)stable structures for the step edge structure with different bias-dependent STM images (One of them is shown in Fig. 1 (c)). Moreover the same step edge structures were predicted also for germanium surface.

The present research demonstrates the hierarchical investigation as a promising theoretical approach for nano-material process, which covers different length scales.

[1] T. Hoshi, Y. Iguchi and T. Fujiwara, Phys. Rev. B**72**, 075323 (2005).
[2] R. Takayama, T. Hoshi, T. Sogabe, S-L. Zhang and T. Fujiwara, Phys. Rev. B**73**, 165108 (2006).
[3] Y. Iguchi, T. Hoshi and T. Fujiwara, Phys. Rev. Lett. **99**, 125507 (2007).
[4] T. Hoshi and T. Fujiwara,
Preprint (http://arxiv.org/abs/0903.1819)
[5] http://www.damp.tottori-u.ac.jp/%7Ehoshi/elses/;
http://www.elses.jp/

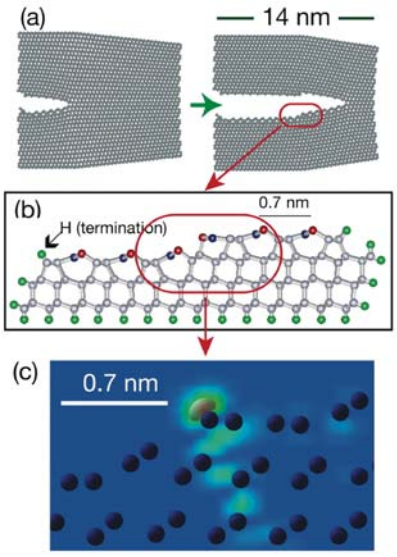

Figure 1: An example of the hierarchical investigation in electronic structure theory among different length scales. (a) Ultra-large-scale calculation of silicon cleavage process. [1] The resultant surface contains a stepped (111)-2 × 1 surface. (b) *Ab initio* calculations of the stepped (111)-2 × 1 surface with the hydrogen termination. (c) A step-edge wavefunction on the (111)-2 × 1 surface that gives a bias-dependent STM image.

Suppression of indefinite peaks in InAs/ GaAs quantum dot spectrum by low temperature Indium-flush method

N. Kumagai [a], S. Ohkouchi [a, b], S. Nakagawa [a, d], M. Nomura [a], Y. Ota [a, d], M. Shirane [a, b], Y. Igarashi [a, b], S. Yorozu [a, b], S. Iwamoto [a, c, d], and Y. Arakawa [a, c, d]

[a] *Institute for Nano Quantum Information Electronics (INQIE), Univ. of Tokyo, Tokyo, Japan*

[b] *NEC corp., Tsukuba, Japan,* [c] *Institute of Industrial Science (IIS), Univ. of Tokyo, Tokyo, Japan*

[d] *Research centre of advanced science and technology (RCAST), Univ. of Tokyo, Tokyo, Japan*

Keywords: InAs QDs, molecular beam epitaxy, low density, single dot spectroscopy, Indium-flush

Growth condition of QD itself and capping condition as overgrowth have been actively investigated, since tailoring optical properties of InAs quantum dots (QDs) is important. Although impact of capping condition to form a QD shape was reported recently by G. Costantini *et al* [1], relation between a shape of single QD and its optical property has been hardly studied experimentally as far as we know. Tailoring property of a single QD is significant for progress not only in quantum information but also in cavity quantum electrodynamics.

In this study, we have systematically investigated the effect of growth temperature of thin GaAs capping layer in Indium-flush (In-flush) process [2], on relation between a shape of QD and its optical property by micro photoluminescence (μ-PL) and atomic force microscopy (AFM). In-flush is a certain overgrowth technique to shorten emission-wavelength below 1μm where high-sensitive silicon photo-detectors are available.

InAs QDs were grown at 485 °C on GaAs buffer layers by molecular beam epitaxy. After QD growth, we performed the In-flush process. Thin GaAs capping layers of ~1.6 nm were grown at various temperatures from 435 to 485 °C. Then, InAs QDs were covered by 80 nm thick GaAs with the same condition for μ-PL measurement. For AFM observation, InAs QDs with 1nm thick GaAs cap were grown on the top layers with the same conditions as those for μ-PL measurement. After the growth of 1nm-thick GaAs capping layer, QDs changed their shape from isotropic to elongated one as the capping temperature increased. Accordingly, the PL spectrum changes. Figure 1 shows typical AFM images and μ-PL spectra at 10K corresponding for the samples fabricated by high- and low-temperature capping processes. In the case of the high temperature cap, the capped QD shape was elongated and flattened, and PL spectrum showed several peaks accompanied with broad and indefinite peaks. This broadening may be caused by proximity of states as quantum well due to thin and stretched deformation. On the other hand, the low temperature case, the shape was kept in isotropic and PL spectrum showed distinctive peaks without definite peaks. Probably, isotropic shape of QD brings electron to 3 dimensional well-confinement. These results indicate that low temperature capping is effective to keep an isotropic shape of QD and suppress indefinite peaks.

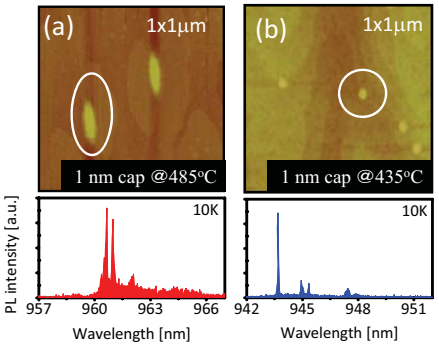

Fig.1 AFM images and μ-PL spectra of the grown samples. Thin GaAs capping layers were grown at (a) 485 °C and (b) 435°C. Excitation power density was 142 μW/cm^{-2} for PL measurements. Typical QD density of both samples was ~5x10^{8} cm^{-2}.

This work was accomplished by the Special Coordination Funds for Promoting Science and Technology.

References

[1] G. Costantini *et al*., Phys. Rev. Lett. **96**, 226106 (2006)

[2] Z. R. Wasilewski *et al*., J. of Cryst. Growth, **201/202**, 1131 (1999).

Polarization conversion of excitonic photoluminescence under zero and nonzero magnetic field in a single InAlAs quantum dot

T. Shindo, R. Kaji, S. Adachi, S. Muto
Department of Applied Physics, Hokkaido University, Sapporo, Japan

Keywords: quantum dot, optical alignment, optical orientation, InAlAs, fine structure

Investigation of spin-related phenomena in semiconductor nanostructures keeps a lot of attention, prompted both by the fundamental aspects of the role of electron spin in physical processes and by the possibility of making use of the spin of free carriers in electronic devices. Since, in such devices, the electronic (or the excitonic) spin state carries information, it is essential that the spin coherence remain intact as long as possible. Detailed knowledge of the spin properties of semiconductors is a necessary prerequisite for the study of spin-based effects on these structures. Furthermore, for spin-based applications used a few QDs, individual property of the QDs has to be investigated by the single QD spectroscopy.

In an ideal QD, the exciton eigenstates $_z = \pm 1$ are coupled to circularly polarized photons, but in actual QDs, some symmetry reduction such as in-plane deformation of the nanostructure as well as any other asymmetry of the localizing potential generally lifts the exciton degeneracy between two linearly polarized states $|\ \rangle$ and $|\ \rangle$, which are dipole active in the two perpendicular directions and by the fine structure splitting (FSS) $_b = \hbar\Omega_{\mathrm{exc.}}$. The localizing potential creates excitons with the preferential orientation of spins, while linearly polarized light produces excitons with the definite direction of the oscillating dipole moment. Conversion between optical orientation and optical alignment has been already demonstrated in ensemble QDs under zero [1] and nonzero magnetic field [2].

In this work, we investigated the polarization conversion of photoluminescence from a single InAlAs QD. The used QD sample has an $In_{0.75}Al_{0.25}As$ QD layer embedded in $Al_{0.3}Ga_{0.7}As$ barrier layers and was held at 5 K under zero and nonzero magnetic field in Faraday geometry. Figure shows the degree of linear polarization (DLP) of the PL under the circular excitation as a function of magnetic field for a QD with the FSS of 30 eV. The DLP has the maximum value and the behavior is different depending on the direction of the magnetic field. This can be explained by the spin precession around the external field and the effective in-plane field Ω_{exc} caused by the anisotropic exchange interaction. The calculated result (bottom panel) coincides with the experimentally obtained one, which indicates the ratio, exciton spin relaxation $_s$ / exciton lifetime $_r$, is 5∼6. The $_r$ was found to be 0.8 ns in this single QD by the measurement using a streak camera. Also, the similar measurements were done for many QDs with different FSS. As a result, QDs with smaller FSS indicated large conversion ratio and the dependence on FSS agreed well with the predicted one with the same model. This gives the valuable information to the applications such as a single photon source.

[1] G.V. Astakhov, T. Kiessling, A.V. Platonov et al., Phys. Rev. Lett. **96**, 027402 (2006).
[2] R. I. Dzhioev, B. P. Zakharchenya, E. L. Ivchenko et al., Phys. Solid State **40**, 790 (1998).

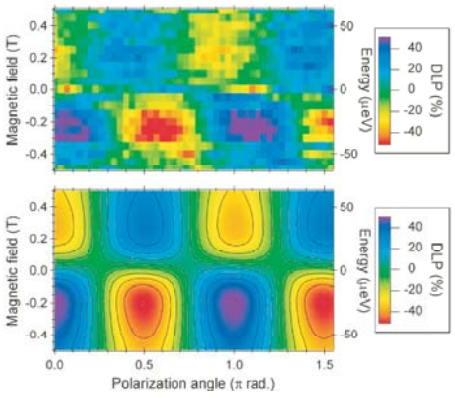

Figure 1: 2D-plot of DLP as functions of external field and polarizer angle under the circular excitation. The lower panel is a calculated result by the spin precession model using the following parameters: $_s = 5$ ns, $_r = 0\ 8$ ns, $_b = 30$ eV, $^{\mathrm{h}}_{\mathrm{z}} = 2\ 54$, and $^{\mathrm{e}}_{\mathrm{z}} = -0\ 37$. The latter four parameters are the values obtained by independent measurements.

Experimentally probing dephasing of zero dimensional exciton-polaritons

A. Laucht, N. Hauke, J. M. Villas-Bôas, F. Hofbauer, M. Kaniber,

G. Böhm, and J. J. Finley

Walter Schottky Institut, Technische Universität München, 85748 Garching, Germany

Keywords: Quantum dot, photonic crystal, strong coupling, dephasing

We present detailed investigations of electrically tunable single quantum dot - photonic crystal nanocavity systems operating in the strong coupling regime of the light matter interaction. Unlike previous studies, where the exciton-cavity spectral detuning was varied by changing the lattice temperature, or by the adsorption of inert gases at low temperatures, we employ the quantum confined Stark-effect to control the exciton-cavity detuning by varying a gate voltage [1]. Our devices allow us to systematically probe the photoluminescence spectrum of the strongly coupled system as a function of the level of incoherent excitation and lattice temperature, revealing new information about the dephasing of 0D exciton polaritons.

The samples investigated consist of a single layer of $In_{0.4}Ga_{0.6}As$ self-assembled quantum dots embedded at the center of a 180 nm thick p-i-n GaAs membrane. Patterning via electron beam lithography and reactive ion etching results in the formation of a photonic crystal slab with a L3 defect nanocavity. Metal contacts on the p- and n-doped GaAs layers provide electrical access, thus allowing us to tune the optical emission of a single exciton using the quantum confined Stark effect.

Optical measurements were performed using confocal microscopy at low temperatures in a helium flow cryostat. In photoluminescence experiments we observe a clear anti-crossing between exciton and mode emission (vacuum Rabi splitting ≈ 120 μeV) when tuning them into resonance, a signature for strong emitter-cavity interaction. When increasing the power of the incoherent optical excitation or the lattice temperature, the vacuum Rabi-splitting remains constant at first and then decreases until only a single broadened peak can be observed in the spectrum. We fit the data with a theoretical model based on work by Laussy et al. [2] and extended by a pure dephasing variable to better describe the experimental situation. The pumping, decay and dephasing rates extracted from simulations of our data enable us to clearly track the degradation of the strong coupling regime, illustrating how dephasing destroys the strong interaction for high pump powers or elevated temperature.

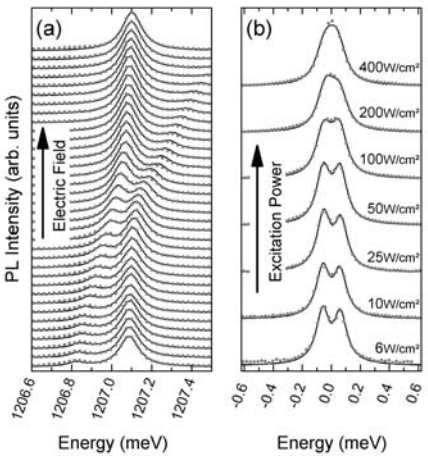

Fig.1 Photoluminescence spectra of the exciton-cavity system for various detunings via changing the electric field (a), and resonance spectra for different excitation power densities (b). The grey circles correspond to the experimental data, while black lines are fits to the theory.

We acknowledge financial support of the DFG via SFB 631 B3, and the German Excellence Initiative via NIM.

References

1. Laucht, A. et al. , NJP 11, 023034 (2009)
2. Laussy, F. P. et al. , PRL 101, 083601 (2008)

Growth and electrical characterizations of semiconducting nanowires

D. Lucot ,G. Faini , J.C. Harmand , D. Mailly, G. Patriarche

Laboratoire de Photonique et de Nanostructures, CNRS, Marcoussis

Keywords: Nanowires, VLS growth, high mobility transistor

Currently, there is intense interest in one-dimensional nanostructures, such as nanowires (NWs) and nanotube, in the search for potential candidates to replace CMOS technology. Studies on carbon nanotubes have demonstrated some potential for devices such as field effect transistors [1]. However, there are important limitations to nanotubes since specific growth of metallic or semiconducting tubes is not possible nowaday. Furthermore, controlled doping of semiconducting nanotubes is impossible, although it is potentially critical for devices applications. Semiconductor NWs, however, can overcome these limitations. They will remain semiconducting independent of diameter and, moreover, it is possible to take advantage of the vast knowledge from the semiconductor industry to dope them and control the surface states

We will present our work on the growth and the electrical characterization of III-V nanowires. Molecular Beam Epitaxy using gold dots as catalyst have been used to produce well diameter controlled InAs wires. After cutting the wires and dispersing them on an insulating substrate we have used electron beam lithography to attach electrical contact and place a gate on the top of a single wire .

We have performed device characterizations on these nanowires.

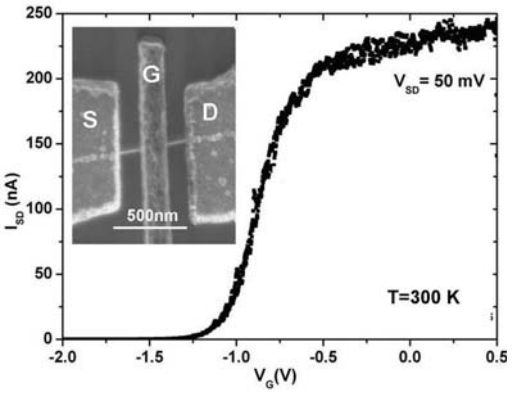

Fig.1 Transfert characteristic of a 15nm diameter InAs wire at a biais of 50mV for gate voltages varying from 0.5V to -2.0V at T=300K.

Figure 1 shows a typical transfert characteristics of a transistor made with a 15nm diameter InAs wire. The on/off current ratio is as high as 10^4 and the mobility reach 3000V/cm^{2}s.

Finally we will report on the first transport measurement at low temperature and high magnetic field of GaAs/GaAlAs core-shell nanowires [2] directly connected on the growth substrate.

References

[1] Tans, S. J.; Verschueren, A. R. M.; Dekker, C. Nature 1998, 393, 49.
[2] Patriarche, G.; Glas, F.; Tchernycheva, M.; Sartel, C.; Largeau L.; Harmand, J.C.; Cirlin, G.E. Nano letters 2008, 8, 1638.

Formation of InAs quantum dots at ultra-high growth rates

Kouichi Akahane, Naokatsu Yamamoto

* *National Institute of Information and Communications Technology, Tokyo, Japan*

Keywords: Quantum dot, molecular beam epitaxy

Remarkable progress has been made in the fabrication of semiconductor quantum dots (QDs) by using the self-assembly method, which is based on the Stranski–Krastanow (S-K) growth mode [1]. However, in the fabrication of very-high-performance optical devices, the problem of improving QD size uniformity still remains. QD size fluctuation is essentially inevitable in the self-assembly technique, and much effort has been devoted to reducing the fluctuation. For example, the self-size-limiting effect of QDs obtained with a low growth rate and low As flux has successfully been used to reduce size fluctuations, resulting in a narrow full-width half maximum (FWHM) of photoluminescence (PL) from QDs [2]. In such cases, the FWHMs of PL spectra have been reduced to less than 20 meV by optimizing the growth conditions. However, in the fabrication of QDs at a low growth rate, the growth of QD structures such as the active layer of semiconductor lasers is time-consuming. Further, the fabrication of QDs at a low growth rate sometimes accelerates the formation of large-size island structures (coalescent dots); this degrades the quality of QDs. Therefore, some efforts were made to prevent the coalescence of QDs [3]. To overcome the abovementioned problems, we investigated the growth of QDs at a high growth rate. This topic has not been studied, even though it is expected to solve the problem of long growth time and prevent the coalescence of QDs.

All the samples were fabricated on GaAs(001) substrates by molecular beam epitaxy. After a GaAs buffer layer was grown, a 2-ML InAs layer was grown to fabricate self-assembled QDs at 500 °C. We used various growth rates ranging from 0.04 ML/s to 1 ML/s to fabricate QDs. Then, a 50-nm-thick GaAs cap layer was grown. The post-growth surface morphology of the sample without the GaAs cap layer was observed using an atomic force microscope (AFM). Further, photoluminescence (PL) measurement was carried out at room temperature.

The insets in fig. 1 show the AFM surface images of InAs QDs grown at (a) 0.04 ML/s and (b) 1.0 ML/s (1 μm × 1 μm). The structures of the InAs QDs in both samples were observed. The lateral size (W), height (H), and density (N) of the QDs in the two samples were (a) W = 43.5 nm, H = 7.1 nm, and N = 3.6×10^{10} cm^2 and (b) W = 38.0 nm, H = 6.5 nm, and N = 2.4×10^{10} cm^2, respectively. Under these conditions, the fluctuations in the QD lateral size and height for sample (b) were smaller than those for sample (a).

Figure 2 shows the PL measured at room temperature. The spectra of the sample when QDs were grown at 0.04 ML/s and at 1.0 ML/s are shown in Figures 2(a) and 2(b), respectively. In both samples, emissions from the QDs were observed at around 1.0 eV. The FWHMs of the ground state emissions in the two spectra are (a) 26.4 meV and (b) 23.5 meV, respectively. The emission from QDs that were grown at a high growth rate also has a small FWHM. Therefore, high-quality QDs can be fabricated by using high as well as low growth rates.

References

1. L. Goldstein, F. Glas, J. Y. Marzin, M. N. Charasse, and G. Le Roux, Appl. Phys. Lett. **47** (1985) 1099
2. T. Kaizu, and K. Yamaguchi, Jpn. J. Appl. Phys. **40** (2001) 1885
3. N. Yamamoto, K. Akahane, H. Sotobayashi, and M. Tsuchiya, Proceedings. of the Opto-Electronics and Communications Conference 2008 TuH-3

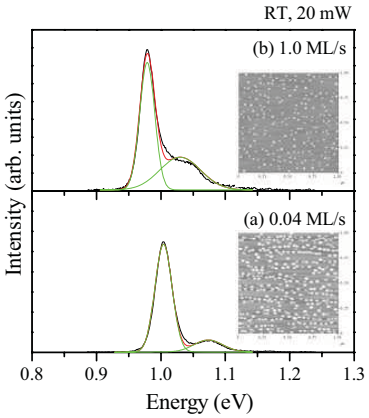

Fig.1 PL spectra of InAs QDs grown at (a) 0.04 ML/s and (b) 1.0 ML/s. Insets: AFM images of InAs QDs.

Photoluminescence properties of annealed and non-annealed InAs quantum dots

S. Hiratsuka*, Y. Mizoguchi*, S. Takeda*, S. Saravanan**, and N. Ohtani*

* *Department of Electronics, Doshisha University, Kyoto, Japan*

** *ATR Wave Engineering Laboratories, Kyoto, Japan*

Keywords: Quantum dots, photoluminescence, thermal annealing

Semiconductor lasers containing quantum dots (QDs) in the active regions are well known to be useful to realize very low threshold lasing. We have reported that the photoluminescence (PL) intensity of InAs QDs can be improved by thermal annealing [1]. In addition, the emission wavelength of the thermally annealed InAs QDs reveals a blue-shift. Thus, the thermal annealing is a powerful tool to improve the performance of QD-lasers. In this report, we discuss PL properties of annealed and non-annealed InAs QDs.

The samples studied contain stacked InAs QDs. In the following expression of (x, y), x denotes the number of the stacking layers, while y denotes the thickness of the spacer layer on the order of nm. Thus, the sample structures are A=(1, 0), B=(2, 10), C=(2, 20), D=(2, 30), E=(2, 40), and F=(6, 40), respectively. Fig. 1 shows PL spectra of these six samples. They were not annealed. It is clear that sample F reveals the maximum PL intensity because the density of QDs in sample F is also maximum due to the largest number of the stacking layer. However, the PL intensities of samples B, C, D, and E are different, although their densities of QDs are equal. The PL intensities of these four samples depend on the thickness of the spacer layer. In addition, the full width of the half maximum (FWHM) of the PL spectra of samples B and C reveal is larger than that of samples D and E. This means that the size of QDs in samples B and C is not uniform due to the thin spacer layers, leading to the weak PL intensities and large FWHM. The PL intensity of sample F is only 5 % stronger than that of sample E, although the density of QDs in sample F is three times larger than that of sample E. In addition, the FWHM of sample F is larger than that of sample E. These results indicate that with increasing the number of the stacking layers, the size of QDs becomes larger.

Next, we investigated the thermal annealing effect on PL properties of sample F. The annealing temperatures were varied from 700 to 1000 deg. The observed PL spectra were drastically changed by changing the annealing temperature. The PL peaking-wavelength of non-annealed sample is around 1200 nm. However, the peaking-wavelength is drastically blue-shifted with increasing annealing temperature. The strongest PL intensity is observed from the sample annealed at 875 deg. This PL intensity is more than seven fold compared with that of the non-annealed sample. We would like to report the details of the thermal annealing effect on PL properties of other samples at the conference.

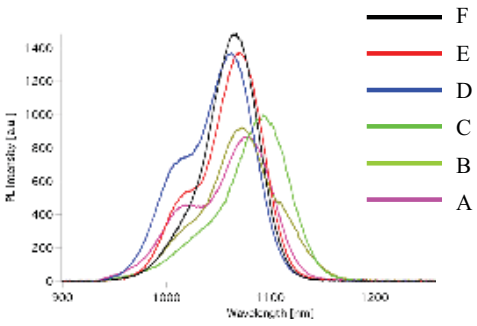

Fig.1 PL spectra of non-annealed InAs QDs.

References

1. S. Hiratsuka, et al., Phys. Stat. Sol. **6**, 189 (2009).

Magneto-photoluminescence spectroscopy of single InAs/AlAs quantum dots

D. Sarkar[1], H. P. van der Meulen[1], J. M. Calleja[1], J. M. Meyer[2], R. J. Haug[2] and K. Pierz[3]

[1]*Departamento de Física de Materiales, Universidad Autónoma de Madrid, E-28049 Madrid, Spain*

[2]*Institut für Festkörperphysik, Leibniz Universität Hannover, D-30167 Hannover, Germany*

[3]*Physikalisch-Technische Bundesanstalt Braunschweig, D-38116 Braunschweig, Germany*

Keywords: Quantum dots, InAs/AlAs, magneto-photoluminescence spectroscopy, strong localization

We present non-resonant, polarization-resolved magneto-photoluminescence (PL) measurements up to 12 T on single InAs/AlAs quantum dots (QDs). We observe (i) typical g-factors between 1 and 2, (ii) very low diamagnetic shifts due to strong exciton localization and (iii) low-energy sidebands, which are attributed to the piezoelectric exciton-acoustic phonon interaction. The sample is grown by MBE and consists of a single layer of self-assembled InAs QDs embedded in a 40-nm wide AlAs matrix.

Figure 1 shows circularly polarized micro-PL spectra for magnetic fields up to 12 T of two individual QD excitons. Spectra are vertically shifted for clarity. Gray and black curves show σ+ and σ- polarized spectra, respectively. We observe that:

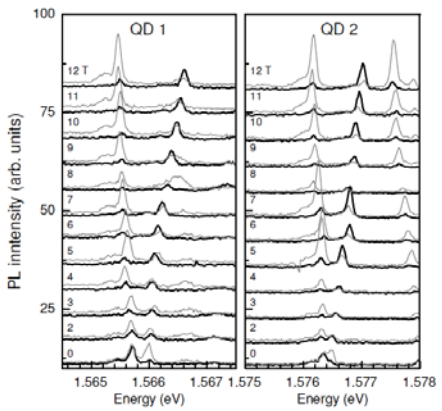

Fig.1 Left (black) and right (gray) polarized PL spectra of two individual exciton doublets QD1 and QD2 for a series of magnetic fields up to 12 T. Spectra are taken at 10 K.

(i) For increasing magnetic fields, the energy separation of zero-field split exciton doublets increases due to the Zeeman interaction. For high magnetic fields the splittings are linear and correspond to g-factors of 1.3 and 1.7, which are in the range of the values typically observed for self-assembled QDs.

(ii) The center of the Zeeman split doublet shifts quadratically to higher energies (diamagnetic shift). The diamagnetic coeffcient of our dots is γ_2 = 1.3 and 1.4 $\mu eV/T^2$. These values are well below those of InAs/GaAs QDs, as a consequence of the stronger localization of the exciton wavefunction due to the high AlAs barriers and also due to reduced intermixing [1].

(iii) The magneto-PL measurements reveal that the narrow sidebands observed 0.25 meV below the zero-phonon-lines (ZPLs) are not due to dark exciton emission: The separation between the ZPLs and their sidebands is fairly constant for magnetic fields up to 12 T. For dark exciton recombination, this can only occur in the unlikely case where either the electron or the hole g-factor is zero. Instead, these narrow low-energy sidebands are features of the ZPLs themselves and are attributed to the interaction of the QD exciton with acoustic phonons via the piezoelectric coupling mechanism [2].

References

1. D. Sarkar et al, Appl. Phys. Lett. **92,** 181909 (2008).
2. D. Sarkar et al, Phys. Rev. B **78,** 241305(R) (2008).

Control of tunnel coupling strength between InAs quantum dots and nanogap metallic electrodes through In-Ga intermixing

K. Shibata*, M. Jung*, K. M. Cha*, M. Sotome*, and K. Hirakawa*, **

* *IIS and INQIE, University of Tokyo, 4-6-1 Komaba, Meguro-ku, Tokyo 153-8505, Japan*

** *CREST-JST, 4-1-8 Honcho, Kawaguchi, Saitama 332-0012, Japan*

Keywords: Electron tunnelling, Quantum dot, InAs, Kondo effect

Transport properties of single quantum dots (QDs) have attracted much attention in the context of their application to quantum information processing. Recently, it was reported that self-assembled InAs QDs directly probed by nanogap Au electrodes operate as single electron transistors (SETs) [1], exhibiting clear shell filling [2] and the Kondo effect at very high temperatures (~80 K) [3]. For further novel functionalities such as gate-controlled superconducting proximity effects, the control of tunnel resistance is crucial. Although it was reported that the junction resistances of QD-SETs strongly depend on the size of the QDs [1], the origin of the observed strong QD-size dependence of the junction resistance has not been clarified yet.

In this work, we have systematically investigated the growth temperature (T_G)-dependence of the electronic states in single self-assembled InAs QDs coupled to nanogap electrodes. We compared the transport properties of QD-SETs for T_G = 470 °C and 500 °C. We have found that the orbital quantization energies and the pinch-off gate voltage of QDs strongly depend on T_G of the QDs and that the effective confinement size of electrons in QDs for T_G = 500 °C is smaller by ~15 nm than that for T_G = 470 °C, due to the intermixing between In and Ga atoms during QD formation; when T_G = 500 °C, a large composition gradient from GaAs to InAs is formed above the wetting layer and electrons are pushed toward the apex of the QDs, which makes the effective confinement size of electrons in QDs smaller than the metallurgical size, as schematically shown in the inset of Fig. 1.

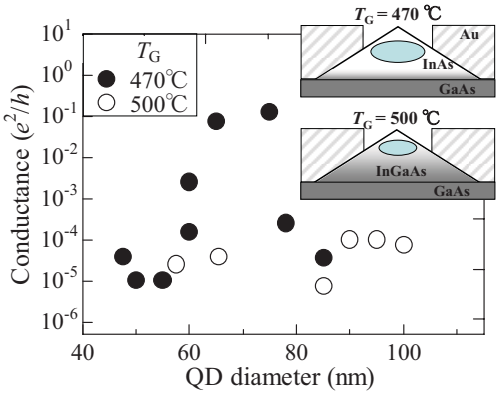

Fig. 1 The QD-diameter dependence of the conductance of the first Coulomb peak for T_G = 470 °C and 500 °C. The insets show schematic illustrations of the sample geometries and the electron wave functions.

Furthermore, since the tunnel junctions between QD and nanogap electrodes are formed near the bottom of the QDs (see the inset of Fig. 1), the tunnel resistance is strongly influenced by the degree of the intermixing in the QDs. In fact, most of the QD-SETs for T_G = 470 °C showed much higher conductance (in some cases, three orders of magnitudes) than those for T_G = 500 °C, as shown in Fig. 1. This implies that the transparency of the tunnel junctions is controllable over a very wide range by simply changing the growth temperature of QDs. Indeed, when QDs were grown at T_G = 470 °C, strong QD-electrodes coupling was realized and the Kondo effect up to 10 K was observed even in small QDs of ~ 45 nm in diameter.

References

1. M. Jung, et al., Appl. Phys. Lett. **86**, 033106 (2005).
2. M. Jung, et al., Appl. Phys. Lett. **87**, 203109 (2005).
3. K. Shibata et al., Appl. Phys. Lett. **93**, 062101 (2008).

Two-color quantum dot infrared photodetector using Fowler-Nordheim tunneling

W. Q. Ma*, X. J. Yang*, M. Chong*, T. Yang*, L. H. Chen*, J. Shao**, X. Lü**, W. Lu**, C. Y. Song***, and H. C. Liu***

* *Laboratory of Nano-Optoelectronics, Institute of Semiconductors, Chinese Academy of Sciences, P.O. Box 912, Beijing 100083, P. R. China*

** *National Laboratory for Infrared Physics, Shanghai Institute for Technical Physics, Chinese Academy of Sciences, Shanghai 200083, P. R. China*

*** Institute for Microstructural Sciences, National Research Council, Ottawa, Canada K1A 0R6

Keywords: Quantum dot, photodetector, Fowler-Nordheim tunneling, two-color

We report here an observation of Fowler-Nordheim (FN) tunneling [1] reflected in the photocurrent (PC) spectra of our InAs/GaAs quantum dot infrared photodetector (QDIP) device working under the normal incidence irradiation [2]. We find that the QDIP device is characteristic of two-color detection by only tuning the applied bias voltage. For a small positive bias, the PC spectrum shows a symmetric peak at 5.5 μm; with increasing the bias above 0.7 V, another peak at 7.0 μm appears while the peak at 5.5 μm reduces. The broad peak at 5.5 μm is photovoltaic arising from the intersubband transition of electron from the ground state of QDs to a high continuum state while the peak at 7.0 μm is photoconductive, which is attributed to the transition between the ground state of QDs and the wetting layer state. The FN tunneling is involved in this photoconductive transition since only at a large bias, can the absorbed electrons at the wetting layer state escape into continuum state contributing to a photocurrent. The FN tunneling is also evidenced that the photoconductive peak at 7.0 μm is asymmetric showing a broad feature on the higher energy side due to a decrease of the tunneling escape time of electron with increasing the photon energy. Our results indicate that bias tunable two-color QDIP can be realized by using FN tunneling mechanism.

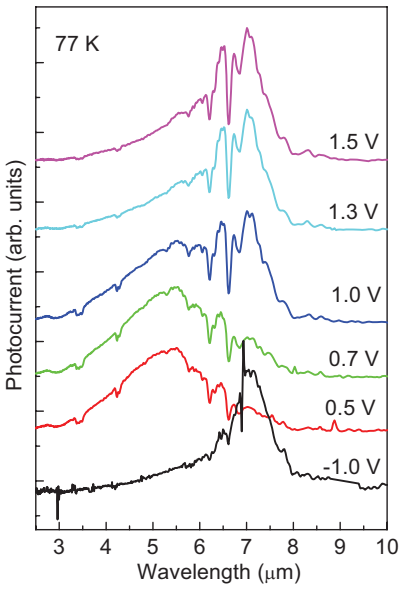

Fig.1 PC spectra of the QDIP at different bias voltages measured in the normal incidence geometry at 77 K.

References

1. R. H. Fowler and L. W. Nordheim, Proc. R. Soc. London, Ser. A. **119**, 173 (1928).

2. W. Q. Ma, X. J. Yang, M. Chong, T. Yang, L. H. Chen, J. Shao, X. Lü, W. Lu, C. Y. Song, and H. C. Liu, Appl. Phys. Lett. **93**, 013502 (2008).

MBE-VLS growth of a catalyst-free GaAs/AlGaAs core-multishell nanowire on (111)silicon substrate

J. H. Paek, T. Nishiwaki, M. Yamaguchi and N. Sawaki

Department of Electronics, Nagoya University, Furo-cho 3C-1, Chikusa-ku, Nagoya 464-8603, Japan

Keywords: GaAs nanowires, MBE-VLS, catalyst-free, heterostructure

Compound semiconductor nanowires (NWs) attract attention to be used in novel optoelectronic integrated devices. Vapour-Liquid-Solid (VLS) method is adopted to grow NWs using Au catalyst [1]. In this method, however, the metal contamination might deteriorate the electrical and optical characteristic of the NWs. In this respect, catalyst-free process is desirable [2]. Recently, we succeeded in the formation of GaAs/AlGaAs core-shell nanowires (CSNW) by growth interruption [3]. In this study, we have tried to make a GaAs single quantum well (SQW) in the AlGaAs shell layer of a GaAs/AlGaAs core-shell NW.

First, a GaAs NW was grown for 10min at 580°C on a (111)Si, followed by growth interruption for 5min under As flux. By the interruption, the Ga droplet on the tip of the NW was diminished by additional growth of GaAs on the top. Thus further growth of the NW by the VLS mode will not occur [3]. Then AlGaAs/GaAs/AlGaAs layers were grown on the wall of GaAs NW for 30 min/100 sec/30 min. The growth temperature of the GaAs and AlGaAs layers were 580°C and 620°C, respectively.

By scanning electron microscopy (SEM) observation, the length and the diameter of the NW were estimated to be ~ 4-5 μm and 300 nm, respectively. The shape of the NW was of hexagonal symmetry with {110} facets. Figure 1 shows typical cross-sectional reflected electron microscopy (REM) images of the samples. The diameter of the GaAs core (initial GaAs NW) is 60 nm. On the GaAs core, the AlGaAs shell (Fig.1(a)) or a GaAs SQW in the AlGaAs shell has been formed successfully. Figure 1(c) shows cathodeluminescence (CL) spectra of the samples at 4.2 K. The

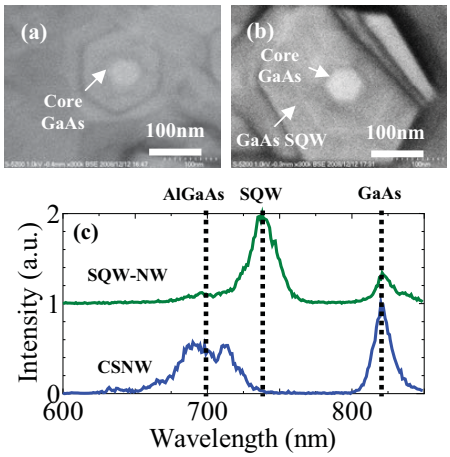

Fig.1 REM images of the cross section of (a) GaAs/AlGaAs CSNW (b) GaAs SQW in AlGaAs shell layer. (c) CL spectra of CSNW and SQW-NW.

peak at 821nm comes from the GaAs core. The Al composition of the AlGaAs shell layer was estimated to be 22% by the spectral peak due to AlGaAs layer. The emission at 738nm is attributed to the 2nm thick GaAs SQW. We found that the spectral peak for the SQW sits at 738nm through out the NW. This suggests that the uniform GaAs SQW layer has been achieved in the AlGaAs shell layer.

References

[1] S. G. Ihn, J. I. Song, Y. H. Kim, and J. Y. Lee, Appl. Phys. Lett. **89**, 053106 (2006)

[2] A. Fontcuberta i Morral, C. Colombo, and G. Abstreiter, Appl. Phys. Lett. **92**, 063112 (2008)

[3] J. H. Paek, T. Nishiwaki, M. Yamaguchi, and N. Sawaki, phys. stat. sol. (c) **6**, 2009 (in press)

Temperature dependent single photon emission in InP/GaInP quantum dots

A. K. Nowak*, E. Gallardo*, D. Sarkar*, D. Sanvitto*, H. P. van der Meulen*, J. M. Calleja*, J. M. Ripalda**, L. González**, and Y. González**

*Departamento de Física de Materiales, Universidad Autónoma de Madrid, E-28049 Madrid, Spain,

**Instituto de Microelectrónica de Madrid, Centro Nacional de Microelectrónica, Consejo Superior de Investigaciones Científicas, Isaac Newton 8, PTM Tres Cantos, E-28760 Madrid, Spain.

Keywords: quantum dot, dark exciton, single photon emitter

Intensity correlation measurements on single InP/GaInP quantum dots (QD) show antibunching at zero delay time, indicative of single photon emission. The antibunching time shows a thermally activated behaviour.

The samples have been grown by molecular beam epitaxy on GaAs (001) substrates. The growth sequence was 100 nm GaInP, 2ML GaAs, 2.2 ML InP, repeated twice. The second, uncapped layer of QDs was used for atomic force microscopy characterization. The QD average diameter and height before capping are 35 and 6 nm, respectively. The critical thickness for QD nucleation at 470ºC was 2 ML of InP at a growth rate 0.05 ML/s.

Hanbury-Brown-Twiss (HBT) measurements show a clear antibunching peak in the second order correlation function, given by:

$$g^{(2)}(\tau) = 1 - \beta \exp\left(-|\tau| / \tau_R\right) \qquad (1)$$

The antibunching time is constant (τ_R = 0.4 ns) at low temperature and rises above 30 K, as shown in Fig.1 (black dots). The same behaviour is observed in the exciton emission intensity I_X normalized to the sum of I_X and the biexciton emission intensity I_{XX} (open squares in Fig.1). This intensity increase has an activation energy of 43 meV close to the LO phonon energy of InP. A similar intensity trend has been attributed to a thermally activated dark – bright exciton (DX → BX) transition [1].

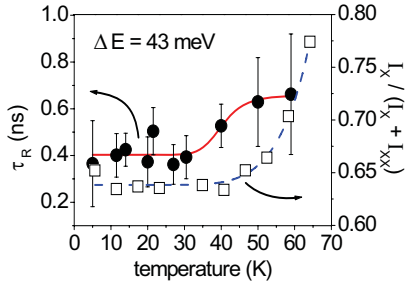

Fig.1 Left axis: antibunching rise time of an InP quantum dot as a function of temperature (●). Right axis: normalized μ-PL intensity I_X / (I_X+I_{XX}) vs. temperature (□). The lines are the corresponding fits.

The origin of the temperature dependent increase of τ_R is discussed in terms of thermally activated DX → BX transitions by LO phonons (solid line in Fig.1). Other possible mechanisms, as 1) thermal population of excited hole states [2] and 2) temperature dependent transition probabilities and state mixing in the QD are also discussed.

The present results are relevant for the use of single InP/GaInP QD as single photon emitters.

References

1. M. Reischle et al. Phys. Rev. Lett. **101**, 146402 (2008),

2. A. Malko et al. Phys. Rev.B **72**, 195332 (2005).

Quantum correlation spectroscopy of single quantum rings embedded in photonic crystal microcavities

E. Gallardo*, L.J. Martínez**, A.K. Nowak*, D. Sarkar*, D. Sanvitto*,
H.P. van der Meulen*, J.M Calleja*, I. Prieto**, A.R. Alija**, D. Granados**,
A.G. Taboada**, J.M. García**, P.A. Postigo**

**Departamento de Física de Materiales, Universidad Autónoma de Madrid, E-28049 Madrid, Spain*
***Instituto de Microelectrónica de Madrid, Centro Nacional de Microelectrónica, Consejo Superior de Investigaciones Científicas, Isaac Newton 8, PTM Tres Cantos, E-28760 Madrid, Spain*

Keywords: quantum ring, photonic crystal cavity, single photon emitter.

InAs/GaAs self-assembled quantum rings (QRs) are demonstrated to be single photon emitters by auto- and, for the first time, cross-correlation measurements based on a Hanbury-Brown and Twiss interferometer. The QRs have been fabricated by molecular beam epitaxy (MBE) [1]. Their average diameter and height are 30 and 3 nm respectively. The QRs are located in a photonic crystal microcavity of H1 *calzone* type [2]. This cavity displays two linearly counter-polarized cavity modes (CMs) with Q factor near 3000.

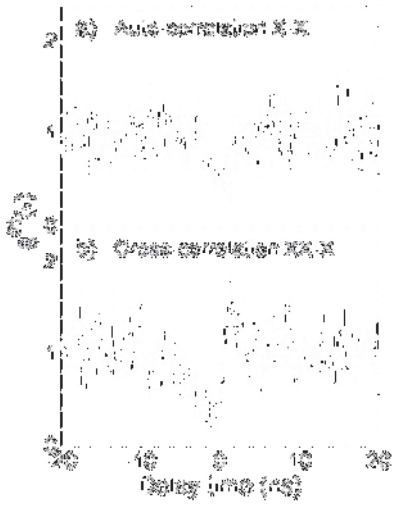

Fig.1 (a) Auto-correlation function of the X emission and (b) cross-correlation function between X and XX emissions of a single InAs/GaAs QR.

Second order auto- and cross-correlation functions of the exciton (X) and biexciton (XX) lines of a single QR are shown in figure 1. Clear antibunching is observed in X (Fig 1-a) and XX (not shown) auto-correlation spectra. The asymmetric shape of the XX-X cross-correlation (Fig 1-b) indicates sequential emission in the XX-X transition cascade.

We also present results on the QRs coupled to the microcavity. By tuning the QR exciton energy with temperature and the CM by thin-film condensation, no energy anti-crossing is observed, indicating weak coupling between QR and CM. A large intensity increase is observed in both X and CM emission lines when they are brought in resonance. They present the same linear polarization, even when their spectral detuning amounts several CM linewidths. This effect gives evidence of the remaining mode influence on the off-resonance QR emission [3].

These results are relevant for developing emitters of single photons and entangled photon pairs based on semiconductor QRs.

References

1. D. Granados et al, APL **82**, 2401 (2003).
2. K. Hennessy et al, APL **89**, 041118 (2006).
3. R. Oulton et al, Optics Express **15**, 17221 (2007).

Intentionally positioned self-assembled InAs quantum dots in an electroluminescent p-i-n-junction diode

M. Mehta*, D. Reuter**, A. Melnikov**, A. D. Wieck**, S. Michaelis de Vasconcellos*, T. Baumgarten*, A. Zrenner*, and C. Meier*

* *Physics Department, University of Paderborn, Paderborn, Germany*

** *Applied Solid State Physics, Ruhr-University of Bochum, Bochum, Germany*

Keywords: Quantum dots, molecular beam epitaxy, focused ion beam

Over the last years, self-assembled InAs quantum dots (QDs) have successfully been demonstrated as building blocks for novel nanooptoelectronic devices such as single photon sources or optical qubits [1]. However, for many applications a controlled positioning of the QDs in the device is necessary.

In this contribution, we present our approach for intentional positioning of optically active quantum dots using site-selective growth by a combination of molecular beam epitaxy (MBE) and focused ion beam (FIB) implantation in an all-ultra-high-vacuum (UHV) setup. A square array of periodic holes on GaAs substrate was fabricated with FIB of 30 keV Ga^+ ions followed by an *in-situ* annealing step. Subsequently, the patterned holes were overgrown with an optimized amount of InAs in order to achieve site-selective growth of the QDs on the patterned holes. Under well optimized conditions, a selectivity of *single* quantum dot growth in the patterned holes of 52% was achieved.

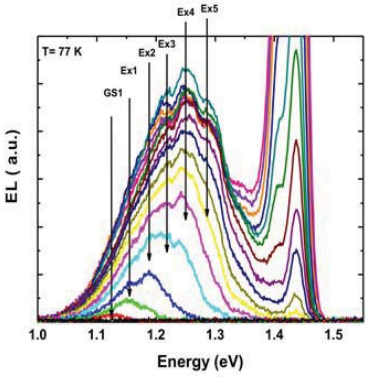

Fig.1 EL spectra from selectively positioned QDs in a p-i-n diode under different bias (from bottom to top: 1.0 V…..4.0 V).

Thereafter, carrier injection and subsequent radiative recombination from the positioned InAs/GaAs self-assembed QDs was investigated by embedding the QDs in the intrinsic part of a GaAs-based p-i-n junction device. In the I/V traces, rectifying behaviour is observed at room temperature as well as at low temperatures (LT). Photoluminescence characterization shows that in spite of the focused ion beam (FIB) implantation, the devices are still optically active.

Finally, we have studied the LT electroluminescence (EL) spectra to prove the performance of the QD based devices under electrical injection. We find that the investigated devices show significant EL. We can observe ground state recombination and up to five excited states from excitonic transitions in the QDs. EL down to the single quantum dot level was demonstrated. Thus, these results suggest a promising pathway for further devices based on single or pairs of coupled InAs QDs. Financial support by the BMBF via the NanoFutur grant 03X5509-NanoPhox and the NanoQuit program.

References

1. Z. Yuan, B. E. Kardynal, R. M. Stevenson, A. J. Shields, C. J. Lobo, K. Cooper, N. S. Beattie, D. A. Ritchie and M. Pepper, Science **295**, 102 (2002).

Γ-X crossover in InGaAs/GaAs quantum dots due to the indentation of a flat cylindrical nanoprobe

Lixia Xu*, Kazunari Ozasa**, H. Kakoi*, Y.H. Liang*, Yoshio Arai* and Wakako Araki*

* *Department of Mechanical Engineering, Saitama University, 255 Shimo-Ohkubo, Sakura-ku, Saitama 338-0825, Japan*

** *RIKEN (The Institute of Physical and Chemical Research), 2-1 Hirosawa, Wako, Saitama 351-0198, Japan*

Keywords: Γ-X crossover, PL quenching, nanoprobe indentation, finite element method

The optical properties of quantum dots (QDs) can be modified by the nano-scale strains. The low-temperature (10K) photoluminescence (PL) of self-assembled InGaAs/GaAs QDs was measured under the indentation of a flat cylindrical nanoprobe (500 or 600 nm in radius). With the increment of indentation force, the PL peak energy of single QDs was linearly blueshifted, while the intensity was firstly increased, then decreased and finally quenched. The observed quenching force, at which a PL peak disappears, shows a variation QD by QD as well as the blueshift rate (shift of PL peak energy per unit force).

In order to clarify the PL-quenching mechanism, a numerical simulation of the strain field induced by the lattice mismatch and indentation was carried out by a 3-dimensional finite element method (FEM). The modifications of the band structures of GaAs and InGaAs due to strains were then calculated based on the deformation potential theory. The diversely distributed strain fields related to the QD location from the probe centre [1] are responsible for the variations of blueshift rate and quenching force as observed in the experiments. The calculation of the band edge energies shows that the Γ conduction band (InGaAs) crossovers with the X or L band (InGaAs) around the probe edge due to the indentation-induced strains. We compared the experimental result to the simulated crossovers by determining the QD location according to the experimental blueshift rate.

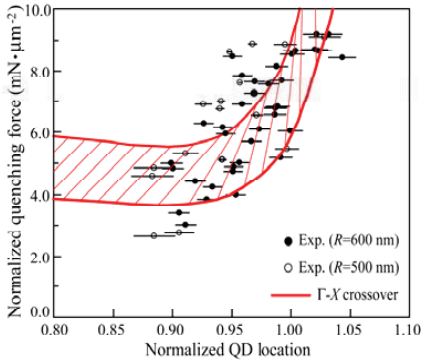

Fig.1 Dependence of quenching force on QD location. The experimental data are plotted with an error bar in the QD location. The Γ-X crossover is given as a band with uncertainty of the bowing parameter (0.6~0.9 eV), providing the boundary of direct to indirect transition.

Figure 1 shows the comparison between the experimental result and the calculation of Γ-X crossover. In Fig. 1, the experimental data indicate that the quenching force increases as the QD location increases. The simulation result of Γ–X crossover agrees well with the experimental result.

From the comparison, we concluded that the quenching of PL peaks observed in our experiment is caused by the Γ (InGaAs) versus X (InGaAs) crossover, rather than the Γ (InGaAs) versus X (GaAs) crossover as reported in the traditional experiment of hydrostatic pressure. The bowing parameter of InGaAs for the X band gap energy is deduced to be from 0.6 to 0.9 eV.

References

1. Y. H. Liang *et al.*, Simultaneous measurement of nanoprobe indentation force and PL of InGaAs/GaAs quantum dots and its simulation, Physica E 36, 1(2007).

Modulation-doping effect on the optical characteristics of vertically coupled InGaAs quantum dots

K.Y. Chuang, C. Y. Chen, T. E. Tzeng, David J. Y. Feng, and T. S. Lay*

Department of Photonics, National Sun Yat-Sen University, Kaohsiung 804, Taiwan

**E-mail address: tslay@mail.nsysu.edu.tw*

Keywords: Quantum dot; Modulation doping; Molecular beam epitaxy

Recent results suggest that vertically stacked quantum dots (QDs) multiple layers provide the favourable optoelectronic characteristics for the fabrications of photonic devices [1]. The growth of vertically coupled QDs would improve the uniformity of QDs arrays. Adding modulation doping (MD) to QDs shows improved characteristics of laser structure [2]. Here, we investigate the luminescence and absorption properties of strongly vertical-coupled InGaAs QDs with p- (n-) MD. Fig. 1 shows the schematic structures of the triple-layer QDs grown on n^+-GaAs (100) substrates by molecular beam epitaxy (MBE). The self-assembled $In_{0.75}Ga_{0.25}As$ QDs are of 3.4 ML coverage at a growth rate of 0.1ML/sec. After the growth of QDs at substrate temperature (T_s) of 510°C, a 10-nm $In_{0.1}Ga_{0.9}As$ capping layer was directly grown on the QDs at the same T_s. Then, the T_s was raised to 580°C for the growth of 5-nm-thick GaAs spacer layer. In the middle of each GaAs spacer, p-type (Be: $4x10^{11}$ cm^{-2}) or n-type (Si: $4x10^{11}$ cm^{-2}) MD were added. The same epi-structure of undoped spacer was also grown for the study. TEM pictures show the vertical alignment of the QDs.

Figures 2(a), (b) and (c) show the room temperature normalized electroluminescence (EL) spectra. For the strong-coupling QDs of un-doped spacer layers, the emission of ground state transition (S_0) is at λ =1269 nm, and the first excited state transition (S_1) is at λ =1189 nm. The energy separation of ($S_1 - S_0$) is about 66 meV. Because of the strong vertically coupling of QDs, a coupled state transition (X) is observed at λ =1236 nm. The EL spectra show that the S_1 transition becomes the dominant peak as the injection current increases. However, for the MD samples, the emission from the coupled state is enhanced. For the p-MD sample, the EL spectra show that the X-state transition has higher gain than the ground state. The photocurrent (PC) spectra are shown in Figs. 2(d), (e) and (f). Two clear absorption peaks corresponding to S_0 and S_1 are observed for the un-doped sample. For the p-MD sample, the signatures of absorption transition become weak. For the n- MD sample, no transition marks is observed in the PC spectrum. The results are attributed to the state filling effect and built-in electric field distribution by the MD.

References

1. M. V. Maximov et al., J. Appl. Phy. **83**, 5561 (1998).

2. K. C. Hall, T. F. Boggess, D. G. Deppe and O. B. Shchekin, Appl. Phy. Lett. **85**, 4570 (2004).

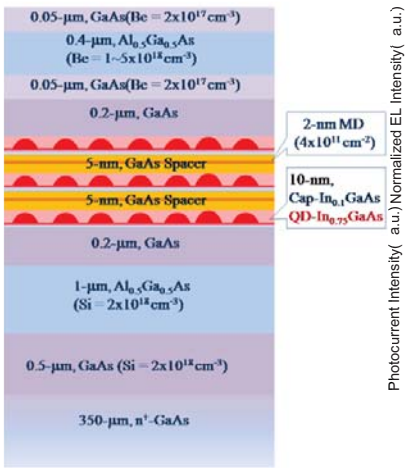

Fig. 1 Schematic structure of the vertically coupled QDs.

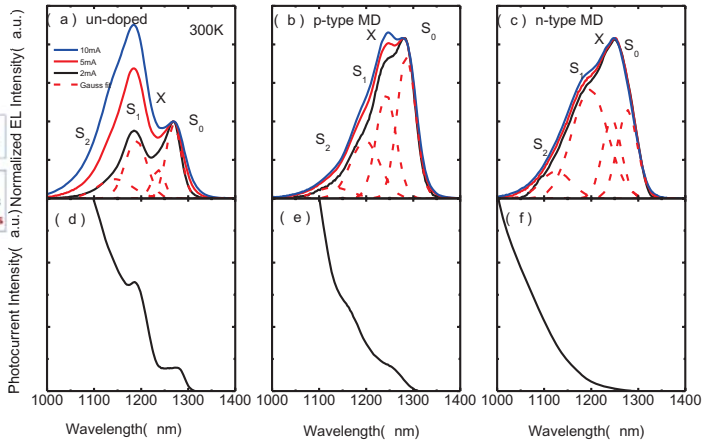

Fig. 2 EL and PC spectra for the vertically coupled QDs of un-doped, p-type MD, and n-type MD.

Optical transitions in AlGaAs/GaAs quantum wires on GaAs(631) substrates studied by photoreflectance spectroscopy*

E. Cruz-Hernandez[a], J. Hernandez-Rosas[b], J.S. Rojas-Ramirez[b], R. Contreras-Guerrero[b], R. Mendez-Camacho[c], C. Mejia-Garcia[c], V.H. Mendez-Garcia[d], and M. Lopez-Lopez[b]

[a]*Graduate School of Science and Engineering, Ehime University, Matsuyama, Japan.*

[b]*Physics Department, CINVESTAV-IPN, Mexico DF, Mexico.*

[c]*Superior School of Physics and Mathematics-IPN, Mexico DF, Mexico.*

[d]*Optical Communications Research Institute, UASLP, San Luis Potosi, Mexico.*

Keywords: Quantum Wires, MBE, Optical transitions, Photoreflectance

We present the synthesis and characterization of a system of self-assembling GaAs Quantum Wires (QWRs) embedded in $Al_xGa_{1-x}As$ barriers. The samples were grown by molecular beam epitaxy on GaAs substrates with (631) orientation. We employed the high index substrate of GaAs(631) due to the interesting diffusion properties of adatoms on this surface [1]. We first induced the self-assembling of a nano-grooved surface by growing GaAs on GaAs(631) substrates under suitable growth conditions. The nano-grooves are oriented along the [-5, 9, 3] direction with average dimensions of 25 nm in width, and 1.5 nm in height. After that, we grew a quantum well structure consisting of 40 nm-AlGaAs/ 20 nm-GaAs/ 40 nm-AlGaAs. The initial corrugation induces a lateral modulation in the thickness of the GaAs QW layer, thus producing the QWRs system.

We studied the optical transitions in the QWRs as a function of temperature (T) by photoreflectance (PR) spectroscopy. The energy transitions were extracted from the PR spectra employing the third-derivative functional form developed by Aspnes [2], and they were compared with the transitions theoretically calculated from a model of QWRs with a cylindrical geometry. The results show a good agreement between experimental and theoretical data and, from this comparison, we were able to identify each transition in the PR spectra and study its behaviour with temperature.

We were able to identify up to 12 different transitions in the PR spectra. The behaviour of the QWRs transitions presents the depopulation of the higher energy transitions when temperature decreases from 300 to 150 K. When the temperature was lowered down to 8 K, the narrowing of the PR lines allowed us to observe two additional transitions. We also discuss the possibility of using this kind of QWRs in devices such as QWRs-based Vertical Cavity Superficial Emitting Lasers.

*) This work was partially supported by Conacyt-Mexico and ICTDF-Mexico.

References

1. E. Cruz-H, J. Crys. Grow. **301–302,** 884 (2007).
2. F.H. Pollak, Surf. Interface Anal. **31,** 938 (2001).

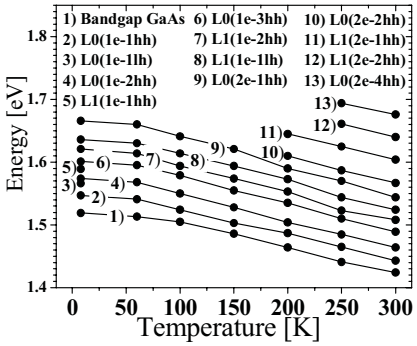

Fig.1 Energy position of the QWRs transitions as a function of T obtained experimentally by PR. The optical transitions are named as L(me-m'h), where L is the radial, and m and m', are the angular momentum quantum numbers of the electrons (e) and hard (hh) and light (lh) holes.

Photovoltaic response in multi-stack $In_xGa_{1-x}As$ quantum dots

T. E. Tzeng, K. Y. Chuang, C.Y. Chang, David J. Y. Feng, and T. S. Lay*

Department of Photonics, National Sun Yat-Sen University, Kaohsiung 804, Taiwan

**E-mail address: tslay@mail.nsysu.edu.tw*

Keywords: InGaAs Quantum Dots, Photovoltaic effect, III-V solar cell, Molecular beam epitaxy

Self-assembled quantum dots (QDs) structures are attractive in III-V solar cells to increase the photovoltaic response in the infrared regime. Appropriate energy-band engineering for the QDs and buffer layers has been proposed to enhance the solar cell efficiency by the intermediate band effect [1]. In this paper, we present the study for the growth and photovoltaic response of multi-stack InGaAs QDs. The multi-layer InGaAs QDs are designed have different In and Ga compositions to have absorption peaks ranging from λ = 1.1 to 1.3 μm. Photocurrent spectroscopy, and current vs. voltage (J-V) characteristics are investigated.

The samples were grown by using solid source molecular beam epitaxy (MBE) on n^+-type (001)GaAs substrate. Figure 1 shows the schematic diagram of the epi-structures. Sample C243 comprises a 0.5μm-thick n^+-GaAs buffer layer grown on the substrate at 580°C to produce a flat surface. QDs/cap pairs of $In_{0.64}Ga_{0.36}As$/GaAs, $In_{0.75}Ga_{0.25}As/In_{0.1}Ga_{0.9}As$, and InAs/GaAs were grown consecutively as the active region. The QDs/cap compositions were prepared to have PL peaks at λ = 1.17 μm (InAs/GaAs), 1.25 μm ($In_{0.64}Ga_{0.36}As$/GaAs), and 1.31 μm ($In_{0.75}Ga_{0.25}As/In_{0.1}Ga_{0.9}As$). Sample C239 is of dots-in-a-well (QDwell) structure as shown in Fig. 1(b). The QDs/cap compositions are the same as C243, besides a 2-nm-thick $In_{0.1}Ga_{0.9}As$ quantum well is inserted beneath each QDs layer. J-V measurements for C243 and C239 are shown in Fig. 2. The short circuit current density (J_{SC}) and open circuit voltage (V_{OC}) are 0.65mA/cm^2 and 0.48V for C243, and 0.55mA/cm^2 and 0.43V for C239. The filling factor (FF) for C243 is 67.9% larger than FF = 61.0% for C239.

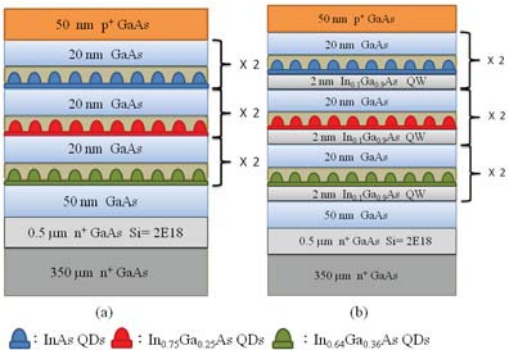

Fig. 1 Schematic diagram of (a) C243 multi-stack $In_xGa_{1-x}As$ QDs structure (2x3) and (b) C239 QDwell structure (2x3) consisting of three pairs of different QDwell types.

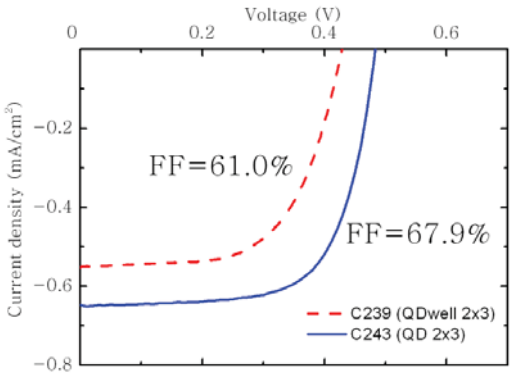

Fig. 2 Current vs. voltage J-V characteristics of C243 and C239.

References

1. A. Luque, A. Marti, N. Lopez, E. Antolin, and E. Canovas, Appl. Phys. Lett. **87**, 083505 (2005).

Modulation spectroscopy on metamorphic InAs quantum dots

E. Y. Lin, C. Y. Chen, S. L. Chen, T. E. Tzeng, David J. Y. Feng, and T. S. Lay*
Department of Photonics, National Sun Yat-Sen University, Kaohsiung 804 , Taiwan
**E-mail:tslay@mail.nsysu.edu.tw*

Keywords: photoreflectance, electroabsorption, metamorphic quantum dots, molecular beam epitaxy

Self-assembled InAs quantum dots (QDs) prepared by Stranski-Krastanow growth are reported to have low threshold currents, and reduced temperature sensitivity in diode laser applications. The metamorphic InAs QDs on GaAs offer an alternative gain medium to achieve long wavelength emission beyond $\lambda > 1.3$ μm [1, 2]. In this paper, we investigate the modulation spectroscopy of the metamorphic InAs QDs with different indium content in the InGaAs capping layers. The metamorphic InAs QDs were grown on GaAs substrate by molecular beam epitaxy (MBE). After the growth of a 0.5 μm GaAs buffer layer at 580°C, metamorphic layers including 0.6 μm $In_{0.16}Ga_{0.84}As$ layer and 0.6 μm $In_{0.16}Al_{0.34}Ga_{0.5}As$ layer were grown. AlAs protective layer was grown for the in-situ thermal annealing at 700°C. The InAs QDs of 3 ML coverage were grown on $In_{0.16}Ga_{0.84}As$ buffer layer with a growth rate 0.05 ML/s at 510°C. After the QDs formation, an $In_{0.4}Ga_{0.6}As$ capping layer was grown. The TEM image reveals that the QDs has a rectangular shape of height = 14 nm and width = 23 nm. The AFM image for the surface QDs shows that the dot density is ~ 2×10^{10} cm^{-2}.

The room-temperature photoreflectance (PR) and electroabsorption (EA) spectra of $In_{0.6}Ga_{0.4}As$/InAs quantum dot structures are shown in Figs. 1(a) and (b). The PR spectrum exhibits several transitions related to the metamorphic InAs QDs and the wetting layer. The results are consistent with EA spectra. As the bias increases from -1 to -4V, a red-shift (~23 nm) of Δα was observed at λ ~1100 nm, indicating a quantum-confined Stark effect (QCSE) in the wetting layer. However, no red-shift is observed for the QD interband transitions. The Δα value has a maximum of 20 cm^{-1} at 1410 nm. Figure 1(c) shows that the electroluminescence (EL) spectra have an emission peak at λ = 1424 nm. The intensity of excited state for metamorphic InAs QDs increases as the injection current increases. The full width half maximum (FWHM) of the EL spectrum is 182 nm at injection current = 40mA. It suggests the possibility to develop novel QD devices on GaAs substrates for optical communication in the λ = 1.55 μm region.

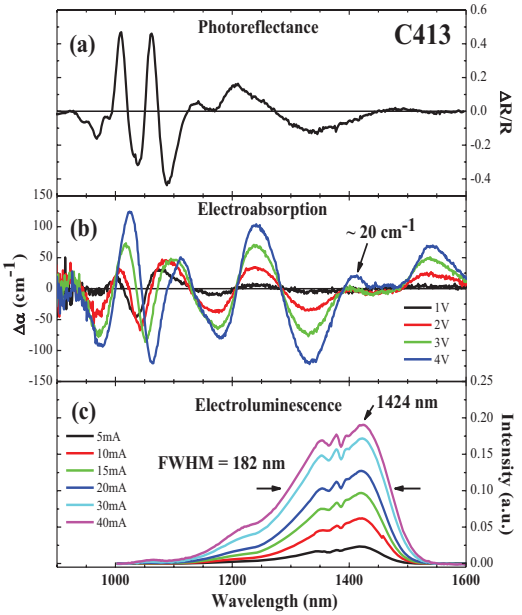

Fig.1 (a) and (b) Photoreflectance and Electro-absorption spectra of InGaAs/InAs QD structures are obtained. Δα has a maximum value ~20 cm^{-1} at 1410 nm. (c) Electroluminescence spectra are shown with different injection current.

References

1. A. E. Zhukov, A. R. Kovsh, V. M. Ustinov, N. N. Ledentsov ,and Zh. I. Alferov, *Microelectron. Eng.*, 81, 229-237(2005).
2. Z. Mi, P. Bhattacharya, and J. Yang, *Appl. Phys. Lett.,* 89, 153109 (2006).

Time-Resolved Photoluminescence Study of ZnO Nanocrystals Embedded in a Hybrid Polymer Composite Layer

Y. Saeki*, Y. Nakazato*, S. Izumi*, T. Nukui*, A. Tackeuchi*,
J. H. Jung**, J. H. You**, T. W. Kim** and Y-H. Kim***

** Department of Applied Physics, Waseda University, 3-4-1 Okubo, Shinjuku-ku, Tokyo 169-8555, Japan*
*** Division of Electronic and Computer Engineering, Hanyang University, Seoul 133-791, Korea*
**** Division of Materials Science and Engineering, Hanyang University, Seoul 133-791, Korea*

Keywords: ZnO; Nanocrystal; Lifetime; Interface recombination

ZnO has attracted much attention as a promising material for ultraviolet optoelectronic devices. Recently, Li et al. reported that the ultraviolet emission at 3.3 eV of self-organized ZnO nanocrystals was significantly enhanced in a hybrid polymer composite layer [1]. In this paper, we report the time-resolved photoluminescence (PL) study of ZnO nanocrystals. The observed nanosecond PL decay demonstrates the high quality of the ZnO nanocrystals.

The ZnO nanocrystals are embedded in a 100-nm-thick polyimide and polyvinylcarbazole hybrid layer. A high-resolution transmission electron microscope image shows that the sizes of the ZnO nanocrystals range from approximately 4 to 6 nm and that the surface density is 8×10^{11} cm^{-2}. In the time-resolved PL measurement, frequency-tripled (4.66 eV) femtosecond optical pulses generated from a Ti-sapphire laser were used for photoexcitation. The PL was time-resolved using a streak camera with a time resolution of 15 ps.

Figure 1 shows the time evolution of the ultraviolet PL (3.3 eV) of the ZnO nanocrystals at 10 K. The PL decays biexponentially with nanosecond time constants. The PL decay time of ZnO nanocrystals dispersed in t-butanol was reported to be 100 - 300 ps [2]. The observed nanosecond relaxation time shows that the interface condition is better than that of nanocrystals in t-butanol, resulting in strong ultraviolet emission. The energy dependences of the two PL decay times have been measured. The slower decay time, τ_2, is found to decrease monotonically with energy, although τ_1 is almost constant. This energy dependence of τ_2 can be explained as being due to the fast interface recombination.

Acknowledgement The work at Hanyang University was supported by the Korea Science and Engineering Foundation (KOSEF) grant funded by the Korea government (MEST) (No. R0A-2007-000-20044-0).

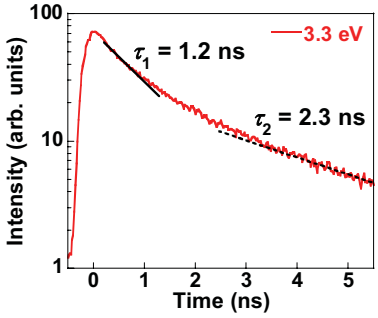

Fig.1 Photoluminescence time evolution of ZnO nanocrystals detected at 3.3 eV at 10 K.

References

[1] Fushan Li et al., J. Appl. Phys. **103** (2008) 073511.
[2] Sekika Yamamoto et al., J. Lumin. **126** (2007) 257.

The effect of spacer layer thickness on vertical alignment of InGaAs/GaNAs quantum dots grown on GaAs(311)B substrate

Y. Shoji [*,***], R. Oshima [*], A. Takata [**], A. Uedono [***] and Y. Okada [*,**]

[*] *Research Center for Advanced Science and Technology (RCAST), The University of Tokyo, Tokyo, Japan*

[**] *Graduate School of Engineering, The University of Tokyo, Tokyo, Japan*

[***] *Institute of Applied Physics, University of Tsukuba, Ibaraki, Japan*

Keywords: Quantum dots, Molecular beam epitaxy, Semiconducting III-V materials

Recently, studies on self-assembled quantum dots (QDs) have attracted increasing attention because of their potential for a variety of applications. For a QD intermediate band solar cell (QD-IBSC), homogeneous QDs should ideally be positioned periodically in all three dimensions, which as a result, lead to the formation of an intermediate band or a miniband [1]. In this work, we investigated on the structural properties of 10 stacked layers of strain-compensated $In_{0.35}Ga_{0.65}As$ QDs/GaNAs on GaAs (311)B substrates from the viewpoint of the effect of spacer thickness on vertical alignment.

All samples were fabricated by atomic hydrogen-assisted RF-molecular beam epitaxy (H-MBE). 7.6 monolayers (MLs) of $In_{0.35}Ga_{0.65}As$ QD layer and d nm thick of GaNAs spacer layer were consecutively grown in pair up to 10 multiple cycles on GaAs (311)B substrate [2]. The growth rate of QD layer was 0.1 μm/h, and growth temperature was 480°C. The GaNAs layer thickness was varied between d = 20, 30, and 40 nm.

Figure 1 shows the cross-sectional high-angle annular dark-field (HAADF) STEM image for the stacked QD structure with d = 40 nm viewed along [-233]. We observe that vertical alignment of QDs is inclined at 22° to the growth direction. This is thought to be caused by in-plane elastic anisotropy of GaAs(311)B substrate [3].

Figure 2 shows the inclination alignment determined by (a) STEM image, and (b) resonant diffuse scattering (RDS) sheets in reciprocal space mapping around GaAs (311) lattice point as function of spacer layer thickness, respectively. For d = 40 nm, the result from RDS sheet of 21° is in good agreement with STEM result of 22°. Further, we observe that the inclination angle becomes monotonously smaller with decreasing the spacer layer thickness. This suggests that the inclination of vertically stacked QD is strongly dependent on the spacer layer thickness and hence local strain.

References

[1] A. Luque *et. al*, Phys. Rev. Lett. **78** (1997) 5014.
[2] R. Oshima *et. al*, J. Crystal Growth, *in press*.
[3] H. Z. Xu *et. al*, Appl. Surf. Sci. **185** (2001) 92.

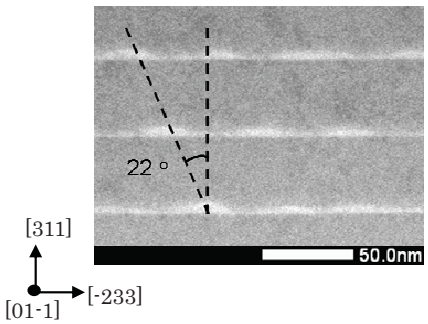

Fig.1 Cross-sectional HAADF STEM image for QDs structure with 10 stacked and d = 40 nm viewed along [-233].

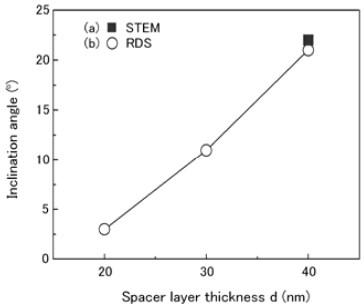

Fig.2 The inclination angle of vertical alignment of QDs determined by (a) STEM image and (b) RDS sheets as a function of spacer layer thickness, respectively.

Growth of multi-stacked InAs/GaNAs quantum dots grown with As_2 source in atomic hydrogen-assisted molecular beam epitaxy

A. Takata,* R. Oshima,** Y. Shoji,**,*** and Y. Okada*,**

* *School of Engineering, The University of Tokyo, Tokyo, Japan*

** *Research Center for Advanced Science and Technology, The University of Tokyo, Tokyo, Japan*

*** *Institute of Applied Physics, University of Tsukuba, Tsukuba, Japan*

Keywords: Semiconducting III-V materials, Quantum dots, Molecular beam epitaxy.

Recently, integration of GaAs material-based long-wavelength optoelectronics has been investigated for future optic fiber communication systems. In the case of InAs/GaAs system, one of the challenging technological issues today is to increase the total QD density while maintaining the quality of QD structure. To overcome this problem, we take advantage of a strain-compensation growth technique by using InAs/GaNAs system. Previously, we reported on improved crystalline quality of GaNAs material by using As_2 source instead of As_4 source[1]. In this work, we study the effect of As_2 source on the properties of stacked layers of InAs/GaNAs QDs fabricated on GaAs(001).

All growths were done by atomic hydrogen-assisted molecular beam epitaxy (H-MBE). After the oxide removal followed by a 250 nm-thick GaAs buffer layer at 580°C, a 30 nm-thick GaNAs strain compensating layer (SCL) and 1.7 ML of InAs QD layer were consecutively grown in pair up to 10 multiple cycles at 480 °C.

Fig.1 show the AFM images of the topmost InAs QDs grown As_2 and As_4 source. We observe a mono-modal QD size distribution with a higher sheet density for the sample grown with As_2. The QD height, diameter and sheet density are 6.8 nm, 28.8 nm, 5.8×10^{10} cm^{-2}, respectively. On the other hand, a bimodal size distribution is observed for the sample grown with As_4 with a lower density. By using As_2, an atomically flat GaNAs surface with a high density of steps is observed, which act as nucleation sites of QDs formation. Therefore, higher density QDs can be formed in InAs/GaNAs grown with As_2 source.

The photoluminescence (PL) spectra measured at 77K show a narrower linewidth of 42 meV for the sample with As_2 compared to 65 meV for the sample with As_4 as shown in Fig.2. Furthermore, we observe a stronger PL intensity for As_2 sample than that for As_4 by a factor of 3.5, which is as a result of both an increase in QD density and improvement of material quality of GaNAs layer.

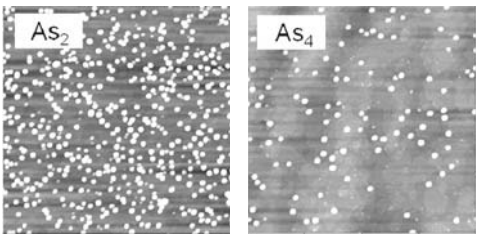

Fig.1 AFM image of the topmost surface for 10 stacked layer of InAs QDs grown with As_2 and As_4, respectively.

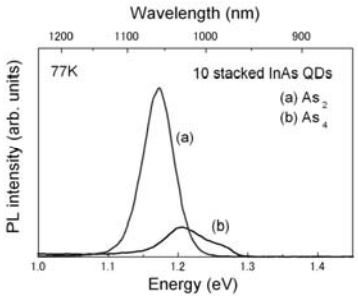

Fig.2 PL spectrum measured at 77K for 10 stacked layer of InAs QDs grown with (a)As_2 and (b)As_4, respectively.

References

1. A. Takata et al, J. Crystal Growth **310** 3710 (2008).

Excitons and biexcitons in type-II InP/GaAs quantum dots

Bhavtosh Bansal*,†, S. Godefroo†, M. Hayne**, G. Medeiros-Ribeiro††, and V. V. Moshchalkov†
*IMM, High Field Magnet Laboratory, University of Nijmegen, Toernooiveld 7, 6525 ED Nijmegen, The Netherlands
†INPAC-Institute for Nanoscale Physics and Chemistry, KU Leuven, Celestijnenlaan 200D, Leuven B-3001, Belgium
**Department of Physics, Lancaster University, Lancaster LA1 4YB, UK
††Laboratório Nacional de Luz Síncrotron, P.O. Box 6192, 13084-971 Campinas-SP, Brazil

Keywords: type-II quantum dots, excitons, biexcitons, magnetophotoluminescence

Excitons in quantum dots (QDs) with type-II band allignment (e.g. GaSb/GaAs, InP/GaAs) are qualitatively different from those in the usual type-I systems. In type-I QDs, the confining potential dominates the physics, while its role in a type-II system is essentially limited to spatially-separating the electrons and the holes. For example, InP/GaAs QDs can only confine the electrons, and are thus effectively capacitors on the nanoscale. But once charged, they can weakly bind the complementary particle to form an excitonic bound state. At higher excitation powers, the QDs can be doubly-charged and thus form four-particle bound states (biexcitons). In the atomic physics language, while the usual biexciton is analogous to a hydrogen molecule, the biexciton in type-II QDs is more like a helium atom[1].

We have measured the photoluminescence (PL) spectra from an InP/GaAs QDs ensemble[2] in high magnetic fields ($\leq 50T$) [Fig.1(a)]. Magneto-PL experiments were performed with the excitation power varied over about six orders of magnitude. At the lowest excitation power, when the QDs are guaranteed to be singly-occupied, we used magneto-PL to infer the excitonic characteristics by fitting the data to a hydrogenic exciton model[1]. The average values for the diamagnetic shift coefficient, the binding energy, and Bohr radius for the excitonic ground states in the QD ensemble are $\Gamma = 42\,4 \pm 0\,5 \quad T^{-2}$, $E_B = 1\,5 \pm 0\,1$meV and $= 15\,0 \pm 0\,1$nm respectively. A comparison with the corresponding values for bulk InP ($E_B = 4\,8$meV, $= 12$nm) and type-I InP/InGaP[4] ($\Gamma = 2 - 8 \;\; e \;\; T^{-2}$) QDs, shows that the Coulombic binding is significantly reduced. This is consistent with the expected spatial separation of the electrons and the holes in type-II systems.

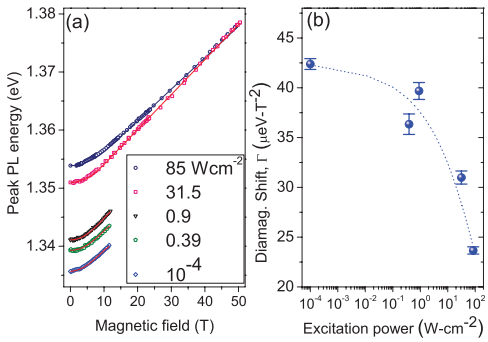

Figure 1: (a) The measured PL peak position as a function of excitation power at different magnetic field. Solid lines are fits to the model of hydrogenic exciton[1]. (b) Changing diamagnetic shift coefficient is a result of many-particle effects. The dotted line is a guide to the eye.

At an incident power density of about (10^{-1} Wcm^{-2}), emission from the four-particle states also becomes significant. This is apparent from the blue-shift of the PL peak position (due to the capacitive charging energy) and the super-linear scaling of the integrated PL intensity with excitation power. In this regime, we observe a strong monotonic decrease in the diamagnetic shift coefficient to about 24 eVT^{-2} at the highest excitation power [Fig.1(b)]. The results prove a strong dependence of the excitonic radius on the charge state of the dot, as is expected from the atomic physics analogy: the Bohr radius of the hydrogen atom is five times larger than for helium. In type-I QDs, on the other hand, confinement usually renders the diamagnetic shift independent of the charge in the dot[3].

References

[1] M. Hayne et al., Appl. Phys. Lett. **82**, 4355 (2003).
[2] R. L. Maltez et al., J. Appl. Phys. **94**, 3051 (2003).
[3] N. I. Cade et al., Phys. Rev. B **73**, 115322 (2006).
[4] M. Sugisaki et al., Phys. Rev. B **66**, 235309 (2002).

Electron-hole complexes in semiconductor nanorods

M. Royo, J.I. Climente, J.L. Movilla, F. Rajadell and J. Planelles
Departament de Química Física i Analítica, Universitat Jaume I, Castelló, Spain.

Keywords: Semiconductor, nanostructures, photoluminescence.

Semiconductor nanorods are elongated nanocrystals grown by wet chemistry [1] which present several advantages as compared to the usual spherical quantum dots, both in optics and transport properties.[2] The theoretical understanding of these structures has so far relied on the well-known physics of spherical nanocrystals, the experimental deviations in the response of nanorods being usually interpreted in terms of the different single-particle energy structure arising from the anisotropic shape.[3-5]

For excitonic complexes, however, the large length of the rod moves the system into a one-dimensional weak confinement regime, where correlation effects become important.[6] This effect is even more pronounced when the dielectric mismatch between the semiconductor nanorod and its surroundings is taken into account, as this greatly enhances the Coulomb interaction energies, explaining the observed differences between transport and optical gaps.[5]

In this work we investigate theoretically the emission properties of excitons, singly charged excitons and biexcitons in CdSe nanorods. Coulomb correlations and dielectric confinement effects are accounted for exactly by means of an effective mass-configuration interaction method which includes the images charges originating from the dielectric mismatch.

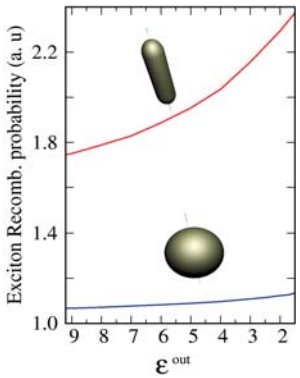

We show that, contrary to spherical quantum dots, the luminescence of excitons in nanorods is enhanced by the dielectric confinement (see Figure), and new excited resonances may appear in the emission spectrum due to the strong correlations.[6] The presence of an external ZnS shell is also considered. It is shown that although the external shell slightly reduces the effect of the dielectric confinement, the latter is still noticeable on the luminescence of excitons.

We further study the binding energies of trions and biexcitons in nanorods and compare our results with the multiline spectra reported in.[7] It is found that the strong Coulomb correlations minimize repulsions and enhance attractions in the system, so that the exciton always shows up on the high-energy side of the spectrum. This would invalidate the tentative assignment proposed in Ref.[7] experiment.

References

1. X. Peng, L. Manna, W. Yang, J. Wickham, E. Scher, A. Kadavanich and A.P. Alivisatos, Nature (London) **404**, 59 (2000).
2. U. Woggon, J. Appl. Phys. **101**, 081727 (2007).
3. D. Katz, T. Wizansky, O. Millo, E. Rothenberg, T. Mokari and U. Banin, Phys. Rev. Lett. **89**, 086801 (2002).
4. J. Li and L. Wang, Nano Lett. **3**, 1357 (2003).
5. A. Shabaev and Al.L. Efros, Nano Lett. **4**, 1821 (2004).
6. J.I. Climente, M. Royo, J.L. Movilla and J. Planelles, submitted.
7. N. Le Thomas, M. Allione, Y. Fedutik and U. Woggon, Appl. Phys. Lett. **89**, 263115 (2006).

Efficient injection-type ballistic rectification in Si/SiGe cross junctions

D. Salloch*, U. Wieser*, U. Kunze* and T. Hackbarth**
*Werkstoffe und Nanoelektronik, Ruhr-Universität Bochum, D-44780 Bochum, Germany
** DaimlerChrysler Forschungszentrum Ulm, Wilhelm-Runge-Straße 11, D-89081 Ulm, Germany

Keywords: Si/SiGe, ballistic transport, ballistic rectification, cross junction

We demonstrate a substantial efficiency increase in an optimized injection-type ballistic rectifier with a near-ideal V-shaped voltage-current transfer characteristic.

The rectifier is as a nanoscale asymmetric cross junction consisting of a straight voltage stem (2 μm long and 490 nm wide) and two pairs of opposing 200 nm wide injectors which merge under 30° into the central stem [Fig. 1(a)]. The starting material is a Si/SiGe heterostructure with a two-dimensional electron gas 30 nm below the surface. The electron mobility and density measured on a mesa-etched Hall bar with top gate ($V_G = 0.15$V) at a temperature of $T = 1.5$ K amounts to $1.25 \cdot 10^5$ cm^2(Vs)$^{-1}$ and $2.3 \cdot 10^{11}$ cm^{-2}, respectively. Nanoscale patterning is performed by using a mix-and-match process which combines high-resolution electron-beam lithography and UV-lithography. The resulting resist pattern is transferred into the heterostructure with a low-damage CF_4/O_2 plasma step. After the preparation of ohmic contacts two local nanoscale Schottky split gates are deposited on top of the device [Fig. 1(b)].

A rectified inertial ballistic voltage develops between the upper and lower end of the central stem upon injecting a current between the branches [1]. The voltage is

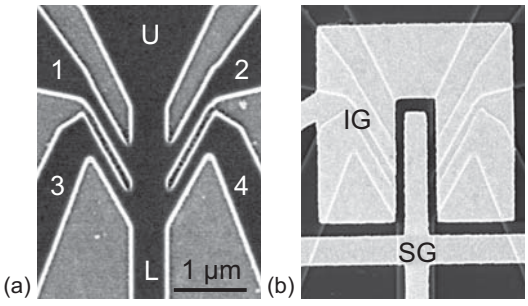

Figure 1: Scanning electron micrograph of the ballistic rectifier (a) before and (b) after split gate deposition with current leads (1 – 4), upper (U) and lower (L) voltage probe, injector gate (IG) and stem gate (SG).

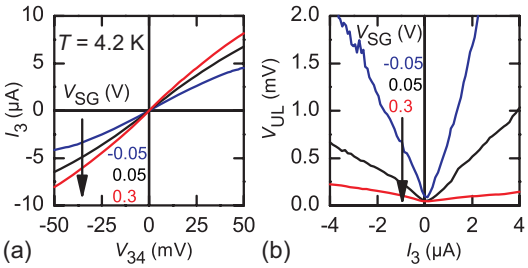

Figure 2: (a) Current I_3 as a function of V_{34} at an injector gate voltage of $V_{IG} = 0.3$ V for different stem gate voltages V_{SG}. (b) V_{UL} as a function of input current I_3 with stem gate voltage V_{SG} as parameter, $V_{IG} = 0.3$ V.

caused by the momentum component of the injected ballistic electrons, which is directed towards the lower part (L) of the stem and therefore is independent of the input bias polarity. The electron density in the injectors and the stem is adjusted by the gate voltages V_{IG} and V_{GS}, respectively [Fig. 1(b)].

Figure 2 shows the DC characteristics of the device for different V_{SG} at constant $V_{IG} = 0.3$ V ($T = 4.2$K). The nonlinear I_3-V_{34} input characteristic in Fig. 2(a) is caused inter alia by carrier heating. For both pairs of injectors the rectified signal $V_{UL} = V_U - V_L$ as a function of input current I_3 respectively I_1 roughly starts parabolic [Fig. 2(b)] followed by a linear characteristic whose slope is widely controlled by the stem gate voltage V_{SG}.

An optimum rectification efficiency as indicated by the transfer resistance R_T (V_{UL} divided by I_1) is achieved if the injecting channels are low-resistive and the stem is close to the threshold voltage. The resulting R_T in excess of 800 Ω at a current of only $I_3 = 2$ μA represents the highest value ever reported for ballistic rectifiers.

References

[1] M. Knop *et al.*, Appl. Phys. Lett. **88**, 082110 (2006).

A two-dimensional electron gas as a sensitive detector to observe the charge carrier dynamics of self-assembled QDs

B. Marquardt*, M. Geller*, A. Lorke*, D. Reuter**, and A. Wieck**

*Experimental Physics & CeNIDE, University Duisburg-Essen, Duisburg, Germany

** Department of Applied Physics, Ruhr-University, Bochum, Germany

Keywords: time-resolved, electron tunneling, quantum dots, two-dimensional electron gas

In the last few years, the electrical readout of quantum dot states by an adjacent electron channel has become a powerful tool to study charge, spin and entanglement in confined few electron systems [1]. These studies were mostly performed on *lateral* and lithographically defined structures. No corresponding read-out scheme was demonstrated for the otherwise widely studied self-assembled quantum dots (QD). Here, we show that the conductance of a two-dimensional electron gas (2DEG) can be used as an efficient and sensitive detector to study the charging dynamics of self-assembled InAs QDs with single-electron charge resolution and a time resolution ranging from microseconds to several ten seconds.

An example is shown in Fig. 1. The sample consists of a MISFET structure [2] with embedded self-assembled InAs QDs, which are separated by an $Al_{0.34}Ga_{0.66}As$/GaAs-tunneling barrier from a 2DEG, as schematically depicted in the left inset. The operation starts with a 600 ms long charging pulse (U_p= 0.6 V) applied to the gate electrode. This brings the Fermi-level E_F above the highest (p-) state of the dots, so that the QD-states are filled with electrons from the nearby 2DEG by tunneling through the barrier. The charge in the QDs screens the gate potential and thus depletes the 2DEG, resulting in a smaller conductance. At t=600 ms, a detection bias of U_{det}= -0.7 V is applied, which brings the Fermi-level E_F below the lowest (s-) states in the dots, as schematically depicted in the left inset, and tunneling from the QD states to the 2DEG takes place. As shown in the main part of the figure, tunneling takes place on very different time scales, corresponding to exponential dependence of the tunneling process on the thickness and height of the barrier. We find tunneling times of 30 ms, 13 ms and 0.6 ms for the s1, s2 and the p-states respectively (see solid lines), in good agreement with frequency-dependent CV measurements [3] on the same sample (not shown here).

Furthermore, a boxcar evaluation method is used to compare the time-resolved measurements with standard CV measurements. The clear charging signal of all 6 QD states (see right inset) confirms that the transients are indeed caused by tunneling from the different many-particle states in the self-assembled QDs.

Contrary to CV measurements, the present readout scheme is scalable without great loss of signal-to-noise ratio. This, together with the high transient amplitudes (up to 10 %) gives us confidence that our technique will make single dot readout possible in the near future.

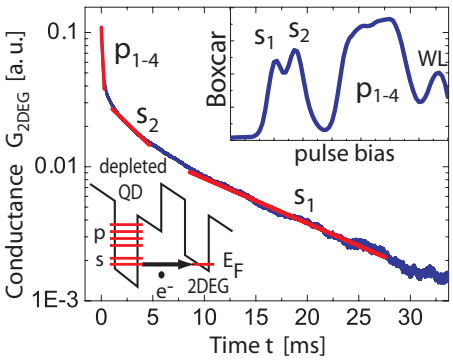

Figure 1: Charge emission transient of QDs, measured by a change of the conductance in a nearby 2DEG.

References

[1] see M. Elzerman et al., Nature **430**, 431 (2004); S. Gustavsson et al., Phys. Rev. Lett. **96**, 076605 (2006) and references therein.

[2] M. Russ et al., Phys. Rev. B **73**, 115334 (2006).

[3] R. J. Luyken et al., Appl. Phys. Lett. **74**, 2486 (1999).

Holes in double quantum dots: effects of the spin-orbit interaction

J. I. Climente*, M. F. Doty**, M. Korkusiński***, M. Scheibner****, A.S. Bracker****, D. Gammon****, and P. Hawrylak***

*Department of Physical and Analytical Chemistry, Universitat Jaume I, Castellón, Spain

** Department of Materials Science, University of Delaware, Newark, USA

*** Institute for Microstructural Sciences, National Research Council, Ottawa, Canada

**** Naval Research Laboratory, Washington, USA

Keywords: quantum dot molecule, hole, spin-orbit interaction

Tunneling of carriers between vertically coupled quantum dots enables the formation of hybridized, molecular-like orbitals which are important in many quantum dot-based devices, including those aiming at optically controlled quantum information storage.[1]

The differences in size and composition of the quantum dots is overcome by the application of a vertical electric field, which brings the two quantum dot levels into resonance and induces either electron or hole tunneling.[2] While early works investigating coupled quantum dots used resonant electrons, recently it has become apparent that the use of resonant holes poses a number of advantadges, such as slower decoherence rates[3] and improved suitability for local spin manipulation using electric fields[4].

Many of the differences in the behavior of holes as compared that of electrons arise from the strong spin-orbit interaction of the valence band. In this work we illustrate a few such instances affecting double quantum dots, and show that they can be understood by describing holes as Luttinger spinors.

We show that the spin-orbit interaction is responsible for the formation of molecular ground states with anti-bonding character, a situation that never occurs in natural molecules.[5] This peculiar phenomenon is confirmed by magneto-photoluminescence experiments.[6] We next show that the tunnel-coupling strength -a key parameter for applications of quantum dot molecules- can be controlled at will by modulating the spin-orbit interaction strength via longitudinal magnetic fields.[7] This is a most useful tool as it can be applied after growth, is fully reversible and -unlike transversal fields- does not interfere with protocols for optical spin manipulation and non-destructive measurements.[8] Finally, we investigate the influence of structural deformations of the double quantum dot on the spin of the holes. It is shown that the strong coupling of spatial and spin degrees of freedom makes the hole spin purity sensitive to such deformations.

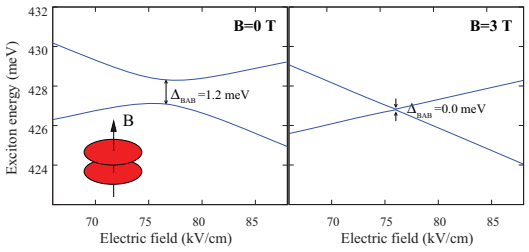

Figure 1: Exciton energy vs. an electric field inducing resonant hole tunneling in a double quantum dot. A longitudinal magnetic tunes the gap between bonding and antibonding states.

References

[1] M. Bayer et al., Science **291**, 451 (2001); E.A. Stinaff et al., ibid **311**, 636 (2006).

[2] A.S. Bracker et al., Appl. Phys. Lett. **89**, 233110 (2006).

[3] B.D. Gerardot et al., Nature **451**, 441 (2008).

[4] M.F. Doty et al., Phys. Rev. Lett. **97**, 197202 (2006); T. Andlauer, and P. Vogl, Phys. Rev. B **79**, 045307 (2009).

[5] J.I. Climente et al., Phys. Rev. B **78**, 115323 (2008).

[6] M.F. Doty et al., Phys. Rev. Lett. **102**, 047401 (2009).

[7] J.I. Climente, Appl. Phys. Lett. **93**, 223109 (2008).

[8] D. Kim et al. Phys. Rev. Lett. **101**, 236804 (2008).

Optical anisotropy of a triexciton in a quantum dot

A. Babinski*, A. Golnik*, T.Tite*, P.Kossacki*, J.Gaj* S.Raymond**, and Z. Wasilewski**

* *Institute of Experimental Physics, University of Warsaw, Warsaw, Poland*

** *Institute for Microstructural Sciences, National Research Council, Ottawa, Canada*

Keywords: optical anisotropy, quantum dots, triexciton

Quantum dots (QDs) are often referred to as “artificial atoms”. However their electronic and optical properties are influenced by symmetry properties of the confining potential and the atomic crystal structure. The in-plane anisotropy leads to the splitting of excitonic emission, which can be used to identify the corresponding charge states. The optical anisotropy of a neutral exciton and biexciton, as well as charged excitons has been thoroughly investigated. Less information is available on excited states, which through configuration mixing, influence the energy shell structure of all bound states. In this communication we report on polarization sensitive spectroscopy of the *p*-shell related emission attributed to the triexciton recombination in a single neutral QD.

Typical emission spectrum of a single QD excited non-resonantly with a low power density consists of emission due to neutral (X) and charged (X*) single excitons, as identified by polarization-sensitive measurements.

Under stronger excitation new features emerge both in the *s*- and *p*- shell emission energy ranges (see Fig. 1a). Studies under different excitation regimes, which favoured particular charge state of the QD allowed us to attribute the 2X and 3X emission to its neutral-charge. Power-dependent measurements sug-gested the attribution of the 3X feature to a triexcitonic complex.

There are two emission lines corresponding to the ground state of the triexciton. As confirmed by measurements in magnetic field, the 3X line is related to the *p*-shell of the QD. The 3X emission line comprises two components, which are linearly polarized in perpendicular directions (see Fig. 1b). The splitting between the components as found from Gaussian fits was in the range of 60..100 μeV. In all investigated cases the splitting was considerably larger than the splitting of a single exciton in the same QD (lower than 20 μeV). We relate the splitting to electron-hole exchange interaction. The splitting results from in-plane anisotropy of localizing potential. The observation may intuitively be understood by larger extent of a *p*-shell-related wavefunction as compared to its *s*-shell-related counterpart. Less intuitive is an explanation of the splitting sign. The splitting corresponds to the triexcitonic complex, as the lowest energy final state of the triexciton is a spin-singlet biexciton. Therefore the effect of the localizing potential asymmetry on the triexcitonic complex is opposite to its effect on the exciton.

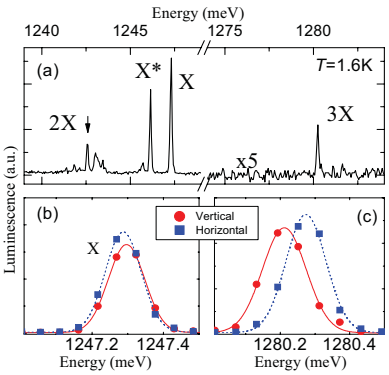

Fig.1 Typical spectrum of a single QD excited nonresonantly (a). Polarization-sensitive spectra of the exciton X (b), and triexciton 3X (c) are also shown.

We believe that our experimental results may spark theoretical work in order to better understand the electronic structure of self-assembled QDs.

Temperature dependence of electronic energy transfer in PbS quantum dot films

W. Lü, and I. Kamiya

Toyota Technological Institute, Nagoya 468-8511, Japan

Keywords: PbS quantum dots, photoluminescence, energy transfer

PbS is an important direct-gap material with a small band gap and a small effective mass allowing controlled light emission tuning from about 3μm to the visible range by decreasing their size, making them attractive candidates for optically active materials in the near-infrared regime. In close-packed film of quantum dots (QDs), energy transfer (ET) between QDs can occur, which is an important process in actual applications. However, the measurements on ET in QD solids have mainly been performed at room-temperature till now. In this work, in order to clarify temperature dependence on ET mechanisms, we investigated temperature-dependent photoluminescence (PL) of PbS QDs in close-packed film without matrix and in polystyrene (PS) film.

PbS QDs were synthesized using an organometallic route previously reported [1]. The samples of PbS QDs in close-packed film and PS film were prepared by drop casting and evaporation in vacuum or nitrogen. The 740 nm beam from a continuous-wave Ti:sapphire laser was used as an excitation source and steady-state PL spectra were measured between 5 K and 300 K. For time-resolved fluorescence measurements, the samples were excited at a repetition rate of 80 kHz by Ti:sapphire laser pulses with 1.5ps pulse width at 740 nm.

The average size of synthesized PbS QDs is about 2.9 nm determined from the first absorption feature. The PL peak of close-packed sample show an obvious redshift compared with that of PS sample. The redshifted emission line is one of the signatures of ET from smaller to larger QDs due to their size distribution in ensemble. However, for the temperature-dependent PL spectra, the integrated PL intensity of close-packed sample increases from 5 to 120 K, then decrease till 300 K, while PS sample keep decreasing from 5 to 300 K as shown in Fig. 1. This difference can be explained by considering a thermally activated ET mechanism. We propose a model involving a trap state to explain the carrier dynamics in the close-packed PbS QD film. Depending on the available thermal energy and the local barrier height, the charge carriers at the trap state may decay to ground state or tunnel to excited state of neighboring larger QDs. This model is supported by time-resolved fluorescence measurements.

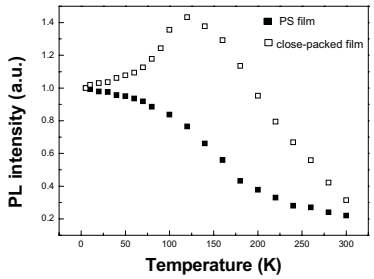

Fig.1 The variation of integrated PL intensities of PbS QDs in PS film (solid squares) and in close-packed film (void squares).

Reference

1. M. A. Hines, and G. D. Scholes, Adv. Mater **15,** 1884 (2003).

InAs/GaNAs strain-compensated quantum dots stacked over 50 layers for use in high-efficiency solar cell

R. Oshima*, A. Takata**, Y. Shoji*, ***, and Y. Okada*,***

* *Research Center for Advanced Science and Technology (RCAST), The University of Tokyo, Tokyo, Japan*

** *Graduate School of Engineering, The University of Tokyo, Tokyo, Japan*

*** *Institute of Applied Physics, University of Tsukuba, Tsukuba, Japan*

Keywords: Quantum dots, Molecular beam epitaxy, Semiconducting III-V materials

Studies on self-assembled quantum dots (QDs) have attracted intense research owing to their potential for significant improvements on the performance of optoelectronic devices. One of the present challenges is to develop a technique to stack the QD structures in order to increase the QDs density. To this end, we previously reported on the growth method to embed each layer of InAs self-organized QDs by a GaNAs strain compensating layer (SCL) in stack configuration. In this work, we report on the structural and optical properties of multiple-stacked InAs/GaNAs QDs on GaAs (001) substrate with up to 50 stacked layers.

All growths were done by atomic hydrogen-assisted RF-molecular beam epitaxy [1]. After the growth of a 300 nm-thick GaAs buffer layer at 580°C, 1.7 ML of InAs QD layer and a 30 nm-thick $GaN_{0.007}As_{0.993}$ SCL were consecutively grown in stack up to 50 multiple cycles at 480 °C on GaAs (001) substrate.

Figure 1 show the STEM image of a part of 50 stacked layers of InAs QD. The mean QD diameter, height, size dispersion in diameter, and sheet density are determined to be 33.8 nm, 6.2 nm, 12.2 %, and 4.4 $\times 10^{10}$ cm^{-2}. No dislocations are observed in the STEM image, which would otherwise be generated if the build-up of lattice strain exceeded the critical limit during stacking [2]. Thus, ultra high density of QDs of 2.2×10^{12} cm^{-2} has been obtained.

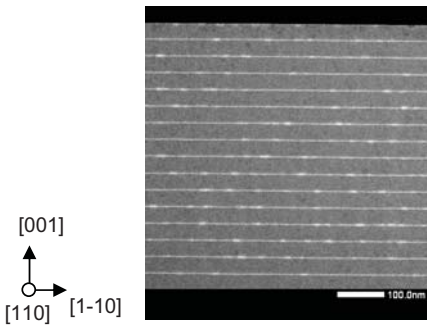

Fig. 1 STEM image of 50 stacked layers of InAs/GaNAs strain-compensated QDs

Figure 2 show the PL spectra for stacked QD samples at 77 K with (a) 10, (b) 30, and (c) 50 layers of stacking, respectively. Almost the same PL peak position observed at 1060 nm with a narrow PL linewidth of ~40 meV indicates that the degradation in homogeneity of QD size has not occurred. Further, PL intensity becomes stronger by increasing the number of stacks which suggests that a good crystalline quality is maintained even after 50 layers of stacking.

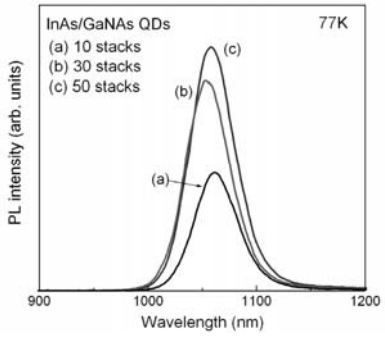

Fig. 2 PL spectra at 77 K for stacked QD samples with (a) 10, (b) 30, and (c) 50 layers of stacking, respectively.

References

[1] R. Oshima *et al*., J. Appl. Phys. **100**, 083110 (2006).
[2] A. Marti *et al*., Appl. Phys. Lett. **90**, 233510 (2007).

Thermal annealing of GaSb quantum dots in GaAs formed by droplet epitaxy

T. Kawazu*, T. Mano*, T. Noda* and H. Sakaki*,**

*National Institute for Materials Science, Tsukuba, Japan

**Toyota Technological Institute, Nagoya, Japan

Keywords: Nanostructures, Quantum dots, Molecular beam epitaxy, Semiconducting III-V materials

10 nm-scale self-assembled quantum dots (QDs) have been the subject of intensive research for more than 15 years due to their importance in physics and device applications. Type-II GaSb QDs in GaAs are quite attractive, as their unique band alignment lead to unique electronic or optical properties. In this work, we investigate effects of annealing on GaSb QDs formed by droplet epitaxy.

GaSb QDs were formed on semi-insulating GaAs (100) substrates by a modified molecular beam epitaxy method. After growing a 300-nm-thick GaAs layer at T_s = 590 ºC, 3.75 mono-layers of Ga atoms were deposited at T_s = 200 ºC to form Ga droplets. Then, Sb_4 molecules were supplied to let Ga droplets react with Sb atoms and also to form a polycrystalline Sb layer on the surface. Then the sample was annealed for 1 minute to remove the excess Sb layer by desorption. Two samples S1, S2 were formed via this annealing step at 340 and 380ºC. GaSb QDs thus formed were embedded by growing a 150 nm-thick GaAs. GaSb QDs were again formed on the surface by repeating the steps identical to those used for buried QDs.

The surface morphology of these samples was studied by atomic force microscope (AFM). Figures 1(a) and 1(b) show their AFM images. On average, GaSb dots on S1 are 60 nm in diameter $\langle d \rangle$ and 7.4 nm in height $\langle h \rangle$, and their density N_{QD} is about 14.3 × 10^9 cm^{-2}, while $\langle d \rangle$ is 74 nm, $\langle h \rangle$ 9.2 nm, and N_{QD} 7.8 × 10^9 cm^{-2} for S2. On average QDs on S2 is larger than those on S1 by about 24 % in length and twice in volume, suggesting that the coalescence of GaSb QDs occurs during the annealing process.

Photoluminescence (PL) measurements were carried out in a closed cycle helium cryostat at 4 K with a frequency doubled Nd:YAG laser. Figure 2 shows the PL spectra of S1 and S2 measured by setting the excitation power density P at about 0.88 W/cm^2. The PL peak of GaSb QDs is observed at about 1.02 eV only for sample S2 annealed at T_s = 380 ºC, indicating that the annealing process plays an important role in forming high quality GaSb QDs.

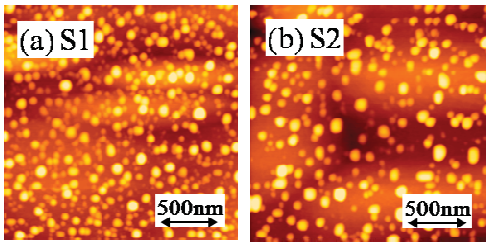

Fig. 1 AFM images (2 μm×2 μm) of GaAs QDs on S1 (a) and S2 (b).

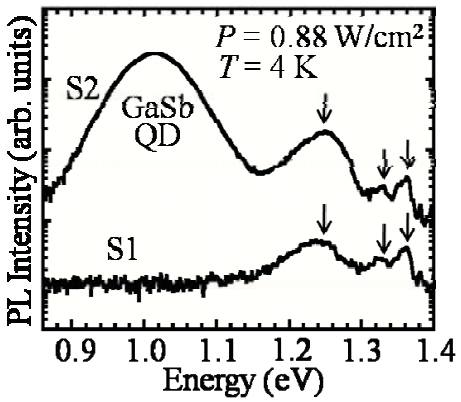

Fig. 2 PL spectra of S1 and S2 at T_s = 4 K, P = 0.88 W/cm^{-2}.

Growth and luminescence characterization of self-assembled InGaAsN/GaPN quantum dots for photonics applications on Si

K. Umeno, R. Noma, Y. Furukawa, S. Mitsuyoshi, H. Okada, A. Wakahara and H. Yonezu

Department of Electrical and Electronic Engineering, Toyohashi University of Technology, Aichi, Japan

Keywords: quantum dots, silicon photonics, dilute nitride semiconductors, molecular beam epitaxy

Novel monolithic optoelectronic integrated circuits (OEICs) will be realized by combining specific features between III-V photonic devices and Si electronic devices. GaP based alloys are key materials to fabricate the OEICs, especially dilute GaPN can be lattice-matched to Si [1]. We already fabricated a dislocation-free GaPN based LED on Si [2]. However, the optical transition of GaPN is similar to indirect one and thus direct-transition materials should be applied to the active layer. When the GaPN is a barrier layer, dilute InGaAsN alloys are extremely suitable for the quantum dot (QD) active layer in the OEICs. In this work, we have investigated the growth and luminescence characterization of self-assembled InGaAsN/GaPN QDs grown by molecular beam epitaxy (MBE).

The multiple stacked $In_{0.5}Ga_{0.5}As(N)/GaP(N)$ QD samples were grown by solid-source MBE on semi-insulating undoped GaP (001) substrates. The growth temperatures of the $In_{0.5}Ga_{0.5}AsN$ QD layer and the 40-nm-thick GaPN or GaP barrier layers were 460 and 500°C, respectively. The N composition of the $In_{0.5}Ga_{0.5}AsN$ was approximately estimated to be 1~2% by the photoluminescence (PL) measurement of InGaAsN/GaAs quantum well samples grown on GaAs (001) substrates with the same growth condition. The QD samples were evaluated by TEM and AFM. PL spectra were measured using a 532-nm solid-state laser.

Fig. 1 shows the cross sectional TEM (XTEM) image for the $In_{0.5}Ga_{0.5}AsN/GaP$ QD sample. The QD density per one QD layer was 8.0×10^{10} cm^{-2}. The average QD height and diameter were estimated to be 4 and 20 nm, respectively. No structural defects were detected by the XTEM observation. Fig. 2 shows temperature dependence of the PL spectra for the $In_{0.5}Ga_{0.5}AsN/GaP$ QD sample. The PL peak photon energy was red-shifted with increasing temperature and clear PL emission was observed up to room temperature (RT). A similar RT PL spectrum was also measured for the $In_{0.5}Ga_{0.5}AsN/GaP_{0.99}N_{0.01}$ QD sample, while we could not detect the PL emission for the $In_{0.5}Ga_{0.5}As/GaP$ QD sample even at 18 K. This result suggests that the N incorporation into the QD layer leads a type-I band alignment and strong quantum confinement since the conduction band offset increases with increasing the N composition.

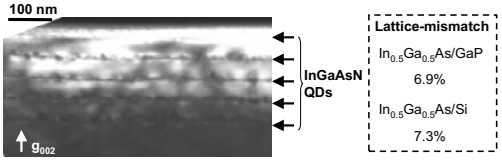

Fig. 1 A dark field XTEM image for the multiple InGaAsN/GaP QD sample stacked up to 5QD layers. The XTEM image was taken along the [1-10] direction under the $\mathbf{g_{002}}$ diffraction condition.

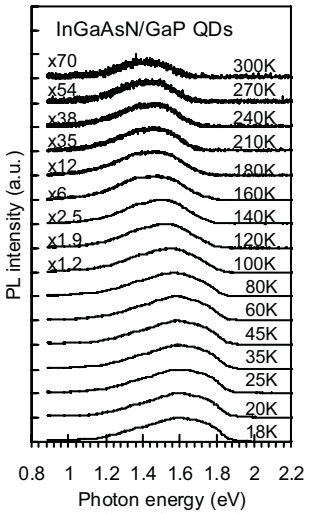

Fig. 2 Temperature dependence of the PL spectra for the multiple InGaAsN/GaP QD sample shown in Fig. 1.

References

1. H. Yonezu, Semicond. Sci. Technol. **17**, 762 (2002).
2. Y. Furukawa, *et al.*, Jpn. J. Appl. Phys. **45**, L920 (2006).

Channel length dependence of Single-walled carbon nanotube multi-functional quantum transistor characteristics

T. Kamimura*, **, ***, and K. Matsumoto*, ***, ****

* *National Institute of Advanced Industrial Science and Technology, Tsukuba, Japan*

** *JSPS, Chiyoda-ku, Japan*

****CREST-JST, Kawaguchi, Japan*

*****ISIR, Osaka University, Ibaraki, Japan*

Keywords: Single-walled carbon nanotube, resonant tunnelling transistor, single-hole transistor, Schottky barrier

The channel length dependence of single-walled carbon nanotube (SWNT) multifunctional quantum transistor characteristics are measured. This transistor can operate as a resonant tunnelling transistor (RTT) and also as a single-hole transistor (SHT). Both devices need tunnelling barriers at both sides of the quantum island. The RTT needs strong coupling while the SHT needs weak coupling between the quantum island and the electrodes. Usually, these tunneling barriers are made from thin oxide layers, etc. Therefore, the thickness of the tunneling barriers and the coupling strength cannot normally be controlled in a given device. In the present device, however, the Schottky barriers act as the tunneling barriers between the SWNT quantum island and electrodes. Therefore, the thickness of the tunneling barriers and the coupling strength between the SWNT and electrodes can be controlled by the applied gate voltage V_G. Fig. 1(a) and 1(b) shows Coulomb diamond characteristic of the SHT mode with 73 nm and 114 nm channel at 6.3 K, and inset shows device diagram. The period of the Coulomb diamonds ($\bullet V_G$) are $\bullet V_G$ = 0.53 V and 0.26 V, respectively. The periods are depending on the channel lengths.

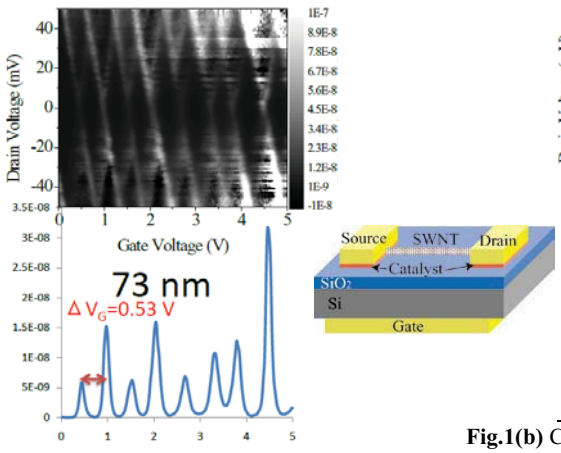

Fig.1(a) Coulomb diamond characteristics of the device with 73 nm channel length and corresponding Coulomb oscillation characteristic. The period of Coulomb diamond is 0.53 V. Inset is the device diagram.

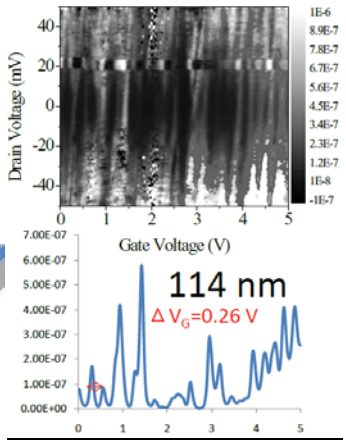

Fig.1(b) Coulomb diamond characteristics of the device with 114 nm channel length and corresponding Coulomb oscillation characteristic.. The period of Coulomb diamond is 0.26 V.

References

1. T. Kamimura, Y. Ohno, and K. Matsumoto, Jpn. J. Appl. Phys. **48,** 015005 (2009).

Doping effect on photocarrier lifetime in InAs quantum dots with strain-relaxed InGaAs barriers grown by molecular beam epitaxy

T. Kitada, A. Mukaijo, T. Takahashi, T. Mukai, K. Morita and T. Isu

Center for Frontier Research of Engineering, Institute of Technology and Science, The University of Tokushima, 2-1 Minami-josanjima-cho, Tokushima 770-8506, Japan

Keywords: photocarrier lifetime, quantum dots, III-V materials, molecular beam epitaxy

An ultrafast all-optical switch operating in the 1.55 μm waveband is one of key devices in the high-bit-rate optical fiber communication system. Recently, we have proposed a planar-type optical Kerr gate switch based on a GaAs/AlAs multilayer cavity with InAs quantum dots (QDs) embedded in strain-relaxed $In_{0.35}Ga_{0.65}As$ barriers. [1] Strong optical Kerr signal could be realized owing to the large optical nonlinearity of the InAs QDs at 1.55 μm and the strong optical field in the multilayer cavity. Moreover, photocarriers generated in the QDs quickly relax into the nonradiative centers arising from the crystal defects related to the lattice-mismatch, [2] which greatly reduces pulse pattern effects under high-bit-rate operation. In this paper, we have investigated doping effect on photocarrier lifetime in self-assembled InAs QDs with strain-relaxed $In_{0.35}Ga_{0.65}As$ barriers grown by molecular beam epitaxy (MBE).

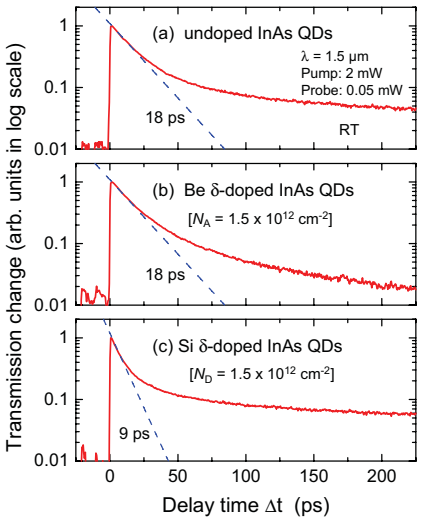

Figure 1: Delay-time dependence of transmission change measured for (a) undoped, (b) Be δ-doped, and (c) Si δ-doped QD samples.

All QD samples were grown on semi-insulating (100) GaAs substrates by a solid-source MBE. After GaAs/AlAs buffer layers were grown at 580°C, 20-nm-thick $In_{0.35}Al_{0.65}As$, 3-nm-thick $In_{0.35}Ga_{0.65}As$ layers, and 3.4 monolayer InAs QDs were grown at 400°C. Relaxation of the lattice-strain was induced in the 20-nm-thick $In_{0.35}Al_{0.65}As$ layer. The average height and density of the QDs were 8 nm and 4×10^{10} cm^{-2}, respectively. Si or Be δ-doping ($\sim 1.5 \times 10^{12}$ cm^{-2}) was performed after the formation of the InAs QDs. The 20-layer stack of the δ-doped QDs separated by 20-nm-thick $In_{0.35}Ga_{0.65}As$ spacers was prepared for optical characterization.

Time-resolved transmission change at $\lambda = 1.5$ μm was measured by a pump-probe method using 0.1 ps pulses with a 100 kHz repetition rate. (Fig. 1) Temporal behavior of the transmission change consists of two decay components. The fast decay observed near $\Delta t = 0$ comes from photocarrier relaxation into the nonradiative centers arising from the crystal defects related to the lattice-strain relaxation. The small component with a slow decay time (a few hundred ps) is attributed to the radiative recombination process in the QDs. Decay time (18 ps) of the fast component of the Be δ-doped QD sample is the same as that of the undoped QD sample, while the slow decay component is rather suppressed by Be δ-doping. This suggests that intentionally doped holes are strongly localized in the radiative QDs. On the other hand, a faster decay time of 9 ps was observed for the Si δ-doped QD sample, suggesting that barrier potential between the QDs and nonradiative centers might be screened by free electrons generated by intentional Si δ-doping.

References

[1] T. Kitada et al., Appl. Phys. Express **1**, 092302 (2008).

[2] T. Kitada et al., to be published in J. Cryst. Growth (2009).

High Performance Multi-Nano-Pillar Vertical MOSFET Scaling from 50nm to 15nm Node

Tetsuo Endoh
Center of Interdisciplinary Research, Tohoku University, Sendai, 980-8578, Japan, JST-CREST

Keywords: Vertical MOSFET, Nano Pillar, Nano Wire, Nano-CMOS

In this paper, the device performance of Multi-Nano-Pillar Vertical MOSFET [1] is numerically analyzed. Multi-Nano-Pillar Vertical MOSFETs are constructed by connecting several Single Vertical MOSFETs [2][3] together in parallel and share a common gate, source, and drain, as shown in Fig. 1.

The device performances of 90nm gate length Multi-Nano-Pillar Vertical MOSFETs with different silicon pillar diameters are analyzed. Fig. 2 shows SEM photograph of fabricated Multi-nano-silicon pillar with diameter of 50nm and height of 280nm.

Fig. 3 shows the driving current characteristics of Multi-Nano-Pillar Vertical MOSFETs with different silicon pillar diameters standardized by the fixed footprint with a 3-D device simulator. The number of silicon pillars inside the Multi-Nano-Pillar Vertical MOSFET can be increased as the design rule of the silicon pillars is scaled down; therefore, the total channel width increases inside the fixed footprint as shown in Fig. 1. This is a unique structural merit of the Multi-Nano-Pillar Vertical MOSFET. Because the total channel width inside the fixed footprint increases as the silicon pillar diameter is scaled down, driving current of the Multi-Nano-Pillar Vertical MOSFET increases by more than about 3 times as the diameter scales down from 50nm to 15nm. Moreover, it is shown the sub threshold characteristics of Multi-Nano-Pillar Vertical MOSFETs. As the silicon pillar diameters are scaled down, the cutoff leakage current of Multi-Nano-Pillar Vertical MOSFETs is suppressed by more than 1/10 even though the total leak pass increases. It is because in Multi-Nano-Pillar Vertical MOSFETs, the gate controllability increases as the silicon pillar diameter is scaled down.

From all, it is shown that by using Multi-Nano-Pillar Vertical MOSFET technology, the performance of CMOS circuits will be drastically improved. Therefore, Multi-Nano-Pillar Vertical MOSFETs can be inferred as one of the key candidate devices for future nano-scale VLSI.

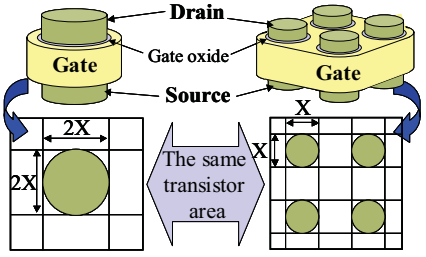

The total channel width becomes two

Fig. 1. Multi-Nano-Pillar Vertical MOSFET with fixed transistor footprint.

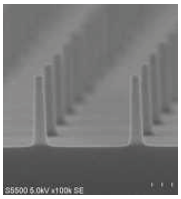

Fig. 2 SEM photograph of fabricated Multi-nano-silicon pillar with of 50nm

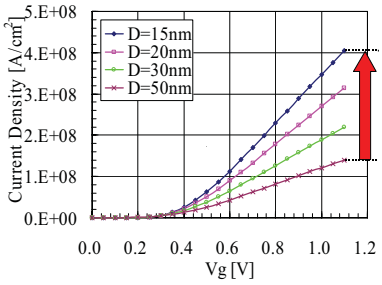

Fig. 3. The Id-Vg Characteristic of M-Vertical MOSFETs standardized by Footprint.

Acknowledgment:

This work was partly supported by JST-CREST (Research of Innovative Material and Process for Creation of Next-generation Electronics Devices).

References

[1] T. Endoh, et al.: IEICE Trans. On ELECTRONICS, Vol. J80-C-II, No. 8, 284-285, August, 1997.
[2] T. Endoh, et al.: IEEE Trans. On ELECTRON DEVICES, Vol. 50, No. 4, 945, April, 2003.
[3] Y. Norifusa, T. Endoh: IMFEDK Technical Digest 2007, 25-26, April, 2007.

Hybrid polymer nanowire based electronic devices: correlated characterization

L. Gence*, V. Callegari**, A. Dinescu***, S. Melinte*, and S. Demoustier-Champagne**

*Lab DICE, Université catholique de Louvain, Louvain-la-Neuve, 1348, Belgium

**Lab Poly, Université catholique de Louvain, Louvain-la-Neuve, 1348, Belgium

***National Institute for R&D in Microtechnologies IMT, Bucharest 077190, Romania

Keywords: PEDOT, Polypyrrole, Nanowires, Electron-beam induced deposition

In the recent years, many studies have been devoted to the structural and electronic characterization of low dimensional materials. Among them, nanowires (NWs) and nanotubes have been intensely scrutinized because of their potential use in various applications requiring miniaturization. Nevertheless, the manipulation and characterization of such single objects are quite challenging. We review our work [1, 2] on the structural and electronic properties of hybrid metal-Polypyrrole(PPy) NWs (40 to 130 nm in diameter) and report on electrical measurements of novel single multisegmented polymer nanowires electrochemically synthesized by the template-based strategy. As an example, the Figs. 1.A and B give the current-voltage ($I-V$) characteristics of tri and four-segmented (Au-PEDOT-Au and Au-PEDOT-PPy-Au) NWs. Interestingly, after an oxidative treatment, the four-segmented NWs exhibit a rectifying behavior. Complex multisegmented nanowires have been characterized using differents contacting techniques. Standard e-beam lithography (Fig. 1.C), dielectrophoretic trapping and electron-beam-induced deposition (EBID) (Fig.1.D) have been used to interrogate single NWs and are thoroughly discussed. It is known that interfaces and morphology greatly affect the transport properties at the nanoscale. The understanding of such complex NWs could be improved by combining the structural characterization with the electrical measurements. In this respect, we designed microdevices to correlate structural (TEM, SEM, atomic force microscopy) and electrical data for single NWs. We show that these devices, fabricated using silicon micromachining techniques, completed with EBID processing offer a unique tool for studying the properties of NWs.

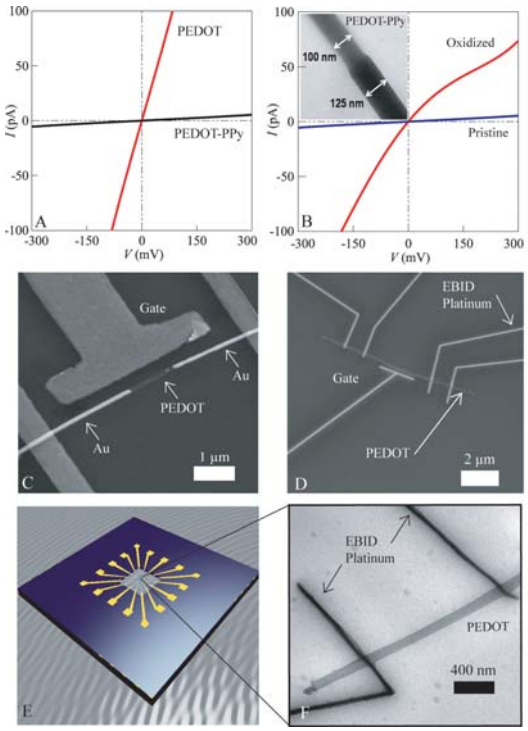

Figure 1: A) $I-V$ curves of Au-PEDOT-Au and Au-PEDOT-PPy-Au nanowires. B) $I-V$ curves of a four-segmented NW as synthesized (blue curve) and after chemical oxidation (red curve). The polymer junction exhibits a diode-like behavior. C) and D) Single PEDOT NWs contacted by different lithographic techniques as revealed by scanning electron microscopy (SEM). E) 3D view of a microdevice for correlated physical characterization and F) Transmission electron microscopy (TEM) of a single PEDOT nanowire contacted by EBID inside a microdevice.

References

[1] L. Gence *et al.*, Phys. Rev. B, **76**, 115415 (2007).

[2] L. Gence *et al.*, Phys. Stat. Sol. (a), **205**, 1447 (2008).

Electrical characterization of multilayered SiC nano-particles for application as tunnel barrier engineered non-volatile memory

Dong Uk Lee*, Eun Kyu Kim*, Goon-Ho Park**,Won-Ju Cho**

* *Quantum-Function Spinics Laboratory and Departments of Physic, Hanyang, University, Seoul, Korea*

** *Department of Electronic Materials Engineering, Kwangwoon University, Seoul, Korea*

Keywords: SiC, non-volatile memory, tunnel barrier

The tunnel oxide thickness has a difficult problem to scale down for the improvement of endurance and charge retention properties of the non-volatile memory. Also, the nano-floating gate memory applications require the tunnel barrier to have relatively low applied voltage for long retention time and fast speed [1]. Generally, the single layered Si or metal nano-crystals are creating the quantum well between control and tunnel oxide layers by their work function difference. To improve the density of charge to use non-volatile memory, we have been proposed the structure of nano-floating gate memory with multilayered SiC nano-particles [2].

The nano-floating gate capacitors with SiC nano-particles were fabricated on *p*-type Si substrate. Structure and thickness of the barrier engineered tunnel layer were $SiO_2/Si_3N_4/SiO_2$ (ONO) and 2 nm/ 2 nm/ 3nm, respectively. Subsequently, the SiC layer on the tunnel layer with a thickness of 8 nm was deposited by using sputtering at room temperature. The additional SiO_2 layer with a thickness of 50 nm was deposited at 300 ^oC. After post-annealing at 900 ^oC for 3 min under N_2 gas, the multilayered SiC nano-particles created in the additional SiO_2 layer as shown in Fig. 1. The average size of SiC nano-particle was about 5 nm. After this process, the control oxide layer with 20-nm-thickness was deposited. Finally, the Al gate electrode of 150-nm-thickness was evaporated by using thermal evaporator system

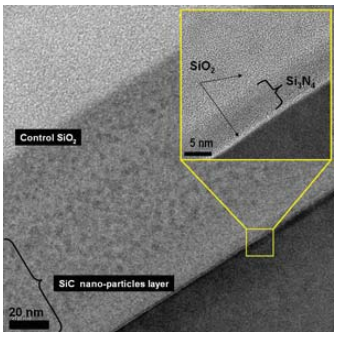

Fig.1 Cross-sectional TEM of multilayered SiC nano-particles with ONO tunnel barrier.

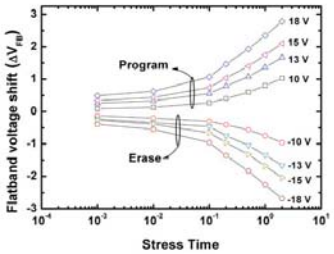

Fig.2 Flatband voltage shifts of the multilayered SiC nano-floating gate capacitor with ONO tunnel barrier as function of applied program/erase voltages and pulse times

Figure 2 shows program/erase speed of the nano-floating gate capacitor with the multilayered SiC nano-particles with ONO tunnel barrier as function of applied voltages. The flatband voltage shifts was about 1 V at 10 ms after applied at ±13V.

In this study, we characterized the electrical properties and discussed the reliability of the nano-floating gate capacitors, which have the charge stored quantum structure by multilayered SiC nano-particles and the tunnel barrier engineered layer.

References

1. K. K. Likharev, Appl. Phys. Lett. **73**, 2137 (1998)
2. T. H. Lee, D. U. Lee, S. P. Kim, and E. K. Kim, Jpn, J. Appl. Phys. **47**, 4992 (2008).

Optical signatures of neutral and charged excitons in inorganic semiconducting nanotubes

D. Kammerlander[1,2], G. Ferrari[1,3], F. Troiani[1], and G. Goldoni[1,2]

[1] *CNR-INFM Research Center for nanoStructures and bioSystems at Surfaces (S3), Via Campi 213/A, 41100 Modena, Italy*

[2] *Dipartimento di Fisica, Università di Modena e Reggio Emilia, Via Campi 213/A, 41000 Modena, Italy*

[3] *CNISM Research Unit of Modena, 41100 Modena, Italy*

Keywords: optical excitation, nanotube, trion.

Among emerging nanostructures with innovative design, inorganic semiconductor nanotubes (NT), where electronic states are confined in a shell with a cylindrical symmetry, stand for their applications, e.g., in phase-based electronic devices. These may be obtained, e.g., from the multi-layer overgrowth of a free-standing nanowire [1] or from the strain-induced wrapping of a conventional quantum well [2].

In this work we present theoretical predictions of the optical properties of semiconducting, hollow NT by use of exact diagonalization of the electron-hole interaction. In particular we investigate the stability and spectral signatures of neutral excitons and singly charged excitons (trions) confined in a hollow cylinder as a function of tube radius for a broad range of semiconducting materials. We include the possibly strong dielectric modulation of the material by an exact Green's function of the Poisson equation for a cylindrical shell. In this way we take the screening properties of the core (either vacuum or a semiconducting material), the semiconducting confining layer, and the environment into account. We found, in particular, that the stability of trions depends on the sign of its charge, the material through the electron hole mass ratio, and the diameter of the tube. Stable triplet states are found for positively charged excitons for all kind of tubes (see Fig. 1), while negative triplet states are unstable for several materials. With small tube diameter these latter states are most stable for tubes with a dielectric core. We will also discuss how the discrete symmetry of the core, as in core multi-shell nanowires, may affect the optical properties of the system.

References

[1] A. Fontcuberta i Morral et al., small, **4**, 899 (2008).

[2] O. G. Schmidt et al., Nature **410**, 168 (2001).

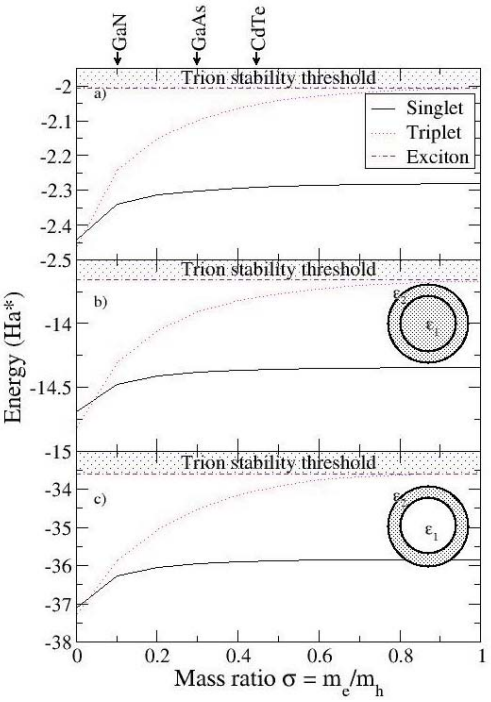

Figure 1: Energy of positively charged excitons confined in a cylindrical shell as a function of the electron hole mass ratio. Results are reported for cylinders with diameter $d = 1a_B^*$; a_B^* being the exciton Bohr radius. Calculations were done for three different dielectric configurations: a homogeneously distributed dielectric constant (a)), a filled cylinder with vacuum outside (b)) and a hollow cylinder with vacuum outside its shell (c)). The energy is found to be dependent on the dielectric configuration: the less screening, the lower the energy. The triplet state depends in all cases strongly on the mass ratio.

Large optical Kerr signal of GaAs/AlAs multilayer cavity with InAs quantum dots embedded in strain-relaxed barriers

K. Morita, T. Takahashi, T. Kanbara, S. Yano, T. Mukai, T. Kitada and T. Isu

Center for Frontier Research of Engineering, Institute of Technology and Science,
The University of Tokushima, 2-1 Minami-jyosanjima-cho, Tokushima, 770-8506, Japan

Keywords: Optical Kerr effect, GaAs/AlAs multilayer cavity structures, self-assemble InAs quantum dots

All-optical Kerr switches using the semiconductor multilayer cavity structures are one of the promising devices for optical communications. In the structure, an internal optical filed of the cavity mode is strongly enhanced in the cavity layer, which results in the large optical Kerr signal intensity. We have shown that the signal intensity of the cavity mode is expected to be extremely enhanced when a strong nonlinear material is inserted only in the $\lambda/2$ cavity layer [1]. To realize the high-bit rate optical switches with the large signal, InAs quantum dots (QDs) with a fast carrier relaxation are one of the strong candidates for the material in the $\lambda/2$ cavity layer [1]. Recently, we have successfully grown the self-assemble InAs QDs embedded in the strain-relaxed barriers and demonstrated the fast carrier relaxation time (~ 18 ps) [2]. In this work, GaAs/AlAs multilayer cavity which includes the self-assemble InAs QDs embedded in the strain-relaxed barriers for the $\lambda/2$ layer (InAs QDs cavity) was fabricated, and the ultrafst response of optical Kerr signal was demonstrated at 1.5μm range. GaAs/AlAs multilayer cavity which includes the $\lambda/2$ GaAs layer (GaAs cavity) was also measured and the optical Kerr signal enhancement of the InAs QDs cavity was evaluated.

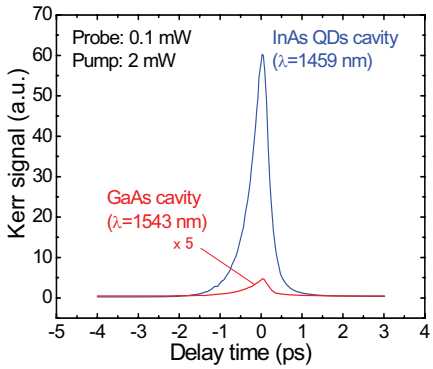

Fig.1 The optical Kerr signals for the InAs QDs cavity and GaAs cavity.

The samples were grown by molecular beam epitaxy on GaAs(001) substrates, and $\lambda/2$ layer which consists of 2 layers of self-assemble InAs QDs and InGaAs strain-relaxed barriers were inserted in the 26 pairs of GaAs(111 nm)/AlAs(130 nm) multilayer. Time-resolved Kerr signals were measured by a cross-Nikol configuration using 100 fs pulses with 100 kHz reputation rate. The spectral width of pulse was ~35 nm and the wavelength was tuned at the center of each cavity mode. Figure 1 shows temporal profiles of the optical Kerr signals for the InAs QDs cavity and the GaAs cavity. The strong optical Kerr signals were observed for the both cavities, and the response time-widths (< 1 ps) of the optical Kerr signals were restricted to the photon life-time of the each cavity. Although only two InAs QDs layers were inserted in the $\lambda/2$ layer, the optical Kerr signal intensity of the InAs QDs cavity was about 60 times larger than that of the GaAs cavity at $\Delta t = 0$. We also observed the large transmittance change due to the saturable absorption in the presence of the excited pump pulse for the InAs QDs cavity. This assures us that the large optical Kerr signal of InAs QDs cavity come from the strong cavity effect and the large optical nonlinearity of the resonant InAs QDs in the $\lambda/2$ cavity layer.

References

1. T. Kitada *et al.*, Appl. Phys. Express **1**, 092302 (2008).
2. T. Kitada *et al.*, to be published in J. Cryst. Growth (2009).

Polarization anisotropy of dynamic quantum wires formed by surface acoustic waves

T. Sogawa, H. Sanada, H. Gotoh, H. Yamaguchi, S. Miyashita*, and P. V. Santos**

NTT Basic Research Laboratories, NTT Corporation, Japan

** NTT Advanced Technology Corporation, Japan*

*** Paul Drude Institute, Germany*

Keywords: surface acoustic wave, dynamic quantum wire, polarization anisotropy

Recently, dynamic quantum dots [1] and dynamic quantum wires (DQRs) [2,3] formed by the spatial modulation of the piezoelectric potential and strain induced by surface acoustic waves (SAWs) have attracted much attention from the view point of low-dimensional physics and their device application. In this study, we investigate the dynamic polarization anisotropy of photoluminescence (PL) properties in GaAs/AlAs DQRs formed by SAWs.

SAWs were generated by inter-digital transducers formed on high-quality GaAs/AlAs quantum wells with various well thicknesses. Mode-locked pulses (1.5 ps, 82 MHz, 720 nm) from a Ti-sapphire laser synchronized with the SAW frequency of 820 MHz were used to photo-generate carriers. Low-temperature (4 K) spatial-resolved PL spectra were measured using a micro-PL setup with a spatial resolution of about 1-2 μm. Figures 1(a) and (b) show spectra for the polarization averaged PL, ($I_{[1\text{-}10]} + I_{[110]}$), and the PL degree of polarization $\rho=(I_{[1\text{-}10]} - I_{[110]})/ (I_{[1\text{-}10]} + I_{[110]})$, respectively, measured while scanning the laser spot along the [1-10] direction. Here, the PL component polarized along the [1-10] ([110]) direction is denoted by $I_{[1\text{-}10]}$ ($I_{[110]}$). Figures 1(a) and (b) clearly show that the PL intensities and transition energies as well as ρ periodically change in space due to the SAW-induced modulation of the band structure. In addition, ρ exhibits opposite signs between the lower- and higher-energy sides of each PL emission, as shown in Fig. 1(b), where the transition energies in the absence of SAW are indicated by arrows. Figures 2(a) and (b) show time-resolved PL and ρ spectra measured by a streak camera, respectively, demonstrating that the PL polarization changes in time. These spatially dependent and electrically-controlled polarization properties are unique features of the dynamically-modulated structures.

References

1. F. Alsina, et al., Solid State Commun. **129**, 453 (2004).
2. T. Sogawa, et al., Phys. Rev. B**63**, 121307(R) (2001).
3. P. V. Santos, et al., Phys. Rev. B**69**, 155318 (2004).

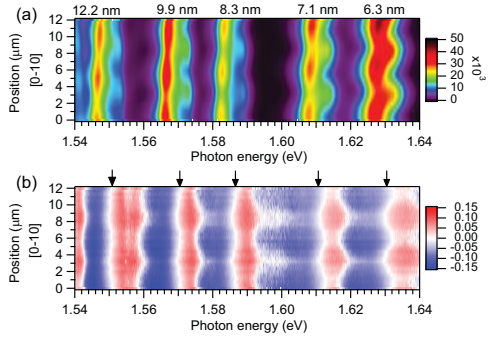

Fig. 1 (a) Spatially-resolved PL spectra for DQRs, and (b) degree of polarization.

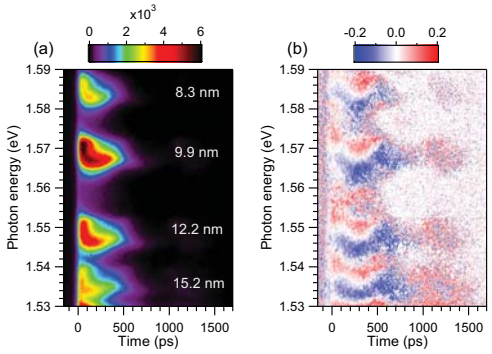

Fig. 2 (a) Time-resolved PL spectra for DQRs, and (b) degree of polarization.

Suppression of non-radiative recombination up to room-temperature in long-lived GaN/AlN quantum dots

J. Renard, H. Mariette, E. Monroy and B. Gayral

CEA-CNRS "Nanophysique et semiconducteur" group, CEA-Grenoble, INAC/SP2M

17 rue des Martyrs, 38054 Grenoble, France

Keywords: quantum dots, GaN, time-resolved photoluminescence

One of the advantages of quantum dots (QDs) over quantum wells (QWs) for light emission applications is the fact that three-dimensional confinement hinders carrier diffusion towards non-radiative recombination centers. This is especially important for low crystalline quality materials such as III-N. Indeed a QD-like localization behavior probably explains the high luminescence efficiency of InGaN/GaN QWs, despite the high dislocation density.

Regarding GaN/AlN heterostructures, it is known that due to the large spontaneous and piezo-electric polarization discontinuities, low-temperature (T = 4 K) photoluminescence (PL) decay times can reach very high values, up to 200 µs for 4 nm high QDs [1]. These long decays already prove that non-radiative recombination is not an efficient relaxation mechanism at low temperature. One might then wonder how the non-radiative decay rates evolve with temperature in such heterostructures. Due to the very large band offsets between GaN and AlN, non-radiative recombination should not occur for carriers trapped inside such QDs even at room temperature, but this statement has not been demonstrated so far.

In this work, we present temperature-dependent time-resolved PL measurements of GaN/AlN QD superlattices emitting in the 350-460 nm range. The samples were grown by plasma-assisted MBE on AlN-on-sapphire templates. At T = 4 K, we observe decay times in the range of 10 to 600 ns, depending on the QD size. When raising the temperature, we found that the PL decay curves show no evolution between 4 K and 300 K (see Fig. 1 for the largest QDs). As a comparison, in the case of GaN/AlN QWs emitting in the same wavelength range, the onset of non-radiative recombination is observed at much lower temperature (typically around 100 K) in time-resolved PL.

From this experiment, we conclude that non-radiative recombination in GaN/AlN QDs remains negligible up to room-temperature: for instance, a lower limit of 5 µs can be estimated for the non-radiative recombination time from the data presented in figure 1. Moreover, the stability of the decay curves demonstrates that thermalization towards excited states of the QDs does not affect the radiative recombination time, which is dominated by the electron-hole overlap along the growth axis.

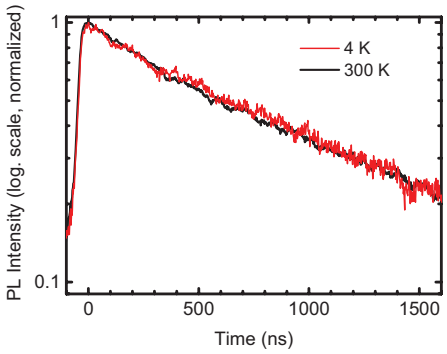

Fig.1 Photoluminescence decay for GaN/AlN QDs emitting around 460 nm, at 4 K and room temperature.

These results are the first demonstration of the suppression of non-radiative recombination in GaN QDs at room temperature, thanks to efficient carrier localization.

References

1. T. Bretagnon *et al.*, Phys. Rev. B **73**, 113304 (2006)

Hydrogenic impurity states in zinc-blende InGaN/GaN cylindrical quantum-well wires

Hailong Wang *, Liming Jiang *, Huiting Wu *, Qian Gong** and Songlin Feng**

* *College of Physics and Engineering, Qufu Normal University, Qufu, P.R. China*

** *Key laboratory of wireless sensor network & communication, Shanghai Institute of Micro-system and Information Technology, Chinese Academy of Sciences, Shanghai, P.R. China*

Keywords: InGaN/GaN, Quantum-well wire; Hydrogenic impurity; external electric field

The wide-band-gap zinc-blende (ZB) InGaN/GaN material system has attracted increasing attention for potential application on high-temperature and/or high-power electronic devices. It has been recognized that the built-in electric field is absent in the ZB InGaN/GaN quantum heterostructures. Impurity states play a very important role in the semiconductor optoelectronic devices. Without impurities, there would be no diode, no transistor, or any semiconductor science and technology. Research on the electronic structure properties of quantum-well wires (QWWs) under the external electric field can provide useful information on the potential application of semiconductor QWWs.

In the framework of effective-mass envelope-function approximation theory, calculations of electronic states usually adopt the variational method. A uniform method to study the electronic states of a hydrogenic donor impurity in semiconductor nano-structures in the framework of effective-mass envelope-function theory using the plane wave basis has been proposed [1]. The method can be widely applied in the calculation of the electronic states of hydrogenic donor impurities in nano-structures of various shapes and can easily be extended to study the effects of external fields and other complex cases. In the previous, we have calculated the electronic structure properties of quantum dots (QDs) using this method [2,3].

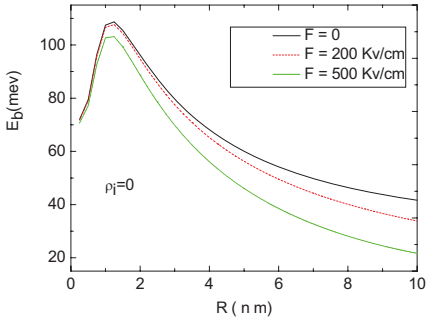

Fig.1 Binding energy E_b of hydrogenic impurities in positions $\rho_i = 0$ as a function of the radius R of ZB $In_{0.2}Ga_{0.8}N/GaN$ cylindrical QWWs..

In this paper, we calculate the binding energy of the hydrogenic impurity in ZB InGaN/GaN QWWs in the framework of effective-mass envelope-function theory using the plane wave method. It is shown that the donor binding energy is highly dependent on the impurity position, the radius of QWWs and the external electric field. In addition, the Stark shift of the binding energy is also calculated. We hope that our calculation results are helpful for further investigations of the physics and device applications of group-III nitrides.

References

1. S.S. Li and J.B. Xia, Phys. Lett. A 366, 120 (2007)
2. H.T. Wu, H.L. Wang, L.M. Jiang, Q. Gong and S. L. Feng, Physica B 404, 122 (2009)
3. L.M. Jiang, H.L. Wang , H.T. WU, Q. Gong and S. L. Feng, Chin. Phys. Lett. 25, 3017 (2008)

Photoluminescence of trions in quantum dots: the dominant role of valence band correlations

J.I.Climente[1,2], A. Bertoni[2] and G. Goldoni[2,3]

[1] *Departament de Química Física i Analítica, Universitat Jaume I, Castello, Spain*
[2] *CNR-INFM research center for nanoStructures and bioSystems at Surfaces, Modena, Italy*
[3] *Dipartimento di Fisica, Università di Modena e Reggio E., Modena, Italy*

Keywords: quantum dots, charged excitons, correlation, valence states

Singly-charged excitons – trions – show spectral signatures which can be easily resolved, or may even the dominant ones, among inter-band excitations in quantum nanostructures. Being the result of delicate cancellations between competing attractive electron (e) – hole (h) interactions and repulsive e-e or h-h interactions, their spectral signatures (position and intensity) with respect to, e.g., the corresponding neutral excitonic states, expose direct informations on the Coulomb forces of the system. In semiconductor quantum dots (QDs), trions are involved in important applications such as the optical preparation of pure spin electrons or holes, and are the natural source of single photons with pure circular polarization. Despite their importance, the spectral properties of trions have been less investigated and understood than those of the corresponding neutral excitations.

Here we discuss recent theoretical predictions for trion energetics and radiative recombination rates in semiconductor QDs, from the strong to the weak confinement regime, i.e., where Coulomb interactions are dominating. Using a Full Configuration-Interaction approach we treat exactly Coulomb interactions within an envelope function description of the electronic states, and we evaluate energy and recombination rates of positively ($1e$+$2h$, X^+) and negatively ($2e$+$1h$, X^-) charged excitons for different classes of samples, representing different correlation regimes. We show that in the weak confinement regime the enhanced PL of neutral excitons (X^0) is partially quenched for X^- and completely suppressed

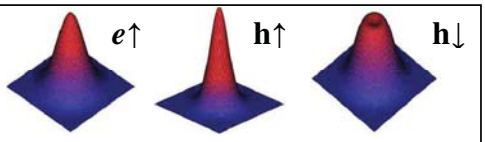

Charge density of particles constituting the trion complex X^+. The hole with antiparallel spin exhibits a dip at the electron position, indicating strong hole correlation and quenched radiative recombination, which does not happen for X^-.

for X^+, which is traced to the strong h-h correlations[1] (see figure). Indeed, recent[2] observed spectral features in self-assembled structures can only be explained with significant correlations in the valence states[3]. We also show that correlations in the valence band may show up as a peculiar temperature dependence of satellite X^+ lines, which differentiates the spectral signatures of X^+, X^- and X^0.

We also investigate different confining regimes, to study the effect of asymmetric e and h confinement lengths on the PL spectrum. We show that this e-h asymmetry brings about qualitative changes in both the relative spectral position and recombination rates confirmed by recent measurements[4].

References

1. J.I. Climente, A. Bertoni, G. Goldoni, Phys. Rev. B **78**, 155316 (2008)
2. P. A. Dalgarno *et al*., Phys. Rev. B **77**, 245311 (2008)
3. M. Ediger *et al*, Nature Phys. **3**, 774 (2007)
4. M.-F. Tsai *et al*, Phys. Rev. Lett. **101**, 267402 (2008)

Surface recombination processes of GaN crystallites

T. Okuhata*, T. Sakka*, S. Taguchi*, A. A. Yamaguchi** and T. Honda*

** Department of Electrical Engineering and Electronics, Graduate School of Engineering, Kogakuin University, Tokyo, Japan*

*** Research Laboratory for Integrated Technological System, Kanazawa Institute of Technology, Tokyo, Japan*

Keywords: GaN, crystallites, surface recombination, photoluminescence

Nano-scale GaN-based structures, such as quantum dots, nano columns, have much attention for the application to light-emitting devices[1]. These structures have a larger surface/volume (S/V) ratio than their bulks or epilayers. In particular, a crystal structure of conventional GaN-based materials is hexagonal; whose low symmetry causes spontaneous polarization along the c-axis. This symmetry also causes Piezo-electric polarization in the case of the strain conditions[2]. Those electric fields enhance the surface recombination in the C-planes of GaN-based materials. It is predicted that the surface recombination in the C-planes. In this paper, the effect of the surface recombination rate for the photoluminescence (PL) is discussed. The reduction of the surface recombination using the surface coating for GaN crystallites is also discussed.

Three types of GaN were prepared. The first was a thick (~300 μm) GaN layer grown by HVPE. The second was GaN pieces, which were formed by the cleaving of GaN crystals grown by HVPE. The third was GaN crystallites fabricated by the reaction of Ga metal and ammonia. The crystallites were annealed in vacuum and were wet-etched using an HCl solution. The GaN pieces and crystallites were deposited on the Si substrates by the sedimentation technique[3]. Time-resolved PL was measured at the temperature of 4 K and 300 K. The time-resolved measurements were performed by the time-correlated single-photon counting technique[4]. The excitation wavelengths were 355 nm, and the excitation power density was about 300 W/cm^2.

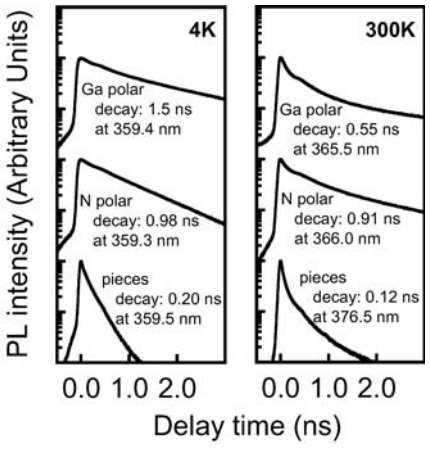

Fig.1 Time-resolved PL measurements of GaN single crystal and pieces.

The PL intensity decays of GaN epilayers and pieces around the bandedge emission are shown in Fig.1. Because the crystalline qualities of the pieces were almost equal to those of the epilayers, the results indicate that the increase of S/V ratio leads to the increase of the surface recombination. The decay time of GaN crystallites showed same tendencies.

The surface coating is one of the techniques to reduce the surface recombination. Thus, gallium-oxide coating for the GaN crystallites were performed. Those decay time was recovered, which indicates the reduction of surface recombination. This is due to the reduction of carrier diffusion into the surface by formatting the gallium-oxide blocking layer or the introduction of strain by the formation of the oxide layer.

References

1. H. Sekiguchi, K. Kishino, A. Kikuchi, APEX, **1**, 124002 (2008).
2. R. Katayama, K. Onabe, H. Yaguchi, T. Matsushita and T. Kondo, Appl. Phys. Lett. **91**, 061917 (2007).
3. M. Akiyama, S. Egawa, K. Matsukawa, T. Honda and H. Kawanishi, J. Vac. Sci. Technol. B**22**, 2201 (2004).
4 A. A. Yamaguchi, M. Mochizuki, M. Mizuta, Jpn. J. Appl. Phys. **39**, 2402 (2000).

Electric-field-tunable electronic properties of graphene quantum dots

R. B. Chen*,C. P. Chang**, and , M. F. Lin***
*Center of General Studies, National Kaohsiung Marine University, Kaohsiung, Taiwan
**Center of General Education, Tainan University of Technology, Tainan, Taiwan
***Department of Physics, National Cheng Kung University, Tainan, Taiwan

Keywords: graphene, quantum dot

Electric-field-tunable low-energy electronic properties of $(\mathrm{N_a}, \mathrm{N_z})$ zero-dimensional finite-sized graphene quantum dot (GQD) are investigated by employing the tight-binding model. $(\mathrm{N_a}, \mathrm{N_z})$ is used to denote the dimer and zigzag lines along the x and y axis, respectively. The electric field (F) will change state energies, alter energy gaps, and induce energy gap modulations. State energies and energy spacings vary significantly with the field strength and direction. State energies oscillate significantly with the field strength. Their oscillating amplitude and period are modified by the alteration of field direction. Such a characteristic results from the spatial anisotropy of the graphene quantum dot. Moreover, The electric-field-tunable electronic properties will be directly revealed in the density of states (DOS). The numbers and frequencies of peaks in DOS are strongly dependent on the field strength and direction.

An $(\mathrm{N_a} = 13, \mathrm{N_z} = 8)$ finite-sized graphene quantum dot is chosen for a model study. Its geometrical structure is shown in Fig.1 (a). Now, an electric field **F** parallel to the plane is applied to a GQD. It simply adds an electric potential $= -e\mathbf{F} \bullet \mathbf{r}$ to the site energy of a carbon atom[1, 2]. The Hamiltonian equation of the system is $= \sum_{i,j} {}_i(\mathbf{F})\ {}^{+}_{i}\ {}_i + {}_0\ {}^{+}_{i}\ {}_j$, where ${}^{+}_{i}$ (${}_j$) is the creation (annihilation) operator, which creates (annihilates) an electron at i ( ) sites. ${}_0 = 2\,598$ eV is a hopping integral[1]. Electric-field-tunable electronic properties of the $(\mathrm{N_a} = 13, \mathrm{N_z} = 8)$ GQD are shown in Fig.1 (b). They are tunable and controlled not only by the field strength[3] but also by the field direction. The electronic properties of the $(\mathrm{N_a}, \mathrm{N_z})$ GQD varying with the field strength and direction will be intensively examined.

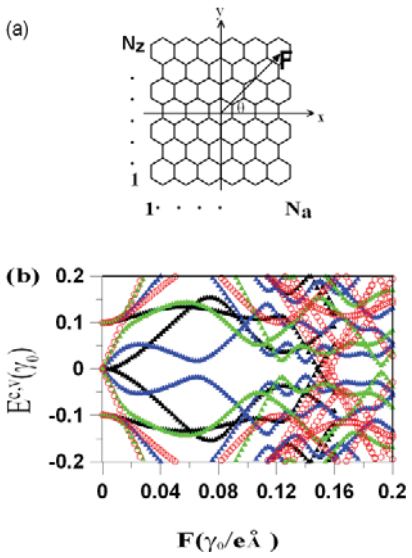

Figure 1: (a) The geometrical structure of $(\mathrm{N_a} = 13, \mathrm{N_z} = 8)$ finite-sized graphene quantum dot. The angle represents the direction of the electric field. (b) The state energies vs. electric fields at $= 0^o$, 30^o, 60^o, and 90^o are shown in black, blue, green, and red dots, respectively.

References

[1] C. P. Chang, Y. C. Huang, C. L. Lu, J. H. Ho, T. S. Li, and M. F. Lin, Carbon **44**, 508 (2006).

[2] Y. C. Huang, C. P. Chang, and M. F. Lin, J. of Appl. Phys. **104**, 104, 103714 (2008).

[3] T. S. Li, S. C. Chang, Y. C. Chuang, Kelan H. J. Wu, and M. F. Lin, Physica B: Physics of Condensed Matter, **404**, 305 (2009).

Strain fields and transition energies for single and vertically stacked InAs/GaAs semiconductor quantum dots

K. B. Hong*, M. K. Kuo* and T. R. Lin**

* *Institute of Applied Mechanics, National Taiwan University, Taipei, Taiwan*

** *Department of Mechanical & Mechatronic Engineering, National Taiwan Ocean University, Keelung, Taiwan*

Keywords: Semiconductor quantum dots, InAs/GaAs, induced strain, optoelectronic transition energy

This study analyzes the strain fields and transition energies of single and vertically stacked InAs/GaAs semiconductor quantum dots based on the linear elasticity theory and strain-dependent $\boldsymbol{k}\cdot\boldsymbol{p}$ theory, respectively, using finite element methods [1]. The three-dimensional steady-state effective-mass Schrödinger equation is then modified by incorporating the effects of strain fields into the carrier confinement potential. Effective mass also depends on strained semiconductor bandgap. The calculated results show that the hydrostatic strain is negative within the InAs quantum dots while the biaxial strain is positive. The biaxial strain is smallest in the middle part of the fivefold-stacked quantum dots. The transition energies of single and fivefold-stacked quantum dots with 30-nm thick GaAs spacer are in excellent agreements with previous experimental photoluminescence studies [2, 3]. Numerical results also suggest that transition energy decreases as the GaAs spacer thickness increases.

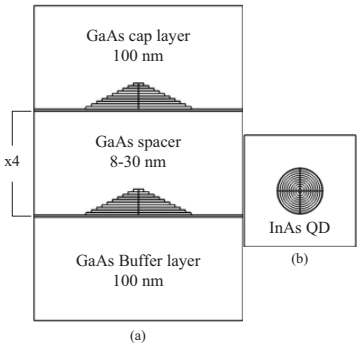

Fig.1 Geometry of fivefold-stacked InAs quantum dots: (a) side view, and (b) top view.

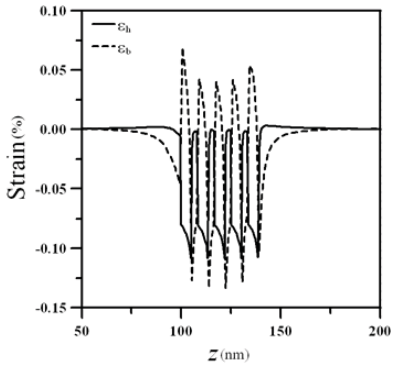

Fig.2 Hydrostatic and biaxial strains plotted along the z-axis.

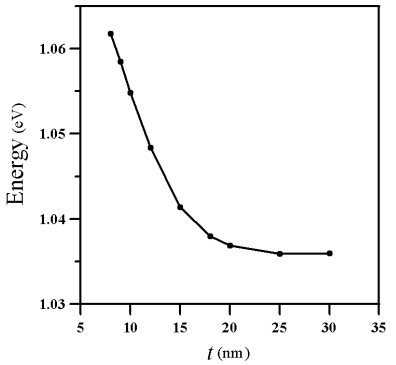

Fig.3 Transition energies as function of GaAs spacer thickness *t*.

References

1. M. K. Kuo, T. R. Lin and K. B. Hong, J. Appl. Phys. **103**, 073705 (2008).

2. Y. Lee, J. D. Song, J. M. Kim, K. S. Chang, Y. T. Lee and T. W. Kim, Mater. Res. Bull. **39**, 135 (2004).

3. J. S. Kim, J. Cryst. Growth **290**, 384 (2006).

Sensitive detection of photoexcited carriers by resonant tunnelling through a single quantum dot

E.E. Vdovin[*,**], O. Makarovsky[*], L. Eaves[*], Yu.N. Khanin[**], A. Patanè[*]

** School of Physics and Astronomy, The University of Nottingham, Nottingham NG7 2RD, UK*

***Institute of Microelectronics Technology RAS, 142432 Chernogolovka, Russia*

Keywords: quantum dots, resonant tunnelling, photoexcitation, InAs

We show that the tunnel current through a single quantum dot (QD) is very sensitive to photoexcited holes that are bound in the vicinity of the dot. These holes can fully open/close the current carrying channel, an effect which has potential for charge-sensitive photon counting detectors [1].

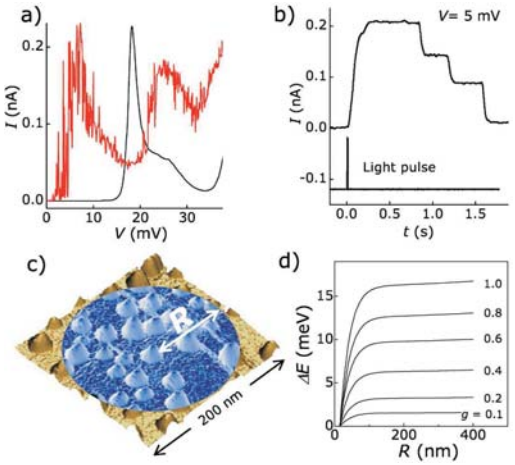

Fig. 1 a) $I(V)$ curve at T = 4.2 K in the dark (black) and under illumination (red) with laser light (λ = 660 nm). b) Time-dependence of the current following photoexcitation with a light pulse. c) STM image of InAs QDs. The circle highlights an area of radius R=100 nm. d) Calculated shift, ΔE, of the energy level of an empty dot versus R for different values of the occupancy, g, of the dots with photoexcited holes.

In our diode, a layer of self-assembled InAs QDs is incorporated in an (AlGa)As tunnel barrier and gives rise to an ensemble of discrete states through which electrons can tunnel, thus leading to sharp peaks in the current-voltage curves $I(V)$. Here we focus on a resonance in $I(V)$ due to tunneling of electrons into the energy level of a single QD. As shown in Fig. 1a, with light illumination, the QD resonance shifts to lower bias. This shift is accompanied by step-like transitions in the current between two or more discrete values, an effect generally referred to as telegraph noise. The current can be reset to its initial "dark" value by applying a short negative bias reset-pulse. The response of the tunnel current to illumination is further illustrated in Fig. 1b. Following excitation of the diode with a short (<10 ms) light pulse, the current increases to its peak value and then falls to zero, through multiple-steps over time intervals of about 0.1s.

To explain these data, we model the effect on the tunnel current of a random distribution of photoexcited holes bound by QDs. We find that the presence of holes adjacent to an empty dot (<100 nm) can shift the QD energy level by several meV (Fig.1c-d). In turns, this provides a means of fully opening/closing the current channel with a very high on/off ratio (>50/1), Fig. 1b. This photoresponse differs from that reported in previous studies [2-3], where the capture of photoexcited carriers on QDs gives rise to small step-like changes (<1%) in the conductivity of a two-dimensional electron gas [2] or in the resonant tunnelling current through the quantum well of a tunnel diode [3]. In our devices, we exploit the tunnel current through a single QD to achieve a much higher level of sensitivity (>1000%).

References

1. EE Vodvin et al., submitted to Nature Phys. (2009).
2. EJ Gansen et al., Nature Photonics **1** 585 (2007).
3. JC Blakesley et al., Phys.Rev.Lett.**94** 067401 (2005).

Luminescence from InAs/GaAs surface related states

K. Fukui and I. Kamiya

Toyota Technological Institute, Nagoya 468-8511, Japan

Keywords: Surface, photoluminescence, InAs quantum dot, InAs wetting layer

Recent reports showed evidence for surfaces and interfaces inducing drastic changes in the optoelectronic properties of semiconductor nanocrystals (NCs) [1, 2]. While such results are expected to lead to tune the properties of nanostructures through surface modifications, detailed analysis is prevented due to the difficulties encountered in determining the surface conditions on the NCs. Therefore, crystals grown in ultra-high vacuum (UHV), where well-defined surfaces can be readily prepared, are adopted in this study.

Here, InAs/GaAs surface QDs (SQDs) were prepared by molecular beam epitaxy (MBE) to discuss electronic state distribution and carrier dynamics through inference for the relaxation and excitation processes. Following growth of 100 nm-thick GaAs buffer layer on s.i.-GaAs(001) substrate at 590°C at a rate of 0.47 ML/s, SQDs were formed by depositing 1.7 ML InAs at 480°C at a rate of 0.014 ML/s.

Photoluminescence (PL) measurements were performed using Ti:sapphire laser with an optical power density of 8 W/cm^2 as an excitation source on liquid nitrogen-cooled samples (77 K).

PL spectra of SQDs, measured at excitation wavelengths (λ_{ex}) of 800 nm (solid line) and 835 nm (dashed line), are shown in Fig.1 (a). When λ_{ex} is 800 nm, an emission is observed at 1260 nm, which is attributed to InAs SQDs whose peak is redshifted from the buried QDs as reported in ref. 3. When λ_{ex} is 835 nm, emission peaks appear at 910 nm, 990 nm, and 1100 nm. The peaks at 910 nm and 1100 nm are attributed to copper impurity and defects/impurities in GaAs after previous report [4] and measurement on a GaAs reference sample, respectively. Distinguished from other electronic states, e.g. defects/impurities in GaAs, quantized states in InAs, and GaAs defects induced by InAs growth [5, 6], the origin of the 990 nm peak is attributed to InAs QD surface related-state (SRS).

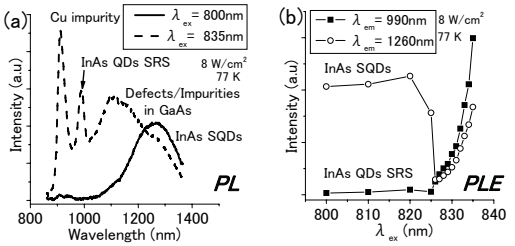

Fig.1 PL spectra recorded at λ_{ex} 800 nm (solid line) and 835 nm (dashed line) (a), and PLE spectra obtained by detecting at 990 nm (solid square) and 1260 nm (open circle) (b).

Photoluminescence excitation (PLE) spectra of SRS and InAs SQDs, detected at emission wavelengths (λ_{em}) of 990 nm and 1260 nm, are shown in Fig.1 (b). As λ_{ex} exceeds 825 nm, corresponding to the GaAs bandgap, SRS emission rises drastically, while the emission from InAs SQDs sharply declines. It is suggested that the emission intensity of InAs SQDs strongly depends on the absorption in GaAs, while SRS emission is almost independent of absorption in GaAs indicating lack of carrier transfer between InAs SQDs and SRS. Hence, SRS emission is considered to be enhanced by the direct excitation and relaxation processes through SRS.

We will also report results of temperature and excitation intensity dependent PL and PLE measurements. The energetic distribution of SRS will be discussed together with the excitation-relaxation processes.

References

1. C. B. Murray, *et al*., J. Am. Chem. Soc. **115**, 8706 (1993).
2. S. Hong, and T. Ha, J. Am. Chem. Soc. **126**, 1324 (2004).
3. H. Saito, *et al*., Appl. Phys. Lett. **73**, 2742 (1998).
4. B. Monemar, *et al*., Phys. Rev. B **31**, 7919 (1985).
5. S. W. Lin, *et al*., Phys. Rev. B **72**, 165302 (2005).
6. M. Kaniewska, *et al*., Mater. Sci. Engineer. C **26**, 871 (2006).

Structural transition of InP nanowires in selective-area metalorganic vapor phase epitaxy

Yusuke Kitauchi[1], Katsuhiro Tomioka[1,2], Yasunori Kobayashi[1], Shinjiro Hara[1,2], Takashi Fukui[1,2], and Junichi Motohisa[1]

[1]*Graduate School of Information Science and Technology, Hokkaido University,*

[2]*Research Center for Integrated Quantum Electronics, Hokkaido University,*

North 14, West 9, Sapporo 060-0814, Japan, e-mail: motohisa@ist.hokudai.ac.jp

Keywords: nanowire, selective-area epitaxy, crystal structure, photoluminescence

InP-based nanowires (NWs) are promising for photonic devices because their band gap energy is compatible with optical fiber telecommunication. So far, most of the NWs are grown by catalyst-assisted vapor liquid solid (VLS) growth method, and crystal structures and properties of InP NWs are discussed rather controversially, for instance, whether they take zincblende (ZB) or wurtzite (WZ) crystal structures[1, 2]. On the other hand, we have reported that InP NWs grown by catalyst-free selective-area metalorganic vapor phase epitaxy (SA-MOVPE) exhibit WZ structures[3]. Recently, control of crystal structures by doping in InP NWs are reported in VLS growth mode[4]. In this report, we show that the SA-MOVPE grown InP NWs exhibits structural and crystallographic transitions depending on the growth conditions.

Growth of III-V NWs by SA-MOVPE is reported in previous publications[3, 5]. For InP NWs, we started with InP (111)A substrates partially covered with SiO_2 mask. The mask had periodic array of holes and their opening pitch was changed from 0.5 μm to 3 μm. The diameter of holes was about 100 nm. InP NWs were grown with trimethylindium (TMIn) and tertiarybutylphosphine (TBP) as source materials. The partial pressure of TMIn was 4.4×10^{-6} atm and that of TBP was changed from 8.1×10^{-5} to 2.4×10^{-4} atm, giving V/III ratio between 18 and 55. The growth temperature T_g was varied from 570°C to 660°C.

Uniform array of NWs with hexagonal cross sections were grown at two distinctive growth conditions, and they exhibited completely different shapes. For low V/III ratio and high T_g (V/III=18 and T_g=660°C, growth condition A), the edges of the hexagons were parallel to the $\langle 211 \rangle$ direction of the ZB InP substrate. Since this growth condition was similar to that for WZ NWs as previously reported[3], we concluded that WZ NWs with $\{1\bar{1}00\}$ facets were formed. Formation of WZ crystal structure was confirmed by cross-sectional transmission electron microscopy (TEM) and by low-temperature photoluminescence (PL) measurement, where the PL peak was blue-shifted as compared to ZB InP by about 83 meV[6, 7]. It is also noted that the thickness of the NWs was almost equal to the size of mask opening but with small tapering. In contrast, we observed thicker, shorter, and untapered hexagonal NWs with $\{\bar{1}10\}$ facet sidewalls at higher V/III ratio and lower T_g (V/III=55 and T_g=600°C, growth condition B). TEM study revealed that the crystal structures were ZB with stacking faults, and the stacking faults were introduced by every few monolayers in average. In addition, PL peak energy form NWs was the same as that of InP substrates.

Such transition of the crystal structure has not been observed in other SA-MOVPE grown NWs and only in InP which has the largest ionicity among other conventional III-V semiconductors. Therefore, it is considered that InP favors WZ stacking more due to stronger Coulomb interaction between the second-nearest pair of In and P atoms. Based on this assumption, we will explain the crystallographic transition at the conference.

References

[1] M. Mattila *et. al.*, Appl. Phys. Lett. **90**, 033101 (2007).

[2] A. Mishra, *et. al.*, Appl. Phys. Lett. **91**, 263104 (2007).

[3] P. Mohan *et. al.*, Nanotechnology **16**, 2903 (2005).

[4] R. E. Algra *et. al.*, Nature **456**, 369 (2008).

[5] J. Motohisa *et. al.*, J. Cryst. Growt **272**, 180 (2004).

[6] Y. Kobayashi *et. al.*, Physica E. **40**, 2204 (2008).

[7] M. Murayama and T. Nakayama, Phys. Rev. **B 49**, 4710 (1994).

Atomistic theory of electronic and optical properties of self-assembled quantum dots

M. Korkusinski*, M. Zielinski*, E. Kadantsev*, and P. Hawrylak*

* *Institute for Microstructural Sciences, National Research Council of Canada, Ottawa, Canada K1A0R6*

Keywords: self-assembled quantum dot, electronic and optical properties, e-e interaction

Self-assembled quantum dots involve millions of atoms and their electronic properties cannot at present be computed using ab-initio methods, such as, e.g., GW-BSE approach [1]. One of the approximate methods, VFF-tb-CI discussed here, involves three steps [2,3]: (a) calculation of equilibrium position of constituent atoms using valence force field model (VFF), (b) calculation of quasi-electron and quasi-hole states (equivalent to the GW step) using a linear combination of atomic orbitals approach in a tight binding approximation (tb), and (c) inclusion of the effect of final state interactions by defining an effective Hamiltonian of interacting excited quasi-particles, solved using the configuration interaction method (CI). The approximate nature of such an approach requires careful analysis of results, and in particular an analysis of sensitivity of results to approximations taken. Benefits include predictive capability allowing us to understand the dependence on size, geometry, composition, and external electric and magnetic fields of the electronic and optical properties of self-assembled quantum dots (SADs).

In this paper we present new results of the VFF-tb-CI methodology applied to InAs/GaAs SADs, with convergent strain distribution computed using the VFF approach for 100s of millions of atoms, the electron and hole single-particle states computed using the 20-band sp3d5s* tight-binding model for millions of atoms, and energies, states and emission spectra from up to ten multiexciton complexes obtained in the configuration-interaction method.

In the VFF calculation we use the Keating model with material parameters derived from bulk elastic constants c_{ij}[4]. The tb parameters for unstrained InAs and GaAs are obtained by fitting of the tb bulk band edges and effective masses to those obtained in experiment or by ab-initio calculations, with the valence band offset (VBO) built into the parameter set [3]. The dependence of band edges on lattice deformation computed using DFT [5] is used to find strain corrections to tb parameters. We generate two sets of parameters corresponding to two DFT results predicting opposite behavior of the valence band edge. The Coulomb matrix elements for CI are obtained with tb wave functions involving ~10^8 orbitals, with onsite and nearest-neighbor terms computed by approximating the tb basis with Slater orbitals. The interactions are screened by a distance-dependent dielectric function. In the CI step, typically ~10^4 configurations are used as a basis for each multiexciton system, while emission spectra are calculated from Fermi's Golden Rule.

We illustrate the method by computing the electronic and optical properties of a lens-shaped and an Indium-flushed (disk-shaped) SAD. We find that in both cases the quasielectron states are organized in degenerate shells, a result independent of the VBO and strain parameters. The quasihole states are sensitive to these constants and reveal a shell structure only for the Indium-flushed dot. We study the signatures of this sensitivity in multiexciton emission spectra. In particular, we focus on the dependence of the fine structure of s- and p-shell multi-exciton spectra on the structure and geometry of the sample.

References

1. C. Spataru et al., Phys. Rev. Lett. **92,** 077402 (2004).
2. M. Korkusinski et al., J. Appl. Phys. (in press); W. Sheng, et al., Phys. Rev. **B71**, 035316 (2005).
3. G. Klimeck et al., Superlatt. Microstruct. **27,** 519 (2000).
4. C. Pryor et al., J. Appl. Phys. **83,** 2548 (1998).
5. S. Wei and A. Zunger, Phys. Rev. B **60, 5**404 (1999).

Resonant enhancement of excitonic photoluminescence via biexciton process in stacked InAs quantum dots

M. Mamizuka*, O. Kojima*, T. Kita*, O. Wada*, and K. Akahane**

* *Department of Electrical and Electronics, Graduate School of Engineering, Kobe University, Kobe, Japan*

** *National Institute of Information and Communications Technology, Tokyo, Japan*

Keywords: Quantum dot, Solar cell, Multiple exciton generation, Biexciton.

Quantum dots (QDs) are attracting strong interests to realize solar cells with high conversion efficiency beyond the Shockley-Queisser limit, where we can expect multiband effects and the multiple exciton generation (MEG) process originated from the low dimensionality [1]. Recently, we demonstrated interconnecting behavour along vertically aligned QD chains in highly stacked InAs QD layers [2] fabricated by the strain compensation technique [3]. Such high density QDs are necessary in order to increase the conversion efficiency [4]. Moreover, the MEG process in QDs promises a further dramatic nonlinear enhancement of the conversion efficiency. A key factor of the MEG processes is the generation of biexcitons. In this work, we have investigated the contribution of the biexciton process to the excitonic photoluminescence (PL) in high density stacked InAs QDs.

We used two samples of InAs self-assembled QDs with 30 layers grown on an InP (311)B substrate by molecular beam epitaxy using the strain compensation technique [3]. The spacer layer thicknesses d in between the QD layers are 20 and 40 nm. In PL excitation (PLE) measurements, the excitation light was produced by combination of a 100-W halogen lamp and a 7-cm single monochromator. The signal was detected at the PL peak energy. At all excitation energies, the excitation photon numbers were kept constant.

Figure 1 shows the PLE spectrum in the d=20 nm sample at 5 K. The closed circles indicate the experimental result and the solid curve is a guide for eyes to see change in the PL intensity. The bottom abscissa is normalized by the typical exciton energy of 0.87 eV. The PL intensity reaches a peak at ~1.8 eV. This resonant energy almost corresponds to twice the typical exciton energy. In the d=40 nm sample, on the other hand, PL intensity has been found to show a peak at ~1.9 eV corresponding to twice the typical exciton energy (0.94 eV) of this QDs. Since the resonant photon energy shows the dependence on the own exciton energy, these PL enhancement can be attributed to the biexciton relaxation process. However, the direct one-photon excitation of the biexciton state is forbidden. Therefore, we need to consider "virtual biexciton" [5]. The resonant PL enhancement implies the MEG via the biexciton states in stacked InAs QDs.

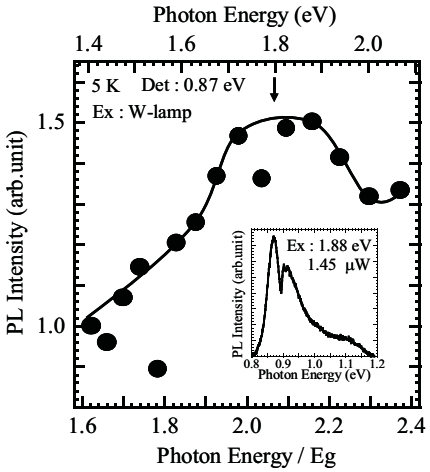

Fig.1 The PLE spectra and the PL spectra in the stacked QDs at 5 K.

References

1. R. D. Schaller and V. I. Klimov, Phys. Rev. Lett., **92**, 186601 (2004). 2. K. Akahane *et al*., J. Cryst. Growth, **245**, 31 (2002). 3. O. Kojima *et al*., J. Appl. Phys., **103**, 113504 (2008). 4. R. Oshima, A. Takata, and Y. Okada, Appl. Phys. Lett., **93**, 083111 (2008). 5. V. I. Rupasov and V. I. Klimov, Phys. Rev. B, **76**, 125321 (2007).

Spectral diffusion of type-II excitons in InP/InAs/InP core-multishell nanowires

Yasuaki Masumoto*, Ken Goto, Bipul Pal, Michio Ikezawa,

Institute of Physics, University of Tsukuba, Tsukuba 305-8571, Japan

Premila Mohan, Junichi Motohisa, and Takashi Fukui

Research Center for Integrated Quantum Electronics, Hokkaido University, Sapporo 060-8628, Japan

Keywords: InP/InAs/InP core-multishell nanowire, type-II exciton, Spectral diffusion

We study type-II exciton dynamics in wurtzite InP/InAs/InP core-multishell nanowires composed of two-dimensional quantum wells (QW) and one-dimensional quantum wires (QWR) by using time- and spectrally-resolved photoluminescence (PL), PL excitation (PLE) and single wire spectroscopy. The PL spectrum of the structures contains bands of type-II excitons consisting of holes in the InAs ultrathin, strained inner shell and electrons in the InP core and the InP outer shell [1]. PL and PLE spectra of the nanowires are composed of multiple bands due to monolayer (ML) scale variation in the InAs layer thickness. Carrier diffusion between regions of different ML thickness is evident from the PLE spectra. Large Stokes shift between PL and PLE spectra and slow decay of PL with a decay time tail of 100 ns indicates a type-II band lineup. Single wire spectroscopy confirms that inhomogeneous broadening exists even in a single wire and that PL is linearly polarized in perpendicular to the wire axis in consistent with the wurtzite crystal structure. Inhomogeneous broadening arises in a wire due to short range interface roughness at the interface. Disorder induced potential fluctuation causes localization of type-II excitons in both QW and QWR. Time- and spectrally-resolved PL is shown in Fig.1 together with the time-dependent average energy of type-II excitons. Constant energy-loss rate is 2×10^6 eV/s at the initial stage, in rough agreement with that of the type-I excitons in GaAs QW [2,3]. The time-dependent redshift of PL is interpreted as slow spectral diffusion of type-II excitons due to acoustic-phonon-assisted relaxation of excitons between the localized states within the inhomogeneous broadening. Time-dependent energy-loss shows a clear kink at 1.3ns indicated by an arrow and its rate is slowed down by an order of magnitude later. Critical slowing down of energy-loss rate is ascribed to crossover from spectral diffusion of type-II excitons in two-dimensional QW to that in one-dimensional QWR.

References

1. B. Pal, K. Goto, M. Ikezawa, Y. Masumoto, P. Mohan, J. Motohisa, and T. Fukui: Appl. Phys. Lett. **93** 073105 (2008).

2. Y. Masumoto, S. Shionoya, and H. Kawaguchi: Phys. Rev. B **29**, 2324 (1984).

3. Y. Masumoto, S. Shionoya, and H. Okamoto: Proc. 17th Int. Conf. on the Physics of Semiconductors (San Francisco, 1984), p.349.

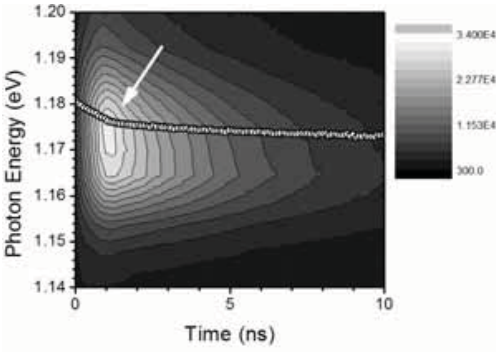

Fig.1 A contour map of time- and spectrally-resolved photoluminescence of InP/InAs/InP core-multishell nanowires. The average energy is shown by circles.

Magnetotransport in MBE-grown III-V nanowires

E. Storace*, J. Weis* and K. v. Klitzing*
S. De Franceschi**,***
F. Jabeen***, S. Rubini***, F. Capotondi***, and F. Martelli***
**Max-Planck-Institut für Festkörperforschung , Heisenbergstrasse 1, D-70569 Stuttgart, Germany*
*** CEA, INAC/SPSMS/LaTEQS, 17 Rue des Martyrs, 38054 Grenoble, France*
****Laboratorio Nazionale TASC-INFM-CNR, Area Science Park, S.S. 14, km. 163.5, I-34012 Trieste, Italy*

Keywords: Nanowires, InAs, GaAs, Magnetotransport

In recent years the number of methods which can be used for the fabrication of nano-scaled devices has increased with demand for smaller structures.
At present, we have performed a first magneto - electrical characterization of different types of III-V semiconductor nanowires (NWs) grown via vapor-liquid-solid method, where the gaseous semiconductor reactants are generated by Molecular Beam Epitaxy (MBE) technique from solid targets [1], [2].
Firstly, we focused on Indium Arsenide (InAs) NW systems that, due to their combination of material properties, present themselves as optimal candidates for addressing two challenges that triggered a wide interest among many research groups: further development of semiconductor transistors and of spintronic devices. We observed that in 20-nm thick InAs NWs low-temperature electron transport is dominated by Coulomb Blockade effect. For sufficiently small separation between the source and drain electrodes (100 nm), the nanowires behave as single quantum dots with typical charging energies of 10 meV and comparable level spacing.
Secondly, we investigated Beryllium doped Gallium Arsenide (Be-GaAs) NWs grown using either Manganese or Gold as catalyzer. The choice of such a material was aiming towards the development of ferromagnetic semiconductors for spin-electronic devices by introducing magnetic elements into nonmagnetic semiconductors. These type of materials, also known in literature as diluted magnetic semiconductors, are characterized by the fact that their magnetic properties are driven by the spin-exchange interactions between the magnetic ions and the free holes.

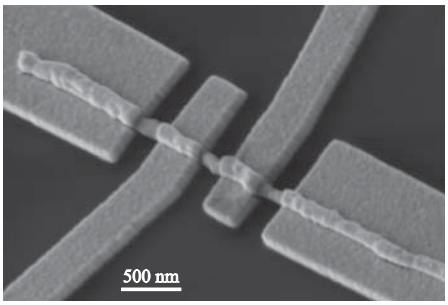

Figure 1: Scanning Electron Microscope image of a typical Be doped Mn-GaAs NW system.

The Be doped GaAs NWs have a diameter ranging from 50 nm to 150 nm and they are contacted in a four-terminal configuration (300 nm distance between adjacent contacts). The four-terminal resistance of the NWs has been measured as a function of the temperature T. Several transport regimes arise in a highly reproducible manner for different devices, interpreted by us as related to different scattering mechanisms: phonon scattering for high T, impurity scattering for intermediate T and weak antilocalization for temperatures below 60 K, as indicated by a pronounced positive magnetoresistance.
In summary, we succeeded in defining and characterizing extremely small InAs NW systems and in tuning the spin-orbit coupling in GaAs NW systems by acting on its temperature.

References

[1] F. Martelli *et al.*, Nano Lett. **6**, 2130 (2006).
[2] M. Piccin *et al.*, Physica E **37**, 134 (2007).

Photocurrent-spectroscopy of CdSe quantum dot photodiodes

M. Panfilova, S. Michaelis de Vasconcellos, A. Pawlis, K. Lischka and A. Zrenner

Department of Physics, University of Paderborn, Paderborn, Germany

Keywords: Photodiode, CdSe quantum dots, photocurrent, Stark effect

Semiconductor quantum dots (QD) receive a lot of attention in applied and fundamental research on nanoscale systems due to their unique properties. If a QD is resonantly excited it can be treated as a two level system that has applications in quantum information technology such as single photon sources and detectors [1-3]. The integration of QDs in the active region of a photodiode (PD) plays thereby an important role. First single QD PDs were realized with III–V semiconductors [4]. However, these III–V based devices are limited to low temperatures. Alternatively, in CdSe QDs, the Coulomb correlation energy is about 10 times higher as compared to typical III-V systems [5]. This enhancement will be essential for PD applications at higher temperatures. Furthermore, coherent manipulations of III–V QD systems are typically limited to excitations with ps-laser pulses due to the small biexciton binding energy. The advantage of CdSe QDs results therefore from the possibility, that 100 fs laser pulses can be used for coherent manipulations, without introducing significant interaction between exciton and biexciton states.

In this contribution we report about investigations on CdSe/ZnSe QDs incorporated into n-i-Schottky PDs. Figure 1 shows a schematic view of a PD with an e-beam written shadow mask and a semitransparent Schottky contact for optical access to single CdSe QDs. We observed a leakage current in our diodes in the order of some pA up to sufficiently high reverse bias voltages at room temperature. Our photoelectrical measurements on a resonantly excited ensemble of QDs clearly reveal the expected photocurrent from the QDs. The photocurrent form GaAs is thereby negligible due to the band offset in the valence band as shown schematically in the band diagram in Figure 2. By tuning the excitation wavelength to the spectral absorption of a single QD and applying sufficiently a high reverse bias voltage, the photocurrent of a single QD is monitored at T=5K.

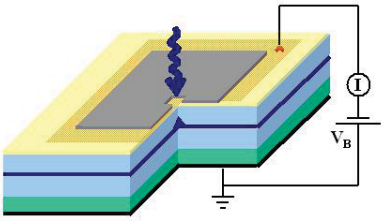

Fig.1 Schematic view of a n-i-Schottky diode with shadow mask for optical access to single CdSe QDs.

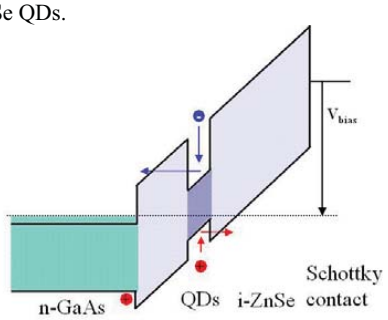

Fig.2 Schematic band diagram of a single QD Schottky PD for photocurrent experiments.

References

1. D. Bouwmeester, A. Ekert, A. Zeilinger, The Physics of Quantum Information, Springer, Berlin, 2000.

2. P. Michler, A. Kiraz, C. Becher, W.V. Schoenfeld, P.M. Petroff, L. Zhang, et al., Science **290**, 2282 (2000).

3. R.M. Stevenson, R.J. Young, P. Atkinson, K. Cooper, D.A. Ritchie, A.J. Shields, Nature (London) **439**, 179 (2006).

4. A. Zrenner, E. Beham, S. Stufler, F. Findeis, M. Bichler, and G. Abstreiter, Nature **418**, 612 (2002).

5. S. Michaelis de Vasconcellos, A. Pawlis, C. Arens, M. Panfilova, A. Zrenner, D. Schikora, and K. Lischka, Microelectronic J. **40**, 215 (2008)

$ZnO/Mg_{0.2}Zn_{0.8}O$ Coaxial Nanorod Heterostructures for High Performance Electronic Nanodevice Applications

Chul-Ho Lee*, Jinkyoung Yoo*, Yong-Joo Doh* and Gyu-Chul Yi**

** Department of Materials Science and Engineering, POSTECH, Pohang, Gyeongbuk 790-784, Republic of Korea*

*** National Creative Research Initiative Center for Semiconductor Nanorods, Department of Physics and Astronomy, Seoul National University, Seoul 151-747, Korea*

Keywords: ZnO, MgZnO, metal oxide nanostructure, electronic device

Tremendous demand has arisen for fabrication of field effect transistors (FETs) with high carrier mobility, large current on/off ratio, and small subthreshold swing for transparent electronic nanodevice applications. The bottom-up method to use metal oxide nanostructures has recently demonstrated the ability to exploit nanostructures as building blocks for transparent device applications.

In particular, high-quality ZnO nanorods have been employed for fabricating FETs [1] and logic gates [2]. The device characteristics of ZnO nanorod FETs are significantly enhanced by passivating the ZnO surfaces with an insulating polymer [1] and inorganic dielectric layers because the high-density surface states of metal oxide nanostructures cause hysteresis in the electrical characteristics and reduce minority carrier lifetime. However, significantly better device performance is expected with the use of heteroepitaxial $ZnO/Mg_{1-x}Zn_xO$ coaxial nanorod heterostructures. Here, we report on fabrication and device characteristics of FETs based on heteroepitaxial $ZnO/Mg_{0.2}Zn_{0.8}O$ coaxial nanorod heterostructures.

As shown in Fig. 1, excellent electrical characteristics of the coaxial nanorod heterostructure FETs were observed [3]. As compared to bare ZnO nanorod FETs, coaxial nanorod heterostructure FETs exhibited the enhanced mobility of 110 cm^2/Vs. In addition, coaxial nanorod heterostructure FETs exhibited remarkably small subthreshold swing (S) value of 200 mV/dec at room temperature, which is in contrast with much larger value of 1900 mV/dec for bare nanorod FETs. Also notable in the I_{ds}–V_g characteristic curves for coaxial nanorod FETs was negligible hysteresis even at room temperature.

Such desirable behavior by an oxide coaxial nanorod heterostructure device was mainly attributable to both *in-situ* surface passivation and carrier confinement effects through the heteroepitaxial growth of a lattice-matched $Mg_{0.2}Zn_{0.8}O$ shell layer with a wider band gap than ZnO nanorods. Furthermore, these oxide coaxial nanorod heterostructures would greatly increase the versatility and power of building blocks for the fabrication of numerous electrical nanodevices based on the oxide heterostructures.

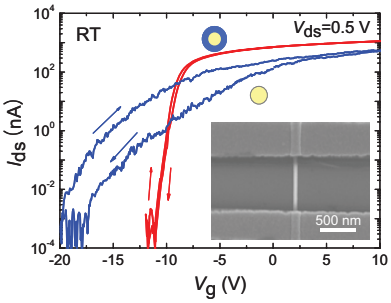

Fig.1 Semi-log plot of transfer characteristics of both bare and coaxial nanorod heterostructure FETs at room temperature. (Inset) A FE-SEM image of a device.

References

1. W. I. Park, J. S. Kim, G.-C. Yi, M. H. Bae, and H.-J. Lee, Appl. Phys. Lett. **85**, 5052 (2004).
2. W. I. Park, J. S. Kim, G.-C. Yi, and H.-J. Lee, Adv. Mater. **17**, 1393 (2005).
3. C.-H. Lee, J. Yoo, Y.-J. Doh, and G.-C. Yi, Appl. Phys. Lett. **94**, 043504 (2009).

Electron transport in gated InGaAs/InP and InAsP/InP quantum well ridge structures fabricated by nanotemplate technology

G. Granger, S. A. Studenikin, A. S. Sachrajda,

A. Kam, P. J. Poole, G. C. Aers, and R. L. Williams

Institute for Microstructural Sciences, National Research Council, Ottawa, Canada

Keywords: Transport, Nanotemplates, InAsP, InGaAs

Electron transport properties of gated 2DEG ribbon-like wires made of $In_xGa_{1-x}As$ and $InAs_xP_{1-x}$ quantum wells inserted in InP ridge structures have been investigated. These structures are grown by chemical beam epitaxy on pre-patterned InP substrates [1].

The long term objective of this work is to develop a new material system for making quantum dot electronic circuits for quantum information applications. Compared to GaAs/AlGaAs structures, the potential advantages of the studied material systems are the large values for the effective electron g*-factor and the spin-orbit interaction that make them attractive for fast spin qubit devices.

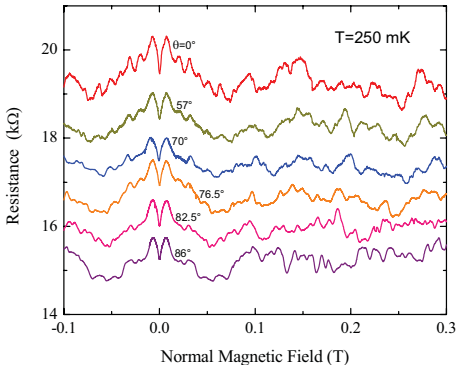

Fig.1 Example of mesoscopic oscillations in an InGaAs wire of 0.5 µm width as a function of normal magnetic field for different tilts.

To optimize the growth and fabrication processes, we first explore the contact resistance, electron density, and mobility of the wires as a function of the wire width and growth parameters. The electron mobility reaches values of up to 100,000 cm^2/Vs comparable to planar InGaAs/InP 2DEG structures. Therefore, ridges are suitable for the fabrication of quantum dot structures.

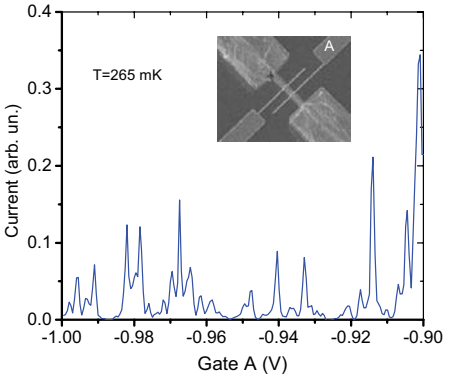

Fig.2 Example of Coulomb blockade oscillations through a quantum dot formed in a ridge shown in the inset.

Next, based on electrostatic modelling of the potential profile, we fabricate gated ridge structures with top finger gates. Preliminary measurements exhibit good gating and pinch-off characteristics.

At temperatures down to 250 mK, the ridge structures reveal mesoscopic conductance fluctuations (Fig. 1) which change in tilted magnetic field possibly due to spin effects. Using the finger gates, the wires can be split to form a quantum dot detected as Coulomb blockade peaks in transport measurements (Fig. 2). Charging and magnetotransport characteristics will be discussed in detail.

References

1. P. J. Poole, G. C. Aers, A. Kam, D. Dalacu, S. Studenikin, and R. L. Williams, J. Crystal Growth 310, 1069-1074 (2008).

Evidence of different doping modes in tapered VLS nanowires by studying axial distribution of carrier concentration in Si-doped InAs nanowires

Guoqiang Zhang, Kouta Tateno, Satoru Suzuki, Hideki Gotoh, and Hidetoshi Nakano
NTT Basic Research Laboratories, NTT Corporation, 3-1 Morinosato-Wakamiya, Atsugi, 243-0198, Japan

Keywords: nanowire, carrier concentration, InAs, field effect transistor

Semiconductor nanowires (NWs) are expected to play an important role as functional device elements in nanoscale devices. Particle-seeded method via the vapor-liquid-solid (VLS) [1] mode has been widely used for the growth of NWs [2]. These NWs normally have a tapering shape and this is believed to be mainly induced by growth of the core part in VLS mode and vapor phase epitaxy (VPE) growth on NW sidewalls (see Fig. 1a) [3]. Due to the different growth modes of VLS and VPE, doping atoms may have different incorporation ways. However, up to now there is no study about the doping distribution induced by different growth mechanisms. Here, we show the evidence of different doping modes in tapered VLS NWs grown by studying axial distribution of carrier concentration in Si-doped InAs NWs.

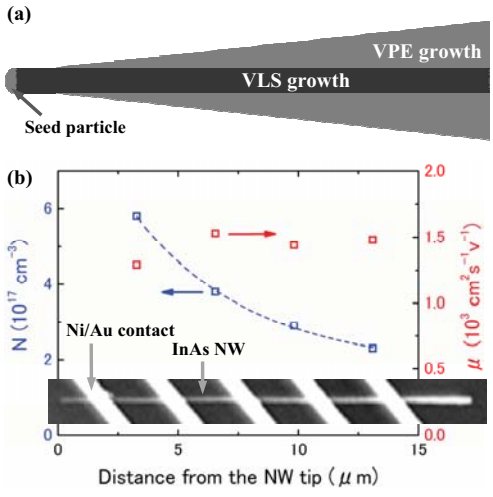

Fig. 1 (a) Schematic diagram of a tapered NW including VLS and VPE growth parts. (b) N and μ as a function of the distance from the NW tip. The inset is a SEM image of InAs:Si NW FET with five electrode contacts. The four NW segments between these contacts correspond to the data points.

The Si-doped InAs NWs were grown using 40-nm Au colloids as catalysts in a low-pressure (76 Torr) MOVPE system [2,3]. InAs NW-channel field effect transistors (FETs) were then fabricated with Ni/Au electrodes [4]. The inset in Fig. 1 shows a SEM image of NW- FET with five electrode contacts on a single NW. Four-terminal measurements show a specific contact resistivity of 2.0×10^{-7} Ω-cm^2. The performances of NW-channel FETs were evaluated at room temperature. The carrier concentration (N) and mobility (μ) of these NW segments can be estimated based on the performances of NW-channel FETs [4]. Figure 1b shows an axial distribution of carrier concentration and mobility in a single NW. The carrier concentration decreases and mobility shows a little increase with increasing diameter. We applied a simple growth model including VLS and VPE parts. By fitting the data and extrapolating the formulation, we obtained N values in Au-seeded VLS and VPE parts in the NW, 1.37×10^{18} and 1.5×10^{17} cm^{-3}, respectively. This indicates a large difference of dopant concentration exists in the NW and Si atoms are more easily incorporated via Au-seeded VLS mode compared with VPE mode on NW sidewalls.

References

1. Wagner and Ellis, Appl. Phys. Lett. **4**, 89 (1964).
2. Tateno, et al., Appl. Phys. Lett. **85**, 1808 (2004).
3. Zhang, et al., J. Appl. Phys. **103**, 014301 (2008).
4. Zhang, et al., TuB III-4, p.142, ISCS2007, Japan.

Boron and Germanium Distribution in Individual Boron-doped $Si_{1-x}Ge_x$ Alloy Nanowires Grown by a Vapor Liquid Solid process

Chiharu Nishimura*, Go Imamura*, Minoru Fujii*, Takahiro Kawashima**, Tohru Saitoh**, and Shinji Hayashi*

** Department of Electrical and Electronic Engineering, Kobe University, Kobe, Japan*

*** Panasonic Corporation, Osaka, Japan*

Keywords: $Si_{1-x}Ge_x$ alloy nanowires, Raman spectroscopy,

$Si_{1-x}Ge_x$ alloy nanowires (SiGeNWs) synthesized by the vapor-liquid-solid(VLS) growth process have been attracting increasing interests because the electronic properties can be tailored in an extended range, and they can be used as transistors, chemical sensors, and light emitting devices. For these applications, precise control of the composition and the impurity profile, and the development of the technique to characterize the profiles are indispensable. In this work, we employ micro Raman spectroscopy to characterize concentration and distribution of Ge and electrically-active B in in-situ boron (B)-doped SiGeNWs synthesized by gold (Au)-catalyzed chemical vapor deposition (CVD).

Fig. 1(a) and 1(b) show Raman spectra of undoped and B-doped single SiGeNWs, respectively. The Raman spectra are measured from the catalyst side (A) to the substrate side (E or F) of the SiGeNWs. Three major peaks are observed at 500-520, 400-410, and 280-290 cm^{-1} due to the vibrations of adjacent Si-Si, Si-Ge, and Ge-Ge pairs, respectively. In B-doped SiGeNWs, the Raman spectra change drastically by changing the measurement position. The relative intensity of the Ge-Ge and Si-Ge Raman modes increase from the catalyst side to the substrate side. From the intensity ratio, the Ge composition can be estimated. In addition to the intensity ratio, the spectral shape changes depending on the measurement position. The Si-Si mode of B-doped SiGeNWs has a long tail towards a high-wavenumber side. This asymmetric spectral shape is attributed to Fano resonance between discrete phonon Raman scattering and continuous electric Raman scattering caused by the excitation of holes in the valence band. To evaluate the concentration of active B atoms from the asymmetric spectral shape, the spectra are fitted by Fano resonance formula and asymmetry parameters are extracted. The comparison of the asymmetry parameter with those obtained for reference samples, i.e., B-implanted Si, allow us to estimate the concentration of active B atoms. We show that there is strong correlation between the concentrations of Ge and B, i.e., high Ge concentration region of B-doped SiGeNWs is always more heavily B doped. This correlation combined with transmission electron microscopy observation suggests that supply of B_2H_6 during the VLS growth enhances conformal deposition of high Ge and B concentration layers on the side wall of VLS grown SiGeNWs. The co-existence of axial VLS-growth and conformal geowth results in the formation of conical SiGeNWs with strong distribution of Ge and B in axial and radial directions.

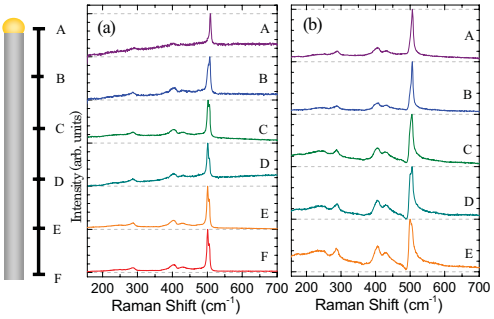

Fig. 1 Raman spectra of (a) undoped and (b) B-doped SiGeNWs measured from the catalyst side (A) to the substrate side (E or F).

Critical exciton kinetic energy in InAs/GaAs quantum dot sample by infrared time resolved spectroscopy

M. H. Abdellatif*, O. S. Kopylov, Jin Dong Song, Won Jun Choi, Nam Ki Cho, Jung Il Lee

**Nano Device Research Center, Korea Institute of Science and Technology, Seoul 136-791, Korea*

Keywords: InAs/GaAs Quantum dot, radiative and non-radiative decay time, Photo-luminescence, migration enhanced S-K growth.

InAs quantum dot is grown by Migration Enhanced Molecular Beam Epitaxy (MEMBE). Photoluminescence (PL) and time-resolved photoluminescence are carried out at different laser powers and temperatures. The temperature varied from 14K up to 200K. We found two emission peaks near 1.096ev, 1.172ev the emission energy is found to red shift with increasing temperature while there is no change in the peak position with varying laser power. Decay time analysis revealed effective life time at the ground state transition of 512ps at 14K and laser power of 15mW. At the same temperature, the decay time decreases slightly as the laser power increases to reach 503ps at 200 mW laser power. We also investigated the radiative and non-radiative recombination time by varying temperature and laser power. The low value of the radiative recombination time explains the higher PL intensity at low temperature. As the temperature increases the PL peak intensity decreases and radiative life time increases.

The radiative and non-radiative decay times are calculated on the basis of Feldmann[1] theory. The non radiative recombination becomes more effective, through phonon scattering and crystal vibrations, which increases as KT increases. At low temperature radiative and non radiative decay times are of the same order, and excitons kinetic energy is less than critical value Δ, that favours radiative recombination. As the temperature increases the radiative decay slows down with respect to the non-radiative one. That variation of the radiative decay time with respect to the non-radiative is the main reason for the PL intensity decrease with increasing temperature. The critical temperature, at which the exciton kinetic energy exceeds its critical limit Δ, which determines the effectiveness of the radiative and non-radiative channels, is obtained from the point where the slope changes. The temperature is around 120K for emission from ground state and 60K for the first excited state. The critical exciton kinetic energy is calculated and tabulated.

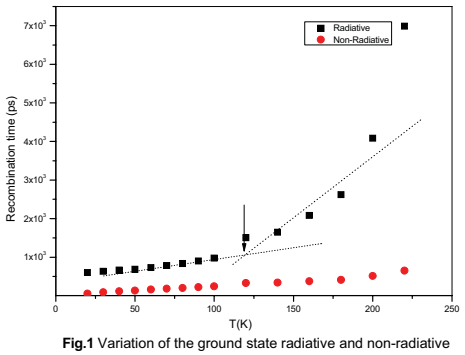

Fig.1 Variation of the ground state radiative and non-radiative recombination time with temperature

References

1. J.Feldmann, G.Peter, E.O. Gobel, P. Dawson, K. Moore, C. Foxon, and R.J.Elliot, Phys.Rev.Lett. **59**, 2337 (1987).

Observation of excited states in a p-type GaAs quantum dot

M. Csontos*, Y. Komijani*, T. Ihn*, K. Ensslin*, D. Reuter** and A. D. Wieck**

*Solid State Physics Laboratory, ETH Zurich, Switzerland

** Angewandte Festkörperphysik, Ruhr-Universität Bochum, Germany

Keywords: p-type GaAs, AFM lithography, quantum dots, electrical transport

Quantum dots (QDs) implemented in GaAs heterostructures represent promising candidates for the realization of quantum information processing, as well as various spintronic devices. Low-dimensional hole-doped systems are especially interesting due to the more pronounced spin-orbit as well as carrier-carrier Coulomb interactions compared to n-type systems. We fabricated a p-type dot in a C-doped GaAs heterostructure with a small number of holes and studied the electric transport through single-particle excited states important for the all-electrical manipulation of individual hole spins. As a first step towards single-hole charge and spin dynamics studies we successfully implemented and tested a quantum point contact (QPC) charge detector which is capacitively coupled to the dot.

We fabricated the quantum dot in a p-type GaAs heterostructure by AFM oxidation lithography (Fig. 1). Clear and reproducible Coulomb resonances were observed at weak coupling to the leads (Fig. 2). From the Coulomb diamond measurements charging energies up to 2 meV were found at elevated plunger gate voltages indicating a small number of the confined holes. Lines of resonant conductivity in the charge stability diagram outside the Coulomb blockaded region of the dot are resolved for the first time [1]. They are attributed to sequential tunneling through single-hole excited states which may open new routes to all-electrical manipulation of individual hole spins. From the energy-separation of the excited states we estimate a dot diameter of 50-100 nm corresponding to 1-10 confined holes. Our preliminary experimental results indicate that the QPC-based non-invasive charge detection scheme known from n-type QDs can be successfully implemented also in p-type systems. This opens the way to study single-hole charge- and spin dynamics as well as the back action of the charge detector QPC in various p-type nanodevices.

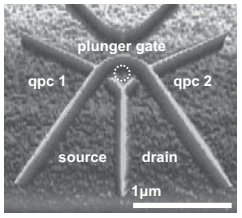

Figure 1: AFM image of the sample topology. The 15 nm high oxide lines are prepared by local anodic oxidation and create insulating barriers in the underlying 2DHG separating it into electrically disconnected areas. The dashed circle indicates the location of the QD which is connected to source and drain contacts by two QPCs. The couplings of the dot to the leads are tuned individually by the in-plane gates qpc1 and qpc2 while the electrochemical potential of the dot can be varied by applying a voltage on the nearby plunger gate.

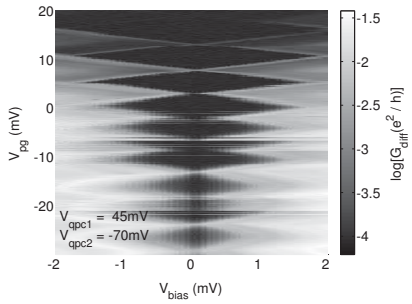

Figure 2: Logarithmic gray scale plot of the Coulomb blockade diamonds observed in the differential conductance of the dot. The charging energy associated with the size of the diamonds increases with the plunger gate voltage. The measurement was performed at 60 mK base temperature.

References

[1] Y Komijani, M. Csontos, T. Ihn, K. Ensslin, D. Reuter and A. D. Wieck, Europhys. Lett. **84**, 57004 (2008).

July 21 (Tuesday)

9:00 – 10:30

Session M2

Terahertz dynamics and devices

International Conference Room

MSS-EP2DS Parallel session

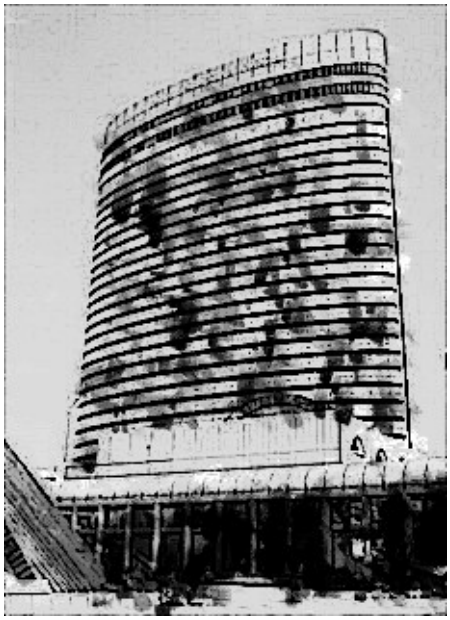

Kobe Portpia Hotel

Non-adiabatic control of intersubband cavity polaritons

R. Huber*, A. A. Anappara*, A. Sell*, G. Günter*, G. Biasiol**, L. Sorba**,
S. De Liberato***, C. Ciuti***, A. Tredicucci**, and A. Leitenstorfer*

** Department of Physics and Center for Applied Photonics, University of Konstanz, Germany*

*** Laboratorio NEST CNR-INFM and Scuola Normale Superiore, Pisa;*
Laboratorio Nazionale TASC CNR-INFM, Trieste, Italy

**** Laboratoire Matériaux et Phénomènes Quantiques, Université Paris Diderot – Paris 7 and CNRS, Paris;*
Laboratoire Pierre Aigrain, Ecole Normale Superieure, Paris, France

Keywords: cavity quantum electrodynamics, ultrafast dynamics, intersubband polaritons, terahertz spectroscopy

Intersubband cavity polaritons in a quantum well waveguide structure are optically generated within less than one cycle of light by a femtosecond near-infrared pulse. Mid-infrared probe transients trace the non-adiabatic switch-on of ultrastrong light-matter coupling and the conversion of bare photons into cavity polaritons directly in the time domain.

Photonic microcavities have been exploited to tailor the interaction of light with material excitations. In the strong coupling regime, a photon may be absorbed and spontaneously reemitted by an elementary excitation many times before dissipation becomes effective. This process gives rise to new eigenstates of mixed light-matter character, so-called cavity polaritons. The characteristic energy anticrossing, known as vacuum-field Rabi splitting $2\hbar\Omega_R$, is a direct measure of the strength of light-matter interaction [1].

Recently intersubband resonances of semiconductor quantum wells (QW) hybridized with the mid-infrared photon mode of a planar waveguide have entered a new regime of ultrastrong interaction, where Ω_R amounts to a significant fraction of the bare eigenfrequencies ω_{12} themselves [2,3]. The resulting squeezed two-mode quantum vacuum is expected to give rise to a variety of novel quantum electrodynamical (QED) effects [4]. In particular, ultrafast switching of the Rabi frequency Ω_R has been predicted to release correlated photon pairs out of the vacuum, reminiscent of the intriguing, yet unobserved dynamic Casimir effect [4].

Up to now, however, non-adiabatic phenomena – classical or QED in nature – remained an academic curiosity since there has been no laboratory capable of controlling light-matter interaction on a sub-cycle scale. Here, we report an all-optical pump – terahertz probe scheme for the first implementation of femtosecond control of ultrastrongly coupled cavity polaritons [5].

The sample contains 50 identical, undoped GaAs QWs

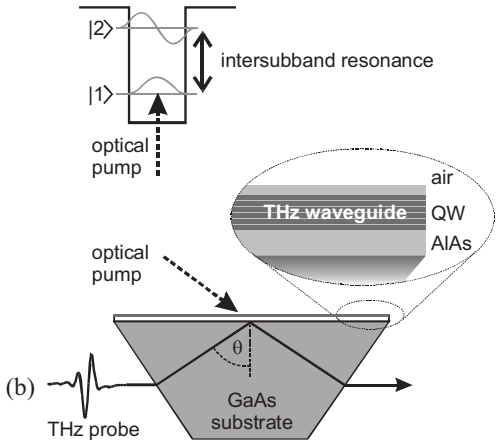

Fig. 1: (a) Schematic band diagram of a GaAs/AlGaAs QW; broken arrow: interband excitation populates subband $|1\rangle$; double-headed arrow: intersubband transition. (b) Sample geometry: The THz waveguide is resonant with the intersubband transition for light propagation at $\theta = 65°$. THz probe pulses coupled through the substrate are reflected off the waveguide.

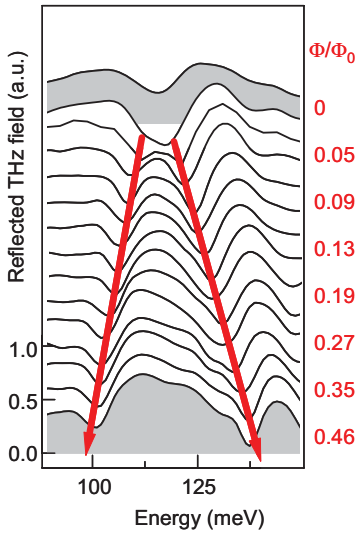

Fig. 2 All-optical in-situ tuning of light-matter interaction. THz reflectance spectra measured at room temperature for various fluences Φ (vertically offset) of the control pulse (t_D = 2 ps). Minima indicate eigenmodes of the system. For Φ = 0, only the bare photon mode is observed at $\hbar\omega_c$ = 113 meV; both branches of the intersubband cavity polaritons are discernible for Φ ≥ 0.05 Φ_0 (Φ_0 = 0.1 mJ/cm^2).

separated by $Al_{0.33}Ga_{0.67}As$ barriers. The electronic wave functions are quantized along the growth direction forming subbands [Fig. 1(a)]. The subbands of quantum number n = 1 and n = 2 are connected by radiative transitions featuring a narrow absorption line at a photon energy of $\hbar\omega_{12}$ = 113 meV (wavelength λ = 10 μm) and a strong dipole moment oriented along the growth direction. The multi-QW structure is designed as a planar step index waveguide for mid-infrared light [2]. Radiation is confined between a top-cladding ($Al_{0.33}Ga_{0.67}As$)-air interface (n_{air} = 1, n_{QW} = 3.1) on one side and a low refractive index AlAs layer (n_{AlAs} = 2.9) on the other. The effective thickness of the entire waveguide is chosen to be λ/2 at an internal angle of θ = 65°. Photon modes with electric field components in growth direction (TM polarization) may resonantly couple to intersubband transitions provided the subbands are populated. The vacuum Rabi frequency is known to scale with the electron sheet density N_e in level $|1\rangle$ as $\Omega_R \sim N_e^{1/2}$ [4]. In previous work, N_e was provided by static doping or gate injection [3], both of which are difficult to modulate with sufficiently high bandwidths for the non-adiabatic coupling regime.

We employ a low-noise Ti:sapphire laser system generating amplified 12-fs pulses (central photon energy: 1.55 eV) to photoinject electrons from the valence band into the lowest conduction subband of the QWs [Fig. 1(a)], activating the intersubband oscillator. Since the inverse frequency of the latter transition amounts to 37 fs, we activate it within less than half a cycle of light.

The subsequent ultrafast dynamics of the non-equilibrium cavity at room temperature is traced by multi-terahertz (THz) spectroscopy [6]: A second part of the laser output generates phase-locked THz pulses covering the spectral window from 80 meV to 150 meV by optical rectification in a 50-μm-thin GaSe emitter [7]. TM polarized field transients are coupled through the prism-shaped substrate and internally reflected off the photoexcited area of the waveguide under incidence angles around θ = 65° [Fig. 1(b)]. The pulse front of the near-infrared pump is tilted to match the geometry of the THz phase surfaces. The oscillating electric field of the reflected THz transient is resolved in the time domain via phase-matched electro-optic sampling [7]. Fourier transformation provides amplitude and phase spectra in the mid infrared. The eigenmodes of the cavity are identified via their characteristic minima in the amplitude reflectivity [2].

In a first step, we demonstrate that light-matter coupling is continuously tunable via the control fluence Φ. The spectra of Fig. 2 are recorded at a fixed delay t_D = 20 ps between the near-infrared control and the multi-THz probe pulse. In equilibrium (Φ = 0), a single reflectance minimum at $\hbar\omega_c$ = 113 meV (top curve) attests to the sole resonance of the unexcited cavity, the bare photon mode. For Φ > 0.05 × Φ_0, Ω_R exceeds the widths (FWHM ~ 5 meV) of intersubband and cavity resonances and two strongly coupled cavity polariton branches are discernible. Further increase of the fluence enhances the separation of the minima to as much as 50 meV (see e.g. bottom curve of Fig. 3), corresponding to a fraction of 44% of the bare photon frequency. The apparent mode separation is not identical with the vacuum Rabi splitting at the anti-crossing point [2]. Only a quantitative simulation of the energy position of the polariton dips allows for extraction of Ω_R. For a

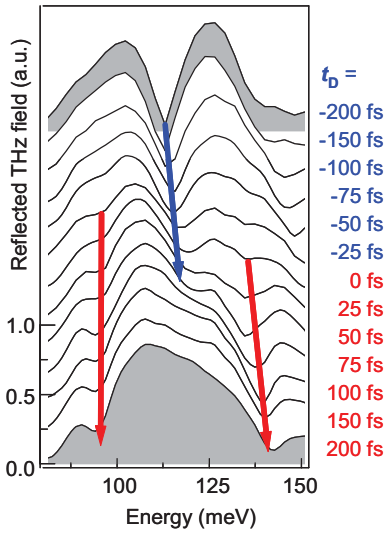

Fig. 3 2-dimensional optical pump – THz probe data: amplitude reflectivity spectra at T_L = 300 K for various delay times t_D (control fluence: Φ = 0.1 mJ/cm^2). The arrows serve as guides to the eye for the position of the cavity and polariton resonances.

correct description of our data, the theory has to go beyond the rotating wave approximation and include antiresonant terms in the light-matter Hamiltonian. These contributions describe the simultaneous creation or annihilation of two excitations with opposite in-plane wave vector k and give rise to a two-mode squeezed quantum vacuum [4]. By comparison with this theory we determine a maximum splitting $2\Omega_R = 0.18 \times \omega_{12}$ for our experiments. This value is comparable to the record achieved in doped structures [2] and clearly fulfills the criteria of ultrastrong coupling.

The central question is: How rapidly may ultrastrong coupling be activated? In order to address this issue, we repeat the experiments for various delay times t_D between near-infrared pump and multi-THz probe pulses. For $t_D \leq$ -50 fs the spectra are dominated by a single dip located at 113 meV which we may unequivocally assign to the photonic waveguide mode. Photoinjection of electrons into the lower subband induces dramatic changes of the spectra of order unity. The initial bare photon eigenstate is replaced, on a ten femtosecond scale, by two ultrastrongly coupled cavity polariton modes appearing simultaneously at energies of 94 meV and 143 meV, respectively (red arrows in Fig. 3). Most remarkably, the new resonances do not develop by gradual bifurcation out of the bare cavity mode as in Fig. 2. In contrast, switching occurs discontinuously once subband $|1\rangle$ is populated.

Femtosecond activation of the light-matter Hamiltonian is predicted to give rise to yet unexplored effects on pre-existing photon states and the quantum vacuum itself [4]. In order to appreciate the impact of sub-cycle control, we prepare a coherent photon state in the bare cavity and perturb the radiative relaxation by ultrafast switching. On a sub-cycle scale, the photon population converts into ultrastrongly coupled coherent polaritons [5]. Electro-optic sampling directly monitors this phenomenon for the first time (not shown). A quantitative theory including anti-resonant terms of the light-matter Hamiltonian as well as the extremely non-equilibrium carrier dynamics is currently under way.

In conclusion, we have demonstrated the first non-adiabatic switching scheme of cavity-polaritons, reaching the regime of ultrastrong light-matter coupling on a sub-cycle scale. The experiments provide a benchmark for latest theories in the ultrastrong coupling regime, point out a viable route towards novel QED phenomena such as the observation of Casimir-type vacuum radiation, and demonstrate an optical switching device at the ultimate speed.

References

1. C. Weisbuch et al., Phys. Rev. Lett. **69**, 3314 (1992).
2. D. Dini et al., Phys. Rev. Lett. **90**, 116401 (2003). A. Anappara et al., arXiv:0808.3720, to appear in Phys. Rev. B **79**, 2009.
3. A. A. Anappara et al., Appl. Phys. Lett. **87**, 051105 (2005); Appl. Phys. Lett. **89**, 171109 (2006).
4. C. Ciuti, G. Bastard, and I. Carusotto, Phys. Rev. B **72**, 115303 (2005); S. De Liberato et al., Phys. Rev. Lett. **98**, 103602 (2007).
5. G. Günter et al., Nature **458**, 178 (2009).
6. R. Huber et al., Nature **414**, 286 (2001); Phys. Rev. Lett. **94**, 0274011 (2005); C. Kübler et al., Phys. Rev. Lett. **99**, 116401 (2007).
7. C. Kübler, et al., Semicond. Sci. Technol. **20**, 128 (2005) and references therein.

Breakdown of the semiclassical miniband picture for transient electron transport in GaAs-based superlattices

T. Unuma[1,2], Y. Ino[3], M. Kuwata-Gonokami[3], and K. Hirakawa[1]

[1]*Institute of Industrial Science and INQIE, University of Tokyo, Tokyo 153-8505, Japan*

[2]*Department of Applied Physics, Nagoya University, Nagoya 464-8603, Japan*

[3]*Department of Applied Physics and INQIE, University of Tokyo, Tokyo 113-8656, Japan*

Keywords: terahertz, superlattice, Bloch oscillations, Wannier-Stark ladder

There are two physical pictures to describe Bloch oscillations in semiconductor superlattices (SLs), i.e., the semiclassical miniband picture and the Wannier-Stark ladder picture. However, the equivalence between them has been confirmed only for a few properties in steady states. In this work, we have investigated the time-evolution of transient electron transport in GaAs-based SLs for various initial electron distributions by time-domain terahertz (THz) emission spectroscopy.

The samples used in this study were undoped GaAs-based SLs with *m-i-n* diode structures. Electrons were photoexcited into the ground miniband at 10 K by Ti:Sapphire laser pulses (temporal width: ~100 fs), and transient THz waveforms emitted from the samples under dc bias electric fields F were recorded using a ZnTe electro-optic sensor with a flat sensitivity up to 3.5 THz. The excitation photon energies E_{ex} were changed between the values corresponding to electron creations near the bottom and top of the miniband.

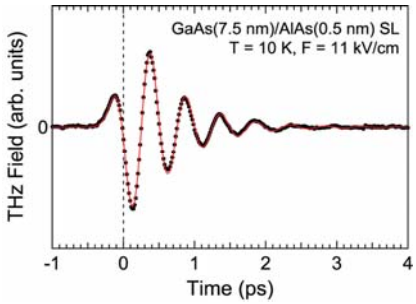

Fig.1 (dots) Observed THz waveform emitted from a GaAs/AlAs SL. The vertical dashed line denotes the time origin determined by the maximum entropy method. (solid curve) Simulated THz waveform expected for a damped $\cos\omega_B t$ current.

Figure 1 shows the THz waveform (dots) emitted from a GaAs(7.5 nm)/AlAs(0.5 nm) SL at F = 11 kV/cm for the lowest photoexcitation of E_{ex} = 1.538 eV. The observed damped oscillation has a frequency of 2.0 THz, nearly equal to the expected Bloch frequency eFd/h (d: SL period) [1]. However, we have found that the observed THz waveforms are very insensitive to the change in E_{ex} (not shown here), contrary to the common expectation from semiclassical electron distributions in k-space. The vertical dashed line in the figure denotes the time origin (t = 0) determined by the maximum entropy method [2], indicating that the oscillatory THz signal evolves nearly as damped $-\sin\omega_B t$ (ω_B: Bloch frequency). Also shown in the figure is a simulated THz waveform dJ/dt (solid curve) calculated from a damped $\cos\omega_B t$ current $J(t)$ with a reasonable temporal broadening. As seen in the figure, the agreement between the observed and simulated THz waveforms is excellent. The damped $\cos\omega_B t$ current $J(t)$ requires the semiclassical miniband picture to assume an *unrealistic* electron distribution around the middle of the miniband at t = 0 even for the lowest value of E_{ex}.

We will show that the spatially uniform electron distribution on the Wannier-Stark ladder states with translational symmetry is essential for the obtained transient current.

References

1. T. Unuma *et al*., Appl. Phys. Lett. **89**, 161913 (2006).
2. E.M. Vartiainen *et al*., J. Appl. Phys. **96**, 4171 (2004).

Magnetic field assisted sub-THz quantum cascade lasers

A. Wade*, D. Smirnov*, S. Kumar**, B.S. Williams***, Q. Hu**, and J.L. Reno***

* *National High Magnetic Field Laboratory, Tallahassee, Florida 32310, USA*

** *Massachusetts Institute of Technology, Cambridge, Massachusetts 02139, USA*

*** *University of California at Los Angeles, California 90095, USA*

**** *Sandia National Laboratories, Albuquerque, New Mexico 87185-0601*

Keywords: semiconductor lasers, quantum cascade lasers, FIR and THz lasers

Quantum cascade lasers (QCLs) exploit the concept of a cascade of radiative transitions between size-quantized subbands in a multi-quantum-well structure. The motivation for the development of low-energy QCLs (1THz ~ 4meV) is driven by their potential for remote sensing and imaging, spectroscopy, and communications. THz QCLs now cover a frequency range between 1.2 THz and 5 THz, though cryogenic cooling is still required [1]. Progress towards the realization of sub-THz and/or high temperature operation becomes exceedingly difficult because it requires achieving lasing action in a system with closely spaced 2D electronic subbands.

Recently there has been much focus on utilizing a magnetic field to create additional lateral quantization in QCLs. A sufficiently strong magnetic field B breaks subbands' in-plane continuum of states into a set of discrete, equidistant, 0D-like Landau levels (LLs) separated by the cyclotron energy $\hbar\omega_C = \hbar eB/m^*$. Here we exploit this field-controlled confinement in a threefold way. First, it allows suppressing LO phonon emission, thus increasing the electron's lifetime in the initial state of the laser transition. Second, by adjusting the magnetic field one can resonantly decrease the final state lifetime. Such control of electronic lifetimes makes it possible to obtain laser action at significantly reduced thresholds and/or higher temperatures. Finally, making the LLs separation bigger than the emission energy, $\hbar\omega_C >> h\nu$, eliminates the reabsorption of light, and opens up a possibility of achieving extremely low emission energies.

We studied two sets of GaAs/$Al_{0.15}Ga_{0.85}As$ THz QCLs based on a "resonant-phonon" extractor and a double-well (single-well) injector operating at ν=3.1THz (ν=1.9THz) at the designed zero-field bias [2,3]. Above laser threshold, the bias voltage per a QCL period, V^*, is essentially pinned such that $eV^* \approx h\nu + \hbar\omega_{LO}$. As the increasing magnetic field splits the 2D parabolic subbands into discrete LLs and breaks the traditional resonant tunnelling regime, one can apply much greater biases. Then the QCLs develop new plateaus in the I-V curves indicating new stable alignments of the energy levels that cannot be achieved without a magnetic field.

In a narrow range of fields of about 20T, the devices with a two-well injector design show strong dual-frequency lasing (at 0.97THz with sidebands down to 0.68THz, and at 3THz) that originates from the simultaneous emission from two cascaded optical transitions in each QCLs period. Moreover, 1THz laser action is observed at record high temperatures up to 215K (19T), and 3THz lasing up to 225K (31T). The devices with a one-well injector also show field-assisted emission at ~17T and sufficiently high electrical bias. This resulted in single-line lasing at 600GHz, the lowest ever recorded from a QCL.

References

1. B.S. Williams, Nature Photonics **1**, 517 (2007).
2. B.S. Williams et al., Opt. Express **13**, 3331 (2005)
3. S. Kumar et al., Appl. Phys. Lett. **88**, 121123 (2006).
4. A. Wade et al., Nature Photonics **3**, 41 (2009).

Fabrication and operation of a metal-metal waveguide GaAs terahertz quantum cascade laser

Tsung-Tse Lin, Keita Ohtani, and Hideo Ohno

Laboratory for Nanoelectronics and Spintronics, Research Institute of Electrical Communication, Tohoku University, 2-1-1 Katahira, Aoba-ku, Sendai 980-8577, Japan

Keywords: metal-metal waveguide, terahertz, quantum cascade laser, GaAs

Quantum cascade lasers (QCLs) are a promising candidate for a terahertz (THz) source because of its compact, high power, and narrow emission linewidth. However present maximum operation temperature (T_{max}) is 178 K [1] which restricts their practical application. A waveguide with high optical confinement and low loss is essential to increase T_{max} because reducing threshold current density (J_{th}) increases a current density dynamic range of the device. Here we describe the fabrication process of a metal-metal waveguide THz QCL, which exhibits high optical confinement and small waveguide loss [2], and report on its laser operation. The emission properties are also compared with those of the device utilizing a single plasmon waveguide structure.

The GaAs/$Al_{0.15}Ga_{0.85}As$ QCL structure was grown by molecular beam epitaxy (MBE). The growth sequence started with 600 nm-thick $Al_{0.6}Ga_{0.4}As$ etch-stop layer and was followed by a 100 nm-thick *n*-GaAs layer (n=5.0×10^{18} cm^{-3}), 175 repeats active/injection layers, and a 60 nm-thick *n*-GaAs layer (n=5.0×10^{18} cm^{-3}). The active/injection layers were designed using a longitudinal optical phonon depopulation scheme [2]. After MBE growth, the QCL sample was cleaved into 1cm^2 dies and a Ti/Au (20 nm/800 nm) metal contact was evaporated. The wafer was then bonded for 25 min at 250 ˚C in a N_2 atmosphere to the SI-GaAs substrate with deposited layers of Ti/Au/In (20 nm/75 nm/1400 nm). The bonded wafer was lapped down to 100 μm. All sides of the bonded wafer were coated with a photoresist to protect the edges from lateral etching. A citric acid based solution was used to remove the GaAs substrate. After removing $Al_{0.6}Ga_{0.4}As$ etch-stop layer by a diluted HF, the bonded wafer was processed into 230 μm-wide ridge structure by wet etching and photolithography. A Ti/Au (20 nm/200 nm) contact was deposited on the top of ridges.

Lasing at 3.4 THz was observed at 4 K. As shown in Fig. 1, J_{th} at 4 K was 0.8 kA/cm^2, which is smaller than J_{th} (=1.3 kA/cm^2 at 4 K) obtained from the separated devices utilizing single plasmon waveguide with identical active/injection layers. This is attributable to its large optical gain by increasing optical confinement factor. The observed T_{max} was 130 K, which indicates that reduction of J_{th} makes it possible to operate at higher temperature compared with T_{max} (=85 K) of the single plasmon waveguide device.

This work was supported by a Grant-in-Aid for Scientific Research (A) (No. 19206033) from JSPS and the GCOE Program at Tohoku University Electro-Related Department.

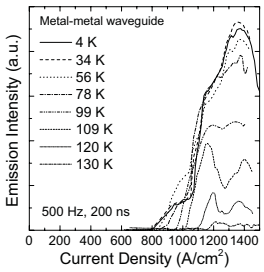

Fig.1 Current density-light output characteristics of the fabricated metal-metal waveguide THz QCL.

References

1. M. A. Belkin, J. A. Fan, S. Hormoz, F. Capasso, S. P. Khanna, M. Lachab, A. G. Davies, and E. H. Linfield: Opt. Express **16** (2008) 3242.

2. B. S. Williams, S. Kumar, H. Callebaut, Q. Hu, and J. Reno: Appl. Phys. Lett. **83** (2003) 2124.

Tailored beams in quantum cascade ring lasers

E. Mujagić*, S. Schartner*, M. Nobile*, H. Detz*, A. M. Andrews*, P. Klang*, W. Schrenk*, C. Deutsch**, K. Unterrainer**, M. P. Semtsiv***, W. T. Masselink***, and G. Strasser*,****

* *Institute for Solid State Electronics, Vienna University of Technology, Vienna, Austria*

** *Photonics Institute, Vienna University of Technology, Vienna, Austria*

*** *Department of Physics, Humboldt University Berlin, Berlin, Germany*

**** *Department of Electrical Engineering and Physics, State University of New York, Buffalo, New York, USA*

Keywords: quantum cascade laser, beam shaping, surface emission

Quantum-cascade lasers (QCLs) are well established as reliable laser sources from the midinfrared (MIR) to the terahertz (THz) spectral range. The fingerprint region of molecular absorption is significantly pronounced in both regimes of the electromagnetic spectrum, which makes the QCLs attractive as compact light sources for several applications like chemical sensing and medical imaging. Due to small dimensions and elongated shape of the resonator, the emitted light of standard Fabry-Perot and surface emitting QCLs is typically broad and asymmetric. Especially for THz QCLs, the sub-wavelength dimensions of laser ridge facet lead to an inhomogeneous diffractive-like pattern, thus reducing the light collection efficiency. However, symmetric far fields and low beam divergence are of special interest since they make bulky and expensive optics obsolete.

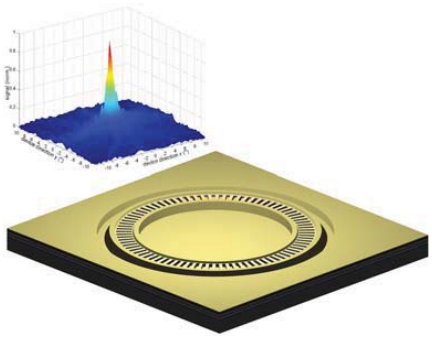

Fig.1 Illustration of a surface emitting ring QCL. Inset shows a 2D far-field plot.

We present a concept to lower the divergence of the output beam by using a ring-shaped resonator with a radial, light out-coupling grating on top (Figure 1). The emitting area naturally forms a circularly shaped far field and the overall large emission area narrows the beam [1, 2].

In order to demonstrate the beam shaping effect, we fabricated ring QCLs, designed for an emission wavelength of ~4 μm. A second order grating on top of the lasers allows for surface emission. The QCLs exhibit robust single mode operation. Due to the symmetric waveguide, the far-field patterns are circularly symmetric. By varying the grating period the shape of the beam is tuned, resulting in spot and ring-shaped patterns. The highly symmetric beams have a full width at half maximum of ~3°.

Preliminary results demonstrate that this beam shaping concept can successfully be applied to THz QCLs.

References

1. E. Mujagić, S. Schartner, L. K. Hoffmann, W. Schrenk, M. P. Semtsiv, M. Wienold, W. T. Masselink and G. Strasser, Appl. Phys. Lett. **93**, 011108 (2008).

2. E. Mujagić, L. K. Hoffmann, S. Schartner, M. Nobile, W. Schrenk, M. P. Semtsiv, M. Wienold, W. T. Masselink and G. Strasser, Appl. Phys. Lett. **93**, 161101 (2008).

July 21 (Tuesday)

11:00 – 12:30

Session M3

Physics and devices for quantum information processing

International Conference Room

MSS-EP2DS Parallel session

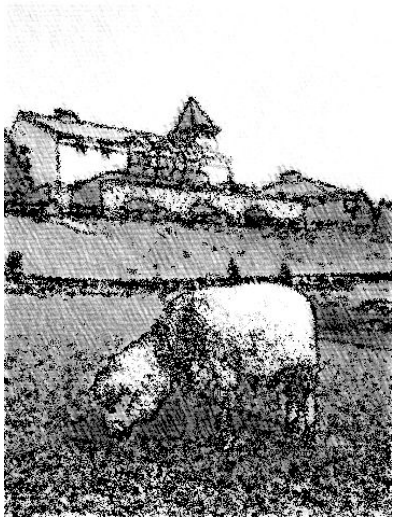

Rokko farm

Coherent Hole Spin in a Semiconductor Quantum Dot

R. J. Warburton*, Daniel Brunner*, Brian D. Gerardot*, Paul A. Dalgarno*,
Nick G. Stoltz**, and Pierre M. Petroff**
*School of Engineering and Physical Sciences, Heriot-Watt University, Edinburgh EH14 4AS, UK
**Materials Department, University of California, Santa Barbara, California 93106, USA

Keywords: quantum dot, spin

Spin is potentially highly coherent in a semiconductor. By confining an electron to a nano-sized quantum dot, spin dephasing via the phonons, the dominant source of dephasing in bulk semiconductors and quantum wells, can be highly suppressed. This leads to long spin relaxation times: T_1 1 s has been achieved on single electron spins in an electrostatically-defined quantum dot [1]. Furthermore, in a self-assembled quantum dot, the spin can be initialized, manipulated and read-out with purely optical techniques. However, despite the long T_1 times, the electron spin coherence time T_2^* is disappointingly small, typically $\sim$ 10 ns. The origin of the fast dephasing is the hyperfine interaction, the coupling of the electron spin to the nuclear spins of the host material. The nuclear spins create an effective magnetic field, the Overhauser field. Spin precession about the randomly fluctuating Overhauser field leads to a rapid loss of electron spin coherence. The rapid loss of coherence of the electron spin represents a major stumbling block to coherent manipulation.

One possibility is to use not an electron spin but a hole spin. The hole has a p-like atomic Bloch state with a node at the location of the nuclei, conveniently removing the contact part of the hyperfine interaction. The dipole-dipole part of the hyperfine interaction remains however but its effect on the hole spin coherence has yet to be probed in any detail. We show here that the hole spin is remarkably coherent: we determine a lower limit to the hole spin T_2^* time of about 1 s at 4.2 K and in an in-plane magnetic field of 3 T.

Our experiment involves, first, trapping a single hole in a quantum dot using a vertical charging device with p-type back contact, and, second, probing the hole spin with two coherent lasers. Optical pumping is used to initialize the hole spin with a fidelity of well over 99%, demonstrating that the hole spin T_1 is large even without an external magnetic field [2]. A quantitative analysis of our data shows that $T_1 \sim 1$ ms [2]. In order to probe T_2^*, we have used a quantum interference, coherent population trapping, the atomic process which underpins electromagnetically-induced transparency. We couple the two hole spin states to a common exciton state by applying an in-plane magnetic field. When both transitions are driven with coherent lasers, pump and probe, we observe a spectacular dip in the probe absorption spectrum. The dip corresponds to a destructive interference of the two absorption processes, and the high visibility of the interference implies a highly coherent system. Modeling the data allows us to set a lower bound on the hole spin T_2^*. A very positive feature of this experiment is that the dip is just a few tens of MHz wide despite the much larger inhomogeneous broadening, several GHz, of the exciton transition.

References

[1] S. Amasha *et al*., Phys. Rev. Lett. **100**, 046803 (2008).

[2] B. D. Gerardot *et al*., Nature **451**, 441 (2008).

Phase and coherence of entangled photon pairs from a single quantum dot

A. J. Bennett*, R. M. Stevenson*, A. J. Hudson*,**, R. J. Young*, C. A. Nicoll**, D. A. Ritchie** and A. J. Shields*

* *Toshiba Research Europe Limited, Cambridge Research Laboratory, 260 Science Park, Milton Road, Cambridge, CB4 OWE, U. K.*

** *Cavendish Laboratory, Cambridge University, JJ Thomson Avenue, Cambridge, CB3 0HE, U K.*

Keywords: Entanglement, quantum dots, coherence

The exciton-biexciton cascade in a quantum dot has been shown to be a practical system for entangled photon pair generation [1]. The degree of entanglement is dependent upon information which distinguishes the two decay paths (see Fig.1, insert), such as the fine structure splitting in the dot, and the coherence of the intermediate exciton-photon state. Here we discuss an experimental investigation of the parameters that determine the fidelity of entanglement, using a quantum dot where we tune the fine structure splitting by application of an external magnetic field [2]. Our measurements show that the entanglement of the photon pair is robust to the dephasing of the intermediate exciton state responsible for the first-order coherence time.

We then go on to show that for finite fine structure splittings we observe time-varying quantum correlations in the emitted photons, which are attributed to the spin-dependent phase acquired in the intermediate, non-degenerate, exciton-photon state [3]. The results show strong oscillations in fidelity with the expected Bell state as a function of time (Fig. 1). We conclude that the emission of photon pairs emitted by a typical quantum dot is entangled in a time evolving fashion, and not classically correlated as previously regarded. Thus, the expected Bell state for any pair of photons can be determined by the delay between them. Furthermore, time-independent states may be temporally selected limiting the undesirable influence of background light and dark counts, in addition to improving the time-integrated entanglement fidelity.

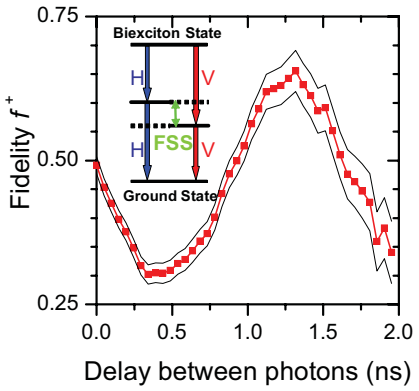

Fig.1 (inset) decay paths in a non-degenerate (split) quantum dot with finite fine structure splitting (FSS). (main panel) Evolution of entanglement fidelity f^+ with the maximally entangled state ($|HH\rangle+|VV\rangle)/\sqrt{2}$, as a function of the time delay between the first (biexciton) and second (exciton) photon emitted by a quantum dot with polarization dependent splitting of 2.5μeV. Bands indicate errors dominated by Poissonian noise.

References

1. R. M. Stevenson *et al,* Nature 439 (2005) 179.
2. A. J. Hudson *et al*, Phys. Rev. Lett. 99 (2007) 266802
3. R. M. Stevenson *et al*, Phys. Rev. Lett., 101, (2008) 170501.

Microcavity quantum dot single photon source electrically driven at 1 GHz

E. Stock*, A. Lochmann*, J. A. Töfflinger*, W. Unrau*, A. Toropov**, A. Bakarov**, A. Kalagin**, V. Haisler** and D. Bimberg*

** Institut fuer Festkoerperphysik, Technische Universitaet Berlin, Germany*

***Institute of Semiconductor Physics, Novosibirsk, Russia*

Keywords: Single photon source, quantum cryptography, quantum dots,

Self-organized quantum dots (QDs) demonstrated their excellent capability for a compact single photon device based on well established semiconductor technology [1, 2] and will be a key device for quantum cryptography. An ideal source must have a high single photon rate combined with a high outcoupling efficiency.

Our device consists of a layer of InAs/GaAs QDs grown by MBE with a density of $5x10^8$ cm^{-2} embedded in a pin diode structure. The current is constricted by an AlO_x aperture which allows pumping of a single QD [2]. In order to increase the outcoupling efficiency and to decrease the exciton lifetime a microcavity consisting of 12/5 DBR mirrors on the bottom/top of the device was grown.

The electroluminescence spectra demonstrate individual sharp lines from well separate QDs. At bias conditions, where the exciton emission is saturated, the count rate of our avalanche photodiodes (APDs) is ten times higher than from previous devices without cavity under comparable bias [2]. The photonic modes of the cavity couple to the electronic state in the cavity and lead to a preferred emission direction.

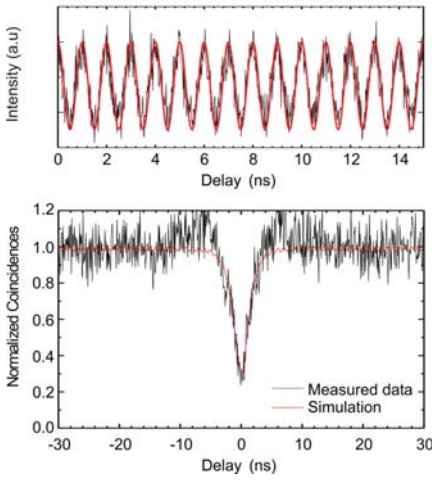

Although the additional DBR mirrors increase the serial resistance and the capacity of our device in comparison to simpler devices and may reduce the bandwidth, we are able to drive our device with 1 GHz and a pulse width of 350 ps (Fig.1 top). The optical response of our device to the electrical pulse agrees very well with theoretical simulations of a pulse train with a FWHM of 400 ps. The exciton life time without cavity is in the order of 1 ns and the short optical response of our device demonstrates, an appreciable reduction of the life time by the Purcell effect. The time resolution of our APD is 350 ps, thus presently still limiting the measured optical response.

For photon correlation measurement two APDs for the start and stop signal must be used, thus reducing the time resolution by the factor 2 and the measured correlation function (Fig.1 bottom) looks similar to cw excitation. The measured $g^2(0)$ value of 0.25 is again limited by the time resolution of our setup. The photon correlation agrees excellent with a simulation of a pulsed perfect single photon device ($g^2(0) = 0$) with 1 GHz repetition rate, taking into account the limited time resolution of 0.7 ns of our setup.

References

1. Bimberg, D. Elect. Lett. 44, 390 (2008)
2. Shields, A. Nature Photonics 1, 215 (2007)
2. Lochmann, A. et al. Elect. Lett 47, 774 (2006)

Demonstration of an optoelectronic quantum phase gate

S. Michaelis de Vasconcellos*, S. Gordon*, M. Bichler**, D. Reuter***, A. Wieck*** and A. Zrenner*

*Department of Physics, University of Paderborn, Paderborn, Germany

** Walter-Schottky-Institute, TU Munich, Garching, Germany

*** Applied Solid State Physics, Ruhr-University Bochum, Bochum, Germany

Keywords: Quantum dot, quantum gate, coherent control

Quantum gates acting on one or more qubits are critical components of quantum processors. As recently shown, excitons in semiconductor quantum dots (QDs) are interesting implementations of qubits [1]. In the past, one and two qubit gates have been demonstrated by performing all-optical manipulations [2].

In our contribution, we demonstrate the manipulation of the phase of an exciton in a single QD by electric signals. Thereby it is possible to implement an optoelectronic one qubit phase gate, controlled by the amplitude and phase of a high frequency electric signal.

We use a single InGaAs/GaAs QD embedded in the intrinsic region of a n-i-Schottky diode and separately addressable through a shadow-mask. The exciton ground state represents a two-level system (e.g. a qubit) and can be coherently prepared by ps laser pulses. Its occupancy can determined quantitatively with high accuracy by current measurements [3].

We proof the performance of our quantum gate by Ramsay-like experiments [4]. An excitation with a first $\pi/2$ laser pulse creates a coherent superposition between $|0\rangle$ and $|1\rangle$. The phase of this superposition is stored in the QD and can be detected by a second $\pi/2$ pulse. This setup is highly sensitive to manipulations of the exciton phase between the two optical pulses.

In order to demonstrate the optoelectronic gate operation, we apply a 2.4 GHz electric signal to the photodiode, which is phase locked to the laser pulses. By varying only the delay of this electric signal in relation to the first laser pulse, we are able to switch the quantum interference from constructive to destructive. This means we are able to add a phase shift of π to the quantum phase of the exciton qubit.

The amount of this phase shift is controlled by the electric pulse area, which is defined as the time integral of the electric gate signal between the ps laser pulse pair.

To confirm the experimental results we performed theoretical calculations based on the optical Bloch equations. These show a very good agreement with the experimental data.

We acknowledge financial support by the BMBF via Grant No. 01BM466 (NanoQUIT)

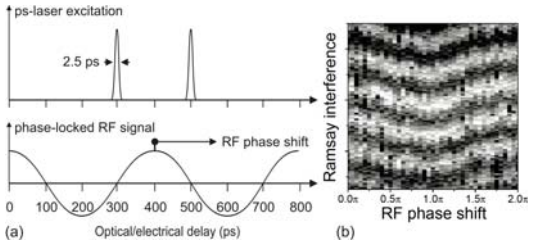

Fig. 1: (a) Timeline of the experiment. The two laser pulses are at fixed delay, while the electric signal can be shifted in relation to the laser pulses. (b) Ramsay interference are recorded for each phase shift of the RF signal. A phase shift of π of the electric signal results here in the inversion of the Ramsay interference pattern.

References

[1] A. Zrenner, P. Ester, S. M. de Vasconcellos et al., J. Phys.: Condens. Matter **20**, 454210 (2008)

[2] X. Li, Y. Wu, D. Steel, D. Gammon, et al., Science **301**, 809 (2003)

[3] A. Zrenner, E. Beham, S. Stufler, et al. Nature **418**, 612 (2002)

[4] S. Stufler, P. Ester, A. Zrenner, M. Bichler, Phys. Rev. Lett. **96**, 037402 (2006)

Lateral single electron transport in capped self-assembled quantum dots

T. Nakaoka[a,b,c], K. Watanabe[a], N. Kumagai[a] and Y. Arakawa [a,c]

[a] *Institute for Nano Quantum Information Electronics, the University of Tokyo, Japan*
[b] *PRESTO, Japan Science and Technology Agency, Japan*
[c] *Institute of Industrial Science, the University of Tokyo, Japan*

Keywords: Single electron transistor, quantum dot, opto-electronic device

Electrons and photons hold great potential in quantum information science. Electrons can be used to store and process quantum information while photons are ideal candidates to transmit quantum information. In this paper, we present a single electron transistor (SET) with capped self-assembled quantum dots for controlling both electrons and photons.

Our device structure has self-assembled InAs quantum dots with a thin *capping* layer of GaAs [Fig. 1(a)]. The n-type GaAs substrate is used as a back-gate. The source and drain metal electrodes on top of the sample are separated by a nanogap of about 20 nm. The structure is very similar to a SET demonstrated in *uncapped* self-assembled dots with nanogap electrodes directly deposited on top of the dot surfaces [1,2]. The optical properties of the *capped* dots are generally much better than the *uncapped* dots, which enables to add optical functionality to the SET. Electrical contact to the *capped* dots is made by thermal diffusion of metal atoms in the nanogap electrodes. We find that the device structure allows for controlling electron tunneling, photocurrent and photoluminescence.

Figure 1(b) and (c) display typical current-voltage characteristics measured in the nanogap structures. A calculation in the framework of the orthodox model shows that the charge stability diagrams are for single self-assembled dot and for electrostatically-coupled double-dots, respectively. In addition to the electron transport properties, we have observed gate-dependent photoluminescence and photocurrent from the dots near such nanogap structures. The results demonstrate that the device structure is suitable to realize the SET with optical functionality, which will be important for future quantum information technology.

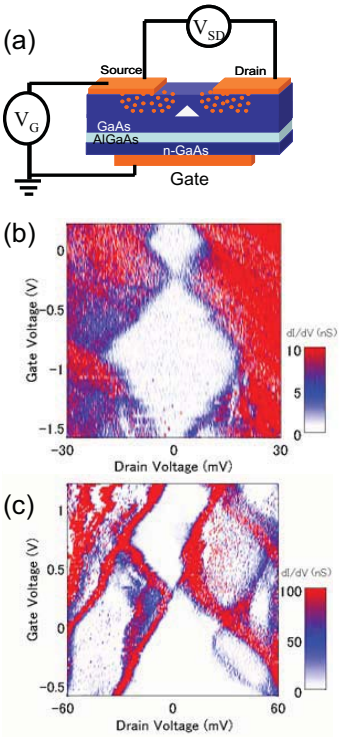

Fig. 1 (a) Schematic illustration of our device structure with capped self-assembled quantum dots. (b) and (c) show the differential conductances at 4 K as a function of the bias voltage and the gate voltage.

This work was supported by Special Coordination Funds for Promoting Science and Technology.

References

1. M. Jung , T. Machida, K. Hirakawa, S. Komiyama, T. Nakaoka, S. Ishida, Y. Arakawa, Appl. Phys. Lett. **87**, 203109 (2005).
2. T. Nakaoka, S. Kako, S. Tarucha and Y. Arakawa, Appl. Phys. Lett. **90**, 162109 (2007).

July 21 (Tuesday)

14:00 – 16:00

Session M4

Optical properties of quantum dots

International Conference Room

MSS-EP2DS Parallel session

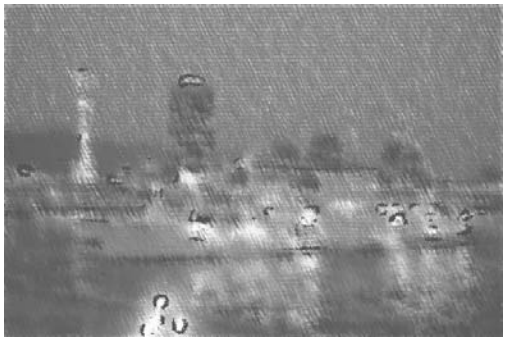

Night view of port Kobe

Two-photon interference from the resonance fluorescence of a single quantum dot in a microcavity

S. Ates*, S. M. Ulrich*, S. Reitzenstein**, A. Löffler**, A. Forchel** and P. Michler*
*Inst. für Halbleiteroptik und Funkt. Grenzflächen, Universität Stuttgart, Allmandring 3, 70569 Stuttgart, Germany
** Technische Physik, Universität Würzburg, Am Hubland, 97074 Würzburg, Germany

Keywords: Quantum Dot, Resonance Fluorescence, Mollow Triplet, Photon Indistinguishability.

Single-photon applications like linear optics quantum computation and quantum teleportation are based on the effect of two-photon interference of two single-photon pulses on a beamsplitter [1]. An essential precondition for the realization of these applications is the possibility to generate indistinguishable photons. For pulsed operation, the two photons need to be Fourier transform-limited and identical in terms of pulse width, spectral bandwidth, carrier frequency, polarization, transverse mode profile, and arrival time at the beamsplitter. The critical ingredient to create such 'ideal' photons is the initial excitation process of the emitter, which strongly influences the coherence properties and, consequently, indistinguishability of the emerging photons.

For our investigations we have applied purely resonant continuous-wave optical laser excitation to coherently prepare an excitonic state of a single semiconductor quantum dot (QD) inside a high quality pillar microcavity. To ensure Fourier transform-limited photon emission with negligible background signal we use an orthogonal geometry of laser excitation and photon detection, together with stabilized low-temperature operation at $T \geq 10$ K. By utilizing the tunable weak coupling between a single QD and the fundamental cavity mode in terms of a significant reduction of the emitter radiative lifetime T_1 (Purcell-enhancement), a strong suppression of phonon-mediated 'pure' dephasing could be achieved.

As a direct proof of single QD resonance fluorescence, the gradual evolution from a narrow and purely Lorentzian transition line $\hbar$ $_0$ to a characteristic Mollow triplet [2] with additional satellite peaks at $\hbar($ $_0 \pm \Omega)$ (Ω: Rabi frequency) has been observed in power-dependent high-resolution measurements (HRPL, Fig. 1a). In accordance with the theory of such a 'dressed state' [2], the spectral splitting of the side peaks reveals a linear dependence on the square-root of the excitation power (Fig. 1c).

Second-order correlation measurements under resonant excitation conditions (not shown) have revealed a pronounced antibunching dip of $^{(2)}(0) = 0\ 08$ (deconvoluted), demonstrating the nearly pure single-photon nature of the collected signal. From time-resolved measurements we inferred a $T_2/2T_1$ ratio of $0\ 91\ \pm 0\ 05$ which is very close to the ideal Fourier-transform limit of 1. The indistinguishability of the photons has been measured by linear polarization-dependent two-photon interference measurements, revealing high visibility degrees of $= 0\ 90 \pm 0\ 05$. This demonstrates the high potential of QDs in pillar microcavities as a source for quantum optics experiments and in quantum information science.

References

[1] B. Lounis and M. Orrit, Rep. Prog. Phys. **68**, 1129-1179 (2005).

[2] B. R. Mollow, Phys. Rev. **188**, 1969 (1969).

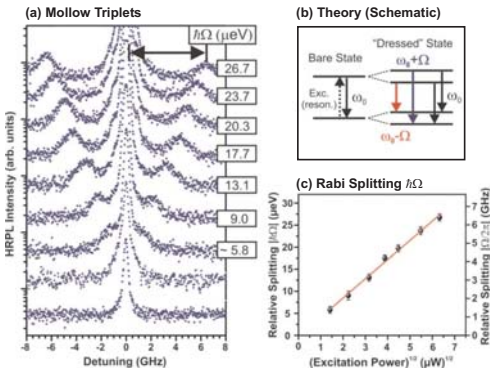

Figure 1: (a) Mollow triplet emission spectra of the resonance fluorescence from a single QD under increasing excitation power. (b) Schematic representation of the 'dressed state' and its optical emission under purely resonant excitation. (c) Excitation power-dependent Mollow side-band splittings $\hbar\Omega \sim (\text{power})^{1/2}$ extracted from (a).

Quantum statistics of correlated two photons with biexciton-exciton cascades: saturation effect

T. Kuroda*, T. Mano*, T. Belhadj*,**, M. Abbarchi*,***, C. Mastrandrea***, M. Gurioli***,
B. Urbaszek**, T. Amand**, X. Marie**, N. Ikeda*, Y. Sugimoto*, K. Asakawa*, and K. Sakoda*
*Quantum Dot Research Center, National Institute for Materials Science, Tsukuba 305-0044, Japan
** Université de Toulouse, LPCNO, INSA-CNRS-UPS, 135 avenue de Rangueil, 31077 Toulouse Cedex 4, France
*** Dipartimento di Fisica, CNISM, Università di Firenze, and Europian Laboratory for Non-Linear Spectroscopy, Via Sansone 1, I-50019, Sesto Fiorentino, Italy

Keywords: Photon statistics, bunching, biexciton, quantum dot

Correlated two photons associated with biexciton - exciton relaxation cascades are attracting considerable attention, since they can realize polarization-entangled photons on demand. Numerous attempts have been made to develop the correlated photon source, and to achieve the high degree of quantum correlation. In this contribution, we report the visibility of bunching statistics crucially depends on excitation intensity, and a significant bunching is only present at extremely low excitation [1]. This is quite surprising because a regulated sequence of correlated two photons does not show any bunching feature, although such a light source should be favorable for practical applications.

The experiments were carried out in GaAs quantum dots (QDs) grown by droplet epitaxy, being embedded in photonic crystal defect cavities [2]. Emission spectra from a single QD after pulsed excitation revealed the biexciton (B) and exciton (X) transition lines. Time correlation between the arrivals of B and X photons is integrated.

An example of coincidence histograms is presented in Fig. 1. At low excitation with 40 μW, the histogram shows a central peak following sequential backgrounds. The presence of a high coincidence peak confirms that two photons were generated with a single radiative cascade. The sequential background is due to coincidence counts between photons in temporally separated pulses. The bunching visibility, i.e., the ratio of a coincidence peak to background side peaks, is evaluated to be 2.7 ($\pm$0.1).

When excitation intensity increases to 80 μW, we find a remarkable reduction in the height of a bunching peak. The visibility in this case is evaluated to be 1.3 ($\pm$0.05). For excitation intensity at 120 μW, the coincidence peak further decreases to 1.06 ($\pm$0.02), as shown in the bottom panel of Fig. 1.

We analyze the power dependence of coincidence histograms in terms of photon number statistics: Our model predicts the height of a bunching peak being determined by the inverse of probability of finding more than one exciton, showing excellent agreement with the observed trend.

References

[1] T. Kuroda et al., Phys. Rev. B **79**, 035330 (2009).

[2] T. Kuroda et al., Appl. Phys. Lett. **93**, 111103 (2008).

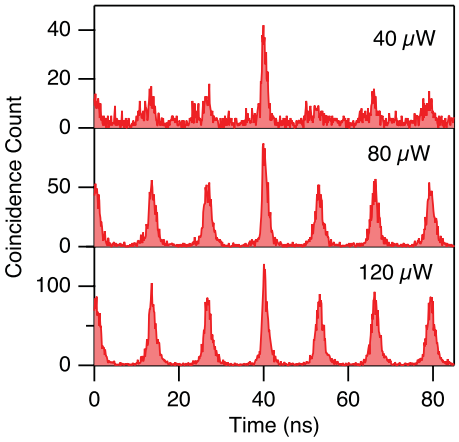

Figure 1: Histograms for the coincident arrival of two photons with biexcitonic and excitonic transitions.

Carrier relaxation in quantum dots: strong energy dependence in the terahertz domain

T. Grange[1], E. A. Zibik[2], B. A. Carpenter[2], N. E. Porter[2], R. Ferreira[1], G. Bastard[1], D. Stehr[3], S. Winnerl[3], M. Helm[3], H. Y. Liu[4], M. S. Skolnick[2] and L. R. Wilson[2]

[1] *Laboratoire Pierre Aigrain, Ecole Normale Supérieure, CNRS, Paris, France*

[2] *Department of Physics and Astronomy, University of Sheffield, UK*

[3] *Institute of Ion Beam Physics and Material Research, Dresden, Germany*

[4] *EPSRC National Centre for III-V Technologies, Sheffield, UK*

Keywords: Quantum dot, Energy relaxation, Electron-phonon interaction, Terahertz

Semiconductor quantum dots (QDs) are highly attractive for terahertz (THz) applications because of their expected long excited state lifetimes. Devices incorporating semiconductor QDs have the potential to overcome many of the limitations of quantum well-based devices. Yet, their potential use as emitters in the THz domain depends critically on their energy relaxation times. However, to date, carrier relaxation in self-assembled QDs has only been studied over a limited range of sublevel energy separations, typically above the Reststrahlen band.

We present here the first investigation of intersublevel relaxation dynamics in n-doped InGaAs self-assembled quantum dots in the THz spectral domain, which reveals variations of 3 orders of magnitude in decay time, with longest measured lifetime exciding 1ns. Experimental data are in good agreement with our calculations. Our model is based on a microscopic description of anharmonic decay of QD polaron[1]: the Fröhlich polar coupling between confined electron and optical phonon leads to the formation of polaron states. Due to the anharmonicity of the lattice vibrations, these polaron states can disintegrate into a combination of two phonon. Our calculation show that the efficiency of this process depends critically on the transition energy in the THz regime. Moreover, we show that the anharmonic polaron decay is expected to be the dominant mechanism down to the 1 THz regime.

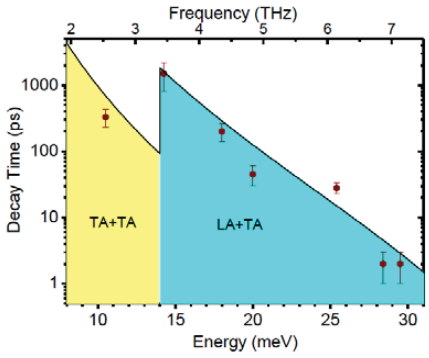

Fig.1 Intersublevel relaxation time as a function of the transition energy in annealed self-assembled quantum dots: Decay time extracted from pump-probe experiments (symbols) and calculations (solid line) based on a microscopic model of anharmonicity induced polaron decay.

References

1. T. Grange, R. Ferreira, G. Bastard, Phys. Rev. B **76**, 241304 (2007).

Time-Resolved Optical Studies of the Charge Carrier Dynamics in Lateral InGaAs Quantum Dot Molecules

C. Hermannstädter*, G. J. Beirne*+, M. Witzany*, L. Wang**, A. Rastelli***, W.-M. Schulz*, M. Jetter*, O. G. Schmidt*** and P. Michler*

*Inst. für Halbleiteroptik und Funkt. Grenzflächen, Universität Stuttgart, Allmandring 3, 70569 Stuttgart, Germany

** Max-Planck-Institut für Festkörperforschung, Heisenbergstr. 1, 70569 Stuttgart, Germany

*** Institut für Integrative Nanowissenschaften, IFW Dresden, Helmholtzstr. 20, 01069 Dresden, Germany

+ now: Cavendish Laboratories, University of Cambridge, J. J. Thomson Ave., Cambridge, CB3 0HE, UK

Keywords: coupled quantum dots, time-resolved photoluminescence, charge carrier dynamics

The charge carrier configuration and dynamics in coupled quantum dot systems are the essential properties that need to be understood for gaining the ability to coherently manipulate the coupling in the system using external fields, such as, electric, magnetic or light.

In the presented work the time-resolved photoluminescence (PL) of single self-assembled lateral quantum dot molecules (QDMs) is investigated. Due to their specific growth mode [1] all QDMs are aligned along the same crystallographic axis $[1\bar{1}0]$. This allows to apply a lateral electric field using parallel electrodes on top of the sample to manipulate the band structure and thus the charge distribution and coupling within the QDMs, as well as, to reversibly switch between different emission lines [2]. To be able to measure the spectral and temporal excitonic emission characteristics simultaneously the QDMs have been placed inside a low-Q planar -cavity to obtain a higher PL extraction efficiency and thus sufficient signal for using a Streak camera at the typical emission energies of ≈1.3 eV. The decay characteristics of the neutral exciton X1, which is displayed Fig. 1 (c), shows a clear difference for the two tuning situations where X1 is the dominant line (left panel - "single-dot case") and where two neutral excitons X1 and X2 are equally intense (mid panel - "alignment case"). Whereas the "single-dot case" reveals a cascaded emission of XX1 and X1 similar to a single QD, the "alignment case" clearly deviates from such mono-exponential decay behavior due to bi-directional inter-dot-tunneling of charge carriers. The full charge dynamics is treated using a rate-equation model including all states up to 2 electrons and 2 holes in the QDM, pump- and radiative decay-rates (experimental parameters), as well as, tunnel-rates under consideration of the different Coulomb exchange energies (fit parameters).

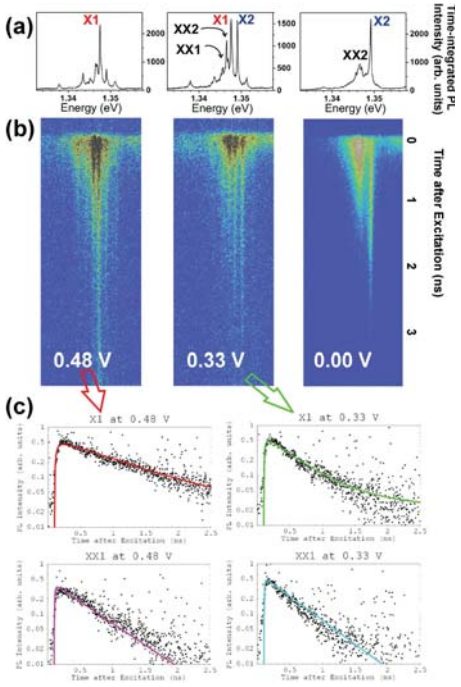

Figure 1: (a) PL spectra of a single QDM under non-resonant excitation: the application of different electric fields (electrode bias voltages given as insets) results in three different tuning situation; (b) the corresponding Streak camera spectra; (c) the time-traces (points) for the exciton X1 and biexciton XX1 at 0.48 V and 0.33 V (alignment) and the best-fit model-results (lines).

References

[1] R. Songmuang et al., APL **82**, 2892 (2003); L. Wang et al., New J. Phys. **10**, 045010 (2008).

[2] G. J. Beirne et al., PRL **96**, 137401 (2006).

Excited-state spectroscopy of charged quantum dots in magnetic field

H. Sanada, T. Sogawa, H. Gotoh, Y. Tokura, H. Yamaguchi, H. Nakano, and H. Kamada
NTT Basic Research Laboratories, NTT Corporation, Japan

Keywords: trion, charged exciton, quantum dot

Spin states in semiconductor nanostructures are expected to act as quantum information carriers in solid-state systems. One approach that allows us to access single electron spin in semiconductor quantum dots (QDs) is to use negative trions, which serve as an intermediary for the initialization [1] and readout [2] of single electron spins. Most experimental studies have focused on their *lowest* radiative states, however, their *excited* states have a rich variety of configurations because Coulomb and/or exchange interactions between different shells are quite different from those in the lowest shells. In this study, we investigated the magneto-photoluminescence (PL) properties of excited trions in a charge-tunable QD [3].

Our sample consists of monolayer-fluctuation GaAs QDs embedded in an n-i-Schottky diode grown by molecular beam epitaxy. For micro-PL measurements, the sample was cooled to 6 K in a cryostat placed in a magnetic field B, which was applied to the sample in the Faraday geometry. A Ti:sapphire laser excited QDs within an aperture in the metal mask/electrode, and the PL spectra were measured with a monochromator and CCD detector.

Figure 1 shows a magnetic field dependence of PL spectra measured at a bias voltage of 0.25 V. In addition to the ground exciton (X^0) and trion (X^-) emissions, we found several PL lines (labeled A, B, and C), most of which exhibit much complex B dependencies. The most noteworthy is the line A, whose energy decreases as $|B|$ increases. To understand the origin of these PL lines, we consider shell and spin configuration of excited trions [Fig. 2(a)]. From a configuration-interaction calculation using an elliptic Fock-Darwin model, we obtained the B dependence of trion and electron energies [Fig. 2(b)], and found that the transitions $(sp_-)_{\rm t}p_- \rightarrow s$, $(sd_+)_{\rm t}s \rightarrow d_+$, and $(sp_-)_{\rm s}s \rightarrow p_-$ are possible assignments for lines A, B, and C, respectively. We believe that the present work opens the possibility of developing a novel scheme for the optical control of single electron spins using the excited states of trions in QDs.

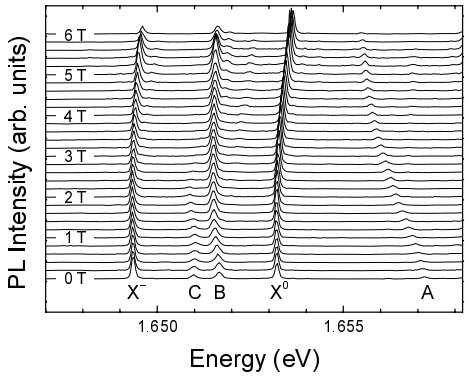

Figure 1: PL spectra obtained in a magnetic field range of $0 < B < 6$ T at a bias voltage of 0.25 V.

This work was partly supported by the Japan Society for the Promotion of Science (JSPS).

References

[1] M. Atatüre *et al.*, Science **312**, 551 (2006).
[2] J. Berezovsky *et al.*, Science **314**, 1916 (2006).
[3] H. Sanada *et al.*, Phys. Rev. B **79**, 121303(R) (2009).

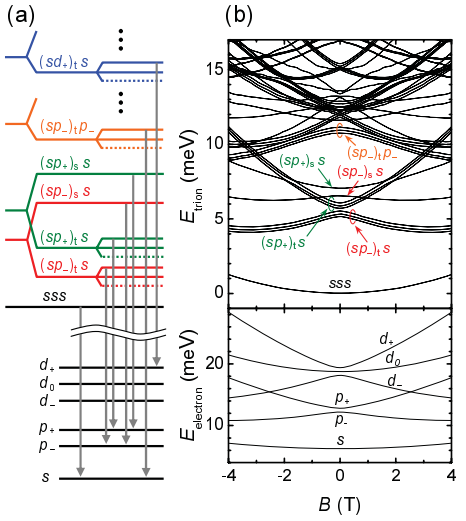

Figure 2: (a) Energy diagram for a single electron and trion. (b) Calculated total energy vs B. $(e_1e_2)_{\rm t(s)}h$ describes the shell-configurations with two electrons (e_1e_2) and a hole (h), and subscript t(s) represents spin-triplet (singlet) of two electrons.

Size-dependent exciton g-factor in self-assembled InAs/InP quantum dots

J. van Bree*, N. A. J. M. Kleemans*, P. J. van Veldhoven*, R. Nötzel*, A. Yu. Silov*, C. Pryor**, M. E. Flatté** and P. M. Koenraad*

*Photonics and Semiconductor Nanophysics, COBRA, Eindhoven University of Technology, The Netherlands

** Department of Physics and Astronomy and Optical Science and Technology Center, University of Iowa, USA

Keywords: self-assembled quantum dots, -factor, diamagnetic shift, anisotropy splitting

Self-assembled quantum dots are suggested as building blocks in quantum information processing. Control over the exciton -factor ($_{ex}$) is therefore highly desirable for the realization of individual qubits [1]. The self-assembly process of quantum dots gives rise to a distribution in size, shape, and composition of the dots and therefore leads to a dot to dot variation in $_{ex}$. This opens the possibility of utilizing the growth conditions to engineer $_{ex}$. However, up to now experiments on InAs/GaAs quantum dots did not reveal a strong correlation between emission energy and $_{ex}$.

We have studied the size dependence of the exciton -factor in self-assembled InAs/InP (100) quantum dots [2]. For these dots the emission wavelength is compatible with the telecommunication wavelengths. Photoluminescence measurements on a large ensemble of these dots indicate a multimodal height distribution. Cross-sectional scanning tunneling microscopy measurements have been performed and support the interpretation of the macrophotoluminescence spectra. More than 160 individual quantum dots have systematically been investigated by analyzing the Zeeman splitting of single dot magnetoluminescence between 1200 and 1600 nm in magnetic fields up to 10T.

A direct relationship between the exciton -factor and the emission energy E_0 has been found (see Figure 1), which is unique for self-assembled quantum dots. It is noteworthy that around 830 meV $_{ex}$ even changes sign. We have demonstrated that the exciton -factor is strongly correlated with the height of the quantum dots. The measured diamagnetic shift, which is a measure for the lateral extension of the quantum dot, was found to be only weakly correlated to the emission energy. This supports the argument that the dependency of $_{ex}$ versus E_0 is due to the height variation and the distribution of $_{ex}$ at a given energy is related to the diameter of the quantum dots. The observed correlations agree with calculations using 8-band $\mathbf{k}\cdot\mathbf{p}$-theory [3]. Furthermore, we have found a size-dependent anisotropy splitting of the exciton emission in zero magnetic field.

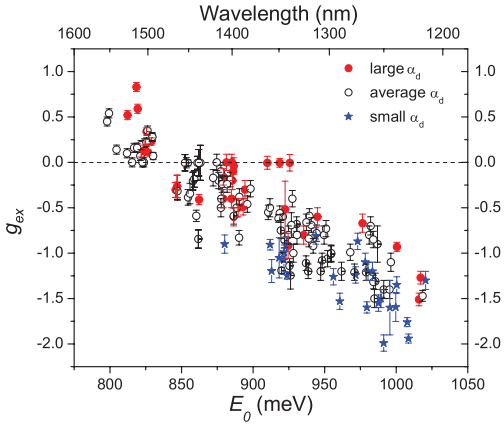

Figure 1: The exciton -factor $_{ex}$ as function of the emission energy E_0 for 164 quantum dots. Quantum dots having a small height and small diamagnetic shift, thus having a small lateral size, have a more negative -factor as compared to dots having a large height and large lateral size. The colors represent different intervals of the diamagnetic shift.

References

[1] D. Klauser, W. A. Coish and D. Loss, Adv. Solid State Phys. **46**, 17 (2007).

[2] N. A. J. M. Kleemans, J. van Bree, P. J. van Veldhoven, P. A. Nouwens, R. Nötzel, A. Yu. Silov, M. E. Flatté, and P. M. Koenraad, Phys. Rev. B **79**, 045311 (2009).

[3] C. E. Pryor and M. E. Flatté, Phys. Rev. Lett. **96**, 026804 (2006), and erratum **99**, 179901(E) (2007).

Magnetic-field control of exciton fine structure splitting in nitrogen δ-doped GaAs

Yukihiro Harada, Osamu Kojima, Takashi Kita, and Osamu Wada
Department of Electrical and Electronics Engineering, Graduate School of Engineering, Kobe University, Rokkodai 1-1, Nada, Kobe 657-8501, Japan

Keywords: nitrogen doping, bound exciton, fine structure splitting, Zeeman effect

The electronic states created by nitrogen (N) related centers in III-V semiconductors cause substantial localization of excitons. In particular, in the impurity limit, the localized electronic states relating to N pairs and N clusters show the extremely narrow bandwidth luminescence [1–3]. These impurity centers in a semiconductor have been attracting a strong interest in single photon sources with a certain emission wavelength. Recently, we have reported the linearly polarized fine structure splitting (FSS) of the exciton bound to N pair centers in GaAs [4]. On the other hand, we have observed photoluminescence (PL) lines showing superlinear excitation power dependence [3]. The FSS is, therefore, a key issue for demonstrating the entangled photon pair generation by using the biexciton-exciton cascade process. In this work, we have studied a magnetic-field control of the FSS by magneto-PL spectroscopy and performed theoretical calculations taking into account the *J*-*J* coupling, local field, exciton population, and Zeeman effects.

The nitrogen δ-doping has been performed on the (3×3) N stable surface of GaAs(001) by molecular beam epitaxy. Linearly polarized magneto-PL measurements have been carried out by using the 488 nm line of an argon-ion laser at 2.5 K. Magnetic field was applied along the [-110] direction in the Voigt configuration, which is perpendicular to the N pair direction. The resolution limit of our spectroscopy system is 0.1 meV.

Figure 1(a) displays magneto-PL spectra detected by the [-110] polarization. With applying the magnetic field, the PL spectrum splits into several signals and changes their intensities. Calculated Zeeman splittings of a center with the C_{2v} symmetry are shown for the [-110] polarization in Fig. 1(b). The results reproduce qualitatively the measured magneto-PL spectra. Figure 1(c) shows the detailed polarization-selection characteristics of the exciton energies related to the $A_{\pm1}$ (bright exciton) and $B_{\pm2}$ (dark exciton in our measurement configuration) levels defined in Ref. 4. Solid and dashed lines represent the [-110] and [110] polarizations, respectively. The exciton energies indicated by arrows in Fig. 1(b) correspond to the solid lines. The exciton states having the orthogonal linear polarization components degenerate at about 3 T. This result points out the possibility of the entangled photon pair generation by using the biexciton-exciton cascade process in the nitrogen δ-doped GaAs.

References

[1] T. Makimoto *et al.*, Appl. Phys. Lett. **67**, 688 (1995).
[2] S. Francoeur *et al.*, Phys. Rev. Lett. **93**, 067403 (2004).
[3] T. Kita *et al.*, Phys. Rev. B **74**, 035213 (2006).
[4] T. Kita *et al.*, Phys. Rev. B **77**, 193102 (2008).

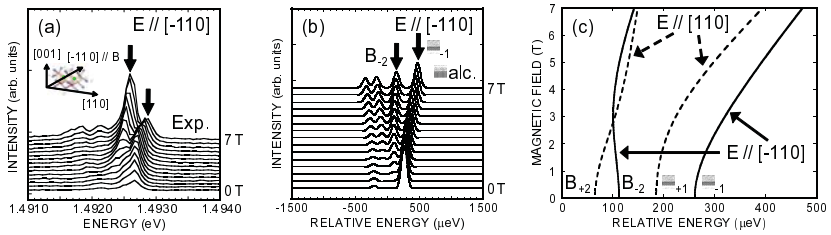

Figure 1: (a) Linearly polarized magneto-PL spectra detected by the [-110] polarization. (b) Calculated Zeeman splittings of a center with the C_{2v} symmetry for the [-110] polarization. (c) Polarization-selection characteristics of the exciton energies in the magnetic field. Solid and dashed lines represent the [-110] and [110] polarizations, respectively.

Widely tunable intense MIR photoluminescence mission from epitaxial Pb(Sr)Te quantum dots embedded in CdTe

S. Kriechbaumer, G. Springholz, T. Schwarzl, A. Hochreiner, W. Heiss, E. Kaufmann, M. Simma, H. Groiss, F. Schäffler, T. Wojtowicz, K. Koike*, H. Harada*, M. Yano*

Institut für Halbleiter- und Festkörperphysik, Johannes Kepler University, Linz, Austria

**) Osaka Institute of Technology, Asahi-ku Ohmiya, Osaka 535-8585, Japan*

Keywords: Quantum dots, heterostructures, optical and electronic properties, novel structures

The narrow gap IV-VI semiconductors are well suited for mid-infrared optoelectronic devices due to their symmetric conduction- and valence bands as well as small Auger recombination rates. For such devices, quantum dot active regions are desirable, however, conventional IV-VI Stranski-Krastanow quantum dots only exhibit weak luminescence emission due to the strain-induced type-II band alignment. As alternative, we have developed a novel synthesis method for epitaxial PbTe quantum dots embedded in wide gap CdTe matrices. PbTe and CdTe are essentially lattice matched but differ in their crystal structure. Thus, quantum dots are produced by phase separation rather than by strain [1]. The resulting quantum dots exhibit a number of extraordinary properties such as highly symmetric shapes, atomically abrupt interfaces as well as intense luminescence emission due to the very large quantum confinement due to the high CdTe energy barriers.

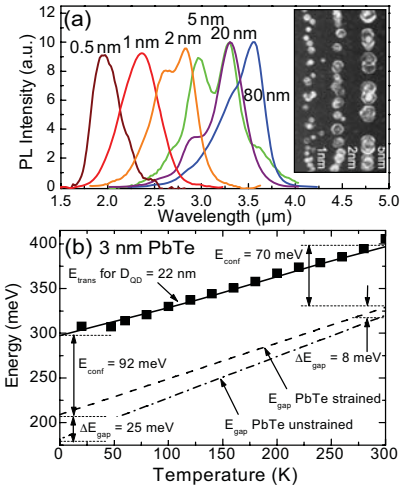

Fig. 1: (a) PL emission spectra of PbTe/CdTe QDs with different size (see cross-sectional TEM insert). (c) Temperature dependence of emission (■) of PbTe QDs with ~22 nm diameter compared to strained and unstrained PbTe band gap.

In this work, we have focused on the optical emission and tuning of the wavelength over a wide spectral region by control of the quantum dot size as well as composition. All samples were grown by molecular beam epitaxy on high quality CdTe buffer layers predeposited on GaAs (001) substrates. As demonstrated in Fig. 1(a), by changing the PbTe layer thickness from 0.5 to 80 nm, the dot emission at room temperature can be tuned from 1.8 to 4 μm. This corresponds to a change of the diameter of the nearly spherical dots from 8 to 30 nm [1], as shown by the cross-sectional TEM image of Fig. 1. Alloying with Sr leads to a further blue shift of the QD emission due to the rapid increase of the PbSrTe band gap with Sr content, while the strong room temperature emission is maintained. In fact, for 1 nm PbSrTe/CdTe layers, the PL signal is even stronger as compared to a 1 nm PbTe reference sample, despite the shorter emission wavelength. For small PbSrTe dots, the blue shift is somewhat less than expected, indicating that part of the Sr is incorporated in the CdTe matrix material. At cryogenic temperatures, the PL efficiency increases and reaches a maximum at around 50 to 100 K in dependence of the dots size [2]. We suggest that this behaviour arises from the splitting of the ground state into a higher lying bright state and a lower lying dark state, as was also observed in chemically synthesized QDs. The strong temperature shift of the PL peak shown in Fig. 1(b) agrees very well to model calculations taking into account the thermal strain as well as non-parabolicity effects. Thus, our dots provide very promising perspectives for realization of novel mid-infrared optoelectronic devices

References

1. H. Groiss, *et al.*, Appl. Phys. Lett. **91**, 222106 (2007).
2. T. Schwarzl, *et al.*, Phys. Rev. B **78**, 165320 (2008).

July 21 (Tuesday)

16:00 – 18:00

Poster Session Tu-mP

Meeting Room 501, 502

MSS-EP2DS Parallel session

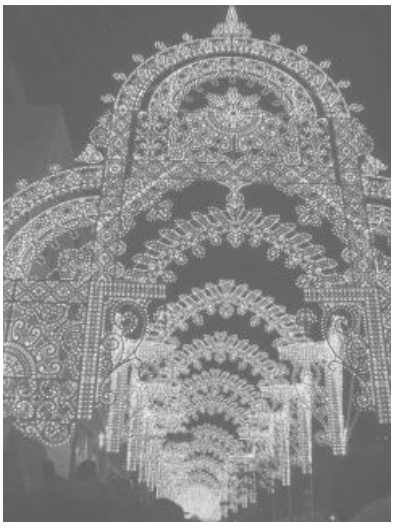

Kobe luminarie
(December)

Polarization controlled emission from stacked InAs quantum dots

T. Inoue *, N. Yasuoka*,**, O. Kojima*, T. Kita*, and O. Wada*

* *Department of Electrical and Electronics Engineering, Kobe University, Kobe, Japan*

** *Fujitsu Laboratories Ltd., Atsugi, Japan*

Keywords: Quantum dot, Polarization control, Electronic coupling, Molecular beam epitaxy

Self-assembled InAs quantum dots (QDs) have been attracting much attention for semiconductor optical amplifiers (SOAs). QD-SOA is expected to realize high saturation power, multi-channel processing, and high-speed response. However, in the conventional QDs, the significant polarization dependence in the optical gain is caused by the flat shape and the biaxial compressive strain, in which polarization fluctuation of the input signal is regenerated in the amplified output. Therefore, control of the polarization sensitivity is indispensable. We proposed columnar QDs [1,2], where QD layers were stacked with very thin intermediate layers. On the other hand, recently we reported enhancement of the transverse magnetic (TM) polarization component in highly stacked QD layers with relatively thick spacer layers of 20 nm. The polarization change is attributed to electronic coupling in the vertical direction [3]. In this work, we have studied effects of electronic coupling on the polarization properties of QD-SOA structures including double-stacked QD layers.

Samples were grown on GaAs (001) substrates by using solid-source molecular beam epitaxy. On a GaAs buffer layer, double-stacked InAs QDs were grown. The GaAs spacer layer thickness in between the QD layers was controlled. Finally, a 150 nm-GaAs capping layer was grown. Furthermore, SOA structures with the same double-stacked QD layers were fabricated to confirm the polarization change in the edge electroluminescence (EL).

Figure 1 displays the transmission electron microscope (TEM) image of the double-stacked QDs, where the spacer thickness is 16 monolayers (MLs). Vertically aligned QD pairs are formed perfectly. Figure 2 shows photoluminescence (PL) spectra obtained from the (001) surface. The PL spectrum of the stacked QD sample shows a slightly narrower signal than that of a sample with a single QD layer. In addition, the energy separation between the ground state (solid bars) and the first excited state (dotted bars) has been found to be reduced in the stacked QDs. That is considered to be due to vertical coupling of the electronic states in the vertically coupled QDs. Furthermore, we have confirmed in the SOA devices that the polarization difference in the edge EL is reduced as compared with a reference device containing a single QD layer.

References

1. T. Kita *et al.*, Jpn. J. Appl. Phys. **41**, L1143 (2002).
2. T. Kita *et al.*, Appl. Phys. Lett. **88**, 211106 (2006).
3. O. Kojima *et al.*, J. Appl. phys. **103**, 113504 (2008).

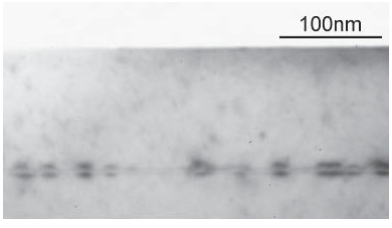

Fig.1 TEM images of double-stacked QDs with spacer layer thickness of 16 MLs.

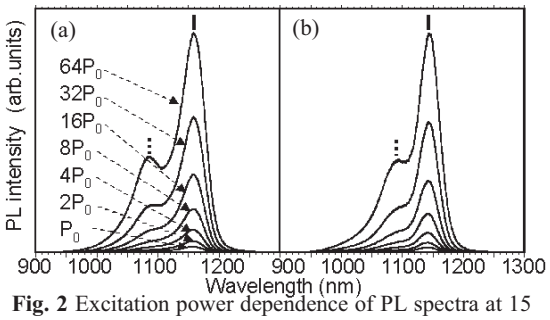

Fig. 2 Excitation power dependence of PL spectra at 15 K of (a) single QDs and (b) double-stacked QDs with spacer layer thickness of 16 MLs. P_0= 0.5 mW.

Structural properties of GaP anti-quantum dots on the GaAs grown by droplet epitaxy

J. Y. Lim*,**, J. D. Song*, W. J. Choi*, J. I. Lee*, S. H. Han*, H. S. Yang**, and J. S. Kim***

** Nano Science Research Division, Korea institute of Science and Technology, Seoul,Korea*

*** Department of Physics, Chung-ang University, Seoul, Korea*

**** Department of Physics, Yeungnam University, Gyeongsan, Korea*

Keywords: GaP, anti-quantum dot, droplet epitaxy, molecular beam epitaxy

We report structural properties of anti-quantum dots (AQDs) – nano-sized structure with larger bandgap compared with that of the sandwiching materials - made of GaP on GaAs as a function of P_2 injection substrate temperature (T_f) and P_2 flux (F_p). The GaP anti-QDs show various shapes according to the change of T_f, and F_p.

All samples were grown using molecular beam epitaxy with droplet epitaxy method [1]. Surface oxide of GaAs substrate was removed at 600°C, and ~ 100 nm-thick GaAs buffer layer was grown at 580°C. Substrate temperature was decreased to 180 °C for the formation of Ga metal. Chamber's vacuum is lower than 1 x 10 $^{-9}$ torr during injection of Ga metal. The flux of Ga is equivalent to the growth rate of GaAs of 0.14nm/s. The density of AQDs is determined at this stage. Sequentially, P_2 is introduced on the metal droplet. Atomic force microscopy (AFM) and scanning electron microscopy (SEM) observations were performed to study structural properties of self aligned nano size GaP AQDs..

The result of measurement shows that the height of GaP AQDs is decreased and the density of GaP AQDs is almost same as the T_f increases from 75°C to 180°C. Furthermore, if substrate temperature is higher, a GaP AQD is divided by 2 or 4 flods. (see Fig. 1)

Details of properties of these noble structures will be discussed in the presentation.

References

1. Mano, T. et al., Nano Lett. 2005, v. **5**, pp. 425 (2005).

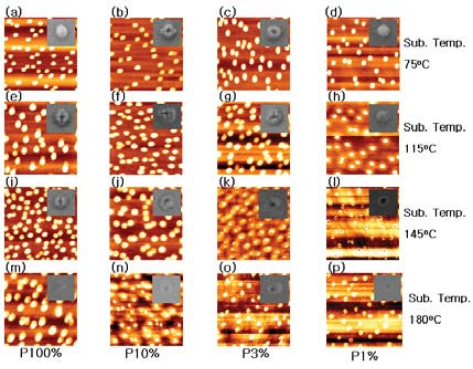

Fig.1 1um x 1um AFM images of GaP anti-QDs classified by P_2 injection substrate temperature and P_2 flux. Inset is SEM data.

Corresponding ; jdsong@kist.re.kr

Controlled growth of InAs nanowires on engineered substrates

S.Roddaro *, P.Caroff**, G.Biasiol***, F.Rossi****, C. Bocchi****, K.Nilsson**, L.Fröberg**, J.B.Wagner**, L.Samuelson**, L.-E.Wernersson** and L.Sorba*

* *NEST INFM-CNR and Scuola Normale Superiore, P.za S.Silvestro 12, 56127 Pisa, Italy*

** *Solid State Physics & the Nanometer Structure Consortium, Lund University, P.O.Box 118 Lund, Sweden*

*** *TASC INFM-CNR Laboratory, Area Science Park, 34012 Trieste, Italy*

**** *Istituto CNR IMEM, Parco Area delle Scienze 37/A, 43100 Parma, Italy*

Keywords: semiconductor nanowires, Au-seeded growth, engineered substrates

Recent years have witnessed the emergence of semiconductor nanowires (NWs) as a new promising platform for nanoelectronics [1]: the small radial extension of the NW structure makes strain constraint looser and allows novel heterostructure combinations [2]; the strong surface effects during NW growth can lead to high-quality nanostructures from both crystalline and geometrical point of view [3].

Our work focuses on the the Au-seeded growth of InAs NWs on engineered substrates as a crucial step in the development of novel NW-based devices. Two specific cases are discussed: farbrication of NWs starting from AlGAs/GaAs (111)B heterostructures capped by a 50nm-thick InAs layer grown by molecular beam epitaxy and from 2μm-thick InAs buffer layer grown on Si (111) by metal-organic vapour phase epitaxy. Morphological and structural properties of the substrates are investigated by atomic force and transmission electron microscopy (TEM). nm-scale surface roughness for the first case and large atomically-flat regions for the second were measured. Both substrates offer specific advantages with respect to bulk InAs(111)B substrates such as integration of NWs on Si-based electronics as well as for the development of micromechanical structures incorporating NW elements.

InAs NWs were successfully grown by chemical beam epitaxy on both substrates. Figure 1 shows a 30°-tilted scanning electron microscopy (SEM) image of InAs NWs grown on InAs/Si. No significant difference was observed for NWs grown on engineered substrates with respect the ones obtained starting from standard InAs(111)B (Fig.1a and b, respectively). The quality of NW crystal structure was evaluated by high resolution TEM. Figure 1c demonstrates that NWs crystallize in the usual hexagonal wurzite phase, with a very low density of stacking faults (<< 1μm^{-2}). Our results indicate a new route for the integration of NWs in advanced devices.

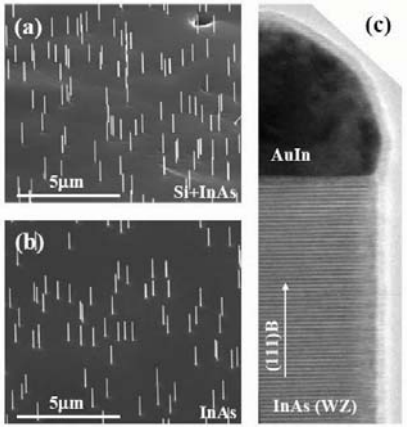

Figure 1 (a) SEM image of InAs NWs grown from Au nanoparticles on InAs on Si(111). (b) SEM image of InAs NWS grown on a standard InAs(111)B substrate. Both images were taken at a tilt angle of 30°. (c) High resolution TEM image of an InAs NW grown on InAs/Si substrate.

References

1. T. Bryllert *et al*, Nanotechnology **17**, s227 (2006).
2. M.T. Björk *et al,* Nano Lett. 2, 87 (2002)
3. M.W. Larsson at el, Nanotech. **18**, 015504 (2007).

Photoluminescence from single isoelectronic traps in nitrogen delta-doped GaAs grown on GaAs(111)A

T. Fukushima[1], M. Ito[1], Y. Hijikata[1], H. Yaguchi[1], S. Yoshida[1], M. Okano[2], M. Yoshita[2], H. Akiyama[2], S. Kuboya[3], R. Katayama[3], and K. Onabe[3]

[1] *Saitama University, Saitama, Japan*
[2] *ISSP, The University of Tokyo, Kashiwa-shi, Chiba, Japan*
[3] *Department of Advanced Materials Science, The University of Tokyo ,Kashiwa-shi, Chiba, Japan*

Keywords: Isoelectronic trap; Single photon; δ-doping

Single-photon sources are expected to play a key role in the field of quantum information science and technology, such as quantum cryptography and quantum computing. Single isoelectronic traps in semiconductors are promising candidates for single-photon sources because sharp emission lines are obtained from isoelectronic traps, for instance, formed by nitrogen pairs in dilute III-V-N alloys (GaAs:N and GaP:N). In previous studies, we have succeeded in observing exciton emission lines from single isoelectronic traps in N δ-doped GaAs layers grown on GaAs(001) surface [1], and reported twin emission lines which are linearly polarized in the [1-10] and [110] directions, respectively [2]. In the present paper, we have studied photoluminescence from isoelectronic traps in N δ-doped GaAs grown on GaAs (111)A substrates in order to obtain randomly polarized photons suitable for the application the quantum cryptography.

The samples used in this study were N δ-doped GaAs layers grown on GaAs (111)A substrates by metalorganic vapor phase epitaxy. We have measured micro photoluminescence (PL) spectra at 4 K using a diode-pumped solid-state laser (532 nm) as the excitation source. We have also carried out polarization measurements of the PL spectra.

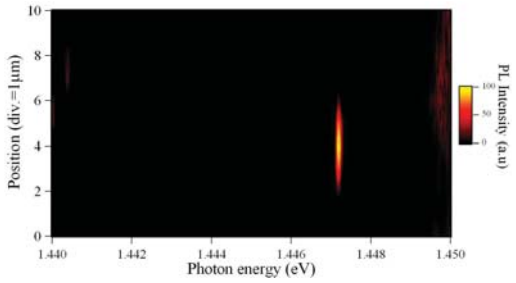

Fig.1 PL intensity map of N δ-doped GaAs grown on GaAs(111)A.

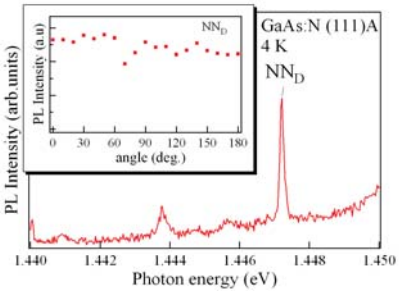

Fig.2 PL spectrum and PL peak intensity as a function of polarization angle.

Figure 1 shows a PL intensity map of N δ-doped GaAs grown on a (111)A substrate obtained by scanning the sample in one direction. As can be seen from this figure, one PL line with a narrow linewidth of less than 50 μeV is observed at a specific position, clearly indicating that the emission from a single isoelectronic trap can be successfully detected. This PL line is located at 1.447 eV, which is in close agreement with the energy reported for emission line due to NN_D [3]. As shown in Figure 2, the emission line shows a single-peak character, unlike twin PL peaks observed from isoelectronic traps in N δ-doped GaAs grown on (001) surface.

The inset in Figure 2 shows the PL intensity as a function of polarization angle. It is found from the almost constant PL intensity that randomly polarized photons can be obtained. This polarization property is completely different from that observed for isoelectronic traps in N δ-doped GaAs on (001). The results obtained for (111) indicates the in-plane strain is isotropic, which is consistent with the crystal symmetry.

References

[1] Y. Endo *et al.*, J. Cryst. Growth **298**, 73 (2007).
[2] Y. Endo *et al.*, Physica E **40**, 2110 (2008).
[3] T. Makimoto *et al.*, Jpn. J. Appl. Phys. **36**, 1694 (1997).

Growth of low density InGaAs quantum dots using MEMBE

N. K. Cho, S. J. Park, J. D. Song, W. J. Choi and J. I. Lee

Nano Device Research Division, Korea Institute of Science and Technology, Seoul, Korea

Keywords: Quantum dots, MEMBE, Density

Recently communication methods utilizing the quantum nature of photons have been suggested for enhancing security. For the realization of optical communication using quantum cryptography, the single photon sources are essential [1]. Trapped single atoms or ions, single molecules, and single semiconductor quantum dots (QDs) have been researched for the single photon sources. Nowadays, the single photon emission from nano-structure cavity containing single QD has been reported [2]. The InGaAs QDs embedded in GaAs layer can emit the light used in the optical fiber communication. Therefore, the single photon sources using InGaAs QDs have compatibility to the technology in use.

In this presentation, we suggest the migration enhanced molecular beam epitaxy (MEMBE) to the reducing of density of InGaAs QDs and characterize the optical properties of low density InGaAs QDs.

For the formation of InGaAs QDs using MEMBE growth mode, we applied the migration enhancing times between the supplies of In, Ga, and As [3]. As the migration enhancing time increases from 30 seconds to 120 seconds, the density of InGaAs QDs is decreased from ~ 350 QDs/μm^2 to ~ 3 QDs/μm^2. In case of QDs with migration enhancing time of 120 seconds, height is ~ 7 $\pm$ 1 nm and diameter is ~ 105 $\pm$ 15 nm. The size of InGaAs QDs is increasing as the migration enhancing time increases. The optical properties of low density InGaAs QDs was measured by photoluminescence (PL) at 10K. The ground emission and first excited emission of the QDs is measured at 981nm and 940nm separately.

The measured data shows that the InGaAs QDs grown by MEMBE have low density and good optical properties for the realization of the single photon sources.

References

1. P. Michler, A. Kiraz, C. Becher, W. V. Schoenfeld, P. M. Petroff, L. Zhang, E. Hu, and A. Imamoglu, Science **290**, 2282 (2000).

2. M. Pelton, C. Santori, J. Vuckovic, B. Zhang, G. S. Solomon, J. Plant, and Y. Yamamoto, Phys. Rev. Lett. **89**, 233602 (2002).

3. N. K. Cho, S. P. Ryu, J. D. Song, W. J. Choi, J. I. Lee, H. Jeon, Appl. Phys. Lett. **88**, 133104 (2006).

Edge localization, Landau levels and Aharonov-Bohm oscillations in core multi-shell nanowires

Giulio Ferrari[1,2], G. Cuoghi[3], A. Bertoni[1], G. Goldoni[1,3], and E. Molinari[1,3]
1*CNR-INFM S3 Research Center on nanoStructures and bioSystems at Surfaces, Modena, Italy*
2*CNISM Research Unit of Modena, Italy*
3*Department of Physics, University of Modena and Reggio Emilia, Italy*

Keywords: core multi-shell nanowires, Landau levels, Aharonov-Bohm oscillations, radial heterostructure

Core multi-shell nanowires (NWs) have recently been demonstrated experimentally for GaN/InGaN [1], InP/InAs [2] and GaAs/AlAs [3]. Here, 2D electronic states (2DESs) are formed at the interface between different semiconductor layers, as in usual planar hetero-structures, but wrapped around the NW core, resulting in a 2DES with prismatic shape which reflects the symmetry of the underlying free-standing NW used as a substrate.

Here we show that the prismatic symmetry leads to edge-localized states formation, so that a prismatic 2DES behaves as a set of quasi-1D quantum channels (see Figure 1 (a)), with inter-channel coupling dictated by the geometric details. We show how such edge-localized states can be manipulated by strong magnetic fields either in the axial or in the normal configuration, and rationalize how results in terms of Aharonov-Bohm (AB) oscillations or Landau level formation, respectively.

In our approach, the 2DES is modeled as a strictly 2D electronic system confined around a prismatic core, by use of a geometric potential [4] which takes into account the local curvature of the system. Experimental imaging information [1, 2, 3] is fed into the model, and numerical simulations for prismatic 2DESs based on GaAs, InAs, and InGaN with triangular, square and hexagonal symmetries have been performed, and the behavior of the localization energy and inter-channel tunnel coupling is predicted as a function of symmetry, local curvature γ at the edges, and radius R of the NW.

The geometric potential approach allows to include a magnetic field in arbitrary configurations [5, 6]. We will show that an axial field induces AB oscillations of the energy subbands (see Figure 1 (b)), analogous to those found in Carbon nanotubes [7]. Here, however, the discrete prismatic symmetry induces gap openings (which depend on R and γ) between n-fold energy levels, corresponding to the n-fold symmetry of the NW.

On the other hand, we will show that a magnetic field normal to the NW axis induces Landau level formation and the 2DES behaves as a pair of quasi-1D channels. Depending on the field direction with respect to the NW facets, these Landau levels are localized along the facets or edges of the NW, consistently enhancing or diminishing the edge localization discussed above.

References

[1] F. Qian *et al.*, Nano Lett. **4**, 1975 (2004).

[2] K. Tsumura *et al.*, Jpn. J. Appl. Phys. **46**, L440 (2007).

[3] A. Fontcuberta i Morral *et al.*, Small **4**, 899 (2008).

[4] H. Jensen *et al.*, Ann. Phys. **63**, 586 (1971).

[5] G. Ferrari *et al.*, Phys. Rev. Lett. **100**, 230403 (2008).

[6] G. Ferrari *et al.*, Phys. Rev. B **78**, 115326 (2008).

[7] A. Bachtold *et al.*, Nature **397**, 673 (1999).

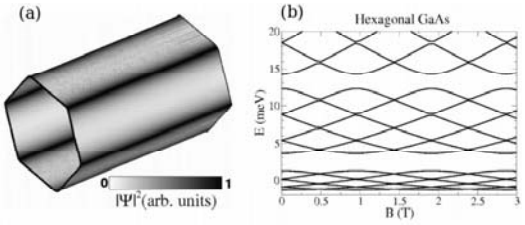

Figure 1: (a) Charge density of the ground state of a carrier in an hexagonal core multi-shell NW (gray scale), showing localization along the edges (darker regions). (b) Energy levels vs axial field intensity for an hexagonal GaAs 2DES ($R = 40$ nm, $\gamma = 0.29$ nm^{-1} [3]), showing AB oscillations.

Oscillations of electron density in the quantum dot with large number of electrons in high magnetic field

A.A. Vasilchenko

Kuban Stase Technological University, Krasnodar, Russia

Keywords: screening, Kohn-Sham equations

We have performed self-consistent calculations of the nonlinear screening of donor impurity charge by two-dimensional spin-polarized electrons in the perpendicular magnetic field using a density functional theory. The calculations are based on self-consistent solutions of the Kohn-Sham equations. Many-body effects are taken approximately into account by the use of local effective exchange energy.

For spin-polarized electrons Kohn-Sham equations is presented in the following form (atomic system of units is used)

$$\{-\frac{\partial^2}{\partial r^2}-\frac{1}{r}\frac{\partial}{\partial r}+\frac{r^2}{4L^4}+\frac{m^2}{r^2}-\frac{m}{L^2}+V_{eff}(r)\}\psi_m(r)=E_m\psi_m(r)$$

where

$$V_{eff}(r)=2\int\frac{n(r')}{|\boldsymbol{r}-\boldsymbol{r}'|}d\boldsymbol{r}'-2\int\frac{n_m(r')d\boldsymbol{r}'}{|\boldsymbol{r}-\boldsymbol{r}'|}+\sqrt{\frac{\pi}{8}}4\pi L(n(r)-n_m(r))+V_{ext}(r)$$

$$V_{ext}(r)=-\frac{2z_0}{r}+\frac{\omega_0^2}{4}r^2\ ,\ n_m(\rho)=\psi_m^2(\rho),\ n\ (r)=\sum_{m=0}^{N-1}n_m(r)\cdot$$

m is the angular momentum of electron, L is magnetic length.

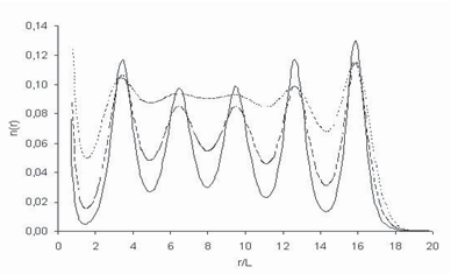

Fig.1 Profiles of electron density in quantum dot with N =140, z_0 = 1 (solid line - B = 2.6 T, dashed line - B= 3 T, dotted line - B= 4 T)

The external potential is created by impurity with the charge z_0 and positively charged disk of density n_+. Confining potential of charged disk was being replaced by parabolic potential with $\omega_0 = 2(\pi n_+)^{3/4}/N^{1/4}$. Self-consistent calculations were done for $n_+ = 1/(2\pi L^2)$ and $z_0 = 1$.

Figure 1 presents the results of calculations for the quantum dot with the number of electrons N = 140 for different quantities of magnetic field. It can be seen, that profile of electron density has an oscillatory form, and the cycle of oscillations and the period of oscillation is approximately equal πL. With decreasing quantity of magnetic field (or mean density of electrons) the amplitudes of these oscillations increase.

This work was supported by the RFBR and administration of Krasnodar region (№ 09-01-96507).

Strong competition between thermal and tunneling emission processes in self-assembled quantum dots

A. Schramm*,**, S. Schulz**, T. Zander**, Ch. Heyn**, and W. Hansen**
*Optoelectronics Research Centre, Tampere University of Technology, Tampere, Finland
** Institute of Applied Physics, University of Hamburg, Hamburg, Germany

Keywords: quantum dots, thermal emission, tunneling, deep level transient spectroscopy

Understanding the charge exchange between quantum dots and adjacent reservoirs is of fundamental interest for applications. Measurements of the escape rates in electric fields clearly resolve the level structure of quantum dots [1, 2]. The emission and capture of charge carriers from and into self-assembled quantum dots (QDs) can be quite complex since several emission (capture) paths are apparent. For the escape of electrons from QDs embedded in a Schottky or *pn* diode thermal, tunneling, and thermally assisted tunneling processes may be distinguished as sketched in the inset of Fig. 1. In thermally assisted tunneling processes the electron tunnels from an intermediate state that is energetically elevated with respect to the ground state. They compete with pure tunneling processes depending on the temperature and the electric field across the diode. Here we study the emission processes by means of deep level transient spectroscopy (DLTS) on InAs QDs embedded in Schottky diodes in strong electric and magnetic fields. The experiments reveal that the emission rates strongly depend on both, an applied electric-field as well as the charge state of the dot shells. The behavior can be quantitatively understood with a thermally assisted tunneling model (TAT) in which the tunnel barrier is assumed to consist of a Coulomb barrier arising from the charge within the dot and a triangular contribution from remote charges (Fig. 1). The analysis applied to the emission from the s and the p shell of self-assembled InAs quantum dots reveals, that the activation energies obtained from a conventional Arrhenius analysis of the transients depart from the barrier height at high electric field and quantum dot occupation. By applying magnetic fields parallel to the QD layer, we obtain valuable information about the nature of the competing emission paths in the thermally assisted tunneling processes [3]. Our results demonstrate that tunneling contributions to the escape rate drastically increases with increasing occupation of the QDs.

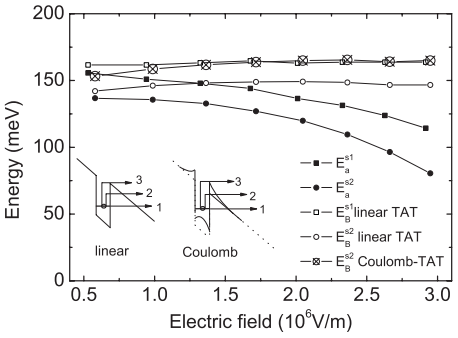

Figure 1: Experimentally determined activation energies E_a and barrier heights E_B of QD s1 and s2 electrons calculated within different models. The insets show schematically the Coulomb-field influence on the effective barrier for an electron escaping from singly (left) and multiply (right) charged quantum dots. 1: tunneling, 2: thermally assisted tunneling, 3: thermal emission.

References

[1] S. Schulz, S. Schnüll, Ch. Heyn, and W. Hansen, Phys. Rev. B **69**, 195317 (2004).

[2] A. Schramm, S. Schulz, J. Schaefer, T. Zander, Ch. Heyn, and W. Hansen, Appl. Phys. Lett. **88**, 213107 (2006).

[3] A. Schramm, S. Schulz, Ch. Heyn, and W. Hansen, Phys. Rev. B **74**, 033311 (2008).

Dislocation-induced electron and hole levels in InAs quantum-dot Schottky diodes

A. Schramm*, V. Polojärvi*, A. Tukiainen*, A. Aho*, and M. Pessa*
**Optoelectronics Research Centre, Tampere University of Technology, Tampere, Finland*

Keywords: quantum dots, defects, deep level transient spectroscopy

Self-assembled InAs/GaAs quantum dots (QDs) are fascinating nano-objects that exhibit intriguing electronic and optical properties. These can be tailored by growth parameters during the molecular beam epitaxy (MBE) process. The formation of coherently strained and defect-free QDs, which are essential for device applications as well as for studying fundamental electronic properties, takes place only in a small window of growth parameters, e.g., the amount of InAs deposited is restricted to $1.7 < \theta < 2.5$ monolayers (ML) [1, 2], with the nominal coverage θ of InAs. Growth beyond or at the edge of optimal parameters may result in plastically relaxed QD structures that introduce electrically active defects. A detailed knowledge of the nature of these electron and hole trap levels is necessary in order to reduce the amount of defects or even to utilize them.

Here intentionally introduced electron as well as hole trap levels are studied by means of deep level transient spectroscopy (DLTS). We vary the amount of deposited InAs, change the QD growth method (interrupted or continuously), and the species of arsenic (As_2 and As_4) in the growth process of QDs embedded in n- and p-type GaAs host material.

The QDs were embedded in slightly n- or p-type GaAs grown either on undoped, n- or p-doped GaAs(100) substrates by MBE. A second QD layer with the same growth parameters as for the embedded QDs was grown on the sample surface for atomic force microscopy (AFM). Schottky contacts for electrical characterization were formed onto samples by evaporation of 100 nm chromium.

In Fig. 1 we exemplarily show DLTS measurements of n- and p-type Schottky diodes with embedded QDs grown with $\theta = 2$ and 3 ML InAs in the range of $100 < T < 400$ K. Whereas no DLTS signal is observed in the 2 ML sample, broad DLTS spectra with overlapping peaks and shoulders are observed for the 3 ML samples in the entire temperature range in both, n- and p Schottky diodes. These DLTS signals are associated with multiple defects levels mainly introduced by the formation of dislocation in the plastically relaxed QDs. The electron and the hole traps are spatially localized in the proximity of the QD layer and can interfere with the intrinsic electron or hole QD levels in n- and p-doped Schottky diodes, respectively.

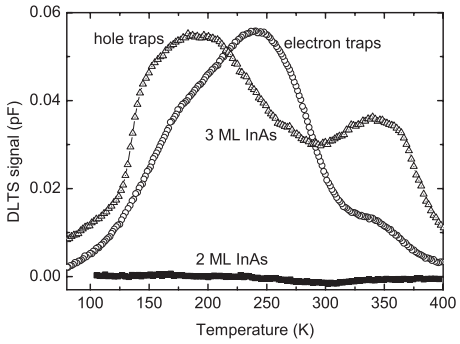

Figure 1: Electron and hole traps in n- and p-doped GaAs Schottky diodes with 3 ML InAs QDs due to dislocation-induced defects.

References

[1] Ch. Heyn, Phys. Rev. B **64**, 165306 (2001).

[2] P. Frigeri *et al.*, J. Appl. Phys. **102**, 083506 (2007).

Nanogap formation of indium oxide core/shell heterostructure nanowires

M. Jung*, W. Song*, J. S. Lee*, N. Kim*, B. -C. Woo*, J. Kim* and K. Hirakawa**

* *Korea Research Institute of Standards and Science, Daejeon, Korea*

** *IIS and INQIE, University of Tokyo, Tokyo, Japan*

Keywords: Nanowire, Core/shell heterostructure, Nanogap, Indium oxide

The electron transport through single molecules and nanoparticles has been studied intensively for the last decade due to the importance of theses studies in fundamental physics and device applications [1–3]. In order to measure the conductance of single molecules or nanoparticles, the fabrication of metal electrodes with gaps of a few nm is a key issue. So far, various techniques [1–3] for such nanogap electrodes have been demonstrated. They include electromigration, mechanical break junction, controlled electrochemical plating, nanoconstriction (nanopore), electron-beam lithography, dip-pen lithography, and strain-induced break junction. Although these techniques have been shown to be useful to measure the electron transport through nano-sized materials, major drawbacks include their complexity, high cost, and low yield.

Here, we report a simple nanogap-fabrication method using electrical breakdown of a core/shell heterostructure nanowire. The heterostructure nanowires used in this work, consisting of a crystalline In_2O_3 core and an amorphous InO_x shell (or In-rich), were synthesized by a chemical vapor deposition method. We fabricated both substrate-supported and suspended nanowire devices (Inset of Fig. 1) whose electrical breakdown behavior and subsequent nanogap formation were studied. The current–voltage (*I–V*) characteristics of the fabricated devices exhibited two distinguished current drops, which were attributed to the breakdowns of the more conductive shell part and the less conductive core part, respectively (Fig. 1). After the electrical breakdown, gaps of a few nm to tens of nm-size formed in the nanowire, as shown in the inset of Fig. 1. The size of gap depended strongly on the width and length of the nanowires and on the structure of devices. The breakdown temperature In_2O_3/InO_x core/shell nanowire was estimated. Finally, the usefulness of this technique was demonstrated by fabricating pentacene-field-effect transistors.

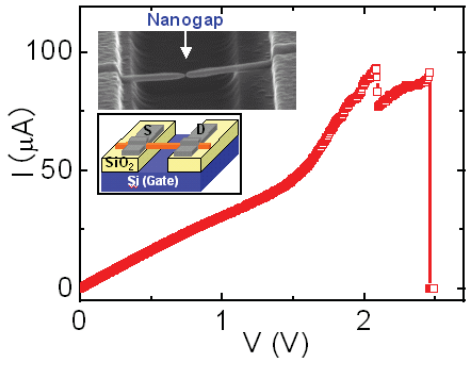

Fig.1 The *I-V* curve of a substrate-supported core/shell nanowire. The current exhibited two abrupt drops. The upper inset shows a SEM image of broken nanowires. The lower inset shows a schematic of a substrate-supported device.

References

1. C. Joachim, J. K. Gimzewski and A. Aviram, Nature **408**, 541 (2000).

2. A. Nitzan and M. A. Rather, Science **300**, 1384 (2003).

3. J. R. Heath and M. A. Rather, Phys. Today **5**, 43 (2003).

Two-mode photon interference in a quantum-dot single photon emitter

H. Kumano*,**, H. Nakajima*, S. Ekuni*, H. Sasakura* and I. Suemune*,**

* *Research Institute for Electronic Science, Hokkaido University, Sapporo, Japan*

** *Japan Science and Technology Corporation (CREST), Kawaguchi, Japan*

Keywords: two-mode interference, single photon, which-path information, quantum dot

Young's double slit experiments for photons have been demonstrated with both attenuated coherent light [1] and single photons [2]. They have revealed one of the most fundamental aspects of quantum mechanics such as wave-particle duality. In the above experiments, two modes to generate interference are prepared *outside* the photon sources, while interference between photon modes prepared *in* a photon source is not so far demonstrated.

In this work, single photon interference analogous to the Young's double slit experiment is demonstrated. Interference occures between two photon polarization modes rather than space modes, which stem from non-degenerated neutral exciton states in a solid-state single photon emitter. It is clarified that interference between two modes appears when the single photon could not be labeled by its transition energy in principle to identify "which-path", and the photon state can be described as a superposition of two modes, i.e., $|V\rangle + e^{i\phi}|H\rangle$. We investigated two $In_{0.75}Al_{0.25}As$ quantum dots (QDs) with different exciton fine structure splitting (FSS) at 20 K. Quantum nature of photon emission for both dots was confirmed by observing photon antibunching with independent measurements [3].

For studying single photon interference between two polarization modes, polarization of neutral exciton emission under non-resonant excitation (1.687 eV) was analyzed by two separate detection systems; (i) a 0.64-m triple-grating spectrometer equipped with a Si charge-coupled-device detector (energy resolution of this detection system < 5 μeV) and (ii) single photon counting module with a filter to select specific emission line. Figure 1 shows PL spectra of the two QDs measured with V/H polarizations as well as their emission energy and integrated intensity at each polarization angle. In striking contrast to QD A where the spectral overlap is relatively small, QD B shows large spectral overlap enough not to make transition energy labeling to the two polarization modes possible. In the QD B, FSS and linewidth are 30 μeV and 100 μeV, respectively. As a result, integrated intensity exhibits clear periodic variation with the same period to the transition energy. Furthermore, $\pi/2$ phase shift is obvious, where the intensity is maximized at $\pi/4+n\pi$ (n: integer). This behavior is a clear indication of two-mode photon interference in a single photon emitter.

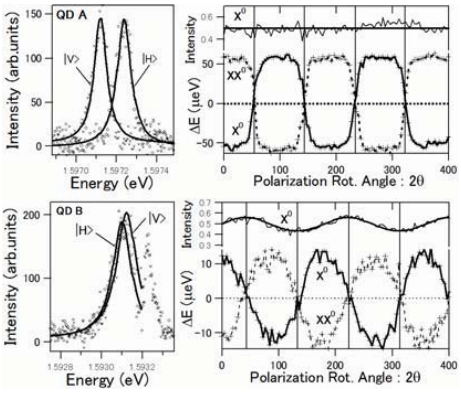

Figure 1: (a),(c) PL spectra of X^0 for both polarization modes |V>/|H>. (b),(d) Detection polarization dependence of the relative X^0 and XX^0 energy and normalized PL intensity of the X^0 integrated over both polarization modes.

References

1. R. L. Pfleegor and L. Mandel, Phys. Rev. **159**, 1084 (1967).
2. V. Jacques, E. Wu, T. Toury, F. Treussart, A. Aspect, P. Grangier, and J.-F. Roch. Eur. Phys. J. D **35**, 561 (2005).
3. H. Kumano, S. Kimura, M. Endo, H. Sasakura, S. Adachi, S. Muto, and I. Suemune, J. Nanoelectron. Optoelectron. **1**, 39-51 (2006).

Polarization phenomena in the asymmetric double layers of self-assembled quantum dots

Taehee Yoo*, Sanghoon Lee*, M. Dobrowolska** and J. K. Furdyna**

* *Department of Physics, Korea University, Seoul, Korea*

** *Department of Physics, University of Notre Dame, Notre Dame, IN 46556, USA*

Keywords: Polarization, quantum dot, Photoluminescence

Spin related phenomena of semiconductor quantum dot (QD) have received a great deal of attention during last decade due to the possibility of using them in the new spintronic devices. Specifically, spin states of the QD was proposed as quantum bits in quantum commutation. [1] One of the best way investigating spin properties of QD system is the optically technique, in which polarization of the signal is selectively detected. The spin polarization of carriers and the exchange interaction between them in the QD system have been investigated by using such optical experiments.

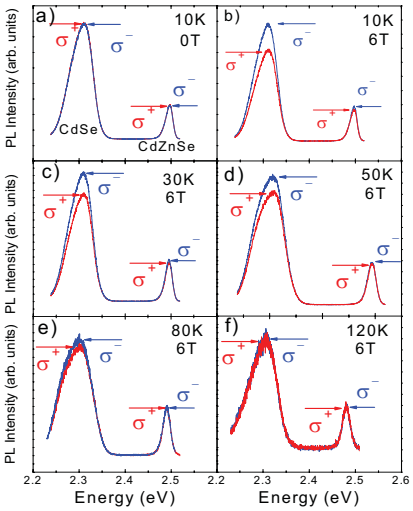

Fig.1 (a) PL spectra obtained with two different circular polarizations at zero magnetic field. on the double-layer QD system. (b)-(f) Magneto-PL spectra obtained with σ^- and σ^+ polarizations in the presence of 6 T magnetic field.

In this paper we have adapted polarization selective magneto-photoluminescence (PL) measurement to investigate the phenomena of an asymmetric double-layer self-assembled QD system made of the CdSe and the CdZnSe QD layers. The asymmetric QD structure was specially designed for the experimental observation of interaction between the two QD layers. The excitation power dependent PL measurement are carefully performed to investigate the carrier transfer phenomenon occurring between the two QD layers.

The photoluminescence peaks from two QD layers are well resolved in the spectra. The relative PL intensity of the two QD layers strongly depends on the excitation power indicating carrier transfer between the two QD layers. The intensity of the PL peak undergoes significant change when the one circular polarization is selected under a magnetic field. Specifically, the PL from both QD layers shows stronger intensity for the σ^- than for the σ^+ circular polarizations due to the spin polarization of carriers in the presence of magnetic field as shon in Fig. 1. The difference of PL intensity between the two polarizations showed significant dependence both on the excitation power and on the temperature. Furthermore, the degree of polarization from the CdSe QDs was much larger than from the CdZnSe QDs. Such polarization phenomena of PL were discussed in terms of thermal effect and spin interaction between the carriers in the pairs of QDs in the system.

References

1. D. Loss, and D.P. DiVincenzo, Phys. Rev. A **57**, 120 (1998).

(GaMn)As Nanowires- A Synchrotron-based investigation

I. Ulfat I.[1,2,3], J.Adell [1,2], J. Sadowski [2], L. Ilver L. [2] and J. Kanski J. [2]

[1] *Department of Applied Physics, Chalmers University of Technology, SE-41296 Göteborg, Sweden.*
[2] *MAX-lab, Lund University, SE-22100 Lund, Sweden.*
[3] *Department of Physics, University of Karachi, Karachi-75270, Pakistan.*

Keywords: Nanowires, Synchrotron radiation

Self-assembled one-dimensional structures such as nanowires are currently subject of an intense research activity as they are expected to possess great capabilities for a wide range of potential applications. The nanowires are usually grown on substrates covered with nanodots of a metal catalyst [1-5]. However in some cases also catalyst-free nanowire growth has been reported [6]. In view of these perspectives it is highly important to understand and control the physical mechanisms leading to self-assembled nanowires growth.

Our studies are mainly focused on nanowires fabricated on substrates with ferromagnetic epilayers namely (GaMn)As. It was recently found that the MBE-deposition of (GaMn) As at intermediate substrate temperatures (typically 350 °C) results in formation of nanowires [7]. Nanowires formed of (GaMn)As are particularly interesting, as they open prospects of integrating spintronics in nanostructures.

In this poster we present a study of the electronic structure of such nanowires, with focus on the Mn 3d states. We have employed a combination of techniques (PES, XAS and XES) utilizing synchrotron radiation. All the experiments were performed at Swedish National Synchrotron Facility – the MAX-lab. These investigations not only reveal that solid MnAs particles segregated due to Mn over-saturation but also show that with the development of the nanowires the electronic properties of the Mn atoms change considerably.

References:
1. Xiangfeng D. et al., Appl. Phys. Lett. **76**, 1116 (2000)
2. Björk M. T. et al., Nano Lett. **2**, 87 (2002)
3. Gao P. X. et al, Science **309**, 1700 (2005)
4. Li Y. et al, Appl. Phys. Lett. **87**, 183107 (2005)
5. Jun Zhang and Lide Zhang, J. Vac. Sci. Technol. B **21**, 2415 (2003)

6 Khorenko V. et al., Appl. Phys. Lett. **85**, 6407 (2004)

7. Sadowski J. et al., Nano Lett. **7**, 2724 (2007)

All-optical switching using InAs/GaAs quantum dots within a vertical cavity structure

C. Y. Jin[1], O. Kojima[2], T. Kita[2], O. Wada[1, 2], M. Hopkinson[3] and K. Akahane[4]

[1]*Division of Frontier Research and Technology, CREATE, Kobe University, Kobe, Japan*
[2]*Department of Electrical and Electronic Engineering, Graduate School of Engineering, Kobe University, Kobe, Japan*
[3]*Department of Electronic and Electrical Engineering, EPSRC National Center for III-V Technologies, University of Sheffield, Sheffield, UK*
[4]*National Institute of Information and Communications Technology, Tokyo, Japan*

Keywords: Quantum dot, Vertical cavity, Optical switching, Ultra-fast

The unique nature of atom-like energy states in three dimensional confined quantum dots (QDs) leads to novel application in photonic devices. As an optical nonlinear source, InAs/GaAs QDs have been proposed to demonstrate optical switching with ultra-low power consumption in a Mach-Zehnder interferometer.[1] However, the low density of QD states requires large size of such lateral transmission type devices and makes it difficult to be integrated into a compact device. A vertical structure is therefore desirable, and has been theoretically analyzed recently for an optical Kerr effect inside QDs.[2] In this work, we investigate a reflection-type GaAs/AlAs vertical cavity structure for ultra-fast optical switching by utilizing the nonlinear absorption saturation in InAs/GaAs QDs.

When a train of optical pulses pumps at a front mirror of a vertical cavity, saturated absorption of QDs will shift the energy position of the cavity resonant mode. This yields a fast switching of the input signal.

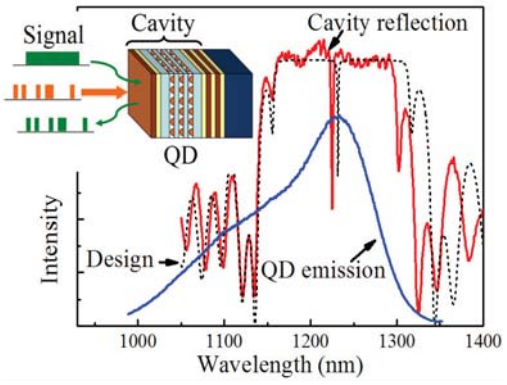

Fig.1 Cavity reflection and QD emission. The inset shows a schematic structure of QDs within a vertical cavity.

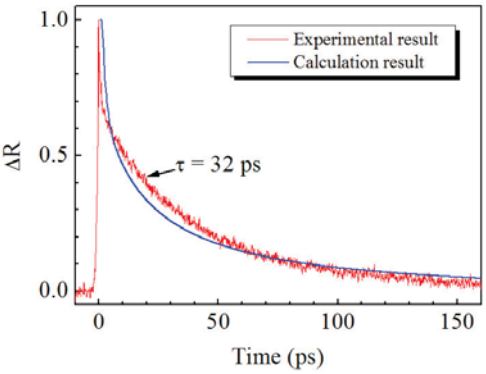

Fig.2 Differential reflection signal as a function of time delay at room temperature determined from the pump-probe measurement and calculation.

Based on this mechanism, an InAs/GaAs QD structure consisting of 9 QD layers has been integrated into a vertical cavity, which has 10 GaAs/AlAs pairs for the front mirror and 25 pairs for the back mirror. InAs QDs give a photoluminescence (PL) emission around 1.23 μm, which is well matched by a cavity resonant mode at 1.225 μm, as shown in the reflection spectra in Fig.1 (solid curve: experiment, dashed curve: theoretical design). Conventional pump-probe measurement at the same wavelength as the cavity resonant mode has shown a fast switching process with a time constant of ~32 ps (Fig. 2). Calculation results from a FDTD and rate equation model have been also shown in the figure for comparison. These results support QD materials to be useful for compact ultra-fast all-optical switches.

References

1. R. Prasanth *et al*, Appl. Phys. Lett. **84**, 4095, 2004.
2. T. Kitada *et al*, Appl. Phys. Exp. **1**, 092302, 2008.

Control of ensemble effect on Rabi oscillations in quantum dots

M. Kujiraoka[1,2], J. Ishi-Hayase[1,3,4], K. Akahane[1], N. Yamamoto[1], K. Ema[2], M. Sasaki[1]

1. *National Institute of Information and Communications Technology, Tokyo, Japan*
2. *Department of Physics, Sophia University, Tokyo, Japan*
3. *The University of Electro-Communications, Tokyo, Japan*
4. *PRESTO, Japan Science and Technology Agency (JST), Saitama, Japan*

Keywords: quantum dot, Rabi oscillation, four-wave mixing spectroscopy

Optical Rabi oscillations (ROs) play crucial roles in coherent control of excitons in semiconductor quantum dots (QDs). Most reported ROs of QD excitons were observed in a single QD [1] because inhomogeneous Rabi frequencies make it difficult to observe ROs in a QD ensemble. Thus QD ensembles have been considered disadvantageous for coherent manipulation. In this study, we propose a new way to control macroscopic coherent phenomena by taking advantage of the characteristics of QD ensembles. We demonstrated that the ensemble average of ROs of excitonic polarization can be changed drastically by selecting spatial distributions of input electric fields. We show that the changes in ensemble averages were caused by polarization interference and the results of our experiments agree with our calculations.

In order to observe ROs of excitonic polarization, we detect four-wave mixing (FWM) signals from the QD ensemble as a functions of the input pulse area $\Theta_i = \mu \overline{E_i} \Delta T/\hbar$. The area is generally changed by varying the spatially averaged electric field $\overline{E_i}$, while maintaining a constant temporal duration for the excitation pulse ΔT. If the beam to excite a large number of QD is spatially distributed like a Gaussian function, the QDs are excited not by the same $\overline{E_i}$ but by different field strengths depending on their positions $E_i(x,y)$. This results in a spatial distribution of the pulse area for each QD at each different position $\Theta_i(x,y)$. In this study, the inhomogeneity of transition dipole moment μ is assumed to be negligible compared to the distribution of $E_i(x,y)$. We calculated the FWM signals averaged over the ensemble of ROs, including the spatial distributions of input pulse areas. Fig. 1 shows the calculated FWM signals as a function of the average area of the first excitation pulse, $\overline{\Theta}_1$, which is defined as $\iint E_i(x,y)dxdy/\pi R^2$ (R: beam radius). The average area of the second excitation pulse, $\overline{\Theta}_2$, was fixed to π. The Inset of Fig. 1 shows the distribution functions of the excitation beam used in the calculation. The average RO excited by rectangular beams coincides with $\sin\overline{\Theta}_1$ in an ideal two level (dot line). The average RO excited by Gaussian TEM 00 beam damps strongly at $\overline{\Theta}_1 > \pi$ due to interferences of excitonic polarizations (solid line). We experimentally demonstrated this polarization interference (not shown here). The average RO excited by Gaussian TEM 10 beam vanishes at every $\overline{\Theta}_1$ because negative and positive polarizations are cancelled out completely. This result demonstrates that a macroscopic coherent response from a QD ensemble can be controlled by changing the spatial distribution of excitation beams.

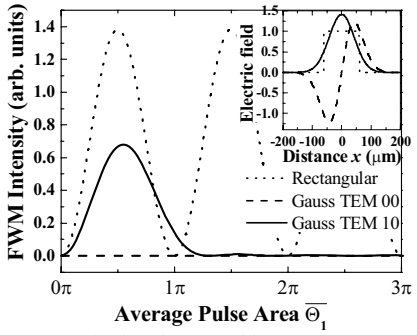

Fig.1 Calculated ensemble average of Rabi oscillations of excitonic polarization for various spatial distributions of beams (see the inset).

References

1. B. Patton, U. Woggon and W. Langbein, Phys. Rev. Lett. **95**, 266401 (2005).

Silicon nanowires: functionality at the nanoscale

M.Mongillo[a], G.Katsaros[a], P.Spathis[a], C.Mouchet[b], P.Gentile[c], E.Rouviere[b] and S. de Franceschi[a]

[a]CEA, *INAC/SPSMS/LaTEQS, F38054 Grenoble, France*

[b]CEA, *DRT/LCH, F38054 Grenoble, France*

[c]CEA, *INAC/SiNAPS, F38054 Grenoble, France*

Keywords: Silicon nanowires, transistors,electrostatic doping

Nanowires have attracted wide interest during the last few years due to their exciting properties associated with their low dimensional character [1]. Furthermore, they are receiving attention in view of their potential for future functional nanodevices such as high performance FETs, nanoscale photodetectors, sensors, logic circuits [2]. A key step in the fabrication of nanowire-based devices is to obtain an efficient carrier injection into the semiconducting material by overcoming the Schottky barrier at the metal-semiconductor interface. One approach in order to obtain sufficiently transparent contacts is to heavily dope the semiconductor in proximity to the metallic leads [3]. A different approach we are currently investigating is based on the use of local fields [4] acting independently on the two contacts.

Here we present our studies on the transport properties of silicon nanowires grown from catalytic gold nanoparticles. The Silicon nanowires are contacted by means of conventional lithographic techniques with Nickel electrodes. After a thermal annealing [5] we form a metallic alloy of Nickel and Silicon close to the contacts. A pair of split gates act electrostatically at the interface between the alloyed extensions and the semiconductor in a Gate-All-Around geometry (Fig.1a). The capability to address independently the local electrostatic field at the two contacts offers the possibility to embed in a single device different functionalities such as a high performance Field Effect Transistor, a p-n junction and a Schottky diode.

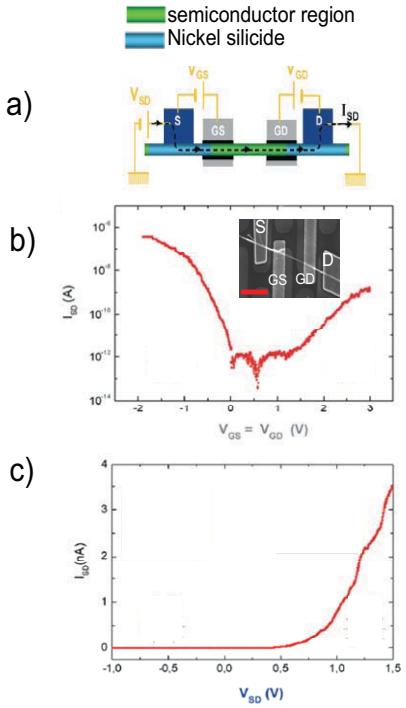

Fig.1 a) Schematic view of the sample: S=Source, D=Drain, GS=source-gate, GD=drain -gate. **b)** Output characteristic of the device (inset, scale bar 1µm) working as a transistor; **c)** Characteristic of the device working as a pn diode.

References

1. Zhong et al., **Nano Lett**.,5, 6,1143-1146, (2005)
2.Y.Li et al., **Materials Today**, 9,18-27(2006)
3. Tsung-ta Ho et al., **Nano Lett., 8,** 12,4359(2008)
4.J.Appenzeller et al., **PRL**,93,196805(2004)
5.Weber,W.M., et al.,**NanoLett., 6**, 12, 2660-2666(2006)

Magnetic field dependence of exciton fine structures in InAs/GaAs quantum dots: exchange vs. Zeeman splittings

T. Saito, T. Nakaoka and Y. Arakawa
Institute for Nano Quantum Information Electronics, The University of Tokyo, Tokyo, Japan

Keywords: exciton fine structures, magnetic field, InAs, quantum dots

The exciton energies in a self-assembled InAs/GaAs quantum dot (QD) split into two bright-state energies and two dark-state ones due to the electron-hole exchange interaction. The splitting between the two bright-state energies, *i.e.* the fine structure splitting (FSS), increases with a longitudinal magnetic field while it decreases with an in-plane magnetic field. The detailed understanding of the magnetic field dependence of the exciton fine structures is important for controlling the FSS as well as for analyzing the magneto-photoluminescence(PL) data. In this study, we calculate the exciton fine structures in InAs/GaAs QDs under the magnetic field using the **k**·**p**-based configuration interaction (CI) method.

The QD structure is modeled as a pyramidal InAs QD (base length 15 nm, height 7.5 nm) embedded in a GaAs matrix. Firstly we calculated the strain distribution and strain-induced piezoelectric potential in the QD structure. Next we carried out a single-particle calculation of electron and hole states under the longitudinal magnetic field, B, using the 8-band **k**·**p** method including the Zeeman Hamiltonian [1]. Finally we calculated many-body exciton states and energies using the CI method [2].

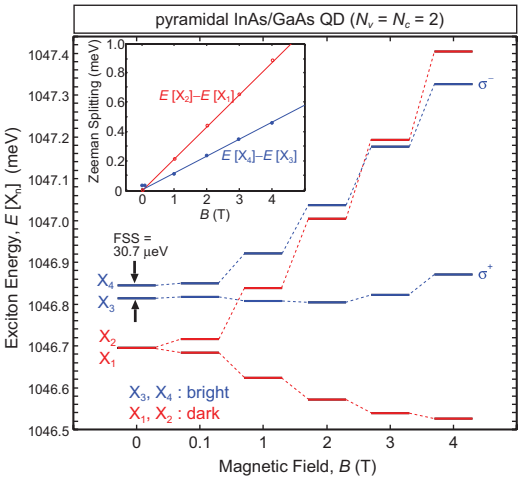

Figure 1: Lowest four exciton energies versus the longitudinal magnetic field, B, in the pyramidal InAs/GaAs QD. The inset shows the Zeeman splitting versus B.

Figure 1 shows the calculated exciton energies for the lowest four states, $X_1 \sim X_4$, versus B. The X_3 and X_4 are bright excitons while the X_1 and X_2 states are dark ones, which is revealed from a spin configuration of excitons. At $B = 0$, the splitting between the bright-state energies, FSS, is 30.7 μeV, while that between the dark-state energies is almost zero. At $B = 0.1$ T, the FSS changes little, while the dark-state energies split due to the Zeeman effect. The electron-hole exchange interaction still dominates in the bright excitons; the Zeeman effect dominates in the dark ones.

At $B \geq 1$ T, the bright-bright and dark-dark splittings increase almost linearly with B due to the Zeeman effect (see the inset). The X_3 (X_4) state has σ^+ (σ^-) polarization. From the linear fit to the Zeeman splitting, we obtain the exciton g-factor, g_{ex}; $g_{ex} = -1.99$ (-3.77) for the bright (dark) exciton. The dark-state energy of X_2 crosses the bright-state energies of X_3 and X_4. At $B = 4$ T, the dark state X_2 (X_1) becomes the highest (lowest) exciton state. We have observed the magneto-PL data which support this calculation [3].

In conclusion, in the exciton fine structures in the InAs/GaAs QD, the exchange interaction determines the splittings at $B = 0$ giving FSS = 30.7 μeV. The Zeeman effect dominates at $B \geq 1$ T with the different g_{ex} values for the bright and dark excitons. The intermediate case is found at the weak field of $B = 0.1$ T. The present method can be applied to a wide range of study such as the exciton fine structures under an in-plane magnetic field, and the fine structures in coupled QDs.

This work was accomplished by the Special Coordination Funds for Promoting Science and Technology.

References

[1] T. Nakaoka *et al.*, Phys. Rev. B **70**, 235337 (2004).
[2] R. Seguin *et al.*, Phys. Rev. Lett. **95**, 257402 (2005).
[3] T. Nakaoka *et al.* (unpublished).

Effect of Oxygen on the Low-Frequency Noise in ZnO Nanowire Devices

Seon hee Kim*, Byung-Yong Yu**, Jungil Lee*, and Gerard Ghibaudo***

** Nano Device Research Center, Korea Institute of Science and Technology, 39-1 Hawolkok Seongbuk, Seoul, Korea*

***Advanced Metal Research Center, Korea Institute of Science and Technology, 39-1 Hawolkok Seongbuk, Seoul, Korea*

****IMEP-MINATEC, INPG-CNRS, 3 rue Parvis Louis Neel, BP257, 38016 Grenoble, France*

Keywords: Low-frequency noise, ZnO nanorod, surface states, random walk of electrons

In this study, we investigated the effect of oxygen on the noise density in ZnO nanowire devices. Experimental results from literature are analyzed based on the random walk model involving surface states.

Wang et al. [1] reported the increase in the value of the Hooge parameter from $5x10^{-3}$ in mild vacuum to $4x10^{-2}$ in dry oxygen ambient in their back-gate ZnO nanowire field-effect transistor, where most of the nanowire surface is exposed to the ambient. Wang et al conjectured that the oxygen species at the surface of the nanowire could be the major noise sources based on the 8 times increase of the Hooge parameter from mild vacuum to dry oxygen ambient. Lee et al. [2] reported the change of Hooge parameter with the bias conditions and deviation from 1/*f* behavior in back-gate ZnO nanowire field-effect transistors after exposing the devices to air for many months.

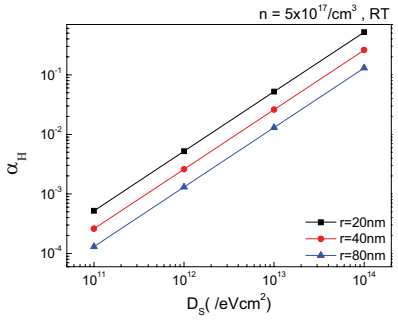

Fig.1 Current dependence of the normalized noise density at 10 Hz, room temperature.

Random walk of electrons involving surface states can contribute to the generation of 1/*f* noise [1]. One can easily derive a scaling law concerning the relation between the Hooge parameter and the radius, carrier concentration, and the surface states density as shown in Fig. 1.

Based on this scaling law, the density of surface states was evaluated from the measured noise density. From ref. [1] the surface states densities were estimated to be $2.3x10^{12}$/eVcm^2 for mild vacuum, and $1.6x10^{13}$/eVcm^2 for dry oxygen, respectively. From Ref. [2], the surface states density varied within $10^{12\sim14}$/eVcm^2 depending on the bias condition. Along with the deviation from 1/*f* noise it can be concluded that after long time exposure to air, both energetically and spatially non-uniform surface states are generated possibly due to the reaction of oxygen with the ZnO nanowire surfaces.

References

1. W. Wang et al., J. Appl. Phys. 101, 044313 (2007).
2. J. Lee et al., Phys. E 40, 2147 (2008).
3. O. Jaentsch, IEEE Trans, Electron Dev. **ED-34**, 1100 (1987).

Characterization of $Zn_{1-x}Cr_xO$ nano crystals grown by catalytic ECH processes

K. Shimoda*, T. Yasui*, Y. Kuroki** and M. Takata**

* *Department of Mechanical Engineering, Nagaoka University of Technology , Nagaoka, Japan*

** *Department of Electrical Engineering, Nagaoka University of Technology , Nagaoka, Japan*

Keywords: $Zn_{1-x}Cr_xO$: catalytic growth: photoluminescence:

In recent years, the ZnO crystals doped with transition metals (TM = V, Cr, Fe, Co or Ni) as dilute magnetic semiconductors (DMS) have been expected to be advance alternative uses in spintronics devices [1,2]. We have presented advantages of catalytic electric current heating (ECH) processes to grow the $Zn_{1-x}Cr_xO$ nano crystals [3,4]. In our previous report, $Zn_{1-x}Cr_xO$ nano crystals with Cr up to the compound ratio (x) of 9%, which means quite high compound ratio, were successfully synthesized [4]. Guozhen et al. reported that the sulphur doped ZnO showed an increase of green emission intensity, being caused by the increase of oxygen vacancy introduced by the lattice distortion with the doping [5]. The purpose of this study was to investigate Cr compound ratio (x) in $Zn_{1-x}Cr_xO$ nano crystals. In this paper, the relationship between x and the green emission intensity for $Zn_{1-x}Cr_xO$ nano crystals has been reported.

The ECH process [3] was formed the Cr dispersed ZnO ceramic bar as a sublimation source using a direct current (50 A/cm^2) in Ar/H_2 flow with a mixture ratio of balance /0.1 % [4]. The w_s in the ceramic bar were varied from 0 to 12 mass%. The growth conditions such as temperature, time and the distance between the ceramic bar and Au coated (50 nm) sapphire (0001) substrate were 800 °C, 10 min and 5 mm, respectively. The Photoluminescence (PL) spectra were measured at room temperature.

Figure 1 shows PL spectra for $Zn_{1-x}Cr_xO$ nano crystals formed on the sapphire substrate. The UV emission at about 380 nm and the green emission at about 500 nm were observed. The spectra were normalized using the intensities of UV emission. The intensity ratio of the green to UV emission increased with increasing w_s. It suggests the increase of x in the $Zn_{1-x}Cr_xO$ crystals because of the similar mechanism of the sulphur doped ZnO [5]. This result strongly supports the high x (9%) of $Zn_{1-x}Cr_xO$ crystals. The detailed quantitative analysis of x in $Zn_{1-x}Cr_xO$ is now under investigation using XRD and EPMA.

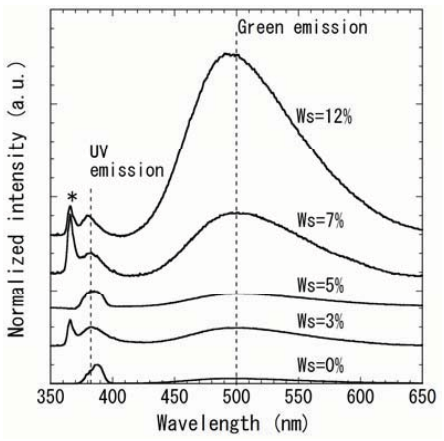

Fig.1 PL spectra of $Zn_{1-x}Cr_xO$ nano crystals on sapphire substrate measured at room temperature. The w_s were Cr compositions in the sublimation sources of ZnO. The symbol * indicates an excitation line from the Hg lamp.

References

1. R.P. Borges et.al, J. Magn. Magn. Mater. **316**, e191(2007).
2. K. Sato et.al, Jpn. J. Appl. Phys. **39**, L555(2000)
3. D. Nezaki et.al, J. Ceram. Soc. Jpn. **112**, 5958(2004)
4. K. Shimoda et.al, Appl. Surf. Sci. **254**, 7993(2008)
5. Gouzhen Shen et. al, j. Phys. Chem. B. **109**, 5491(2005)

Importance of Electronic State of Two-Dimensional Electron Gas for Electron Injection Process in Nano-Electronic Devices

M. Muraguchi*, T. Endoh*, Y. Takada**, Y. Sakurai**, S. Nomura**, K. Shiraishi**, M. Ikeda***, K. Makihara***, S. Miyazaki***, and Y. Shigeta ****

* *Center for Interdisciplinary Research, Tohoku University, Sendai, Japan*

** *Graduate School of Pure and Applied Science, University of Tsukuba, Tsukuba, Japan*

*** *Graduate School of Advanced Sciences of Matter, Hiroshima University, Hiroshima, Japan*

**** *Graduate School of Life Science, University of Hyogo, Hyogo, Japan*

Keywords: Electron Tunneling, Si-Dots Floating Gate MOS Capacitor, Two-Dimensional Electron Gas

In this paper, we suggest that the spatial distribution of electron density in the electrode would work as a new controllable state for the electron injection in nano-electronic devices. To extract a mechanism of electron injection process from the electrode to the nano-structure, we have investigated the transient injection current from the substrate to the Si-dots in a Si-dots floating gate MOS capacitor [1] with 3.5nm tunneling oxide [the inset of Fig. 1]. Figure 1 shows the observed transient electron injection currents as functions of the effective gate voltage [Gate Voltage (V_g)-Flatband Voltage (V_{fb})]. We can observe clear peaks, which correspond to the electron injections from the two-dimensional electron gas (2DEG) to the Si dots, where the first peak occurs at V_g-V_{fb} =5.0V at 160K and 3.8V at 240K. Conventionally, the tunneling probability in the direct tunneling region was thought to be determined independently from the temperature [2]. This large voltage shift in the peak as shown in Fig. 1 cannot be explained by the temperature dependencies of material properties. Note that the clear temperature dependence of electron tunneling can be observed due to the large potential barrier height at the Si-SiO_2 interface.

To explain this phenomenon, we focused on the spatial mismatch in the shape between the Si-dots and the 2DEG, where the 2DEG is spread two-dimensionally, whereas the Si-dots cover only a part of the 2DEG. Thus, the electrons are inevitably injected from the large area to the small area. We clarified how the spatial distribution of electronic state in the 2DEG affects the electron tunneling from the 2DEG to the Si-dot by Monte Carlo Simulations. As a result, we obtain a good agreement with the experiment when we introduce a finite time for electron tunneling. These

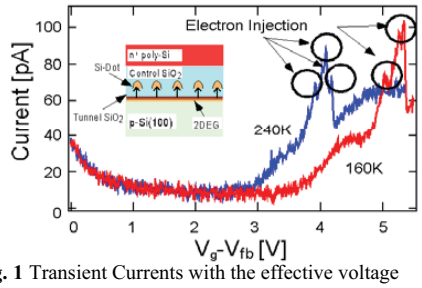

Fig. 1 Transient Currents with the effective voltage in a Si-dots floating gate MOS capacitor (inset).

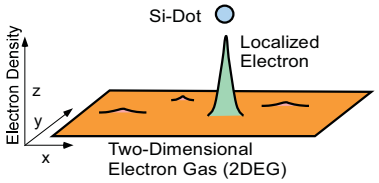

Fig. 2 Schematic illustration of considerable electron injection process.

results indicate that the spatial and temporal fluctuation of the electronic state in the 2DEG plays a crucial role for the temperature dependence of electron tunneling as shown Fig. 2. This implies that the modulation of the spatial density distribution of electronic state in 2DEG enable us to control the electron injection process. These features are derived from our simplified model for Si-dot system. However, electron density in the electrode is not in equilibrium for all type devices. Therefore, the initial density distribution dependence of electron injection can be projected to a generalized system.

Acknowledgements: This work is supported by Grant in Aid for Scientific Research No. 18063003 and 20760019 of the MEXT, Japan.

References:

1. S. Miyazaki *et al*, Thin Solid Films, **369,** 55 (2000).
2. Y. Takahashi, *et al*, IEEE Trans. Electron Device, 43,1213 (1996)

Tailoring of the Wave Function Overlaps and the Carrier Lifetimes in InAs/GaAs$_{1-x}$Sb$_x$ Type-II Quantum Dots

Wei-Ting Hsu[1], Yu-An Liao[1], Shu-Kai Lu[1], Shun-Jen Cheng[1],
Pei-Chin Chiu[2], Jen-Inn Chyi[2], and Wen-Hao Chang[1]

[1)] *Department of Electrophysics, National Chiao Tung University, Hsinchu, 300 Taiwan*

[2)] *Department of Electrical Engineering, National Central University, Chung-li, 320 Taiwan*

Keywords: Quantum Dots, Type-II, PL, TRPL

Recently, many experimental evidences indicated that InAs self-assembled quantum dots (QDs) covered by a thin GaAs$_{1-x}$Sb$_x$ layer (with x >14%) can exhibit type-II optical transitions between electrons confined in the QDs and holes localized in the GaAsSb layer. Due to the spatial separation of electrons and holes in the type-II QDs, the carrier lifetime are much longer than their type-I counterparts. The long carrier lifetimes and the confinement of only one carrier species make the type-II QDs very promising for many applications, such as solar cells and optical memory devices. Tailoring of the band alignment, the wave function overlaps and hence the carrier dynamics is therefore an important subject for practical applications.

In this study, we employed postgrowth thermal annealing to manipulate the emission properties of type-II InAs/GaAsSb QDs. Apart from large blueshifts and a pronounced narrowing of the QD emission peak, the annealing induced alloy intermixing also leads to enhanced radiative recombination rates and reduced localized states in the GaAsSb layer. By using the energy-dependent, power-dependent and temperature-dependent photoluminescence (PL) and time-resolved PL measurements, we are able to clarify the effects of hole localizations on the emission properties of the type-II QDs. With the increasing annealing temperature, the type-II QD structure gradually evolved into a type-I alignment. In particular, we found that it is possible to manipulate between type-I and type-II recombinations in annealed QDs by using different excitation powers to control the Coulomb potential produced by the non-equilibrium electrons in the QDs. We demonstrate that postgrowth thermal annealing can be used to tailor the band alignment, the wave function overlaps, and hence the recombination dynamics in the InAs/GaAsSb type-II QDs

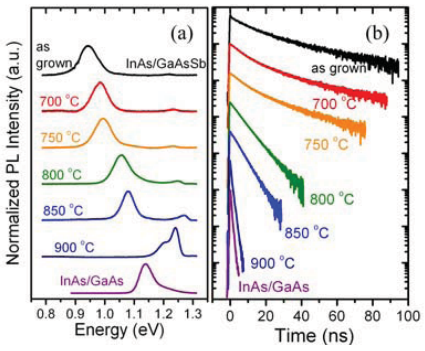

Fig.1 PL spectra (a) and TRPL decay traces (b) for the as-grown and annealed InAs/GaAsSb QDs, together with the reference type-I InAs/GaAs QDs.

References

1. H. Y. Liu, *et al.*, Appl. Phys. Lett. **86**, 143108 (2005); C. Y. Jin, *et al.*, Appl. Phys. Lett. **91**, 021102 (2007); Y. D. Jang, *et al.*, Appl. Phys. Lett. **92**, 251905 (2008).
2. W.-H. Chang, Y.-A. Liao, W.-T. Hsu, M.-C. Lee, P.-C. Chiu, and J.-I. Chyi, Appl. Phys. Lett. **93**, 033107 (2008).
3. Y.-A. Liao, W.-T. Hsu, P.-C. Chiu, J.-I. Chyi and W.-H. Chang, Appl. Phys. Lett. **94**, 053101 (2009).

Growth and characterization of ZnO/ZnTe core-shell nanowire and its device applications

H. Y. Chao[1], J. H. Cheng[1], J. Y. Lu[1], S. H. You[1], Y. H. Chang[1*], C.L.Cheng[1], Y. F.Chen[1], and C. T. Wu[2]

[1]*Department of Physics, National Taiwan University, Taipei 106, Taiwan*
[2]*Center for Condensed Matter Sciences, National Taiwan University, Taipei 106, Taiwan*

Keywords: ZnO, ZnO/ZnTe, nanowire, core-shell

One-dimensional ZnO nanowires have attracted much attention for their potential applications in making electronic and opto-eletronic devices. As the nanowires have large surface to volume ratio, the surface effect, especially the effect of surface defects on the performance of ZnO-nanowire-based device cannot be overlooked. For example, it is well-known that chemisorption of ambient gases, primarily oxygen, has a strong effect on the electrical properties of ZnO nanowire. In order to improve the stability of the performance of the ZnO-nanowire-based devices it is desirable to passivate the surface of the ZnO nanowire. In this paper we report the growth and characterization of ZnO-ZnTe core-shell nanowires and their electrical and opto-electronical properties. In this structure the ZnTe layer not only serve the purpose of passivating the ZnO surface, it also forms a type -II semiconductor heterosructure with the ZnO core layer . The separation of electron and hole in the type-II heterostructure is expected to enhance the light induced photo-conductivity for the core-shell nanowire.

A two-step synthesis was used to fabricate ZnO/ZnTe core/shell nanowire. In the first step, the ZnO nanowires were grown for 40 minutes at T= 930 °C in a furnace by chemical vapor deposition with a gold thin film as catalyst. After the sample was cooled down, it was then transferred to the MOCVD chamber for the deposition of ZnTe shell on ZnO core for 300 sec at T= 550 °C. The morphology and size distribution of the ZnO/ZnTe core/shell nanowire arrays were studied by scanning electron microscopy and it was found that the surfaces of the well-aligned ZnO nanowires became rougher after the growth of ZnTe layer and the diameter of the nanowire increase from 70-100 nm to 150-300 nm. The x-ray diffraction and transmission electron microscope measurements show that the ZnO core has wurtzite structure, the ZnTe shell has zinc-blende structure and both materials have good crystalline quality.

The nanowire was then placed on top of a 300 nm SiO_2 layer which in term was on top of a n-type Si substrate to form a field effect transistor with the heavily doped silicon substrate served as a metal gate. Metallic electrodes consisting of Ti /Au were then deposited on the two ends of the nanowire by an electron beam evaporator and defined as source and drain electrodes by a photolithography and lift-off process. Wavelength-dependent photoconductivity of the nanowire was then studied by dispersing the light emitted from a Xe lamp with a monchromator. It was found that the ZnO-ZnTe core-shell narrowire show improved device performance over ZnO nanowire both as a field effect transistor and as a photoconductor.

Anomalously Induced-Charge on a Domain Wall of a Semiconductor-Dot Atom

I. Kanazawa

*Department of Physics, Tokyo Gakugei University, Tokyo, Japan

Keywords: domain wall, semiconductor, dot atom

Self-assembled InAs quantum dots(SAQD) have proven to be highly interesting quantum structures both from a technological as well as from a fundamental physics point of view. Due to the relatively strong confinement in lateral direction, SAQD can be regarded as artificial atoms. In most experiments, SAQD have been investigated by optical spectroscopy, in particular photoluminescence(PL). PL experiments on single dots are well established, which overcome the inhomogeneously broadened line widths in typical ensemble measurements. Brocke et al.[1] have investigated InAs self-assembled quantum dots(SAQD) by resonant inelastic light scattering. By applying a gate voltage between amatallic front gate and a back electrode, they can charge the quantum dots with single electrons. With resonant inelastic light scattering, they can directly observe the elementary electronic excitations of the few-electron quantum-dot atoms, which are formed by the SAQD. They observe excitations which they identify as transition of electrons from the s- to the p-shell(s-p transitions) and from the p- to the d-shell(p-d transitions) of the quasiatoms. They explain the shift and broadening of the s-p transitions of collective excitations in the experiment to be due to additional excitations at lower energies, which can not be individualy resolved, on a domain wall surronding the few-electron quantum-dot atom. Recently, the present author[2] has indicated the importance of the photo-induced domain-wall in anomalous properties in diluted magnetic semiconductors in low-dimensional geometry. In this study, we will discuss the additional excitations in the quantum dot from collectively induced-charge effects on a domain wall around the dot atoms, extending the previous formula[2-4].

References

1. T. Brocke et al. Physica E**22,** 478(2004).
2. I. Kanazawa, Physica E**40**, 277(2007).
3. C. Callen, J. Harvey, Nucl Phys. B**250**, 427(1985).
4. D. Boyanovsky et al., Nucl Phys. B**285**, 340(1987).

Magnetic-field asymmetry of nonlinear mesoscopic transport in channels coupled to a single metallic gate

L. Worschech, B. Brandenstein-Köth, S. Lang, S. Höfling and A. Forchel

Technische Physik, Universität Würzburg, 97074 Würzburg, Germany

Keywords: Non-linear transport, magnetic field asymmetry, hybrid quantum wires, magnetoconductance

According to the Onsager-Casimir symmetry relations, in the linear transport regime the conductance G=I/V of a two-probe conductor, defined as the ratio of the current I through the conductor to the voltage V between the probes, remains unaffected for a reversal of an external magnetic field [1]. Recently, it has been found that an odd part in the magnetic field of nonlinear I-V characteristics of mesoscopic metallic systems can exist, for which all spatial symmetries are broken [2]. The appearance of nonlinear magnetoconductance was principally associated with electron-electron interaction or screening, which also effectively results in electron-electron interaction. As boundaries of conductors can be described by a superposition of electron potentials, an interesting question arises as to whether or not the interaction of an electron in a conductor with its boundaries can give rise to an asymmetry in nonlinear mesoscopic transport [3]. Here we demonstrate large magnetic-field asymmetries in quantum wires coupled asymmetrically to a single metallic gate. The asymmetric conductance reaches values on the order of e^2/h.

The structure is based on a modulation doped GaAs/AlGaAs heterostructures. As sketched in the upper part of Fig.1, a narrow trench was etched down through the two-dimensional electron gas (2DEG). In a second lithographic step a metallic top gate was defined. As a result one boundary of the channel is defined by applying a negative voltage to the top gate (V_{tg}). The other boundary is caused by the etched trench. The adjacent unconstrained 2DEG is used as side gate (V_{sg}). By applying a magnetic field, for small bias voltages of a few mV the conductance is symmetric with respect to B=0T. Large asymmetric conductance is found for large bias voltages attributed to a coupling to a single metallic gate.

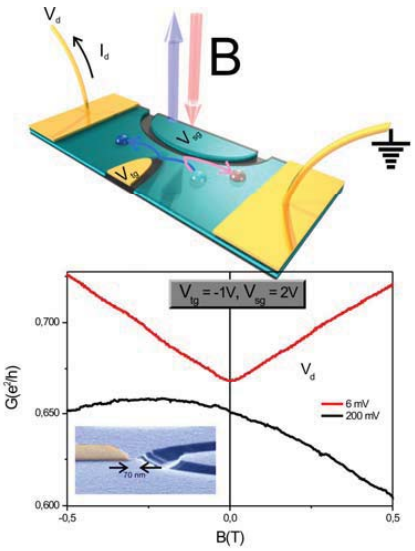

Fig.1 Top: Sketch of a studied channel. One boundary is realized by an etched trench down through the 2DEG of the modulation doped GaAs/AlGaAs heterostructures. A metallic top gate was used to define the other boundary. An electron can sustain different scattering in the channel (forward/backward) due to a change of the magnetic field direction. Bottom: The conductance for small bias voltage is almost symmetric as regards B=0T, in contrast a large magnetic field asymmetry takes place for large bias voltages.

References

1. L. Onsager, Phys. Rev. 38, 2265 (1931).
2. D. Sánchez and M. Büttiker, Phys. Rev. Lett. 93, 106802 (2004).
3. D. Hartmann, L. Worschech, A. Forchel, Phys. Rev. B78, 113306 (2008).

Anisotropic modal gain spectra of GaAs self-assembled quantum-wire laser structures on (775)B GaAs substrates

S. Shimomura*, T. Fujita**, S. Imadu*, and T. Kitada***

* *Graduate School of Science & Engineering, Ehime University, Matsuyama, Japan*

** *Graduate School of Engineering Science, Osaka University, Toyonaka, Japan*

*** *Institute of Socio Technoscience, the University of Tokushima Graduate School, Tokushima, Japan*

Keywords: quantum wires, modal gain spectra, laser structure, variable stripe method

Self-assembled quantum-wires (QWRs) grown on (775)B GaAs substrates by molecular beam epitaxy are attracting researchers' interest because their large anisotropic optical gain is expected to lift the problem that the polarization-direction of light from vertical-cavity surface-emitting-lasers (VCSELs) switches by 90 degrees dependent on the excitation current.[1] Recently we have demonstrated room-temperature lasing of self-assembled quantum-wire VCSELs without polarization switches.[2] Actual anisotropy of the gain of the QWRs is not investigated under current excitation. In this work, we have fabricated a QWR laser structure and measured the anisotropic modal gain.

An active region of a laser structure consists of five sets of a nominally 3-nm-thick GaAs QWR layer sandwiched by $(GaAs)_4(AlAs)_2$ barrier layers. Figure 1 shows amplified spontaneous emission spectra and modal gain spectra which were measured when an excitation current of 710 mA flew via 500 μm and 500 + 500 μm long stripe segment contacts. The peak modal gain was 10 cm^{-1} was obtained. Fig. 2 shows peak modal gain as a function of current density when the stripe direction is parallel to the QWRs and normal to the QWRs. Large anisotropy of the modal gain was observed in all range of the excitation current.

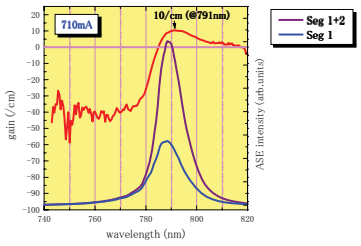

Fig.1 Amplified spontaneous spectra (ASE) of 500-μm-long stripe (Seg 1) and 500 + 500 μm long stripe (Seg 1+2) were excited. Modal gain spectrum is deduced from the two ASE spectra.

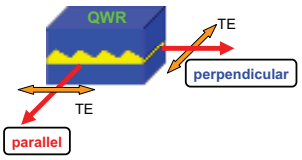

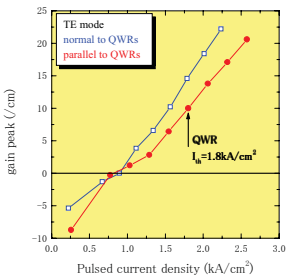

Fig.2 Stripe direction dependent gain peak as a function of current density.

References

1. Y. Ohno, S. Shimomura, S. Hiyamizu, Y. Takasuka, M, Ogura, and K. Komori, J. Vac. Sci. Technol. B **22**, 1526 (2004).

2. Y. Higuchi, S. Osaki, T. Kitada, S. Shimomura, Y. Takasuka, M. Ogura, and S. Hiyamizu, Solid State Electron. **50**, 1173 (2006).

Influence of the number of turns and the distortion of the shape on the optical properties of semiconductor microtubes.

Y. Mizoguchi*, S. Hiratsuka*, S. Takeda*, S. Saravanan**, M. Hosoda*** and N. Ohtani*

* *Department of Electronics, Doshisha University, Kyoto, Japan*

** *ATR Wave Engineering Laboratories, Kyoto, Japan*

*** *Department of Applied Physics, Osaka City University, Osaka, Japan*

Keywords: semiconductor microtubes, quantum well, photoluminescence

Semiconductor microtubes are expected to be novel low threshold laser diodes [1,2]. In this report, we have fabricated semiconductor microtubes and evaluated the influence of the number of turns and the distortion of the shape on the optical properties of microtubes by micro-photoluminescence (μ-PL) investigation.

A multilayered thin semiconductor film is grown on a (100)-oriented GaAs substrate by molecular beam epitaxy (MBE). Starting from the substrate, the sample consists of a GaAs buffer layer, an $Al_{0.52}Ga_{0.48}As$/AlAs digital alloy sacrificial layer, an $In_{0.19}Ga_{0.81}As$ strained layer, a 7-ML GaAs/AlGaAs quantum well (QW). Next, the sacrificial layer is selectively etched with HF:H_2O (1:10). Then, the upper layer is released from the substrate and rolled up from the cleavage surface due to the strain relaxation effect of the InGaAs layer. We successfully rolled up an approximately 40-nm thick semiconductor layer containing a QW into a miccrotube of several microns in diameter. We performed spatially resolved μ-PL investigations, because the microtube was photoexcited by using a cw He-Ne laser through a 100x objective lens.

PL emission cannot be observed in the unreleased area, because the band alignment of the 7-ML QW is indirect. However, the PL emission from semiconductor microtubes can be clearly observed. This result suggests that the band alignment of the QW was changed as direct due to the influence of uniaxial-strain caused by the rolling-up process [3].

In addition, the PL intensity depends on the number of turns. Fig.1 shows the PL spectra of three samples, in which the number of turns are 1.9, 3.2 and 6.7. The PL intensity becomes stronger with increasing the number of turns. This result clearly suggests that the overlap of the QW layer enhances the PL intensity.

The shift of PL wavelength depends on the position of the microtubes. This indicates that the strain distribution in the microtubes is not uniform because the shape of microtubes is distorted. We confirmed that the edge of the microtubes is elliptical by using a scanning electron microscope (SEM).

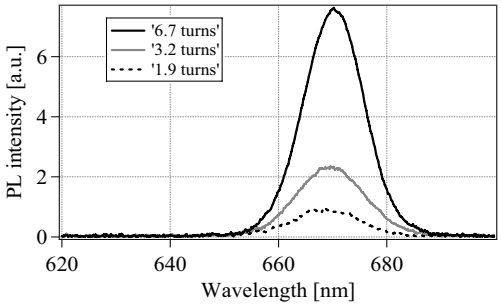

Fig. 1. PL spectra of three microtubes in which the number of turns are 1.9, 3.2 and 6.7.

References

[1] T. Kipp, et al., Phys. Rev. Lett., **96**, 077403 (2006).

[2] M. Hosoda et al., Appl. Phys. Lett., **90**, 181107 (2007).

[3] N. Ohtani, et al., Physica E, **21**, 732 (2004).

Self-assembled Quantum Dots in a liquid-crystal-tunable microdisk resonator

K. A. Piegdon, C. Meier, M. Urbanski, A. Hoischen, H.-S. Kitzerow, S. Declair, J. Foerstner, and T. Meier

Center for Optics and Photonics Paderborn (CeOPP), Department of Physics and Department of Chemistry, University of Paderborn, 33098 Paderborn, Germany

Keywords: Photonic resonators, microdisks, quantum dots, liquid crystals

Photonic devices employing quantum dots have proven to be highly attractive. Their use ranges from fundamental investigations of weak or strong coupling with a photonic cavity mode to device applications. However, the spectral resonance between the quantum dot emission and the cavity mode is vital for all these applications.

In this contribution, we will present our approach employing hybrid devices made from photonic semiconductor cavities and liquid crystals in order to add tunability to photonic devices.

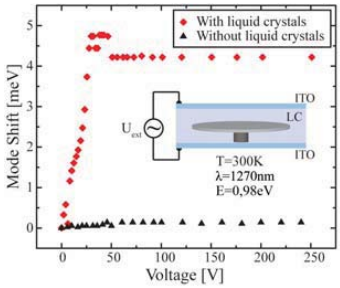

Fig.1 Electrical tunability of a resonant cavity mode in a microdisk immersed in liquid crystal.

GaAs-based microdisk resonators with an embedded layer of InAs quantum dots have been fabricated. The microdisks are embedded in a liquid crystal, which undergoes a phase transition when it is heated above the clearing temperature T_c. Above the clearing point, the liquid crystal is in its isotropic phase. Below T_c, the liquid crystal is in an ordered nematic phase, which exhibits an uniaxial optical and dielectric anisotropy. We have studied the resonant mode spectra when heating the device above the clearing point. It turns out that in the range of the clearing temperature, the phase transition of the liquid crystal has great impact on the observed wavelength of the photonic mode, for which a tunability as large as $\Delta\lambda$=7nm can be observed. Additionally, we have embedded the liquid-crystal-immersed cavities in capacitor-like device structure, which allow to apply an electric field in the growth direction. We find that in the nematic phase, the alignment of the liquid crystal molecules changes the dielectric environment of the photonic resonator, causing an electric field-induced shift of the resonant modes. The total mode shift observed is in the same order of magnitude as the phase transition-induced shift described before. To understand the interaction of the liquid crystal with the resonant cavity modes in greater detail, we have performed director-field measurements by means of fluorescence confocal polarizing microscopy, which probes the alignment of the rod-like liquid crystal molecules in the vicinity of the microdisk. The experimental results are reproduced by numerical calculations using the finite differences time-domain (FDTD) method. The quantum dots were in previous work already successfully described using a nonlinear approach [2]. Moreover, we take the dielectric anisotropy of the liquid crystal in its nematic phase into account and investigate the nonlinear coupling dynamics of the quantum dots with the resonant electromagnetic fields.

Support by the BMBF via NanoFutur grant 03X5509-NanoPhox, the DFG via the Emmy-Noether program, and the European Science Foundation (Self-Organized Nanostructures 2, LC-NANOP).

References

1. K. A. Piegdon, H. Matthias, C. Meier, and H.-S. Kitzerow, Proc. SPIE **6911**, 6911OJ (2008).
2. C. Dineen, J. Förstner, A.R. Zakharian, J.V. Moloney, S.W. Koch, Optics Express **13**, 4980 (2005).

Spontaneous formation and imprinting of vortices in the microcavity optical parametric oscillator

D.N. Krizhanovskii[1], D.M. Whittaker[1] , E.Cerda[2] , R.A. Bradley[1], A.P.D. Love[1], K. Guda[1], P.Santos[2], M.S. Skolnick[1], J.S.Roberts[3]

[1]*Department of Physics & Astronomy, University of Sheffield, Sheffield S3 7RH, United Kingdom.*
[2]*Paul-Drude-Institut für Festkörperelektronik, Berlin, Germany*
[3]*EPSRC National Centre for the III-V Technologies, University of Sheffield, Sheffield, United Kingdom*

Keywords: Polariton, Vortex, Parametric Scattering

Topological defects occur in many areas of science, including particle physics, cosmology, condensed matter physics and optics. Vortices are typical examples, which occur in bosonic condensates, such as dilute gases, liquid helium, superconductors and polariton BECs[1].

We report the observation of spontaneous vortex formation in the microcavity optical parametric oscillator (OPO) carrying finite Orbital Angular Momentum (OAM). We also demonstrate that a weak probe beam carrying OAM enables imprinting of a vortex state on to macroscopically occupied polariton states.

In the OPO "signal" and "idler" states are formed due to polariton-polariton pair scattering from the pump. These states exhibit quantum properties similar to those of polariton Bose-Einstein condensates, such as coherence and superfluidity. However, the distinctive property of the OPO system is that it is strongly non-equilibrium and involves three coupled states.

The OPO was excited using a laser beam without OAM. Figure 1a shows an image of the "signal" emission at k=0 in real space above threshold. At the edge of the emission a defect is formed with a dip in the emission intensity (region A). Figure 1b shows the interference pattern between the "signal" image in Fig.1a and the same image inverted in so that region A is mixed with region B. The fork-like dislocation indicates the spontaneous formation of a quantised vortex with finite OAM (L=1) in the signal. The phase relationship between pump, signal and idler results also in an anti-vortex in the idler state of OAM L=-1.

The vortex state observed is stable in time (on a few sec timescale) and its formation strongly depends on the position across the sample. At lower excitation powers

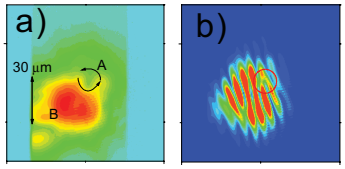

Fig.1 a) Real space image of signal emission at k=0. b) Interference pattern demonstrating vortex state

the vortex state disappears. Such observations indicate that the fluctuations in transverse photonic potential and the strong nonlinear interactions between OPO states play an essential role in spontaneous formation of vortices. The physical origin of the observed effect is an in-plane continuous polariton flow from the region of high to low density and decay in the non-equilibrium OPO. Potential disorder introduces boundary conditions, which transform such a flow into a stable rotary behaviour. Using numerical modeling which takes into account photonic potential fluctuations we are able to obtain spontaneous formation of stable vortices, as in experiment.

Finally, we demonstrate that using a probe beam with intensity 10 times smaller than that of the signal we are able to imprint a vortex of L=1 or 2 onto the signal, which thus results in formation of the antivortex L=-1 or -2 in the idler. Our work demonstrates that microcavity polaritons can be utilized for optical gates, which convert and amplify orbital angular momentum of light beams.

References

[1] K.G. Lagoudakis et al, *Nature Phys.* **4**, 706–710 (2008).

Study of Optical Bistability and Bimodal Lasing in Coupled Microdisks

S. N. Ghosh*, B.B. Buckley**, N. Samarth***, D.D. Awschalom**, and S. Ghosh*

* *School of Natural Sciences, University of California, Merced CA 95340, USA*

** *Department of Physics, University of California, Santa Barbara, CA 93106, USA*

*** *Materials Research Institute, Penn State University, University Park, Pennsylvania 16802, USA*

Keywords: GaAs, Microcavity, Quantum dot, Optical bistability.

Semiconductor microcavities offer unique means of controlling light-matter interactions in confined geometries, resulting in a wide range of applications in optical communications. We have previously demonstrated low threshold lasing [1] and modulation of electron spin coherence [2] in single GaAs/(Al,GaAs) microdisk cavities with quantum wells (QW) containing interface-fluctuation quantum dots (QDs) in the active region. Here, we report bi-stable lasing in coupled microdisks and present our technique of optically toggling the coupled system between its two states.

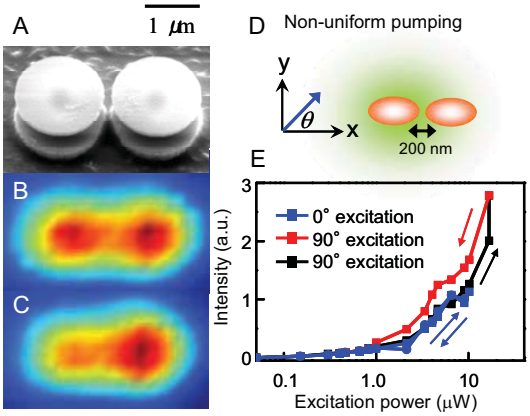

Fig.1 (A) SEM image of coupled GaAs/(Al,Ga)As microdisks with QDs. Scanning PL microscopy images of above sample at T = 10 K showing (B) a delocalized high Q emission mode, and (C) localized low Q mode. (D) Schematic representing the principle of non-uniform pumping used to achieve saturable gain, where the excitation spot uniformly illuminates one disk but the other partially. The excitation is linearly polarized and the polarization angle θ is varied with respect to the coupling axis. (E)Emission intensity of the delocalized mode as a function of excitation power for different polarizations. θ = 0° (blue) shows no hysteresis. θ = 90° shows a hysteretic emission dependence as power is increased (black)

Figure 1A is an SEM image of a coupled microdisk sample. The individual disk diameters are 2 μm and the inter-disk separation is 200 nm. Evanescent coupling of whispering gallery modes between the disks results in mode-splitting, with the higher energy resonance persistently achieving higher mode Q (~ 5000). This emission mode is also spatially delocalized, as shown in fig. 1B. In contrast, the lower energy mode is preferentially localized (fig. 1C). When the pair is illuminated non-uniformly (fig. 1D) the emission intensity of the higher energy mode exhibits hysteresis as a function of excitation power when the incident pump is polarized perpendicular to the coupling axis (fig. 1E, 90° excitation). This bi-stability disappears when the incident pump is polarized along the coupling axis (fig. 1E, 0° excitation).

Using polarization control, we leverage this dependence to demonstrate controllable gain modulation. Our results could be useful for applications in optical memories and computing, and in next generation of low-threshold, scalable optoelectronic devices.

References

1. W. H. Wang, et al Phys. Rev. B **71**, 155306 (2005).
2. S. Ghosh et. al, Nature Materials **5**, 261 (2006).

High Purcell factor microcavity containing quantum dots : how to measure the Q-factor?

B. Gayral and J.-M. Gérard

CEA-CNRS "Nanophysique et semiconducteur" group, CEA-Grenoble, INAC/SP2M

17 rue des Martyrs, 38054 Grenoble, France

Keywords: quantum dots, microcavity, Purcell effect

The quantum dot (QD)/microcavity system has been studied for more than 10 years. It allows in particular to implement quantum optics experiments with semiconductor emitters, thereby being a first step towards practical devices that make use of cavity quantum electrodynamics effects.

One key parameter of an optical microcavity is its quality factor (Q) that measures the photon lifetime within the cavity. The most direct way of measuring Q is to perform a transmission experiment through the bare cavity, as is done in atomic physics. This is however difficult to implement in semiconductor microcavities. One more appealing possibility in this case is to perform a photoluminescence (PL) experiment, in which the quantum dots inside the microcavity behave as an internal light source, which is then spectrally filtered by the cavity [1].

It was so far admitted that in such an experiment, the microcavity modes appear as positive peaks in the PL spectrum with a linewidth yielding the quality factor [1]. We show theoretically that in the case of high enough Purcell factor (F_p>1) microcavities, this is not the case [2]. At low excitation power, the spectral shape of the mode in PL is broader than the natural shape of the mode (as measured in transmission) by a factor $(F_p+1)^{1/2}$. It is only at high excitation power when the fundamental transition of all QDs is saturated that the natural linewidth of the cavity is recovered in the PL spectrum (see Fig. 1). Moreover, we show that under particular experimental conditions, the microcavity mode can appear as a spectral dip (instead of a peak) in the PL spectrum. This is obtained when the leaky modes of the cavity are collected preferentially over the resonant modes. Both these effects allow in particular to demonstrate directly the Purcell effect in simple continuous wave PL experiments.

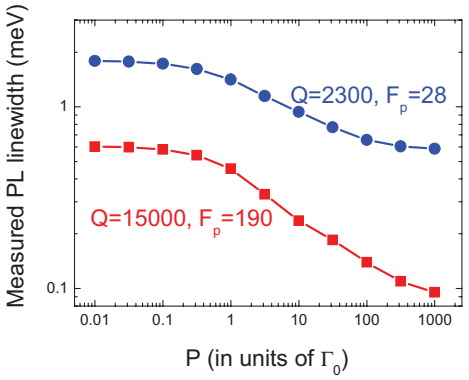

Fig.1 Evolution of the measured microcavity mode peak linewidth in PL for two different cavities, as a function of the excitation power per QD (in units of Γ_0 : the natural radiative decay rate of the considered QDs).

It thus appears that measuring the Q of a high Purcell factor microcavity in PL is not straightforward, and we shall discuss strategies to correctly measure the Q in such structures.

References

1. J.-M. Gérard *et al.*, Appl. Phys. Lett. **69**, 449 (1996)
2. B. Gayral and J.-M. Gérard, Phys. Rev. B **78**, 235306 (2008).

Cavity Quantum Electrodynamics in Electrically Contacted Quantum Dot-Micropillar Cavities

S. Reitzenstein, C. Kistner, T. Heindel, A. Rahimi-Iman, C. Schneider, S. Höfling, and A. Forchel
*Technische Physik, Universität Würzburg, Am Hubland, D-97074 Würzburg

Keywords: quantum dot, microcavity, strong coupling, electro-optical tuning

In recent years quantum dot-microcavity systems have attracted considerable attention with respect to the implementation of cavity quantum electrodynamics (cQED) effects on a solid state platform. In particular, weak [1] and strong coupling [2] have been realized in optically pumped micropillar cavities allowing either to enhance the spontaneous emission or to realize a coherent exchange of energy between light and matter.

In this contribution we report on electrically excited or electro-optically tuned high-quality (Q) factor micropillar cavities featuring pronounced cQED effects, such as electro-optical tuning in strong coupling regime. In addition, these structures allow for single photon emission and low threshold lasing which reflects their potential for integrated nonclassical light sources and nanolasers.

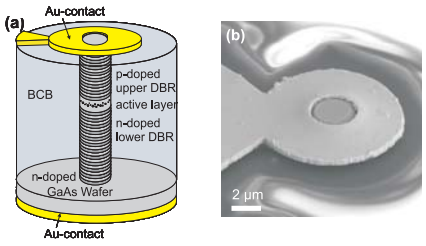

Figure 1: (a) Schematic view of an electrically contacted micropillar cavity. (b) Scanning electron microscope image showing the upper part of a fully processed electrically contacted micropillar cavity.

The electrically contacted high-Q micropillar cavities are based on doped planar AlAs/GaAs microcavity structures with a low density layer of InGaAs QDs in the active region. The structures were grown by molecular beam epitaxy on n-doped GaAs substrate. In order to realize electrically pumped devices as sketched in Fig. 1(a) several nano-processing steps are necessary, including metallization of the n-contact, plasma etching of the pillar structures, planarization and patterning of a ring-shaped Au p-contact at the top of the structure (cf. Fig. 1(b)).

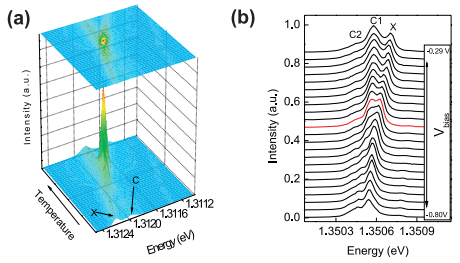

Figure 2: (a) EL intensity map showing the temperature tuning of a single QD exciton (X) into resonance with the fundamental mode (C). (b) Demonstration of strong coupling via electro-optical resonance tuning.

The processed devices are studied at low temperature via micro electroluminescence (EL) and photoluminescence (PL) experiments. Devices with Q factors up to 16.000 paves the way for a wide range of applications including deterministic single photon sources (SPS) relying on pronounced single QD resonance effects. In fact, temperature tuning shows strong enhancement of the excitonic emission intensity on resonance with the cavity mode due to the Purcell effect (c.f. Fig 2(a)). Photon autocorrelation measurements (not shown) reveal clearly photon antibunching.

Furthermore the structures are very suitable for electro-optical resonance tuning of single QDs taking advantage of the quantum confined stark effect (QCSE) and allows for tuning speed in the GHz range - significantly faster the conventional tuning methods such as temperature tuning. Electro-optical resonance tuning in the strong coupling regime is presented in Fig. 2(b).

References

[1] J. M. Gérard et al, Phys . Rev. Lett. **81**, 1110 (1998).

[2] J. P. Reithmaier et al., Nature **432**, 197 (2004).

Highly efficient extraction of spontaneous emission through coupling of evanescent waves

X.-L. Wang*, S. Furue*, M. Ogura*, V. Voliotis**, M. Ravaro**, A. Enderlin** and R. Grousson**

* *Nanotechnology Research Institute, National Institute of Advanced Industrial Science and Technology (AIST), Tsukuba Central 2, Tsukuba 305-8568, Japan*

** *Institut des Nanosciences de Paris, CNRS UMR 7588, Université Pierre et Marie Curie, Campus Boucicaut, 140 rue de Lourmel, 75015 Paris, France*

Keywords: spontaneous emission, extraction efficiency, evanescent wave, coupling

It is a very challenging task to extract spontaneous emission generated in semiconductors to air owing to the existence of strong total internal reflection (TIR) that occurs at the semiconductor-air interface. This represents a serious problem limiting the efficiency of various optoelectronic devices, especially light-emitting diodes. In this paper, we report that spontaneous emission in semiconductors can be extracted to air with an efficiency exceeding 50% through a novel coupling effect of evanescent waves.

The sample used is a GaAs/AlGaAs quantum well (QWL) grown on a V-grooved GaAs substrate (see inset of Fig. 1). It is very surprising to find that the 4.5K photoluminescence (PL) intensity per unit area of the QWL formed on the flat facet between V grooves increases drastically when the width of the flat facet was reduced to less than 1μm. We found through quantitative analysis of the PL data of Fig. 1 that the QWL emission of the 0.5-μm-wide sample escaped to air with an efficiency of greater than 50% [1]. This is an extraction efficiency about 20 times higher than that of a flat-substrate sample.

Theoretical simulation has revealed that the high extraction efficiency is the result of a novel coupling effect of evanescent waves. Shown in Fig. 2 is a series of images simulated by using the finite-difference time-domain (FDTD) method, demonstrating the evolution of electromagnetic field with time around the ridge top. Two evanescent waves (yellow arrows in Fig. 2) were generated on the two sidewall facets accompanied by TIR when the uniform wave from a point source placed in the QWL center (red dots in Fig. 2) arrives at the ridge-air interface. The two evanescent waves move towards the ridge top along the sidewall facets. When they meet at the narrow ridge top facet, the two evanescent waves couple together and are transformed efficiently into light propagating in air. Spatial distribution of PL intensity similar to Fig. 2(d) was experimentally observed in angle-resolved PL [1].

References

1. X.-L. Wang et al., APL **94** (2009) 091102-1.

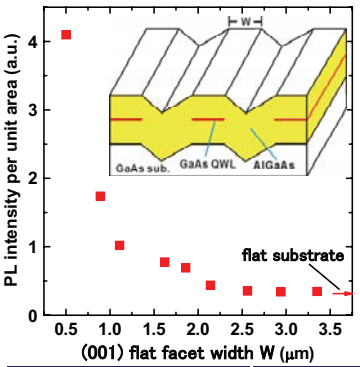

Fig.1 PL intensity as a function of flat facet width

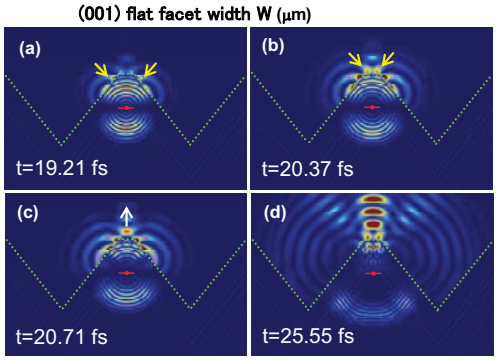

Fig.2 FDTD simulation results

Fabrication and optical characterization of photonic crystal nanocavities with InAs quantum dots bonded on silicon substrates

K. Tanabe, M. Nomura, D. Guimard, S. Iwamoto and Y. Arakawa

Institute for Nano Quantum Information Electronics, Research Center for Advanced Science and Technology, and Institute of Industrial Science, University of Tokyo, Tokyo, Japan

Keywords: quantum dot, photonic crystal, silicon photonics, semiconductor laser

Photonic crystal (PhC) lasers with quantum dot (QD) gain exhibit extremely low operation threshold [1] and their monolithic devices coupled with silicon waveguides would be promising to realize highly integrated optical circuits. We report fabrication of a two-dimensional PhC GaAs slab with InAs QDs inside on a Si substrate through wafer bonding and layer transfer (Fig. 1) and its optical characterization. Continuous-wave (CW) lasing in air-bridge PhC nanocavities was also demonstrated under optical pumping at room temperature (RT).

A 220-nm-thick GaAs slab embedding three layers of InAs QDs with a density per layer of 4×10^{10} cm^{-2} following a 700-nm-thick $Al_{0.7}Ga_{0.3}As$ layer was grown on a GaAs substrate by antimony-mediated metal-organic chemical vapor deposition [2]. The QD slab was layer transferred onto a Si substrate with a SiO_2 layer on top through direct wafer bonding and selective etch of the GaAs substrate and the AlGaAs layer. Defect-shifted L3 type two-dimensional PhC nanocavities [3] were then formed in the QD slab.

Photoluminescence spectra taken at RT included sharp peaks identified to emission stemming from nanocavity optical modes coupled with the QDs verified through the peak wavelength dependence on PhC structure variations (Fig. 2) and polarization states. Quality factors < 1000 for the PhC nanocavities on SiO_2 were enhanced up to ~8000 by removing SiO_2 to form air-bridge structures due to reduction of vertical evanescent optical leakage from the QD slab into the Si substrate as well as vertical-asymmetry-induced TE-TM mode coupling loss, resulting in RT CW lasing. This is the first demonstration of CW PhC nanocavity lasers on silicon operating at RT.

References

1. M. Nomura et al, Phys. Rev. B **75**, 195313 (2007).
2. D. Guimard et al, Appl. Phys. Lett. **89**, 183124 (2006).
3. Y. Akahane et al, Nature **425**, 944 (2003).

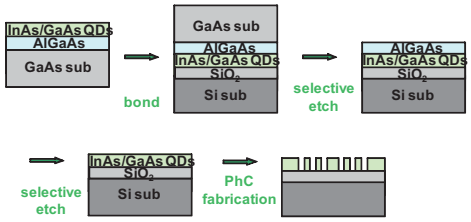

Fig.1 Cross-sectional schematic of the PhC fabrication process.

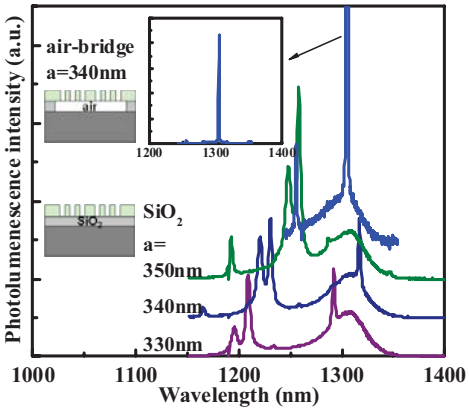

Fig.2 RT photoluminescence spectra with 30 μW pumping power for the PhC nanocavities on a 1-μm-thick air layer and a 300-nm-thick SiO_2 layer with varied PhC lattice constants. The cavity mode emission peaks red-shift with PhC lattice constant increment according to the scaling law.

Comparison between semiclassical and quantum carrier transport analysis of THz quantum cascade lasers

A. Mátyás*,***, C. Jirauschek*,**, P. Lugli** and T. Kubis***

* *Emmy Noether Research Group "Modeling of Quantum Cascade Devices", TU München, München, Germany*

** *Institute for Nanoelectronics, TU München, München, Germany*

*** *Walter Schottky Institute, TU München, Garching, Germany*

Keywords: Monte-Carlo simulation, coherent transport, quantum cascade laser, terahertz source

While Quantum Cascade Lasers (QCLs) hold great potential as compact THz sources, a further improvement, e.g., with respect to the temperature performance, requires a deep understanding of the microscopic processes, as obtained by detailed device modelling [1,2]. Various methods with differing degrees of complexity have been developed for carrier transport simulations in QCLs. The semiclassical Ensemble Monte-Carlo (EMC) method is well established for investigating and optimizing QCL structures [1]. On the other hand, the Non-Equilibrium Green's Function (NEGF) method is the most general approach to carrier transport analysis, covering quantum transport and scattering-induced decoherence effects on equal footing [2]. However, NEGF routinely neglects electron-electron (e-e) scattering, due to its increased computational complexity as compared to single-electron processes. For THz QCLs, quantum coherence effects as well as e-e scattering can play a major role. For the first time, we compare full-fledged EMC and NEGF results to each other, and discuss the agreement with experimental data. We assess the influence of the neglected effects in either method.

We investigate a phonon depopulation THz QCL emitting at 2.75 THz [3], accounting for interface roughness (IR) and electron-(acoustic and LO) phonon (e-p) scattering. While NEGF naturally includes quantum coherence, the EMC analysis can assess the influence of e-e scattering. In both methods, all mechanisms are evaluated self-consistently apart from IR scattering, which is not accessible to direct experimental characterization and thus has been described phenomenologically via its mean height Δ. In Fig. 1(a), the best fit for the EMC (with Δ=0.48 nm) and NEGF (Δ=0.3 nm) calculated laser current are presented and compared to experimental data. Both methods can reproduce the experimental result for realistic, similar values of Δ. The differences in the optimum Δ reflect the lack of coherent transport in the EMC and e-e scattering in the NEGF method, as shown in Fig. 1(b), where Δ is set to 0. For reference also the EMC result without e-e scattering and the ballistic (i.e., no scattering at all) NEGF result are also displayed, which demonstrates that both coherent transport and e-e scattering do contribute significantly to carrier transport, as will be discussed in more detail at the conference.

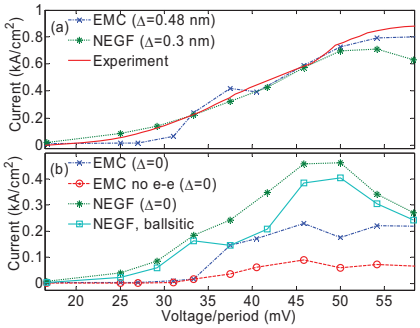

Fig.1 (a) Comparison of EMC and NEGF results to experimental current. (b) Simulated currents for Δ=0 (i.e., no IR scattering).

References

1. C. Jirauschek et al., J. Appl. Phys. **101**, 086109 (2007).

2. T. Kubis, C. Yeh and P. Vogl, J. Comput. Electron. 7, 432 (2008).

3. A. Benz et al., Appl. Phys. Lett. **90**, 101107 (2007).

Discrete or Continuous Energy Tuning of Amplified Spontaneous Emissions from Conductive Polymer Films

Y. Kamiyama*, A. Tomioka*, T. Anzai*, and K. Iwamoto*

*Osaka Electro-Communication University, 18-8 Hatucho, Neyagawa, Osaka 572-8530, Japan

Keywords: amplified spontaneous emission, π-conjugated polymer, vibrational mode, energy tuning

Conductive π-conjugated polymer films are promising material also for photonic applications: large transition moment that accompanies with the long π-electron conjugation assures the advantage of the material. Based on the successful demonstration of the material's versatility, e.g. luminescence energy tuning by molecular structure design, energy tuning of the same polymer film [1] will be the next challenge.

In this respect, most of the reports on amplified spontaneous emissions (ASE) from π-conjugated polymer film described the emission at the energy presumably corresponding to the 0-1 transition between the vibrational modes along the π-conjugation that is strongly coupled to the electric polarization oscillating at the optical frequency in excited states of the molecule. Since the $\nu = 0$ state in the ground level is almost full with electrons at room temperature, induced emission is expected as the 0-1, 0-2, etc. transitions. Energy selection to the 0-1 transition was assumed to reflect the optically allowed transition of a harmonic oscillator based on the quantum mechanical model. There have been only few reports which detected weak ASE at 0-2 transition. In the present study, efficient ASE's as 0-2, 0-3, or 0-4 transitions was successfully observed using thick polymer films. Previous report [2] on thick film ASE described that the ASE energy can be varied continuously depending on the film thickness, where the ASE was achieved as a leaky mode of the polymer film cavity and, therefore, the ASE energy was argued to be near the cutoff energy of the guided mode in the cavity. We have deposited a poly[2-methoxy-5-(2'-ethyl-hexyloxy)-*p*-phenylene-vinylene] (MEH-PPV) film on a glass substrate, where the optical confinement in the polymer film was found to be insufficient: majority of the emission was observed on the edge of the glass substrate, which indicates that the ASE leaked from the polymer film and that the glass substrate served as a waveguide. When the film thickness was thinner than 100nm, the observed energy of ASE was always at 630nm, which seemed to correspond to 0-1 vibrational transition. While the film thickness was thicker than 100nm, however, the ASE exhibited itself at different energies that seemed to correspond to the 0-2, 0-3, and 0-4 vibrational transitions [Fig. 1].

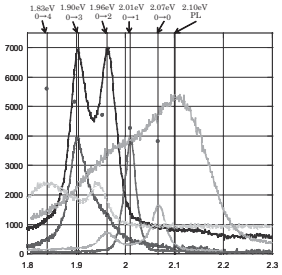

Fig.1 Discrete energy tuning of ASE's from thick MEH-PPV films spin-cast on a glass substrate.

When the optical excitation power was incremented above the ASE threshold, the ASE energy increased continuously, which was an indication of phase space filling of the excited states: under higher excitation power, more electrons are pumped up to the excited states whose band will be filled with electrons from the bottom, leading to ASE from higher energy states in the excited band.

References

1. Y. Kamiyama, A. Tomioka, T. Mizutani, M. Yamazaki and K. Morimoto, IEICE Trans. Electron., E91-C No.12 **463,** 1869 (2008).
2. D. Yokoyama, M. Moriwake and C. Adachi, J. Appl. Phys. 103, 123104 (2008).

Control of thermal radiation using intersubband transitions in quantum wells

M. De Zoysa, T. Asano, and S. Noda

Department of electronic science and engineering, Kyoto University, Kyoto, Japan

Keywords: thermal radiation, intersubband transition, emissivity control, Kirchhoff's law

Thermal radiation generally contains an extremely wide rage of spectral components. A great deal of research has gone into controlling thermal radiation in order to realize emission from only desired spectral components having very high emissivity close to the black body. However, since most of these researches were based on the modification of the optical density of states [1-2], realizing sufficient control of thermal radiation has proven to be a challenge. This is because control over the optical density of states is difficult to achieve over a wide spectral range. Here, we propose a novel approach based on the modification of electronic states of a material. Our method is based on Kirchhoff's law which states that a material's emissivity equals its absorptivity, and thus we put forward that the thermal radiation should be controlled by tailoring its absorption spectrum. To demonstrate this idea, we employed an intersubband transitions (ISB-T) in a quantum well (QW), which has a very strong, narrow peak absorption spectrum. In the following, we demonstrate experimentally that an ISB-T is indeed very useful for emitting a single thermal emission peak, while significantly suppressing undesired spectral components.

We prepared an n-type modulation doped GaAs/$Al_{0.3}Ga_{0.7}As$ multiple quantum well (MQW, 64 layers) sample. The widths of the well and barrier layers are 23 and 46ML, respectively. Only the barrier layer is doped with Si at a density of 5×10^{17} cm^{-3}. The ISB-T wavelength is calculated to be 9.2 μm. Figure 1 (a) shows the sample's absorption spectrum measured under the Brewster condition (θ_B=73°) at room temperature. The results show that a narrow (FWHM=10 meV) strong absorption dip exists at 9.1μm which is close to the designed value (9.2 μm). Next we heated the sample by an external heater to 100 °C and measured the thermal radiation spectrum from the sample's end-facet under the Brewster condition (Fig.1 (b)). It is seen in the figure that a strong radiation peak exists at 9.5 μm only for transverse magnetic (TM) polarization. This peak is attributed to ISB-T because the wavelength and the polarization coincide with the ISB-T absorption properties. We also compared the sample's radiation spectrum with that of a quasi-black body and found that the radiation peak has nearly the same intensity. Therefore, we can conclude that thermal radiation can be manipulated with high emissivity close to the black body in design wavelengths by using ISB-Ts of QWs.

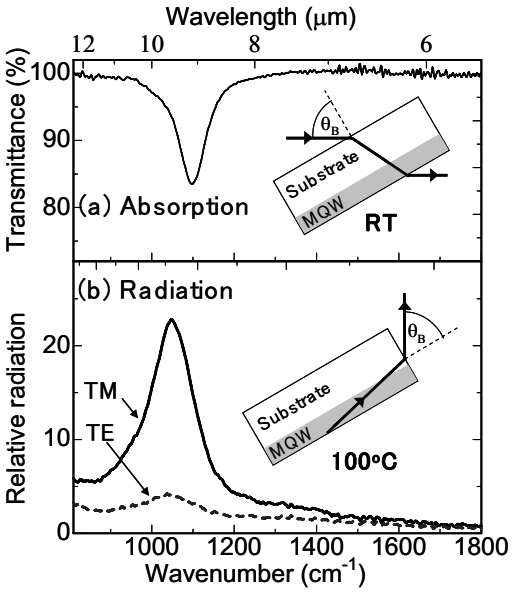

Figure 1: (a) Absorption spectrum, measured at RT. (b) Thermal radiation spectra from the MQW sample's end-facet, measured under Brewster condition (θ_B=73°) at 100 °C.

References

1. J.F. Waymouth, J. Light & Vis. Env. **13**, 51(1989)

2. S.Y. Lin, J.G Fleming and I.El-Kaddy, Appl. Phys. Lett. **83**, 380(2003)

Tuneable surface plasmon modes in core (dielectric)-shell (metal) nanocylinder pair

J. Y. Lu, H. Y. Chou, J. C. Wu, S. Y. Wei, and Y. H. Chang

Department of physics, National Taiwan University, Taipei, Taiwan

Keywords: metals, nanoshell, dispersion, FDTD, Raman scattering

The optical response of metal nanoparticles depends on the size, shape, and the local dielectric environment of the nanoparticles. Therefore, nanoparticles can be used to guide, enhance, emit, and modify the incident electromagnetic wave, and have many technological applications. Recently, the optical response of core (dielectric)-shell (metal) nanostructures has attracted much attention. Compared to solid gold particles of similar size, these core-shell nanostructures exhibit a red-shifted localized surface plasmon that can be tuned over an extended wavelength range by varying the thickness of the shell and the measured wavelength variation is interpreted as originating from coupling of localized surface plasma modes at the inner and outer surfaces of the core-shell structure. [1]

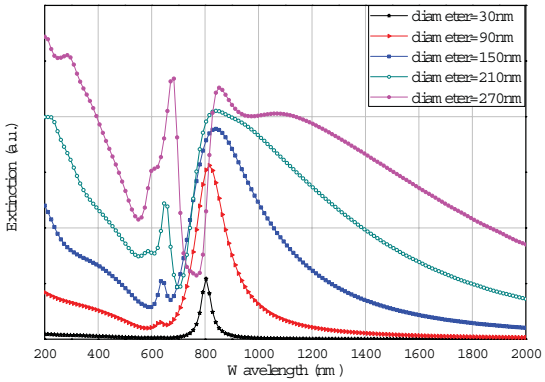

Fig. 1 Extinction spectra of a pair of core shell nanocylinder with different diameters excited by incident wave propagating perpendicular (electric field parallel) to the axis of the pair.

In this work, we use the 2-D finite difference time domain method (FDTD) in conjunction with the efficient dielectric function (CP3 model) [2] to study the optical properties of core-shell nanocylinders with the emphasis on the optical coupling between a pair of core-shell nanocylinders. In this study the ratio of the outer radius to inner radius is fixed at 6:5 and the ratio between the outer radius and the inter-nanocylinders spacing is fixed at 5:1. The perfect medium layers condition is used as radiation boundary condition for simulating the propagation of the electromagnetic wave. Both extinction spectrum and near field intensity associated with the coupling resonance as a function of nanocylinder diameter are studied.

Three major resonance modes were observed for a pair of core-shell nanocylinders. In addition to the core-shell dipole-dipole and quadruple-quadruple symmetric interaction modes, a new mode appears when the diameter of the nanocylinder exceeds 250 nm. This new mode is similar to the dipole-dipole interaction mode of a pair of gold nanocylinder because the charge distribution of this mode indicates that there is no polarized charge in the inner surface of the core-shell nano-cylinder. In addition, an interesting intensity distribution can be found when the incident field is propagating parallel to the axis of the nanocylinder pair and can be related to the resonance inside a cavity.

References

1. J. Aizpurua, P. Hanarp, D. S. Sutherland, M. Kall, G. W. Bryant, and F. J. Garcia de Abajp, Phys. Rev. Lett. **90**, 057401 (2004).
2. J. Y. Lu and Y. H. Chang submitted.

Anderson localization of light in random configuration of dielectric circular cylinders

Y. Inose[*1], T. Ohtsuki[*1,2,3], H. Kunugita[*1,2,3], K. Ema[*1,2,3], M. Sakai[*1,2,3], A. Kikuchi[*1,2,3] and K. Kishino[*1,2,3]

*1 *Department of Engineering and Applied Sciences, Sophia University*

*2 *Sophia Nanotechnology Research Center, Sophia University*

*3 *CREST, Japan Science and Technology Agency*

Keywords: Anderson localization of light, pseudogap map, finite-difference time-domain, nanocolumn

There has been an increase of the research for photonic crystal recently. On the other hand, in the case of random medium, the overall picture of Anderson localization of light [1] is less well understood. Here we obtain a pseudogap map adopting the parameters of nanocolumn samples [2], which indicates the parametric dependence of the localization effect.

We have simulated the light propagation in random media using the two-dimensional finite-difference time-domain method [3]. The simulation system was 4.5 μm square, which consisted of random arrays of parallel dielectric cylinders with a constant radius (r = 50 nm) and a constant refractive index (n = 2.35), and they were embedded in a vacuum. Several values of the filling fraction of cylinders Φ have been considered. We have irradiated a Gaussian white pulse onto the whole sample area at t = 0, and fields at each location were recorded via array of 400 antennas evenly spaced in the system. After the simulation, we have obtained localized light spectra by averaging several power spectra which are Fourier transformed from each field signal (see Fig. 1). Furthermore, to create a pseudogap map, we calculated Q factors using localized light spectra of different time windows.

The pseudogap map we have succeeded in obtaining is shown in Fig. 2. This is the first detailed report of the overall picture. We can estimate optimal parameters for strong localization effect from the map. We can prepare GaN nanocolumn ensemble with the optimal parameters. Actually such samples show random lasing.

References

1. S. John, Phys. Today **44**, No. 5, 32 (1991).
2. M. Yoshizawa et al., Jpn. J. Appl. Phys., Part 2 **36**, L459 (1997).
3. A. Taflove, Computational Electrodynamics: *The Finite-Difference Time-Domain Method* (Artech House, 2005).

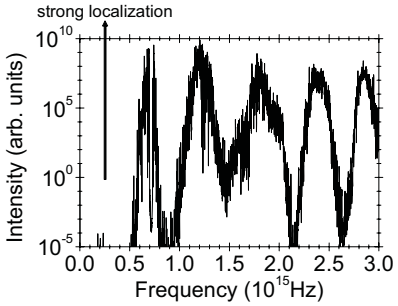

Fig.1 An example of a localized light spectrum, where Φ = 0.4 and time window [2, 4 ps].

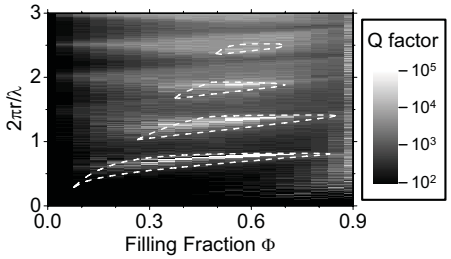

Fig.2 A pseudogap map for random medium using Q factors. The dashed lines are band edges for hexagonal photonic crystal.

Enhancement of photoluminescence from germanium by utilizing air-bridge type photonic crystal slab

Shigeru Nakayama[a,c], Satomi Ishida[b], Satoshi Iwamoto[a-c] Damian Bordel[c], Emmanuel Augendre[d], Laurent Clavelier[d] and Yasuhiko Arakawa[a-c]

[a] *Research Center for Advanced Science and Technology, University of Tokyo, Japan*
[b] *Institute of Industrial Science, the University of Tokyo, Japan*
[c] *Institute for Nano Quantum Information Electronics, the University of Tokyo, Japan*
[d] *CEA, LETI, Minatec, F38054 Grenoble France*

Keywords: photonic crystal, germanium, photoluminescence, air-bridge

Silicon photonics technologies have been receiving much attention due to their potential applications in the future electronics and in other fields. Especially, it is a hot research topic to realize silicon-based efficient light emitting devices, which should be compatible with the silicon technology. Germanium is an attractive material as light emitter in silicon photonics technology. Germanium shows the direct-transition emission at telecom wavelength (~1.55μm) at room temperature. Recently, photoluminescence (PL) characterizations of germanium on insulator (GeOI) with micro cavity resonator [1] and vertically asymmetric slab photonic crystal (PhC) cavities [2] have been reported. In this work, we report on the first demonstration of large enhancement of PL intensity from "air-bridge type" germanium PhC slab. The peak PL intensity from the air-bridge type PhC is about 10 times stronger than that from a non-processed substrate.

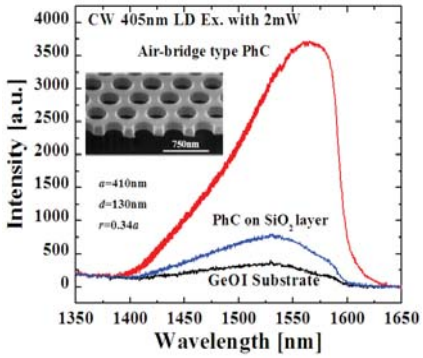

Fig. 1. Room temperature μ-PL spectra from air-bridge type Ge PhC, Ge PhC on SiO_2 layer and non-processed substrate. The inset shows a scanning electron micrograph image of an air-bridge structure.

Air-suspended germanium PhCs were fabricated on GeOI substrate, which consists of a 130-nm-thick germanium layer and a 500-nm-thick buried SiO_2 layer, by common silicon processing techniques. The samples were characterized by μ-PL measurement at room temperature using a CW laser diode (λ=405nm) as a pump light source with 2mW excitation power. Figure 1 shows the PL spectra from air-bridge type germanium PhC slab, germanium PhC slab on SiO_2 layer (Both of them have lattice constant a=410nm and radius r=0.34a.) , and non-processed GeOI substrate.

PL from non-processed substrate shows a typical PL spectrum of germanium. By introducing PhC structures we observed enhancement of PL signals. Especially peak PL intensity from the air-bridge type PhC is ~10 and ~2 times larger than those from the unprocessed area and from PhC slab on SiO_2 layer, respectively. This large enhancement in air-bridge PhC can be attributed to the suppression of light leakage into the lower side of the slab due to larger index contrast between air(1.0) and germanium(~4.2) and the improvement of extraction efficiency into the collection lens in the optical setup due to the diffraction effect caused by photonic crystal structure. .

Acknowledgments This work was supported by Spatial Coordination Funds for Promoting Science and Technology. We thank CEA-Soitec for the fabrication of the germanium on insulator substrates.

References

[1] P. H. Lim,*et al*. Appl. Phys. Lett. **93**, 041103 (2008).
[2] T-P. Ngo,*et al*. Appl. Phys. Lett. **93**, 241112 (2008).

Drastic Enhancement of Luminescence from InAs Quantum Dots Embedded in Niobium Metal

M. Takada[*], Y. Idutsu[*,**], D. Kato[*], S. Ida[*], S. Ito[*], H. Sato[*], J.-H. Huh[*,***], H. Sasakura[*,**], H. Kumano[*,**], and I. Suemune[*,**]

** Research Institute for Electronic Science, Hokkaido University, Sapporo, Japan*

*** CREST, Japan Science and Technology Agency, Tokyo, Japan, ***GCOE, Hokkaido University, Japan*

Keywords: Quantum dot, Photon extraction, Metal cavity, Photon generation

Photon extraction efficiency from semiconductors with high refractive indices is usually limited to a few % due to internal total reflections. This is a very important issue not only to realize highly efficient light emitting diodes (LEDs) but also to realize on-demand single photon emitters. This is also a crucial issue for highly efficient entangled photon-pair generation. Cavities based on photonic crystals and pillar microcavities have been studied for this purpose. In this paper, a metal cavity burying semiconductor pillars is proposed. Drastic enhancement (>30 times) of luminescence from InAs quantum dots (QDs) is reported.

InAs QDs buried in GaAs were prepared into pillar structures with the diameter below 1μm and they were buried in a niobium (Nb) metal. The reason why Nb was selected is due to the future expectation of the enhanced radiative recombination with the Nb superconductivity. One example is shown in Fig. 1. The height of the pillars was ~500nm. Photoluminescence (PL) measurements were performed at 4 K with the excitation of Ti: Sapphire laser emitting at the wavelength of 850nm. The emission wavelength of the InAs QDs was around 1100 nm and discrete sharp peaks were observed for the smaller pillar diameters.

The exact evaluation of the photon extraction efficiency from a single InAs QD is difficult, since the efficiency will be dependent on the relative position of QDs in the pillar structure. The strategy in this work is the evaluation of ensemble of QDs in the pillars. This will average out the position dependence of the luminescence efficiency, which will be proportional to the average QD numbers and therefore the pillar cross-sectional area.

Fig.1 GaAs pillar with InAs QDs inside buried in Nb.

The integrated PL intensities measured on two kinds of samples are plotted in Fig. 2. One sample (A) is bare GaAs pillars with InAs inside and the other (B) buried in Nb. The dashed lines are the maximum for the A sample and the average for the B sample. More than 30-times enhancement of the luminescence intensity will be evident by burying with Nb. For the two dashed lines to be parallel, it was necessary to shift the data for the B sample by 300nm. This suggests the presence of 150nm-wide dead layer near the Nb interface, but the uniformity of the data is improved in the B samples. These measurements are analyzed with FDTD simulations and more detailed of the improved photon extraction efficiency from single InAs QDs will be discussed during the conference.

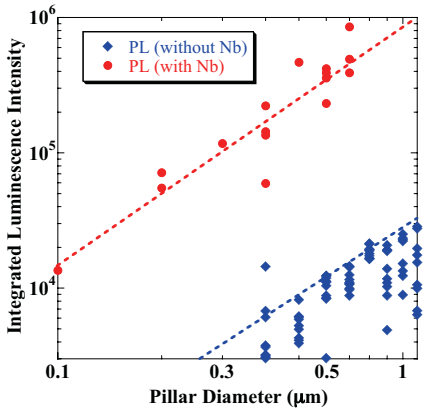

Fig.2 Integrated PL intensities measured on two kinds of samples plotted against GaAs pillar diameter.

Rolled-up metal/semiconductor microtubes as hyperlenses working in the visible

M. Bröll, S. Schwaiger, D. Heitmann, and S. Mendach

Institute of Applied Physics, University of Hamburg, Hamburg, Germany

Keywords: optics, metamaterials, rolled-up microtubes, hyperlensing

Metamaterials gained considerable interest in the science community since the beginning of the century. Their optical properties can be arbitrary tailored by designing their artificial building blocks with size and wavelength smaller than the wavelength of interest giving rise to envisioned applications like, e.g. object cloaking or sub wavelength imaging. One promising route towards magnifying sub wavelength lenses is the concept of hyperlensing. Hyperlenses for ultra violet light have been created by subsequently evaporating alternating layers of Ag and Al_2O_3 onto a cylindrically shaped ridge in a transparent substrate [1].

Here we present a bottom-up concept for free-standing hollow hyperlenses working in the visible. We employ the method of self-rolling strained layers [2, 3] to produce well-defined radial Ag/InGaAs superlattices (RSLs) with accurately tuneable curvature, lattice constants and layer thickness aspect ratios. For wavelengths much larger than the lattice constant (typically some ten nanometers) the transmission through the superlattice can be described by the effective permittivity tensor which shows a strong anisotropy with respect to the radial component ε_r and the tangential component ε_t. Sub-wavelength imaging is obtained for an operating wavelength λ_O chosen such that $\varepsilon_r >> \varepsilon_t = 0$. Figure 1 shows finite difference time domain simulations for a rolled-up radial superlattice with 25 cells of 4 nm Ag and 6 nm InGaAs. The operating wavelength λ_O of the system is 685 nm. As expected from the effective medium picture the electromagnetic field is radially channelled and the near field of the dipoles located at the inner perimeter is transmitted to the outer perimeter, i.e. the RSL exhibits hyperlensing. In the image on the outer perimeter of the RSL the distance of the dipoles is magnified by the ratio of the outer and the inner bending radius from 250 nm to 425 nm.

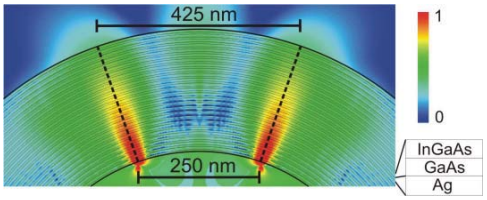

Fig.1 Finite difference time domain simulations on a hyperlens working at visible frequencies based on a rolled-up Ag/(In)GaAs radial superlattice (RSL). Two dipoles at the inner perimeter of the RSL emit at the working wavelength λ_O = 685 nm with H polarized along the RSL rolling axis. The value of H_z represents the wavefield normalized to the dipol sources and is given by a logarithmic color plot. At the outer perimeter of the RSL a magnified image of the dipoles is obtained.

The experimental feasibility of our concept is substantiated by transmission and reflection measurements on first realized structures similar to the one shown in Fig. 1. These measurements are in good agreement with an effective medium approach and confirm that the working wavelength λ_O with $\varepsilon_r >> \varepsilon_t = 0$ can be tuned over a broad range in the visible and near infrared by varying the Ag and InGaAs layer thickness ratio [4].

References

1. Z. Liu, H. Lee, Y. Xiong, C. Sun, and X. Zhang, Science **315**, 1686 (2007).
2. A. Cho, Science **313**, 164 (2006)
3. S. Mendach, J. Podbielski, J. Topp, W. Hansen, and D. Heitmann, Appl. Phys. Lett. **93**, 262501 (2008).
4. S. Schwaiger, M. Bröll, A. Krohn, A. Stemmann, C. Heyn, Y. Stark, D. Stickler, D. Heitmann, and S. Mendach, submitted to Phys. Rev. Lett.

Direct observation of nuclear spin pumping dynamics in a single InAlAs quantum dot

S. Furukawa, R. Kaji, S. Adachi, S. Muto, and H. Sasakura*
Department of Applied Physics, Hokkaido University, Sapporo, Japan
**Research Institute for Electronic Science, Hokkaido University, Sapporo, Japan*

Keywords: quantum dot, nuclear spin, InAlAs, time-resolved measurement

Since the first proposal of using nanostructures for quantum information processing, the semiconductor quantum dots (QDs) have been attracting a lot of attention. Single spin manipulation in a QD has been recently demonstrated by time-resolved Kerr (Faraday) rotation and electron spin resonance, evidencing clearly the long electron spin coherence to which the nuclear spin fluctuation plays an important role. Beginning with the first observation of large nuclear spin polarization in self-assembled InAlAs QDs [1], research of the nuclear spins in QDs proceeds swiftly, and the hysteretic response was also observed [2]. However, the detailed spin dynamics in the coupled electron-nuclear spin system is still unclear.

In this work, optically pumped nuclear spin polarization in single InAlAs quantum dots was investigated in detail through the time-resolved measurements of the formation process. The QD sample has an $In_{0.75}Al_{0.25}As$ QD layer embedded in $Al_{0.3}Ga_{0.7}As$ barrier layers and was held at 5 K under the magnetic field up to 5 T in Faraday geometry. For the single QD spectroscopy, small mesa structures with a top lateral size of ∼150 nm were fabricated. A cw Ti:sapphire laser was tuned to the tail of the wetting layer. In order to achieve zero nuclear spin polarization as the initial condition, alternating cross-circular excitation with an EO modulation frequency of 10 Hz was employed. Then, changing the excitation polarization to σ_- by which the nuclear field creates in antiparallel to the external field, PL spectra were obtained sequentially every 100 ms. The dependences on external field and excitation power of the Overhauser shift (OHS) of positive trion (X^+) PL are depicted in Fig. 1. OHS is induced by the nuclear field proportional to the nuclear spin polarization. The jump to the upper stable branch of OHS is observed clearly in its temporal evolution and the calculated results considering the spin dynamics in hole-X^+ system coincide with the experimental ones. Degree of circular polarization (DCP) can be also reproduced in the same model. In the conference, we will discuss the spin flip-flop process between electron and nuclear spins and verify the model and some assumptions.

[1] T. Yokoi, S. Adachi, H. Sasakura, S. Muto et al., Phys. Rev. B **71**, R041307 (2005).
[2] A. I. Tartakovskii, T. Wright, A. Russell et al, Phys. Rev. Lett. **98**, 026806 (2007), R. Kaji, S. Adachi, H. Sasakura, S. Muto, Appl. Phys. Lett. **91**, 261904 (2007), Phys. Rev. B **77**, 115345 (2008).

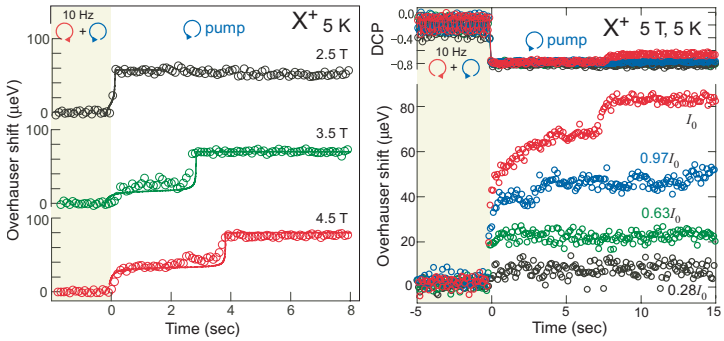

Figure 1: Temporal evolution of nuclear spin pumping process observed via OHS. OHS of X^+-PL at 5 K was plotted as parameters of external field (left) and excitation power (right). Solid lines in a left panel are the calculated curves.

Transient grating studies of phase and spin coherences of excitons in GaAs single quantum wells

K. Tomoda, Y. Nakano, S. Adachi, and S. Muto
Department of Applied Physics, Hokkaido University, Sapporo, Japan

Keywords: exciton spin, exchange interaction, GaAs, coherence

The spin relaxation processes of excitons and electrons in semiconductor nanostructures have been a topic of intense experimental and theoretical investigations. Possible spin-based applications such as quantum information processing boost up the studies of spin coherence, especially, in QDs since quantitative information on spin relaxation or spin lifetime is essential to the design and successful implementation of such applications.

Based on the investigations since about 1990, exciton spin relaxation mechanism effective for GaAs QWs gets settled; for room temperature the scattering during the precession in the effective magnetic field originating from the spin splitting in conduction band and for low temperatures the exchange interaction between electron and hole in an exciton because of the increased wavefunction overlap and the ability of exciton to acquire appreciable momentum during it's longer lifetime. The former is analogous to the D'yakonov-Perel'(DP) mechanism and the latter is the QW version (Maialle-Andrada-Sham (MAS) mechanism [1]) of the Bir-Aronov-Pikus (BAP) mechanism for electron spin relaxation in bulk semiconductors, respectively. However, there exists only a few reports on the well width dependence of spin coherence, which corresponds to change the wavefunction overlap. Furthermore, in most of their reports, phase coherence has been assumed as a constant regardless of the well width [2-5].

In the present work, the exciton spin and phase coherences at low temperatures in GaAs/AlGaAs single QWs were investigated by using transient grating technique. This technique allows us to obtain the exciton lifetime, spin relaxation, and phase relaxation in the same setup. The character that spin coherence depends strongly on the scattering events gives rise to a sample-to-sample distribution of the experimental spin relaxation times. The extent of localization also should affect significantly to the spin coherence through the change of scattering. In order to minimize such risks, a series of single QWs with different well width separated by 200-Å-thick $Al_{0.3}Ga_{0.7}As$ layers were grown on a (001) GaAs substrate. Figure shows the experimental values of spin relaxation times for four single QWs under the same exciton density at 10 K. The phase relaxation times T_2 for individual QWs are also indicated in the figure. Solid lines are the theoretical prediction according to MAS mechanism. Both coincide well and the motional narrowing behavior is clearly demonstrated.

[1] M. Z. Maialle, E. A. de Andrada e Silva, and L. J. Sham, Phys. Rev. B **47**, 15776 (1993).
[2] A. Vinattieri, J. Shah, T. C. Damen et al., Phys. Rev. B 50, 10868 (1994).
[3] P. Perozzo and A. Miller, Proc.of SPIE **2694**, 51 (1996).
[4] A. Tackeuchi, Y. Nishikawa, and O. Wada, Appl. Phys. Lett. **68**, 797 (1996).
[5] A. Malinowski, R. S. Britton, T. Grevatt et al., Phys. Rev. B **62**, 13034 (2000).

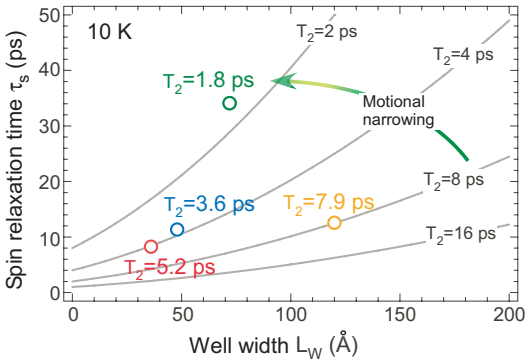

Figure 1: Spin relaxation times of four single QWs with different well width are plotted. The phase relaxation time T_2 of their QWs are also indicated. The solid curves are the theoretical prediction considering the exchange interaction

Controllable Dresselhaus field in microscopically inversion symmetric quantum wells

Masahiko Murata, Takuma Tsuchiya

Hokkaido University (Hokudai), Graduate School of Engineering, Sapporo 060-8628, Japan

Keywords: Dresselhaus field, quantum wells, inversion symmetry, tight-binding method

The Rashba effective magnetic field is controlled by the external electric field and is used to control the electron spin precession in compound semiconductors, such as GaAs and InAs. On the other hand, the Dresselhaus field, arises from special inversion asymmetry of the crystal structures, can not be controlled externally. This field, however, is sometimes comparable to the Rashba field and becomes an obstacle to the coherent spin precession.

In this study, we proposed a method to control the Dresselhaus field, using microscopically inversion-symmetric quantum wells of compound semiconductors. As shown in Fig. 1, two mono-layers of Ge at the center of the well is sandwiched by GaAs layers, and the both side of the Ge layer are Ga ones. In this structure, the Dresselhaus field should vanish, because the structure has global spatial inversion symmetry. Further, if we apply the electric field along the growth direction, the Dresselhaus field appears, because the electron wave function is distorted, and the global inversion symmetry is lost. As a result, it is possible to control the Dresselhaus field, but the strength and the behaviour of the field is not known. Thus, we perform an sps* tight-binding calculation, to demonstrate the validity of this method.

Figure 2 shows the spin splitting of the ground conduction subband for 8.62 nm well. The total magnetic field, sum of the Dresselhaus and the Rashba field, vanishes for applied electric field of 0 V/m, as has been expected. It increases in proportional to the applied field to the strength sufficient for spin control. Wave-vector dependence of the effective magnetic field, shown in Fig. 3, shows a characteristic shape of comparable Dresslhaus and Rashba field.

These results show that the Dresselhaus field in the present structure has sufficient strength for spin control, and we can controll it effectively by the applied electric field.

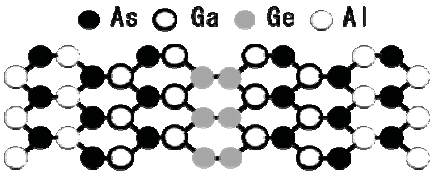

Figure 1 Schematic illustration of the crystal structure of the microscopically inversion symmetric quantum well.

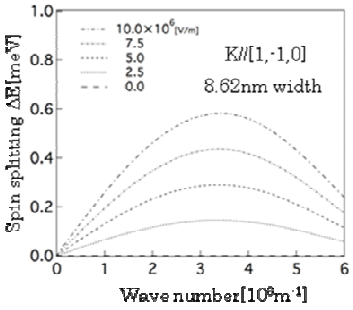

Figure 2 Spin splitting of the ground subband of 8.62 nm well for applied electric field of 0 to 10^7V/m.

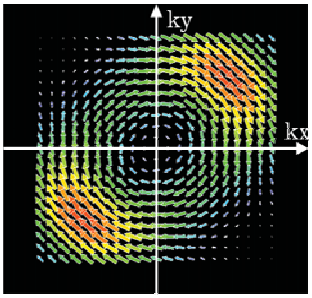

Figure 3 Wave vector dependence of the effective magnetic field for 8.62 nm well and applied electric field of 10^7V/m.

Efficient room temperature spin filter based on GaNAs quantum wells

X.J. Wang*, Y. Puttisong*, I.A. Buyanova*, H. Carrére*,**, F. Zhao**, A. Balocchi**, X. Marie**, C.W. Tu***, and W.M. Chen*

** Department of Physics, Chemistry and Biology, Linköping University, 58183 Linköping, Sweden*

*** Université de Toulouse, LPCNO: INSA, UPS, CNRS, 135 avenue de Rangueil, 31077 Toulouse cedex, France*

**** Department of Electrical and Computer Engineering, University of California, La Jolla, CA92093, USA*

Keywords: spin filter, GaNAs, spintronics, defect-engineering

Generating electron spin polarization and coherence at room temperature is one of the most important as well as the most challenging issues for future spintronics and spin-based quantum information technology, which has attracted intense global research efforts during recent years. Many approaches have been attempted with a varying degree of success. Spin filtering has been demonstrated by employing ferromagnetic metals, diluted magnetic semiconductors, quantum point contacts, quantum dots, carbon-nanotubes and multiferroics, etc., though so far unfortunately mostly with a limited efficiency and primarily at a low temperature or under applied magnetic fields.

Here, we present and demonstrate a new approach for an efficient electron spin filter by defect-engineering of a non-magnetic semiconductor. Our preliminary results were recently published in Nature Materials [1]. Such a spin filter is shown to be capable of generating >40% electron spin polarization at room temperature in GaNAs epilayers and quantum wells (QW), without requiring a magnetic layer or external magnetic fields. We provide direct experimental proof for the exact physical mechanism leading to the observed spin filtering effect. It is shown that an electron spin-polarized defect, such as a Ga self-interstitial in dilute nitride GaNAs, can effectively deplete conduction electrons with an opposite spin orientation and can thus turn the non-magnetic semiconductor into an efficient spin filter. The identification of the spin-filtering defects is unambiguously established by their unique spin-resonance signatures derived from the hyperfine interaction between the localized unpaired electron spin and nuclear spins (I=3/2) of the Ga atom with two naturally abundant isotopes ^{69}Ga and ^{71}Ga. We demonstrate how the spin-filtering effects can be engineered by varying the concentration of the responsible defects, which can be achieved by varying N composition and growth condictions, and also by post-growth treatments. We also demonstrate how the spin-filetering effect can be controled by varying the QW width. These results shed light on the directions for further improvements and optimization of the efficiency of such defect-engineered spin filters. We also illustrate another attractive feature of this new approach - the spin direction of such spin filters can easily be switched at will by orienting electron spins of the spin-filtering defect at a preferred direction. Possible applications of such spin-filtering on improving efficiency of light-emitting devices will be discussed. More importantly, the present work has demonstrated the potential of such a defect-engineered, switchable spin filter as an attractive alternative to generate, amplify and detect electron spin polarization at room temperature without a magnetic material or external magnetic field, i.e. under the conditions that will be found desirable for practical device applications in future spintronics.

References

1. X.J. Wang, I.A. Buyanova, F. Zhao, D. Lagarde, A. Balocchi, X. Marie, C.W. Tu, J.C. Harmand and W.M. Chen, Nature Materials 8, 198 (2009).

A method for detecting polarity of wurtzite semiconductor

Q. Zhang*, X.Q. Wang*, X. W. He*, C. M. Yin*, B. Shen*, Y. Ishitani, ** A.Yoshikawa**

**State Key Laboratory of Artificial Microstructure and Mesoscopic Physics, School of Physics, Peking University, Beijing 100871, China*

*** Department of Electronics and Mechanical Engineering, Chiba University, 1-33 Yayoi-cho, Inage-ku, Chiba 263-8522, Japan*

Keywords: Polarity, wurtzite semiconductors, InN, CPGE.

Wurtzite semiconductors, such as GaN, InN and ZnO, have wide application in optoelectronic and electric field. One of important issue for these materials is polarity which greatly influences the growth mode, impurity incorporation, chemical stability and so on[1]. Therefore, it is very important to accurately detect and control the polarity. In this presentation, a method based on circular photogalvanic effect (CPGE) for detecting polarity of wurtzite semiconductors is proposed [2].

Experiments were carried out on InN films grown by molecular beam epitaxy (MBE) on c-plane sapphire substrates. Polarity of InN was controlled by that of GaN buffer layer, where Ga/N polar GaN buffer layers led to In/N polarity InN. Electrodes were made by indium contact. A diode pumped solid state laser with a wavelength of 1064 nm was used as excitation source while a quarter wave plate was used to change helicity of the incident light.

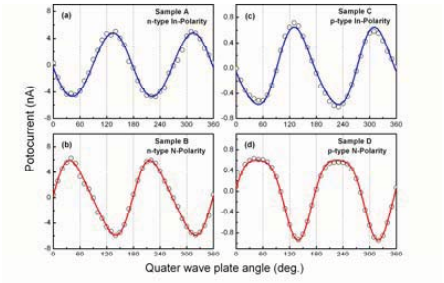

Fig.1 Opposite photocurrents in four typical InN samples with different polarities as a function of 1/4λ plate angle φ. It is shown that polarity can be clearly identified in both n-type and p-type samples. Incidence angle in all experiments is +25 degree.

Fig. 1 show the CPGE current of four InN samples as a function of 1/4λ plate angle φ. As shown in Fig. 1(a) and 1(b), the photocurrent directions at the same 1/4λ plate angle φ are opposite for n-type InN with different polarities. Furthermore, their dependence on angle φ is also opposite due to that the reversed spin splitting for different polarity InN layers. CPGE currents of p-type InN layers with different crystalline polarities were also measured and shown in Fig. 1(c) and 1(d). It is obvious that the same results were obtained for p-type samples, showing that the CPGE current does not depend on the conduction type. The smaller current shown in p-type layer is caused by the fast momentum relaxation due to the large scattering rated in p-type layer with low mobility.

In summary, a new method to detect crystalline polarity of wurtzite semiconductor is provided. It is worth noting that it is very easy to set up measurement system with low price and measurement itself is also very simple. This method is operated at ambient condition with high sensitivity and is not destructive to samples. In addition, this detection method based on CPGE is applicable for almost all semiconductors with crystalline polarity such as GaN, ZnO and so on, though we just show the result of InN here.

References

1.X. Wang, A. Yoshikawa, Prog. Cryst. Growth Character. Mater. **48/49**, 42 (2004).

2.S.D. Ganichev, W. Prettl, J. Phys. Condens. Matter.**15**, R935 (2003).

Influence of antiferromagnetic interactions and of alloy disorder on the ferromagnetic properties of p-(Cd,Mn)Te quantum wells

C. Simserides[1], A. Lipińska[2], A. Majhofer[3], K. N. Trohidou[1] and T. Dietl[2,4]

[1] *Institute of Materials Science, NCSR Demokritos, Athens, Greece*

[2] *Institute of Physics, Polish Academy of Science, Warszawa, Poland*

[3] *Institute of Experimental Physics, University of Warsaw, Warszawa, Poland*

[4] *Institute of Theoretical Physics, University of Warsaw, Warszawa, Poland*

Keywords: Magnetic II-VI semiconductors, Monte Carlo methods, Exchange and superexchange interactions

Modulation-doped *p*-type (Cd,Mg,Zn)Te/(Cd,Mn)Te quantum wells (QWs) are a unique medium allowing to probe carrier-induced Ising-like ferromagnetism in the two-dimensional case, as in this system the mean free path is longer than the QW width [1]. However, a surprising result is the absence of hysteresis loops below the Curie temperature, T_C. To obtain information on the mechanisms controlling spin dynamics, we have extended our previous Monte Carlo simulations combining the Metropolis algorithm with the determination of hole eigenfunctions at each Monte Carlo sweep [2].

The numerical calculations show that short-range antiferromagnetic superexchange interactions between Mn spins, which compete with the hole-mediated long-range ferromagnetic coupling, play an important role in magnetization relaxation of the system. Moreover, we reveal that the effect of antiferromagnetic interactions becomes much reduced if the thickness of the layer containing Mn spins is narrower than the extend of the hole wave function [3]. This implies that magnetic hysteresis should be recovered in QWs, if the thickness of the Mn layer is smaller than the region visited by the holes.

Furthermore, we analyze theoretically the role of spin-independent alloy disorder [3] and we find that it reduces T_C, particularly in the range of low hole concentrations. We have performed simulations for repulsive as well as for attractive alloy potential, δV. The attractive potential washes the ferromagnetism virtually entirely out because holes get localized for the chosen magnitude of δV. Hence, our results substantiate the view that delocalized or weakly localized carriers are indispensable to set a long-range order between diluted spins. Obviously, smaller amplitude of the attractive potential or greater hole concentrations will lead to carrier delocalization and the re-entrance of a ferromagnetic order. Interestingly, the repulsive potential $\delta V > 0$, the case of (Cd,Mn)Te, also leads to reduced magnitudes of T_C comparing to the values determined for $\delta V = 0$. We interpret this finding by noting that in the presence of a repulsive potential, the amplitude of the wave function at Mn ions is decreased compared to the case $\delta V = 0$. This reduces the *p-d* coupling and shifts the appearance of the carrier-mediated ferromagnetic order to lower temperatures.

References

1. H. Boukari, P. Kossacki, M. Bertolini, D. Ferrand, J. Cibert, S. Tatarenko, A. Wasiela, J. A. Gaj, and T. Dietl, Phys. Rev. Lett. **88**, 207204 (2002).

2. D. Kechrakos, N. Papanikolaou, K. N. Trohidou, and T. Dietl, Phys. Rev. Lett. **94**, 127201 (2005).

3. A. Lipińska, C. Simserides, K. N. Trohidou, M. Goryca, P. Kossacki, A. Majhofer, and T. Dietl, arXiv:09020406.

Optical spin injection in novel InAs quantum dots structures

J. Beyer*, I. A. Buyanova*, S. Suraprapapicha ** , C. W. Tu**, and W. M. Chen*

** Department of Physics, Chemistry and Biology IFM, Linköping university, Linköping, Sweden*

***Department of Electrical and Computer Engineering, University of California at San Diego, La Jolla, USA*

Keywords: spin injection, InAs, quantum dot

Quantum dots (QDs) are often considered as a suitable candidate for applications in a variety of novel devices with spin-enabling functionality, e.g. for spin filtering and spin quantum computation, owing to slow spin relaxation of carriers and high efficiency of optical transitions. Among key challenges for these applications is our ability to preserve spin orientation of carriers or excitons during their injection into the QDs. The latter can be accomplished either through injection of individual carriers or via exciton transfer. The aim of this work is to characterize spin injection efficiency of these processes in novel, laterally arranged self-assembled InAs/GaAs QDs structures, by using optical orientation measurements in combination with tuneable laser spectroscopy.

Three different sample structures were studied. They are self-assembled single QDs (SQD), lateral double QDs (DQD), and QD rings (QDR) with five to seven dots per ring – see the upper part of Fig.1. The structures were nominally undoped and were grown by molecular beam epitaxy on a (001) semi-insulating GaAs substrate. Photoluminescence (PL) and PL excitation (PLE) spectra were measured using a tunable Ti:Sapphire-laser as an excitation source.

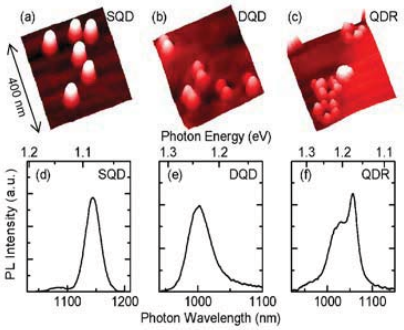

Fig.1 Atomic force microscopy topographs (the upper part) and PL spectra (the lower part) of the studied QDs structures. The PL spectra were measured at 6K under photo–excitation of the wetting layer.

PL spectra of the samples are shown in the lower part of Fig.1. Emissions from the excitonic ground state of the SQD, QQD and QDR can be seen as the dominant PL peak in these spectra. In order to analyse efficiency of spin injection to these structures, combined optical orientation and PLE measurements were performed. It was found that excitation of the InGaAs wetting layer by circularly polarized light leads to circular PL polarization (up to 10%) of the QDs, due to spin injection to the charged QDs within the QD ensemble. Furthermore, the polarization degree was strongly dependent on excitation photon energy. A higher efficiency of spin injection from the wetting layer was observed when the excitation photon energy was tuned to preferably generate free electrons and holes. In sharp contrast, spin injection was found to be significantly less efficient under the condition that the excitons in the wetting layer were selectively created. This shows that the spins of uncorrelated carriers are better conserved during the spin injection than the spins of correlated electrons and holes in an exciton. We attribute to this finding to an electron-hole exchange interaction of the excitons, which facilitates spin relaxation of the electrons and holes via a flip-flop process. The same tendency was observed for all structures. Our findings suggest that separate carrier injection, such as that employed in electrical spin injection devices, is more advantageous for spin conserving injection in novel quantum devices with spin functionality.

Optical manipulation of a single Mn spin in a CdTe quantum dot

M. Goryca*,***, T. Kazimierczuk*, M. Nawrocki*, A. Golnik*, J. A. Gaj*, P. Wojnar***, G. Karczewski*** and P. Kossacki*,***

* *Institute of Experimental Physics, University of Warsaw, Warsaw, Poland*
** *Grenoble High Magnetic Field Laboratory, CNRS, Grenoble, France*
*** *Institute of Physics, Polish Academy of Sciences, Warsaw,Poland*

Keywords: spin manipulation, spin memory, quantum dot, single magnetic atom

Quantum dots (QDs) containing single magnetic ions have recently attracted significant interest as systems close to the ultimate limit of information storage miniaturization. An efficient optical read-out of the Mn spin state [1] as well as the studies of dynamics of this state [2] were demonstrated. However, the writing and storing of the information in the Mn spin state has received less attention so far.

In this work we demonstrate optical writing of information in the spin state of a single Mn ion and we test the storage time in the range of a few tenths of a ms.

The sample used in our experiments was grown by molecular beam epitaxy [3]. The Mn content was adjusted so it was possible to select a significant number of dots, each containing single Mn ion. Among the identified QDs with single Mn ions we selected those exhibiting a sharp resonance in photoluminescence excitation (PLE) spectra. Similar resonances were found previously in CdTe/ZnTe QDs without Mn ions and interpreted as related to transfer of excitons between a smaller and a larger QD [4]. It was also shown that the spin of the exciton was conserved during this transfer. We use this process as a tool for optical writing of information in the Mn spin. Carriers created by defined circular polarization of light act on the Mn ion via exchange interaction and orient its spin. The Mn spin orientation appears as a nonuniform distribution of intensities between the 6 exciton lines, each of them being related to a specific Mn spin state (Fig. 1). The orientation is much more efficient in presence of a magnetic field of about 1 T, due to suppression of fast spin relaxation channels [5].

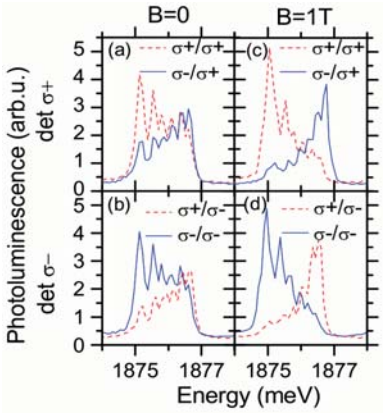

Fig.1 Exciton photoluminescence spectra excited at the resonance, using indicated excitation/detection polarizations and magnetic field.

Storage time of the information in the Mn spin was analyzed in a time-resolved experiment in which the intensity and polarization of excitation were modulated. The spin relaxation in the dark was found to be suppressed by application of a static magnetic field, with relaxation time reaching hundreds of microseconds at 1 T.

References

1. L. Besombes *et al.*, Phys. Rev. Lett. **93**, 207403 (2004).
2. L. Besombes *et al*., Phys. Rev. B **78**, 125324 (2008).
3. P. Wojnar *et al.*, Phys. Rev. B **75**, 155301 (2007).
4. T. Kazimierczuk *et al*., to appear in Phys. Rev. B.
5. M. Goryca *et al.*, Phys. Rev. Lett. **102**, 046408 (2009).

g-factors and exchange energy of few-electron single and double quantum dots defined in an InGaAs/InP heterostructure

M. Larsson, H. A. Nilsson and H. Q. Xu

Division of Solid State Physics, Lund University, Box 118, S-221 00 Lund, Sweden

Keywords: Quantum dot, InGaAs, Exchange energy, Zeeman energy

Quantum dots fabricated from semiconductor materials are promising candidates for solid-state two-state quantum systems (quantum bits or qubits) and have been widely studied in recent years. Quantum dots made from InGaAs and InAs based materials are specifically of interest, because large g-factors and spin-orbit interaction are present in these material systems [1-3]. Here we present the first study on both few-electron single and double quantum dots made from an InGaAs/InP heterostructure by low temperature transport and magnetotransport measurements.

The sample was fabricated on a high-mobility InGaAs/InP quantum well structure. First, an 800 nm long and 300 nm wide quantum wire defined by etching trenches was made. A layer made of cross linked PMMA was used as a gate dielectric. Finally five local Ti/Au finger gates with a pitch of 100 nm were defined on top of the quantum wire.

The formation of few-electron single quantum dots in these devices was studied in a dilution refrigerator at a temperature of 60 mK by transport measurements. In order to create quantum dots in the wire we apply negative voltage to the local gates to induce electrostatic barriers along the electron transport direction. A few-electron quantum dot was formed using three of the gates. Shell filling resulting in variation in Coulomb diamond size was clearly seen in the charge stability diagram reflecting that the dot is in the few-electron regime. However, the dot could not be emptied completely of electrons. To extract the electron g-factors for the states in the dot magnetotransport measurements were performed by looking at the evolution of the Coulomb blockade peaks as function of magnetic field applied parallel to the quantum well. The splitting for a simple spin filling sequence alternating between ↑ and ↓ is given by $g_n^* \mu_B B$ for odd-number electron occupation and by $\Delta\varepsilon_n(0) + g_n^* \mu_B B/2 - g_{n-1}^* \mu_B B/2$ for even-number electron occupation. Previous investigations for lateral InGaAs quantum dots in the many-electron regime have shown effective g-factors of around 1 to 2 [2]. Our measurements show a spin filling for the first visible states of ↑↑↓↓↑↓↑↓ indicating the formation of orbital-degenerate or nearly orbital-degenerate energy levels in the dot for the first 4 fillings due to the exchange interaction being larger than the single particle level spacing. Using a simple model for the charging energy E_c and the knowledge of the spin filling sequence we determine the charging energy E_c = 3.54 meV as well as the single particle level spacing $\Delta\varepsilon$ and exchange energy ε_x to be $|\varepsilon_x| - \Delta\varepsilon = 0.21$ meV. The latter lead to $|\varepsilon_x| \geq 0.21$ meV since $\Delta\varepsilon$ is always positive. The measured g-factors give $|g^*_n| = 3.28$, $|g^*_{n+1}| = 2.56$, $|g^*_{n+2}| = 2.69$ and $|g^*_{n+3}| = 3.96$, all of which are larger than those of the larger InGaAs dot presented in [2].

Double dots in the wires were formed using five gates. Standard conductance maps using two gates as energy level probes showed that a single big dot system could be tuned to a weakly coupled double dot system by simply changing the voltage on the middle barrier gate. This illustrates good tunability of the inter-dot coupling with the middle barrier gate.

References

1. M. Larsson, D. Wallin, H. Q. Xu, JAP 103, 086101 (2008).
2. J. Sun, M. Larsson, I. Maximov, H. Hardtdegen, H. Q. Xu, APL 94, 042114 (2009).
3. T. Koga, J. Nitta, T. Akazaki, H. Takayanagi, PRL 89, 046801-1 (2002).

Width and temperature dependences of lithographically induced magnetic anisotropy in (Ga,Mn)As wires

J. Ogawa*, M. Kohda*, **, F. Matsukura***, Y. Ohno***, H. Ohno***, and J. Nitta*

* *Department of Materials Science, Tohoku University, Sendai, Japan*

** *PRESTO, Japan Science and Technology Agency, Kawaguchi, Japan*

*** *Laboratory for Nanoelectronics and Spintronics, Research Institute of Electrical Communication, Tohoku University, Sendai, Japan*

Keywords: (Ga,Mn)As, narrow wire, magnetic anisotropy, anisotropic magneto-resistance

Ferromagnetic semiconductor (Ga,Mn)As shows in-plane cubic (⟨100⟩) and uniaxial ([110] or [-110]) magneto-crystal anisotropies. Recently, it was shown that an additional magnetic anisotropy can be introduced in submicron-sized (Ga,Mn)As structures [1-3]. In (Ga,Mn)As wires, this lithography-induced magnetic easy axis is along wire-direction, which is originated from shape anisotropy [4] and/or anisotropic strain relaxation [2]. In this work, we have investigated the temperature dependence of magnetic anisotropies in (Ga,Mn)As wires with different width through the anisotropic magneto-resistance (AMR) effect.

A 35 nm-thick $Ga_{0.957}Mn_{0.043}As$ layer was grown on a semi-insulating (001) GaAs substrate by molecular beam epitaxy. The Curie temperature T_C of as-grown sample was 80 K. The sample was processed into wire structures with different width of w = 20, 1.0, and 0.4 μm, while the wire length is fixed to 40 μm. Longitudinal direction of the wire is set along [100] direction. AMR was measured in the temperature range from 5 to 75 K by rotating the sample in an in-plane magnetic field H. ϕ_H is the angle between magnetic field and [100] direction. Figures 1 (a) and (b) show ϕ_H dependence of AMR in 1.0 μm-wide wire at T = 15 and 60 K, respectively. AMR signals show the distortion from the sine-shaped curve at both temperatures indicating the existence of sizable magnetic anisotropies. In addition to ⟨100⟩ cubic and [-110] uniaxial anisotropies, anisotropy along [100] direction is observed in the wires with the width of 1.0 μm and 0.4 μm. We used a coherent magnetization model to determine the magnetic anisotropy constants. The solid lines in Fig. 1 show the results of the fit. All the anisotropy constants decrease as temperature increases, and the dominant contribution becomes lithographically induced anisotropy at T = 60 K, which results in the asymmetric AMR behaviour between [100] and [0-10] directions. We found also that the magnetic field dependence of magneto-resistance can be reproduced by using obtained anisotropy constants, where magnetization direction is along wire-direction at zero magnetic field in narrow wires.

References

[1] S. Hümpfner *et al*., Appl. Phys. Lett. **90**, 102102 (2007).
[2] J. Wenisch *et al*., Phys. Rev. Lett. **99**, 077201 (2007).
[3] K. Pappart *et al*., Nat. Phys. **3**, 573 (2007).
[4] K. Hamaya *et al*., J. Appl. Phys. **99**, 123901 (2006).

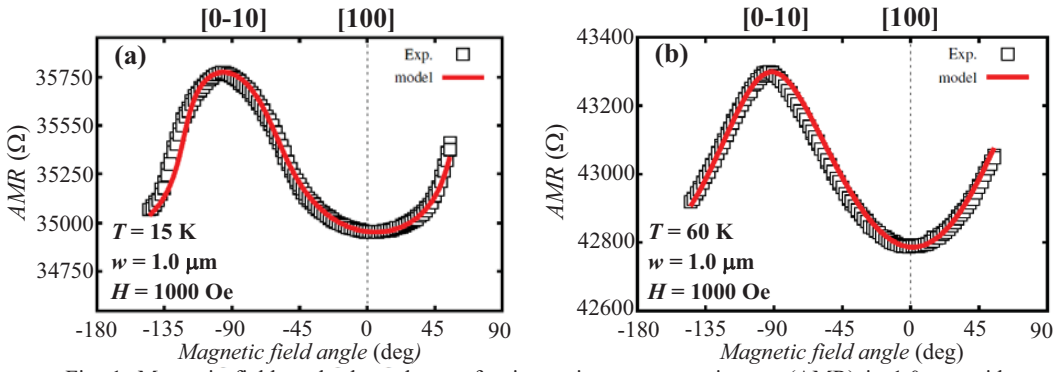

Fig. 1. Magnetic field angle dependence of anisotropic magneto-resistance (AMR) in 1.0 μm-wide wire at (a) T = 15 K and (b) T = 60 K.

Layer thickness dependence of magnetic anisotropy in (Ga,Mn)As

T. Horii, Y. Inoue, J. Okabayashi and J. Yoshino

Department of Physics, Tokyo Institute of Technology, Meguro-ku, Tokyo, Japan

Keywords: (Ga,Mn)As, magnetic anisotropy

Magnetic/non-magnetic multilayer structures (MMSs) offer a variety of significant features, such as large magneto-resistance and magnetization dynamics based on the interaction between spin-polarized current and magnetization. (Ga,Mn)As-based MMSs are essentially important for related researches, since they can be prepared in single crystalline form. Although the properties of (Ga,Mn)As have been extensively studied, there still remained a lot of issues to be clarified, such as the origin of uniaxial magnetic anisotropy. We found that characteristics of magnetoresistance hysteresis observed in (Ga,Mn)As-based double barrier magnetic tunnel junctions strongly depend on the layer thickness [1]. In this paper, we report on systematic study on the layer-thickness dependence of magnetic anisotropy in (Ga,Mn)As layers based on magneto-resistance and planer Hall effect measurements.

The samples studied are grown by molecular beam epitaxy on semi-insulating GaAs (001) substrates. (Ga,Mn)As layers are grown at a substrate temperature of about 250 °C. Manganese concentration in (Ga,Mn)As layers is about 5 %. Thicknesses of the (Ga,Mn)As layers are 30 nm (sample A), 5 nm (sample B), and 3 nm (sample C). To maintain the resistances of all samples at similar range, samples B and C includes 6 and 10 (Ga,Mn)As layers, respectively, separated by 4 nm-thick-GaAs spacer layers. For magneto-transport measurements, Hall bridges were prepared along [1-10] direction.

Apparent hole concentrations estimated by Hall measurements at room temperature are to be 1×10^{20} in sample A, 3×10^{20} in sample B, and, 1×10^{20} cm^{-3} in sample C. The figure 1 shows the magnetoresistance and planer Hall resistances measured applying magnetic filed along [110], [100], and [1-10] directions. Two distinguish features are found in these characteristics: Firstly, in samples B and C, $\rho_{//}$ is smaller than $\rho_{\perp}$, while in sample A, $\rho_{//} > \rho_{\perp}$. The latter is consistent with previous reports on bulk (Ga,Mn)As [2]. Secondly, the areas enclosed by hysteresis loop in planer Hall characteristics are decreased with the decrease of the layer thickness, suggesting the decrease of both cubic and uniaxial components of magnetic anisotropy energy.

In the presentation we will discuss the origin of these behaviours in terms of Curie temperature, carrier concentration, and size quantization.

References

[1] M. Watanabe et al., Physica E40, 335 (2007).
[2] H.X. Tang et al., Phys. Rev. Lett., 90, 107201 (2003).

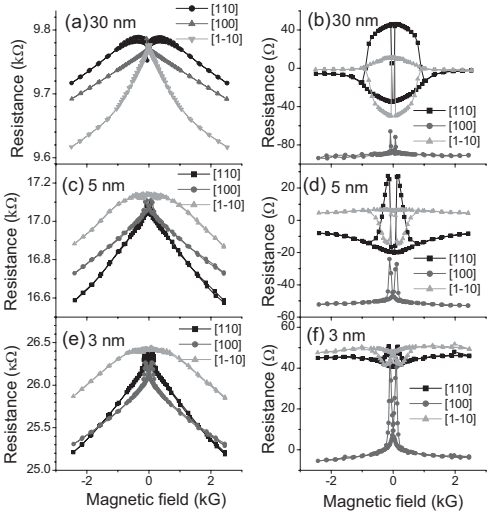

Fig.1 Magnetoresistance (left) and planer Hall resistance (right) in sample A: (a), (b), in sample B: (c), (d), and sample C: (e), (f), measured applying magnetic field along [110](square), [100](circle) and [1-10](triangle) directions.

Magnetic control of Rashba splittings in symmetric InAs quantum wells

T. Matsuura*, N. Monta** and T. Koga*,**
*Creative Research Initiative "Sousei", Hokkaido University, Sapporo, 001-0021, Japan
**Graduate School of Information Science and Technology, Hokkaido University, Sapporo, 060-0814, Japan

Keywords: Rashba spin-orbit interaction, spintronics, quantum well, narrow-gap semiconductor

There have been much interest on spin-orbit interactions in narrow gap semiconductors for manipulating quantum spin state without magnetic field. Especially, a spin-orbit interaction, called Rashba effect, has been expected to provide a useful way of spin control by electric field. Since, for the Rashba effect to be present, the presence of interfacial electric field is essential, most researches have focused on asymmetric quantum well potentials, i.e., the systems *without* structural inversion symmetry. Recently, a new type of the Rashba effect was proposed for *symmetric* quantum well systems, i.e., systems *with* structural inversion symmetry, where the two lowest subbands in the quantum well are coupled each other by the modified Rashba Hamiltonian, $H_R = \alpha(z)(k_y\hat{\sigma}_x - k_x\hat{\sigma}_y)$, $\alpha(z)$ being the position-dependent Rashba spin-orbit coupling constant [1].

In this paper, we investigate spin and subband energy splittings of symmetric quantum wells of AlSb/InAs/AlSb heterostructures [Fig. 1(a)] under in-plane magnetic field $\mathbf{B} = (0, B, 0)$. The Hamiltonian we consider is

$$H = \frac{1}{2m^*}(\hat{\mathbf{p}} + e\mathbf{A})^2 + V(z) + \frac{1}{2}g\mu_B B\hat{\sigma}_y + H_R,$$

where the third term is the Zeeman coupling term.Various thicknesses between 20 and 100 nm are chosen for the quantum well and, for each, the symmetric confinement potential $V(z)$ includes a Hartree potential due to homogeneous charge distribution of $N_s = 3 \times 10^{16}$ m^{-2}.

Shown in Figure 1 (b) is the spin splittings of the subbands as a function of the magnetic field at $k_x = 3 \times 10^8$ m^{-1} ($\sim k_{\rm F}$) and $k_y = 0$. We find that the spin degeneracy of each subband at $B = 0$ is lifted by applying the magnetic field and a level-anticrossing phenomenon takes place between the lowest two subbands with a specific (up) spin. This clearly demonstrates the magnetic control of the Rashba splittings in symmetric quantum wells. We also find that the physical origin of the subband gap between $E_{1\uparrow,\downarrow}$ and $E_{2\uparrow,\downarrow}$ at $B = 0$ is changed continuously from the quantum confinement origin for the narrow wells ($d_{\rm QW} \lesssim 40$ nm), to the Rashba interaction origin for relatively thick quantum wells ($d_{\rm QW} \gtrsim 40$ nm). This smooth transition would provide an intriguing way of studying the well-known mystery of the Shubnikov-de Haas beating problem [2].

This work is supported by KAKENHI, Grant-in-Aid for Young Scientists (A), No. 19684009.

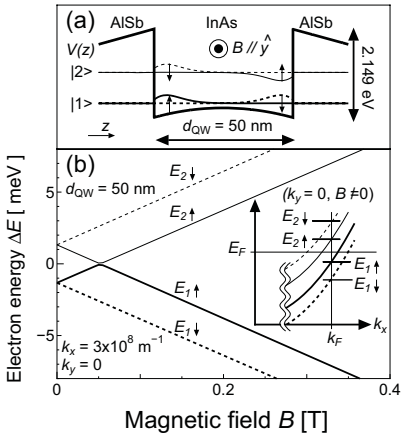

Figure 1: (a) Symmetric quantum well. The values of the effective mass $m*$, g-factor g and conduction band offset are chosen to be $0.03m_e$, -14 and 2.149 eV, respectively. (b) Magnetic field dependencies of subband energies at the Fermi wave number. (Inset) Schematic diagram to show the meanings of $E_{1\uparrow}$, $E_{1\downarrow}$, $E_{2\uparrow}$ and $E_{2\downarrow}$. Spin axes for $|\uparrow\rangle$ and $|\downarrow\rangle$ are chosen to be $\pm\hat{y}$, respectively.

References

[1] E. Bernardes, et al, Phys. Rev. Lett. **99**, 076603 (2007). T. Koga, et al, Phys. Rev. Lett. **88**, 126601 (2002).

[2] S. Brosig, et al, Phys. Rev. B. **60**, R13989 (1999). A. C. H. Rowe, et al, Phys. Rev. B. **63**, 201307(R) (2001).

Current-Induced Spin Polarization in Gallium Nitride

W. Koehl*, C. Poblenz*, M. H. Wong*, U. Mishra*, J. Speck*, and D. D. Awschalom*

* *Center for Spintronics and Quantum Computation, University of California, Santa Barbara CA 93106 USA*

Keywords: Gallium nitride, spintronics, spin-orbit coupling, spin coherence

Current-Induced Spin Polarization (CISP) is a phenomenon in which carriers become spin polarized as they are transported through a semiconductor. The net spin polarization generated is spatially uniform throughout the material, and the physical mechanism underlying this phenomenon, which is seemingly distinct from the spin Hall effect, is not well understood. Previously, CISP has been observed in both GaAs [1] and ZnSe [2], two materials with widely separated bandgaps but with similar spin-orbit splitting parameters. Intriguingly, CISP was observed to exist even at room temperature in ZnSe, a wide-bandgap material.

GaN is a III-V semiconductor with a bandgap even wider than that of ZnSe and with an exceedingly small spin-orbit splitting. We directly observe CISP in GaN and characterize the phenomena in order to further explore the degree to which CISP depends on the band structure and spin lifetimes of a material. A series of n-type GaN epilayers are grown in the wurtzite phase both by molecular beam epitaxy (MBE) and metalorganic chemical vapor deposition (MOCVD) with a variety of doping densities chosen to modulate the transverse spin lifetime, T_2^*, across its full available range. Using the Kerr effect, CISP is then measured in both types of epilayers as a function of electrical excitation energy over a range of temperatures [3].

References

1. Y. Kato, et al., Phys. Rev. Lett. **93**, 176601 (2004).
2. N. P. Stern, et al., Phys. Rev. Lett. **97**, 126603 (2006).
3. W. Koehl, et al., in preparation (2009).

Magnetic anisotropy in a ferromagnetic (Ga,Mn)Sb thin film

Y. Nishitani, M. Endo, F. Matsukura, and H. Ohno

Laboratory for Nanoelectronics and Spintronics, Research Institute of Electrical Communication, Tohoku University, Sendai, Japan

Keywords: spintronics, magnetic semiconductor, (Ga,Mn)Sb, magnetic anisotropy

III-V based magnetic semiconductors show hole-induced ferromagnetism[1]. It was shown experimentally that controlling hole concentration by electric-fields E brings about the change of their magnetic properties[2]. Recently, we succeeded to control the magnetization direction by E thorough the change of magnetic anisotropy[3], which is promising for the application to new scheme of magnetization switching. However, there have been only a few reports on magnetic anisotropy in other III-V magnetic semiconductors than (Ga,Mn)As. In this work we have investigated the magnetic anisotropy of a thin (Ga,Mn)Sb layer .

A 10-nm $Ga_{0.98}Mn_{0.02}Sb$ thin film was grown by low temperature molecular beam epitaxy on 4 nm GaSb / 100 nm $Al_{0.76}Ga_{0.24}Sb$ / 200 nm AlSb (from the surface side) onto semi-insulating GaAs (001) substrate. The sample was processed into a Hall-bar geometry to determine its magnetic anisotropy through the anomalous Hall effect.

Figure 1 shows magnetic field $\mu_0 H$ dependence of Hall resistance R_{Hall}. The applied $\mu_0 H$ was parallel to [001] direction. At low-temperature T (< 20 K), clear hysteresis curves with negative anomalous Hall coefficient were observed[4]. The Curie temperature T_{C} was determined to be ~27 K from the Arrott plots. By

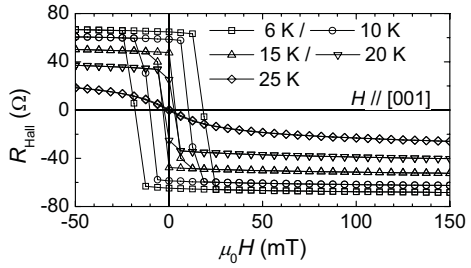

Fig.1 The magnetic field $\mu_0 H$ (// [001]) dependence of Hall resistance R_{Hall}.

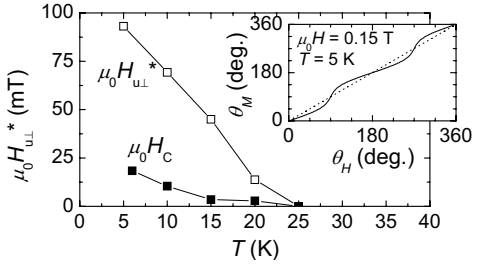

Fig.2 Temperature T dependence of perpendicular anisotropy field $\mu_0 H_{\mathrm{u}\perp}$*. The inset shows the relation between magnetic field angle θ_H and magnetization angle θ_M at T = 5K.

rotating the magnetic field (0.15 T) around the sample, we measured the angle dependence of R_{Hall} to determine its perpendicular magnetic anisotropy field $\mu_0 H_{\mathrm{u}\perp}$*. θ_{H} is the angle of $\mu_0 H$ with respect to [001] direction in the plane perpendicular to the current. By assuming the coherent magnetization model and using $R_{\mathrm{Hall}} \propto \cos\theta_{\mathrm{M}}$ (θ_{M} is the magnetization angle from [001]), we fit the data to obtain the temperature dependence of $\mu_0 H_{\mathrm{u}\perp}$*. Figure 2 shows that the obtained magnetic easy axis is perpendicular to plane in whole temperature range and its magnitude is smaller than coercivity $\mu_0 H_{\mathrm{C}}$ as same as (Ga,Mn)As films[5].

This work was supported in part by Grant-in-Aids from MEXT/JSPS, the GCOE Program at Tohoku University, and JSPS Research Fellowships for Science for Young Scientists.

References

1. T. Dietl *et al.,* Science **287**, 1019 (2000).
2. H. Ohno *et al.*, Science **281**, 951 (1998).
3. D. Chiba *et al*., Nature **455**, 515 (2008).
4. W. L. Lim *et al*., Physica E **20**, 346 (2004).
5. D. Chiba *et al*., Appl. Phys. Lett. **89**, 162505 (2006).

Spin relaxation in high In content InGaAs/GaAs quantum wells

H. Nosho*, T. Asami*, T. Okamoto*, T. Umi*, S. L. Lu **, Z. C. Niu*** and A. Tackeuchi*

* *Department of Applied Physics, Waseda University, Tokyo, 169-8555, Japan*

** *Suzhou Institute of Nano-tech and Nano-bionics, Chinese Academy of Sciences, Suzhou, 215125, China*

*** *State Key Laboratory for Superlattice and Microstructure, Institute of Semiconductors, Chinese Academy of Sciences, Beijing, 100083, China*

Keywords: InGaAs/GaAs; Quantum well; High In content; Spin relaxation

High indium content InGaAs/GaAs quantum wells were successfully grown by optimizing the molecular beam epitaxy growth conditions.[1] The critical thickness of the strained $In_{0.475}Ga_{0.525}As$/GaAs quantum wells (QWs) is raised to 7nm. In this paper, we report the spin relaxation time of the high indium content $In_{0.425}Ga_{0.575}As$/GaAs multi-quantum wells.

The sample has three periods of 7 nm thick InGaAs well with an indium molar fraction of 42.5% and 20 nm thick GaAs barrier grown by molecular beam epitaxy on GaAs substrate. The time-resolved spin-dependent photoluminescence (PL) measurement was done using a streak camera. The spin polarized carriers were photoexcited by the circularly polarized femtosecond Ti-sapphire laser pulse. The excitation laser wavelength was tuned to near the band gap energy of GaAs. The collected luminescence passes through an analyzer consisting of an achromatic quarter-wave plate and a linear polarizer arranged so that right- or left-circularly polarized emission can be selected.

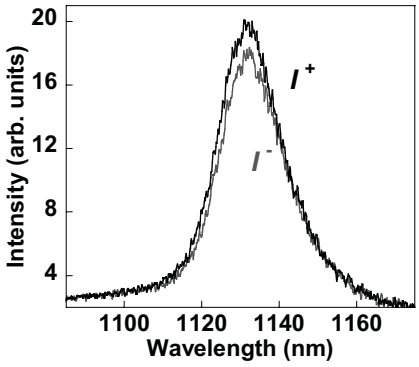

Fig.1 PL spectra of InGaAs/GaAs QWs at 10 K for the excitation power of 20 mW. I^+ and I^- indicate the PL intensity of the same and opposite circular polarizations from the pump laser, respectively.

Figure 1 shows the spin-dependent PL spectra of InGaAs/GaAs QWs at 10 K for the excitation power of 20 mW. The wavelength of PL peak is 1132 nm. I^+ and I^- indicate the PL intensity of the same and opposite circular polarizations from the excitation laser, respectively. The difference between the two curves corresponds to the spin polarization. Figure 2 shows the time evolution of spin-dependent PL at 10 K for the excitation power of 20 mW. The spin relaxation time is obtained to be 280 ps using a single exponential fitting. This is one order of magnitude slower than the 43 ps spin relaxation of InGaAs/InP MQWs at 13 K.[2] This result suggests that the difference of the barrier material affects on the spin relaxation mechanism.

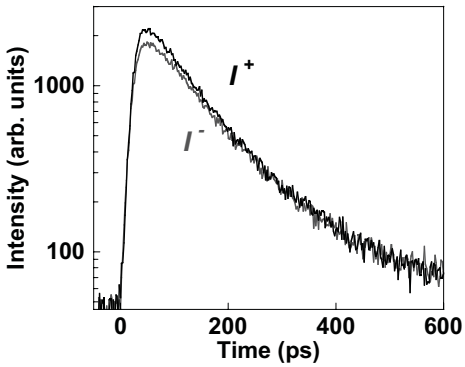

Fig.2 Time evolution of spin-dependent PL for the excitation power of 20 mW

References

1. H. Q. Ni, Z. C. Niu, X. H. Xu, Y. Q. Yu, W. Zhang, X. Wei, L. F. Bian, Z. H. He, Q. Han, and R. H. Wu, Appl. Phys. Lett. 84, 5100 (2004).

2. S. Akasaka, S. Miyata, T. Kuroda, and A. Tackeuchi et al., Appl. Phys. Lett. 85, 2083 (2004).

Coherent spin precession of electrons and excitons in charge tunable InP quantum dots

Yasuaki Masumoto, Keisuke Kawana and Shinichi Tomimoto
Institute of Physics, University of Tsukuba, Tsukuba 305-8571, Japan

Keywords: Spin precession, exciton, InP, quantum dot

Spins in semiconductor quantum dots (QDs) has attracted considerable attention recently, since it is expected to be used for quantum information processing. Highly sensitive time-resolved Kerr rotation spectroscopy enables us to observe coherent spin precession of electrons in semiconductors. In this contribution we report coherent spin precession of electrons and *excitons* in charge tunable InP QDs.

The sample we studied is charge tunable InP QDs embedded in InGaP grown on an n^+-GaAs substrate. With the change of the electric bias across the sample structure, InP QDs become either neutral or doped by electrons [1,2]. For the time-resolved Kerr rotation measurement, 2ps pump and probe pulses from a mode-locked Ti:sapphire laser were used. Resonant excitation of InP QDs at 1.734eV was used. A quarter wave plate, a photo-elastic modulator operating at 42kHz, a Wollaston prism, balanced detectors for 2 circularly polarized signals and 2 tandem lock-in amplifiers were used for the sensitive detection of the Kerr signal. The sample was set in a superconducting magneto-optic cryostat in the Voigt geometry. The magnetic field B was applied up to 10T.

When InP QDs are doped by 1 electron under the electric bias of U = -0.15V, the time-resolved Kerr rotation signal oscillates at the period T_e under the non-zero magnetic field. The oscillation continues for more than 2 ns which is longer than the lifetime of trion 260ps [3]. The long-term oscillation means that the oscillation comes from the spin precession of doped electrons. The corresponding energy separation h/T_e increases in proportion to B. The slope gives $g_{e\perp} = h/\mu_B B T_e = 1.53$ to the electron g-factor for the magnetic field perpendicular to the crystal growth direction.

When InP QDs are neutral under the electric bias of U = -0.85V, the oscillation period T_{ex} is slightly different from the period T_e. The oscillation fades away at 100ps. The corresponding energy separation h/T_{ex} increases with the increase of B, but does not increase in proportion to B. Alternatively, the corresponding energy separation h/T_{ex} is well expressed by the form $[\delta^2 + (g_{ex\perp}\mu_B B)^2]^{1/2}$. This fact clearly indicates that the oscillation comes from the spin precession of excitons in InP QDs. Here $g_{ex\perp}$ is the exciton g-factor for the magnetic field perpendicular to the crystal growth direction and δ is the electron-hole exchange energy. In neutral QDs, electron-hole exchange interaction holds the correlation between electron and hole spins and therefore spin precession of excitons is observed. The fitting gives $g_{ex\perp} = g_{e\perp} - g_{h\perp} = 1.52$ and $\delta = 0.18$meV. Because $g_{e\perp} = 1.53$ is given by the spin precession of electrons, very small hole g-factor $g_{h\perp} = 0.01$ is obtained.

References

1. E. Kozin, V. G. Davydov, I. V. Ignatiev, A. V. Kavokin, K. V. Kavokin, G. Malpuech, H. -W. Ren, M. Sugisaki, S. Sugou, and Y. Masumoto, Phys. Rev. B**65**, 241312(R) (2002).
2. I. A. Yugova, I. Ya. Gerlovin, V. G. Davydov, I. V. Ignatiev, I. E. Kozin, H. W. Ren, M. Sugisaki, S. Sugou, and Y. Masumoto, Phys. Rev. B**66**, 235312 (2002).
3. M. Ikezawa, B. Pal, Y. Masumoto, I. V. Ignatiev, S.Verbin, and I. Ya. Gerlovin: Phys. Rev. B**72**, 153302-1 (2005).

SQUID magnetometry of the effect of electric-field on magnetization of (Ga,Mn)As

F. Matsukura*,**, M. Sawicki*,***, D. Chiba**,*, A. Korbecka****, Y. Nishitani*, J. A. Majewski****, T. Dietl***,****,**, and H. Ohno*,**

* *Laboratory for Nanoelectronics and Spintronics, Research Institute of Electrical Communication, Tohoku University, Sendai, Japan*

** *Semiconductor Spintronics Project, Exploratory Research for Advanced Technology, Japan Science and Technology Agency, Tokyo, Japan*

*** *Institute of Physics, Polish Academy of Sciences, Warszawa, Poland*

**** *Institute of Theoretical Physics, University of Warsaw, Warszawa, Poland*

Keywords: magnetic semiconductor, (Ga,Mn)As, electric-field, magnetization measurement

Ferromagnetism of (Ga,Mn)As is brought about by the exchange interaction among Mn spins and holes. Accordingly, magnetic properties, such as the Curie temperature T_C, coercive force, and magnetic anisotropy are a function of the hole concentration p, and thus can be controlled by the application of an electric field E_G to the gate of metal-insulator-semiconductor (MIS) structures[1-3]. So far, magnetic properties of (Ga,Mn)As MIS structures have been examined through magnetotransport properties. In this work, we report on the effect of gating on the magnetism in (Ga,Mn)As probed directly by magnetization measurements which, in addition to T_C, allow us to determine a dependence of the spontaneous magnetic moment on E_G.

A 3.5-nm $Ga_{0.93}Mn_{0.07}As$ thin film was grown by molecular beam epitaxy on a semi-insulating GaAs (001) substrate. Then a gate insulator, 38-nm HfO_2/Al_2O_3 (dielectric constant ~ 20), was deposited by atomic layer deposition, and finally Au/Cr gate electrode was evaporated to complete the MIS structure. The gated area of the samples is about 10 mm^2. T_C at E_G = 0 is determined to be 34 K for the processed sample. We have measured the magnitude of magnetization by superconductor quantum interference device (SQUID) magnetometer under the gate voltage V_G up to ±12 V.

We have found that not only T_C but also the magnitude of spontaneous magnetic moment m vary with V_G. This implies that the interfacial electric field affects the width of the hole channel as well as points to the existence of a surface depletion layer (because no increase of saturation moment is expected if all the Mn moments participate in the ferromagnetic order).

We adapt the *p-d* Zener model[4] for the case when the phase coherence length is longer than the magnetic layer width and determine the hole density profiles $p(z)$ along the growth direction under various V_G by employing a Poisson solver. This approach provides us with $T_C(V_g)$ and to $m(V_g)$, the latter proportional to the thickness of the channel populated by the holes. The model can reproduce our experimental findings by adjusting the concentration of interface states at (Ga,Mn)As/insulator border and the net concentration of acceptors in (Ga,Mn)As.

The work was supported in part by Grant-in-Aids from MEXT/JSPS, the GCOE Program at Tohoku University, the Research and Development for Next-Generation Information Technology from MEXT, JSPS Research Fellowships for Science for Young Scientists; NANOSPIN and FunDMS ERC Advanced Grant from EU, and Polish Ministry of Science and High Education.

References

1. H. Ohno *et al*., Nature **408**, 944 (2000).
2. D. Chiba *et al*., Appl. Phys. Lett. **89**, 162505 (2006).
3. D. Chiba *et al*., Nature **455**, 515 (2008).
4. T. Dietl *et al*., Science **287**, 1019 (2000).

Epitaxy and characterization of Co doped ZnO on ZnO substrate

Y. Guo*,**, F. Matsukura**,*, K. Ohtani**, and H. Ohno**,*

* *Semiconductor Spintronics Project, Exploratory Research for Advanced Technology, Japan Science and Technology Agency, Tokyo, Japan*

** *Laboratory for Nanoelectronics and Spintronics, Research Institute of Electrical Communication, Tohoku University, Sendai, Japan*

Keywords: magnetic semiconductor, Co doped ZnO, electric-field, magnetization measurement

After the theoretical prediction of a candidate for ferromagnetic semiconductors with the Curie temperature T_C above room temperature (RT)[1,2], ZnO based magnetic semiconductors have been investigated extensively. Ferromagnetism in Co doped ZnO at RT has been reported by some research groups[3], while paramagnetic or spinglass phase by others[4]. Although some reports suggested that the ferromagnetism is enhanced by the presence of donors[5], the origin of the observed ferromagnetism and its correlation with electron concentration n are not fully established. In this work, in order to investigate the influence of n on magnetism, we grew ZnO:Co by molecular beam epitaxy on O-polar ZnO (000-1) substrates[6] and changed n by doping with Ga and by the application of electric filed in metal-insulator-semiconductor (MIS) structures.

ZnO:Co films with thickness of 10-40 nm were grown at 450°C. The Co composition was 8, 10, 12, 16, and 20%. The 10% and 20% samples were doped with Ga (n-type dopant) with its composition 0, 0.004, and 0.01%. The wurtzite structure of the samples was confirmed by reflection high energy electron diffraction (RHEED) pattern during growth. The surface morphology observed by atomic force microscope showed a flat surface with atomic monolayer steps. Some of the samples were processed into MIS structure with 50-nm thick Al_2O_3 insulator deposited by atomic layer deposition and Au gate electrode.

The magnetic properties were investigated by superconducting quantum interference device (SQUID) magnetometer. The samples without Ga showed paramagnetism down to 10 K, except for the samples with x = 20% which showed ferromagnetism at RT. We found that the Ga doping increases the magnitude of the magnetization for both paramagnetic (x = 10%) and ferromagnetic (x = 20%) samples.

The magnetization of MIS structures under gate voltage V_G up to ±10 V was measured to investigate the influence of the change of n on magnetic properties[7]. From the transport measurements, n can be modulated by a few-tens of percents by V_G. We found that no effect of V_G on magnetization of neither paramagnetic nor ferromagnetic samples. The results suggest that the donor doping affects on the distribution of Co ions in the samples during growth[8], while there is no relationship between the magnetism and the electron concentration once the material is synthesized.

The work was supported in part by Grant-in-Aids from MEXT/JSPS and the GCOE Program at Tohoku University.

References

1. T. Dietl *et al*., Science **287**, 1019 (2000).
2. K. Sato and H. Katayama-Yoshida, Jpn. J. Appl. Phys. **40**, L334 (2001).
3. K. Ueda *et al*., Appl. Phys. Lett. **79**, 988 (2001); G. L. Liu *et al*., *ibid.* **81**, 4040 (2007); H. J. Lee *et al*., *ibid.* **81**, 4020 (2002).
4. J. –H. Kim *et al*., J. Appl. Phys. **92**, 6066 (2002); M. H. Kane *et al*., *ibid.* **97**, 023906 (2005).
5. H. –H. Huang *et al*., J. Appl. Phys. **101**, 09H116 (2007); K. R. Kittilstved *et al*., Phys. Rev. Lett. **97**, 037203 (2006).
6. H. Xu *et al*., Appl. Phys. Lett. **89**, 071918 (2006).
7. H. Ohno *et al*., Nature **408**, 944 (2000).
8. S. Kuroda *et al*., Nature Mater. **6**, 440 (2007); T. Dietl *et al*., Phys Rev. B **76**, 155312 (2007).

Optical detection of zero-field spin precession of high mobility two dimensional electron gas in a gated GaAs/AlGaAs quantum well

T. Takahashi, S. Matsuzaka, Y. Ohno and H. Ohno

Laboratory for Nanoelectronics and Spintronics, Research Institute of Electrical Communication, Tohoku University, Sendai, Japan

Keywords: spintronics, spin-orbit interaction, time-resolved Kerr rotation, GaAs

Spin-orbit interaction, which originates from the space inversion asymmetry of potential in the bulk crystal structure and heterostructures, plays an important role in semiconductor spintronics. The spin-orbit interaction results in the spin splitting in the conduction band, which enables generation of spin current in zero magnetic field: For example, spin injection in a quantum point contact has been proposed [1]. In this context, we focus our attention on the generation and optical detection of spin current in quantum nanodevices based on a high mobility two dimension electron gas (2DEG). In this work, we investigate the internal effective magnetic field induced by spin-orbit interaction in a gated modulation-doped GaAs/AlGaAs quantum well (QW) structure. We measured the zero-field precession of the optically-injected electron spins by a time-resolved Kerr rotation (TRKR) technique [2] as a function of the gate voltage V_g.

The sample is a modulation-doped, 20 nm-thick GaAs/$Al_{0.3}Ga_{0.7}As$ single QW structure grown on a semi-insulating (001) GaAs substrate by molecular beam epitaxy. The electron concentration and mobility measured at 3.2K are 4.6×10^{11} cm^{-2} and 8.8×10^{5} cm^2/Vs, respectively. A semi-transparent Schottky gate was formed by deposition of a thin gold film (10 nm) on the epilayer. The source of the light is generated by a mode-locked Ti:sapphire laser: the pulse width was ~ 3ps and the repetition frequency was 76MHz. The sample was set in the cryostat, and cooled by direct flow of the He gas. In the TRKR measurement, the wavelength of circularly-polarized pump and linearly-polarized probe beam was set at the vicinity of the edge of the higher-energy side of the photoluminescence spectra.

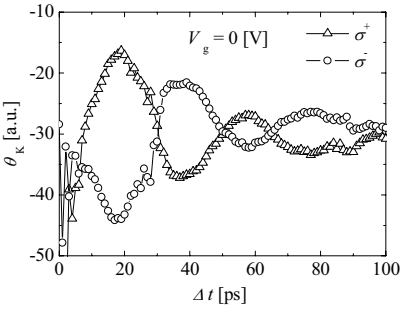

Fig.1 Experimental results of TRKR measurement in the zero magnetic field and zero gate voltage .

Figure 1 shows the TRKR result measured by 3.3K in zero magnetic field and zero gate voltage (V_g). We observed an exponentially-decaying oscillation in the TRKR signal, which reflects the precession of photoexcited electron spins by internal in-plane effective magnetic field. When negative V_g was applied and the 2DEG density was decreased, the dephasing time of the TRKR oscillation becomes short and the frequency was decreased almost linearly with V_g. As V_g < -0.4 V, no TRKR oscillation was resolved. The V_g dependence of the internal effective magnetic field will be discussed.

References

[1] M. Eto *et al*., J. Phys. Soc. Jpn. **74**, 1934 (2005).
[2] M. A. Brand *et al*., Phys. Rev. Lett. **89**, 236601 (2002).

Spin transistor and spin Hall effects in CdF_2 nanostructures

N. T. Bagraev*, O.N. Guimbitskaya **, L. E. Klyachkin*, A. M. Malyarenko*,
A. I. Ryskin***, A. S. Shcheulin *** and I. A. Shelykh**

* *Ioffe Physical-Technical Institute, St. Petersburg, 194021, Russia*

** *Polytechnical University, St. Petersburg, 195251, Russia*

*** *St.Petersburg University of Information Technologies, Mechanics and Optics, St. Petersburg, Russia*

Keywords: spin polarization, quantum well, superconductor barriers, spin transistor effect

Planar CdB_xF_{2-x} - *p*–CdF_2 - CdB_xF_{2-x} sandwich structures prepared on the *n*-CdF_2 substrate are studied to register the spin transistor and quantum spin Hall effects at room temperatures. The current-voltage characteristics of the ultra-shallow *p*+-*n* junctions verify the CdF_2 gap, 7.8 eV, and the subbands of the 2D holes in the *p*–CdF_2 quantum well. The results obtained are evidence of the important role of the subbands of the 2D holes in the proximity effect that is due to the Andreev reflection in the CdB_xF_{2-x} - *p*–CdF_2 - CdB_xF_{2-x} sandwich structures which represent the ultra-narrow quantum well confined by the superconductor barriers. The longitudinal emf exhibits the resonance behavior in week magnetic fields perpendicular to the *p*–CdF_2 quantum well plane, which verifies the high spin polarization of the 2D holes. The studies of the 2D hole conductance by varying the value and orientation of the magnetic field perpendicular to the *p*–CdF_2 quantum well plane allow the findings of the anti-crossing points for the background singlet and excited triplet sublevels that belong to the dipole boron centers responsible for the spin hole polarization in the one-dimensional channels along the edges of the *p*–CdF_2 quantum well. The high spin hole polarization in the edged channels identifies the mechanism of the current-voltage characteristics of the spin transistor and quantum spin Hall effects induced by varying the top gate voltage which is also able to control the Bychkov-Rashba spin-orbit interaction value.

Finally, the Shubnikov – de Haas oscillations and the quantum staircase of Hall resistance are found in the *p*–type CdF_2 confined by the δ- CdB_xF_{2-x} barriers prepared on the *n*–CdF_2 substrate. Owing to the ultra-low effective mass of 2D holes, the quantum Hall observation became to be possible at room temperatures.

0.7 feature in p-type quantum point contacts tuned by combined in-plane and top gates

M. Csontos*, Y. Komijani*, T. Ihn*, K. Ensslin*, D. Reuter** and A. D. Wieck**
*Solid State Physics Laboratory, ETH Zurich, Switzerland
** Angewandte Festkörperphysik, Ruhr-Universität Bochum, Germany

Keywords: p-type GaAs, AFM lithography, atomic layer deposition, quantum point contacts

Low-dimensional hole-doped systems have more pronounced spin-orbit as well as carrier-carrier Coulomb interactions compared to n-type systems. The experimental investigation of such systems has been rather challenging mostly due to the technological difficulties in fabricating stable p-type nanostructures. Here we present a nano-fabrication technique which enables the realization of highly tunable devices. The high tunability of these structures is provided by the combined electrostatic effect of intrinsic in-plane gates created by local anodic oxidation lithography and evaporated metallic top gates. We tested devices fabricated with this new technique by electrical conductance spectroscopy. Measurements on various p-type quantum point contacts (QPCs) revealed a rich variety of 0.7-like features.

Nanodevices defined on p-type GaAs with conventional split-gate techniques show significant gate instabilities. This is presumably due to the fact that metallic Schottky barriers on p-type GaAs are leaky and exhibit a highly hysteretic behavior, making them unsuitable for high-precision tuning of the devices. Instead, we fabricate stable p-type nanostructures by local anodic oxidation lithography. Oxide lines are created on the wafer surface by using the charged tip of an atomic force microscope (AFM) in a humid environment. Oxide lines as high as 15 nm locally deplete the two-dimensional hole gas (2DHG) situated 45 nm below the surface, thereby separating the 2DHG into laterally disconnected regions connected individually to metallic leads. Voltages in the range of [-200 mV, +200 mV] can be applied between separated regions without any significant leakage current across the oxide line. This allows to tune the electrical properties of the holes confined in different nanoconstrictions with in-plane gates.

The tunability of the AFM-defined nanostructures can be greatly improved by local top gates separated from the wafer surface by a thin insulating layer which prevents leakage. For this purpose we grow a 10-20 nm thick Hafnium-oxide layer by the atomic layer deposition (ALD) method. This is followed by electron beam evaporation of a 5-8 nm thick Ti layer which can be patterned in a second AFM lithography step creating local top gates. Although such metallic gates have little effect on the hole density of the bulk 2DHG, our experience shows that they can significantly increase the tunability of the electrical properties of confined hole systems.

The effect of the combined side- and top gate electrodes on the tunability of low-dimensional hole systems has been first tested on different QPCs defined by AFM- as well as by electron beam lithography (EBL). The yield of the tunable devices is considerably higher than in case of the only in-plane structures and clear conductance quantization is observed with pronounced 0.7-like features. The latter have been extensively studied as a function of the gate configuration, QPC bias, in-plane- and perpendicular magnetic field as well as temperature. By the application of an in-plane transverse electric field to the QPC we can separate the standard 0.7 plateau from resonances at impurity states, while finite bias spectroscopy measurements at finite magnetic field reveal a considerable in-plane – out-of-plane anisotropy of the hole g-factor as expected from two-dimensional spin 3/2 systems.

Excited-state spectroscopy of single spins in diamond

G. D. Fuchs*, C. D. Weis**, D. M. Toyli*, T. Schenkel** and D. D. Awschalom*

* *Center for Spintronics and Quantum Computation, University of California, Santa Barbara, CA 93106, USA*

** *Lawrence Berkeley National Laboratory, Berkeley, CA 94720, USA*

Keywords: Nitrogen-vacancy, Diamond, Electron spin resonance, Single spin

Nitrogen-vacancy (N-V) defect centers in diamond have garnered increasing scientific attention in recent years due to the long room temperature spin coherence times in this system and the capacity to optically initialize and read out the spin states of N-V centers at room temperature. These properties have facilitated experiments studying the dynamics of a single N-V center spin and its interactions with proximal electronic and nuclear spins. However, the desire to further apply N-V center spins in quantum information science experiments necessitates the development of a means to reliably position N-V centers within the diamond host and also requires a more detailed understanding of the defect's electronic structure. Here we address both of these challenges in two related experiments. In the first we combine the spatial resolution of scanning force microscopy with ion implantation to controllably generate N-V centers with both spatial and isotopic control [1]. In the second experiment we utilize single spin resonance to probe the electronic structure of the N-V center's orbital excited state [2]. This allows for a direct measurement of the excited-state zero-field splitting, g-factor, and transverse anisotropy splitting of an individual NV center. We also demonstrate strong hyperfine coupling between the N-V center electronic spin and the nitrogen nuclear spin.

Figure 1 shows an optically detected spin resonance trace taken at B = 720 G. The data show two dips corresponding to resonant transitions between spin triplet levels of the N-V center in it's orbital ground state and it's orbital excited state.

The knowledge of the N-V center's excited-state electronic structure obtained in this work is critical to quantum control schemes utilizing the N-V center's orbital excited state.

References

1. C. D. Weis et al., J. Vac. Sci. Technol. B **26**, 2596 (2008).
2. G. D. Fuchs et al., Phys. Rev. Lett. **101**, 117601 (2008).

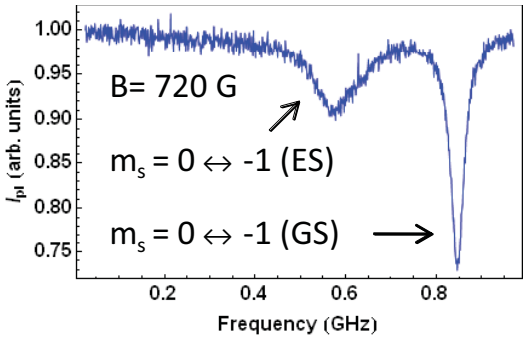

Fig.1 Optically detected spin resonance trace taken at B = 720 G showing transitions between spin triplet states of the N-V center in both it's orbital ground state (GS) and it's orbital excited state (ES).

Detection of local electron and nuclear spin dynamics by time-resolved Kerr microscopy

S. Matsuzaka*, Y. Ohno* and H. Ohno*,**

* *Research Institute of Electrical Communication, Tohoku University, Japan*

** *Exploratory Research for Advanced Technology, Japan Science and Technology Agency, Japan*

Keywords: time-resolved Kerr microscopy, (110) quantum well, electron spin, nuclear spin

Nuclear magnetic resonance (NMR) with high sensitivity and high spatial resolution is a powerful tool for investigation of nuclear spin physics in semiconductors. Recently, novel approaches for highly-sensitive detection of NMR have been demonstrated by both electrical and optical means. So far, we demonstrated an optical detection of NMR by a time-resolved Kerr rotation technique in GaAs quantum wells (QWs) [1]. In order to achieve higher spatial resolution, we implemented time-resolved Kerr microscopy (TRKM) with about 1 μm spatial resolution for observation of coupled electron-nuclear spin dynamics such as dynamic nuclear polarization (DNP) in local area of the laser spot.

In this work, we prepared a 9 nm-thick n-doped GaAs/$Al_{0.3}Ga_{0.7}As$ single QW grown on (110) substrate by molecular beam epitaxy. In our TRKM system, we used a mode-locked Ti:Sapphire laser which generates ~110 fs pulses at a repetition rate of 76MHz to produce circularly polarized pump and linearly polarized probe pulses. The pump and mechanically time-delayed probe pulses were focused onto the same position of the sample by an objective lens with a spot size of a full width at half-maximum of 1.5 μm. For high sensitive detection of the Kerr rotation angle of reflected probe beam, we employed heterodyne detection technique by using acousto-optical modulators (AOMs) for modulation of both pump and probe beams at different frequency. The Kerr rotation signal was detected by a balanced detector.

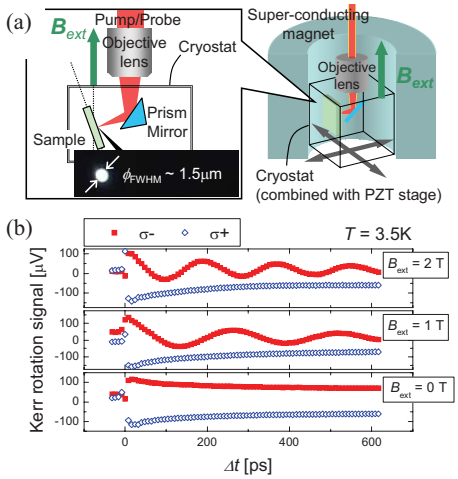

Fig.1 (a)Schematic figure of the optical configuration around the sample. (b)TRKR results of local electron spin dynamics in a laser spot size of about 1 μm.

Figure 1(a) schematically shows an optical configuration. The sample was set in a He-flow cryostat combined with superconducting magnet which can apply a magnetic field (B_{ext}) up to 5 T. The sample was set so that the (110) QW plane is tilted by about 20 degree between the [001] crystalline axis and B_{ext} to enhance the dynamic nuclear polarization. The path of the laser light was bent by a prism mirror placed near the sample. Figure 1(b) shows the experimental results of TRKM measurements done at T = 3.5 K and various B_{ext}. The pump (probe) power was 50 (250) μW. Larmor precession of electron spins injected by σ+ and σ- pump pulses was detected. The difference of the precession frequency between σ+ and σ- pumping corresponds to the polarization-dependent nuclear magnetic field caused by DNP. This indicates that we successfully detected coupled electron-nuclear spin dynamics in local area of the laser spot size of ~ 1 μm,.

Furthermore, we will discuss the pump and probe power dependence of DNP in high optical density region. All-optical NMR is also demonstrated by arbitral frequency by controlling AOM.

References

1. H. Sanada, *et al*., Phys. Rev. Lett. **96**, 067602 (2006).

Electric-field control of the anomalous Hall effect in (Ga,Mn)As thin films

D. Chiba[1,2,3], M. Endo[2], Y. Nishitani[2], F. Matsukura[2,1], and H. Ohno[2,1]

[1]*Semiconductor Spintronics Project, ERATO, Japan Science and Technology Agency, Japan*

[2]*Laboratory for Nanoelectronics and Spintronics, RIEC, Tohoku University, Japan*

[3]*Institute for Chemical Research, Kyoto University, Japan*

Keywords: Anomalous Hall effect, (Ga,Mn)As, Electric-field control of ferromagnetism

The anomalous Hall effect (AHE) is one of the most fundamental but still much debated issues in physics of transport properties in ferromagnetic materials[1,2,3]. In order to clarify the origin of AHE, the anomalous Hall conductivity σ_{AH} under various temperatures or in various samples has been conventionally investigated[4]. Here we show the AHE of (Ga,Mn)As thin films under electric fields to alter the carrier concentration.

We used a capacitance structure to apply gate electric field E to (Ga,Mn)As, which consists of a gate electrode / insulator / t nm $Ga_{1-x}Mn_xAs$ from the top. Hall measurements were performed to determine the magnitude and the sign of σ_{AH} of (Ga,Mn)As channel layer as a function of E. The σ_{AH} of almost all the samples is positive and increases with the conductivity σ when E is changed.

A few samples, however, show unusual behavior. One of them is shown in Fig. 1, which is the result of Hall measurements under various E from -5.0 to +5.0 MV/cm at 10 K (Curie temperature of this sample is ~130 K at $E = 0$), for the sample with $x = 0.12$ and $t = 4.0$ nm. The positive E indicates the direction of depletion of carriers (holes). Square hysteresis loops are observed in all the Hall resistance curves, which indicate that perpendicular-to-plane direction is the easy axis for the magnetization. The most interesting point is that the direction of the loop changes around $E = \sim+1.5$ MV/cm from counter-clockwise to clockwise when E is changed. This shows that the magnitude and the sign of σ_{AH} depend on the hole concentration, thus σ, as shown in Fig. 2. The details of the observed phenomena together with the origin of this behavior[5] will be discussed.

References

1. R. Karplus and J. M. Luttinger, Phys. Rev. **95**, 1154 (1954).
2. T. Jungwirth *et al.*, Phys. Rev. Lett. **88**, 207208 (2002).
3. S. Onoda *et al.*, Phys. Rev. Lett. **97**, 126602 (2006).
4. W. Lee *et al.*, Science **303** 1647 (2004).
5. A. Werpachowska and T. Dietl, ICPS2008, Th-A3c-2.

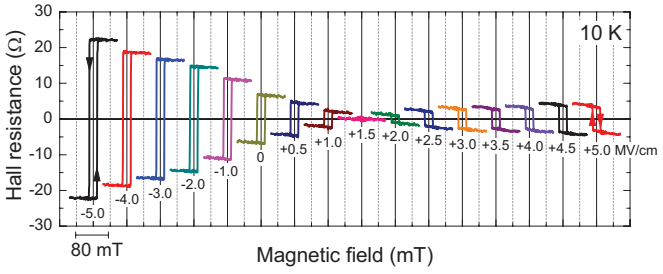

Fig. 1 Results of Hall measurements performed under various gate electric fields at 10 K.

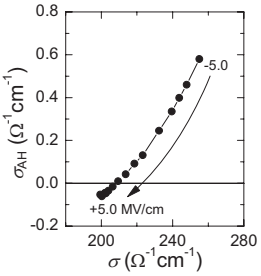

Fig. 2 Conductivity σ dependence of the anomalous Hall conductivity σ_{AH} at 10 K.

Room temperature ferromagnetic semiconductor Co-doped TiO_2 films grown on glass by sputtering method

T. Fukumura[1,2], T. Yamasaki[1], Y. Yamada[1], K. Ueno[3], M. Nakano[1], T. Makino[3] and M. Kawasaki[3,1,4]

[1] *Institute for Materials Research, Tohoku University, Sendai 980-8577, Japan*

[2] *PRESTO, Japan Science and Technology Agency, Saitama 332-0012, Japan*

[3] *WPI Advanced Institute for Materials Research, Tohoku University, Sendai 980-8577, Japan*

[4] *CREST, Japan Science and Technology Agency, Tokyo 102-0075, Japan*

Keywords: Spintronics, room temperature ferromagnetism, oxide semiconductor, cobalt-doped TiO_2

Ferromagnetic semiconductor is one of the promising materials for the semiconductor spintronics. Recently, wide gap ferromagnetic oxide semiconductors are extensively studied because of their potential to realize room temperature ferromagnetism. Among ferromagnetic oxide semiconductors with high Curie temperature, magnetic properties of Co-doped TiO_2 ($Ti_{1-x}Co_xO_{2-\delta}$: δ is oxygen vacancy) have been comprehensively investigated by using a systematic series of epitaxial films on single crystal substrates. However, growth of the films on glass is rather important because the semitransparent nature of the film could ultimately lead to transparent spintronics even on window glasses.

Here, we report on the properties of $Ti_{1-x}Co_xO_{2-\delta}$ films grown on glass substrates by sputtering method. Rutile $Ti_{1-x}Co_xO_{2-\delta}$ polycrystalline films were grown on glass and *r*-sapphire substrates by a dc magnetron sputtering method, where details were described elsewhere.[1,2]

Figure 1 shows magnetization versus magnetic field curves at 300 K for the $Ti_{0.95}Co_{0.05}O_{2-\delta}$ films with different electron density *n* grown on glass substrates. The magnetization is negligible for the lowest *n* film, whereas the substantial magnetization appears for higher *n* films. The saturation magnetization is close to 3 μ_B/Co that is an ideal value of Co^{2+} high spin state, obviously excluding possible segregation of Co metal (1.7 μ_B/Co). Inset of Fig. 1 shows the magnetic-field dependence of Hall resistivity at 300 K for the high *n* films, representing appearance of anomalous Hall effect.

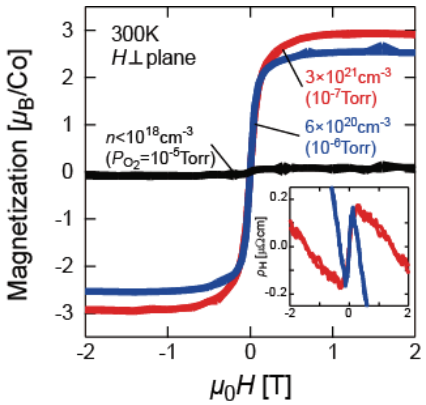

Fig.1 *M-H* curves at 300 K for $Ti_{0.95}Co_{0.05}O_{2-\delta}$ films with different electron density *n* grown on glass substrates. Inset shows Hall resistivity ρ_H -*H* curves for the same ferromagnetic films at 300 K. Magnetic field is perpendicular to the film plane. P_{O2} denotes oxygen pressure during growth.

In this paper, gigantic magneto-optical effect in a magnetophotonic crystal with $Ti_{1-x}Co_xO_{2-\delta}$ layer will be also presented.

References

1. T. Yamasaki *et al.*, Appl. Phys. Express **1**, 111302 (2008).
2. T. Yamasaki *et al.*, Appl. Phys. Lett. in press.

String-like self-assembly in $Ge_{1-x}Mn_x$

D. Bougeard*, J. M. LeBeau**, D. Saxey***, S. Ahlers*, N. Sircar*, V. Lang*,
A. Cerezo***, G. Abstreiter*, and S. Stemmer**

* *Walter Schottky Institut, Technische Universitaet Muenchen, Germany*

** *Materials Department, University of California, Santa Barbara, USA*

*** *Department of Materials, University of Oxford, UK*

Keywords: magnetic semiconductors, self-assembly

Magnetic materials made in molecular beam epitaxy from an alloy of Ge with Mn have recently attracted growing attention due to promising reports about the realization of $Ge_{1-x}Mn_x$ magnetic semiconductors. These materials, fabricated at conditions far from thermal equilibrium, exhibit above room temperature Curie temperatures while displaying an unperturbed Ge diamond-type crystal lattice and no signs of precipitation of known ferromagnetic, intermetallic Ge_xMn_y phases. Electron microscopy studies showed that the alloying of Ge with Mn in these crystals results in an inhomogeneous distribution of the Mn atoms in the Ge lattice: self-assembled nanometer-sized Mn-rich regions appear in a Ge-rich matrix containing less than 1% of Mn. Similar self-assembly phenomena in single crystals have since then also been observed in other magnetic materials such as Ga(Fe)N or (Zn, Cr)Te.

With proper crystal growth control in molecular beam epitaxy the process of self-assembly can be controlled in the case of $Ge_{1-x}Mn_x$, opening apparently the possibility to form columnar structures extending over the whole film thickness while conserving single crystallinity. Apart from above room temperature Curie temperatures the $Ge_{1-x}Mn_x$ single crystals reveal promising magnetic and electrical properties making them attractive candidates for the realization of a multifunctional material for room-temperature, all-semiconductor spintronics applications as well as a model system for self-assembly in other material systems.

We have recently achieved a closer analysis of the apparently columnar and crystallographically coherent Mn-rich areas through a combination of atom probe tomography (APT), annular dark field scanning electron transmission microscopy (ADF STEM) and magnetometry. We observe a string-like self-assembly perpendicular to the epitaxy plane of nanometer-sized Mn-rich dots in $Ge_{1-x}Mn_x$ which are the origin of the magnetisation of the material. Although apparently showing signs of crystallographic coherence with the Ge-rich matrix in cross-sectional and plan view TEM, we present converging evidence for strong structural disorder within these dots from ADF STEM and magnetometry. Each Mn-rich dot presents a core-shell structure with a crystallographically disordered core. Our results suggest that structural disorder leads also to magnetical disorder and the observed magnetical inactivity of a non-negligible fraction of Mn atoms. We propose that the disordered core of a Mn-rich dot is magnetically inactive, while the observed magnetization stems from magnetically active Mn in its shell. Strong strain fields induced by the Mn-rich dots induce a string-like stacked self-assembly along the direction perpendicular to the growth plane.

A deeper understanding of the formation mechanism of the disordered dots seems to be key to an improvement of the self-assembly process on the one hand and a further engineering of the magnetic and electrical properties of this promising magnetic semiconductor on the other hand.

InSb-based switching device operating at room temperature using magnetic controlled avalanche process for the application to magnetologic devices

J. D. Song*, J. K. Hong**, S. J. Joo*·**, S. H. Shin*, S. H. Han*, K. H. Shin*

** Nano Science Research Division, Korea institute of Science and Technology, Seoul 136-791, Korea*

*** Department of Display Semiconductor, Korea University, Chungnam 339-700, Korea*

Keywords: InSb, magneto conductance, logic deivce

A magnetologic device stands for an electronics device using magnetic information (such as magnetic alignment direction) as a gate or an input. The output signal can be change of current, voltage or magnetic information etc. Recently, this magnetologic device attracts a great attention, because it has re-configurable, low-power and non-volatile characteristics with high re-configuration speed faster than 1 GHz, where, in this device, logic and memory operations are not well-separated, rather, those can be manipulated by the same device. Therefore, with it, the idea of chameleon processor – the function of logic devices changes by request - has been introduced [1].

Therefore, many researchers focus on this topic. MIT group expected that TMR devices used in MRAM can be enhanced to be a magnetologic device.[1] Paul-Drude group suggested magnetic resistance phenomena as an engine of a magnetologic device and exhibited AND, OR, NAND, NOR etc. with a single device.[2] UC San Diego group depicted magnetic logic device based on non-local method using accumulation of spin introduced to semiconductor from magnetic metal.[3] European teams led by Bielefeld Univ. group focus on this topic with the title of "Exploring the Frontiers of Magnetic Logic". They showed many result based on MTJ or Hall effect.[4] There are many other researchers working on this topic with single electron transistor, carbon nano tube, magnetic wall motion, etc.

Until now, although all the technologies described above can be candidates to realized magnetologic devices, MTJ surpasses others in the number of activities and researchers. However, this also has a hurdle to jump; too small MR to fabricate array device such as CMOS.

In this presentation, we will report an InSb-based switching device using magnetic controlled avalanche process. The device was designed to reduce Hall voltage in it, and grown in MBE. It shows large change magneto-conduction (MC) over 400%, where the MC also can be controlled by bias voltage. Furthermore, the direction of the change of MC can be selected into positive or negative one in a single device. An important point of this device is that this InSb-based device is operated at room-temperature. We hope that this device shall be another good candidate for a re-programmable and non-volatile magnetologic device

This work is supported by KIST institutional research project of SPINTRONICS.

References

1. J. Moodera and P. Leclair, Nature materials **2**, 707 (2003).
2. A. Ney, C. Pampuch, R. Koch and K. H. Ploog, Nature **425**, 485 (2003).
3. H. Dery, P. Dalal, L . Cywinski and L. J. Sham, Nature **447** (2007).
4. V. Höink, D. Meyners, J. Schmalhorst, G. Reiss, D. Junk, D. Engel and A. Ehresmann, Appl. Phys. Lett. **91**, 162505 (2007).

Comparison between spin splitting obtained with an 8×8 matrix and various 2×2 matrices

D. M. Gvozdić*, N. Čukarić* and U. Ekenberg**

* *Faculty of Electrical Engineering, University of Belgrade, 11120 Belgrade, Serbia*

** *School of Information and Communication Technology, Royal Institute of Technology, Kista, Sweden*

Keywords: Spin splitting, Rashba effect, Dresselhaus effect, spin-orbit interaction

In spintronics there is strong interest in electric-field-induced spin splitting of electron subbands. The mechanisms include the Rashba effect due to structure inversion asymmetry and the Dresselhaus effect due to the bulk inversion asymmetry. For electrons these effects are frequently studied using various 2×2 matrices. In the simplest form one obtains two terms, both linear in the in-plane wave vector k.

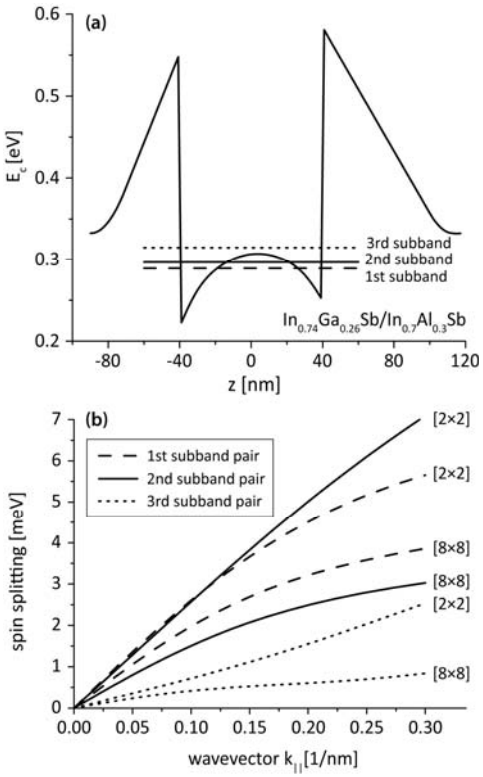

Fig.1 (a) Band diagram of an asymmetric modulation-doped quantum well and (b) corresponding spin splittings calculated by 8×8 k·p and 2×2 Hamiltonians for three lowest subbands.

Using the process called downfolding various approaches of deriving two-component equations have been obtained starting from larger matrices, typically 8×8 or 14×14 matrices. In this work we compare such approximations to numerical multiband calculations obtained by an 8×8 k·p matrix including the conduction, heavy-hole, light-hole and split-off bands. We include interface contributions via the Burt-Foreman boundary conditions [1].

We apply these models to a wide modulation-doped quantum well (Fig. 1(a)). As is shown in Fig. 1(b) the spin splittings are clearly different for the different subband pairs. The 2×2 model tends to overestimate the spin splitting. There is also a clear deviation from a linear k-dependence obtained in simple but frequently used models.

In previous work [2] we have demonstrated interesting anticrossing phenomena in slightly asymmetric quantum wells. Such phenomena would not occur in simple 2×2 models including the lowest subband only. A way to improve such models by including the two lowest electron subbands was recently presented by Bernardes et al [3]. We relate the results in this model to the 8×8 matrix approach.

References

1. M. G. Burt, J. Phys.: Condens. Matter **4**, 6651 (1992); B. A. Foreman, Phys. Rev. B **48**, 4964 (1993).

2. D. M. Gvozdić and U. Ekenberg, Physica E **40**, 2081 (2008).

3. E. Bernardes, J. Schliemann. M. Lee, J. C. Egues and D. Loss, Phys. Rev. Lett. **99**, 076603 (2007).

Effect of interface structure on current spin-polarization in narrow gap semiconductor heterostructures

Satofumi Souma and Matsuto Ogawa
Deparatment of Electrical and Electronics Engineering, Kobe University, Kobe Japan

Keywords: Spin-orbit coupling, Spin-polarized current, Resonant Tunneling Structure

Control of the spin-degree of freedom in semiconductor nanostructures has attracted a great attention recently. Especially, many attentions have been paid to the idea to generate spins in semiconductors by controlling the spin-orbit interaction electrically without use of any magnetic materials. One simple and efficient way is to use the spin-dependent resonant tunneling current through narrow gap semiconductor heterostructures, where two different types of spin-orbit coupling mechanisms play essential roles. One is the structural inversion asymmetry (SIA) described by the Rashba term [1], while the other is the bulk inversion asymmetry (BIA) described by the Dresselhaus term [2]. Since both of two mechanisms cause the conduction band spin-splitting and then the spin-polarized tunneling current in a complicated way, it is very important to understand how to enhance the spin-polarization of the current by utilizing these two distinct spin-orbit coupling mechanisms efficiently.

Although many previous theoretical studies have estimated qualitatively the spin-polarization of the output current with the perturbative treatment of the spin-orbit coupling, the quantitative simulation of such spin-device requires us to calculate the spin-splitting in non-perturbative way, especially when the ñon-common-atom interfaceëxists such as for InAs/GaAs interface. With such motivation, we present our study on the atomistic simulation of the spin-polarized electronic current in resonant tunneling heterostructures, where we employ the atomistic sp3s* tight binding Hamiltonian including the intra-atomic spin-orbit interaction [3] for the electronic state calculation and the non-equilibrium Green's formalism for the calculation of the non-equilibrium carrier density. The sp3s* tight-binding Hamiltonian with intra-atomic spin-orbit coupling has been employed it can reproduce the BIA- and the SIA-spin splittings without introducing the phenomenological spin-orbit interaction terms such as Rashba and Dresselhaus terms. As a demonstration of the usefulness of our atomistic approach, we have also studied the cases where ñon-common-atom interfaceëxists such as the case for InAs/GaAs interface.

References

[1] Y. A. Bychekov and E. I. Rashba, J Phys. C**17**, 6039 (1984).

[2] G. Dresselhaus, Phys. Rev. **100**, 580 (1955).

[3] P.Vogl et al., J. Phys. Chem. Solids 44, 365 (1983).

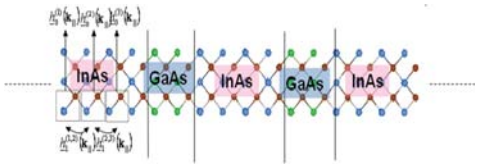

Figure 1: Schematic illustration of the InAs/GaAs double barrier hetrostructure. Periodic bounday condition is assumed along the direction perpendicular to the current.

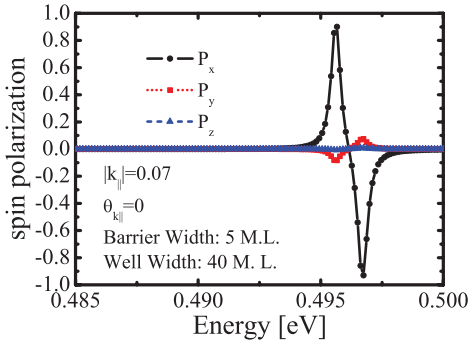

Figure 2: Spin-polarization of the transmission through the InAs/GaAs/InAs/GaAs/InAs heterostructure. The , , and components of the spin-polarization are shown.

Real-time X-ray diffraction measurements during Sb-mediated SK growth and annealing of InAs quantum dots

T. Kaizu*, N. Kakuda**, M. Takahasi***, S. Fujikawa*** and K. Yamaguchi**

* *Quantum Dot Research Center, National Institute for Materials Science, Tsukuba, Japan*
** *Department of Electronic Engineering, The University of Electro-Communications, Chofu, Japan*
*** *Synchrotron Radiation Research Center, Japan Atomic Energy Agency, Sayo-cho, Japan*

Keywords: InAs quantum dot, Sb-mediated method, growth interruption, X-ray diffraction measurement

Semiconductor quantum dots (QDs) have been extensively studied because of their prospective applications such as QD lasers. For fabrication of QD lasers with high performance, high QD density, high uniformity in the QD size and high crystal quality are required. Recently, high-density InAs QDs with a narrow photoluminescence linewidth have been obtained via Sb-mediated Stranski-Krastanov (SK) growth method, and in addition, the formation of giant dots with dislocations during QD growth was suppressed [1]. Growth interruption (G.I.) after the QD formation is also an important process for fabrication of high-quality QDs because coarsening often occurs during the G.I.. In this study, the structural evolution of InAs QDs on Sb-adsorbed GaAs(001) during the InAs growth and annealing under two different atmospheres, antimony and arsenic, was investigated by real-time X-ray diffraction measurements.

Experiments were performed at the synchrotron radiation beamline 11XU at SPring-8, Japan, using an X-ray diffractometer directly connected with a molecular beam epitaxy apparatus [2]. X-ray diffraction from InAs islands was measured with a temporal resolution of about 9 s, and the height of the InAs islands was evaluated. From this analysis, we have shown that, using X-ray diffraction, the structures of coherent dots and giant dots can be characterized separately even when they coexist. Figure 1 shows the temporal evolution of the height of coherent dots and giants dots (a) and the ratio of diffraction intensity from giant dots to the total diffraction intensity (b) during the 5 ML-InAs growth and annealing. When the growth time reaches 160 s, the island formation occurs and the diffraction from coherent dots appears. The height of coherent dots increses up to 7 nm in 140 s after the island formation and keeps a constant value until the stop of InAs growth. In contrast, the diffraction from giant dots begins to appear just before the growth stop. For both samples annealed under Sb and As atmospheres, the ratio of diffraction intensity from giant dots, p, gradually increases during annealing. However, the value of p is smaller under Sb atmosphere. This indicates that the formation of giant dots due to coalescence during annealing is suppressed under Sb atmosphere. The sample with the G.I. under Sb atmosphere, in addition, shows larger photo-luminescence intensity than that under As atmosphere. Therefore, the G.I. under Sb atmosphere is a promising way to maintain the crystal quality of high density InAs QDs.

References

[1] K. Yamaguchi and T. Kanto, J. Cryst. Growth **275** e2269 (2005).
[2] M. Takahasi, Y. Yoneda, H. Inoue, N. Yamamoto and J. Mizuki, Jpn. J. Appl. Phys. **41** 6247 (2002).

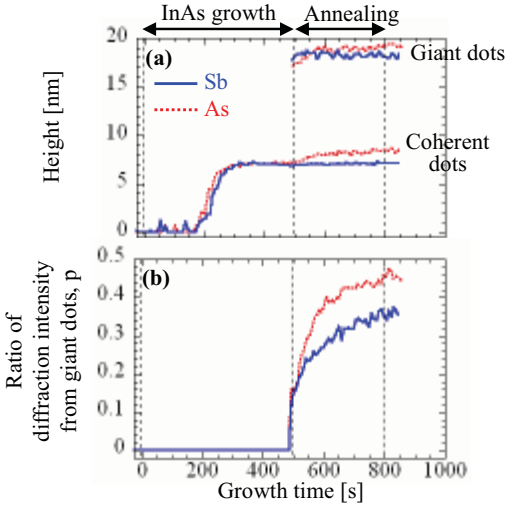

Fig.1 Temporal evolution of the height of InAs islands (a) and the ratio of diffraction intensity from giant dots (b).

Influence of growth and capping layer temperatures on the properties of GaSb/GaAs quantum dots

M. Ahmad Kamarudin*, Q. D. Zhuang*, T. N. Nuytten**, V. V. Moshchalkov** and M. Hayne*

* *Department of Physics, Lancaster University, Lancaster, United Kingdom*

** *INPAC-Institute for Nanoscale Physics and Chemistry, Pulsed Field Group, K. U. Leuven, Leuven, Belgium*

Keywords: III-V Semiconductor, Quantum Dots

The size, density and composition of GaSb self-assembled quantum dots (QDs) are important parameters for applications, e.g. QD memories [1]. We have studied the effect of GaAs capping layer temperatures on GaSb quantum dot samples A to D grown by molecular beam epitaxy at 400˚C, 430˚C, 460˚C and 490˚C. GaSb was deposited for 7 s at a growth rate of 0.3 ML/s on a GaAs buffer layer, and capped with GaAs at the same temperature and growth rate. Finally, a top layer of uncapped GaSb QDs was deposited for atomic force microscopy (AFM) studies.

AFM images show that samples A and D have a low density of QDs with large lateral size but higher in the latter case. Samples B and C have a high density of small dots with a height that is similar to sample A. Low temperature (4.2K) photoluminescence (PL) spectroscopy provides evidence for the dissolution of the dots during the capping process. Sample A, which has a low QD density and capping temperature, emits bright QD PL (see figure). For samples B and C, the overlap between the QD and wetting layer (WL) PL peaks indicates that the dots have been dissolved. For sample D, which was capped at 490˚C, a very weak, but well-resolved QD peak is observed. It hence seems that large QDs with low density survive the capping better than high-density/small-size QDs. It should be noted that typical GaSb QD growth and capping temperatures in the literature range from 450 to 500˚C [2,3,4]. Two more samples were prepared to investigate this further. The QDs on samples E and F were grown at 490˚C and only thinly capped (19 nm) at 430˚C and 490˚C respectively. Using AFM we found elongated features with lengths of ~3 μm on sample F, whereas for sample E round shapes were observed (size ~60 nm). Finally, sample G was prepared for PL measurements, with QDs grown at 490˚C and capped at 430˚C. This sample showed strong low energy QD PL emission well separated from the WL peak.

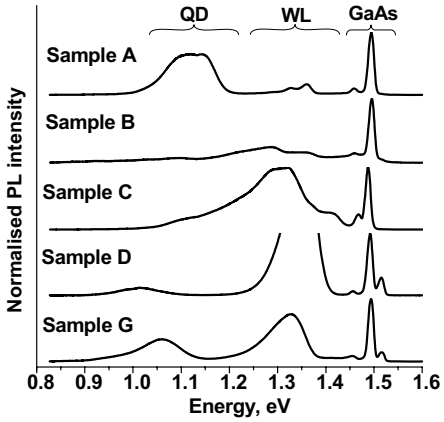

Fig. 1 PL spectra for samples A to D and G. The energy ranges for QD, WL and GaAs PL are shown.

References

1. A. Marent *et al.*, Appl. Phys. Lett. **91**, 242109 (2007)
2. M. Kudo *et al*., Phys. E **21**, 275-278 (2004)
3. C. Jiang *et al*. Phys. E **26**, 180-184 (2005)
4. T. Sato *et al*. Phys. E **32**, 152-154 (2006)

Enhancement of saturation magnetization in GaGdN/AlGaN multiple quantum wells grown by PA-MBE

S. Hasegawa, H. Tani, M. Kin, Y. K. Zhou and H. Asahi

The Institute of Scientific and Industrial Research, Osaka University, Ibaraki, Japan

Keywords: Dilute Magnetic Semiconductor, Multiple Quantum Well, Molecular Beam Epitaxy

Wide bandgap nitride-based dilute magnetic semiconductors (DMSs) have attracted great attention as potential materials for semiconductor spintronics. We have reported that Cr- or Gd-doped GaN shows ferromagnetism even at room temperature [1, 2], and that GaGdN/GaN short-period superlattices have much higher saturation magnetization than single GaGdN layers [3]. Heterostructures with DMS layers can be used to engineer the Gd-Gd exchange interaction mediated by the valence and/or conduction bands. In this presentation, we will report the growth of Gd-doped GaN/AlGaN multiple quantum wells (MQWs) and their optical and magnetic properties.

Samples used in this study were grown on GaN templates by plasma-assisted molecular beam epitaxy (PA-MBE). Elemental metals (Ga, Al, and Gd) and RF plasma-enhanced N_2 were used as group III and group V sources, respectively. Initially, a GaN buffer layer was grown at 700 °C. Then, GaGdN/AlGaN MQWs were grown at 700 °C followed by a GaN capping layer under irradiation of RF plasma-activated N_2 with a flow rate of 1.0 sccm. During the MBE growth, the sample surfaces exhibited sharp (1x1) reflection high-energy electron diffraction patterns indicating atomically flat surfaces.

Figure 1 shows X-ray diffraction $\theta/2\theta$ scan profiles for three samples of GaGdN/AlGaN MQWs with different well thicknesses L_w (1, 2, and 3 nm) and a fixed barrier thickness L_b (9 nm). The cycle number of QWs was 50 and the AlN mole fraction in the barrier layers was set to 0.24. The MQWs samples exhibit well-defined satellite structures. From the profiles, the respective periodic lengths L_w+L_b of the MQWs with L_w = 1, 2, and 3 nm are obtained as 9.4, 10.3, and 11.1 nm, as expected. Figure 2 shows *M-H* curves for the three MQWs taken at room temperature using super-conducting quantum interference device magnetometer. Even at room temperature, the three MQW samples show ferromagnetism. The MQWs with L_w = 3 nm has much higher saturation magnetization than the other two. We will discuss this phenomenon together with their optical properties.

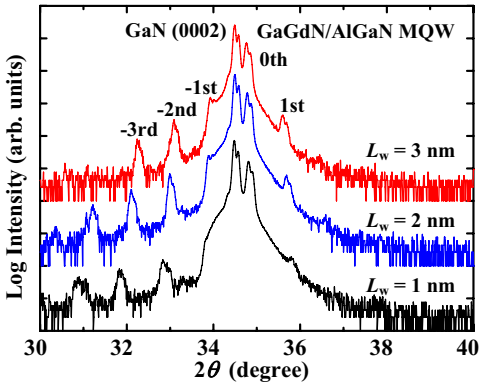

Fig. 1. XRD $\theta/2\theta$ scan profiles for GaGdN/AlGaN MQWs.

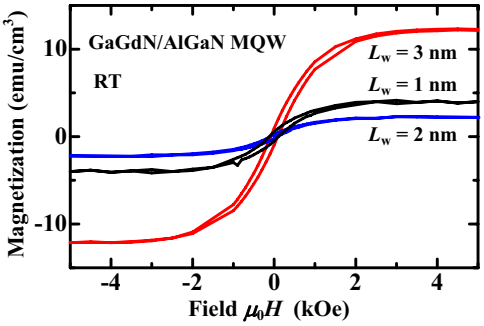

Fig. 2. *M-H* curves for GaGdN/AlGaN MQWs.

References

1. M. Hashimoto *et al*., Solid State Commun. **122**, 37 (2002).
2. N. Teraguchi *et al*., Solid State Commun. **122**, 651 (2002).
3. S. W. Choi *et al*., phys. stat. sol. (a)**203**, 2774 (2006).

July 22 (Wednesday)

9:00 – 10:30

Session M5

Spintronics I

International Conference Room

MSS-EP2DS Parallel session

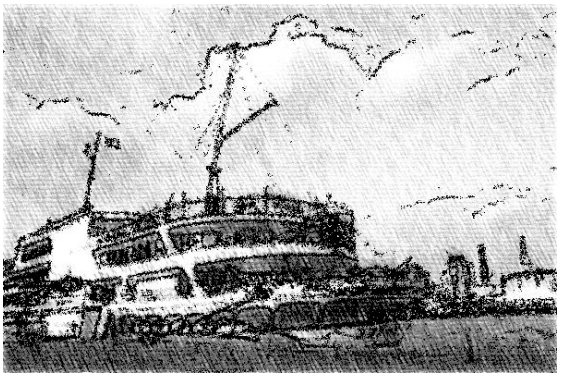

Kobe harbor cruise

Spin-orbit coupling induced magneto-resistance effects in ferromagnetic semiconductor structures

T. Jungwirth*,**

**Institute of Physics ASCR, v.v.i., Cukrovarnická 10, 162 53 Praha 6, Czech Republic*

*** School of Physics and Astronomy, University of Nottingham, Nottingham NG7 2RD, United Kingdom*

Keywords: ferromagnetic semiconductors, magnetoresistance, spin-orbit coupling

In the lecture we will review basic electronic and magnetotransport, properties of ferromagnetic semiconductor (Ga,Mn)As and devices based on this material [1, 2]. The discussion will be based on complementary theories based on the $\mathbf{k} \cdot \mathbf{p}$ kinetic-exchange model, microscopic tight-binding model, and *ab initio* calculations, and on extensive comparisons of the theory results to experiment. Transport effects covered in the lecture will include the Curie point singularity in the temperature derivative of the resistivity and extraordinary magnetoresistance coefficients, namely the anisotropic magnetoresistance, in bulk (Ga,Mn)As. We will then demonstrate how the more direct relation between the spin-orbit coupled exchange-split band structure and transport realized in more complex tunneling or single-electron transistor devices leads to a large enhancement of the magnitude and tunability of the magnetotransport effects. We will discuss the electric-field control of ferromagnetism in DMS transistor structures.

References

[1] T. Jungwirth, J. Sinova, J. Mašek, J. Kučera, A.H. MacDonald, Theory of ferromagnetic (III,Mn)V semiconductors, Rev. Mod. Phys. **78**, 809 (2006).

[2] T. Jungwirth, B. L. Gallagher, J. Wunderlich, Transport properties of ferromagnetic semiconductors, Spintroncs, Semiconductors and Semimetals vol. 82, p. 135-205 (Elsevier, 2008)

Effect of inversion asymmetry on anomalous Hall effect in ferromagnetic (Ga,Mn)As

A. Werpachowska* and T. Dietl*,**
*Institute of Physics, Polish Academy of Sciences, Warsaw, Poland
** Institute of Theoretical Physics, University of Warsaw, Poland

Keywords: anomalous Hall effect, Dresselhaus interaction, ferromagnetic semiconductors

The anomalous Hall effect (AHE) was first observed in ferromagnets by Hall himself [1]. The measured Hall voltage contains a part proportional to magnetization, but possible to explain only by the presence of the spin-orbit coupling. The latter generates a variety of effects investigated as AHE, but it is the "intrinsic" mechanism [2] that was experimentally shown to play a key role in the Hall effect in ferromagnetic semiconductors [3].

We investigate theoretically the intrinsic AHE in ferromagnetic (Ga,Mn)As, which have been hitherto examined [4] employing the 6-band $k.p$ method neglecting the inversion asymmetry of zinc-blende lattices. To describe this phenomenon in the language of topology, we replace the wave function with a triad of vectors. The rotation of such an object during its transport in the reciprocal space can be parameterized by the azimuthal and polar angles. The first is the well-known adiabatic Berry phase giving rise to AHE, while the other describes the tendency of the carrier to change the energy band.

By including the inversion asymmetry in GaAs bulk crystals (resulting in the so-called Dresselhaus k^3 terms and spin-splitting in the Γ_6 conduction band [5, 6]) we reject the notion of AHE proportionality to the magnetization of lattice spins. We explain this effect by analyzing different models of the GaAs band structure (multiband $k.p$ methods [4, 7] and tight-binding approximation [8, 9]), and propose the conditions under which it can be best experimentally observed (Fig. 1). At the same time, we show that the inversion asymmetry has minor effect on Curie temperature and anisotropies in (Ga,Mn)As. These results lead us to distinguish the static and kinetic properties of the system.

This work was supported by Scholarship of the President of the Polish Academy of Sciences for doctoral students and ERC Advanced Grant FunDMS.

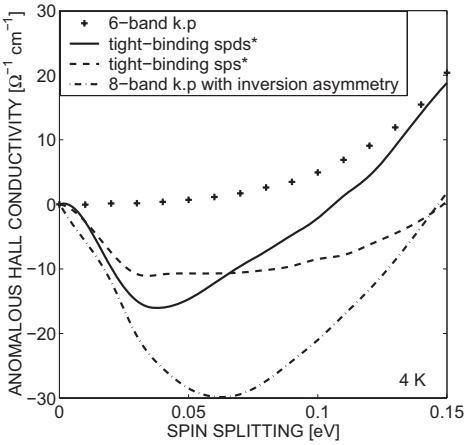

Figure 1: Anomalous Hall conductivity calculated using different models of the (Ga,Mn)As band structure for carrier concentration 0.5 nm^{-3} *vs* spin-splitting. The inversion asymmetry is included in the 8-band $k.p$ and tight-binding methods.

References

[1] E.H. Hall, Philos. Mag. **10**, 301 (1880).

[2] R. Karplus and J. M. Luttinger, Phys. Rev. **95**, 1154 (1954).

[3] W. Lee, S. Watauchi, V.L. Miller, R.J. Cava and N.P. Ong, Science **12** 1647 (2004).

[4] T. Jungwirth, Q. Niu and A.H. MacDonald, Phys. Rev. Lett. **88**, 207208 (2002).

[5] G. Dresselhaus, Phys. Rev. **100**, 580 (1955).

[6] A.G. Malshukov and K.A. Chao, Phys. Rev. B **71**, 121308 (2005).

[7] T.E. Ostromek, Phys. Rev. B **54**, 14467 (1996).

[8] J. Jancu, R. Scholz, F. Beltram and F. Bassani, Phys. Rev. B **57**, 6493 (1998).

[9] A. di Carlo, Semicond. Sci. Technol. **18**, R1 (2003).

Electric control of magnetization via control of carriers' spectrum anisotropy

A. Chernyshov,[1]* M. Overby,[1] L. P. Rokhinson,[1] Y. Lyanda-Geller,[1] X. Liu,[2] J. K. Furdyna[2]
[1] *Department of Physics and Birck Nanotechnology Center, Purdue University, West Lafayette, IN 47907*
[2] *Department of Physics, University of Notre Dame, Notre Dame, IN 46556*
** Tel: (765)-494-5513, Fax: (765)-494-0706, E-mail: achernys@purdue.edu*

The current state of information technology accentuates dichotomy between processing and storage of information, with logical operations performed by charge-based devices and non-volatile memory based on magnetic materials. The major obstacle for a wider use of magnetic materials for information processing is the lack of efficient control of magnetization. Reorientation of magnetic domains is conventionally performed by non-local external magnetic fields or by externally polarized currents [1]. Efficiency of the latter approach is greatly enhanced in materials where ferromagnetism is carrier-mediated [2]. In the latter case anisotropy of carriers' spectrum is transferred into the magnetic anisotropy of magnetic ions. For example, in magnetic semiconductor (Ga,Mn)As magnetic Mn ions have d^5 configuration and their total orbital moment is zero. Therefore, magnetic anisotropy originates from the spin-related anisotropy of the holes spectrum. This anisotropy is strain-dependent [3] and, as we show in this work, can be controlled electrostatically in multi-ferroic strain-coupled devices. In addition, in strained crystalline materials without the center of inversion there is a coupling between spin and kinetic momentum of carriers (spin-orbit interactions), which results in finite polarization and anisotropic modification of hole spectrum in the presence of current [4]. In this work we demonstrated two types of magnetization control in a magnetic semiconductor (Ga,Mn)As: in device A uniaxial strain is applied by a strain-coupled piezoelectric material and magnetization direction is controlled by electrostatic voltages[5]; in device B magnetization is controlled by spin-orbit effective field generated intrinsically by non-polarized dc current[6]. In the latter experiment for the first time we are able to measure magnitude and direction of the effective SO magnetic field ue to holes polarization electrically. For both approaches of hole polarization control we report reversible manipulation of magnetization direction, which demonstrates a direct implementation of a non-volatile memory cell. The reported effects are generic for a wide class of ferromagnetic materials, which raises a prospect for electrical control of magnetization at room temperatures. This work was partially supported by NSF ECS-0348289 (Purdue) and DMR-0603752 (Notre-Dame).

[1] J.C. Slonczewski, J. Magn. Magn. Mater. **159**, 1 (1996); L. Berger, Phys. Rev. B **54**, 9353 (1996)
[2] M. Yamanouchi *et al.*, Nature **428**, 539 (2004)
[3] G. Bir and G. Pikus, Symmetry and strain-induced effects in semiconductors (Wiley, New York, 1974)
[4] A.G. Aronov and Yu.B. Lyanda-Geller, JETP Lett. **50,** 431 (1989), V.K. Kalevich *et al.*, JETP lett. **52**, 230 (1990)
[5] M. Overby *et al.*, Appl. Phys. Lett. **92**, 192501 (2008)
[6] A. Chernyshov *et al.*, arXiv: 0812.3160 (2008)

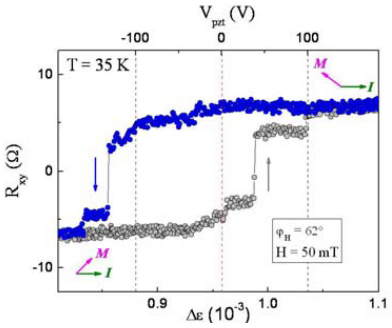

Fig. 1. Electrostatic control of magnetization via piezoelectric coupling

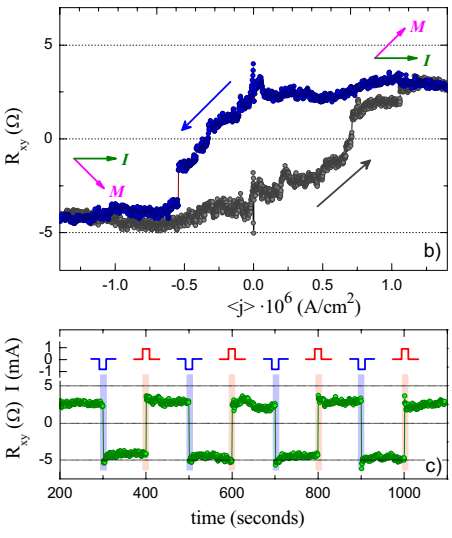

Fig. 2. Current control of magnetization via SO field

Spin currents in diluted magnetic semiconductors induced by THz radiation

P. Olbrich[1], S.A. Tarasenko[2], V.V. Bel'kov[2], Ch. Brinsteiner[1], W. Eder[1], D.R. Yakovlev[2,3], V. Kolkovsky[4], W. Zaleszczyk[4], G. Karczewski[4], T. Wojtowicz[4], D. Weiss[1], and S.D. Ganichev[1]

[1] *Terahertz Center, University of Regensburg, 93040 Regensburg, Germany*

[2] *A.F. Ioffe Physico-Technical Institute, Russian Academy of Sciences, 194021 St. Petersburg, Russia*

[3] *Experimental Physics 2, TU Dortmund University, 44221 Dortmund, Germany*

[4] *Institute of Physics, Polish Academy of Sciences, 02-668 Warsaw, Poland*

Keywords: Diluted magnetic semiconductors, Spin currents

Here we report on the observation of spin currents in diluted magnetic semiconductor (DMS) structures. We show that the free carrier absorption of terahertz (THz) radiation causes a pure spin current formed by oppositely directed and equal flows of spin-up and spin-down electrons. The effect is probed in an external magnetic field which converts the spin current into a net electric current. Such a conversion was previously observed in non-magnetic structures and attributed to the the Zeeman-effect which destroys the cancellation of spin-up and spin-down electron flows [1]. In DMS, the conversion is greatly enhanced. Here, the application of the external magnetic field results not only in a giant Zeeman spin splitting of the conduction band but evokes also spin-dependent exchange scattering of free electrons by magnetic impurities. We demonstrate that the latter effect plays an important role in the current generation.

The spin currents are studied in (Cd,Mn)Te/(Cd,Mg)Te single quantum well (QW) structures grown by molecular-beam-epitaxy on (001)-oriented GaAs substrates. Evenly spaced $Cd_{1-x}Mn_xTe$ thin layers were inserted during the growth of 10 nm wide QW (Fig. 1) applying the digital alloy technique. The photocurrent is detected at low power ($P \approx 0.5$ mW) terahertz radiation of a continuous-wave laser operating at the wavelength of 118 μm [2]. Figure 1 shows the observed voltage signal as a function of the magnetic field strength. As an important result, it was observed that a cooling of the sample changes the polarity of the signal and increases its absolute value by more than two orders of magnitude. Both the temperature and magnetic field dependences of the photocurrent corresponds to typical for DMS structures behavior caused by exchange interaction and polarization of the Mn^{2+} ions localized in the quantum well.

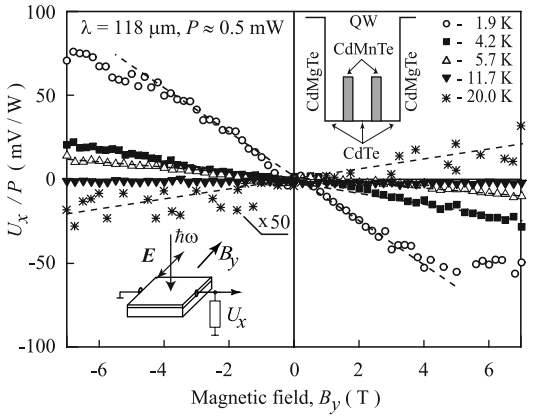

Figure 1: Magnetic field dependence of the photosignal in response to THz radiation. The inset shows the experimental geometry.

We developed the microscopic theory of the phenomena, which describes well the experimental data. It is shown that the carrier exchange interaction with localized magnetic ions in DMS vastly amplifies the conversion of pure spin current into the electric current. Two mechanisms are responsible for that: The giant Zeeman splitting of the conduction-band states and the spin-dependent scattering of free electrons by localized Mn^{2+} polarized by the magnetic field. The data indicate that in a degenerate electron gas at weak magnetic fields the scattering mechanism determines the current generation.

References

[1] S.D. Ganichev, V.V. Bel'kov, S.A. Tarasenko et al., Nature Phys. **2**, 609 (2006).

[2] S.D. Ganichev, S.A. Tarasenko, V.V. Bel'kov et al., arXiv: cond-mat 0811.4327

Tunneling anisotropic magneto-resistance in an epitaxial Co_2MnSi/n-GaAs junction

M. Harada, T. Uemura, Y. Imai, K.-i. Matsuda, and M. Yamamoto

Division of Electronics for Informatics, Hokkaido University, Sapporo 060-0814, Japan

Keywords: tunneling anisotropic magneto-resistance (TAMR), Heusler alloys, Co_2MnSi, GaAs

One Co-based Heusler alloy in particular, Co_2MnSi (CMS), is a promising ferromagnetic electrode for spintronic devices, such as magnetic tunnel junctions (MTJs) and spin injection devices, because of its intrinsically high spin polarization at room temperature (RT). We demonstrated relatively large tunneling magneto-resistance ratios of 179% at RT and 683% at 4.2 K in CMS/MgO/CMS MTJs [1]. To realize spin injection between ferromagnet and semiconductor, basic properties of ferromagnet/semiconductor heterostructures should be clarified. In this study, we investigated the transport properties of a fully epitaxial CMS/n-GaAs Schottky tunnel junction and observed a tunneling anisotropic magnetoresistance (TAMR).

Layer structures consisting of (from the substrate side) i-GaAs (50 nm)/n^--GaAs (Si = 1×10^{16} cm^{-3}, 750 nm)/n^+-GaAs (Si = 3×10^{18} cm^{-3}, 30 nm) were grown by molecular beam epitaxy (MBE) at 580ºC on GaAs(001) substrates. The sample was then capped with an arsenic protective layer and transported to a magnetron sputtering chamber. Prior to film growth, the arsenic cap was removed by heating the sample to 400ºC. A 20-nm-thick CMS film was grown by magnetron sputtering at 200ºC. The magneto-resistance (MR) of the CMS/n-GaAs junction with a size 10 × 50 μm was measured by a conventional four-probe method.

Figure 1 shows the MR curves at 4.2 K for a CMS/n-GaAs junction with two different bias voltages (V) of (a) –2.5 V and (b) 0.3 V. The n-GaAs was grounded. The magnetic field was applied along the [1–10] direction. Strong voltage-dependent MR curves were obtained. The MR curves showed that $R_{110} < R_{1-10}$ when V = –2.5 V, while $R_{110} > R_{1-10}$ when V = 0.3 V, where R_{110} and R_{1-10} stand for the MR value when the magnetization of CMS is oriented to [110] and [1–10] directions, respectively. Since such a complex voltage dependence of the MR cannot be explained by an AMR effect of the CMS electrode or a local Hall effect due to a stray field from CMS to n-GaAs channel, one possible origin is the TAMR effect, which is induced by an anisotropic electronic structure for tunneling electrons due to spin orbit interactions at the CMS/n-GaAs Schottky junction [2].

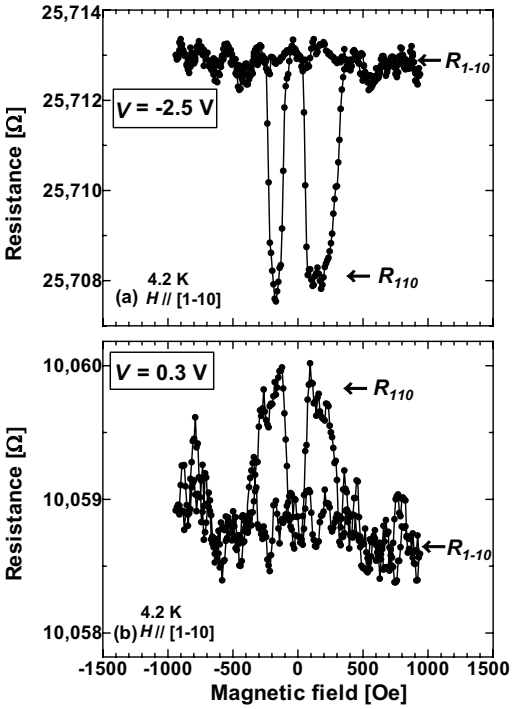

Fig. 1 Magneto-resistance curves at 4.2 K for a CMS/n-GaAs junction for (a) V = –2.5 V and (b) V = 0.3 V.

References

1. T. Ishikawa et al., JAP **93**, 07919 (2008).
2. J. Moser et al., PRL **99**, 056601 (2007).

July 22 (Wednesday)

11:00 – 12:30

Plenary Session 3, 4

Main Hall

EP2DS-MSS Joint session

Ikuta shrine

Outlook over graphene flatland

A. K. Geim*

**Centre for Mesoscience & Nanotechnology, University of Manchester, Oxford Road, Manchester M13 9PL, UK*

Keywords: graphene

Graphene is a wonder material with many superlatives to its name [1-3]. It is not only a new 2D electronic system but the first truly 2D crystal. It is the thinnest material in the universe and the strongest one ever measured. Charge carriers in graphene exhibit the highest known intrinsic mobility, have the smallest effective mass (it is zero) and can travel the longest (micron) distances without scattering at room temperature. Graphene can sustain the highest current densities (million times higher than copper), shows record thermal conductivity and stiffness, is impermeable and reconciles such conflicting qualities as brittleness and ductility. Electron transport in graphene is described by a Dirac-like equation (rather than the standard Schrödinger equation) allowing the investigation of relativistic quantum phenomena in a bench-top experiment.

I will overview our experimental work on graphene concentrating on its fascinating electronic and optical properties and speculate about future applications.

References

1. A. H. Castro Neto, F. Guinea, N. M. R. Peres, K. S. Novoselov, A. K. Geim. The electronic properties of graphene. *Rev. Mod. Phys.* **81**, 109 (2009).

2. A. K. Geim, K.S. Novoselov. The rise of graphene. *Nature Mat.* **6**, 183 (2007).

2. A. K. Geim, A.H. MacDonald. Graphene: Exploring carbon flatland. *Physics Today* **60**, 35 (2007).

Coherence and control of single electron spins in quantum dots

L.M.K. Vandersypen

* Kavli *Institute of Nanoscience, Delft University of Technology, Delft, the Netherlands*

Keywords: electron spin, quantum dots, quantum coherence

Individual electron spins isolated in semiconductor quantum dots are natural two-level quantum systems that could form the basis of a quantum information processor. Using a fully electrical approach, it is now possible to initialize, coherently manipulate and read out the spin state of a single electron in a quantum dot, and to couple it coherently to the spin of an electron in a neighbouring dot. Furthermore, we have come to a quantitative understanding of the timescales and mechanisms by which the spin loses phase coherence. Ongoing work focuses on integrating all buildings blocks in a single experiment, and on either control or elimination of the electron spin environment, in particular the nuclear spins in the quantum dot host material. This should permit using entangled spins as a new resource for quantum information processing.

References

[1] R. Hanson, L.P Kouwenhoven, J.R. Petta, S. Tarucha, and L.M.K. Vandersypen, *Spins in few-electron quantum dots*, Reviews of Modern Physics 79**,** 1217 (2007)

[2] I. T. Vink, K. C. Nowack, F. H. L. Koppens, J. Danon, Yu. V. Nazarov, and L. M. K. Vandersypen, Locking electron spins into magnetic resonance by electron-nuclear feedback, arXiv:0902.2659

[3] F.H.L. Koppens, K.C. Nowack, and L.M.K. Vandersypen, *Spin echo of a single electron spin in a quantum dot*, Phys. Rev. Lett. 100, 236802 (2008)

[4] K.C. Nowack, F.H.L. Koppens, Yu.V. Nazarov and L.M.K. Vandersypen, *Coherent control of a single electron spin with electric fields*, Science 318, 1430 (2007)

[5] F.H.L. Koppens, C. Buizert, K.J. Tielrooij, I.T. Vink, K.C. Nowack, T. Meunier, L.P. Kouwenhoven, and L.M.K. Vandersypen, *Driven coherent oscillations of a single electron spin in a quantum dot*, Nature 442, 766-771 (2006)

July 23 (Thursday)

9:00 – 10:30

Session M6

Spintronics II

International Conference Room

MSS-EP2DS Parallel session

Kobe “Ijinkan”

Electromotive force and magnetoresistance (~100,000%) in magnetic tunnel junctions with zinc-blende MnAs nanomagnets

P. N. Hai[1], S. Ohya[1,2], S.E. Barnes[3], S. Makeawa[4,5] and M. Tanaka[1,2]

[1.] *Department of Electrical Engineering and Information Systems, University of Tokyo, Japan*
[2.] *Japan Science and Technology Agency*
[3.] *Physics Department, University of Miami, USA*
[4.] *Institute for Materials Research, Tohoku University, Japan*
[5.] *CREST, Japan Science and Technology Agency*

Keywords: Electromotive force, magnetoresistance, zinc-blende MnAs, nanomagnets, tunneling

For nanostructures such as magnetic nanowires or spin valves, it is theoretically predicted that an electromotive force (emf) arises from a time-varying magnetization, such as the motion of magnetic domains, even in a *static* magnetic field [1][2]. This reflects the conversion of magnetic to electrical energy. Here we show that such an emf can indeed be induced by a static magnetic field in magnetic tunnel junctions (MTJs) containing zinc-blende (ZB) MnAs quantum nano-magnets for a time scale of 10^2~10^3 sec. Our results strongly suggest that Faraday's Law of induction must be generalized in order to account for purely spin effects in magnetic nanostructures [3].

The studied MTJs consist of ZB MnAs nanoparticles as the bottom electrode, a 2.1 nm-thick AlAs tunnel barrier followed by a 1 nm-thick GaAs spacer, and a 20 nm-thick NiAs-structure hexagonal MnAs thin film as the top electrode, grown by molecular beam epitaxy. The ZB MnAs nanoparticles, with a 2-3 nm diameter, are fabricated by the low-temperature annealing of GaMnAs at 480°C. Spin-dependent tunneling occurs between the nanoparticles and the top MnAs film through the AlAs tunnel barrier. Figure 1 shows, in solid, the zero and, in dashed, the 10 kG magnetic field, current (I) – voltage (V) characteristics of a round 200 μm diameter MTJ, measured at 3 K. The magnetic field was applied along the easy axis of magnetization of the top MnAs thin film (that is the GaAs[110] axes). The polarity of the applied bias voltage is defined as the voltage of the top MnAs film with respect to the substrate. The I – V curve, for 10 kG, is shifted toward the positive bias voltage region by 21 mV. This shift corresponds to an emf of 21 mV generated by the MTJ. The inset in Fig. 1 shows the resistance of the MTJ increased sharply when $|V|$ < 50 mV, implying a Coulomb blockade (CB) energy of ~50 meV. The emf is induced by a co-tunnelling process of electrons and magnetization of ZB MnAs nanomagnets subject to this strong CB [3].

Due to this CB and the emf, a huge magnetoresistance of up to 100,000% or even higher is observed for certain bias voltages [3]. The huge magnetoresistance and emf may find potential applications in a completely new kind of magnetic sensors with ultra high sensitivity, as well as in new active devices such as "spin batteries".

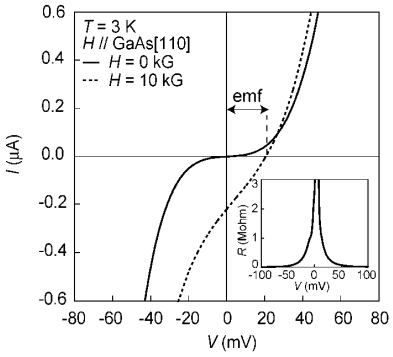

Fig.1 Current (I) – voltage (V) characteristics of a 200 μm-diameter MTJ, measured at 3 K with (dashed curve) and without (solid curve) a magnetic field of 10 kG applied in plane along the GaAs[110] azimuth. A magnetic field of 10 kG induced an emf of 21 mV. The inset shows the voltage dependence of the MTJ resistance at zero-field.

References

[1] S. E. Barnes, J. Ieda and S. Maekawa, Appl. Phys. Lett. **89**, 122507 (2006).
[2] S. E. Barnes and S. Maekawa, Phys. Rev. Lett. **98**, 246601 (2007).
[3] P. N. Hai, S. Ohya, M. Tanaka, S.E. Barnes and S. Makeawa, Nature, doi:10.1038/nature07879.

All optical spin storage and readout in a single quantum dot

V. Jovanov, D. Heiss, F. Klotz, D. Rudolph, M. Bichler, M. S. Brandt, G. Abstreiter and J. J. Finley
Walter Schottky Institut, Technische Universität München, Munich, Germany

Keywords: quantum dot, spin, storage, dynamics

We demonstrate all optical preparation and readout of a single electron spin in an individual self-assembled InGaAs quantum dot (QD). Our methods combine spin to charge conversion with luminescence recycling[1] and are applied to optically probe the spin relaxation dynamics. Importantly, our approach allows us to probe the dynamics of a single spin over ultra long timescales ($\geq 200\mu$s), generally inaccessible to optical single spin readout.

The devices investigated are voltage tunable QD spin memory structures that can be switched between two modes of operation; (i) charging, where optically generated holes are removed from the dot whilst electrons remain stored due to the presence of an AlGaAs barrier and (ii) readout, where excitons optically pumped into the dot recombine to produce luminescence[1, 2]. A single electron is prepared in the dot by setting the device to the charging mode and applying a resonant laser pulse tuned to the X^0 transition. The spin of the electron is controlled via the polarization of the preparation laser with high fidelity since the pure spin X^0 eigenstates are not mixed by the anisotropic electron-hole exchange interaction before hole tunneling escape occurs. After generation, the electron is stored and its spin tested after a controlled delay time via the conditional absorption of a second laser pulse tuned to the X^- transition. This readout pulse converts the spin of the stored electron into a charge occupancy ($1e$ or $2e$), which is then repeatedly sampled during the readout phase of the measurement.

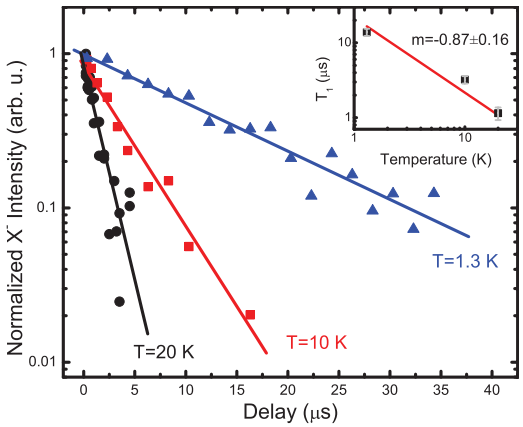

Figure 1: Occupation of the energetically higher Zeeman level as a function of the delay between $1e$ and $2e$ charging steps. Data recorded at T=1.3, 10 and 20K are presented. (inset) Single electron spin lifetimes extracted from polarization dynamics.

Our experiments confirm that the dot can be selectively prepared in a $2e$ state by successive excitation of the X^0 and X^- transitions. The charging and discharging dynamics are probed using time dependent measurements to probe the tunneling escape time of the electron and hole [3]. Furthermore, measurements in high magnetic fields exhibit a clear Pauli blockade in the $1e \rightarrow 2e$ charging step. This blockade can be lifted by delaying the $2e$ charging pulse by times longer than the electron spin T_1 time. The spin lifetime of the stored electron was measured by monitoring the storage time dependence of the blockade (Fig. 1) as the temperature was varied. We observe a $T_1 \propto T^{-0.87\pm0.16}$ dependence (Fig. 1 - inset), very close to the expected T^{-1} [4] for spin relaxation due to phonon mediated spin-orbit interaction. From the equilibrium degree of polarization of X^- and its dependence on temperature an absolute value of $g_e = 0.86 \pm 0.03$ was extracted, in excellent agreement with $\mathbf{k} \cdot \mathbf{p}$ calculations for our QDs. Our first attempts to coherently manipulate the electron spin using ESR-fields will also be presented.

References

[1] D. Heiss *et al.*. Phys. Rev. B **77**, 235442 (2008).

[2] M. Kroutvar *et al.*. Nature **432**, 81 (2004).

[3] D. Heiss *et al.* Appl. Phys. Lett. **94**, 072108 (2009).

[4] A. V. Khaetskii *et al.* Phys. Rev. B **64**, 125316 (2001).

All-eletrical spin injection and detection scheme in an all-semiconductor lateral device

M. Ciorga, A. Einwanger, U. Wurstbauer, D. Schuh, W. Wegscheider and D. Weiss
Institute for Experimental and Applied Physics, University of Regensburg, Regensburg, Germany

Keywords: spin injection/detection, ferromagnetic semiconductor (Ga,Mn)As

We demonstrate a successful all-semiconductor, all-electrical scheme for spin-polarized injection, transport and detection in devices with a lateral geometry[1]. As spin aligning material we use a ferromagnetic semiconductor (Ga,Mn)As forming the part of the Esaki diode structure employed both in injecting and detecting contacts. Thanks to the Esaki tunnelling that p-type material can be used as a source of spin-polarized electrons, which are injected into a non-magnetic GaAs layer.

The experiments were conducted in a non-local configuration i.e. with a detector placed outside the current path. Successful generation and detection of the spin current was confirmed by the measurement of Hanle effect, i.e precession and dephasing of the injected spins under the influence of a transverse magnetic field. A typical curve can be seen in Fig.1. The raw data is shown, which is a sum of the spin-related signal and some background signal, observed in most non-local experiments, origin of which is still not well understood. From those measurements we have estimated spin diffusion length and spin relaxation time in our samples as, respectively, $\sim 3\mu$m and 5 ns at T=4.2K. With increasing temperature the width of the Hanle curves increased in a full agreement with the model, primarily due to decrease in spin relaxation time from 5.5 ns at T=4.2K to 1.69 ns at 30K.

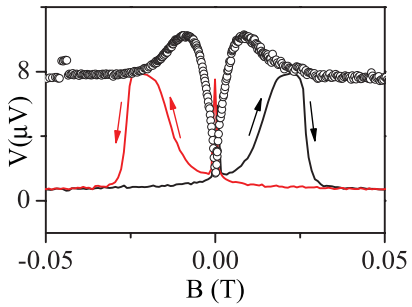

Figure 1: Non-local voltage measured at the detector at a distance of 10μm from the injector for a bias current of -50μA at perpendicular (symbols) and in-plane magnetic field (solid lines).

We obtained relatively high value of spin injection efficiency P_{inj} of $\sim$50% for bias current I$\leq 20\mu$A and in-plane orientation of injected spins, which strongly decreased with the increasing bias, in agreement with other reports[2]. Our studies revealed a small 5% in-plane anisotropy in P_{inj} as well as out-of-plane anisotropy of 40%.

We observed also a spin-valve-like (SV) switching in the non-local signal in an in-plane magnetic field, (see Fig.1). The amplitude of the switching events decays exponentially with the injector-detector separation on the length scale of a spin diffusion length, supporting the claim for its spin-related origin. Our measurements reveal however that the observed SV feature is not due to the parallel-antiparallel switching of magnetizations in injector/detector contacts but it is rather a result of vanishing of the spin signal in the certain range of the magnetic field. It is still to be resolved if the reason for the latter are mutually orthogonal magnetizations in injector/detector contacts or a formation of multi-domain structures therein.

This work has been supported by DFG under SFB 689 project.

References

[1] M. Ciorga, A. Einwanger, U. Wurstbauer, D. Schuh, W. Wegscheider and D. Weiss arXiv:0809.1736.

[2] P. Van Dorpe, W. Van Roy, J. De Boeck, G. Borghs, P. Sankowski, P. Kacman, J. A. Majewski, and T. Dietl, Phys. Rev. B **72**, 205322 (2005).

Exciton transport by moving strain dots in GaAs quantum wells

S. Lazić*, P.V. Santos* and R. Hey*

* *Paul Drude Institute , Hausvogteiplatz 5-7, 10117, Berlin, Germany*

Keywords: indirect exciton, spin, surface acoustic waves, photoluminescence

The strong light-matter interaction mediated by excitons has significant implications for the coherent manipulation of electronic states using photons. In addition, a number of collective phenomena, such as exciton condensation and superfluidity [1], have been predicted for excitons at low-temperatures in low-dimensional semiconductor structures. The control of the excitonic density, motion and dynamics without dissociating the coupled electron-hole pairs, are among the major challenges for the observation of microscopically coherent state of excitonic gas.

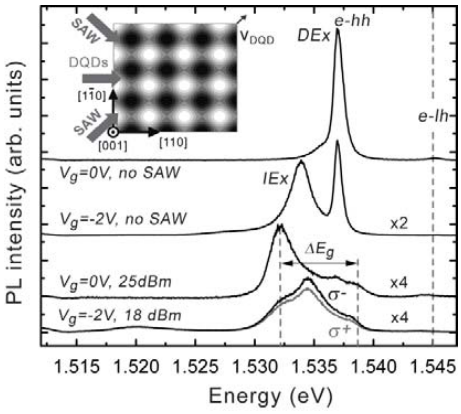

Fig.1 PL spectra from a DQW sample at T=8K under different bias conditions and different SAW powers applied to the IDTs. The inset shows the formation of strain dots for indirect excitons.

In this contribution, we address the simultaneous confinement and transport of excitons using moving microscopic traps created by the strain field of a surface acoustic wave (SAW) [2]. The zero-dimensional traps (strain dots) are formed by interfering two SAW beams (see inset in Fig.1) [3]. The trapping mechanism relies on a dynamic type-I modulation of the conduction and valence band edges via the deformation potential interaction, with a spatial SAW periodicity of a few μm.

The experiments are performed using long-living indirect excitons in a double quantum well (DQW) structure grown by molecular beam epitaxy on (001) GaAs. The exciton lifetime is voltage-tunable via the top gate and is substantially longer than the SAW period. Non-piezoelectric SAWs travelling along a <100> direction of the (001) GaAs sample surface (to avoid exciton dissociation) are generated using interdigital transducers deposited on a thin piezoelectric ZnO island. Optically excited excitons within the modulation region are then captured close to the minima of the bandgap modulation and transported with the well-defined acoustic velocity v_{SAW}. The dynamic bandgap modulation, as well as acoustically induced exciton transport by the strain dots, is investigated using spectrally and spatially resolved photoluminescence (PL). By applying a SAW, the exciton lines shift and split by ΔE_g as a result of the band-gap modulation induced by the moving potential dots, which propagate with velocity $\sqrt{2}v_{SAW}$, thus allowing for a quantitative determination of the strain. For the highest acoustic powers the band-gap shrinks by approximately 6 meV (Fig.1). Moreover, we report on the exciton distribution within the array of moving strain dots and provide experimental evidence of long-range acoustic transport of excitons over distances exceeding 100 μm.

Strong spin polarization of the indirect exciton line is observed under bias, even in the presence of SAW (Fig.1). Spin transport of the indirect excitons originating from the long spin relaxation time and long lifetime associated with interwell transitions is discussed, as well as the use of dynamic quantum dots to control the exciton density required for the observation of exciton-exciton interaction effects.

References

1. J.M. Blatt et al., Phys. Rev. **126**, 1691 (1962).
2. J. Rudolph et al., Phys. Rev. Lett. **99**, 047602 (2007).
3. F. Alsina et al., Solid State Commun. **129**, 453 (2004).

Two-color pump-probe measurements of intersubband excitonic interactions in GaAs/AlGaAs quantum wells

K. Morita*,**, H. Sanada**, S. Matsuzaka**, Y. Ohno**, and H. Ohno*,**

** Exploratory Research for Advanced Technology, Japan Science and Technology Agency, Japan*

*** Research Institute of Electrical Communication, Tohoku University, Japan*

Keywords: Two-color pump-probe measurements, electron spin, intersubband exchange interaction

Many experiments of time-resolved optical spectroscopy have explored exciton and spin dynamics in semiconductors and their quantum wells. Through the optical studies of lowest exciton resonance, phase space filling (PSF) and short-ranged exchange interaction is known as the responsible mechanisms for a modulation of spin-dependent excition resonance absorption in the lowest subband [1]. However, the responsible mechanism of intersubband excitonic interaction in the presence of spin-polarized electrons or excitons is not experimentally studied so far. In this work, we investigate the modulation of the second subband exciton resonance via short-ranged exchange interaction with photoexcited electron spins at the first subband in GaAs/AlGaAs quantum wells (QWs) by two-color pump-probe measurements.

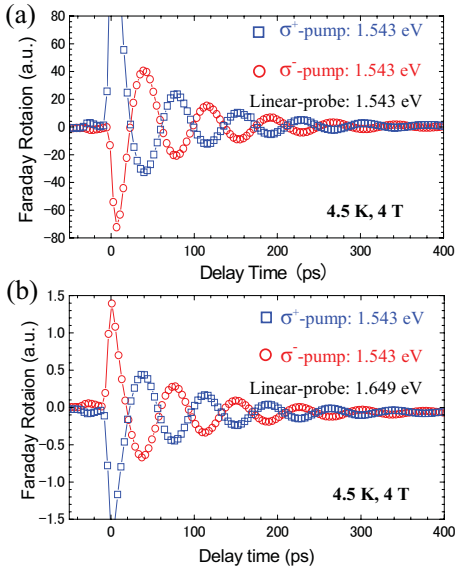

Fig.1 (a) $\theta_F(\Delta t)$ measured at B = 4 T with pump and probe energies set at 1.543 eV (b) $\theta_F(\Delta t)$ measured with the probe energy set at 1.649 eV.

The sample was grown on GaAs (001) substrate and consists of 60 periods of 11 nm-thick undoped GaAs QWs separated by 10 nm-thick $Al_{0.3}Ga_{0.7}As$ barriers. We used synchronized two mode-locked Ti:Al_2O_3 lasers to generate pump and probe pulses (~110 fs) at 76 MHz. The pump beam was circularly polarized and the energy was tuned at the first subband (E_1-HH_1) resonance (1.543 eV). Figure 1 (a) shows time-resolved Faraday rotation angle $\theta_F(\Delta t)$ measured at B = 4 T. The exponentially-decaying oscillations of $\theta_F(\Delta t)$ reveal the absolute value of the electron g-factor $|g|$ = 0.236, and T_2^* ~100 ps. In Fig. 1 (b), we carried out two-color TRFR measurement at B = 4 T by setting the probe energy at 1.649 eV near at the second subband (E_2-HH_2) resonance. We observed clear exponentially-decaying oscillations similar to those when the E_1-HH_1 state is probed. This indicates the polarization-dependence of second-subband exciton resonance on electron spins at the first subband. Further study of time-resolved transmission measurements showed clear polarization-dependent spectra at the second subband exciton absorption after resonant excitation of E_1-HH_1 exciton by σ^+-pump beam. The short-ranged exchange interaction between the first and the second subband excitons is found to play a crucial role in polarization-dependent spectral modulation.

References

1. S. Schmitt-Rink, D.S. Chemla and D.A.B. Miller, Phys. Rev. B **32**, 6601 (1984).

July 23 (Thursday)

11:00 – 12:30

Session M7

Nanostructure growth

International Conference Room

MSS-EP2DS Parallel session

Kobe port tower 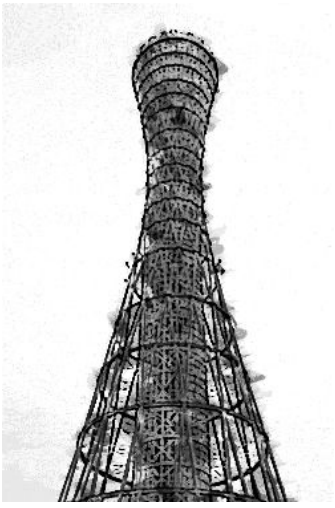

Growth and applications of GaN-based nanocolumns emitting from blue to red

K. Kishino*, **, ***, H. Sekiguchi*, *** and A. Kikuchi*, **, ***

* *Department of Engineering and Applied Sciences, and* ** *Sophia Nanotechnology Research Center, Sophia University, 7-1 Kioi-cho, Chiyoda-ku, Tokyo 102-8554, Japan,*

*** *CREST, Japan Science and Technology Agency, Kawaguchi, Saitama 330-0012, Japan*

Keywords: nanocolumn, InGaN, visible emission, selective area growth

GaN nanocolumns are self-assembled one-dimensional columnar nano-crystals, and were demonstrated by rf-plasma-assisted molecular-beam epitaxy (rf-MBE) [1]. The self-assembly of nanocolumns was employed for fabrication of visible InGaN/GaN nanocolumn LEDs [2,3]; however, random and spontaneous nucleation in the self-assembly process introduces fluctuation in nanocolumn shape and In-composition of InGaN, bringing about broad emission spectra. In order to control the position and the shape of nanocolumns, selective area growth (SAG) of GaN nanocolumns is a key technology to be developed. Recently Ti-mask SAG technology has been developed [4], by which well-arranged GaN nanocolumn arrays have been fabricated [5]. In this talk, emission characteristics of the InGaN/GaN nanocolumn LEDs and the Ti-mask SAG of rf-MBE are described. By use of the Ti-mask SAG, InGaN/GaN nanocolumn arrays with different column diameters and periods were grown, demonstrating controlled emission-color with the size and the period of the nanocolumns.

Prior to the growth, Ti thin films were deposited on GaN surface, in which nanoholes arranged in triangular and square lattices, with various depth and periods, were prepared by focused ion beam (FIB) etching. The Ti mask surfaces were nitrided at 400 ^{o}C, followed by the growth of GaN nanocolumns at temperatures from 880 ^{o}C to 900 ^{o}C. Then 3-period InGaN/GaN multi quantum wells (MQWs) were grown at top regions of the nanocolumns, at 650 ^{o}C.

The SAG of GaN nanocolumns occurred at the growth temperature (T_g) above 900 °C; diffusion and desorption of Ga adatoms on/from nitrided Ti mask was enhanced with the increased T_g, which contributed to the SAG. However, an excessive increase in T_g to above 900 °C at nitrogen flow rate (Q_{N2}) of 3.5 sccm brought about increased inhomogeneity in the nanocolumn shape. Upon reducing Q_{N2} from 3.5 to 1 sccm, uniform nanocolumn arrays arranged in triangular and rectangular lattices were successfully grown around the critical temperature of 900 °C. Thus in this experiment, the GaN nanocolumn arrays were prepared typically at O_{N2} from 1 to 2 sccm.

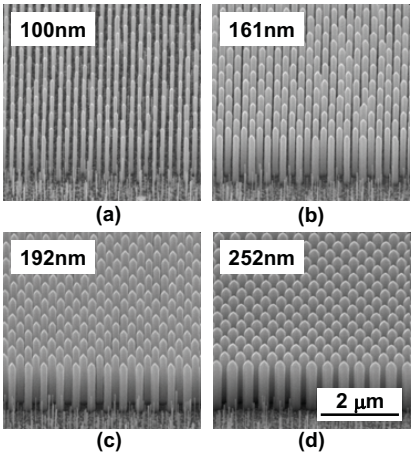

Fig. 1 SEM images of GaN nanocolumns grown at 900^{o}C by Ti-mask selective area growth with Q_{N2}=1sccm. The average column diameter was 100, 161, 192, and 252nm.

GaN nanocolumn arrays with different column diameter and array period were grown on the same substrates. Figure 1 shows bird's eye views of scanning electron microscope (SEM) of nanocolumn arrays. The nanocolumn diameter was precisely controlled from 100 nm to 300 nm at the constant period of 400 nm. The GaN nanocolumns have six-sided pyramid tops

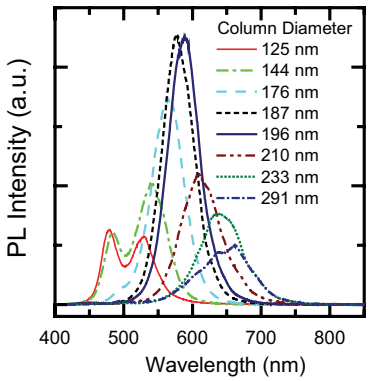

Fig. 2 PL spectra of InGaN/GaN MQW (3-period) nanocolumn arrays with different nanocolumn diameter; the samples were grown at 900 oC and QN2=2sccm.

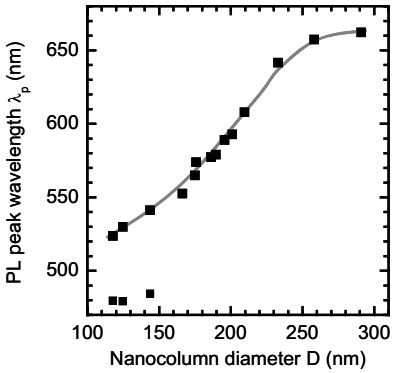

Fig. 3 PL peak wavelength as a function of nanocolumn diameter for the InGaN/GaN MQW nanocolumn arrays

(see Fig. 1), though flat surfaces tend to appear at the apex of the pyramids with increasing the diameter. Six fold side faces of the pyramids can be assigned to {1-101} crystal faces; the nanocolumn diameter was defined as the distance between two parallel hexagonal sides. The room temperature photoluminescence (PL) spectra of the InGaN-MQW nanocolumns are shown in Fig.2; the column diameter of the samples evaluated here changed from 125 nm to 291 nm. They were evaluated with a selective excitation of InGaN QWs by use of an InGaN-based semiconductor laser of 405-nm wavelength. The excitation power density was 0.15kW/cm^2. We note that the PL peak wavelength shifted monotonically from 520 nm to 660 nm with increasing the nanocolumn diameter (see Fig.3). At the same time, the PL peak wavelength of 190-nm-size nanocolumns decreased from 508 nm to 480 nm with increasing the nanocolumn period from 400 nm to 4 μm.

In summary, various InGaN/GaN MQW nanocolumn arrays, having different nanocolumn diameter and array period in the range from 100 nm to 300 nm, and from 400 nm to 4 μm, respectively, were grown on the same substrate by the rf-MBE SAG. The PL emission wavelength of the nanocolumns shifted as a function of the nanocolumn diameter and the array period; it allows us to control the emission color for InGaN-based nanocolumns on the same substrate. This suggests that three primary-color (RGB) nano-LEDs can be monolithically integrated on the same substrate with controlling the nanocolumns diameter.

Acknowledgement

This study was supported by Grants-in-Aid for Scientific Research on Priority Areas No.1806910 from the Ministry of Education, Culture, Sports, Science and Technology, Japan.

References

1. M. Yoshizawa…K. Kishino, Jpn. J. Appl. Phys. **36**, L459 (1997).
2. A. Kikuchi…K. Kishino, Jpn. J. Appl. Phys. **43**, L1524 (2004).
3. K. Kishino et al., Proc. SPIE **6473**, 64730T-1 (2007).
4. K. Kishino et al., Electron. Lett. **44**, 819 (2008).
5. H. Sekiguchi, K. Kishino and A. Kikuchi, Appl. Phys. Express **1**, 124002 (2008).
6. K. Kishino, H. Sekiguchi and A. Kikuchi, J. Cryst. Growth, **311**, 2063 (2009).

Fabrication of InGaN/GaN stripe structure on (111)Si and stimulated emission properties under photo-excitation

B-J. Kim, T. Tanikawa, Y. Honda, M. Yamaguchi, and N. Sawaki

Department of Electronics and Akasaki Research Center, Nagoya University,

Furo-cho 3C-1, Chikusa-ku, Nagoya, 464-8603, Japan

Keywords: GaN, MOVPE, selective epitaxy, LD

Compound semiconductor stripe structures grown by selective MOVPE have been used as a cavity of laser diode (LD). By using the selective MOVPE method, we may fabricate multiple wavelengths LDs on a wafer by adjusting the stripe width[1]. This has, however, not been achieved in III-nitrides. We have been studying the growth of GaN fine structures on Si substrate and found that the dislocation density is much reduced by controlling the growth modes. In this study, we attempt to fabricate a GaN-LD on (111)Si.

The samples were fabricated by MOVPE on a patterned (111)Si substrate. The period of stripe pattern was 10 μm (3 μm wide windows and 7 μm wide masks). The stripe direction was along the <11-2> axis of the Si so that it is parallel to the <1-100> axis of the GaN. GaN stripes were grown selectively via an AlN intermediate layer. In order to reduce the dislocation density, we used FACELO technique[2]. The GaN stripes have been grown by two steps under different growth conditions. The temperature and pressure of the first step were 1010 °C and 600 Torr, while those of the second one were 1130 °C and 400 Torr, respectively. On the thus prepared low dislocation density GaN stripes, three periods of InGaN/GaN QWs were grown at 800 °C embedded between 120 nm thick $Al_{0.16}Ga_{0.84}N$ cladding and 100 nm thick GaN guide layers. The widths of the QW and the barrier layers were 2 and 4 nm, respectively.

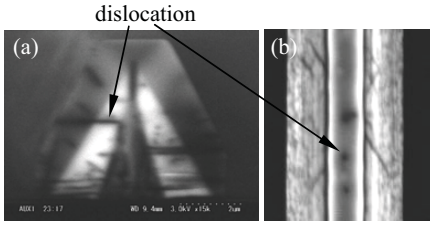

Fig. 1 Cross-sectional (a) and top view (b) CL images

Figure 1 shows cross-sectional (a) and top view (b) CL images of a sample. The dislocation density on the top face, determined by the dark spot density, was 2 x 10^7/cm^2, which is two orders of magnitude lower than those found in planar samples.

Photoluminescence (PL) spectra from the edge of the stripe were investigated at room temperature by using 337 nm line form a N_2 gas laser as the excitation source. The cavity length of the sample was 350 μm. Figure 2 shows the spectra (I) and the integrated PL intensity as a function of the excitation intensity. As shown in Fig. 2, narrowing of the emission peak (FWHM = 2 nm) and a nonlinear increase of the integrated intensity are obvious under excitations higher than 5 MW/cm^2. These suggest that the laser emission has been achieved in this sample and prove the potential of an as grown stripe structure.

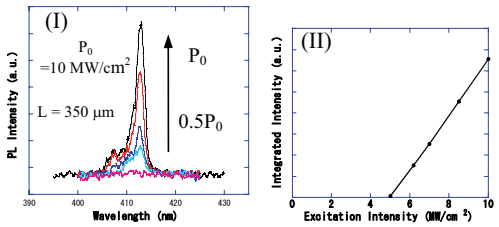

Fig. 2 Pump power dependence of edge emission spectra (I) and integrated intensity (II)

References

[1]M.Arai, et al., Jpn. J. Appl. Phys. **40** (2001) 4056.

[2] K.Hiramatsu, et al., J. Crystal Growth **220** (2000) 316.

Adding functionality to GaAs nanowires: from prismatic heterostructures to band gap engineering with only one material

D. Spirkoska*, M. Heigoldt*, J. Arbiol**,***, J. R. Morante***, G. Abstreiter* and A. Fontcuberta i Morral****
*Walter Schottky Institut, Technische Universität München, Munich, Germany
**TEM-MAT, Serveis Cientificotècnics, Universitat de Barcelona, C/ Lluís Sole i Sabarís 1-3, E-08028 Barcelona, CAT, Spain
***EME/CeRMAE/IN2UB, Departament d'Electrònica, Universitat de Barcelona, C/ Martí i Franquès 1, E-08028 Barcelona, CAT, Spain
****Laboratoire des matèriaux Semiconducteurs, Instiut de Matèriaux, Ecole Polytechnique Fèdèrale de Lausanne, 1015, Lausanne, Switzerland

Keywords: nanowires, molecular beam epitaxy, prismatic heterostructures, band gap engineering

GaAs nanowires grown by the Ga assisted method using molecular beam epitaxy (MBE) posses excellent structural and optical quality [1]. When the properties of these wires are combined together with the versatility of growth modes offered by the MBE technique their functionality can be enormously increased. By tuning the growth conditions after the nanowires have obtained the desired length the side facets can be overgrown with atomic precision. This allows fabrication of complex heterostructures and quantum wells in a prismatic geometry. Figure 1 a) and b) show as an example the cross section of a complicated co axial structure. Furthermore the formed quantum wells show strong and narrow photoluminescence and good homogeneity along the whole nanowire [1].

By fine tuning of the growth conditions, in particular the As pressure the structure of the nanowires can be changed from pure zinc blende (zb) to a mixture of a wurtzite (wz) and zinc blende (see Figure 1 c) and d)) [2]. This affects dramatically the PL properties of the nanowires. Light is emitted at energies bellow the free exciton emission of zb GaAs (1.51 eV), with very narrow emission lines. This is due to the confinement of carriers in the zb or the wz regions. The emission of the nanowires can be tuned from 1.51 eV down to 1.43 eV. The lowest observed energy corresponds to a transition at the wz/zb interface and is in very good agreement with a type II band offset predicted for the wz/zb GaAs interfaces [3]. This work opens a route for achieving band gap engineering using only GaAs.

References

[1] A. Fontcuberta i Morral, D. Spirkoska, J. Arbiol, M. Heigoldt, J. R. Morante and G. Abstreiter, Small **4**, 899 (2008).

[2] A. Fontcuberta i Morral, J. Arbiol, D. Spirkoska et al, submitted.

[3] M Murayama and T Nakayama, Phys. Rev. B **49**, 4710 (1994).

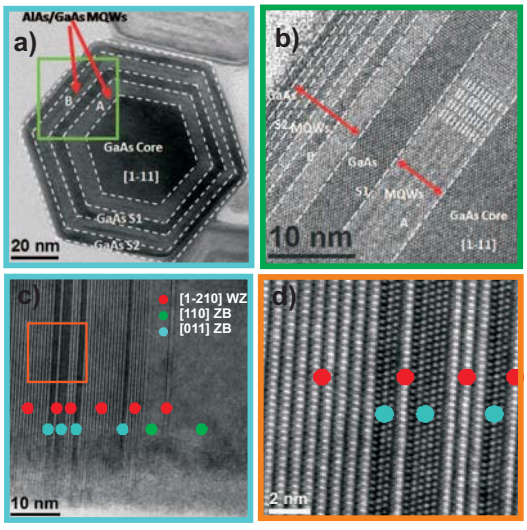

Figure 1: (a) Transmission electron micrograph (TEM) of a cross section of a prismatic heterostructure nanowire. In the region labeled as A and B several layers of AlGaAs and GaAs are grown. b) High resolution (HR) TEM from the selected region in a). c) TEM from a GaAs nanowire with a mixture of wz (red dots) and zb (green and blue dots) structure. d) HRTEM from the selected region in c).

Ordered SiGe islands on Si (001) for spectrally narrow photoluminescence

M. Grydlik*, M. Brehm, N. Hrauda, T. Fromherz, J. Stangl, F. Schäffler and G. Bauer

* *Institute of Semiconductor and Solid State Physics, Johannes Kepler University, A-4040 Linz, Austria*

Keywords: SiGe islands, structural and electronic properties, photoluminescence

The major advantages of Ge islands grown on pre-patterned Si(001) substrates as compared to randomly nucleated islands grown on planar substrates are the control both over the nucleation sites as well as the comparatively narrow size and Ge content distribution of the islands. We demonstrate that those parameters significantly reduce the spectral width of the island photoluminescence (PL) (Fig. 1).

The Si(001) substrates were pit-patterned by e-beam lithography with a period of 400 nm. The dimensions of the pits are 200 nm × 200 nm in lateral and 40 nm in vertical directions. SiGe islands were grown by deposition of 6 ML of pure Ge by solid source molecular beam epitaxy at a growth temperature of 650°C. Si capping at low temperature (300°C) was used to preserve the island shape, size and Ge composition. Both ordered and randomly nucleated islands were grown together in the same MBE growth run. Uncapped samples grown under otherwise identical conditions were used for the determination of the island shapes by atomic force microscopy (AFM). A pronounced narrowing and a blue shift of the PL signal of the ordered islands is clearly observed with respect to the PL of the randomly nucleated islands. Furthermore, we show by extensive x-ray diffraction (XRD) experiments performed on both types of islands that this blue shift is due enhanced strain relaxation and intermixing of the islands grown on the pit-patterned substrates. We have clear evidence that the substrate morphology determines the Ge concentration profiles in the islands grown under otherwise identical conditions.

Based on the structural parameters obtained by XRD and the island shapes determined by AFM investigations, a quantitative modelling of the valence band structure within the islands and the conduction band structure in the surrounding Si matrix based on full 3D simulations using the nextnano[3] package was performed. An excellent agreement between observed and calculated PL transition energies was achieved.

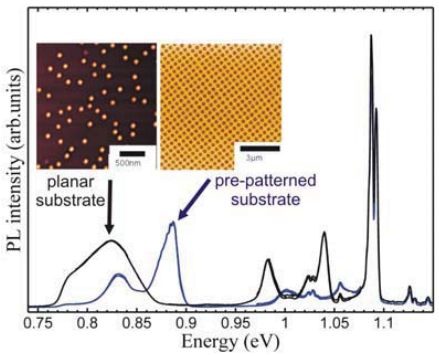

Fig.1 Photoluminescence spectra of islands grown on pre-patterned and planar substrates. A clear narrowing of the island PL (between 0.8 and 0.9 eV) and a pronounced shift of the PL of islands grown on pre-patterned substrate is observed. Insets (a) and (b) show typical AFM micrographs of the patterned and planar samples. Note the different length scales.

Reference

T. U. Schülli, G. Vastola, M. I. Richard, A. Malachias, G. Renaud, F. Uhlik, F. Montalenti, G. Chen, L. Miglio, F. Schäffler, and G. Bauer, Phys. Rev. Lett. **102**, 025502 (2009).

Ordered semiconducting functional polymer nano-architectures with three-dimensional structural control

P. Jedrasik*, U. Södervall*, C. A. Dutu**, D.A. Serban**, P. Guillet***, A. Vlad**, C.-A. Fustin***, J.F. Gohy***, and S. Melinte**

**MC2, Chalmers University of Technology, Göteborg, 41296, Sweden*

***Unité DICE, Université catholique de Louvain, Louvain-la-Neuve, 1348, Belgium*

****Unité CMAT, Université catholique de Louvain, Louvain-la-Neuve, 1348, Belgium*

Keywords: polyaniline, near teradot/inch^2 pattern transfer, 3D nanostructuring, structural self-assembly

We report on a novel protocol for patterning the semiconducting polyaniline (PANI) with an unprecedented areal patterning density exceeding 0.25 teradot/inch^2 (Fig. 1a). A simple two-step process is put forward to hierarchically build a large variety of functional PANI nanostructures on virtually any type of flexible or rigid substrates. Using template confinement, through Pt catalyzed electroless growth, highly-ordered arrays of distinct PANI nanowires are produced with a typical diameter of 15 nm and aspect ratio higher than 20. Complex three-dimensional structural control is achieved through a direct pattern transfer using a novel type of resist- and dose-modulated electron beam lithography (Fig. 1b). The method is scalable [1] and provides a generic approach for nanopatterning surfaces with functional polymers. Aspects of the PANI growth mechanism at nanoscale are discussed and the highly controllable, sub-picogram scale fabrication is emphasized. A simple scheme for the single PANI nanowire fabrication, processing and device integration resolution is presented. The tunable optoelectronic properties achieved through a simple doping/dedoping scheme are considered.

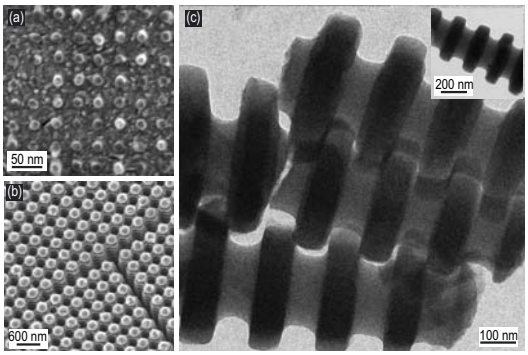

Figure 1: Bottom-up and top-down paradigms are converged to grow single nanoscale polyaniline elements and architectures with a remarkable structural and positional control. (a) Near-teradot/inch^2 pattern transfer. (b) Orthorhombic polyaniline lattice. (c) Geometry-controlled, capillary-driven gear-type self-assembly.

The morphology-modulated nanowires are driven to self-assemble in key-lock type architectures orchestrated by the structural asymmetry and non-uniformity of the capillary forces [2]. The re-entrant topography of the fabricated nanostructures (disc and square-shaped axially modulated as well as branched and hyper-branched pillars) can induce the pinning of the receding contact line of the liquid menisci in the case of an evaporating liquid. This behavior increases the capillary forces exerted between the pillars forming gear-like nanoassemblies (Fig. 1c). The structural matching of the alternated modulations favors compact stacking with very few interstices in between. This morphological asymmetry provides the potential of being further exploited for spherical, helical or tubular functional macroassemblies. Combined with the modulated optoelectronic properties and the straightforward mechanical actuation of the polyaniline, these assemblies could play a role in the design of stimuli-responsive smart materials.

References

[1] A.L. Bogdanov *et al.*, Microelectron. Eng. **67**, 381 (2003).

[2] B. Pokroy *et al.*, Science **323**, 237 (2009).

July 23 (Thursday)

14:00 – 16:00

Session M8

Novel materials and physics

International Conference Room

MSS-EP2DS Parallel session

Nada “sake” brewery

ZnO/MgZnO heterostructures for optoelectronic devices

M. Kawasaki

WPI Advanced Institute for Materials Research (AIMR), Tohoku University, Japan

CREST, Japan Science and Technology Agency (JST), Tokyo, Japan

Keywords: ZnO, Ultraviolet LED, Quantum Hall Effect, Transistor, Polar Interface

ZnO powder is a well-known chemical product used as an additive of automobile-tire rubbers and cosmetics (baby-powders). At the same time, ZnO is a key material for sensor devices and as transparent conducting thin films used in displays and solar cells. We focused our efforts on making epitaxial ZnO thin films with using the knowledge of cutting-edge oxide epitaxy technology [1, 2] aiming at optical functionalities, because ZnO has a direct wide bandgap 3.3eV (ultraviolet regime) and a huge exciton binding energy of 60meV. Actually, stimulated emission [3] and laser action [4] were demonstrated by us to trigger intensive research on ZnO ultraviolet emitting devices world-wide [5]. The bandgap could be tuned by alloying with CdO or MgO [6, 7], enabling heterostructures and superlattices [8]. Clear demonstrations of oxides as tuneable semiconductors drove our motivation into magnetic semiconductors [9-13] and thin film transistors [14] as well. The difficulty was making ZnO into p-type caused by the tendency of naturally n-type character due to defect. We spent much effort for making ZnO as intrinsic as possible [15, 16] and finally succeeded in valence control of ZnO by nitrogen doping and *pn* ZnO homojunction light emitting diodes (LED) [17, 18]. Recent activities are also directed in quantum Hall effect (QHE) [19] that was introduces as an important milestone of oxide electronics [20]. Since ZnO is a polar material and spontaneous polarization does not match at the ZnO/MgZnO interface, two dimensional electron gas (2DEG) is accumulated at the ZnO side of the interface.

These efforts have been made by using a thin film technology called as “Pulsed Laser Deposition (PLD)” that may be unfamiliar to the compound semiconductor researchers. Along with our study, we identified a very critical drawback of PLD for the study of semiconductor heterostructures, *i.e.,* this film purity never to be better than that of sintered ceramics target (usually 100ppm level impurities such as Si and Al). Our fortune during the research above was that we can buy highly pure ZnO single crystals that could be used as a target in PLD. However, we were never be able to grow highly pure MgZnO. We solved this problem by switching to “Molecular Beam Epitaxy. (MBE)”. We could fabricate atomically smooth $Mg_xZn_{1-x}O$ ($0 \leq x \leq 0.44$) films on Zn polar ZnO single crystal substrate. The residual donor densities are less than $10^{15}cm^{-3}$. By using a proper nitrogen agent, *p*-type MgZnO could be grown and clear ultraviolet emission was demonstrated from heterostructure LED. The mobility of 2DEG was also improved quite a lot for MBE grown heterostructures, reaching to $20{,}000cm^2/Vs$ [21, 22]. With spin-coating of poly (3,4-ethylenedioxythiophene) poly (styrenesulfonate) (PEDOT:PSS) on ZnO, nearly ideal Schottky junctions could be formed [23]. These Schottky junctions are useful for visible-blind or solar-blind ultraviolet sensors [24, 25]. From capacitance-voltage (*C-V*) relations of Schottky junction made on MgZnO/ZnO heterostructure, we could profile the carrier concentration along depth that clearly indicated the presence of 2DEG as designed. Metal-semiconductor field effect transistors (MES-FET) with a Hall-bar geometry clearly showed that the quantum transport such as Shubnikov-de Haas (SdH) oscillation and QHE were modulated by the tuning of the sheet charge density in the channel of the MES-FET.

References

1. M. Kawasaki et. al., *Science* **266** 1540 (1994)
2. "New Features" J. Heber, *Nature*, **459** 28 (2009)
3. P. Yu et. al., *Solid State Commun.* **103**, 459 (1997)
4. Z. K. Tang et. al., *Appl. Phys. Lett.* **72**, 3270 (1998)
5. "News": R. Service, *Science*, **276**, 895 (1997)
6. A. Ohtomo et. al., *Appl. Phys. Lett.,* **72,** 2466 (1998)
7. T, Makino et. al., *Appl. Phys. Lett.,* **78,** 1237 (2001).
8. A. Ohtomo et. al., *Appl. Phys. Lett.,* **75,** 980 (1999).
9. T. Fukumura et. al., *Appl. Phys. Lett.,* **75,** 3366 (1999).
10. Y. Matsumoto et. al., *Science*, **291** 854 (2001).
11. T. Fukumura et. al., *Appl. Phys. Lett.,* **78,** 958 (2001).
12. Z. Jin et. al., *Appl. Phys. Lett.,* **78,** 3824 (2001).
13. H. Toyosaki et. al., *Nature Mater.* **3**, 221 (2004).
14. J. Nishii et. al., *Jpn. J. Appl. Phys.*, **42** (2003).
15. A. Ohtomo et. al., *Appl. Phys. Lett.,* **75,** 2635 (1999).
16. A. Tsukazaki et. al., *Appl. Phys. Lett.*, **88**, 152106 (2006).
17. A. Tsukazaki et. al., *Nature Mater.* **4**, 42 (2005).
18. A. Tsukazaki et. al., *Jpn. J. Appl. Phys.*, **44**, L643 (2005).
19. A. Tsukazaki et. al., *Science*, **315**, 1388 (2007).
20. "Perspective" A. P. Ramirez, *Science*, **315**, 5817 (2007).
21. A. Tsukazaki et. al., *Appl. Physics Express,* **1**, 055004 (2008).
22. "News and Views" Y. Tokura and H. Y. Hwang, *Nature Materials*, **7**, 694 (2008).
23. M. Nakano et. al., *Appl. Phys. Lett.,* **91**, 142113 (2007).
24. M. Nakano et. al., *Appl. Phys. Lett.,* **93**, 123309 (2008).
25. M. Nakano et. al., *Appl. Phys. Express,* **1**, 121201 (2008).

New two-dimensional electronic systems at the surface of organic crystals

A.F.Morpurgo

DPMC and Gap, University of Geneva, 24 quai Ernest-Ansermet, CH1211 Geneva, Switzerlands

Keywords: Organic transistors, Frohlich polarons, electron-hole transport, molecular crystals

The investigation of the electronic properties of organic materials is strongly motivated by the relevance of these materials for device applications, such as field-effect transistors, organic light-emitting diodes, solar cells, etc. When considering these devices, it is clear that –in essentially all cases- their performance is determined not by a single organic material, but rather by interfaces between two different materials. In transistors, the key interfaces are those between the organic semiconductor and the gate dielectric (channel) and between the organic semiconductor and a metal (contact). In organic LEDs and solar cells, the interface between two different organic materials is where the relevant processes (light emission and light absorption) take place.

In this talk I will mainly discuss electronic transport at two different interfaces, namely organic/dielectric interfaces and organic/organic interfaces. In the first case, I will show how the polarizability of the gate dielectric crucially determines the mobility of charge carriers in organic transistors. The microscopic mechanism is the formation of interfacial Frohlich polarons, where a hole at the interface self-localizes through the interaction with its polarization cloud in the dielectric, so that hole and polarization cloud act as an individual elementary excitation. At high carrier density we also observe strong coulomb interactions between the polarons, that have a large effect on the electrical characteristics of the transistors. Comparison of data and theory shows that a well-defined macroscopic models captures essentially all aspects of our experiments at an unprecedented quantitative level.

For the case of organic/organic interfaces I will present results on a new system formed by laminating a crystal of TCNQ and a crystal of TTF on top of each other. TCNQ and TTF are both large gap semiconductors and essentially insulators in the bulk. However, we find that at these interfaces a very large charge transfer takes place –comparable to that occurring in bulk TTF-TCNQ- so that the interface of the two materials become conducting. In the highest quality samples, the temperature dependence of the conductivity is metallic down to the lowest temperature at which measurements were done (~40 K). The experiments indicate that these TTF-TCNQ interfaces are a new electronic system where a high density electron gas is facing at a distance of a few Angstroms a high density hole gas, with only very weak electronic coupling.

Finally, if time will allows, I will go very rapidly through several other results recently obtained on organic single-crystal transistors, in which a quantitative understanding of the data has been possible in terms of well-defined microscopic models. This is the case, for instance, for transport across metal/organic interfaces and for the shift of the threshold voltage as a function of channel length (from which we successfully extracted the value of the effective mass of charge carriers in rubrene).

References

1.H. Alves *et al.*, Nature Materials **7**, 574 (2008)
2. S. Fratini *et al.*, New. J. Phys. **10**, 033031 (2008).
3. A.S. Molinari *et al.*, Appl. Phys. Lett. **92**, 133303 (2008)
4. I.N. Hulea *et al.*, Nature Materials **5**, 982 (2006)

Double quantum-dot devices in triple-layer graphene

S. Moriyama*, D. Tsuya*, E. Watanabe*, S. Uji*,
M. Shimizu**, T. Mori**, T. Yamaguchi**, and K. Ishibashi**
* *National Institute forMaterials Science (NIMS), Tsukuba, Japan*
** *Advanced Science Institute, RIKEN, Wako, Japan*

Keywords: Graphene, Semimetal, Quantum dots, Single-electron transport

Graphene, a single atomic layer of graphite, and few-layer graphene (FLG) sheets are one of the attractive two-dimensional (2-D) conducting materials for a new stage of low dimensional physics [1-3]. Electronic properties are expected to differ from the well studied case of the 2-D electron gas in semiconductor hetero-structure. These differences are due to the unique band structure of graphene, so-called 'Dirac Cone', which exhibits electron-hole degeneracy and vanishing carrier mass near the point of charge neutrality [4]. From the application point of view, the ballistic transport and high mobility in graphene and FLG make them possible candidates for future electronic quantum devices. Nanostructures on graphene or FLG sheets can be fabricated by carving out of the graphene sheets directly [5-7]. In addition to that, the spread 2-D sheet structure may open a door to realize the integrated quantum nano-device system.

Here, we demonstrate double quantum-dot devices in triple-layer graphene, which exhibits single-electron transport of two lateral quantum dots coupled in series. Coupled quantum-dot systems have been proposed for various applications as new logic and architectures, such as the quantum computation and the quantum cellular automata. Our results suggest an important step for the realization of the integrated quantum devices in graphene-based nanoelectronics.

Graphene and FLG samples are prepared by micromechanical cleavage of graphite crystals and deposited on the surface of a silicon substrate with a 290 nm thickness of oxidized silicon. Optical microscope contrast and Raman spectroscopy measurements can be used to identify the single-, double-, triple-, and few-layer graphene flakes on the substrate [8]. From the micro-Raman spectroscopy, we confirmed that our devices were fabricated on a triple-layer graphene (TLG) sheet. By using electron-beam lithography techniques, a double-dot device structure was patterned into a thin ZEP resist that protected chosen areas during the oxygen reactive ion etching process. The devices consisted of two isolated island as quantum dots, connected via two short constrictions to wide source and drain regions. Quantum dots were designed in a triangular shape, and the connected constrictions were about 20 nm in length and 15 nm in width. These constrictions were expected to act as tunnel barriers due to the quantum size effect.

Low-temperature transport measurements have been carried out in the double-dot device at the dilution refrigerator. The experimental results revealed the honeycomb charge stability diagrams from weak to strong interdot tunnel coupling regimes. At the conference, the details on the electron transport characteristics of the graphene-based coupled quantum dots will be reported.

References

1. K.S. Novoselov et al., Science **306**, 666 (2004).
2. K.S. Novoselov et al., Nature **438**, 197 (2005).
3. Y. Zhang et al., Nature **438**, 201 (2005).
4. A.K. Geim and A.H. MacDonald, Physics Today **60**, 35 (2007).
5. M.Y. Han et al., Phys. Rev. Lett. **98**, 206805 (2007).
6. C. Stampfer et al., Appl. Phys. Lett. **92**, 012102 (2008).
7. L.A. Pomarenko et al., Science **320**, 356 (2008).
8. A.C. Ferrari et al., Phys. Rev. Lett. **97**, 187401 (2006).

Elementary process of electromigraion at gold nanojunctions

A. Umeno, K. Yoshida, S. Sakata and K. Hirakawa

Institute of Industrial Science and INQIE, Univ. of Tokyo, 4-6-1 Komaba, Meguro-ku Tokyo, 153-8505 Japan

CREST-JST, 4-1-8 Honcho, Kawaguchi, Saitama 332-0012, Japan

Keywords: electromigration, break junction, gold nanojunction

Excess amount of electrical current through metallic wires induces electromigration (EM) of metallic atoms and leads to failures of metal wires. The EM of metallic nanojunctions has been attracting much attention as a method to fabricate nanogaps with spacings less than 1 nm, which can interface quantum states in individual molecules with macroscopic circuitry. However, since the fabrication yield of molecular junctions has been typically no more than 10 %, deeper understanding of underlying physics of EM is highly required [1].

In this work, we have investigated EM at gold nanojunctions as small as several tens of atoms. Junction conductance showed successive drops by one conductance quantum, corresponding to one-by-one removal of gold atoms, only when the junction voltage exceeded certain critical values, V_C. The peak position in the histogram of V_C agreed with activation energy for surface diffusion of gold atoms. This fact indicates that the elementary process of EM in such small junctions is the self-diffusion of a single gold atom driven by microscopic kinetic energy transfer from only one conduction electron.

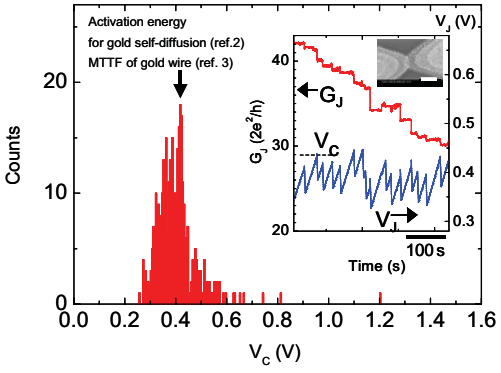

Fig.1 A histogram of the critical voltages, V_C, for inducing step-like drops in junction conductance, G_J. Insets are the time evolution of G_J and junction voltage V_J, and a SEM picture of the gold nanojunction (scale bar 200 nm).

The samples used in the present study were weak gold junctions fabricated by e-beam lithography and subsequent shadow evaporation of gold (Fig. 1 inset). The junctions were subjected to a controlled voltage application with monitoring the junction conductance. When the junction showed a precursor of EM during ramping up the voltage, which appeared as rapid decrease in conductance, the voltage was reduced to settle down the EM. This careful stress-and-relax voltage control was repeated and the junction was gradually broken to form nanogaps.

We have found that as the junction conductance became less than few tens of G_0 (= $2e^2/h$), it began showing step-like drops by G_0 only when the junction voltage exceeded certain critical values, V_C (Fig.1 inset). As shown in Fig. 1, a histogram of V_C was found to exhibit a maximum at 0.4 V, which coincide with the activation energy for diffusion process of surface gold atoms [2] and with the activation energy for the mean time to failure (MTTF) determined empirically from the reliability data for gold wires, 0.42±0.02 eV [3]. These results indicate that the elementary process of the EM is a removal of single metallic atom driven by an energy transfer from only one conduction electron. This view is significantly different from conventional understandings on EM such as cumulative momentum transfer from high-density electron flow (electron wind force). This new insight will help control EM at nanoscale to form molecular junctions with higher yields and better reproducibility.

References

1. H. Park *et al*. Nature (London) **407**, 57 (2000). 2. S. Günther *et al.* Surf. Rev. Lett. **4**, 1103 (1997). 3. M. Etzion *et al.* J. Appl. Phys. 46, 1455 (1975).

Novel Transduction Schemes for Nanoelectromechanical Systems

Q. P. Unterreithmeier, T. Faust, E. M. Weig and J. P. Kotthaus
Fakultät für Physik and Center for NanoScience (CeNS), Ludwig-Maximilians-Universität, München, Germany

Keywords: Nanoelectromechnanics, Nonlinear Mechanics

Micro- and Nanoelectromechanical Systems (NEMS/MEMS) are a rapidly growing field of science. In particular, these systems can be coupled relatively easily to their environment offering unmatched sensitivities concerning e.g. mass, charge and spin. Typically, the sensitivity is inversely proportional to the mass of the resonators; therefore a reduction in size is desirable. However, with decreasing size, the task for actuating the system as well as detecting the resonant motion becomes increasingly difficult. For both, fundamental science as well as applications, it is highly desirable, that a transduction scheme is not bound by specific requirements such as material, geometry or temperature. We present two experiments concerning novel and widely applicable transduction schemes. The first scheme is based on dielectric gradient forces [1]. Here, the nanomechanical resonator is electrostatically polarized by subjacent gold electrodes, that are DC-biased (see Fig. 1). The thereby created inhomogenous electric field, leads to an attractive force towards the electrodes. A superimposed RF signal couples to the influenced dipole moment. This gives rise to an oscillating dipolar force, and can be easily extended to GHz frequencies. Moreover, as the oscillating dielectric force is proportional to both the DC bias as well as the RF voltage, one has two independent parameters to adjust the amplitude of the displacement. We present room-temperature measurements, that prove the actuation scheme to be highly effective. In addition, it is demonstrated to allow easy frequency tuning and quantitative studies of the nonlinear mechanical behaviour.

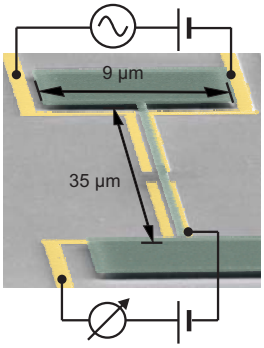

Figure 1: SEM and schematic setup; the gold electrodes and the suspended beam are highlighted for clearance.

By reversing the actuation principle, that is measuring the capacitance between the subjacent electrodes modulated by the mechanical displacement, we are also able to detect the resonant motion of our mechanical element.

We present a second experiment, that equally enables on-chip detection. Here we utilize the mechanical modulation of a locally generated photocurrent. This is implemented by illuminating the sample with monochromatic light. Caused by scattering and interference, the magnitude of the local light intensity is modulated by the oscillation of the mechanical element. To transduct the signal, we process a Schottky contact beneath the resonator. Mechanically generating an oscillating photosignal across the Schottky diode, we achieve a sensitivity of $3\mathrm{pm}/\sqrt{\mathrm{Hz}}$; and are able to detect the Brownian motion of our resonator at room temperature.

References

[1] Q. P. Unterreithmeier, E. M. Weig and J. P. Kotthaus Nature, *in press*

Manipulating the dynamical potential well of a parametric resonator

Imran Mahboob, Charline Froitier and Hiroshi Yamaguchi
NTT Basic Research Laboratories, NTT Corporation, Atsugi-shi, Kanagawa 243-0198, Japan

Keywords: electromechanical oscillator, parametric resonance, non-linear, symmetry lifting

Parametrically modulated resonators can be described in the rotating frame approximation where the resonator's position is expressed as $x(t) \approx P(t)\sin(\omega t)+Q(t)\cos(\omega t)$ with the slowly varying dynamical variables $P(t)$ and $Q(t)$. The energy map of the parametric resonator in PQ space reveals a dynamical (as the resonator is driven and far from thermal equilibrium) double well potential where the two minima correspond to the two stable phases of oscillation (0 and π) separated by π radians. The probability that the system will occupy either state is universally $\frac{1}{2}$ and examples include RLC circuits, electrons in Penning traps as well as mechanical oscillators. Previously, this dynamical potential has been utilised for binary logic and memory applications [1]. Enormous scope exists for exploiting parametric resonators for sensors as well as for the study of quantum physics in macroscopic systems. The key to developing these applications is the ability to control and manipulate the dynamical potential well.

An electromechanical resonator was realised from a GaAs/AlGaAs heterostructure in which parametric resonances could be excited via the piezoelectric effect. Previously, this system was utilised for Parametron based mechanical memory, parametric amplification and ultrasharp mechanical resonances. Here we extend this system architecture and demonstrate for the first time that by applying a weak secondary excitation at exactly half the parametric actuation frequency enables the dynamical potential to be modulated. This enables the number of potential wells and the barrier heights to be controlled as well as enabling the symmetry in the dynamical potential to be lifted with perturbations as small as 10^{-15} J to the barrier resulting in a favoured oscillation phase.

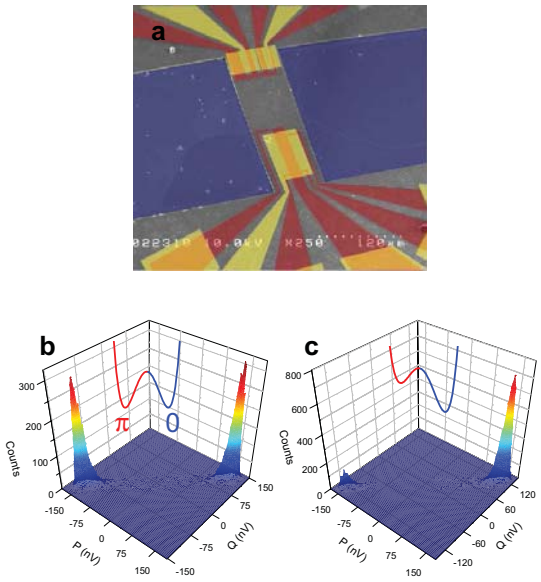

Figure 1: **a** An SEM image of the parametric electromechanical resonator consisting of a GaAs beam embedded with a two dimensional electron system integrated with Schottky contacted Au electrodes. The beam has a length, width and thickness of 260, 84, 1.35 μm respectively and a resonance frequency of 159178.7 Hz with a quality factor of 93000. **b, c** The stability diagram is constructed by plotting the number of events as a function of $P(t)$ and $Q(t)$ and it indicates the amplitude and phase at which the electromechanical resonator is most likely to be found. **b** In the first case, the resonator has two oscillation states with equal occupancy corresponding to 0 and π oscillation phases indicating a symmetric dynamical potential well. **c** However, when the additional field excitation is activated, the stability diagram reveals that the resonator prefers to oscillate only with the 0 phase indicating that symmetry has been lifted in the dynamical potential well.

References

[1] I. Mahboob and H. Yamaguchi, Nature Nanotech. **3**, 275 (2008).

July 23 (Thursday)

16:00 – 18:00

Poster Session Th-mP

Meeting Room 501, 502

MSS-EP2DS Parallel session

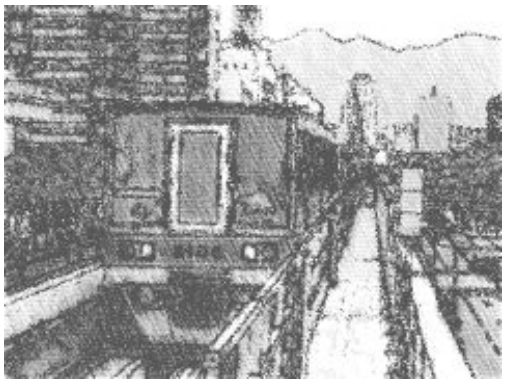

Port liner

Highly-reduced Fine-structure splitting in InAs/InP quantum dots offering efficient on-demand 1.55 μm entangled photon emitter

Lixin He*, Ming Gong*, Chuan-Feng Li*, Guang-Can Guo* and Alex Zunger**
*Key Laboratory of Quantum Information, University of Science and Technology of China, Hefei, China
** National Renewable Energy Laboratory, Golden, Colorado, 410012,USA

Keywords: entangled photon, quantum dots, fine structure, quantum information

Entangled photon pairs distinguished themselves from the classically correlated photons because of their non-locality and therefore play a crucial role in quantum information applications, including quantum teleportation, quantum cryptography and distributed quantum computation, etc. Traditionally, an entangled photon pair is generated through spontaneous parametric down conversion process (SPDC) process. However, this nonlinear process occurs randomly with very low probability, and even worse there is a finite probability of generating more than one photon pair in a excitation cycle. The multiple photon pairs degrade the fidelity of the optical quantum gates. It also opens up a security threat in the quantum communication. Therefore an "event-ready" entangled photon source is highly desirable. Benson *et al*. [1] proposed that a biexciton cascade process in a self-assembled QD can be used to generate the "event-ready" entangled photon pairs, which has recently been demonstrated using the (In,Ga)As/GaAs quantum dot(QD) [2]. However, a genuine finite energy difference between photons with different polarizations, known as the fine structure splitting (FSS), can destroy the entanglement of the photon pairs. To achieve entanglement from (In,Ga)As/GaAs QD, it was, indeed, necessary to cherry-pick a sample with extremely small FSS from a large number of samples, or to apply strong in-plane magnetic field. Furthermore, the emission wavelength of (In,Ga)As/GaAs QD (880 - 950 nm) is mismatched with the 1.55 μm needed for communications using the optical fibers. Using theoretical modeling of the fundamental causes of FSS in dots, we predict [3] that altering the matrix material around the InAs dot from GaAs to InP would simultaneously overcome the above two difficulties in the InAs/GaAs QDs, because (i) the intrinsic FSS of the InAs/InP QDs is predicted to be an order smaller than that in InAs/GaAs QDs and (ii), the excitonic gap matches the 1.55 μm fiber optical wavelength, and far away from the wetting layer background emissions. Combining these advantages, one can expect that the InAs/InP QDs can play a crucial role in the quantum information applications, as a new generation of "on-demanding" entangled photon source.

References

[1] O. Benson et al., Phys. Rev. Lett. **84**, 2513 (2000).

[2] R. M. Stevenson et al., Nature (London) **439**, 179 (2006).

[3] L. He et al. Phys. Rev. Lett. **101**, 157405 (2008).

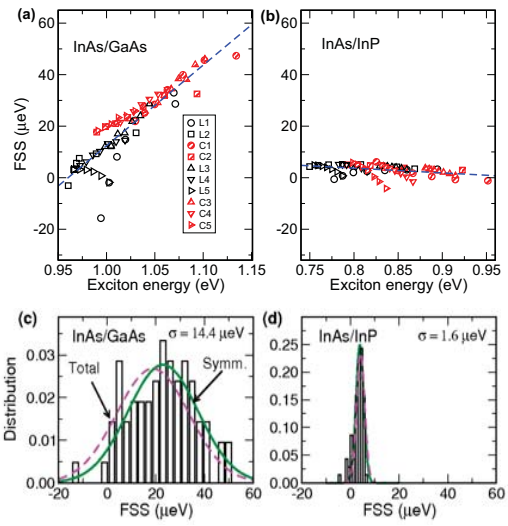

Figure 1: The upper panel shows the FSS vs the exciton energy for (a) InAs/GaAs and (b) InAs/InP QDs. The lower panel shows the FSS distributions for (c) InAs/GaAs and (d) InAs/InP QDs. The solid lines are fitted by Gaussian functions for all shape-symmetric QDs, whereas the dashed lines represent the distributions of the FSS of total samples including also the asymmetric dots. σ is the standard deviation of the distribution.

Interference of photons from a weak laser and a quantum dot

A. J. Bennett*, R. B. Patel*,**, C. A. Nicoll**, D. A. Ritchie** and A. J. Shields*

** Toshiba Research Europe Limited, Cambridge Research Laboratory, 260 Science Park, Milton Road, Cambridge, CB4 OWE, U. K.*

*** Cavendish Laboratory, Cambridge University, JJ Thomson Avenue, Cambridge, CB3 0HE, U K.*

Keywords: Entanglement, quantum dots, coherence

The ability to create photons in defined quantum states is a pre-requisite of optical quantum information processing. To make such schemes scalable it is essential to be able to interfere photons from separate sources. In particular, a practical quantum repeater may require integration of quantum cryptography schemes that rely on weak lasers with more-exotic sources of non-classical photons.

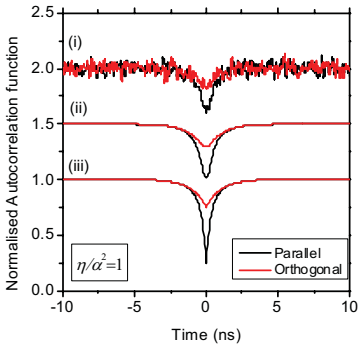

Fig.1 Correlations on the outputs of the beamsplitter as function of delay between the detectors. Data (i) was recorded for the case of equal intensity sources with parallel (black) and orthogonal (red) polarsiations. We also show the predicted correlation functions for infinitely fast detectors (iii) and realistic detectors (ii).

Here demonstrate two-photon interference with photons from two unsynchronized sources operating via different physical processes, with different photon statistics. One source is spontaneous emission from the X^- state of an electrically-driven InAs/GaAs single quantum dot with μeV linewidth, the other stimulated emission from a laser with a neV linewidth. We mix the emission from these sources on a balanced non-polarising beamsplitter and measure correlations in the photons that exit using Si-avalanche photodiodes and a time-correlated counting card. By periodically switching the polarisation state of the weak laser we are able to simultaneously measure the correlation for the case of parallel and orthogonally polarised sources, corresponding to maximum and minimum degrees of interference. One set of data is shown in Fig.1 for the case where the two sources have the same intensity. A reduction in the correlation function at time zero for the case of parallel photon sources clearly indicates we are able to observe this interference effect.

To quantify the degree of interference, we develop a theory that predicts the correlation function. Data and experiment are then compared for a range of intensity ratios. We find that the experimentally measured interference visibility is limited by the relative time scales of the detector response time and the coherence of the quantum dot sources. Based on this analysis we infer a wave-function overlap of 91%, which is remarkable given the fundamental differences between the two sources.

References

1. A. J. Bennett *et al*, in preparation.

Photon correlation spectroscopy of a single quantum dot within a photonic bandgap

M. Shirane[1,2], Y. Igarashi[1,2], Y. Ota[2,3], M. Nomura[2], N. Kumagai[2], S. Ohkouchi[1,2], A. Kirihara[1,2], S. Ishida[2], S. Iwamoto[2,3], S. Yorozu[1,2], and Y. Arakawa[2,3]

[1]*Nano Electronics Research Laboratories, NEC Corporation, Tsukuba, Japan,*
[2]*Institute for Nano Quantum Information Electronics, the University of Tokyo, Tokyo, Japan*
[3]*Research Center for Advanced Science and Technology, the University of Tokyo, Tokyo, Japan*

Keywords: quantum dots, photonic bandgap, photon correlation, biexciton-exciton cascade

Semiconductor quantum dots (QDs) provide the key devices for quantum information processing [1,2], in which the investigation and control of the carrier dynamics is very important. Photonic crystal structures are often utilized to modify the radiative decay rate of excitons confined in the QDs. When the exciton is put within a photonic bandgap (PBG), its lifetime becomes longer compared to that without PBG. This will enable us to access carrier interactions in the QDs, which are hidden in a conventional situation. In this paper, we investigated the carrier dynamics in a single InAs QD within the PBG by the photon correlation spectroscopy.

The sample was grown by molecular-beam epitaxy on a GaAs substrate. A single layer of InAs self-assembled QDs (density of ~3×10^8 cm^{-2}) was put in the center of a 165-nm-thick GaAs membrane on an AlGaAs sacrificial layer. Then a photonic crystal structure of the triangular lattice was made with a 238-nm lattice constant and a 62-nm air hole radius. The two-dimensional PBG lies between 700 nm and 950 nm according to our calculation with the FDTD method. The sample was cooled down to ~10 K and optically excited by a Ti:sapphire laser with a beam spot size of 3 μm.

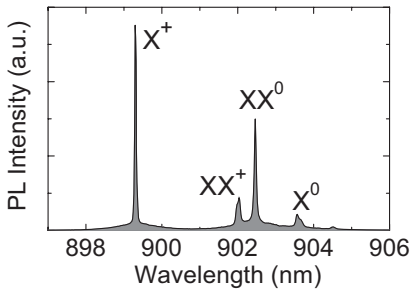

Fig 1: PL spectrum of the single QD in the PBG

Figure 1 shows the photoluminescence spectrum of the QD within the 2D PBG. Based on their pump power dependences and energy differences, the four main peaks were identified as the positively charged exciton (X^+), biexciton (XX^+), and the neutral biexciton (XX^0) and exciton (X^0). The lifetime of X^0 estimated by the time-resolved PL intensity was 4.6 ns, which is ~4 times longer than that of intrinsic QDs. Figure 2 shows the measured photon correlation function of $g^{(2)}(\tau)$ for (a) XX^+-X^+ and (b) XX^0-X^0 using a Hanbury-Brown and Twiss type setup. The observed anti-bunching ($g^{(2)}(\tau)<1$) at $\tau<0$ together with the bunching ($g^{(2)}(\tau)>1$) at $\tau>0$ is a clear evidence of the biexciton-exciton cascade emission. The polarization-dependent $g^{(2)}(\tau)$ was also measured, and our result was explained by the spin-spin interaction of the neutral exciton.

This work was supported by the Special Coordination Funds for Promoting Science and Technology.

References

1. P. Michler et al., Science **290**, 2282 (2000).
2. N. Akopian et al., Phys. Rev. Lett. **96**, 130501 (2006).

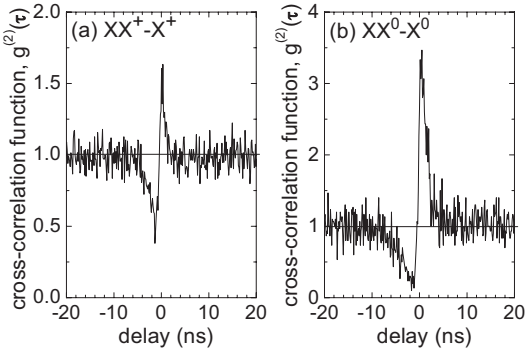

Fig 2: Photon cross-correlation function

Electron – phonon interaction in Quantum Cascade Lasers subjected to a strong magnetic field

Y. Chen*,**, N. Regnault*, R. Ferreira*, Bang - Fen Zhu** and G. Bastard*

* *LPA – ENS Paris (France)*

** *Department of Physics, Tsinghua University, Beijing (China)*

Keywords: Quantum Cascade Lasers, quantum transport, magneto - polarons

We report a theoretical study of the carrier relaxation in Quantum Cascade Lasers subjected to a quantizing magnetic field when the electron energy difference are tuned to the LO phonon energy. The QCL structure is modelled as a single quantum well subjected to a quantizing magnetic field applied parallel to the growth direction. We are interested in the non radiative escape of electrons in the n = 0 Landau level (LL) of the E_2 subband towards the p^{th} Landau state of the E_1 subband. This escape can be resonant when $E_2 - E_1 = p\hbar\omega_c + \hbar\omega_{LO}$. The LL broadening is computed either numerically or by means of the self consistent Born approximation. The static scatterers are the short range alloy fluctuations that are known to be the most efficient scatterers of the $Ga_{0.47}In_{0.53}As$ alloys. The simpler calculation consists in using the Fermi golden≈ rule to compute the escape rate to $|E_1,p>$ LL. Such calculations predict a very fast rate (8.5 ps^{-1} at maximum), as a result of the strong Landau quantization (B ≈ 25T if p = 2). However, these results are unreliable because the ensuing level broadening due to the electron - phonon interaction is comparable to the unperturbed Landau level width.

Actually, LL's that are unbroadened by alloy scattering have highly singular densities of states. This leads to the formation of magneto – polarons when they interact with optical phonons (Fröhlich coupling). The latter are entanglement of $|E_2,0>$ LL states with 0 phonon and the 1LO replica of $|E_1,p>$ states. For p = 2, the magneto – polaron gap is ≈ 4 meV at resonance. We have studied the broadening of the p =2 magneto – polarons due alloy scattering. Results for their widths and densities of states will be detailed at the conference. Since, Fermi golden rule is meaningless for these mixed elementary excitation, we studied the survival probability P_s in the $|E_2,0>$ LL numerically once the carrier has been injected into one of the $|E_2,0>$ state. This survival probability displays oscillations versus time at the Rabi frequency corresponding to the magneto –polaron gap. At resonance, P_s converges to ½ at long time. In other words there is no irreversible departure from the upper Landau level when the alloy broadening effects is taken into account within the polaron basis but only an equalization of the probability of being in $|E_1,p>$ and $|E_2,0>$ Out of resonance, P_s oscillates between 1 and 1 - α to stabilizes at 1 - α/2. This result is analogous to the those found for elastic scattering between LL's belonging to different subbands[1].

Restricting the alloy scattering to the polaron basis is however insufficient. There is a very large number of "uncoupled" states, eigenstates of the interacting electron and phonon Hamiltonian, that are orthogonal to the polaron states and that can be coupled to them by the alloy scattering. They act as a sink for the electrons and make that the survival probability in the $|E_2,0>$ LL converges to zero at long time. This does not imply any validity of the Fermi golden rule because the $|E_2,0>$ LL empties in a non exponential fashion, even displaying some remnant of the polaron oscillations discussed above. Finally, we shall present plots of the long time limit of P_s versus magnetic field. The ΔB width of these plots are compatible with the those of the oscillatory output of the Ga(In)As QCL versus magnetic field[2].

References

1. N. Regnault, R. Ferreira and G. Bastard , Phys. Rev. B **76**, 176121 (2007).
2. A. Leuilet et al. Phys. Rev.**73**, 085311 (2006).

Evidence for photon anti-bunching in acoustically pumped dots

O. D. D. Couto, Jr.*, S. Lazić*, F. Iikawa**, J. Stotz***, R. Hey, and P. V. Santos*

** Paul-Drude-Institut für Festkörperelektronik, Berlin, Germany*

*** Institute of Physics, University of Campinas, Campinas-SP, Brazil*

****Department of Physics, Engineering and Astronomy, Queens University, Kingston, ON, Canada*

Keywords: single photon emitters, acoustic transport, surface acoustic waves

Single-photon-sources (SPSs) are essential components for quantum information processing. Among the different approaches for the realization of semiconductor-based SPSs, an interesting one is based on the transport of photoexcited electrons and holes by surface acoustic waves towards a quantum dot (QD), where they recombine emitting single photons [1]. The repetition rate of these SPS, which can be combined with SAW-based spin transport, is determined by the SAW frequency f_{SAW} and can easily reach 1 GHz.

The realization of a SAW-based SPS requires a high-mobility quantum well (QW) transport channel with an embedded QD. Here, we demonstrated the realization of such channels via the growth of an (Al,Ga)As QW via molecular-beam epitaxy (MBE) on (311)-GaAs substrate pre-structured with mesas. The mesas in form of "wires" and triangular "dots" were defined by optical lithography (cf. Fig.1(a)). The particular growth mode on theses substrates leads to the formation wires at the edges of the mesa. The optical properties of the wires were investigated by generating carriers in the QW in a spot within the SAW beam (G, cf. inset of Fig.1(b)). The SAW transports them to the dots, where they are captured and recombine, giving rise to photoluminescence (PL). The remotely excited, spectrally resolved PL from the dots consists of a series of sharp lines, which indicate the recombination in quantized potentials. These are attributed to potential fluctuations probably located close to the triangle corners. The energetic spacing between the lines $\Delta E \sim 3$ meV corresponds to a thickness change one step height (about 0.43 nm) on the (311) surface. Time-resolved PL traces measured for pulsed excitation in the QW are shown in Fig.1(b). The delay of the PL relative to the excitation pulse corresponds to the SAW propagation time from G to the dots, thus indicating that the electrons and holes are transported with the SAW velocity while trapped in successive maxima and minima of the SAW potential,

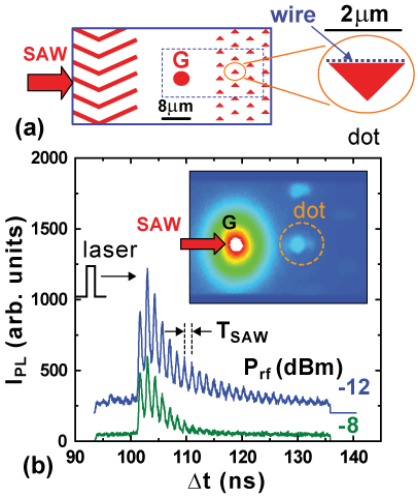

Fig.1 (a) SAW transport of carriers generated at G to triangular dots and (b) time-resolved PL from a single dot. The inset shows a PL image of the acoustic transport.

respectively. The electrons are then captured by the quantized potentials, where they recombine with holes brought in $T_{SAW}/2$ later, giving rise to the PL oscillations with the SAW frequency $f_{SAW}=1/T_{SAW}=750$ MHz. Finally, two-photon correlations studies of the emission from a single dot using a Hanbury-Brown and Twist setup show a reduced probability (by approx. 25%) for the simultaneous emission of two photons. These results demonstrate the feasibility of the concept for the realization of SAW-based SPSs.

References

1. C. Wiele, F. Haake, C. Rocke, and A. Wixforth, *Phys. Rev.* **A58**, R2680 (1998).

*Work supported by the German NanoQUIT consortium.

Spatial coherence effect on transient response of confined excitons in GaAs thin films

O. Kojima*, S. Watanebe*, T. Kita*, O. Wada* and T. Isu**
*Department of Electrical and Electronics, Kobe University, Kobe, Japan
** Department of Nano-Technology, The University of Tokushima, Tokusihma, Japan

Keywords: exciton-polariton, transient response, coherence, GaAs thin film

Ultrafast processes in nanostructured semiconductors are currently the subject of intense research. A large number of studies have been carried out to investigate their application to optical devices, including all-optical switching devices. Recently, we reported the excitonic ultrafast response owing to quantum beats and a possibillity of the ultrafast control of the excitonic states based on the Rabi oscillation in GaAs thin films [1, 2]. For the optical control of the confined excitons towards the ultrafast operating devices, the propagation velocity in mediums slower than the light velocity in vacuum modulates the exciton response. In fact, the propagation of the exciton-polariton causes a slow signal-rise in the negative time region under the exciton excitation conditions [3]. In this work, we reports the detail of the effects of spatial coherence on the transient response of confined excitons in GaAs thin films using a reflection-type pump-probe technique.

We used the double heterostructure (DH) thin films with three periods of GaAs(110nm)/$Al_{0.3}Ga_{0.7}As$(5nm) grown on a (001) GaAs substrate by molecular beam epitaxy. The transient signals were measured by using a reflection-type pump-probe technique in the temperature range from 3.4 K to 40 K. The light source was a mode-locked Ti:sapphire pulse laser with a repetition rate of 80.6 MHz and a pulse width of 100 fs. The excitation energy was 1.5158 eV, which agrees with the $n = 2$ exciton energy of the sample. The pump and probe energy densities were kept at 12 and 1.2 nJ/cm^2, respectively.

A typical transient signal under the exciton-excitation condition is shown in the inset of Fig. 1. The signal shows a rise longer than the pulse width in the negative time region. The negative time delay means that the pump pulses reach at the sample after the probe pulses reach. This rise is attributed to the propagation of the exciton polariton [3]. The signal rise time was plotted as a function of the temperature in Fig. 1. As the temperature increases, the signal rise time almost decreases linearly. This decrease indicates the disappearance of the exciton-polariton propagation triggerd by the spatial decoherence due to the exciton-phonon scattering. Therefore, we conclude that the spatial coherence has a siginificantly effect on the excitonic response in the ultrashort time region. Our results will be important for design of ultrafast devices using exciton response in terms of adjustment of the relation between the thickness and response time.

References

[1] O. Kojima, T. Isu, J. Ishi-Hayase, A. Kanno, R. Katouf, M. Sasaki, and M. Tsuchiya, J. Phys. Soc. Jpn. **77**, 044701 (2008).

[2] O. Kojima, A. Miyagawa, T. Kita, O. Wada, and T. Isu, Appl. Phys. Express **1**, 112401 (2008).

[3] S. Watanabe, O. Kojima, T. Kita, O. Wada, and T. Isu, Phys. Stat. Sol. (c), in press.

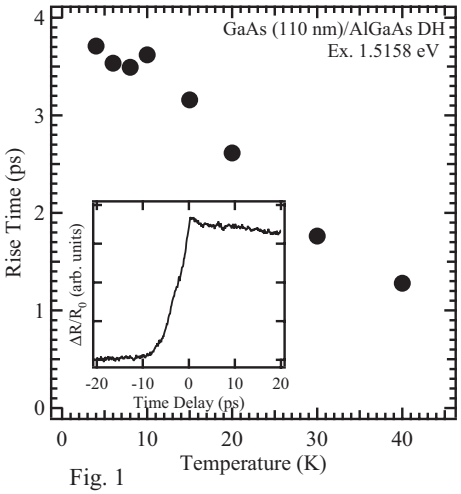

Fig. 1

Magnetoresistance oscillations in triple quantum wells under microwave irradiation

S. Wiedmann*, N. C. Mamani**, G. M. Gusev**, A. K. Bakarov** and J. C. Portal*,***
*LNCMI-CNRS, BP 166, 38042 Grenoble and INSA, 31077 Toulouse, France
** Instituto de Física da Universidade de São Paulo, São Paulo, SP, Brazil
*** Institut Universitaire de France, 75005 Paris, France

Keywords: 2D system, magnetotransport, triple quantum wells, microwave excitation

The discovery of microwave induced resistance oscillations (MIRO) and Zero Resistance States (ZRS) in 2D electron systems has demonstrated a spectacular influence of microwave irradiation on the magnetotransport and attracted much interest in experimental [1] and theoretical studies [2]. These oscillations are periodic in the inverse magnetic field and governed by the ratio between microwave frequency ω to the cyclotron frequency ω_c.

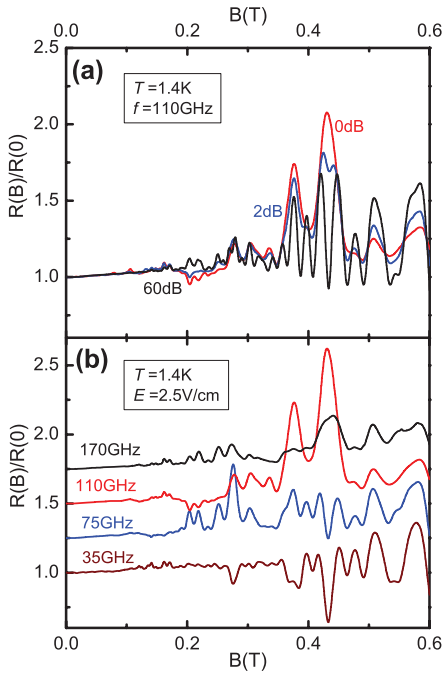

Figure 1: (a) MIS oscillations under a microwave irradiation of 110 GHz for different attenuations. For 60 dB, microwave irradiation can be neglected. (b) Frequency dependence of MIS oscillations: several MIS peaks are enhanced whereas other MIS peaks are damped or even change sign.

Recently, experiments in double quantum wells (DQWs) have shown the peculiar modification of the magneto-intersubband oscillations (MIS) due to two occupied subbands by microwave irradiation [3]. The theoretical analysis, based on the inelastic mechanism [2][3] gives a suitable explanation of the observed features in DQW structures. We have performed magnetotransport measurements in coupled GaAs triple quantum wells (TQWs) with a central well width of 200 nm and lateral well widths of 140 nm separated by a 1.4 nm barrier in a 2D electron gas with a mobility of $5 \cdot 10^5$ cm^2/Vs, exposed to a continuous microwave frequencies from 35 to 170 GHz. Without irradiation, like in DQWs, the magnetoresistance shows MIS oscillations which survive at high temperatures. A progressive irradiation of the sample (see Figure 1(a)) leads to a modified MIS oscillation picture where some MIS peaks are enhanced or suppressed or even change sign for low frequencies (see Figure 1(b)). This is in strong contrast to DQWs under microwave irradiation [3], where always groups of MIS peaks are enhanced or suppressed. In TQWs, MIS peaks behave independently. We therefore believe that this oscillation picture occurs due to special properties of TQWs where an alignment of Landau levels of three quantum wells become possible with increasing perpendicular magnetic field.

References

[1] M. A. Zudov *et al.*, Phys. Rev. B **64**, 201311(R) (2001), R. G. Mani *et al.*, Nature **420**, 646 (2002).

[2] I. A. Dmitriev *et al.*, Phys. Rev. B **71**, 115316 (2005).

[3] S. Wiedmann *et al.*, Phys. Rev. B **78**, 121301(R), (2008).

Growth and characterization of strain-compensated InGaAs/GaAsSb type II multiple quantum wells on InP Substrate

Y. Yonezawa*, R. Hiraike*, K. Miura**, Y. Iguchi**, Y. Kawamura*

* *Frontier Science Innovation Center, Osaka Prefecture University, Osaka, Japan*

** *Transmission Devices R&D Laboratories, Sumitomo Electric Industries, Ltd. Osaka, Japan*

Keywords: Type II, quantum wells, GaAsSb, InP

InGaAs/GaAsSb type II multiple quantum wells (MQWs) on InP substrates are very attractive for low dark current photodiodes in the 2 μm wavelength region, which are expected for many applications such as chemical sensing and medical diagnostics. It was proposed that introduction of strain-compensated structure makes it possible to get longer emission wavelength in InGaAs/GaAsSb type II MQWs [1]. In this work, strain-compensated InGaAs/GaAsSb type II MQWs were grown by molecular beam epitaxy (MBE) and their optical properties were studied. High quality strain-compensated type II MQWs were successfully grown, which have longer emission wavelength than that of lattice-matched type II MQWs.

InGaAs(5nm)/GaAsSb(5nm) type II MQW layers were grown on Fe-doped (100) InP substrates by solid source MBE. The growth temperature was 480°C. Tetramer As_4 and Sb_4 were used for group V beam sources. The room temperature PL intensity and the PL spectral half-width of GaAsSb layers were comparable to those of InGaAs layers.

Figure 1 shows the PL spectra at 300K of the lattice-matched type II MQWs (dash line) and strain-compensated type II MQWs (solid line), where the InGaAs layer has 0.6% tensile strain and GaAsSb layer has 0.6% compressive strain. The observed peak energy shift is 43 meV at 300K, which agrees fairly well with the calculated energy shift of 31 meV. In addition, the PL intensity of the strain-compensated MQWs is comparable to that of the lattice-matched MQWs, suggesting that the crystal quality of the strain-compensated MQWs is good.

Figure 2 shows the temperature dependence of the PL peak energy for both samples. It was found that the PL peak energy of the strain-compensated MQWs is smaller than that of the lattice-matched MQWs in all temperature range from 10K to 300K.

1. R.Sidhu, N.Duan,J.Campbell, and A.Holmes: IEEE Photon. Technol. Lett. **17**, 2715 (2005).

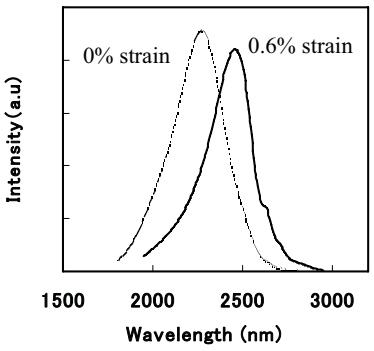

Fig.1 PL spectra at 300K

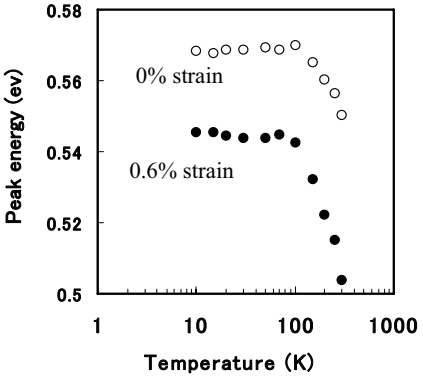

Fig.2 Temperature dependence of PL peak energy

Midinfrared photoluminescence from SnTe/PbTe/CdTe double quantum wells grown by molecular beam epitaxy

Kazuto Koike, Ryo Kawaguchi and Mitsuaki Yano

Nanomaterials Microdevices Research Center, Osaka Institute of Technology, Osaka, Japan

Keywords: SnTe, PbTe, CdTe, double quantum well, MBE

Narrow-gap IV-VI compound semiconductors such as PbTe, PbSe and SnTe has been of great interest to the development of midinfrared optoelectronic devices. These materials have no degenerated heavy hole-bands which degrade high-temperature emission by enhancing inter-valence-band absorption and nonradiative Auger recombinations. From a viewpoint of efficient emission, carrier confinement in quantum well using a newly developed lattice-matched heterosystem of rocksalt-PbTe/zincblende-CdTe can be promising for the application to midinfared optoelectronic devices [1] due to the large bandgap difference over 1.2 eV although these two tellurides crystallize in different structures.

Recently, we grew single-crystalline (100)-oriented $Pb_{1-x}Sn_xTe$/CdTe single quantum wells (SQWs) by molecular beam epitaxy (MBE), and observed midinfrared photoluminescence (PL) with a proportional red-shift to the Sn content x [2]. However, the luminance efficiency became low with increasing x presumably due to the crystallographic deterioration of the $Pb_{1-x}Sn_xTe$ layer by the difference in atomic radii. In this study, we grew SnTe/PbTe/CdTe double quantum wells (DQWs) and observed highly efficient midinfrared PL even at high temperatures.

The epitaxial growth was conducted on (100)-oriented GaAs substrates using an MBE apparatus equipped with compound sources of CdTe, PbTe, and SnTe in Knudsen cells. As illustrated by the band diagram in Fig. 1, SnTe/PbTe heterostructure is known to have type II band alignment. We expected the transition energy between electrons and holes in the DQW to be controlled by changing the SnTe thickness d as well as the PbTe thickness. In this study, we limited the thickness d less than several mono-layers to maintain the pseudomorphic growth to the PbTe layer with a 2.1% larger lattice constant.

Figure 1 shows the PL spectra at 300 K from a series of DQWs with different d values in 10-nm-thick PbTe wells. Each peak locates in a 3 - 5 μm atmospheric window and shifts toward the lower-energy side with increasing d. These emissions were observed even at higher temperatures over 300 K, and their intensities were much stronger than those of the $Pb_{1-x}Sn_xTe$/CdTe SQWs with the same wavelength, indicating the encouragement of the SnTe/PbTe/CdTe DQW structure to light emitting device application.

References

1. K. Koike, T. Tanaka, M. Yano, IPAP Conf. Series 2, Proc. NGS **10**, 39 (2001).
2. K. Koike, T. Hotei, R. Kawaguchi, M. Yano, JCG, in press.

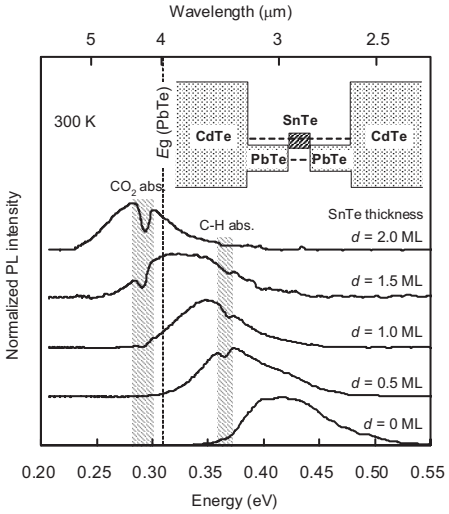

Fig. 1 PL spectra at 300 K from a series of SnTe/PbTe/CdTe DQWs with different SnTe thicknesses in 10-nm-thick PbTe wells. Inset shows a schematic diagram of the DQW band structure.

Enhancement of optical gain in Li:CdZnO/ZnMgO quantum well lasers

Hee Change Jeon[1], Seung Joo Lee[1*], Seoung-Hwan Park[2], Tae Won Kang[1], Doyeol Ahn[3], and G. Ihm[4]

[1]*Quantum-functional Semiconductor Research Center, Dongguk University, Korea*

[2]*Department of Electronics Engineering, Catholic University of Daegu, Korea*

[3]*Institute of Quantum Information Processing and Systems, University of Seoul, Korea*

[4]*Department of Physics, Chungnam National University, Korea*

Keywords: polarization, quantum well, internal field, optical gain

The wide band-gap wurtzite semiconductors have attracted much attention due to their potential applications for optoelectronic devices in blue and ultraviolet regions. Recently, ZnO and related oxides have been proposed as the new wide band-gap semiconductors for short wavelength optoelectronic device applications. With the current progress in the CdZnO material, fundamental properties of the CdZnO/MgZnO quantum well (QW) structures become very important for device applications [1].

Here we report, for the first time, electronic and optical properties of Li:CdZnO/MgZnO QW structures with spontaneous, piezoelectric polarizations, and ferroelectric dipole moment made by Li dopant.

The many-body optical gain in Li:CdZnO/MgZnO QW structures with spontaneous, piezoelectric polarizations, and ferroelectric dipole moment are investigated by using the non-Markovian gain model with many-body effects. We studied the valence band structure and the optical gain of Li:CdZnO/MgZnO QW structures theoretically. As the Cd composition increases, the sign change of the internal field is observed. The CdZnO/MgZnO QW structure with high Cd composition is found to have smaller optical gain because the strain-induced piezoelectric polarization and the spontaneous polarization in the well increase with the inclusion of Cd. Our interesting results indicate that electronic and optical properties of Li:CdZnO/MgZnO QW structures confirm the interaction between the strain-induced piezoelectric polarization and the spontaneous polarization and the ferroelectric dipole moment due to the Li existed in QW. The internal field is found to be cancelled due to the additional polarization by Li in the CdZnO/MgZnO QW structure. The optical gain greatly increases. These results demonstrate that high performance laser diode operation can be realized in Li:CdZnO/MgZnO QW structures with high Cd composition.

ACKNOWLEDGMENT

This work was supported by the Korea Science and Engineering Foundation (KOSEF) grant funded by the Korean government(MEST) (No. R17-2008-024-01000-0).

References

1. T. Makino, K. Tamura, C. H. Chia, and Y. Segawa, M. Kawasaki, A. Ohtomo, H. Koinuma, Appl. Phys. Lett. 81, 2355 (2002).

*Corresponding author e-mail: leesj@dongguk.edu

Upconversion of photoluminescence due to subband resonances in a GaAs/AlAs multiple quantum well structure

T. Hasegawa*, S. Okamoto** and M. Nakayama**

** Department of Material Science, University of Hyogo, Hyogo, Japan*

*** Department of Applied physics, Osaka City University, Osaka, Japan*

Keywords: Upconversion of photoluminescence, subband resonance, multiple quantum well, GaAs/AlAs

In semiconductor quantum well (QW) structures, resonant tunneling between spatially-separated subbands is an outstanding phenomenon under an applied electric field condition. The resonant tunneling produces a nonthermal carrier population in a higher-lying subband with a quantum number $n \geq 2$ due to an injection of carriers from the ground (n=1) subband. From the viewpoint of photoluminescence (PL), the subband resonance leads to an upconversion process from the higher-lying subband, which is also called anti-Stokes PL. Although the upconversion of PL due to the subband resonance was investigated, asymmetric double QW structures were typically used to achieve an efficient carrier injection for the upconversion [1,2]. In addition, the details of effects of subband resonances on the PL upconversion have not been revealed.

In this work, we have investigated the upconversion of PL due to subband resonances in a simple GaAs (15.3 nm)/AlAs (4.5 nm) multiple quantum well (MQW) structure embedded in a *p-i-n* diode structure, where the intrinsic layer consists of the MQW. Figure 1 shows the PL spectra as a function of applied electric field strength and the excitation laser spectrum, where the notation of En_eHHn_h indicates the interband transition between the n_eth electron subband and n_hth heavy-hole subband. The excitation energy corresponds to the E1HH1 transition energy. The upconversion-PL band labeled E3HH1 (E4HH1) sharply appears at ~95 (~150 kV/cm). The theoretical calculation of the subband energies as a function of electric field strength using a transfer-matrix method indicates that the electron subband resonances of E1(+1)-E3(0) and E1(+1)-E4(0) occur at ~95 and ~150 kV/cm, respectively, where the index of "+1" in the parenthesis indicates the first-nearest-neighbour QW on the higher potential side to a given QW with the index of "0". Thus, the appearance of the E3HH1 (E4HH1) PL at ~95 (~150) kV/cm originates from the injection of photogenerated carriers to the E3 (E4) subband from the E1 subband due to the E1(+1)-E3(0) [E1(+1)-E4(0)] resonance. The peaky profiles of the intensities of the E3HH1-PL and E4HH1-PL bands as a function of electric field strength also suggest that the subband resonance dominates the PL upconversion. Note that the E3HH1-PL band appears again at ~150 kV/cm under the E1(+1)-E4(0) resonance condition. This indicates the occurrence of the relaxation of carriers from the E4 subband to the E3 subband.

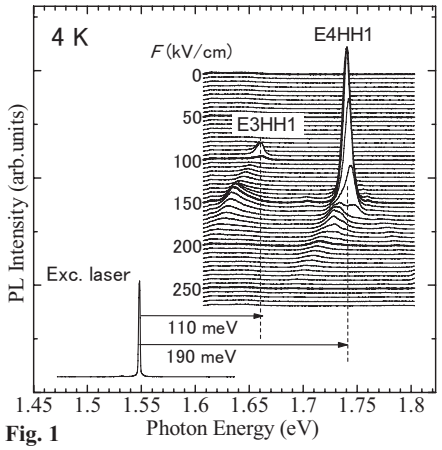

Fig. 1

References

[1] L. Schrottke *et al*., Phys. Rev B **60**, 16635 (1999).
[2] Y. Hirose *et al*., Appl. Phys. Lett, **81**, 3870 (2002).

Photoconductivity of Si/Ge/Si structures with 1.5 and 2ML of Ge layer

O. A. Shegai, V. I. Mashanov, A. I. Nikiforov, V. V. Ulyanov and O. P. Pchelyakov

Institute of Semiconductor Physics, Novosibirsk, Russia

Keywords: photoconductivity, Ge/Si interface roughness, percolation level.

Investigation of low dimensional Si/Ge structures is interesting due to possible applications in Si based technology. Our previous studies of lateral photoconductivity (PC) of Si/Ge structures with self-organized quantum dots allowed observing a stepped PC as a function of interband light intensity. Recently, a stepped and fluctuated PC of Si/Ge structures with narrow Ge layer (4ML) have been observed. In this report we compare PC studies of Si/Ge structures with integral and half-integral monolayers (ML) of Ge layers: 2 and 1.5 ML, respectively.

Si/Ge structures were grown by molecular beam epitaxy. First, a buffer Si layer of 60 nm thickness was grown on Si (100) substrate at T = 700 °C, then a Ge layer with the width of 1.5 and 2ML, respectively, was deposited at T = 450 °C, finally, a capped Si layer with 20 nm was grown at T = 300 °C. Ge layer width was controlled in situ by RHEED oscillations.

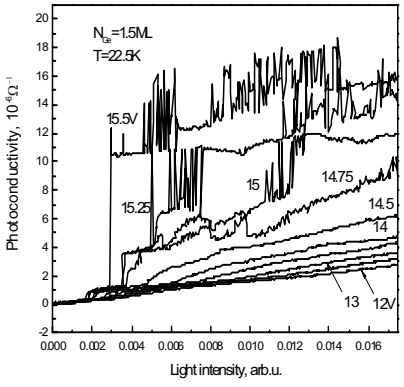

Fig.1 Photoconductivity of Si/Ge/Si structure with 1.5 ML Ge layer on light intensity for the different lateral voltages; T = 22.5 K.

PC measurements were carried out by using red LED and two-contact method, a distance between contacts is about 2 mm and illuminated area is ≈ 2x2 mm^2.

For the Si/Ge structure with 2 ML Ge layer, only monotonous PC growth with the light intensity was observed in large interval of temperatures and lateral voltages (U). Whereas, for Si/Ge structure with 1.5 ML a stepped PC was found, as shown in Fig.1. The number of steps reached four for the T = 22.5 K and U in interval of 12 – 15.5 V. Positions of steps were shifted to lower light intensities with increase in U. In addition, near steps with large amplitude, we observed fluctuations in PC.

Assuming that the studied Si/Ge structures are related to type II structures and photoexcited carriers are vertically separated for the 2 ML structure: holes are localized in Ge and electrons – in Si, respectively. For the 1.5 ML structure, in addition, lateral separation occurred due to a maximal degree of roughness of Si/Ge interface. Stepped PC appears when the carriers reach a percolation level. Few PC steps can be determined by such transitions from localized states to the conductive states on each ground and excited electron sublevels induced by the Coulomb potential of holes situated in the narrow Ge layer. A possible mechanism of a fluctuated PC can be related to electron-hole recombination.

The work is supported by RFBR (# 07-02-01106).

Anti-Stokes and Stokes photoluminescence in non-uniform GaAs-based quantum wells

K. Fujiwara*, A. Satake*, N. Takata*, U. Jahn**, E. Luna**, and H. T. Grahn**

* *Kyushu Institute of Technology, Tobata, Kitakyushu 804-8550, Japan*

** *Paul Drude Institute for Solid State Electronics, Hausvogteiplatz 5-7, 10117 Berlin, Germany*

Keywords: Heterostructures, Anti-Stokes photoluminescence, GaAs, Quantum wells

Anti-Stokes photoluminescence (AS-PL), where the output emission energy is larger than the input photon energy, has received attention in a variety of quantum-well (QW) heterostructures [1-4]. In most of the previous studies asymmetric double QWs with higher and lower energy subband exciton states are used to resonantly excite the lower energy exciton state, and the higher exciton emission is detected due to the nonlinear excitation processes such as Auger excitation as well as two-step two-photon absorption processes. Thus, the AS-PL signal always comes from the low-energy region within a short distance. Here, AS-PL is investigated in a system containing a sequence of GaAs-based QWs [4], where the carrier capture is significantly affected by the distance between the excitation and recombination sites. A sample used for this study consists of three different QWs grown on a GaAs (100) substrate by growth-interrupted molecular beam epitaxy. The nominal widths of the GaAs QWs separated by $Al_{0.2}Ga_{0.8}As$ barriers are 7.8 nm (QW1), 5.5 nm (QW2), and 3.5 nm (QW3). This whole structure is additionally confined by $Al_{0.3}Ga_{0.7}As$ layers. The AS-PL spectra were measured at 15 K using a monochromator (JY HR320), a lock-in-amplifier, and a wavelength-tunable Ti-sapphire laser for excitation.

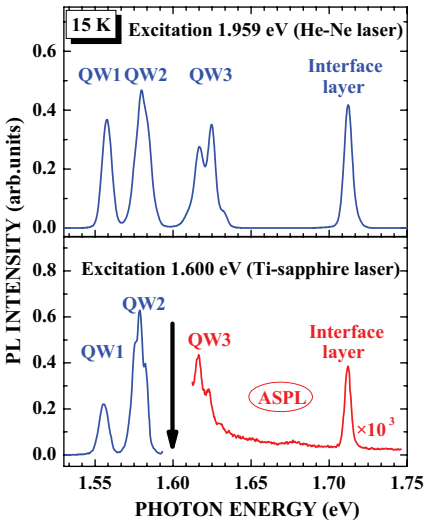

Fig.1 Stokes (top) and anti-Stokes (bottom) photoluminescence spectra of four bands (QW1, QW2, QW3, and an additional emission due to an interface layer between the bottom $Al_{0.2}Ga_{0.8}As$ and $Al_{0.3}Ga_{0.7}As$ layers, as confirmed TEM) at 15 K.

A typical Stokes PL spectrum shown in Fig. 1 (top) indicates four emission bands, including an additional band due to an unintentionally introduced interface well located nearest to QW1, as confirmed by transmission electron microscopy (TEM). Distinct AS-PL signals from QW3 as well as the interface layer (IL) are observed under non-resonant excitation. However, when excited resonantly to QW1, a strong enhancement of the AS-PL signal from the IL is observed relative to the AS-PL signal under resonant excitation of QW2 and QW3. This finding indicates that the capture of nonequilibrium carriers within the QWs plays a very important role for determination of AS-PL signal.

References

1. L. Schrottke *et al.*, Phys. Rev. B 5**6**, R15553 (1997).
2. S. C. Hong *et al.*, Phys. Rev. B **60**, 8883 (1999).
3. T. Kita *et al.*, Phys. Rev. B **59**, 15358 (1999).
4. S. Machida *et al.*, J. Appl. Phys. **98**, 83527 (2005).
5. K. Fujiwara, U. Jahn, and H. T. Grahn, Appl. Phys. Lett. **93**, 103504 (2008).

Terahertz emission from semiconductor superlattices with photonic crystal structures

Y. Sakasegawa, T. Ihara, and K. Hirakawa

Institute of Industrial Science and Institute for Nano Quantum Information Electronics, University of Tokyo, 4-6-1 Komaba, Meguro-ku, Tokyo 153-8505, Japan

Keywords: superlattices, photonic crystals, terahertz spectroscopy,

Recently, an experimental support for terahertz (THz) gain of Bloch oscillating electrons in semiconductor superlattices (SL) have been obtained from time-domain THz spectroscopy [1]. To realize electrically driven Bloch oscillators, it is of prime importance to investigate carrier dynamics of Bloch oscillation in a cavity system. In this work, we have investigated photonic crystal effect on Bloch oscillations in semiconductor superlattices by time-domain THz emission spectroscopy.

Figure 1 shows the GaAs/AlAs superlattice m-i-n (metal-intrinsic-n+-type) diode structures used in this work. We designed the GaAs wells (30ML) and AlAs barriers (2ML) in such a way that the first miniband width, Δ, to be 30meV. The top contact was formed by depositing a semi-transparent 6 nm-thick NiCr Schottky film and a 700 nm-thick gold layer with a photonic crystal structure (sample S1). S1 has a patterned gold layer with a honeycomb lattice of holes, which serves as a THz photonic crystal with a photonic bandgap around 2 THz [2]. Electron wave packet were photo-excited in the bottom of the first miniband by light pulse with a temporal width of 100fs delivered from a mode-locked Ti:sapphire laser, and transient THz waveforms emitted from the sample under dc bias were detected by electro-optic sampling technique [1].

Figure 2 shows the temporal waveforms observed for various dc bias fields, F_{dc}, (left), and their Fourier spectra (right). In a low bias field range (F_{dc} < 9 kV/cm), we observed a single peak that originates from Bloch oscillation and its linear shift with increasing F_{dc} [1]. However, in the high bias field range (F_{dc} > 11 kV/cm), where the Bloch frequency approaches the photonic bandgap, we found that the THz waveforms start showing a beating behavior and their Fourier spectra are strongly deformed with a large dip at 2.4 THz. This is the first step toward understanding of the interaction between Bloch oscillations and photonic crystal cavities.

References

1. N. Sekine, and K. Hirakawa, Phys. Rev. Lett., **94**, 057408 (2005).
2. M. Bahriz et al., Opt. Exp., **15**, 5948 (2007).

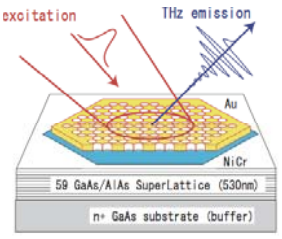

Fig. 1 The sample structure of undoped GaAs/AlAs SL with a THz photonic crystal electrode.

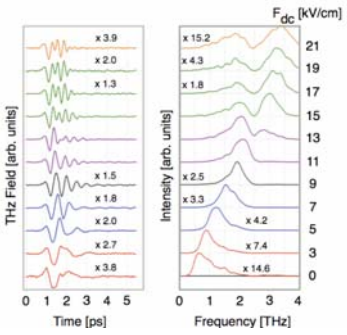

Fig. 2 Temporal waveforms of the THz emission for various bias electric fields (left), and their Fourier power spectra (right). Note the scale change.

Analysis of antenna integrated NDR-DCT oscillator for variable oscillation frequency in THz band

K. Furuya*, O.Numakami**, T. Sugaya*, N.Yagi**, K. Komori*, M. Mori*, Y. Okano** and M.Asada***

* *Photonics Research Institute, National Institute of Advanced Industrial Science and Technology (AIST), Tsukuba, Japan*
** *Faculty of Knowledge Engineering, Tokyo City University, Setagaya, Japan*
*** *Interdisciplinary Graduate School of Science and Engineering, Tokyo Institute of Technology, Meguro, Japan*

Keywords: Negative Differential Resistance Dual-Channel Transistor, Terahertz, Antenna, Slit reflector

Frequency ranges from 100 GHz to 10 THz is called the terahertz (THz) band. The electromagnetic waves within the band show advantages for a great variety of applications[1]. An oscillator device as a THz wave source of easy handling is hoped.

In this study, for such a THz oscillater, the negative differential resistance dual-channel transistor (NDR-DCT) proposed by AIST[2] (Fig. 1) was utilized.

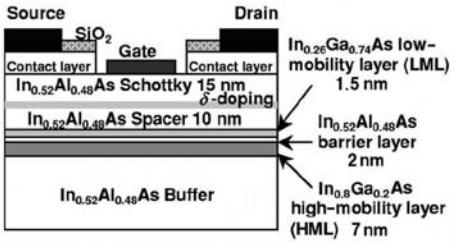

Fig.1 Pattern diagram of NDR-DCT

This device has a three-terminal structure, and the NDR can be controlled by the gate. Figure 2 shows a current-voltage characteristic between source and drain of NDR-DCT. NDR appears within the range of about 0.25-0.4V. The larger the gate voltage, Vg, is, the larger the absolute value of the NDR is.

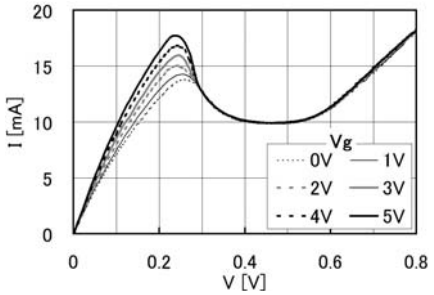

Fig.2 A example of NDR characteristics of the NDR-DCT with the gate length is 120 nm. They depend on the gate voltage.

We previously showed that our oscillator device using NDR-DCT, on which an antenna as a resonant circuit is integrated, can oscillate at about 100 GHz and higher in simulations[3]. The equivalent circuit model in ultrahigh-freauency band of NDR-DCT was derived on the basis of the analogy with RTDs[4]. An antenna on a wafer, which consists of the electrodes of the transistor, could be realized with the slit reflector that we proposed by numerical analysis. Size of the slot antennas are less than about 700 μ m.

The admittance of NDR-DCT and other structures (antenna, and so on), Ydct and Ya, respectively, were analyzed. In order for this device to oscillate, the following conditions must be satisfied simultaneously.

$$\mathrm{Re}(Ydct)+\mathrm{Re}(Ya) \le 0 : \text{Gain condition} \quad (1a),$$

where $\mathrm{Re}(Ydct) < 0$: NDR,

$$\mathrm{Im}(Ydct)+\mathrm{Im}(Ya) = 0 : \text{Phase condition} \quad (1b).$$

Above mentioned admittances which depend on the NDR are also variable as according to the gate voltage. Figure 3 is an example of simulation results of oscillation frequency when the gate voltage is changed. It shows that the frequency is variable within the range of about 10GHz with change from 0 to 5V in Vg. On even other structures for higher oscillation frequency, the simulation results show that the changeable width of about 10 percent of the frequency is achieved.

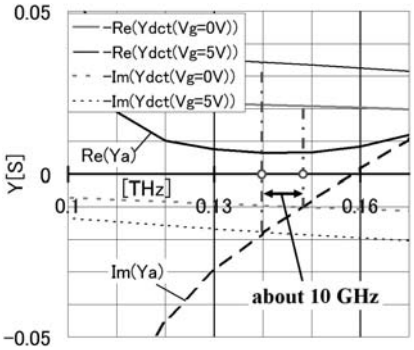

Fig.3 Admittance characteristics of NDR-DCT (Ydct) and resonant circuit (Ya) of the device whose NDR characteristics are in Fig. 2.

The possibility of variable oscillation frequency of our THz oscillation device using NDR-DCT was confirmed. This property is expected to be related to a frequency modulation as an application

References

[1] T. Nagatsuma, IEEJ Trans. EIS, Vol. 128, No. 6, pp.832-837(2008) [in Japanese].
[2] T.Sugaya, et al., Appl. Phys. Lett. 88 (2006) 142107.
[3] K. Furuya, et al., IEICE Trans. Commun., VOL.E91-B, NO.6, pp.1800-1805, JUNE 2008.
[4] N. Orihashi, et al.: Jpn. J. Appl. Phys. **44** (2005) 7809.

Positive and negative electroluminescence in the type II heterostructures with a deep AlSb/InAsSb/AlSb quantum well

M.P.Mikhailova*, K.D.Moiseev*, E.V.Ivanov*, Yu.P.Yakovlev*, E.Hulicius**, A.Hospodkova**, J.Pangrac**, K.Melichar**, T.Šimeček**

** Ioffe Physical-Technical Institute RAS, St.Petersburg, Russia*

*** Institute of Physics AS CR, v.v.i., Prague, Czech Pepublic*

Keywords: heterostructures, quantum well, electroluminescence.

InAs(Sb)/AlSb heterojunction system has attracted an interest for study of physical processes in semiconductors due to a unique band energy diagram which allows to form deep quantum wells (QWs) at the interface [1]. It is also a promising material for near and mid-infrared optoelectronic devices.

We report the first observation of positive and negative electroluminescense (EL) in the type II asymmetric p-InAs/AlSb/InAsSb/AlSb/p-GaSb heterostructures with a deep quantum well (QW) at the interface. The heterostructures were grown on p-InAs: Mn (100) substrate by metal-organic vapor phase epitaxy and consist of 20 nm-AlSb/5 nm-$InAs_{0.84}Sb_{0.16}$/20 nm-AlSb QW and p-GaSb capped layer. Band offsets at the interface were ΔE_c = 1.35 eV and ΔE_v = 0.15 eV, respectively. Transport properties of the samples were studied. Mobility in the structure was found about 5000 $cm^2/(V\ s)$ at 77 K. We estimate the transport broadening $2\Gamma_{tr} = 2\hbar/\tau_{tr}$ according [2] from the mobility value $\mu = e\ \tau_{tr} / m^*$. Effective mass $m^* = 0.018\ m_0$ and energy gap E_g = 0.376 эВ (77 K) for $InAs_{0.84}Sb_{0.16}$ were obtained from low-temperature photoluminescense and magnetotransport data. As a result the values $\tau_{tr} = 10^{-13}$ s and $2\Gamma_{tr}$ = 16 meV were found.

EL spectra were measured both at forward and reverse bias at 77 K and in temperature range 300-380 K. Low-temperature spectra at the forward bias ("+" is at the p-InAs substrate) consist of two positive EL bands with photon energy $h\nu_{max}$ = 0.407 eV and 0.376 eV, which can be written to band-to-band radiative recombination transitions in InAs and from Mn acceptor level (E_a = 31 meV). Full width at a half maximum (FWHM) was about 21 meV for the both bands. High-intensive negative EL was found in temperature range 300-380 K at the reverse bias. Spectra of negative EL were situated in the range 0.3-0.4 eV and similar in shape to ones of positive EL. Dependence of negative EL intensity from drive current value and photon energy was studied. It was established that at high temperature (>75 °C) and drive current up to 100-150 mA the negative EL intensity exceeds the positive one by 60 %. High efficiency of the negative EL was due to the suppression of Auger recombination at temperature increase.

Heterostructures under study are promising for design of light-emitting diodes with switching positive-to-negative EL in the spectral range 3-4 μm for application in gas analysis and ecological monitoring.

Work was supported by RBRF grant # 09-02-0063 and Program of the RAS Presidium.

References

1. A.Nakagawa, H.Kroemer, J.H.English. Appl. Phys. Lett., **54** (19), 1893 (1989).

2. S.Sasa, M.Nakai, M.Furukawa et al. *Proc. 12th Int. Conf. Narrow Gap Semiconductors* (Toulouse, France, 2005) p. 363.

Photoluminescence dynamics due to exciton and free carrier transport in GaAs/AlAs superlattices

R. Kido*, A. Satake*, and K. Fujiwara*

*Kyushu Institute of Technology, Tobata, Kitakyushu 804-8550, Japan

Keywords: Superlattices, Excitons, Time-resolved photoluminescence, Vertical transport

Exciton formation and transport both in vertical and lateral directions in a variety of semiconductor quantum-well (QW) heterostructures have been attracted a great deal of recent attention [1-3]. When excitons are generated from photogenerated electron-hole plasma and the radiative recombination occurs in a QW system with different heterostructures, excitonic radiative recombination processes are expected to be strongly influenced by interplay of exciton formation and exciton transfer times. In this paper, exciton transfer dynamics have been investigated in a set of GaAs/AlAs short-period superlattices (SPSs) with different miniband widths for carrier transport by detecting excitonic radiative recombination in an embedded single QW (SQW) and in SPS.

Nominally undoped GaAs/AlAs SPSs were grown on GaAs (100) substrates by molecular beam epitaxy. The SPS structures consist of 80 periods of 3.18 nm GaAs wells and AlAs barrier thicknesses of 0.90, 1.36, and 1.81 nm [4]. A single GaAs layer in the middle of SPS layers is enlarged to 6.36 nm, which is served as SQW to monitor the transport efficiency. Excitonic absorption spectral features of the SPS and SQW layers were characterized by photoluminescence (PL) excitation spectra. Spectrally and temporally resolved PL transients were measured at 15 and 80 K in a closed-cycle He cryostat using a diode laser at 653 nm with 50 ps pulses for weak excitation (100% maximum average power of 3μW at 1 MHz) and a streak camera system for photon counting detection.

When electron-hole plasma is generated in SPS, they are transported to be formed as excitons and radiatively detected in SQW and SPS. As the miniband width is increased, the transport efficiency is systematically enhanced, which is resulted in the increased SQW intensity relative to SPS, reflecting the tunnelling transport efficiency. At 15 K, the exciton formation is faster and the exciton ambipolar transport is slower. Therefore, the SQW intensity relative to SPS is only dependent on the miniband width. However, coexistence of both excitons and free carriers at 80 K shows unique PL dynamics (Fig.1) which shows a dramatic dependence on the excited carrier density.

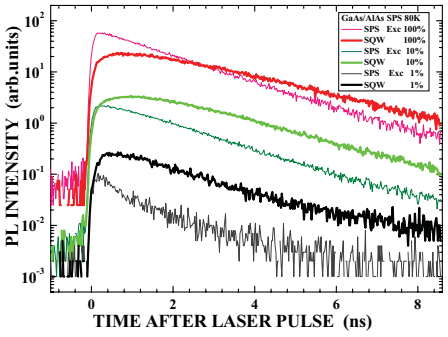

Fig.1 Photoluminescence transients for SQW and SPS emission bands as a function of time under three different excitation powers (100%, 10%, and 1%) at 80 K.

References

1. K. Fujiwara *et al*., Phys. Stat. Sol. (b) **244**, 2926 (2007).
2. J. Szczytko *et al*., Phys. Rev. Lett. **93**, 137401 (2004).
3. 4. M. Stern *et al*., Phys. Rev. Lett. **101**, 257402 (2008).
4. K. Fujiwara *et al*., Phys. Rev. B **40**, 1096 (1989).

Simulation of the interplay between stimulated emission and carrier distribution in quantum-cascade lasers

L. Schrottke, M. Giehler, R. Hey, and H. T. Grahn
Paul Drude Institute for Solid State Electronics, Hausvogteiplatz 5-7, 10117 Berlin, Germany

Keywords: Quantum cascade lasers, transport properties, optical properties

Semiconductor lasers based on electron-hole recombination exhibit, for not too high laser powers, a carrier density locked at its threshold value due to the gain-equals-loss condition. This condition leads to a complete conversion of any additional pumping energy into an increasing laser output power provided that the gain recovery can be considered to be instantaneous. For quantum-cascade lasers (QCLs), however, the population inversion is affected by carrier transport through the injector so that the gain recovery mechanism is qualitatively different from the one in conventional interband lasers. H. Choi *et al.* [1] have shown using pump-probe experiments that for QCLs the gain recovery is determined by the time-dependent transport of electrons through both the active regions and the injector regions connecting them.

The interplay of stimulated emission and carrier transport is expected to modify the electron distribution and consequently the electrical field strength within each QCL period so that the lasing energy may be shifted due to the quantum-confined Stark effect. Therefore, simulations may reveal the influence of the gain recovery behavior on the operation parameters of QCLs. For QCLs with a more complex optically active region, in which several intersubband transitions possess similar energies, the interaction of these transitions mediated by the laser field may also be simulated.

Our model is based on the self-consistent solution of the Schrödinger and Poisson equations. Carrier transport is included by transitions rates $T_{ij} = {}_E(E_{ij})|\ {}_{ij}|^2$ between i-th and -th subbands with the dipole matrix element ${}_{ij}$ and energy E_{ij}. The energy dependent factor ${}_E(E_{ij})$ allows for the empirical treatment of transitions due to scattering. In order simulate the impact of the laser field on the transport, ${}_E(E_{ij})$ is extended by a term for emission or absorption of photons, which is proportional to the number of photons in the cavity modes interacting with the intersubband transition. For the broadening parameter $\Gamma = \Gamma_i + \Gamma_j$ of the Lorentzian of the transition, either externally determined values may be used or the values are calculated within the model by $\Gamma_i \sim \sum_j T_{ij}$.

At the same time, the number of photons ${}_k$ in the -th cavity mode will increase (decrease) when the gain is larger (smaller) than the optical loss . Neglecting spontaneous emission, we assume $d\ {}_k/dt \sim (\ -\ )\ {}_k$. The gain contribution of the transition $i \rightarrow$ is given by $\sim E_{ij}|\ {}_{ij}|^2(\ {}_i -\ {}_j)$ with ${}_i$ denoting the carrier density in the i-th subband. The stationary case is found by a generalized self-consistent solution including these laser rate equations.

For a first qualitative study of the interplay between carrier transport and stimulated emission, we applied the model to a QCL design for the mid-infrared spectral region, in which a diagonal transition contributes significantly to the total gain. The inclusion of stimulated emission leads to a redshift of the gain maximum for field strengths at which the gain would exceed the loss. The gain-equals-loss condition requires a reduction of the carrier density in the upper laser level, which is provided by the faster transition due to stimulated emission. The smaller occupation of this level leads to a lower energy position. At the same time, the stimulated emission results in an increase of the total current density.

We are currently extending the simulations to several designs for THz QCLs including structures which exhibit multiple branches in the gain characteristics. Altogether, we are exploring how this model predicts accurate lasing energies and whether it can be used for the design of, e.g., electrically tunable THz QCLs.

References

[1] H. Choi, L. Diehl, Z.-K. Wu, M. Giovannini, J. Faist, F. Capasso, and T. B. Norris, Phys. Rev. Lett. **100**, 167401 (2008).

Thermal escape process of photogenerated carriers from GaAs single-quantum-well contained in GaAs/AlAs superlattices

A. Satake*, T. Tanigawa*, Y. Tanaka* and K. Fujiwara*

* *Kyushu Institute of Technology, Tobata, Kitakyushu 804-8550, Japan*

Keywords: Superlattice, Quantum well, Time-resolved photoluminescence, Carrier escape

Laser cooling of solids and semiconductors has been received recent attention [1-3]. Laser cooling might work when the energy of the emitted photon is larger than that of the absorbed photon due to phonon absorption processes. This phenomenon is known as luminescence up-conversion or anti-Stokes scattering. In this study, thermal escape process of carriers from a given energy state to higher energy states has been investigated by steady-state and time-resolved photoluminescence (PL) spectroscopy in GaAs single-quantum-well (SQW) contained in GaAs/Alas short-period superlattices (SPSs).

The sample used in this study was grown on a GaAs(100) substrate by molecular-beam epiaxy. The heterostructure consists of an 80-period GaAs (L_W=3.18 nm)/AlAs (L_B=0.90 nm) SPS with an enlarged GaAs SQW layer (L_{SQW}=4.09 nm) in a middle. Steady-state and time-resolved PL measurements were performed for sample temperature (T) between 15 and 300 K in a closed-cycle He cryostat. The steady-state PL spectra were measured using a cw He-Ne laser at 632.8 nm and a miniature fiber optic spectrometer. The time-resolved PL spectra were measured using a diode laser at 653 nm with 50 ps pulses and a streak-scope system for photon counting detection.

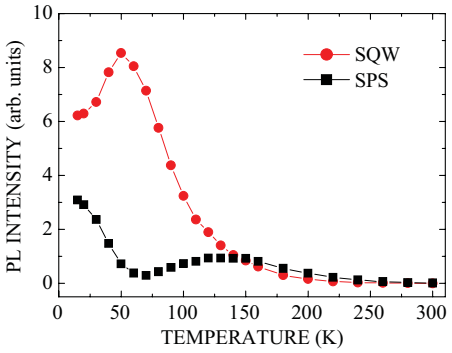

Fig.1 PL peak intensity for SQW (circles) and SPS (squares) as a function of temperature.

A typical PL spectrum indicates two emission bands corresponding to SQW and SPS layers. When the sample temperature is increased from 15 K to higher temperatures, the PL intensity of SQW increases and reaches the maximum value at 50 K, as shown in Fig. 1. On the other hand, the PL intensity of SPS drastically decreases below 60 K and then obviously increases to 120 K with increasing temperature. These results indicate the following processes: In the region of $T < 50$ K, the photogenerated carriers in the SPSs can quickly relax into the SQW due to vertical carriers transport assisted by phonon scattering before radiative recombination within SPSs. In the region of $T > 60$ K, the carriers in the SQW can easily escape into the miniband of SPSs due to thermal excitation. That is, the photogenerated carriers transfer between the subband of SQW and the miniband of SPSs due to the phonon-assisted carrier transport. The suggested processes are also demonstrated by temperature dependence of the time-resolved PL transients and simulating the PL transients based on a two-component rate-equation analysis.

References

1. S. Eshlaghi *et al.*, Phys. Rev. B **77**, 245317 (2008).
2. J. B. Khurgin, Phys. Rev. B **77**, 235206 (2008).
3. E. Finkeißen *et al.*, Appl. Phys. Lett. **75**, 1258 (1999).

Circular and anamorphic microlens array fabricated by selective oxidation of chirped short-period superlattice of GaAs/AlGaAs

K. S. Chang*, Y. M. Song**, Y. T. Lee**, S. C. Yang* and G. H. Kim*

** Division of Instrument Development, Korea Basic Science Institute, Daejeon, Korea*

*** Dept. of Information & Communications, Gwangju Institute of Science and Technology, Gwangju, Korea*

Keywords: Microlens, Selective oxidation, Molecular beam epitaxy, Superlattice

The insatiable demand for higher optical efficiency and newly emerging applications for micro-optical systems and devices have driven the need for advances in fabrication and integration technologies for microlenses [1]. Recently, we developed a novel method for fabricating semiconductor microlenses by selective oxidation of composition-graded digital-alloy AlGaAs [2]. In this presentation, we report the fabrication and optical characterization results of circular and anamorphic microlenses including those with cylindrical, square, elliptical, ring-shaped substrate footprints.

Using molecular beam epitaxy system, 1.3-μm-thick AlGaAs layer was grown on GaAs substrate. The average Al composition was linearly graded from 0.8 to 0.96 along the growth direction. The chirped short period superlattice of GaAs (4ML)/$Al_{0.98}Ga_{0.02}As$ (16 ~ 90ML) in 75 steps was used to grade the composition of AlGaAs. The structure was then capped with a 100-nm-thick GaAs layer. After growth, standard photolithography and dry etching processes were used to form a stripe, circular, square, elliptical, and ring-shaped mesa structures and to expose the composition-graded AlGaAs layer at the mesa side wall for lateral oxidation. A wet thermal oxidation process was carried out at a temperature of 410°C for 60-80min. The Al-oxide covering the AlGaAs microlens was then selectively removed in 1:5 KOH:H_2O solution. Surface profile of the microlenses formed by selective oxidation of linearly composition-graded digital-alloy AlGaAs showed a smooth convex lens shape. The focused spot pattern of the beam after passing through the microlens reveals the strong focusing function of the microlens as shown in Fig 1. This microlens fabrication method is versatile to make a wide range of semiconductor microlens arrays in terms of size, fill factor, and shape, which offer a variety of applications, especially when integrated with photonic devices to achieve required light manipulation.

References

1. S. Sinzinger et al., *Microoptics*, 2nd ed., WILEY-VCH, 2003.

2. K. S. Chang et al., IEEE Phon. Tech. Lett. **18**, 121 (2006).

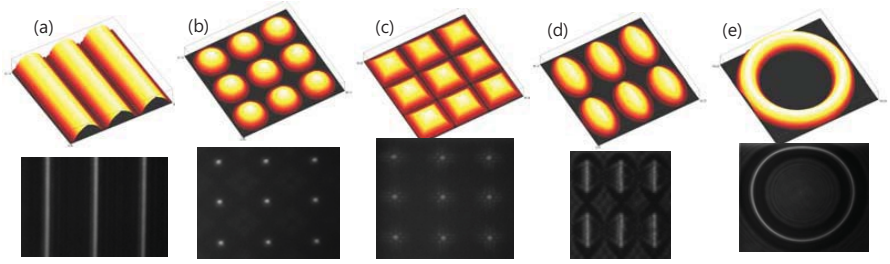

Fig.1 Upper row: 3-D surface profiles of the fabricated microlenses measured by confocal microscopy. Lower row: Focused laser beam images at the focal plane of the microlenses, laser wavelength: 1.55μm. (a) Cylindrical microlens, pitch: 30μm. (b) Circular microlens, pitch: 30μm. (c) Square microlens, pitch: 30μm. (d) Elliptical microlens, long-axis pitch: 40μm, short-axis pitch: 20μm. (e) Micro-ring lens, ring width: 30μm, inner diameter: 100μm.

Photoluminescence properties of exciton-exciton scattering in GaAs/AlAs multiple quantum wells

M. Nakayama*, T. Hirao* and T. Hasegawa**

** Department of Applied Physics, Osaka City University, Osaka, Japan*

*** Department of Material Science, University of Hyogo, Hyogo, Japan*

Keywords: photoluminescence, exciton-exciton scattering, GaAs/AlAs, multiple quantum well

Under intense excitation conditions, exciton-exciton scattering in semiconductors is one of the most interesting excitonic processes because of producing stimulated emission. ZnO- and GaN-based semiconductors have been typical samples for the exciton-exciton scattering [1,2]. The exciton-exciton scattering process causes a photoluminescence (PL) band with its energy lower than the fundamental exciton energy by the exciton-binding energy, which reflects the momentum and energy conservation in the inelastic scattering process. Although numerous studies of PL properties of GaAs/AlGaAs multiple quantum wells (MQWs) have been reported, little has been known about the exciton-exciton scattering process until now [3]. This is our motivation in this study.

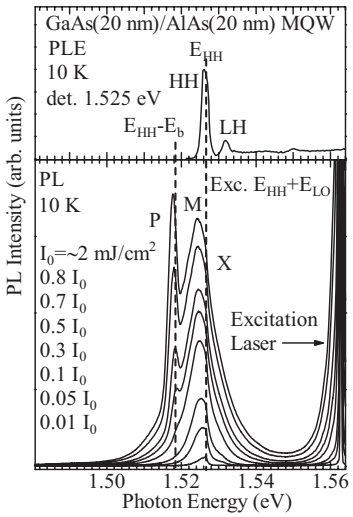

Fig.1: PL spectra of a GaAs(20 nm)/AlAs(20 nm) MQW under various excitation powers at 10 K. The PLE spectrum is shown on the top for the reference of the exciton energies.

Figure 1 shows PL spectra of the GaAs (20 nm)/AlAs (20 nm) MQW under various excitation powers at 10 K, where the maximum intensity I_0 is ~2 mJ/cm^2. The excitation-light source for PL was a pulsed Ti:sapphire laser with a pulse width of 5 ns. The PL excitation (PLE) spectrum is depicted on the top in Fig. 1 to clarify the exciton energies. The excitation energy was tuned to that higher than the heavy-hole-exciton energy (E_{HH}) by the longitudinal-optical (LO) phonon energy (E_{LO}). In the excitation-power region below $0.1I_0$, the well-known biexciton-PL band labelled M is dominant. The noteworthy finding is the appearance of a PL band labelled P with a threshold nature at 0.3 I_0. The energy of the P band is away from E_{HH} by the exciton-binding energy (E_b). These properties of the P band conclusively demonstrate the occurrence of the exciton-exciton scattering process. We will discuss the details of the PL properties of exciton-exciton scattering including the existence of optical gain.

References

1. C. Klingshirn and H. Haug, Phys. Rep. **70**, 315 (1981).

2. M. Nakayama *et al*., Appl. Phys. Lett. **87**, 092106 (2005).

3. T. Hirao *et a*l., J. Lumin. **128**, 960 (2008).

Modulation spectroscopy determined band gap discontinuities in GaInAsSb/Al(In)GaASb quantum wells

M. Motyka*, G. Sęk*, K. Ryczko*, F. Janiak*, J. Misiewicz*, and
S. Belahsene**, G. Boissier**, Y. Rouillard**

** Institute of Physics, Wrocław University of Technology, Wrocław, Poland*

*** Institut d'Electronique du Sud, Université Montpellier 2-CNRS, Montpellier, France*

Keywords: mid-infrared, quantum well, band offset, photoreflectance.

Semiconductor lasers with GaInAsSb/ Al(In)GaAsSb quantum wells (QWs) on GaSb substrate operating in the wavelength region up to 3 µm and beyond are attractive light source for applications including remote sensing, pollutant detection, medical procedures or laser spectroscopy. In spite the room temperature cw operation has been demonstrated for such lasers the optimization of their performance is still limited by unfavourable band gap discontinuities ratio between the conduction and valence band. Therefore, it of crucial importance to be able to determine the band offsets (BO) in such structures reliably. We propose the use of modulation spectroscopy (in a form of photoreflectance) as a high sensitivity technique probing the higher order states in low-dimensional structure as a method which combined with the energy level calculations offers unambiguous band offset determination in contrast to typically used PL studies. The latter detects usually the ground state transition only, which, as occurring between the relatively well confined electron and hole levels, is very weakly sensitive to the band offset ratio change. The observation of the excited state related transitions and those involving the light holes gives several energies to be compared with the results of the calculations in which the BO ratio is treated as the only free parameter. Figure 1 shows an example of such procedure performed for a quinary barrier $Ga_{0.35}In_{0.65}As_{0.32}Sb_{0.68}$/ $Al_{0.25}Ga_{0.50}In_{0.25}As_{0.24}Sb_{0.76}$ QW. The top part is the low temperature photoreflectance spectrum whereas the bottom one is the calculation results in a function of the BO in the conduction band thought for the unstrained materials (chemical band offset). The best agreement has been obtained for about 78 %, which after including the strain (i.e. in the real structure) recalculates into 65 % for the the conduction band. Similar studies has been performed for QWs with different quaternary and quinary barriers giving the insight on the BO dependence. The results have been confronted with the theoretical predictions based on the Van de Walle method [1]. For instance, it has been obtained that the conduction band offset ratio (including the strain effect) would increase to about 90 % for the same quantum well of $Ga_{0.35}In_{0.65}As_{0.32}Sb_{0.68}$ when the barrier is changed into quaternary $Al_{0.30}Ga_{0.70}As_{0.03}Sb_{0.97}$.

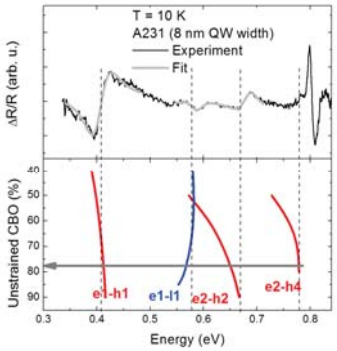

Figure 1. Comparison of the PR spectrum and the calculated transition energies versus the unstrained conduction band offset (CBO) for a 8 nm wide $Ga_{0.35}In_{0.65}As_{0.32}Sb_{0.68}/Al_{0.25}Ga_{0.50}In_{0.25}As_{0.24}Sb_{0.76}$ QW. The horizontal arrow shows the selected band offset

References

C. G. Van de Walle, Phys. Rev. B 39, 1871 (1989).

Optical properties of GaSb-based type II quantum wells emitting in the mid-infrared range

M. Motyka*, G. Sęk*, K. Ryczko*, J. Misiewicz*, T. Lehnhardt**, S. Höfling** and A. Forchel**

** Institute of Physics, Wrocław University of Technology, Wrocław, Poland*

*** Department of Applied Physics, University of Würzburg, Würzburg, Germany*

Keywords: type II quantum well, photoreflectance, mid-infrared semiconductor lasers, gas sensing

Mid-infrared lasers find increasingly applications during last years including for instance gas sensing for detection and control of the presence or concentration of harmful gases like CO_2, SO_x, NH_3, and many others The benefits of laser based methods have been limited mainly by the lack of suitable laser light sources, which have to provide the sensing wavelength in single mode and continuous wave (cw) in order to provide the required wavelength control and intensity. The performance of semiconductor laser emitters based on type I quantum wells operating in mid-wave infrared wavelengths beyond 3µm are restricted by fundamental limitations like unfavourable carrier confinement or small band gaps (comparable with split-off gaps). Therefore, the type II heterostructures employing InAs-GaSb-AlSb family have been proposed as an alternative. This eliminates Auger processes by removing the resonance between energy gap and split-off gap and enhances electronic confinement. Hereby, we present fundamental optical and electronic properties of a type II GaSb/AlSb/InAs/InGaSb/InAs/AlSb/GaSb quantum well system potentially able to cover spectrally the range of 2 to 10 µm (when the thickness of InAs layer is tuned for instance), and possible to be integrated in a photonic sensor unit for gas detection. Spectroscopic experiments at low temperatures, like photoluminescence and photoreflectance, allowed us the detection of the optical transitions, including the spatially indirect ones, and their unambiguous identification after the comparison to the energy level calculations. Based on that, conclusions regarding the band gap discontinuities in such a complex system could also be drawn.

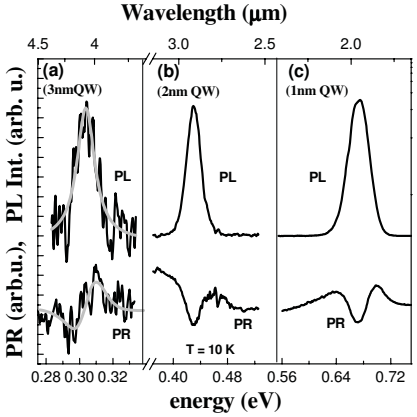

Figure1. Low temperature (10K) PL and PR spectra for the GaSb/AlSb/InAs/GaInSb/AlSb/GaSb type II quantum wells with QW width equal to 3 nm (a), 2nm (b) and 1 nm (c).

Additionally, photoluminescence thermal quenching was analyzed which on the one hand showed that the emission can still be effective at room temperature, and on the other hand that the temperature shift of the optical transitions is significantly smaller than for type I QW system and dependent on the InAs layer thickness. The latter does not follow the energy gap temperature dependence which could be explained when considered that electrons and holes are confined in separate layers.

Anisotropic effective mass and hole transport in *p*-type (311)A thin GaAs quantum wells

T. Noda* and H. Sakaki*, **

* *National Institute for Materials Science, 1-2-1 Sengen, Tsukuba, Ibaraki, 305-0047, Japan*
** *Toyota Technological Institute, 201201 Hisakata, Tempaku-ku, Nagoya 468-8511, Japan*

Keywords: anisotropic effective mass, quantum well, hole, transport

The effective mass m^* of carriers plays a crucial role in determining their mobilities in semiconductors. In most III-V compounds, the mobility μ_h of holes is far lower than that of electrons primarily because the hole mass is much heavier. Note, however, that mobilities of two-dimensional (2D) holes in p-AlGaAs/GaAs heterojunction (SH) formed on (311)A GaAs can get as high as 100 m^2/Vs at low temperatures. Hence the valence band structure of 2D holes on (311)A plane has been studied. For example, by magneto-tunnelling studies in p-type GaAs/AlAs double barrier structures, the valence band structure has been revealed and shown to depend on the crystal orientation and hole concentration p_s [1].

In an earlier work, we reported on the anisotropic transport of 2D holes in very thin GaAs quantum wells (QWs) on (311)A plane and showed that their μ_h -P_s characteristics can be explained by anisotropic interface roughness scattering [2]. Here we focus on the effective mass of such 2D holes and their transport properties at 77K, where the phonon scattering of holes dominate μ.

p-type GaAs/AlGaAs QWs of 4.8nm in thickness were grown on (311)A GaAs substrates by molecular beam epitaxy. Si atoms were introduced as acceptors only in the barrier region (sample A), and in the barrier and well regions (samples B1, B2). The details of sample structures and their growth condition were reported in Ref. [2]. We measured Shubnikov de Haas (SdH) oscillations in sample A whose channel is formed along the [01-1] axis. By analyzing the temperature dependence of SdH oscillations, m^* of 2D holes was estimated to be ~0.27. By combing this value with the mobility ratio along the [-233] and [01-1] directions at 4.2K in sample B, where Si doped in the well is a dominant scatter at low temperature, m^* of 2D holes in 4.8 nm thick QWs was estimated to be ~0.24 and ~0.31 along the [-233] and the [01-1] directions, respectively, when the hole concentration is ~ 2.8 × 10^{11} cm^{-2}.

Mobilities of holes along the [-233] and the [01-1] directions measured at 77K are plotted by solid and open circles, respectively, in Fig.1. For comparison, data for p GaAs/AlGaAs SHs (samples C1, C2) were given by closed and open squares for the channel formed along the [-233] and [01-1] axes, respectively. It was found that μ_h along the [-233] direction is as high as 7500 cm^2/Vs, which was higher than that in that of SH sample. In addition, the dependences of μ_h on *Ps* differ strongly for the two set of samples. This difference is likely to be caused by the modification of valence band structure, resulting from the quantum confinement.

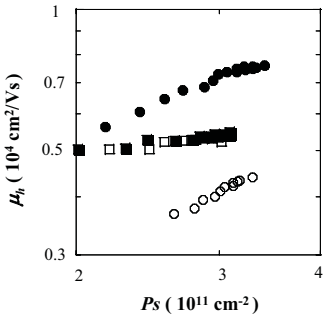

Fig.1 The *Ps* dependence of μ_h for 4.8 nm GaAs QW samples (circles) and GaAs SH sample (squares).

References

1. R. Hayden, et al., Phys. Rev. B46, 15586 (1992).
2. T. Noda, H. Sakaki, Physica E (in press).

Semiclassical and quantum transport in the 2D electron gas in a hard-wall antidot lattice

D. A. Kozlov, Z. D. Kvon, A. E. Plotnikov
Institute of Semiconductor Physics, Novosibirsk, Russia

Keywords: 2D electron gas, antidot superlattice, magnetotransport, hard-wall potential

In all existing theoretical models, the 2D electron gas (2DEG) in the antidot lattice is considered as a system in which 2D electrons move in a field of scattering hard disks (antidots) with a rectangular potential at the 2DEG–antidot interface. At the same time, almost all experiments were performed with the sample in which this interface was smooth due to the boundary effect appearing because the 2DEG is localized at a significant distance (d ≈ 100 nm) from the heterostructure surface. In this work, the AlGaAs/GaAs heterojunction with a 2DEG located at a distance of 25 nm from the structure surface was used as a parent material. The parameters of the 2DEG were $\mu = (2.55–2.65) \times 10^5$ cm^2/(V·s), $n_s = (0.65–0.87) \times 10^{12}$ cm^{-2} and the respective mean free path l_{tr} = 3.3–3.95 μm, depending on the sample illumination. The lattices of 40 nm antidots with the period a = 180 nm were fabricated by means of high-resolution electron lithography followed by low rate plasmochemical etching.

The magnetoresistance of such a sample was measured in the temperature range 0.2–5 K in a magnetic field of up to 10 T with the use of the standard lock-in detection technique. The obtained curves showed in Fig. 1. It is clearly seen that the samples exhibit two commensurate peaks, the main one corresponding to the condition $(2.07–2.12) \times R_c = a$ and the much lower peak corresponding to the condition $R_c = (1.8–1.9) \times a$. However, whereas the position of the main peak coincides with previous results, the position of the second peak displays a substantial disagreement: in all previous experiments, its position was given by the condition $R_c = (1.5–1.6) \times a$. Our result has much more better agreement with theory of delocalized "runaway" trajectories. This fact implies that we succeeded to create a rather sharp potential at the 2DEG–antidot interface in our samples and thus to put their behavior closer to the model of hard-wall billiard.

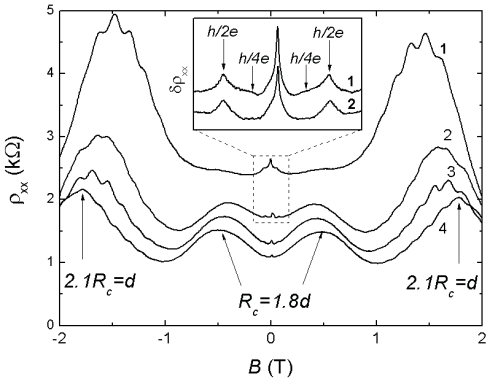

Fig.1. ρ_{xx}(B) curves for the antidot superlattice for different states (marked with numbers; each subsequent state is obtained by illuminating the preceding state) at T = 0.5 K. On insert: quantum interference features in low magnetic fields.

Magnetoresistance curves also show interference features. First, note that the features are observed simultaneously in the low-field region and near the main commensurate magnetoresistance peak. This indicates a much higher quality of the present lattices as compared to the previously studied ones. The low-field oscillation period corresponds, as it must, to the h/2e - quantization of the flux through the unit cell of the lattice. We also notice a weak but quite resolved h/4e feature for the highest resistance state of the sample. Second, in this work we succeeded in discovering a strong magnetic field dependence of the oscillation amplitude near the commensurate peak indicating a strict separation of the trajectories around antidotes and the trajectories colliding with the antidotes due to the sharpness of the 2DEG–antidot interface.

Structural and electrical properties of InAs thin films grown on $AlAs_{0.32}Sb_{0.68}$ meta-morphic buffer layer/GaAs for application as THz emitters

S.Y. Kim*,**, S.H. Shin*, J. D. Song*[+], I. K. Han*, T. W. Kim**, Y. D. Jho***

* *Nano Science Research Division, Korea institute of Science and Technology, Seoul 136-791, Korea*

** *Division of Electronics and Computer Engineering, Hanyang University, Seoul 133-79, Korea*

*** *Dep. of Info. & Comm., Gwangju Inst. of Sci. & Tech., Gwangju 500-712, Korea*

Keywords: InAs, AlAsSb, meta-morphic layer, MBE, THz

InAs materials have emerged as excellent candidates for potential applications in fast Hall sensors or long wavelength sensors due to their excellent physical properties of high mobility and very small bandgap. InAs materials have been currently receiving considerable attention because of their promising material systems to generate THz emission surpassing intensity of THz signal in comparison with conventional InGaAs, GaAs, InP, or Ge [1]. However, when the InAs film is grown on the Si, the GaAs or the InP substrate, there are enherent problems due to substantial lattice mismatches between the substrate and the InAs thin film [2].

In this paper, we focus on the investigations of structural and electrical properties of InAs films grown on a 2.2 μm-thick $AlAs_xSb_{1-x}$ (x = 0.32) meta-morphic buffer layer/GaAs substrate. All samples were grown using molecular beam epitaxy (MBE). The surface oxide was removed from the GaAs substrate by heating the sample at 620°C under As_2 flux, and of a 2.2μm-thick AlAsSb meta-morphic buffer layer was deposited on the GaAs substrate in order to reduce lattice mismatch between the GaAs substrate and the InAs film. Finally, we had grown InAs film varying thickness on the meta-morphic buffer layer.

The AFM and X-ray diffraction results show that the InAs film has considerable homogeneous surface. The root mean square (RMS) roughness of the InAs surface increase with increasing InAs film thickness from 1 to 5 nm.

The origin of the increase for the InAs surface RMS roughness is attributed to residual lattice mismatch between the InAs film and the AlAsSb meta-morphic buffer layer, resulting in the accumulation of the strain. Electron mobility at 300 K increase up to 10,000 cm^2/Vs as InAs film thickness increases up to 1.7 μm.

The possibility of InAs layer grown on meta-morphic AlAsSb/GaAs as THz source by irradiating ultra short pulse laser on the InAs was investigated. This result shows that the characteristic of THz amplitude is about 50 times larger than p-InAs bulk, which is known as the strongest THz emission semiconductor until now [1]. The origin of this strong THz emission is not clearly clarified yet. However, it should be pointed out that the residual strain in InAs may play an important role for the device efficiency. The relationship between the structural and the electrical properties of the samples is described on the basis of the experimental results.

This work is supported by KIST institutional research project of SPINTRONICS, and this work was also supported by the Korea Science and Engineering Foundation (KOSEF) grant funded by the Korea government (MEST) (No. R0A-2007-000-20044-0).

References

1. V. L. Malevich, R. Adomavicius, and A. krotkus, C. R. Physique **9**, 130 (2008).
2. H. Geta, I. Shibasaki, and A. Okamoto, J. C. Growth **278**, 614 (2005).

[+]Corresponding author; JDSONG@KIST.RE.KR

Double Heterojunction of n-ZnO/insulator-MgO/p-Si for Visible-Blind UV Detector

Y. Guo, T. C. Zhang, Z. X. Mei, C. Z. Gu and X. L. Du
Beijing National Laboratory for Condensed Matter Physics, Institute of Physics, Chinese Academy of Sciences, Beijing 100190, China

Keywords: visible-blind, photodetector, heterojunction, ZnO

Recently, UV photodetectors based on a wide band-gap semiconductor material, such as ZnO (E_g = 3.37 eV), have attracted more attentions because of their extensive applications in civil and military areas. Both Schottky contact and p-n junction type of ZnO-based UV photodetectors have been realized and reported. [1-4] However, owing to the lack of stable and controllable p-type ZnO films, in most cases, heterojunctions were used to fabricate ZnO-based UV photodetectors with a different p-type semiconductor, such as NiO, 6H-SiC, Si and so on. Undoubtedly, among all of these p-type semiconductors the commercial silicon is the best candidate for ZnO-based p-n junction UV photodetectors because of its low cost and widely used integrated circuit technology. Nevertheless, reported n-ZnO/p-Si photodetectors remain an obvious photoresponse to visible light, although the UV photoresponse is increased due to ZnO, which would limit its direct application in UV detection under a visible light background.

In this work, we report the fabrication of a visible-blind UV photodetector based on a double heterojunction of n-ZnO/insulator-MgO/p-Si grown by molecular beam epitaxy. The top ZnO (0001) layer of the double heterojunction is an unintentionally doped n-type film with an electron concentration of ~10^{16} cm^{-3} and a thickness of 500 nm, and the substrate is a 2-inch commercial boron doped p-type Si (111) wafer with a hole concentration of ~10^{18} cm^{-3}. A 50nm-thick MgO (111) layer was sandwiched between substrate Si (111) and top ZnO (0001) film to form a double heterojunction of n-ZnO/insulator-MgO/p-Si (p-insulator-n) which retains the in-plane epitaxial relationship $[10\bar{1}0]_{ZnO} \parallel [11\bar{2}]_{MgO} \parallel [11\bar{2}]_{Si}$. The ohmic contact on ZnO film is a circular Ti (~20 nm)/Au (~40 nm) electrode with a diameter of 300 μm. Indium was pasted on the back side of the p-Si wafer with a large area of ~1 mm^2 to serve as the ohmic electrode on p-Si.

The photoresponse spectrum of our device indicates a visible-blind UV detectivity of our devices with a sharp cut off of responsivity at the wavelength of 378 nm. The obvious suppression of photoresponse to visible light is attributed to the high potential barrier (3.2 V) of MgO layer for electrons. We demonstrate that the middle i-MgO layer takes the dual role, i.e. a buffer layer for the epitaxial growth of the p-insluator-n double heterojunction and a barrier layer for the realization of visible-blind UV detectivity of the p-insulator-n photodetector with a high UV/Visible rejection ratio.

[1] S. Liang, H. Sheng, Y. Liu, Z. Huo, Y. Lu, H. Shen, J. Cryst. Growth 225, 110 (2001).
[2] I.-S. Jeong, J. H. Kim, and S. Im, Appl. Phys. Lett. 83, 2946 (2003).
[3] S. Mridha and D. Basak, J. Appl. Phys. 101, 083102 (2007).
[4] C. H. Park, K. S. Jeong, J. H. Kim, and Seongil Im, Appl. Phys. Lett. 82, 3973 (2003).

Bias-induced relaxation-time manipulation in SiGe quantum well structures

P. Rauter*, T. Fromherz*, N.Q. Vinh**, B.N. Murdin***, G. Mussler****, D. Grützmacher****, and G. Bauer*
*Institute of Semiconductor and Solid State Physics, University of Linz, Austria
**FOM Institute for Plasma Physics Rijnhuizen, Nieuwegein, Netherlands
***Advanced Technology Institute, University of Surrey, GU2 7XH, UK
**** Forschungszentrum Jülich, Jülich, Germany

Keywords: SiGe, heterostructures, relaxation time, terahertz

The concept of spatially indirect radiative transitions in quantum cascade structures constitutes a means of increasing the lifetime of the excited state. The emitted wavelength and output power of such structures with diagonal transitions are strongly dependent on the applied bias, implying a variation of the involved transition rates with the voltage. However, up to now neither a direct measurement of the lifetime change nor a lifetime change with applied electric field within one and the same structure has been reported. The measurement of ultrafast relaxation times of electrically active structures has become experimentally accessible by recent photocurrent (PC) pump-pump experiments [1], stimulated by suggestions that light hole (LH)-heavy hole (HH) transitions might be promising as radiating ones for realizing a SiGe quantum cascade laser [2]. In this work [3], we report the first direct measurement of the increase of the lifetime of confined holes due to a change from a spatially direct to an indirect transition within quantum well (QW) structures, and the first direct observation of voltage tuning of an excited state's relaxation time. We have investigated the transition between LH and HH states of two p-type doped SiGe QW structures by performing PC pump-pump measurements using the free electron laser FELIX at the FOM. One period of the investigated sample structures consists of a deep central SiGe well and two symmetric SiGe shallow side wells separated by thin Si barriers. Using six band k.p calculations, the structures were designed in a way that by applying a voltage the lowest light hole (LH1) state of the central QW can be shifted into the side well, therefore decreasing the overlap with the central well's heavy hole (HH1) ground state. The resulting change in the relaxation time between the LH1 and HH1 states was directly measured by exciting a non-equilibrium occupation of the bound LH1 state by the first FEL pulse and probing its decaying occupation via the additional PC excited selectively by a second FEL pulse polarized orthogonally to the first pulse. The experiment was performed for a series of bias voltages. As the bias is increased from 0.2 to 2 V, the LH1-HH1 relaxation time changes from 12 to 25 ps for sample S1 and from 7.5 to 15 ps for the sample S2, where the difference in the initial lifetime is due to the difference in quantum well dimensions and composition. Our experiments demonstrate the continuous tunability of intersubband relaxation times in QW structures with applied electric fields.

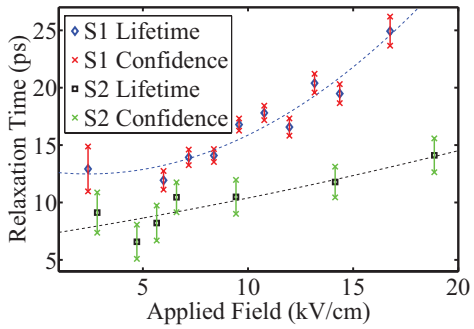

Figure 1: Voltage dependence of the LH1-HH1 relaxation time for two different SiGe quantum well structures S1 and S2. The red and green error bars indicate the 68% confidence limits of the fitted relaxation times.

References

[1] P. Rauter et al., *New J. Phys.* **9**, 128 (2007).

[2] C. Pidgeon et al., *Semicond. Sci. Technol.* **20**, L50 (2005).

[3] P. Rauter et al., *Phys. Rev. Lett.*, accepted for publication (2009).

Intersubband absorption in InGaAs/GaAsSb multi quantum wells

M. Nobile*, S. Schartner*, E. Mujagić*, H. Detz*, A. M. Andrews*, P. Klang*, W. Schrenk* and G. Strasser*,**

** Center for Micro- und Nanostructures, Vienna University of Technology, Floragasse 7, 1040 Vienna, Austria*

*** University at Buffalo, The State University of New York, 332 Bonner Hall, Buffalo, NY 14260, USA*

Keywords: quantum-cascade lasers, multi quantum wells, intersubband transitions

Quantum-cascade lasers (QCLs) [1] are powerful light sources operating in the midinfrared region. High power, high temperature performance QCLs have been demonstrated in the GaAs/AlGaAs system [2] as well as in InP-based materials [3]. However, all these QCLs materials contain a certain fraction of aluminum in the barriers, with the consequence that the effective mass of the electron in the barriers is high.

An aluminum-free material system where the effective mass of the electrons in the barriers is much lower would thus be desirable. Higher optical gain and improved device performance are expected to be the consequence of this. A very promising candidate to this aim is the InGaAs/GaAsSb material system lattice matched to InP. Apart from the results of [4], there is a lack of a detailed study of this material system.

In the present contribution, we report on type I intersubband (ISB) absorption in InGaAs/GaAsSb multi quantum wells. Improvements in the growth technique allow a good control of both layer thicknesses and material composition. Because of the polarization-sensitive nature of the intersubband transitions, pronounced features can be observed in the spectral region where the ISB absorption takes place (Figure 1). The transition energy can then be deduced. By measuring the transition energies for several well widths and by using an envelope function approximation [5] based computer routine, important parameters of the InGaAs/GaAsSb material system can be carried out (Figure 2). The most important of such parameters is the conduction band offset ΔE_c at the InGaAs/GaAsSb heterointerface, which has been determined to be 370meV in good agreement with the value reported in [4].

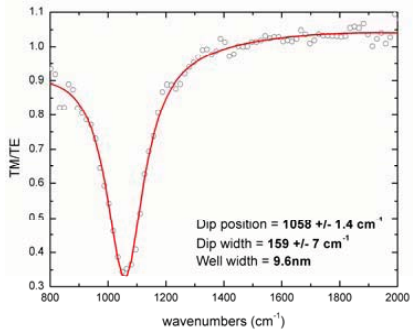

Fig.1 ISB absorption in InGaAs/GaAsSb multi quantum wells (well width: 9.6nm). The circles are experimental data and the solid line is a lorentzian fit.

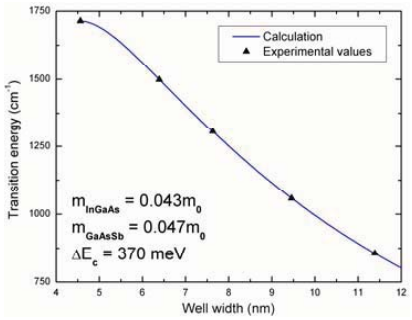

Fig.2 Position of intersubband resonances as a function of well width. The triangles are the experimental values and the solid line represents the fit. The fitting parameters are also reported.

References

1. J. Faist et al., Science, 264, 553 (1994)
2. C. Pflügl et al., Appl. Phys. Lett., vol. 83, 23 (2003)
3. A. Tahraoui et al., Appl. Phys. Lett., vol. 78, 416 (2001)
4. J. Hu et al., Appl. Phys. Lett., vol. 73, 2799 (1998)
5. C. Sirtori et al., Phys. Rev. B, vol. 50, 8663 (1994)

Refractive index of high-carrier-doped InGaAs/AlAsSb coupled double quantum wells

S. Gozu*, T. Mozume* and H. Ishikawa*

**National Institute of Advanced Industrial Science and Technology (AIST), 1-1-1 Umezono, Tsukuba, 205-8568, Japan*

Keywords: Refractive index, InGaAs/AlAsSb coupled double quantum wells, carrier, Kramers-Kronig relation.

Coupled double quantum wells (CDQWs) consisting of InGaAs/AlAsSb have attracted considerable interest for their application to ultrafast all-optical signal processing devices [1]. Since CDQW devices having ISBTs require waveguide structures due to the selection rule of ISBTs, the refractive index contrast between the CDQW core and clad materials should be high, which in turn would yield high optical confinement. Thus, it is desirable to have a large refractive index value of CDQWs. InGaAs wells with high carrier doping are required for achieving high optical absorption (α) due to ISBTs. We have already studied the carrier density dependence of the refractive index of bulk InGaAs [2]. In our previous study, two factors were quantitatively revealed to affect the change in the refractive index: (1) change in α and (2) the carrier plasma effect. However, the results of the previous study cannot be directly applied to the estimation of the change in the refractive index of CDQWs, because the quantum confinement effect in CDQWs modifies these two abovementioned factors. In the present study, the carrier density dependence of the refractive index of CDQWs is examined by an experimental method.

CDQW samples [3] consisted of an $AlAs_{0.56}Sb_{0.44}$ barrier with a 3 nm thickness, an AlAs center barrier comprising 2 MLs, and Si-doped $In_{0.8}Ga_{0.2}As$ wells with a 2.65 nm thickness. In the CDQW samples, α due to the ISBTs appeared at around 1550 nm. The refractive index of the CDQW samples was measured by the prism coupling technique at 1540 nm [4]. Factor (1) was evaluated using differential refractive index spectra (Δn) obtained by the Kramers-Kronig (KK) transformation of differential optical absorption spectra ($\Delta\alpha$). $\Delta\alpha$ was obtained by subtracting α for Si-doped CDQW samples from that for an undoped CDQW sample, where α was measured using a Fourier transform infrared spectrometer. In the measurements of α, light was radiated on samples in a direction normal to the CDQW surface. Factor (2) was evaluated from the plasma reflection that was measured by optical reflectance measurements.

Figure 1 shows the carrier density dependence of Δn. The sum of Δn due to $\Delta\alpha$ and the carrier plasma effect was almost the same as Δn obtained by the prism coupling technique. This indicated that these two factors were the origin of the change in the refractive index. From the carrier density dependence of Δn, it was found that the refractive index of the CDQW samples decreased with an increase in the carrier density. Therefore, in order to increase the refractive index of the CDQW samples, it was essential to decrease their carrier density; however, the carriers were required to have high α due to ISBTs. Therefore, it is important to optimize the carrier density of the CDQW samples.

References

[1] H. Tsuchida *et. al.* Opt. Lett. **32**, 751 (2007).

[2] S. Gozu *et. al.*, J. Appl. Phys. **104**, 07507 (2008).

[3] S. Gozu *et. al.*, to be published in J. Cryst. Growth

[4] T. Mozume, Physica E **40**, 2031 (2008).

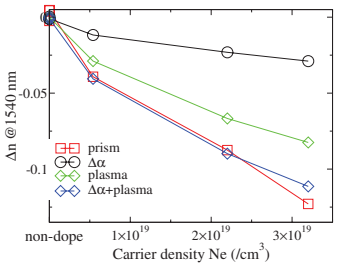

Figure 1: Differential refractive index obtained by prism coupling technique, from $\Delta\alpha$, and by the plasma effect at 1540 nm.

Proposal of a new physical model for Ohmic contacts

Y. Takada*, M. Muraguchi**, T. Endoh**, S. Nomura* and K. Shiraishi*
*Graduate School of Pure and Applied Sciences, University of Tsukuba, Tsukuba, Japan
**Center of Interdisciplinary Research, Tohoku University, Sendai, Japan.

Keywords: Ohmic contacts, two-dimensional electron system

Low resistive Ohmic contacts are crucial for the both device applications and the study of fundamental physics. Especially, Ohmic contacts between two-dimensional electron systems (2DES) embedded in AlGaAs/GaAs heterostuructures and source electrodes are important for studying quantum Hall effects and high electron mobility transistors (HEMT). In this study, we propose a new physical model of Ohmic contacts based on the detailed considerations of a metal/semiconductor interface such as metal induced gap states (MIGS) and the charge neutrality level concept (CNL) [1]. Electronic structure of an Ohmic contact in our new model contains many energy levels in a Schottky barrier, as schematically illustrated in Fig. 1 (a).

Conventionally, electronic structures of Ohmic contacts are explained by the remarkable low Schottky barrier height (Fig.1 (b)). However, it is well-known that the Fermi level of a metal should be pinned to the CNL in Si and GaAs regardless of the metal species, since density of states of MIGS are remarkably large [1]. Above two facts are incompatible each other. Accordingly, the construction of a brand new Ohmic contact model, which includes Fermi level pinning behavior, is inevitable.

Our proposed model contains the many energy levels exist in the Schottky barrier region (Fig. 1(a)). The origin of these energy levels is defects levels in an amorphous layer formed at the metal/semiconductor interface layer. In addition, electrons can tunnel through a barrier by the resonant tunneling that is mediated by these defect levels. Moreover, we also discuss the validity of our model under low temperature and high magnetic field conditions, by comparing the recent experiments [2].

This work is partly supported by KAKENHI 18063003.

References

1. J. Tersoff, Phys. Rev. Lett. **52**, 465 (1984).
2. O. Göktaş et al., Physica E **40,** 1579 (2008).

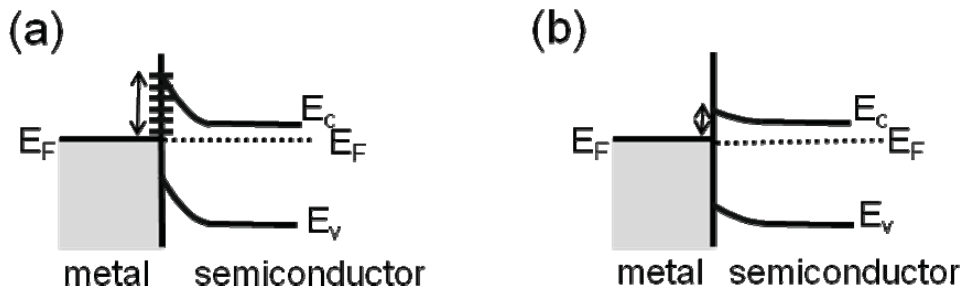

Fig.1 Schematic illustrations of electronic structures of our new Ohmic contact model. (a) Energy band diagram of our Ohmic contact model. (b) Energy band diagram of a conventional Ohmic contact model.

Determination of Band Offsets in a $Ga_{0.5}In_{0.5}P/GaAs_{0.9}P_{0.1}$ Single Quantum Well by Photoreflectance with a Semiconductor Laser

Wataru Susaki, Takahiro Igawa, Takeshi Inada, and Akihiro Tomioka
Osaka Electro-Communication University, Neyagawa 572-8530, Japan

Keywords: Band Offset, GaInP, GaAsP, Photoreflectance,

Band offsets play a key role to confine injected carriers for achieving low threshold and high efficiency in quantum well (QW) lasers. We have determined the band offsets by photoreflectance (PR) using a 410nm InGaN laser modulated by square-wave current at room temperature. The method is applied to determine the band offset of a 660nm-$Ga_{0.4}In_{0.6}P$/$(Al_{0.5}Ga_{0.5})_{0.5}In_{0.5}P$ [1].

The wafers studied here is a single QW 808nm-$Ga_{0.5}In_{0.5}P$ (barrier layer; 500nm) /$GaAs_{0.9}P_{0.1}$ (single QW; 10nm) /$Ga_{0.5}In_{0.5}P$ (barrier layer; 500nm) grown on the GaAs substrates. The QW layer of the sample has a tensile strain of 0.55% between the $Ga_{0.5}In_{0.5}P$ barrier and the $GaAs_{0.9}P_{0.1}$ QW layers. The advantage of the band offset determination by the PR is due to include usually forbidden transitions between the *i*th electron subband level *Ei* and the *j*th heavy hole subband levels *Hj* or the *k*th light hole subband levels *Lk* and enables to determine the band offset value more precise than PL and PLE methods for a few transitions such as *E1-H1* and *E1-L1*. The modulation frequency of the InGaN laser is variable and easily controlled by the square wave current, which is not fixed as in the conventional method using the optical chopper.

The PR spectrum, $\Delta R/R$ (R: reflectivity, ΔR: the change of reflectivity) as the function of the photon energy of the probing light, has been measured at 100 Hz. The subband transition energies, *Ei-Hj*, *Ei-Lk*, have been determined by the separation of PR spectra from 3rd order derivatives for the Lorentzian line shape. The subband levels are calculated numerically using Schrödinger equation by changing the band offset as the parameter to fit the experimental results. Effective masses, energy gaps, and stiffness constants of the respective layers are determined by linear interpolation from the well established values of binary compounds, InP, GaP and GaAs. The electric field is estimated to be 120kV/cm from Franz-Keldysh oscillations in waveguide layers.

The conduction band offset ratio is determined to be 0.45 - 0.50 at the $Ga_{0.5}In_{0.5}P/GaAs_{0.9}P_{0.1}$ interface by fitting the numerical calculation to the experimental results

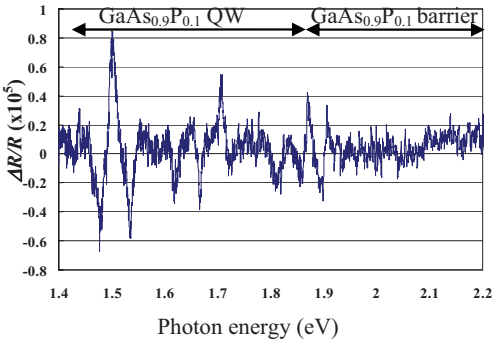

Figure 1. PR spectrum of a GaInP/GaAsP single quantum well

References: [1] W. Susaki, et al., ISCS 2008.

Theoretical investigation for the strain effect on surface structure of InAs(111)*A*

N. Ishimure*, T. Akiyama, K. Nakamura, and T. Ito

* *Department of Physics Engineering, Mie University, Mie, Japan*

Keywords: InAs(111)A, Phase diagrams, Surface structure, Strain effect

InAs/GaAs is an interesting hetero system, since it forms several shapes depend on the growth direction by molecular beam method, and some of them expected for applying quantum devices. On GaAs(001) substrate[1], InAs grows Stranski-Krastanov mode, it configurates 2D island shape, besides on GaAs(111)*A* substrate[2], InAs occasionally forms the dislocation of triangle shape called stacking-fault tetrahedron (SFT), they are expected to application to quantum dots. Especially, SFT has a unique property that the size depends on the film thickness, so it is expected to cut down size dispersion of quantum dots. However, there are few knowledge of mechanism of SFT formation. Joe investigated structural stability of SFT by empirical potential approach[3], and recommend that SFT formed to release distortion due to lattice mismatch between film and substrate. This proposal is one factor of SFT formation, while he did not take into account the effect of surface structure, and it is not enough to give an explanation of the factor of SFT formation. In this study, we apply our *ab initio*-based approach to phase diagram calculations for InAs(111)*A* surface, and investigate the strain effect on surface structure.

Figure 1 shows the calculated phase diagram.The dash line shows a boundary of In-vacancy and As-trimer structure for InAs (111)*A* surface. This shows that In-vacancy structure appears frequently at growth condition[4], it conform with experimental date.The solid line shows a boundary of In-vacancy and As-trimer structure for InAs (111)*A* surface with strain that is due to lattice mismatch beteween GaAs and InAs.This show that In-vacancy structure appears more frequently at growth temperature (700-900 K). This result imply that vacancy site works as a release point of strain. Additionally, InAs surrface with more become more asperity, and that may be good condition for SFT formation.

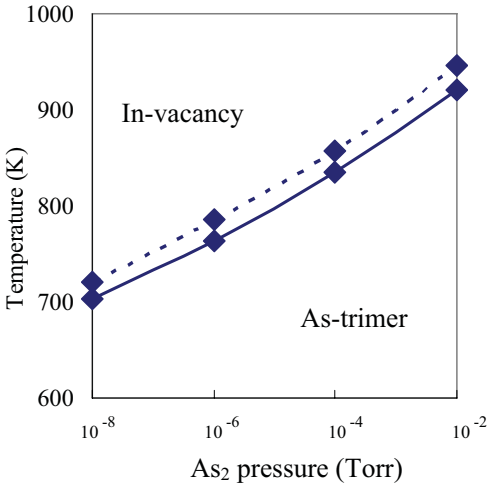

Fig.1 Calculated phase diagram of InAs(111)*A* surface as a function of temperatire and As_2 pressure.

References

1) Y. Q. Wang, Z. L. Wang,, J. J. Shen, and A. S. Brown Solid. Stat Comm**. 122** (2002) 552

2) K. Kanisawa, M. J. Butcher, Y. Tokura, H. Yamaguchi, Y. Hirayama, Phys. Rev. Lett. **87** (2001) 196804

3) H. Joe, T. Akiyama, K. nakamura, K. Kanisawa, and T. Ito, J. Cryst. Growth **301** (2007) 837

4) H. Yamaguchi *et al*. Phys . Rev. B **55** (1996) 1337

Optical properties of fully digital-alloyed 1.3 μm MQW and its application to laser diodes

D. C. Heo*, J. D. Song*, I. K. Han*, J. I. Lee*, J. M. Kim**, Y. T. Lee**
*Nano Science Research Division, Korea institute of Science and Technology, Seoul 136-791, Korea
** Dep. of Info. & Comm., Gwangju Inst. of Sci. & Tech., Gwangju 500-712, Korea

Keywords: Digital-alloy, laser diode, multi quantum well

Digital-alloys, or short-period superlattices (SPSs), consisting of binary or ternary layers with periods of a few monolayers (MLs) have attracted attentions as a solution for molecular-beam epitaxy (MBE) growth of ternary or quaternary materials of various composition with enhanced band-offset, and without additional source cells and laborious change of cell temperature during growth interruption. With the InGaAlAs digital-alloy MBE growth technique, lattice-matched 1.58 μm multi-quantum well (MQW) laser diodes, broadband-emission (1.3 - 1.9 μm) triple-QW light-emitting diodes, strained 1.3 μm MQW lasers, strained 1.55 μm MQW lasers, 1.55 μm vertical cavity surface emitting lasers, avalanche photodiodes, and fully digital-alloyed 1.3 μm MQWs have been successfully grown.[1,2]

In this presentation, optical properties of fully digital-alloyed 1.3 μm MQWs will be covered and electrical properties of fully digital-alloyed MQW laser diodes.

Two compositions of InGaAlAs were used for 1.3 μm MQWs. For separate confinement heterostructure and barriers. $(InGaAs)_{0.4}(InAlAs)_{0.6}$ layers were deposited, and they consisted of the pairs of 6.6 Å thick InGaAs, and 9.8 Å thick InAlAs layers, those are all lattice matched to InP. $(InGaAs)_{0.8}(InAlAs)_{0.2}$ was introduced as well layers, that was made of the pairs of lattice matched InGaAs (15 Å) and InAlAs (3.75 Å). Schematics of laser diode structure was depicted in Fig. 1. The detail of optical, structural and electrical properties of the laser diode will be described on the basis of the experimental results.

Reference

1. J. D. Song et al., Appl. Phys. Lett. **80**, 4650 (2002) and references in it.
2. D.C. Heo et al., J. Kor. Phys. Soc. **43**, 51 (2004).

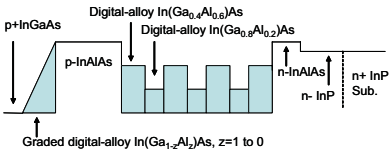

Fig.1 Schematics of laser diodes using fully digital-alloyed MQWs

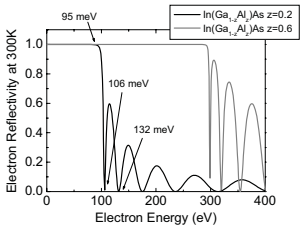

Fig.2 Electron reflectivity as a function of electron energy at 300 K

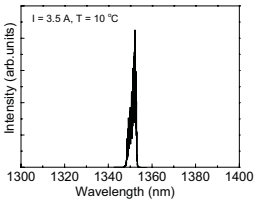

Fig.3 Optical spectrum of broad area laser diode.

Digital-alloy AlGaAs/GaAs distributed Bragg reflector for the application to 1.3 ㎛ surface emitting laser diodes

N. K. Cho*,**, K. W. Kim*, S. P. Ryu*, J. D. Song*, W. J. Choi*, J. I. Lee*, H. S. Jeon**

*Nano Device Research Center, KIST, Seoul 136-791, Korea
** School of Physics, Seoul National University, Seoul 151-747, Korea

Keywords: digital-alloy, AlGaAs, GaAs, distributed Bragg's reflector

Usually in 1.3 μm QD VCSEL structure with In(Ga)As QD on GaAs, they use distributed Bragg reflectors grown by alternatively repeating of GaAs and AlGaAs layer. But, if we use analog method for growing AlGaAs layer on large size wafer, there can be degrading of the compositional uniformity due to thermal inequality on wafer surface. In case of QD VCSEL, the delicate control of the uniformity of the AlGaAs reflector is very important due to the small gain spectrum of QD active layer. But by using the digital-alloy AlGaAs, we can solve these problems. Because only one kind of GaAs or AlAs layer can be grown on the wafer surface in the digital-alloy AlGaAs growing method, the layers do not affected by the thermal inequality on the wafer surface. So, we made the distributed Bragg reflector for 1.3 μm optical devices by digital-alloy AlGaAs.

In this presentation, we will report successful fabrication of digital-alloy $Al_{0.9}Ga_{0.1}As$ with 39 times repetition of 0.283 nm GaAs layer and 2.547nm AlAs layer. The clear formation of interfaces was proven by scanning or transmission electron microscope. With the digital-alloy $Al_{0.9}Ga_{0.1}As$, we evaluated uniformity of 1.3 μm-distributed Bragg reflectors. We found that distribution of reflection spectrum pit over a quarter of 3-inch wafer is less than 0.4%, which was less than half of conventional counter parts. In conclusion, we showed the merit of digital-alloy AlGaAs in good uniformity. In addition, because the digital-alloy method has good repeatability for device production, we can expect better 1.3 μm quantum dot surface emitting devices using digital-alloy AlGaAs layer.

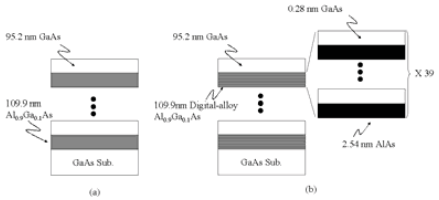

(a) (b)

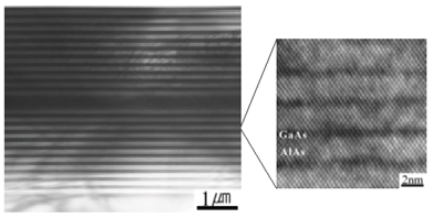

(c)

Fig.1 AlGaAs/GaAs DBR structure using (a) analog-alloy $Al_{0.9}Ga_{0.1}As$ and (b) digital-alloy $Al_{0.9}Ga_{0.1}As$ composed of AlAs and GaAs , (c) TEM image of the $Al_{0.9}Ga_{0.1}As$/GaAs DBR-cavity and the magnified digital-alloy AlGaAs layer.

Room temperature electroluminescence from radiative-defects-engineered InSb-quantum-dot-embedded-Si

Y. Yasutake, J. Igarashi, Y. Terada, N. Tana-ami, and S. Fukatsu

Graduate School of Arts and Sciences, University of Tokyo, Tokyo, Japan

Keywords: Radiative defect engineering, {311}-rod-like-defects, quantum dots, silicon light emitter

Si-based light emitters are a key component in silicon photonics. As opposed to conventional band-gap engineering, which is not so productive in this regard, engineering of *radiative* defects has begun to hold considerable promise. As a matter of fact, G-center defects in a nanopatterned Si permitted light amplification and stimulated emission at 1278 nm at low temperature[1], which stands as a stepping stone in the development of Si-based lasers by utilizing defects.

Among the vast spectrum of the known *radiative* defects in Si, a viable candidate should be color-stable, room-temperature-emitting, possibly with gain, opening the way to *radiative* defect engineering. Here, we focus on the narrow-line 900-meV emission due to {311} rod-like defects (RLDs) [2]. Interestingly, they are a new class of radiative nanostructure, tending to line up with a particular crystal orientation with typical dimensions in the mesoscopic scale. More importantly, they are repeatable enough to be engineered and even exhibiting near-infrared gain [3]. Here is demonstrated the electroluminescence (EL) of {311}-RLDs for the first the time, which persisted up to room temperature.

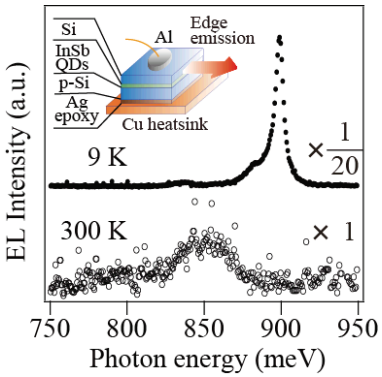

Fig.1 EL spectra of InSb-QD-embedded-Si at 9-K and room temperature. Inset shows schematic sample structure.

InSb-quantum-dot(QD)-embedded-*strained*-Si was prepared by molecular beam epitaxy (MBE). There are 10-bilayers equivalent of InSb in the grown-in p-n junction. The {311}-RLDs were introduced into the epilayers by two-step post-growth annealing processes: (1) extended low-temperature anneal at 300°C for 1 week in vacuum, followed by (2) a furnace anneal at 600-700°C for 30 min in flowing nitrogen. The built-in strain due to the InSb QDs was designed such that the RLDs can be launched into Si without excess damage. This contrasts well with the cases where the RLDs always accompany significant damage, which ruins the radiative properties and has long left EL unchallenged. High-energy ion implantation and electron beam irradiation are the examples that are responsible for this.

Fig. 1 compares the 9-K and room-temperature EL spectra of the InSb-QD-embedded-Si. The sharp EL at 900 meV continuously broadens and tends to lower energies by 50 meV associated with a thermal roll-off of the EL intensity with increasing temperature. The 50-meV shift attributed to the band-gap shrinkage could be repeated by varying the injection current at low temperature, which enables wavelength tuning.

That the MBE-based defect engineering is free from crystal damage has allowed room-temperature EL. Even applicable to various Si-based structures such as strained SiGe, SOI waveguide and photonic crystals, *radiative defect engineering* will provide an avenue towards a viable Si-based light emitter through appropriate microstructuring like heteroepitaxy.

References

1. S. G. Cloutier *et al.*, Nat. Mater. **4**, 887 (2005).
2. T. Mchedlidze *et al.*, phys. stat. sol. (a) **204**, 2229 (2007).
3. S. Fukatsu *et al.*, ACSIN-9 (2006) (unpublished).

Effect of a thin hole-blocking layer on carrier transport and luminescent properties in organic light-emitting diodes

K. Kurata, M. Murata, K. Kashiwabara, and N. Ohtani

Department of Electronics, Doshisha University, Kyoto, Japan

Keywords: organic light-emitting diode, hole-blocking layer, carrier transport

Recently, organic light-emitting diodes (OLEDs) have been researched in expectation of the application to flat panel displays and light illumination sources. The emission color depends on the recombination zone of the device, and a hole-blocking layer (HBL) is utilized to confine the recombination zone. In this study, we fabricated OLEDs with a thin HBL, and investigated carrier transport and luminescent properties of the devices. 2,9-Dimethyl-4,7-diphenyl-1, 10-phenanthroline (Bathocuproine: BCP) was used as a HBL. Besides, we used 4,4',4"-tris(3-methylphenyl-phenylamino)triphenylamine (m-MTDATA) as a hole-transport layer (HTL), N,N'-Di(1-naphthyl)-N,N'-diphenylbenzidine (α-NPD) as a blue emissive HTL, Tris(8-hydroxyquinolinato)-aluminum (Alq_3) as a green emissive electron-transport layer (ETL), and 5,6,11,12-Tetraphenylnaphthacene (Rubrene) as a yellow dopant. The device structures were as follows:

1) ITO/m-MTDATA/BCP(*x* nm)/m-MTDATA/Al,
2) ITO/α-NPD/BCP(*x* nm)/Alq_3/LiF/Al,
3) ITO/α-NPD/BCP(3 nm)/Alq_3+Rubrene(2 %)/LiF/Al.

The total thickness of organic layers was 100 nm. All materials were deposited by vacuum evaporation.

In order to evaluate the hole-blocking properties of BCP, we fabricated device 1 which are hole-only devices with a different thickness of BCP. The current density - voltage (J-V) characteristics indicate that some holes can tunnel through the BCP layer when the thickness is thin enough, particularly less than 5 nm.

An introduction of a thin HBL is effective in controlling electroluminescence (EL) spectra of OLEDs [1]. Fig. 1 shows the EL spectra of device 2. The device without BCP (*x*=0) shows only green emission from Alq_3 (λ_{em}=530 nm). With increasing the thickness of the BCP layer, however, the ratio of blue emission of α-NPD (λ_{em}=440 nm) rises. When the BCP layer is 3 nm, simultaneous emissions from α-NPD and Alq_3 are obtained clearly. The results indicate that the recombination zones are produced in both the α-NPD layer and the Alq_3 layer. Although the accumulation of the holes occurs at the α-NPD/BCP interface, the partial holes are injected into the Alq_3 layer through the thin BCP layer. Consequently, the exciton recombination takes place in two emissive layers. The emission color can be controlled by varying the thickness of the thin BCP layer, because the carrier behavior in the devices is determined by the BCP layer thickness. In addition, device 3 was fabricated as a white OLED. The device exhibited pure white emission using complementary colors, blue emission from α-NPD and yellow emission from Rubrene. The CIE coordinates is (0.31, 0.34).

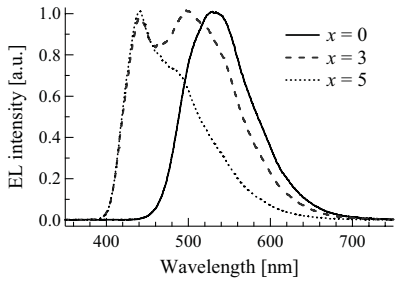

Fig. 1. EL spectra of device 2: ITO/α-NPD/BCP(*x* nm)/Alq_3/LiF/Al.

References

[1] J. Kido, M. Kimura, and K. Nagai: Science, **267**, 1332 (1995)

Improvement of dark current in organic near-infrared photodiodes by mixing a polymer in the active region

K. Nakajima, K. Bando, and N. Ohtani

Department of Electronics, Doshisha University, Kyoto, Japan

Keywords: organic photodiode, near-infrared, dark current

Recently, applications of optical communication in the near-infrared (NIR) region have been extended. Organic NIR photodiodes have an advantage for low-cost production [1]. However, a large dark current is a problem in organic NIR photodiodes, because organic NIR absorption materials have a narrow bandgap. In this study, we fabricated organic NIR photodiodes and improved to reduce a dark current by mixing a polymer in the active region.

The active region of the samples consists of Copper(II)5,9,14,18,23,27,32,36-octabutoxy-2,3-naph -thalocyanine (Cu(II)) which has an absorption peak at around 850 nm. In addition, Poly(N-vinyl -carbazole) (PVK) is mixed in the active region in order to improve a dark current. The active region was fabricated by spin coating method on an Indium-Tin-Oxide (ITO)-coated glass substrate.

Fig.1 shows the dark current characteristics of devices whose Cu(II):PVK ratios are 1:1, 1:3, 1:5, and Cu(II) only, respectively. This result clearly indicates that the dark current decreases with an increase of PVK. Thus, we considered that the carrier injection from each electrode to the active layer was suppressed by mixing PVK, because PVK is a wide bandgap material.

Fig.2 shows photocurrent-voltage characteristics and the corresponding external quantum efficiencies. The Cu(II):PVK ratios are 1:1, 1:3, and 1:5. The samples were irradiated by using a light emitting diode (850 nm) and applied a reverse bias voltage. This result indicates that the photocurrent and the corresponding external quantum efficiency becomes largest when the ratio of Cu(II):PVK is 1:1. In this case, hole transport contributes much more than electron transport, because the mobility of hole in PVK is much higher than that of electron.

In summary, organic NIR photodiodes with the mixture layer of Cu(II) and PVK were fabricated. The dark current and photocurrent can be controlled by changing the mixture ratios of Cu(II) and PVK.

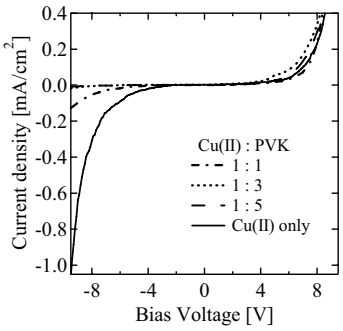

Fig. 1. Dark current characterisitics.

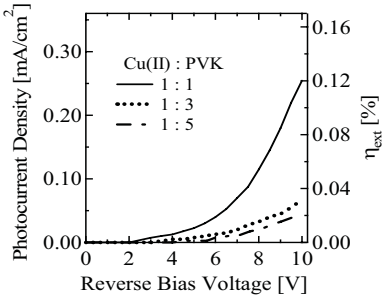

Fig. 2. Photocurrent-voltage characteristics and corresponding external quantum efficiencies.

Reference

[1]. T. Morimune, et al., Jpn. J. Appl. Phys., **45**, 546, (2006)

Memory effect of pentacene field-effect transistors with embedded monolayer of semiconductor colloidal nano-dots

Kaori Kajimoto, K. Uno, and Ichiro Tanaka

Department of Materials Science and Chemistry, Wakayama University, Wakayama, Japan

Keywords: colloidal nano-dot, pentacene, field-effect transistor, memory effect

Organic electronic devices have been intensively studied because of their advantages such as light-weight, flexibility, and low-cost. Besides organic electric luminescent diodes and transistors, memory devices are also attracting much attention [1]. We fabricated pentacene-based memory field-effect transistors (FETs) in which monolayers of semiconductor colloidal nano-dots (NDs) were embedded at the interface of the gate insulator and the active layer as shown in Fig. 1. In their transfer characteristics, considerable shift of the threshold voltage as large as ~ 10 V was obtained after positive writing voltage was applied on the gate electrode.

Approximately 0.01wt% core/shell-type CdSe colloidal NDs were dispersed in chloroform, and ~40 μl of the solution was spread over a water surface. The NDs were considered to aggregate as the solvent evaporated, and formed monolayer over the water surface. The monolayer of NDs were transferred by horizontal lifting method [2] onto a poly (methyl methacrylate) (PMMA) layer spin-coated on a 300-nm-thick SiO_2 layer thermally oxidized on an n^+-Si(001) substrate. It was measured that the surface coverage of the monolayer of colloidal NDs was ~85 % by atomic force microscopy. Then, 30-nm-thick pentacene layer was deposited on the monolayer of NDs by vacuum evaporation. Finally, Au source/drain electrodes were deposited through a metal mask. We investigated memory effect by measuring drain-current (I_D) – gate-voltage (V_G) characteristics before and after a writing voltage of 70 V was applied on the gate electrode for 300 sec. Figure 2 shows $\sqrt{-I_D}$-V_G curves of the memory-FET comprising NDs, in which the dotted and solid lines are curves measured before and after writing, respectively. It is shown that the threshold voltage (V_{th}) is shifted by ~10 V to the positive direction. Also, this large shift of V_{th} was observed even 20 hours after writing; namely the retention time is estimated to be more than 20 hours. However, only small shifts of ~2 V at the maximum were observed with pentacene FETs without embedded NDs. We thus consider that the holes induced at the pentacene/PMMA interface by the electrons, which were trapped in the NDs by applying the writing voltage, caused the positive shift of the V_{th}.

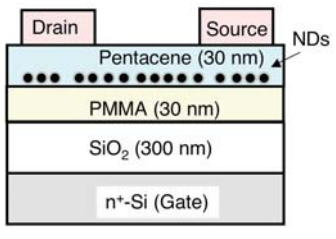

Fig.1 Schematic illustration of memory-FETs with monolayer of colloidal NDs embedded in pentacene layer.

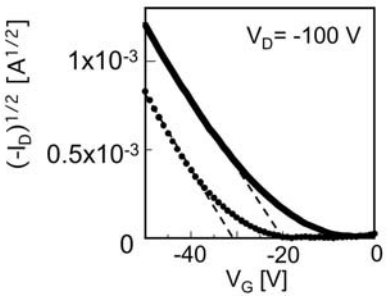

Fig.2 Transfer characteristics of memory-FET. Dotted and solid lines were measured before and after applied writing voltage, respectively.

References

1. Gerwin Gelinck: Nature **445,** 268 (2007).
2. K. Fukuda, H. Nakahara, and T. Kato: J. Colloid Interface Sci. **54,** 430 (1976).

Hybrid nanocomposites based on colloidal PbS quantum dots

L. Turyanska*, U. Elfurawi*, T. D. Bradshaw*,
M. Li**, S. Mann**, N. R. Thomas* and A. Patanè*

* *School of Physics and Astronomy and Centre for Biomolecular Sciences, The University of Nottingham, Nottingham NG7 2RD, UK*
** *Centre for Organized Matter Chemistry, School of Chemistry, University of Bristol, Bristol BS8 1TS, UK*

Keywords: quantum dots, biocompatibility, photoluminescence, PbS

We describe the synthesis, physical properties and biocompatibility of a novel nanocomposite based on a colloidal PbS quantum dot (QD) entrapped in the hollow core of an apoferritin (AFt) protein cage [1-2]. Apoferritin provides the PbS QD with a biocompatible coating and a template for the formation of ordered arrays of nanoparticles. As shown in Fig. 1, AFt acts as a "nanoreactor" for the growth of the PbS nanocrystal and its spherical shape and uniform size facilitate an ordered hexagonal packing of the dots [2].

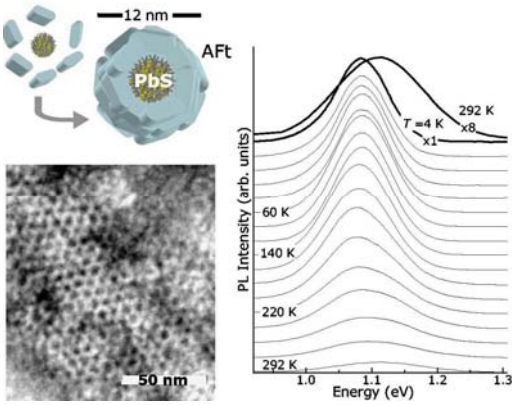

Fig. 1 TEM image and PL spectra of AFt-PbS composites at various temperatures *T*. Top inset: sketch of the AFt-PbS construct showing the PbS core and the subunits of the protein shell.

The encapsulation of PbS in apoferritin allow us to functionalize the protein for fluorescence imaging in the near infrared (NIR) region of the electromagnetic spectrum. This is achieved by exploiting the unique electronic properties of PbS: the large Bohr radius of the exciton (20nm) in bulk PbS and the small dot diameter (<10nm) make possible a regime of strong confinement of carriers, thus leading to large confinement energies for both electrons and holes, and photon emission energies considerably larger than the energy gap of bulk PbS (E = 0.4 eV at T=290K). By tailoring the diameter of the PbS QD during the synthesis or by post-growth thermal annealing, we tune the photoluminescence (PL) emission of the dots in the NIR wavelength range (1000-1300 nm) in which light scattering is significantly reduced and transmission through biological tissues is higher. The QD PL emission is weakly affected by the additional confinement potential provided by a large magnetic field (B up to 14T), but is influenced at high temperatures (T>150K) by the dephasing of the electronic states due to carrier interaction with longitudinal optical phonons.

The AFt-PbS composite presents several advantages over existing biocompatible QD-constructs including water solubility and stability; the same mobility as that of the biocompatible AFt-protein; lower level of toxicity than those reported for other colloidal dots; and stable NIR PL emission. We discuss how these properties can open up prospects of using the AFt-PbS construct as a label for *in vivo* imaging of cells and biological tissues.

References

1. B. Hennequin et al., Adv. Materials **20**, 3592 (2008).
2. L. Turyanska et al., to published in Small (2009).

Sensing near to mid infrared light with an organic/inorganic hybrid hetero–junction

Gebhard J . Matt*, Thomas Fromherz*, Mateusz Bednorz*, Saeid Zamiry**, Christoph Lungenschmied***, Christoph. J. Brabec***, Günther Bauer*

*Institute for Semiconductor and Solid State Physics, Johannes Kepler University, Austria,

**Christian Doppler Laboratory for Surface Optics, Johannes Kepler University, Austria,

***Konarka Austria, Austria

Keywords: organic semiconductors, hybrid structures

Organic and inorganic semiconductors are diverse in many of their physical properties but a combination of these can feature unexpected physical properties. In this work we demostrate an infrared light sensing scheme base on a fullerene derivative (PCBM) / silicon hybrid hetero–junction that is fully compatible with the well established silicon technology. Despite the absent light absorption of silicon and the PCBM in the infrared (IR), a hetero–junction of these materials absorbs and generates a photo–current (PC) in the near to mid IR.

A 140 nm thick PCBM film is spin cast on a single crystalline (001), boron doped ($p \approx 10^{16}\,\mathrm{cm}^{-3}$) silicon substrate ($p$–Si) in an inert gas environment. The fullerene film as well as the p–Si are contacted by aluminium contacts. The current–voltage characteristics of this hetero–junction shows an almost ideal diode behaviour with a reverse current–density smaller than 1 nA/cm^2 at 77 K and a 10^7 times higher current density at a forward bias of 1 V. Despite the absent light absorption of silicon and the PCBM for photon–energies smaller than 1.1 eV and 1.7 eV respectively, the hetero–junction of these materials absorbs in the infrared and generates a PC in the spectral region from 0.56 eV to the fundamental absorption of the p-Si at 1.1 eV. The infrared PC is measured from liquid nitrogen to room–temperature by step–scan Fourier transform spectroscopy. For 0.8 eV photon–energy, the responsivity of a not yet optimized device is in the range of 10^{-5} A/W at 77 K. As shown in the inset of Fig. 1(a), the photo–response at room–temperature is reduced by a factor of only 2 with respect to 77 K.

The spectral dependence of the PC is interpreted as being due to an direct excitation of electrons from the Si valence band–across the interface into conducting states of the PCBM film. Thus the onset of the PC corresponds to the energy barrier between the Si valence–band and the conducting fullerene states. This interpretation is consistent with the thermal activation behaviour of the dark–current measured under reverse bias.

Besides its scientific relevance, the simple fabrication process as well as its compatibility with the well established silicon technology makes the presented hybrid approach a promising candidate for widespread applications.

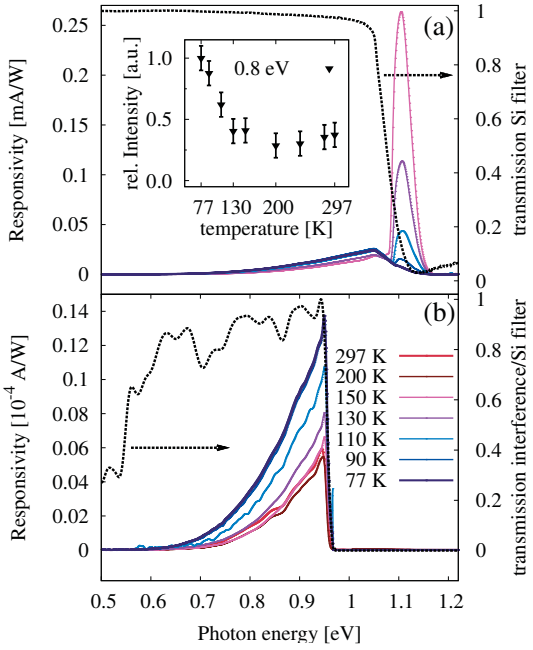

Figure 1: IR PC spectra at 0 V bias of an Al/p–Si/PCBM/Al hetero–junction in the temperature range from 297 to 80 K. In panel (a), the tungsten light–source is spectrally restricted by a Si filter and in panel (b) by an additional low pass filter with a cut–off at 0.95 eV. Filter transmissions are shown by the broken lines in (a) and (b). The normalized PC temperature dependency at 0.8 eV photon energy is shown in the inset of (a).

Carrier transport mechanisms of nonvolatile memory devices fabricated utilizing multi-walled carbon nanotubes embedded in a poly-4-vinyl-phenol layer

Won Tae Kim, Joo Hyung You, Jae Hun Jung, and Tae Whan Kim*

National Research Laboratory for Nano Quantum Electronics, Division of Electronics and Computer Engineering, Hanyang University, 17 Haengdang-dong, Seongdong-gu, Seoul 133-791, Korea

*Corresponding author E-mail: twk@hanyang.ac.kr

Keywords: nonvolatile memory device, MWCNT, PVP, C-V hysteresis, carrier transport mechanism

The electrical properties of multi-walled carbon nanotubes (MWCNTs) with high chemical stabilities have received much attention for fast-response memory devices [1]. Poly-4-vinyl-phenols (PVP)/MWCNT hybrid nanocomposites, which are fabricated by utilizing the combined advantages of chemical stabilities of the MWCNTs and the PVP layer, have been particularly interesting due to their potential applications in nonvolatile flash memory devices. Even though memory effects of nonvolatile memory devices fabricated utilizing CNTs dispersed in an organic layer have been investigated, studies on the carrier transport mechanisms of nonvolatile memory devices fabricated utilizing MWCNTs and embedded in a PVP layer have net yet been performed. Nonvolatile memory devices based on hybrid nanocomposites of MWCNTs embedded in a PVP layer were formed by using a spin-coating method. Transmission electron microscopy images showed that MWCNTs were dispersed in the PVP layer. Capacitance-voltage (C-V) measurements on the Al/MWCNTs embedded in PVP/p-Si (100) devices at 300 K showed a clockwise hysteresis with a large flatband voltage shift due to the existence of the MWCNTs, indicative of memory effects in the device, as shown in Fig. 1. The magnitude of the flatband voltage shift of the C-V curve for the Al/PVP and MWCNT composites/p-Si (100) devices increased with increasing MWCNT concentration, resulting in enhancement of charge storage capacity. Carrier transport mechanisms of the writing and the erasing processes for the Al/MWCNTs embedded in PVP/p-Si devices are described on the basis of the C-V results. These results indicate that the nonvolatile organic memory devices fabricated utilizing the MWCNTs embedded in the PVP layer hold promise for potential applications in next-generation nonvolatile memory devices.

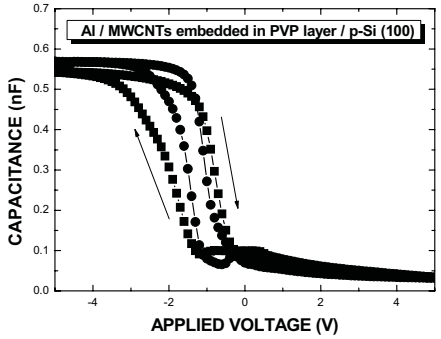

Fig. 1. Capacitance-voltage curves for Al/MWCNTs embedded in the PVP layer/p-type Si (100) devices with MWCNT concentrations of 0.02 (filled circles) and 0.1 wt% (filled rectangles).

Acknowledgements

This work was supported by the Korea Science and Engineering Foundation (KOSEF) grant funded by the Korea government (MEST) (No. R0A-2007-000-20044-0).

References

1. P. G. Collins, M. S. Arnold, and P. Avouris *Science* **292**, 706 (**2001**).

Characteristics of exciton polaritons in a ZnO Microcavity

T. Kawase, S. Komura, K. Miyazaki, D. Kim, and M. Nakayama

Department of Applied Physics, Osaka City University, Osaka, Japan

Keywords: ZnO, microcavity, exciton polariton, temperature dependence

Semiconductor microcavities have been extensively studied from the aspect of controlling exciton-photon interaction [1]. In a strong coupling regime, the mixing of the cavity photon and the exciton results in the formation of cavity polaritons. Recently, ZnO-based microcavities have been developed from the viewpoint of a large exciton binding energy of 61 meV, leading to the high stability of the excitonic system. In the present work, we have investigated characteristics of exciton polaritons in a ZnO microcavity with HfO_2/SiO_2 distributed Bragg reflectors (DBRs).

We adopted rf magnetron sputtering for the preparation of HfO_2/SiO_2 DBRs at the bottom and top of the microcavity. The ZnO active layer was prepared by pulsed laser deposition. For optical properties, the temperature dependence of angle-resolved reflectance and photoluminescence (PL) spectra were measured.

Figure 1 shows the angle-resolved reflectance spectra at 10 K in the effective one-wavelength (λ) thick ZnO microcavity. Four dip structures (●, ▲, ■, ○) appear in the energy region of the stop band of the DBR. The major reflectance dip with the lowest energy shifts to the higher energy with an increase in incidence angle. Furthermore, in the angle-resolved PL spectra, the PL band whose energy just agrees with that of the major reflectance dip is clearly observed. These results indicate that the major reflectance dip is attributed to the lower polariton branch (LPB). The experimental results for the incident angle dependence of the reflectance-dip energies were analyzed by calculating the cavity polariton dispersions with a phenomenological Hamiltonian for the coupling between the cavity photon and three kinds of excitons labeled A, B, and C peculiar to ZnO. The cavity polaritons consist of four branches: the LPB, first middle polariton branch (MPB1), second MPB (MPB2), and upper polariton branch (UPB).

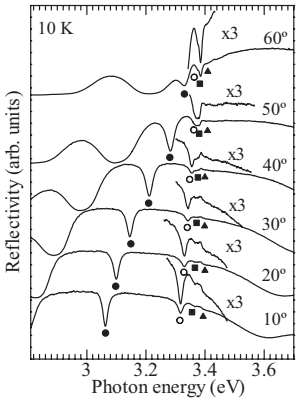

Fig.1 Angle-resolved reflectance spectra at 10 K in the λ-thick ZnO microcavity.

From the comparison of experimental results with the calculated one, it was found that the reflectance dips indicated by ●, ■, and ▲ are assigned to the LPB, MPB1, and MPB2. The UPB could not be observed because mixing effects of the UPB and continuum states may weaken the oscillator strength of the UPB mode and broaden the line shape. From the analysis, the vacuum Rabi splitting energy is estimated to be ~80 meV, which reflects the large exciton oscillator strength of ZnO.

The reflectance dip originating from MPB2 disappear at 77 K, and only LPB signal was observed at room temperature due to the broadening of the line shape with an increase in temperature. We discuss the temperature dependence of the exciton-polariton energies on the basis of the phenomenological Hamiltonian taking account of the temperature dependence of the exciton energies with the Varshni equation.

References

1. For a review, *The Physics of Semiconductor Microcavities*, ed. B. Deveaud (Wiley, 2007)

Tunable coupling of mechanical vibration in GaAs microresonators

H. Okamoto[1], T. Kamada[1,2], K. Onomitsu[1], I. Mahboob[1], and H. Yamaguchi[1,2]

[1] *NTT Basic Research Laboratories, Nippon Telegraph and Telephone Corporation, Atsugi, Japan*

[2] *Department of Physics, Tohoku University, Sendai, Japan*

Keywords: micromechanical resonator, vibration, coupling, tuning

Coupled micromechanical resonators have recently become the focus of research because they allow the study of interesting physical phenomena, such as synchronization and mode localization.[1,2] They also enable new applications in sensors using the dynamics of the coupled system.[3] The coupling efficiency is determined by the eigenfrequency difference in the resonators. Therefore, frequency tuning is important and desired to control the vibrational coupling. Here, we demonstrate the controlled coupling in micromechanical resonators by using photothermal stress. By this method, perfect coupling of micromechanical resonators was realized.

The micromechanical system has two doubly-clamped beams of 40-μm length, 10-μm width, and 0.8-μm thickness [Fig. 1(a)]. The beams consist of top Au gates, AlGaAs/GaAs superlattice, *n*-GaAs, and *i*-GaAs layers. The two beams are mechanically coupled through an etching overhang. Each beam can be actuated separately by the piezoelectric effect by applying an a.c. voltage between the gates and the *n*-GaAs layer. The frequency response of the mechanical vibration was detected using a He:Ne laser via optical interferometry [Fig. 1(a)]. The eigenfrequency of the beams was tuned by adjusting the laser power. These measurements were performed in a vacuum at room temperature.

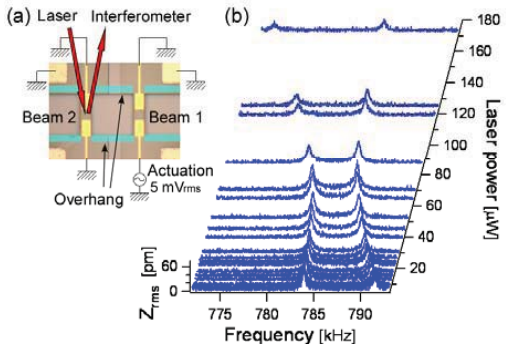

Fig.1 (a) Microscope image of the two mechanically coupled microresonators and an illustration of the measurement setup. (b) Laser power dependence of the resonance spectra of the coupled modes.

Figure 1(b) shows the laser power dependence of the resonance spectra of Beam 2 measured whilst actuating Beam 1. Since the two beams are mechanically coupled, Beam 2 vibrates when Beam 1 is actuated. Two coupled vibrational modes are found around the natural frequency: the nearly symmetric and anti-symmetric vibration for the lower- and higher-frequency, respectively. The coupling efficiency between the beams can be controlled by adjusting the laser power (P). Photo-induced thermal stress modifies the eigenfrequency of the beam with changing its spring constant. Increasing P reduces the eigenfrequency difference between the two beams, therefore enhancing the coupling efficiency. The frequency difference between the two coupled modes decreases with increasing P and is minimized at P = 64 μW [Fig. 1(b)]. At this laser power, the coupling is maximized and purely symmetric and anti-symmetric vibration is realized. For P > 64 μW, the frequency difference again increases with P increase, i.e., the coupled beams are optically detuned. This is the first demonstration of perfectly tunable vibrational coupling in micromechanical resonators.

This work was partly supported by JSPS KAKENHI (20246064).

References

1. S. Shim et al., Science **316**, 95 (2007).
2. C. Pierre, J. Sound Vib. **139**, 111 (1990).
3. M. Spletzer et al., APL **88**, 254102 (2006)

Noise induced phenomena in multi-thread excitable semiconductor 'neuron'

A.S. Samardak*,****, A. Nogaret*, N.B. Janson**, A. Balanov***, I. Farrer*****, D.A. Ritchie*****

* *Department of Physics, University of Bath, Bath, UK*

** *Department of Mathematics, University of Loughborough, Loughborough, UK*

*** *Department of Physics, University of Loughborough, Loughborough, UK*

**** *Department of Electronics, Far Eastern National University, Vladivostok, Russia*

***** *Cavendish Laboratory, University of Cambridge, Cambridge, UK*

Keywords: Quantum Tunneling Amplification, FitzHugh-Nagumo Model, Stochastic Resonance

We report on the stochastic dynamics of an excitable neuron-like structure which propagates and delays electrical pulses via a web of spatially distributed micro-transmission lines [1]. Artificial neurons were synthesized from modulation doped GaAs/AlAs tunnel layers grown by molecular beam epitaxy. Through a combination of selective etching and lithography, we obtain free standing structures [2,3] with artificial soma and dendrites. The 'neuron' emits bursts of electrical spikes whose coherence we study as a function of periodic stimuli and external noise. Noise is found to amplify weak periodic signals thanks to stochastic resonance (SR). SR is demonstrated when the power of the neuron output signal passes through a maximum at an optimum noise value.

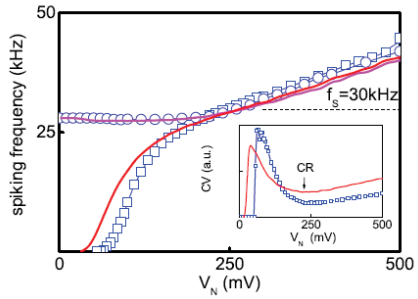

Fig.1 Noise induced synchronization. Frequency of output spikes with entrainment (open circles) and without (open squares). The full lines are the output frequencies computed with the modified FN model, as explained in the text. Entrainment parameters of sinusoidal drive: f_D=28kHz, V_D=90mV. Inset: Coherence resonance minimum at white noise amplitude V_N=220mV (open squares) and theoretical curve (full line).

We demonstrate two additional non-linear phenomena: coherence resonance (CR) and stochastic synchronization. CR is characterized by the activation of regular oscillations at the self-frequency of the neuron oscillator when no periodic drive signal is applied. The variance of inter-spike intervals (CV) is plotted in Fig.1 as a function of noise and shows a minimum at a noise of 220mV where spiking is most regular. This demonstrates CR. Coherence resonance also defines a noise threshold between a pulsing mode synchronized to external forcing and a pulsing mode synchronized to the frequency of self-oscillations. At noise levels below CR, the 'neuron' either synchronizes with the drive signal or remains silent. Above CR, the neuron synchronizes to its internal frequency augmented by noise. Data are quantitatively explained from first principles using a model derived from circuit analysis which relates to the FitzHugh-Nagumo model.

The neuron provides valuable feedback on mathematical models and is found to exploit the power of random noise to enhance the propagation of useful signals. Reproducing this property in the hardware is necessary to create realistic neuron-like structures.

References

1. A. Nogaret, et al., Europhys.Lett. **68**, 874 (2004).
2. A. Samardak et al., APL. **91**, 073502, (2007).
3. A. Samardak et al., New.J.Phys. **10**, 083010 (2008).

Surface State Control of Ⅲ-V Semiconductors using Molecular Modification

F. Yamada, T. Shirasaka, K. Fukui and I. Kamiya

Toyota Technological Institute, Nagoya 468-8511, Japan

Keywords: GaAs/InAs quantum structure, surface state, molecular modification, nano electronics

Surface states of semiconductors play important role in determining the properties of nanostructures and device fabrication. It is known that one of the origins of surface states lies in Fermi level pinning. When electrons and holes are trapped at the surface states, the properties of semiconductor devices such as photoluminescence (PL) or current-voltage characteristics are significantly modified. Hence, we need to distinguish the phenomena that arise from surface states from those of the bulk.

In this paper, we attempt to control the surface states of semiconductors using molecular modification. Yablonovitch et al. reported ammonium sulfide passivation of GaAs surface [1,2], where improvement in current-voltage characteristics was demonstrated. Here, we use thiol molecules, that interact with surface states. In addition, the electronic properties of the thiol molecules can be varied depending on the hydrocarbon group. For instance, benzenethiol is conductive due to the presence of π orbitals [3].

Surfaces of GaAs bare substrate, InAs wetting layer and InAs quantum dots prepared by molecular beam epitaxy (MBE) were treated by octadecanethiol and benzenethiol. The structures and electronic properties of the samples were evaluated by atomic force microscopy (AFM), current-voltage characteristics and surface potential measurements.

Figure 1 shows the surface topography of bare and octadecanethiol coated GaAs surfaces. The presence of octadecanethiol on the GaAs surface was confirmed from surface topography and contact angle measurements. It is known that alkanethiol self-assembled monolayer (SAM) change the surface potential of substrate in proportion to the length of the carbon chain [4]. The potential modification by SAM has strong influence on the surface states of semiconductors. Thus, the degree of Fermi level pinning of the semiconductor surfaces is controlled by the length of the carbon chains.

Benzenethiol was used to not only modify the surface states by potential change but also through interaction with the π-molecular orbital. Results will be shown on the PL and transport through these modified surface states.

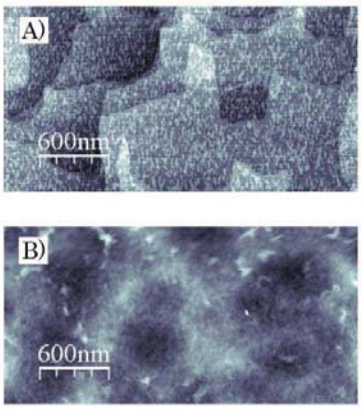

Fig.1 Surface topography of molecular beam epitaxy grown GaAs(001) A) before and B) after octadecanethiol coating.

References

1. E. Yablonovitch, *et al.*, Appl. Phys. Lett. **51**, 439 (1987).
2. Y. Nannichi, *et al.*, Jpn. J. Appl. Phys. **27**, L2367 (1988).
3. S. Datta, *et al.*, Phys. Rev. Lett. **79**, 2530 (1997).
4. R. Ichii, *et al.*, Nanotechnology **15**, S30 (2004).

Effects of mass induced anisotropy on Dirac-Fermions in graphene-based double quantum wires

Cesar E.P. Villegas and Marcos R.S. Tavares
Centro de Ciências Naturais e Humanas, Universidade Federal do ABC, Santo André, SP 09210170, Brazil.

Keywords: Graphene, Quantum wires, Dirac-Fermions

We theoretically investigate the two-dimensional (2D) Dirac Hamiltonian in the presence of an extra confinement potential written in the form

$$H = v_F \begin{pmatrix} mv_F & p_x - ip_y \\ p_x + ip_y & mv_F \end{pmatrix} + V(x), \qquad (1)$$

where v_F is the Fermi velocity, (p_x,p_y) are the momentum operator components, and $V(x)$ is the one-dimensional (1D) confinement potential designed as a double potential well, of a quadratic form, which models the graphene-based double quantum wires of width L_1 and L_2, respectively, and separated by a potential barrier of width L_B and height V_B.

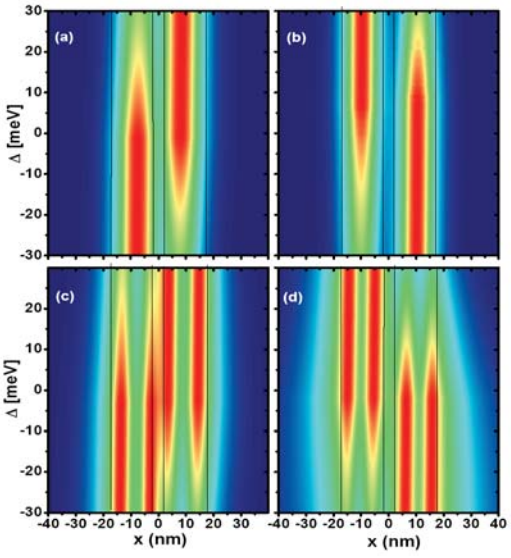

Fig1. Intensity of the probability density function of electrons in the subbands (a) $n = 1$, (b) $n = 2$, (c) $n = 3$,(d) $n = 4$ subbands. The two wires are of $L_1 = L_2$=15 nm wide, separated by a barrier of width L_B=4 nm heigth V_B= 150 meV. Vertical lines denote the confining potential interfaces.

We consider the diagonal massive terms in Eq. 1, mv_F, so that each region (well and barriers) is supposed to have different electronic masses. As a consequence, we can study mass induced anisotropy effects. The diagonal terms in Eq. 1 can actually be related to the energy hopping of the next-nearest-neighbour in the tight binding formalism. [1] We defined the parameter $\Delta = v_F^2(m_b - m)$ to quantify this anisotropy, where m_b and m are the electronic masses in the barrier and in the electrode regions, respectively.

In Fig.1 we show the probability density intensity, as a function of both the x-direction and the parameter Δ, for the first four confined electronic subbands. We are able to mapped out the spatial regions where electrons, in a given subband, have the most chance to be located (red intensity). [2] As the parameter Δ changes, the electron chooses a given wire to be located. Notice also the red intensity in the barrier region in Fig. 1(c), which means strong mixed states (tunneling) in the third confined subband.

Comparison to the zigzag nanoribbon can be provided when one sets the proper pseudo-spinor component to zero at the structure edges. [3] The anisotropy showed in Fig. 1 can indeed be tuned to suit experimental situation where zigzag termination in nanoribbons prevails.

References

[1] G. W. Semenoff, Phys. Rev. Letter **53**, 2449 (1984).

[2] C.E.P. Villegas, and M.R.S. Tavares, to be published.

[3] A.H. Castro Neto *et al*, Rev. Mod. Phys., Vol. 81, No. 1, (2009).

Transport in zigzag graphene nanoribbons modulated by magnetic barriers

N. Myoung*, G. Ihm* and S.J. Lee**

* *Department of Physics, Chungnam National University, Daejeon,305-764, Korea*

** *QSRC, Dongguk University, Seoul, 100-715, Korea*

Keywords: transport, graphene, nanoribbons, magnetic barriers

The physics of monolayer graphene devices has recently attracted a great deal of attention[1]. The relativistic dispersion relation of two-dimensional massless Dirac fermions results in quite different transport properties from electrons of conventional materials. For example, Dirac fermions can not be confined by electrostatic potentials. An electrostatic potential barrier shows no reflection for Dirac fermions incident in the normal direction[2]. Very recently, there has been an alternative approach of using magnetic barriers to overcome such confinement problem[3].

In this study we further develop the latter approach and study the one dimensional transport in zigzag nanoribbons modulated by a magnetic barrier structure such as

$$B_z = B l_B [\delta(x) - \delta(x - L)] \quad , \qquad (1)$$

where l_B is a fixed magnetic length scale. This inhomogeneous magnetic field distribution can be created by the use of ferromagnetic gates and does the exact role of tunneling barrier experienced by Dirac fermions[4].

The conductance is obtained in our structure as a function of incident (Fermi) energy. The results show stepwise increases superimposed upon the characteristic oscillations of order of height $4e^2/h$.

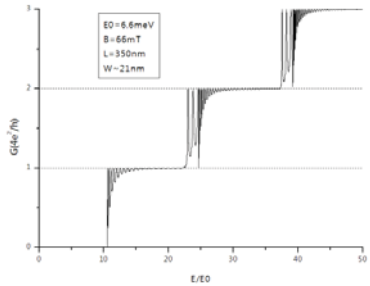

Fig. 1. Conductance as a function of Fermi energy.

References

[1] K. S. Novoselov et al. Science 306, 666(2004); Nature 438, 197(2005).

[2] M. I. Katnelson, K. S. Novoselov, and A. K. Geim, Nature Physics 2, 620(2006).

[3] A. De Martino, L. Dell'Anna, and R. Egger, Phys. Rev. Lett. 98, 066802(2007).

[4] N. Myoung and G. Ihm, to be published.

Selective area growth of ZnO nanorods and enzyme immobilization toward the fabrication of glucose sensors

K. Ogata, H. Dobashi, K. Koike, S. Sasa, M. Inoue and M. Yano

Osaka Institute of Technology, Osaka, Japan

Keywords: ZnO nanorods, selective area growth, enzyme immobilization, XPS characterization

Because of their large surface areas, ZnO nanorods are considered to be one of the candidate materials for high sensitive chemical sensors. Since integration and biofunctionalization are of importance for the fabrication of biosensing devices, selective area growth of ZnO nanorods and enzyme immobilization on their surface were investigated.

ZnO nanorods were grown using aqueous solution via microwave irradiation heating[1]. Photoresist-patterned substrates were prepared for selective area growth. As for the enzyme, glucose oxidaze (GOx), the enzyme of specific detection of glucose, was utilized. In prior to GOx treatment, ZnO nanorods were treated with aminopropyltrimethoxysilane (APTMS) and glutaraldehyde (GA) and GOx treated ZnO nanorods were charatcterized by means of Xray photoelectron spectroscopy (XPS).

As shown in Fig.1, ZnO nanorods were grown on patterned areas after removal of photoresit layer and a magnified image depicted that nanorods with about 200nm diameter were densely grown, indicating that the selective area growth was available. Figure 2 shows XPS spectra of APTMS treated ZnO nanorods and that with GOx in C1s region. Compared with the APTMS-treated ZnO nanorods, two additional peaks at around 287eV were observed in GOx treated ones.

Those results are promising toward the fabrication of high sensitive glucose biosensors based on ZnO nanorods. Considering that N1s peak related with amino group was strongly appeared in GOx treated ones, those two peaks were attributed to the characteristic chemical groups of the proteins[2]. In addition to that, they remained even immersion in phosphate buffered solution (PBS, pH7.4) for 10 min., implying that GOx was successfully immobilized on the surface of ZnO nanorods.

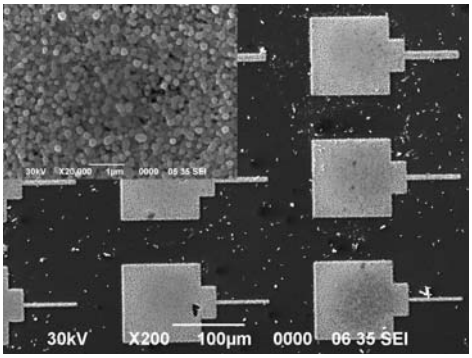

Fig.1 SEM image of ZnO nanorods grown on selective patterned area by photolithography. Inserted is magnified image of ZnO nanorods.

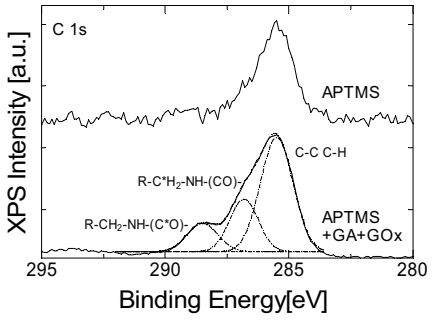

Fig.2 C1s XPS spectra of APTMS treated ZnO nanorods and GOx treated ones with anchoring APTMS and GA molecules.

References

1. K. Ogata *et al.,* Mater. Res. Soc. Symp. Proc. **1035**, L08-16 (2008).
2. S. Libertino *et al.*, Appl. Surf. Sci. **253**, 9116 (2007).

Computational study for growth of GaN on graphite as 3D growth on 2D material

T. Tatani[1,2], H. Asano[1,2],A.Ishii[1,2]

[1]*Group of computational material science*
Department of mechanical and aerospace engineering
Tottori Universiy, Koyama, Tottori 680-8552, Japan
[2]*JST-CREST, 5 Sanbancho, Chiyoda-ku, Tokyo 102-0075, Japan*

Keywords: Catalyst, Pd, GaAs, DFT

Graphene can be a good substrate of nanoscale growth of devices. Recently, the pulsed laser deposition technique has been developed for heteroepitaxial growth. Especially, using the room temperature growth technique, we can apply the pulsed laser deposition for growth of nitrides with various substrates even at room temperatures[1]. The heteroepitaxial gorwth of AlN on carbon-face SiC(0001) using the pulsed laser deposition has been reported[2] and even for graphite substrate, the epitaxial growth of nitride is reported to be possible[3]. The grown nitride on graphite has reported to bind strongly with the substrate graphite and to have enough good crystal quality for light emission device.

In order to improve the quality of grown GaN, theoretical investigation with the first principles calculation is required. In recent theoretical study[4], the adsorption sites and adsorption energies for many atomic species have been reported. In the calculation, graphene is used as surface of graphite. Using the first principles calculation, we investigate the adsorption properties for both Ga and N. The adsorption energy of N is 4.4eV. For Ga, though the predicted adsorption site is H6-site, the migration energy for Ga adatom on graphite is very small. According to the DFT calculation, we found that the N-terminated GaN($000\bar{1}$) growth on graphene is more stable than the Ga-terminated GaN(0001) growth on the graphene. The importance of the growth of this system is the two dimensionality of the substrate, graphite. This two dimensionality make the lattice mismatch not serious.

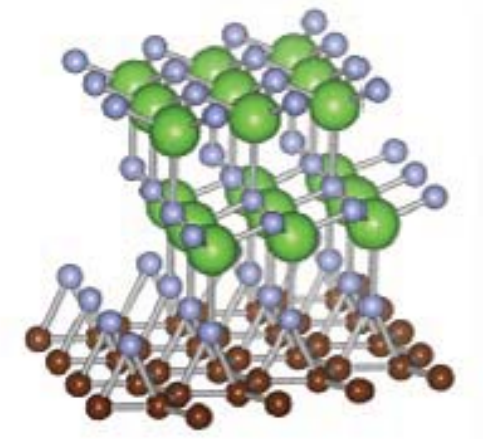

Figure 1: The most stable struture of GaN on graphene. The grown GaN is ($000\bar{1}$).

This work is supported by JST-CREST project.

References

[1] K. Ueno, A. Kobayashi, J. Ohta, and H. Fujioka, Jpn. J. of Appl. Phys. Express Letters, 45, L1139, (2006).;A. Kobayashi, Y. Kawaguchi, J. Ohta, and H. Fujioka, Appl. Phys. Lett., 89, 111918 (2006); G. Li, J. Ohta, K. Okamoto, A. Kobayashi, and H. Fujioka , Appl. Phys. Lett., 89, 182104 (2006); M.-H. Kim, M. Oshima, H. Kinoshita, Y. Shirakura, K. Miyayama, J. Ohta, A. Kobayashi, and H. Fujioka, Appl. Phys. Lett., 89, 031916 (2006); A. Kobayashi, S. Kawano, Y. Kawaguchi, J. Ohta, and H. Fujioka, , Appl. Phys. Lett., 90, 041908 (2007); M.-H. Kim, J. Ohta, A. Kobayashi, H. Fujioka, and M. Oshima, Appl. Phys. Lett. 91, 151903 (2007).

[2] M.-H. Kim, J. Ohta, A. Kobayashi, H. Fujioka, and M. Oshima, Physica Status Solidi - Rapid Research Letters, 2, 13 (2008).

[3] H.Fujioka, private communication

[4] A. Ishii, M. Yamamoto, H. Asano and K. Fujiwara, Journal of Physics: Conference Series 100 (2008) 052087

Band structures of Bernal graphenes modulated by electric fields

S. J. Tsai, J. H. Ho, Y. H. Chiu, and M. F. Lin

Department of Physics, National Cheng Kung University, Tainan 701, Taiwan

Keywords: Bernal graphene, modulated electric field, electronic structure

Recently, there is rising interest in the electronic properties of few-layer graphenes under the modulated magnetic [1,2] and electric fields [3,4]. In this work, the tight-binding model is used to study the influence of modulated electric fields on a bilayer Bernal graphenes (BBG). The effects of interlayer interactions and periodical electric field are investigated in detail.

When a modulated electric field is applied along the armchair direction, the low-frequency energy bands of BBG at R_E=250 (R_E, the period) and V_0=0 (V_0, the field strength) display many parabolic bands, as shown in Fig. 1(a). The conduction and valence bands have weak overlap around the Fermi level (E_F), which induces some Fermi-momentum states at E_F. In addition, the conduction and valence bands are asymmetric about Fermi level. As the field strength increases, as shown in Fig. 1(b), the parabolic bands would oscillate, exhibit some extra band-edge states, and their degeneracy would be broken. The energy dispersions of different modulated periods and directions are also discussed, as shown in Figs. 1(c) and 1(d), respectively. The main features of energy bands would be directly reflected on DOS, as shown in Figs. 2(a)-2(d). DOS presents a lot of prominent peaks originating from extra band-edge states. The finite DOS at Fermi energy resulting from the Fermi-momentum states implies that BBG is semimetallic graphene owing to the interlayer interactions. The dependences of DOS on the field strength, modulated period, and modulated direction are investigated in detail.

References

1. S. Park et al., Phys. Rev. B 77, 075433 (2008).
2. Y. H. Chiu et al., Phys. Rev. B 77, 045407 (2008).
3. J. H. Ho et al., Nanotechnology 19, 035712 (2008).
4. C. H. Park et al., Nature Phys. 4, 213 (2008).

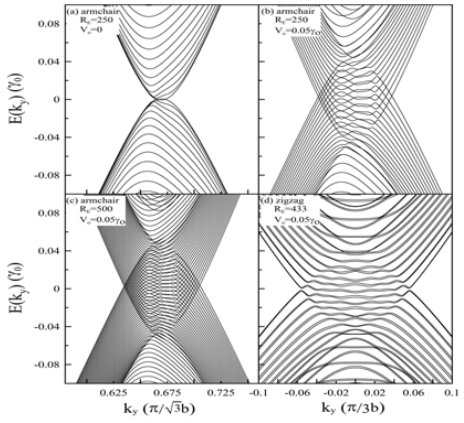

Fig.1 Low-energy bands at (a) R_E=250, V_0=0; (b) R_E=250 and V_0=0.05γ_o; and (c) R_E=250 and V_0=0.05γ_o along the armchair direction. The energy dispersions along the zigzag direction are also shown in (d).

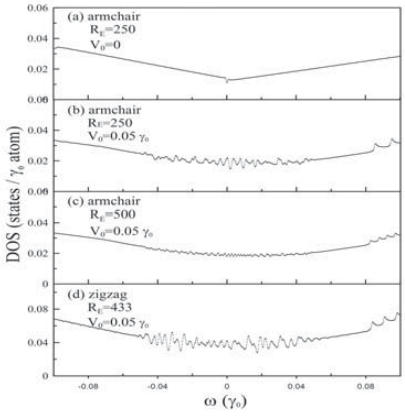

Fig.2 The density of states corresponding to Figs. 1(a)-1(d) are shown in (a)-(d), respectively.

The effects of the modulated magnetic field on the Landu levels of monolayer graphene ribbon

Y.H. Liu, J.Y. Wu, M.F. Lin

Department of Physics, National Cheng Kung University, Taiwan

Keywords: Graphene ribbon, modulated magnetic field, electronic property

Magnetoelectronic properties of one dimensional nanographene ribbon have been investigated by the Peierl tight-binding model recently. The uniform magnetic flux condenses electrons and induces partial flat band (Landau energy band). The Landau flat band could be drastically affected by a weak spatially modulated magnetic field and strongly depend on the field strength, period, and ribbon width. The main features of energy band are directly reflected in density of states (DOS), such as the position, height and the number of dominant strong peaks.

The existence of uniform magnetic field in one layer graphene sheet can transform the parabolic band into the Landau flat band [1]. The same effect can be seen in the nanographene ribbon also. Especially as the larger magnetic field is applied in the ribbon system, the distribution width of wavefunction would become shorter and the effect of ribbon's boundary could be decreased. As a result, the Landau energy level in 1D graphene ribbon would be similar with the one in 2D graphene sheet.

By applying a small modulated magnetic field, the low-energy landau flat bands would be altered into parabolic oscillating bands [2]. In each band, there are two prominent band edge states, one emerges at the maximum and the other appears at the minimum of the modulated magnetic field. Beside these, some edge states appear at both sides of energy band are made by the ribbon's boundary, and they would not be discussed in this article. The band curvature and the position of band edge states could be affected by the modulated field with different period and phase. However, the energy of band edge states only depends on the magnitude of the modulated field.

In the density of states (DOS), the modulated magnetic field could split the prominent peak into two lower peaks and the frequency's difference between the two peaks is dominated by the strength of the modulated magnetic field. The predicable electronic properties are associated with transport properties and magneto-optical spectra which can be measured by experiment.

References

1. C. P. Chang, Y. C. Huang, C. L. Lu, J. H. Ho, T. S. Li, and M. F. Lin, Carbon 44, 508 (2006)
2. J.Y. Wu , J.H. Hoa Y.H. Lai , T.S. Li , M.F. Lin, Physics Letters A 369 (2007) 333–338

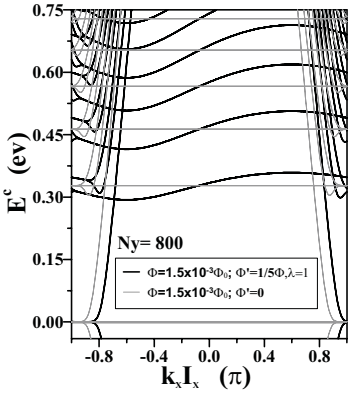

Fig.1 The low electronic structures of the N=800 armchair ribbon with the uniform (modulated) magnetic field $\Phi=1.5x10^{-03}\ \Phi_0$ ($\Phi'=1/5\Phi$, period $\lambda=1$).

Proximity effects in S-Si-QW-S sandwich nanostructures

N. T. Bagraev*, W. Gehlhoff**, L. E. Klyachkin*, A. A. Kudryavtsev*,
A. M. Malyarenko*, V. V. Romanov*** and I. A. Shelykh***

* *Ioffe Physical-Technical Institute, St. Petersburg, 194021, Russia*

** *Institut fuer Festkoerperphysik, Technische Universitaet Berlin, D-10623 Berlin, Germany*

*** *Polytechnical University, St. Petersburg, 195251, Russia*

Keywords: superconductivity, proximity effect, bipolarons, silicon quantum well

Superconductor properties for the S-Si-QW-S sandwich structures that represent the p-type high mobility silicon quantum wells confined by the nanostructured delta - barriers heavily doped with boron on the n-type Si (100) surface are demonstrated by measuring the temperature and magnetic field dependencies of the resistance, thermo-emf, specific heat, magnetic susceptibility and using the technique of the local tunneling spectroscopy.

The studies of the cyclotron resonance (CR) angular dependences, the scanning tunneling microscopy images and the electron spin resonance show that the nanostructured delta - barriers consist of a series of alternating undoped and doped quantum dots, with the doped dots containing the single trigonal dipole centers, B(+) - B(-), which are caused by the negative-U reconstruction of the shallow boron acceptors, 2B(0) =>. B(+) + B(-). The temperature and magnetic field dependencies of the resistance, thermo-emf, specific heat and magnetic susceptibility are evidence of the high temperature superconductivity, T_c =145 K, that seems to result from the transfer of the small hole bipolarons through these negative-U dipole centers of boron at the Si-QW – delta - barrier interfaces.

The oscillations of the upper critical field and critical temperature vs magnetic field and temperature that result from the quantization of the critical current are found using the specific heat and magnetic susceptibility techniques. The value of the superconductor energy gap, 0.044 eV, derived from the measurements of the critical temperature using the different techniques appear to be practically identical to the data of the current-voltage characteristics and the local tunneling spectroscopy.

The extremely low value of the effective mass of the 2D holes in the S-Si-QW-S sandwich structures that is derived from the CR studies, the Aharonov-Casher (AC) oscillations and the temperature dependences of the SdH oscillations seems to be the principal argument for the bipolaronic mechanism of high temperature superconductor properties. The high frequency local phonon mode that is revealed with the superconductor energy gap in the infrared transmission spectra seems to be responsible for the formation and the transfer of small hole bipolarons.

The proximity effect in the S-Si-QW-S structure is identified by the findings of the multiple Andreev reflection (MAR) processes and the quantization of the supercurrent. The value of the superconductor energy gap, 0.044 eV, appears to be in a good agreement with the data derived from the oscillations of the conductance in normal state and of the zero-resistance supercurrent in superconductor state as a function of the bias voltage. These oscillations are found to be correlated by on- and off-resonance tuning the two-dimensional subbands of holes with the Fermi energy in the superconductor delta - barriers. Finally, the studies of the proximity effect in the 'sandwich' S-Si-QW-S structures show that the MAR processes are of great concern in the coherent transfer of the small hole bipolarons both between and along nanostructured delta - barriers confining the Si-QW.

X-ray photoelectron spectroscopy study of interface structure of epitaxial graphene on 4H-SiC(0001)

J. H. Park*, H. Smith*, L. Grazulis*, K. Eyink*, W.C Mitchel*
* Air Force Research Laboratory, Materials and Manufacturing Directorate,
AFRL/RXPS, Wright –Patterson Air Force Base, Ohio, 45433

Keywords: Graphene, Interface, Molecular Beam Epitaxy (MBE), Silicon Carbide (SiC)

The interface properties of epitaxial graphene have been studied by x-ray photoelectron spectroscopy (XPS) measurements. The epitaxial graphene was grown on 4H-SiC (0001) by high temperature molecular beam epitaxy. Various thicknesses of graphene were obtained by varying the substrate temperature from 1200°C to 1700°C. The thickness was estimated by the attenuation model[1] of photoemission lines from SiC and graphene layers.

C1s and Si2p core level spectra were obtained and analyzed. The best curve fit shows that the C1s spectra consists of three components, located at 284eV, 285.1eV, and 285.4eV. The dashed lines shown in Fig.1 are the results from the best curve fits and assigned to interface, graphene, and SiC, respectively. The fitting of Si2p spectra shows that there is one additional component with about a 0.31eV shift toward lower binding energy, which results from Si atoms trapped in the interface layer.

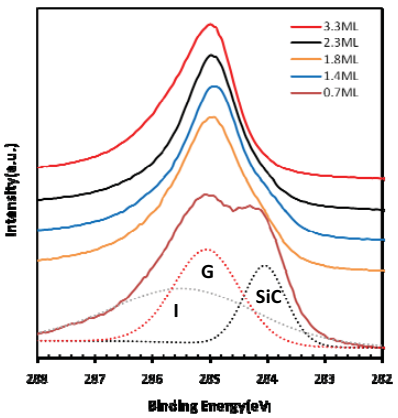

Fig.1 C1s core-level spectra (solid line) for various thicknesses of graphene. The curve fitting (dashed line) of the spectrum from the 0.7ML graphene layer shows theC1s spectrum is made of the three components SiC: SiC component; G: graphene component, I: Interface component.

We found that the interface/SiC C1s and Si2p peak intensity ratio increases as the graphitization progresses. These results suggest a model for graphene growth via an interface layer on the 4H-SiC (0001). At the initial stage of graphene growth, the carbon atoms from thermal decomposition of SiC convert into sp^2-bonded carbon (graphene) and some of atoms go into sp^3 hybrid states (interface), whereas all the Si atoms desorb from SiC surface. This assumption is supported by the existence of the interface layer and no additional components of the Si2p spectrum in the 0.7ML graphene sample. As graphitization progresses, carbon atoms simultaneously convert to graphene (sp^2 hybrids) and interface layer constituents (sp^3 hybrids) by keeping the sp^2/sp^3 concentration ratio constant. Some of Si atoms are trapped in the interface layer and their concentration increases.

In conclusion, graphene layers grown on 4H-SiC (0001) by high temperature molecular beam epitaxy have an underlying carbon rich interface layer and its thickness increases as the graphitization progresses. The interface layer traps a significant amount of Si atoms, whose concentration also increases during the graphitization process.

References

1. Th. Seyller, K. V. Emtsev, K. Gao, F. Speck, L. Ley, A, Tadich, L. Broekman, J.D. Riley, R. C. G. Leckey, O. Radar, A. Varykalov, A. M. Shikin, Surf. Sci. **600**, 3906 (2006).

Charge transport through chains of nanoparticles

T. Lüdtke[1], P. Mirovski[1], R. Hüther[1], Leonid Govor[2], G. H. Bauer[2], J. Parisi[2] and R. J. Haug[1]
[1] *Institut für Festkörperphysik, Leibniz Universität Hannover*
[2] *Institut für Physik, Universität Oldenburg*

Keywords: nanoparticle, transport

To analyze single electron transport through chains of nanoparticles is of great interest especially with decreasing number of particles and smaller particle sizes. We present transport measurements through nanoparticles as well as preparation techniques to contact short chains of nanoparticles.

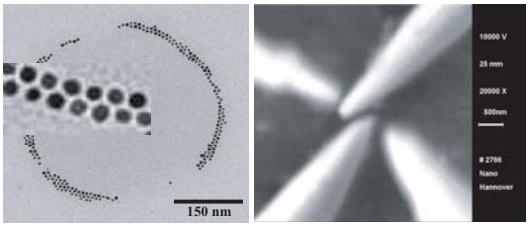

Figure 1: Nanoparticle chain after deposition on a substrate (left) measured with a multi-probe measurement setup (right)

To deposit the nanoparticles used in the measurement a droplet of the solvent containing the particles is put onto the substrate. When the droplet evaporates the nanoparticles along the contact line of the droplet form a ring-shaped chain. The length of the chain as well as the number of chains in parallel is dependent on the concentration of particles in the solvent [1].

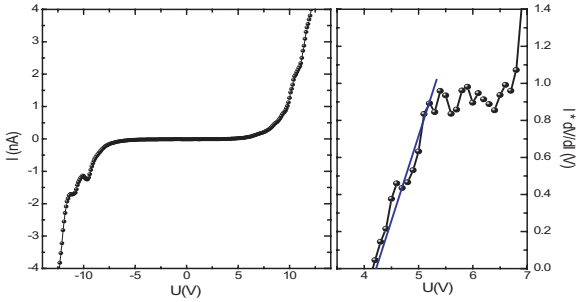

Figure 2: Current-voltage characteristic of a nanoparticle chain. From the $I \cdot d\ /dI$ characteristic threshold and power law scaling is calculated.

We present I-V measurements of nanoclusters at room temperature done inside a electron microscope containing a self-made multi-probe measurement setup. The setup allows contacting nanoparticle chains without using further fabrication steps after the deposition of the nanoparticles onto the substrate. Transport through the nanoparticles shows typical power law scaling known from I-V characteristics in low dimensional systems, originating from multiple conducting channels between the electrodes[2]. Steps in the characteristics indicate single electron tunnelling. Several consecutive measurements were performed at the same location on the sample showing a shift in the threshold voltage for the onset of conduction to lower values. We attribute this to rearrangements of the current paths.

References

[1] L. V. Govor, G. Reiter, G. H. Bauer, and J. Parisi, Appl. Phys. Lett. **84**, 4774 (2004).

[2] Klara Elteto, Xiao-Min Li, and Heinrich M. Jaeger, Phys. Rev. B **71**, 205412 (2005).

Nonlinear Switching Dynamics in Nanoelectromechanical Systems

Q. P. Unterreithmeier, T. Faust and J. P. Kotthaus
Fakultät für Physik and Center for NanoScience (CeNS), Ludwig-Maximilians-Universität, München, Germany

Keywords: Nanoelectromechanics, Nonlinear Nanomechanics

Multistability is a typical phenomenon of nonlinear systems. The resulting states can be utilized to represent a logic bit. Here we present a simple and scalable memory element based on the oscillatory state of a driven nanoelectromechanical system (NEMS).
Oscillating NEMS have been shown to reach high mechanical quality factors, exhibit small drifts and can easily be driven into the nonlinear regime. These characteristics make them ideal to study nonlinear dynamics. Complementary to prior work [1], we investigate the bistability resulting from a driven Duffing oscillator. At room temperature we actuate a doubly clamped string fabricated out of strained SiN with dimensions of $35,0\ 2,0\ 1\ \mathrm{m}$ (length, width, height, respectively) around its resonance frequency with a cw RF signal of about 10 MHz and 35 mV. We employ a novel driving scheme based on dielectric gradient forces. The resulting bistability can be viewed as a bit of information. Using either of the stable states of the driven Duffing oscillator as starting points and applying short and intense RF pulses, we are able to controllably switch between the states. Here, the switching takes approximately 1000 oscillations. This is considerably faster than the relaxation time of the linear system derived from the quality factor corresponding to 120,000 cycles.

We employ this pulsing technique to map out the stability diagram; related experiments have been reported in Ref. [2]. In addition, we utilize a combination of perturbation calculation and numerical integration to simulate the measured data. The approximate solution can be seen to be in close agreement with the experiment, see Fig. 1.

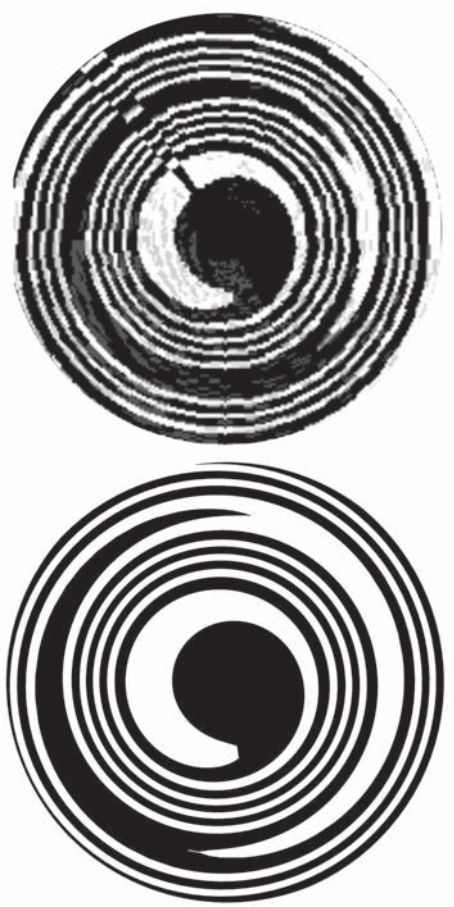

Figure 1: Regions of attraction in the stability diagram. Starting from an initial low amplitude state, an RF pulse of varying puls length (diameter) and phase (angle) is applied. Final low states are depicted in black, high states in white; top: experiment, bottom: simulation

References

[1] I. Mahboob and H. Yamaguchi, Nat. Nanotech. **3**, 275 (2008).

[2] I. Kozinsky, H. W. Postma, O. Kogan, A. Husain and M. L. Roukes, Phys. Rev. Lett **99**, 207201 (2007).

Optical absorption spectra of monolayer graphene in spatially modulated electric potentials

Y. H. Chiu[1], Y. Y. Liao[2], and M. F. Lin[1]

[1]*Department of Physics, National Cheng Kung University, Tainan 70101, Taiwan*

[2]*Department of Applied Physics, National University of Kaohsiung, Kaohsiung 81148, Taiwan*

Keywords: graphene, modulated electric field, optical absorption spectra, gradient approximation

Recently, the electronic properties of few-layer graphenes under the modulated magnetic [1,2] and electric fields [3,4] have attracted many studies. In this work, the low-frequency optical absorption spectra of monolayer graphene in spatially modulated electric fields are investigated by the gradient approximation within the tight-biding model. The modulated electric fields make the energy bands exhibit oscillatory energy dispersions and two kinds of band-edge states μ and ν, as shown in Fig. 1. Such band-edge states could lead to prominent peaks in the density of states, joint density of states, and optical absorption spectra, as shown in Figs. 2(a), 2(b), and 2(c), respectively. The optical absorption spectra are strongly affected by a modulated electric field, and they have not an obvious selection rule. The dependences of the absorption frequency on the modulated period and field strength are investigated in detail. The theoretical predictions could be verified by the experiment of energy-loss spectra and optical measurements.

References

[1] S. Park et al., Phys. Rev. B 77, 075433 (2008).
[2] Y. H. Chiu et al., Phys. Rev. B 77, 045407 (2008).
[3] J. Milton Pereira et al., Phys. Rev. B 75, 125433 (2007).
[4] C. H. Park et al., Nature Phys. 4, 213 (2008).

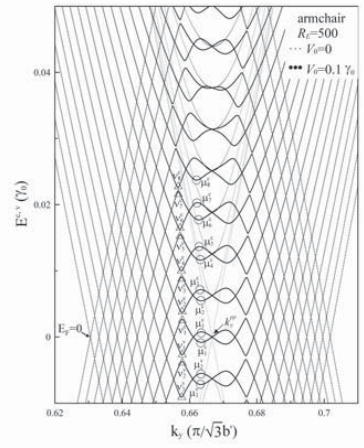

Figure 1. The energy bands of the period R_E=500 and field strength V_0=0.1 γ_0.

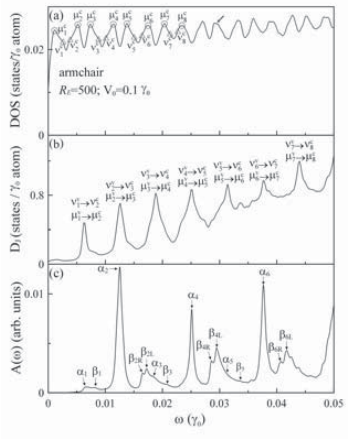

Figure 2. (a) The density of states, (b) joint density of states, and (c) optical absorption spectrum for R_E=500 and field strength V_0=0.1 γ_0.

Low-frequency noise in GaAs Solar Cell with Multi-Quantum Well

S. Kim*, Byung-Yong Yu**, Jungil Lee*, Seong-Il Lim*, Ilki Han* and Gerard Ghibaudo***

** Nano Device Research Center, Korea Institute of Science and Technology, 39-1 Hawolkok Seongbuk, Seoul, Korea*

***Advanced Metal Research Center, Korea Institute of Science and Technology, 39-1 Hawolkok Seongbuk, Seoul, Korea*

****IMEP-MINATEC, INPG-CNRS, 3 rue Parvis Louis Neel, BP257, 38016 Grenoble, France*

Keywords: Low-frequency noise, solar cell, multi-quantum well, deep levels

In this study, we fabricated GaAs single junction solar cells with multi-quantum well (MQW) and measured the photovoltaic response, current voltage characteristics under dark condition, and low-frequency noise characteristics. The current dependence of the noise density was discussed with both mobility and number fluctuation models.

The structures of GaAs single junction solar cell with MQW intrinsic layer were grown on n^+ GaAs substrate via metalorganic chemical vapor deposition (MOCVD), and had *p*-AlGaAs window layer for reduction of recombination velocity and *n*-AlGaAs back surface field layer for reduction of leakage current. The multi-quantum well consisted of three InGaAs and GaAs pairs with 200A of GaAs and 20, 40, and 60A of InGaAs.

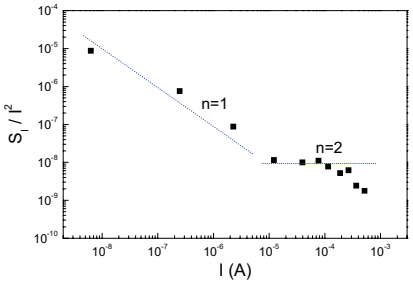

Fig.1 Normalised noise density at 10 Hz as a function of current.

The conversion efficiency was about 13%. I-V curves under dark condition showed typical characteristics of semiconductor *p-n* junction with the ideality factor of about 2.3 and the saturation current of about 10^{-8} A. Noise measurements showed 1/*f* behavior in general with additional Lorentzian components. The corner frequency moved to lower value as the current decreased indicating the existence of deep levels. The current dependence of the spectral density of 1/*f* noise was linear at low current and quadratic at higher currents. The transition current was about 10^{-5} A. At low current region where the noise density is linear, one can estimate the carrier lifetime [1]. At higher current where quadratic behaviour is observed, the tail states density [2] or surface states density [3] could be estimated. The defect states responsible for low-frequency noise might affect the conversion efficiency.

References

1. L. K. J. Vandamme, R. Alabedra and M. Zommiti, Solid-State Elec. **26**, No. 7, 671-674 (1983).
2. A. P. Dmitriev, M. E. Levinshtein, E. N. Kolesnikova, J. W. Palmour, M. K. Das and B. A. Hull, Semicond. Sci. Technol. **23**, 015011 (2008).
3. O. Jaentsch, IEEE Trans, Electron Dev. **ED-34**, 1100 (1987).

Transport characteristics of a single-layer graphene field-effect transistor grown on 4H silicon carbide

Keita Konishi and Kanji Yoh

Research Center for Integrated Quantum Electronics, Hokkaido University, Sapporo, 060-8628 Japan

Keywords: graphene, 4H-SiC, Klein tunnelling,

Epitaxial graphene growth on silicon carbide (SiC) seems to have greater potential of integration because they can be selectively formed on SiC substrates [1]. However, thickness (in number of monolayers) control and grain size control still remain a big challenge. Here we report the fabrication and electrical characterization of single layer graphite films formed on 4H-SiC substrate with increased grain size. Clear ambipolar characteristics and enhanced on/off ratio at cryogenic temperatures were observed. We also report interesting current oscillation in hole conduction mode is achieved by top gate.

Polished Si-face Semi-insulating 4H-SiC wafer is initially H_2 etched at 1370°C. After H_2 etching, we leak nitrogen into chamber and remove H_2 remaining behind with it. Then thin graphite films is formed in vacuum by the decomposition of the surface followed by the synthesis of graphite films with substrate temperature of 1,500°C and base pressure of about 1Pa for 10 minutes. The thin graphite films formation can be verified by AFM, LEED and Low-Energy Emission Microscope (LEEM) measurements [2]. Average of 1.3 monolayer graphene was verified with single layer graphene coverage of 95%. Top gated transistor structures were defined by using conventional photolithography. Ti/Au layer was used as Ohmic contact and gate electrode. Silicon dioxide (2000Å) was used as a gate oxide between the top gate electrode and graphene channel (Fig.1). The Hall measurements revealed carrier concentration of $2.46\times10^{12}/cm^2$ and mobility of $530cm^2/Vs$ a room temperature, respectively. Clear ambipolar characteristics were observed. Current modulation of 40% by gate voltage was observed at room temperature with drain current drivability of 20mA/mm. In addition, we observed increased on/off ratio at cryogenic temperatures suggesting finite band gap opening. The conductance dependence on gate voltage revealed interesting oscillation in p-region by applying negative top gate voltage (Fig.2). It may suggest a possibility of Klein tunnelling in single layer graphene [4].

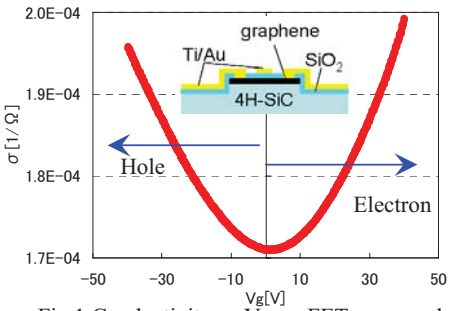

Fig.1 Conductivity vs Vg on FET measured at room temperature. The inset shows a device structure.

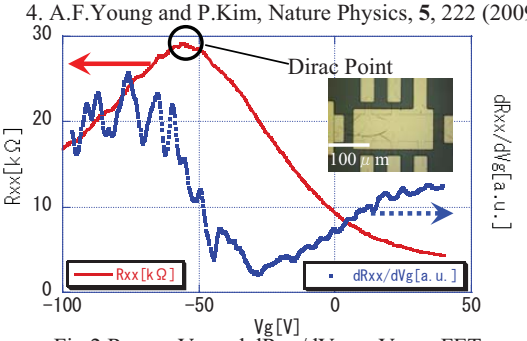

Fig.2 Rxx vs Vg and dRxx/dVg vs Vg on FET measured at 1.6K and at Id=10μA. The inset shows a device image.

References

1. C. Berger et al, J. Phys. Chem. B, **108**, 19912 (2004)
2. H. Hibino et al, Phys. Rev. B **77**, 075413 (2008)
3. K.Yoh, K.Konishi, and H.Hibino, unpublished
4. A.F.Young and P.Kim, Nature Physics, **5**, 222 (2009)

Characterization of supercapacitor of variable content of nitrogen doping in carbon nanotubes with ruthenium dioxide

K.-Y. Lee*,**, Y.-S. Lin**, Y.-M. Chen**, Y.-S. Huang*,**

* *Graduate Institute of Electro-Optical Engineering, National Taiwan University of Science and Technology, Taipei, Taiwan*

** *Department of Electronic Engineering, National Taiwan University of Science and Technology, Taipei, Taiwan*

Keywords: Supercapacitor, Carbon nanotubes, Nitrogen content, Ruthenium dioxide

The supercapacitor, also known as an ultra-capacitor or electrochemical capacitor, has attracted considerable interest due to its high power density, high energy density, and long cycle life [1]. Electric double layer capacitor (EDLC) and pseudo-capacitor are two forms of supercapacitor to store electrical energy. Among the structure of EDLC, the electrode plays an important role on the performance of EDLC.

Multi-walled vertically aligned carbon nanotubes (VACNTs) are extremely suitable for use as EDLC electrodes because of their good electrical conductivity, large effective surface area, and highly regular structure. To enhance the performance of EDLCs, some functional atoms [2] and oxides [3] such as nitrogen and ruthenium dioxide (RuO_2) are attached on the surface of the electrodes to improve the charge-exchange behaviour. In this study, we deposited RuO_2 nanorods on nitrogen-doped VACNTs to investigate the characteristics of the supercapacitors.

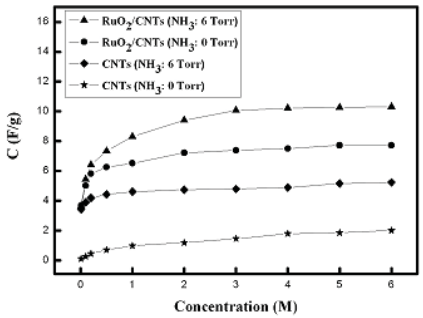

Fig.1 Comparison of the capacitances of pristine VACNTs, nitrogen-doped VACNTs, RuO_2/VACNTs, and RuO_2/nitrogen-doped VACNTs electrodes in different concentrations of KOH electrolyte.

The nitrogen-doped VACNTs were grown, using the thermal chemical vapour deposition (CVD) system, on stainless sheets. C_2H_2 and NH_3 were used as the carbon and nitrogen sources during the VACNTs growth, respectively. The RuO_2 nanorods were synthesized on the nitrogen-doped VACNTs by metal organic CVD. Figure 1 shows the capacitance curves of pristine VACNTs, nitrogen-doped VACNTs, RuO_2/VACNTs, and RuO_2/nitrogen-doped VACNTs electrodes in different concentrations of KOH electrolyte. It reveals that the addition of RuO_2 nanorods to nitrogen-doped VACNTs surface could efficiently increase the capacitance due to the pseudo-capacitor performance and increased surface area from the growth of the RuO_2 nanorod structure.

From the results, the nitrogen-doping and RuO_2 nanorods attachment on VACNTs could effectively enhance the characteristics of EDLC. More details of the research will be presented at the conference.

References

1. B. E. Conway J. Electrochem. Soc. **138**, 1539 (1991).
2. F. Kapteijn, A. J. Moulijn, S. Matzner and H. P. Boehm, Carbon **37**, 1143 (1999).
3. W.-C. Fang, K.-H. Chen and L.-C. Chen, Nanotechnology **18**, 485716 (2007).

Electronic states of atomic monolayers of various materials: Possibility of energy gap engineering

Tatsuo Suzuki*,** and Yushi Yokomizo**

* *Tokyo Metropolitan College of Industrial Technology, Minami-senju, Arakawa-ku, Tokyo,116-0003, Japan*

**Tokyo Metropolitan College of Aeronautical Engineering, Minami-senju, Arakawa-ku, Tokyo,116-0003, Japan*

Keywords: graphene, monolayer, electronic states, energy gap engineering

Graphene [1], an atomic monolayer of carbon atoms arranged in a honeycomb lattice, has been attracting intense interest since quantum Hall effects can be observed even at room temperature [2].

We have been interested in two-dimensional electrons confined within an atomic monolayer, and we calculated the electronic states of atomic monolayers which consist of various materials besides carbon atoms.

A honeycomb lattice was assumed as a crystal structure. The atoms were alternately placed like Fig.1 in case of a two-elements compound. The quantum chemical calculation software *Gaussian03* was used under periodic boundary conditions. The calculation method is LSDA/6-311G(d,p). We tried B3LYP/6-311G(d,p), but the convergence were difficult. The merits of our calculations are structural optimizations, so the effects of the Peierls transition are included.

The materials calculated are C, Si, Ge, GaAs, SiGe, AlP, BN, BAs, SiC, etc. The results are shown as Fig.2.

Fig.3 shows that the change of energy dispersions accompanied by the substitution of the atoms. In the case of Si and C, π bands make *Dirac point* at K point, so the band gap is almost zero. But when the 1/8 of carbon atoms are replaced with Si atoms, the enegy gap becomes open. This fact suggests that the impurity doping to monolayer materials can control the enegy gap of the monolayer materials.

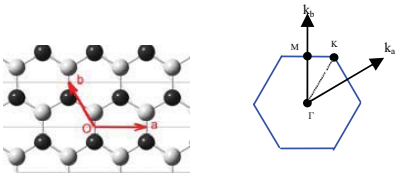

Fig.1 Cristal structure and Brillouin zone

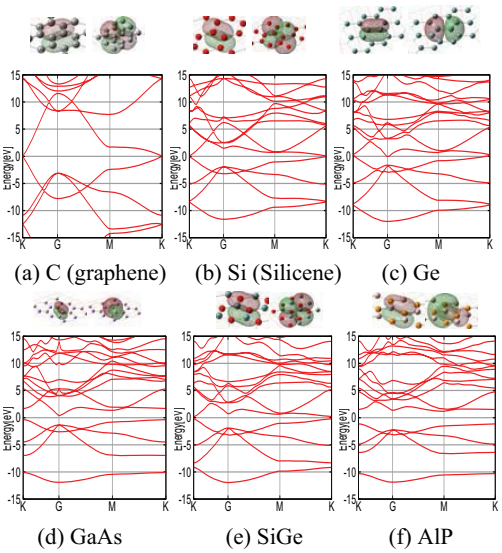

(a) C (graphene) (b) Si (Silicene) (c) Ge

(d) GaAs (e) SiGe (f) AlP

Fig.2 Energy dispersions and wave functions. The origin of energy is the Fermi energy. Left is the wave function of the top of valence band, and right is the wave function of the bottom of conduction band.

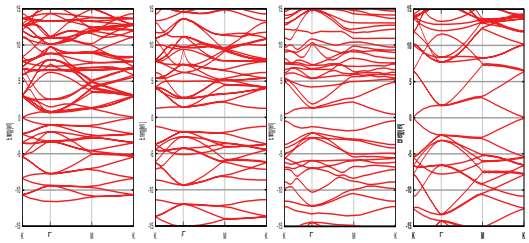

(a) Si (b) SiC (c) $Si_{0.125}C_{0.875}$ (d) C

Fig.3 Energy dispersions of Si, SiC, $Si_{0.125}C_{0.875}$, and C

References

1. K. S. Novoselov *et al*., Science **306**, 666 (2004).
2. K. S. Novoselov *et al*., Science **315**, 1379 (2007).

Statistics and single element processing in nanoporous templates

S. Mátéfi-Tempfli*, M. Mátéfi-Tempfli*, S. Melinte**, and A. Vlad**
*Unité PCPM, Université catholique de Louvain, Louvain-la-Neuve, 1348, Belgium
**Unité DICE, Université catholique de Louvain, Louvain-la-Neuve, 1348, Belgium

Keywords: statistical processing, surface packing optimization, porous alumina, single nanowire resolution

Nanoporous materials and templates have definitely settled the concept of mass production of low dimensional structures. The major drawback that restricts their pervasive integration into real working devices is the mismatch between their dimensionality and today's technological ability. For example, the hexagonal lattice is considered unsuitable for orthogonal arrangements required by the industry standard circuits. Here, we propose a general solution for the ultimate resolution processing of nanoporous templates. No overlay alignment is required to achieve single nanopore resolution and consequently, confined growth of single nanowires, with probabilities as high as 92% upon proper modulation of the patterning mask size.

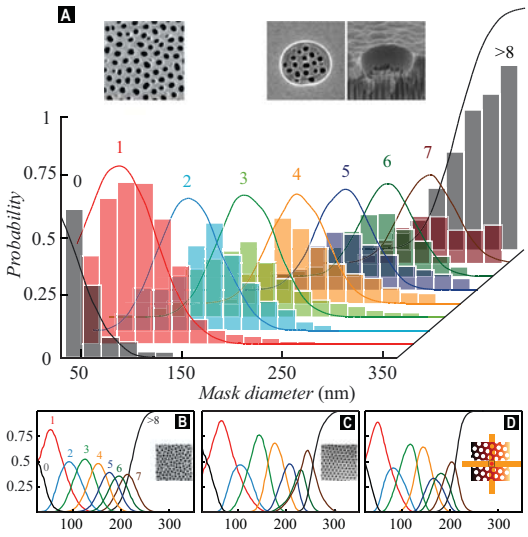

Figure 1: (A) Experimental histograms and simulated probability dispersions for selection and processing of a given number of nanopores inside alumina templates. Simulated probability dispersion for partially (B) and highly-ordered templates (C) using a circular mask or a square mask (D). Insets: 1×1 μm^2 micrographs showing the morphology of the employed templates and masks.

We present a systematic study on the number of accessed nanopores using selective mask processing of anodic aluminum oxide [1, 2]. Modulating the size and geometry of the mask enables statistical, yet accurate control over the achieved resolution. A well-defined probability dispersion, with distinct maxima at integer number resolution (from 0 to more than 8, as shown in Fig. 1A), exists for a given circular mask diameter range. We propose a simple image analysis procedure to simulate the experimental data, enabling fast screening of the processing reliability.

Downscaling the template features translates into a left-side shift of the probability peak positions accompanied by a reduction of the full-width at half maximum (Fig. 1B). Regular packing increases the single nanopore resolution up to 92% interfering only with null- and double-resolution and enhancing the 3, 4 and 7 nanopores bunch selection (Fig. 1C). Important, as well, is that a square mask provides the same degree of processability (Fig. 1D). While, the comprehensive explanation of the experimental and simulated stochastic behavior relies on a straightforward analytical formalism, the technology is interpreted in terms of surface and packing optimization.

Subsequent advanced processing allows for electrical connections to single nanowires with a high yield in a statistically controllable environment. We show that this technology is scalable and enables device design through parallel integration of template-embedded single nanowires.

References

[1] A. Vlad *et al.*, Nanotechnology **17**, 4873 (2006).

[2] A. Vlad *et al.*, Small **4**, 557 (2008).

Detection of Stress distribution using $Ca_2MgSi_2O_7$:Eu,Dy micro-particles

Hongwu Zhang[1)], Nao Terasaki[1)], Hiroshi Yamada[1)], Chao-Nan Xu[1), 2)*]

1) National Institute of Advanced Industrial Science and Technology (AIST), Kyushu, Shuku807-1, Tosu, Saga, 841-0052,JAPAN

2) CREST, Japan Science and Technology Corporation Honcho 4, Kawaguchi, Saitama 32-0012, JAPAN

Keywords: Mechanoluminescence; Stress distribution; $Ca_2MgSi_2O_7$:Eu,Dy; Sensor.

Mechanoluminescence (ML) is an interesting luminescence phenomenon caused by mechanical stimuli such as grinding, cutting, collision, striking and friction,[1] which can convert mechanical energy into visible light efficiently. The ML sensor to detect environmental stress by emitting light can be used widely in various applications such as the forecasting of an earthquake, the damage detection of an air plane or car.[1]

In this study, we prepared mechanoluminescent micro-particles $Ca_2MgSi_2O_7$:Eu,Dy (CMSED) using a sol-gel method. The CMSED micro-particles mixed with optical epoxy were coated on aluminium base using screen-printing method, which is used to detect the stress distribution of aluminium base under the application of stress. From the SEM image (Fig.1), it can be observed that the prepared sample consists of uniform particle with size distribution between 500 nm and 1 um. This results show that good quality luminescent micro particles can be obtained using this sol-gel method.

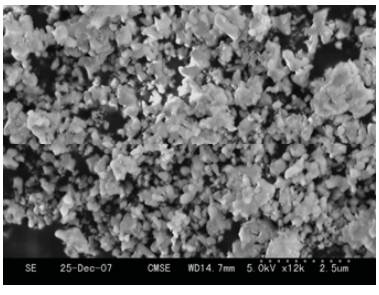

Fig.1. SEM image of CMSED microparticles

Fig. 2 shows the relation between the ML intensity and strain gauge. This figure demonstrates the excellent

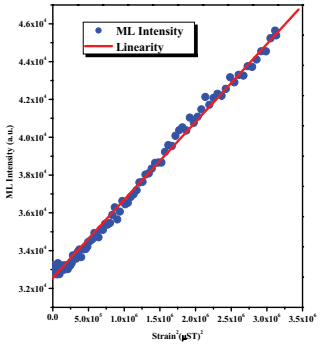

Fig. 2 Relation between ML intensity and strain gauge

linear relationship between the square of strain gauge and the corresponding increase in ML intensity. In other words, the ML intensity of CMSED is linearly proportional to the square of strain gauge, $I = K\varepsilon^2$, K is constant. As reported in previous papers,[2] the strain energy density accords with such an equation $F_\varepsilon = (M_{hkl})\,\varepsilon^2$, where M_{hkl} is the appropriate biaxial modulus, which is constant for the same materials. Thus, it can be noted that strain energy is responsible for the origin of ML, which can explain the excellent linearity between ML intensity and the square of strain gauge. In this way, we can utilize CMSED micro-particles to reflect the stress distribution of object when a stress was applied.

References

1. C. N. Xu, Encycl. Smart Mater. **1-2,** 190(2002).
2.C. Thompson, R. Carel, J. Mech. Phys. Solid. **44,** 657(1996)

Polarity determination of InN by terahertz radiation

K. I. Lin*, J. T. Tsai*, J. S. Hwang*, and M. C. Chen**

** Department of Physics, National Cheng Kung University, Tainan 701, Taiwan*

*** Institute of Nuclear Energy Research, Longtan, Taoyuan 325, Taiwan*

Keywords: indium nitride, terahertz radiation, polarity, spontaneous polarization

Indium nitride (InN) is an important component of the group-III nitride system and has recently received considerable attention due to the lowest effective mass, the highest mobility, and the highest saturation velocity of the group-III nitrides [1]. Recently, many reports indicate that the terahertz (THz) generation mechanism in InN is dominated by the photo-Dember effect [2]. This study investigates the polarity of InN by THz radiation excited by femtosecond optical pulses with a central wavelength of around 790 nm [1,3]. InN samples are grown by metalorganic chemical vapor deposition. An InN layer with a total thickness of approximately 220 nm is grown at 500 °C with an 8 nm GaN buffer layer on the top of sapphire substrates. Fig. 1(a) depicts time-domain wave forms of THz emission from *p*-InAs, *n*-GaAs, *p*-GaAs, and InN samples. The THz wave forms from *p*-InAs and *n*-GaAs have the same polarity, and that from *p*-GaAs and InN are in the reverse direction.

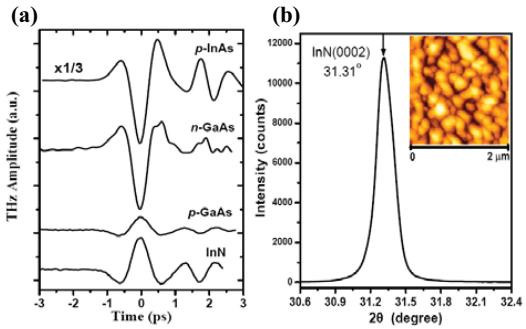

Fig.1 (a) Time-domain wave forms of THz emission from *p*-InAs, *n*-GaAs, *p*-GaAs, and InN samples. (b) X-ray θ-2θ scan of the (0002) diffraction from the InN epilayer. The inset shows the atomic force microscope image.

It is known that the THz radiation mechanism of *p*-InAs is dominated by the photo-Dember effect. The diffusion current (or the photo-Dember field) flows towards the surface of *p*-InAs. For *n*-GaAs, the drift current (or the built-in electric field) also flows towards the surface of the sample [3]. We find that the internal electric field in the InN layer is antiparallel to the electric field in *p*-InAs and *n*-GaAs and parallel to the surface depletion field in *p*-GaAs. This indicates that the dominant radiation mechanism in InN is the drift current induced by the internal electric field at low-density excitation below 590 nJ/cm^2.

The InN surface shows typical grain like morphology often observed in N-polar InN as shown by the inset in Fig. 1(b). The lattice constant c = 5.7091 Å for the InN epilayer is determined by θ-2θ scan of x-ray diffraction. This implies that the InN epilayer is fully relaxed [4]. Therefore, there is no piezoelectric polarization, and we conclude that the internal electric field in the InN layer results from spontaneous polarization. In N-polar InN, the direction of the spontaneous polarization is outward to the surface and the induced electric field has opposite direction in definition [1]. This direction for the induced electric field is consistent with the foregoing inferences from the THz measurements. The internal electric field consists of the surface accumulation field and the spontaneous polarization induced electric field.

References

1. K. I. Lin *et al.*, Appl. Phys. Lett. **93**, 262102 (2008), and references therein.

2. V. Cimalla *et al.*, Phys. Status Solidi B **244**, 1829 (2007).

3. J. S. Hwang *et al.*, Electrochem. Solid-State Lett. **11**, H63 (2008).

4. M. F. Wu *et al.*, J. Vac. Sci. Technol. A **24**, 275 (2006).

Resonant tunneling of electrons through single self-assembled InAs quantum dot studied by conductive atomic force microscopy

Ichiro Tanaka*, Y. Tada*, S. Nakatani*, K. Uno*, I. Kamiya**, and H. Sakaki**

** Department of Materials Science and Chemistry, Wakayama University, Wakayama, Japan*

*** Toyota Technological Institute, Nagoya, Japan*

Keywords: resonant tunnelling, InAs quantum dot, conductive tip, atomic force microscopy

Resonant tunneling of electrons through a quantum level in a self-assembled InAs quantum dot (QD) has been studied by conductive atomic force microscopy (AFM). As shown in Fig. 1(a), we fabricated by molecular beam epitaxy resonant tunneling diodes (QD-RTDs), comprising InAs QDs sandwiched by 1.7 nm-thick AlAs barriers and surface InAs QDs formed on 8.3 nm-thick cap layer as nano-scale electrodes.

Since each surface QD vertically aligns with a buried one, the current flowing via a buried QD can be measured with the conductive tip brought in contact with the surface QD electrode. A negative differential resistance attributed to the resonant tunneling through a buried QD is seen in the current-voltage characteristics, as shown in Fig. 1(b).

Earlier, we have shown that the resonance voltage, at which the current peak appears, becomes smaller as the size of QD electrodes increases [1]. However, it was not clear if the observed tunneling current flowed via the buried QD or the wetting layer. To clarify this point, we investigate here the correlation between the distribution of buried QD size and that of measured resonance voltage.

The size distribution of buried QDs was controlled by adjusting the amount of InAs deposited. Firstly, QDs were formed by depositing 2.2 or 2.7 monolayer (ML) of InAs, and buried in GaAs. Then photoluminescence (PL) spectra of these QDs were measured; the widths of PL peak was ~50 meV for QDs grown with 2.2 ML InAs, and ~90 meV for those with 2.7 ML InAs. Thus, it was found that the QDs grown with 2.7 ML InAs have a wider size distribution than those with 2.2 ML.

Then, we fabricated QD-RTD samples, which have the same structure shown in Fig. 1(a) except 2 MLs of GaAs was inserted between the lower AlAs barrier and buried QDs. Two sets of samples comprising 2.2 or 2.7 ML of InAs deposited were fabricated to prepare ODs of different size distributions. The distribution of resonance voltages was measured on QD-RTDs, and the results are shown in Figs. 2(a) and 2(b). It can be seen that the resonance voltages of the sample fabricated with 2.7 ML InAs are scattered more widely, and that the distribution of the resonant voltages is related with the size distribution of buried QDs.

References

1. I. Tanaka, Y. Tada, S. Nakatani, K. Uno, M. Azuma, K. Umemura, I. Kamiya, and H. Sakaki, Phys. Stat. Sol. (c) **5**, 2938 (2008).

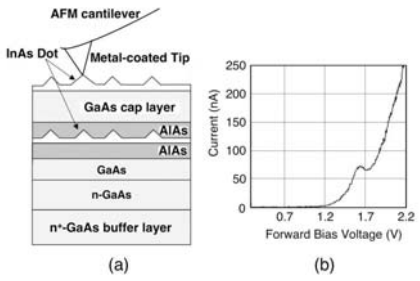

Fig.1 (a) Schematic illustration of the QD-RTD and (b) measured current-voltage characteristics.

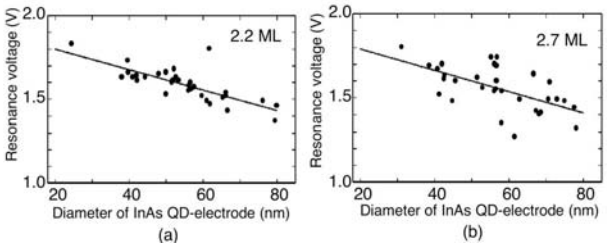

Fig.2 The distribution of resonant voltages measured with QD-RDTs, formed by depositing (a) 2.2 ML and (b) 2.7 ML of InAs.

Characterization of photoelastic effects on the optical properties of strained InN films

J. T. Tsai[*], K. I. Lin[*], Y.T. Lu[*], S. Gwo[**], M. C. Chen[***], G. C. Chi[***] , and J. S. Hwang[*,a)]

[*]*Department of physics, National Cheng Kung University, Tainan 701, Taiwan*

[**]*Department of Physics, National Tsing-Hua University, Hsinchu 30013, Taiwan*

[***]*Institute of Optical Science, National Central University, Jhongli, Taoyunan 320, Taiwan*

Keywords: photoelastic, piezoelectric, strain, phonon

We report a photoelastic screening effect of photo-generated carriers on the strain induced piezoelectric field in indium nitride (InN). MicroRaman and High-resolution x-ray diffraction(HRXRD) measurements are used to characterized the effect. The average variation of the biaxial strain in InN layers is deduced from a detailed analysis of the frequency shift of phonon lines. We find an increase in the optical excitation density is accompanied by a redshift in the frequency of the InN E_2(high) phonon. The frequency of the E_2(high) modes is strongly related to residual stresses induced in the InN epilayer. The underlying mechanism was attributed to the screening of the piezoelectric field by photoexcited carriers.

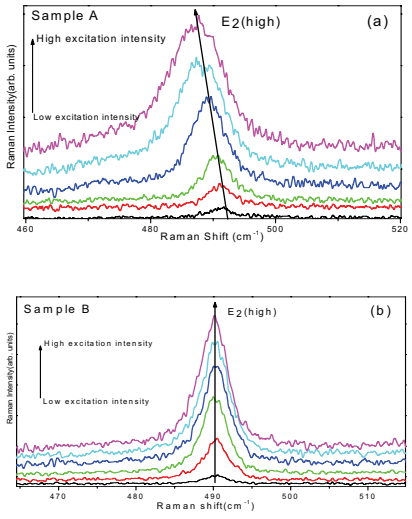

Fig.1. Excitation-intensity-dependent Raman scattering spectra of the strained InN (a) and the fully relaxed InN (b). In (a) the arrows indicate the red-shifts of E_2(high) in strained InN.

The samples A and B studied here are grown by metal-organic chemical vapor deposition (MOCVD) and plasma-assisted molecular-beam epitaxy (PA-MBE) respectively .

HRXRD investigations are performed to to evaluate the room temperature lattice constants *a* and *c*. The in-plane (e_{xx}) and out-of-plane (e_{zz}) strain are determined using the following values for unstrained lattice parameters c_0 = 5.703 Å and a_0 = 3.538 Å [1]: $e_a=(a-a_0)/a_0$ and $e_c=(c-c_0)/c_0$. Our results show that sample B is fully relaxed and the in-plane strains of sample A are generally biaxial compressive and $e_a \sim 10^{-3}$ in magnitude.

All the micro-Raman spectra have been recorded with a Jobin Yvon spectrometer U1000 in backscattering geometry, with excitation achieved using the 532 nm line of a Verdi laser, with incident light powers of between 2 mW and 40mW. As shown in Fig. 1, it is found that the E_2(high) phonon frequencies of the strained InN(sample A) decrease with increasing excitation power, while those of the strain relaxed InN are almost the same at low and high excitation power. We attribute this effect to the screening of the piezoelectric field from the photoexcited carriers. The frequency of the two E_2 modes is strongly affected by residual stresses induced in the InN epilayer. We try to estimate the variation of internal strain by Raman scattering versus excitation intensity. The strength of the internal strain in the InN films can then be estimated from the strain-induced phonon shifts, $\triangle\omega_i$, and the relationship quantified by the following expression[2]: $\Delta\omega=2a\varepsilon_a+b\varepsilon_c$, Apparently, the compressive strain, ε_a , exhibits a reduction 0.59% with increasing excitation intensity.

References

1. Xinqiang Wang, Song-Bek Che, Yoshihiro Ishitani, and Akihiko Yoshikawa, Appl. Phys. Lett. 89,171907(2006).
2. J. M. Wagner, F. Bechstedt, Appl. Phys. Lett. 77, 346(2000)

Electromigration-induced breakage mechanism of Ni nanowires

K. Yoshida*, A. Umeno*, S. Sakata* and K. Hirakawa*, **

* *IIS and INQIE, University of Tokyo, 4-6-1 Komaba, Meguro-ku, Tokyo 153-8505, Japan*

** *CREST-JST, 4-1-8 Honcho, Kawaguchi, Saitama 332-0012, Japan*

Keywords: Electromigration, ferromagnetic nanowire, break junction

Electromigration (EM) due to electrical stress has been widely used as a technique to fabricate metallic electrodes with nanometer-scale gaps essential for single molecular devices [1]. The mechanism of EM has been investigated for a long period and different physics models, such as electron wind force or Joule heating, have been proposed [2,3]. Recently, we proposed a new model that the transfer of kinetic energy from one electron to one atom induces the self-diffusion of atoms [4]. In order to check the validity of this new model for EM, the dependence on metal species must be carefully examined.

In this work, we have investigated EM-induced atom diffusion in Ni nanowires. We applied a feedback-controlled electrical stresses to Ni nanojunctions with ~100 nm-wide constrictions and gradually narrowed the Ni wires. During the EM process, we collected statistical data on the critical junction voltages, V_C, at which discrete step-like decreases in junction conductance by G_0 (= $2e^2/h$) (i.e., one-by-one atom removal from the constricted area) took place. A histogram of V_C obtained from the statistical processing of the data for $G < 30\ G_0$ is shown in Fig.1. It should be noted that a clear peak appears around 0.27 V, which is very close to the surface self-diffusion potential for Ni surfaces (0.30 eV) [5]. We identified this peak voltage as the threshold voltage for EM, V_{EM}. It is found that V_{EM} for Ni is different from that for Au [4], which reflects the chemical trends between Ni and Au.

Next, we investigated how the stability of Ni nanowires depends on the junction voltage, V. We fabricated a pair of Ni electrodes which are bridged by only three Ni atoms ($G = 3G_0$) and applied a bias voltage to the sample. Surprisingly, although the local current density in the atomic-scale constriction was higher than 10^9 A/cm^2, the atomic channel was very stable when $V < V_{EM}$ (see Fig.2, blue region). However, once $V > V_{EM}$ (yellow region), G decreased in a step-wise manner by G_0 in a short time. These results strongly support that EM is indeed induced by kinetic energy transfer from one electron to one atom.

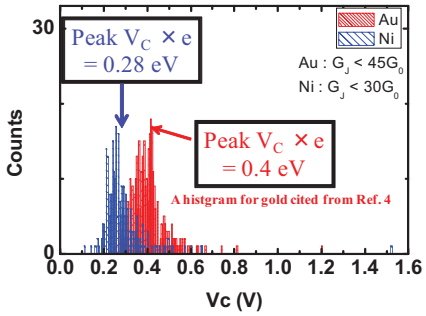

Fig.1 Two histograms of the critical voltage, V_C when junction conductance of Ni (blue) and Au (red) nanowires, G_J, showed discrete decreases by G_0.

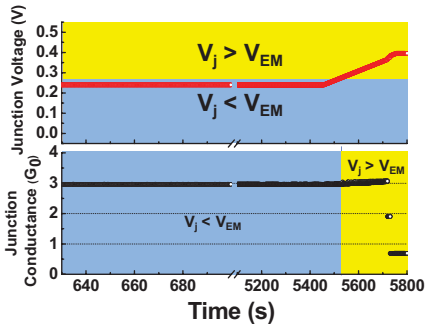

Fig.2 The time evolution of junction conductance and junction voltage of a pair of Ni electrodes contacted with three Ni atoms.

References 1) H. Park et al, Nature (London) **407**, 57 (2000). 2) H. B. Huntington and A. R. Grone, J. Phys. Chem. Solids **20**, 76 (1961). 3) D. R. Strachan et al., Appl. Phys. Lett. **86**, 043109 (2005). 4) A. Umeno and K. Hirakawa, *Submitted.* 5) R.T. Tung and W.R. Graham, Surf. Sci. **97**, 73 (1980).

Study of rolled micro cantilever-like structures based on MBE-grown strained semiconductor layers

H. Iwase*, H. Choi*, S. Yamada*, M. Tanaka** and I. Kimpara***
*Center for Nano Materials and Technology, Japan Advanced Institute of Sci. and Tech.
1-1, Asahidai, Nomi, Ishikawa 923-1292, Japan
** Department of Aeronautics, College of Engineering, Kanazawa Institute of Technology
*** Vice-president, Kanazawa Institute of Technology
7-1, Ougigaoka, Nonoichi-machi, Ishikawa-gun, Ishikawa 921-8501, Japan

Keywords: Bimorph structure, Cantilever structure, Finite element analysis, III-V compound semiconductor.

The most famous representative example of the bimorph structure is a thermostat. The difference between the thermal expansion coefficients is an origin of the internal stress for the bending moment. Today bimorph structure is widely applied to actuator and positioner.

The small rolled nano-structures have been fabricated by using compound semiconductor multi-layer structure with internal stress [1]. In our previous study, we have fabricated the cantilever-like structures based on the multi-layer structure including more than a couple of layer with strain. In such a case, we could make a variety of structures including the straight part, since the layers could cancel their stresses with each other [2]. However, the structures sometimes show unexpected curvatures.

In this study, we fabricated the rolled cantilevers from strain-induced multilayer structure, and compared the deformation of the cantilevers with calculation. We designed the base multi-layer structures with five layers; GaAs 8 nm / $In_{0.5}Ga_{0.5}As$ 1 or 2 nm / GaAs (including two $Al_{0.3}Ga_{0.7}$ As 3 nm) 86 nm / $In_{0.5}Ga_{0.5}As$ 1 or 2 nm / GaAs 8 nm. This structure was grown on GaAs (001) substrate via $Al_{0.7}Ga_{0.3}As$ sacrificial layer. Then the cantilever pattern is defined by lithography, and formed by Cl_2/BCl_3 reactive ion etching. Finally, the cantilever structure was separated by a selective etching of the sacrificial layer. Despite of the symmetrical strains, some of the fabricated structures have finite curvature radius. We considered the upper side InGaAs strained layer might not play it's role, and determined the calculation model of GaAs $h_1 = 96$ nm / $In_{0.5}Ga_{0.5}As$ $h_2 = x$ nm / GaAs $h_3 = 8$ nm.

To discuss the calculated deformation, we compared the primitive method [3] and finite element method (FEM) analysis. In the treatments of experimental results, measured curvature radiuses were converted to the displacements at the cantilever length of calculation model (l_0). As shown in Figure 1, the FEM calculation results explain the experiments better than the primitive calculation extended for three-layers. In the primitive method, only the strain along the direction of cantilever length is considered. However, the FEM results show that the effect of strain along the direction of width cannot be ignored. In the transmission electron microscopy observation, strained layer of the upper side seems to exist but not clear. Even when the effect of the upper side strained layer is neglected, the deformation of the cantilever is still larger than the FEM calculation. This might suggest the damage to the structure surface in the fabrication process.

References

[1] V. Prinz et al., Physica E6(2000)828.
[2] K. Kubota et al., Jpn. J. Appl. Phys. 42(2003)4079.
[3] A. Vorob et al., Jpn. J. Appl. Phys. 42(2003)4024.

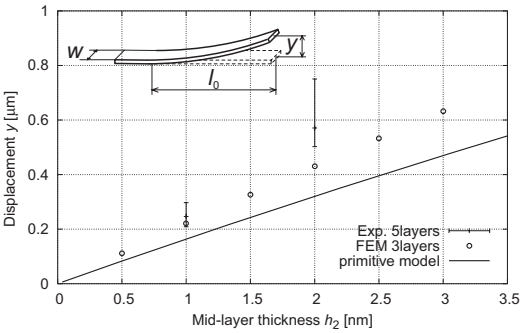

Figure 1: Displacement at and strained layer thickness ($h_1 = 96$ nm, $l_0 = 4.992$ μm, $w = 1$ μm)

Terahertz Si:B blocked-impurity-band detectors by ion implantation

P. Rauter*, T. Fromherz*, S. Winnerl** M. Zier**, A. Kolitsch**, M. Helm**, and G. Bauer*
*Institute of Semiconductor and Solid State Physics, University of Linz, Austria
** Institute of Ion Beam Physics and Materials Research, Forschunsgzentrum Dresden-Rossendorf, Germany

Keywords: terahertz detection, blocked impurity band, solid state photomultiplication, modulated doping

The field of single photon detection in the terahertz frequency range has continued to attract extensive research interest for the last two decades, where the approaches have been manifold [1, 2, 3, 4]. One means of realizing a terahertz single photon detector is constituted by blocked impurity band detectors (BIB) operated as solid state photomultipliers (SSPM) [3]. Conventionally, BIBs are fabricated by epitaxially growing an ultra-pure, highly ohmic Si layer (blocking layer, BL), which prevents the generation of high dark-current, on top of a highly doped impurity layer (IL), which serves as the optically active region of the device. Charge carriers frozen out in the impurity band of the IL, within which hopping transport is possible, are excited by far-infrared radiation into the valence band (*p-type* BIBs). A depletion zone, within which high fields are present, enables an avalanche multiplication of the photoexcited carriers by impact ionization. Up to now, a successful implementation of BIBs operated as SSPMs has been restricted to Si devices fabricated by molecular beam epitaxy (MBE), where the growth of a sufficiently pure BL on top of a highly doped IL is a technologically extremely delicate process. Si BIBs are sensitive to infrared radiation down to 6 THz [5], where the goal to push the sensitivity of BIBs further into the far infrared has induced considerable endeavor to implement the concept in the Ge [6] and GaAs [7] material systems. However, realization was prevented by technological difficulties in growing a BL of sufficient quality.

In this work, we report the fabrication of vertical Si:B BIBs by completely non-epitaxial methods, namely by the ion implantation of a sharply modulated doping profile into a high-ohmic SOI wafer. The implanted boron profile with an approximately constant concentration of 5×10^{17} cm^{-3} down to a depth of 6 μm drops within 2μm below 1×10^{13} cm^{-3} and leaves 2 μm of ultra-pure device layer substrate as a BL. Our samples exhibit highly competitive responsivities of 10 A/W for photon energies of 50 meV, while dark current remains lower than 10^{-10}A. Within a high-gain region our devices feature avalanche gain values of 100, which is of the order required for *single photon detection*. The demonstration of an ion-implanted vertical Si:B BIB opens a highly promising road to technologically simple and cheap BIB array fabrication with implantation substituting the delicate MBE growth of ultra-clean blocking layers.

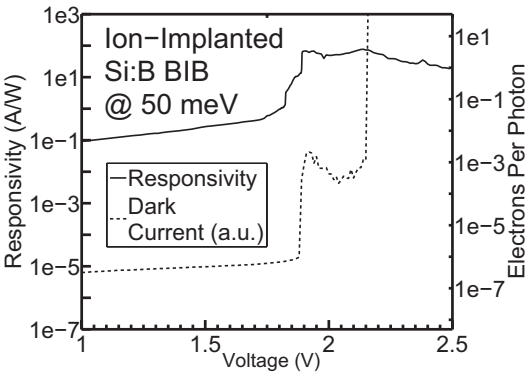

Figure 1: Responsivity and external quantum efficiency at a photon energy of 50 meV. The sample exhibits high peak responsivity values of 65 A/W and gain values of 100, an order of magnitude for which single photon detection is feasible [3].

References

[1] S. Komiyama, *Nature* **403**, 405 (2000).
[2] S. Pelling et al., *Appl. Phys. Lett.* **93**, 073501 (2008).
[3] M. D. Petroff et al., *Appl. Phys. Lett.* **51**, 406 (1987).
[4] O. Astafiev et al., *Appl. Phys. Lett.* **80**, 4250 (2002).
[5] J. Leotin, *Infrared Phys. Technol.* **40**, 153 (1999).
[6] J. Bandaru et al., *Appl. Phys. Lett.* **80**, 3536 (2002).
[7] B. L. Cardozo et al., *Appl. Phys. Lett.* **83**, 3990 (2003).

Efficient photon detectors using surface acoustic waves

S. J. Jiao, P. D. Batista, K. Biermann, R. Hey, and P. V. Santos

Paul-Drude-Institut für Festkörperelektronik, Berlin, Germany

Keywords: photoluminescence, microcavities, surface acoustic waves

The piezoelectric potential (Φ_{SAW}) of a surface acoustic wave (SAW) in a piezoelectric semiconductor creates a type-II modulation of the band edges, which moves along the sample surface. This potential can capture photoexcited electrons (holes) at the position of minimum (maximum) potential and transport them with the acoustic velocity v_{SAW}. Here, we apply this concept for efficient photon detection by quantitatively investigating the efficiency of the ambipolar acoustic transport of photogenerated electrons and holes in (Al,Ga)As structures using spatially resolved photoluminescence and electrical detection by a lateral p-i-n junction. In the experiments (cf. Fig. 1(a)), electrons and holes are photogenerated by a laser spot G located within the path of a SAW generated by an interdigital transducer. The carriers are then attracted to biased metal guides (V_{gn}, V_{gp}), which create independent channels for the transport of electrons and holes towards the lateral p-i-n junction, where they are detected by electrometers. The GaAs transport channel is embedded in a microcavity to ensure the absorption of 71% of the incoming photons. The electrical response of the detector prototype was investigated by measuring I_n and I_p as a function of the illumination intensity (I_L), guide voltages (V_{gn}=-V_{gp}), and acoustic power applied to the IDT (P_{rf}) (Fig. 1(b)). In all cases I_n = -I_p as expected from the generation of the same number of electrons and holes by the incoming photons.

The right vertical scale displays the total photon collection efficiency η, defined as the ratio between the number of detected electron-hole pairs and incident photons. η increases with both $|V_{gn}| = |V_{gp}|$ and P_{rf} due to the improved spatial separation and acoustic transport field, respectively. By taking into account the 71% absorptivity, the η=60% values recorded for low illumination levels (I_L=5 *nW*) imply in a transport and detection efficiency of approx. 85%, thus demonstrating that very few carrier are lost during transport and subsequent detection at the contacts. Interestingly, η increases to values well above 100% for higher I_L - this is attributed to avalanche multiplication the reverse biased pin-junction.

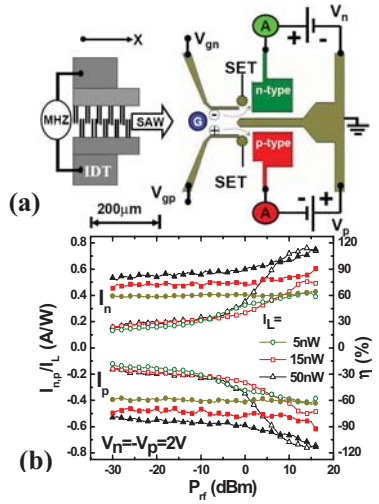

Fig. 1(a) Schematic diagram and (b) dependence of the currents (I_n, I_p) on acoustic power (P_{rf}) for different illumination intensity (I_L) and guide voltages (V_{gn}, V_{gp}). Empty and solid symbols were measured with Vgn=- V_{gp}=0 and 0.5 V, respectively.

In conclusion, the studies demonstrate the efficient ambipolar acoustic transport over hundreds of μm, thus opening the way for application in high sensitivity photon detectors. Efforts are presently underway to apply the concept for single-photon detection by using single-electron transistors (SET, cf. Fig. 1(a)) for charge detection.

*This work is supported by the European Project ACDET2.

Effect of carrier transport on threshold voltage variability in Si MOSFET

Kenji Ohmori[1*], Yasuyuki Ohkura[2], Kenji Shiraishi[3], Keisaku Yamada[1]

1 Nanotechnology Laboratory, Waseda University, Shinjuku, Tokyo, Japan 2 Semiconductor Leading Edge Technologies (Selete), Tsukuba, Ibaraki, Japan 3 University of Tsukuba, Tsukuba, Ibaraki, Japan

Keywords: Si mocroelectronics, nano-scale devices, variability, carrier transport

Variability in electronic devices is one of the crucial issues for nano-scale Si-based device integration and is classified into two categories, extrinsic and intrinsic ones. The former one mostly results from fabrication processes such as a line edge roughness and non-uniformity in gate oxide thickness. On the other hand, the latter one includes the random dopant fluctuation (RDF) in the channel region of devices [1, 2]. The threshold voltage, one of the most important device parameters, is controlled by work function of gate materials and the channel impurity concentration, which fluctuates because of RDF. This is statistically inevitable in nano-scale MOSFET devices where the dopant distribution becomes discrete.

It has been demonstrated that the variability due to the RDF increases as a function of the gate area $(LW)^{-1/2}$ [1, 2]. L and W are the gate length and width, respectively. The experimental fact that still remains obscure is that the magnitude of the variability is certainly larger in n-FETs than in p-FETs [3, 4].

In this paper, we discuss origins of the different magnitude of V_{th} variability between n- and p-FETs. Based on experimental results, we utilize a Monte Carlo (MC) simulation with a novel approach to understand influences of RDF, and propose that the carrier transport of electron and hole, which is mainly affected by impurity scattering, are indeed essential in the difference of the V_{th} variability between n- and p-FETs.

The threshold voltage is estimated using the I_D (drain current)-V_G (gate voltage) characteristics. I_D is expressed as,

$$I_D = \frac{W}{L}\mu C_{OX} f(V_D, V_G, N_I), \quad (1)$$

where μ, C_{OX}, and N_I are the carrier mobility, the oxide capacitance, and the impurity concentration. Note that the I_D value linearly depends on μ, which affects the carrier velocity in the channel. In Fig. 1, our approach for evaluating the influence of carrier transport on the variability is shown.

The mobility shows non-linear dependence on impurity concentration. This indicates that the change in mobility will emerge if the N_I value fluctuates locally in the channel. Therefore, we utilized a MC simulation for obtaining carrier velocities of electron and hole in the bulk Si under uniform electric fields. A HyENEXSS-MC1P simulator was used [5]. The calculated carrier velocities, v, were converted to normalized differential velocity Cv, which is defined as $(dv/dN_I)/(v/N_I)$ (Fig. 2). As the N_I value increases, the $|Cv|$ value increases. In addition, the lesser electric field, the more change in Cv, reflecting that the impurity scattering is dominant in regimes of low carrier velocity (i.e., in a sub-threshold regime). Here, we emphasize that the magnitude of $|Cv|$ for electron is larger than that for hole by a factor of ~2. We consider that the Cv value directly relates to the variability.

By using the parameter Cv, the influences of essential factors such as the carrier transport and scattering phenomena upon the device variability will be discussed together with experimental results from MOSFET measurements.

We are grateful to Front End Process Program in Selete for the fabrication of MOSFET devices and the critical discussions.

References

[1] M. J. M. Pelgrom et al., IEEE J. Solid-State Circuits **24** (1989) 1433. [2] T. Mizuno et al., IEEE Tran. Elec. Dev. **41** (1994) 2216. [3] T. Tsunomura et al., Symp. VLSI Tech. p.156, 2008. [4] A. Asenov et al., IEEE EDL **29** (2008) 913. [5] Y. Ohkura, SISPAD p.287, 2005.

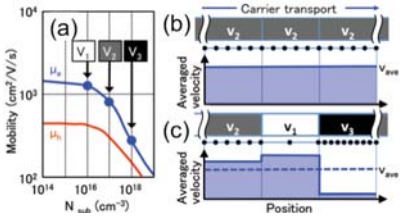

Fig. 1 (a) The carrier mobility shows non-linear dependence on impurity concentration. (b-c) Schematics of impact of N_I fluctuation on the change in the carrier velocity. Compared to the uniform N_I (b), the averaged velocity changes if the carriers experiences local fluctuation of N_I (c).

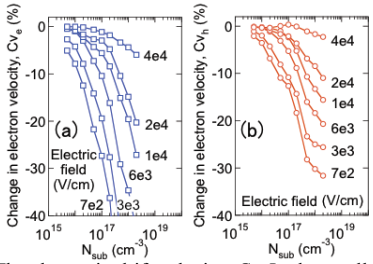

Fig. 2 The change in drift velocity, Cv. In the small electric fields, the $|Cv|$ value increases because the elastic impurity scattering is dominant. The change in the electron velocity (a) is more significant than that of hole (b).

Band properties of $Ga_{1-x}In_xN_yAs_{1-y}$ multiple quantum wells studied by magneto-photoluminescence

T. Nuytten*, M. Hayne**, H. Y. Liu***, M. Hopkinson*** and V. V. Moshchalkov*

** INPAC-Institute for Nanoscale Physics and Chemistry, Pulsed Fields Group, K.U.Leuven, Celestijnenlaan 200D, B-3001 Leuven, Belgium*

*** Department of Physics, Lancaster University, Lancaster LA1 4YB, United Kingdom*

**** Department of Electronic and Electrical Engineering, University of Sheffield, Sheffield S1 3JD, United Kingdom*

Keywords: Dilute nitrides, magneto-photoluminescence, GaInNAs quantum wells, pulsed fields

We have determined the band properties of two dilute nitride $Ga_{1-x}In_xN_yAs_{1-y}$ multiple quantum well (QW) structures of very different optical quality using magneto-photoluminescence (PL) in fields < 50 T. The QW in sample A was grown at 460°C and is embedded between GaAsN barriers, while the QW in sample B was grown at 325°C, with 2.3% In added to the barrier material to provide lattice matching with the QW.

A non-monotonic temperature (T) dependence of the PL energy (Fig. 1), typical for recombination from localised N-states, is present in both samples, but the optimised growth of sample B results in a smoother T-dependence that recovers to the free exciton behaviour much more rapidly. We assert that the zero-field behaviour is essentially governed by the electrons, which migrate from In-rich regions to N-rich regions in the QW causing the red shift at low T. The blue and subsequent red shift is the result of delocalisation of the electrons from N-traps followed by a T-induced reduction in band gap. The properties of the holes are probed by magneto-PL. At low T holes are rapidly released from In-rich regions resulting in a decrease in the exciton Bohr radius with increasing T (inset Fig. 1). At low T, where electrons are localised, a hole effective mass of 0.091±0.001 m_0 for both samples is inferred, consistent with previous reports [1]. The inset to Fig. 1 also shows that the holes in sample B are initially more strongly separated from the electrons, but that the strength of hole localisation is weaker than in sample A. This finding is consistent with transmission electron microscopy data on the effect of growth temperature on the amplitude and periodicity of composition modulation in $Ga_{1-x}In_xN_yAs_{1-y}$ QWs [2]. Finally, we note that at high T the same asymptotic exciton radius of 12 nm is found for both samples, implying that it is characteristic of free excitons. Using the hole mass determined at low T we are thus able to determine an electron effective mass of 0.17 m_0 for dilute nitrides with N in the % range; similar to what was recently reported for $y < 0.02$ [3].

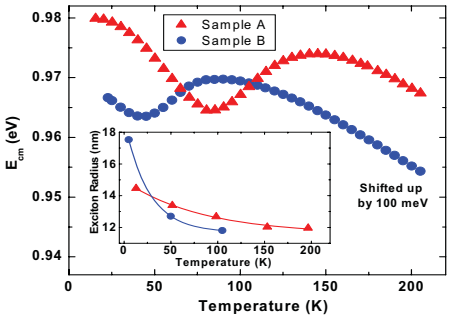

Fig.1 T-dependence of the PL energy for samples A and B, with the data for sample B shifted up by 100 meV for clarity. The exciton radius as a function of temperature is shown in the inset for samples A and B. The solid lines are guides for the eyes.

References

1. A.Polimeni *et al.*, J. Phys. Condens. Matter **16**, S3187 (2004).
2. M. Herrera *et al.*, Semicond. Sci. Technol. **19**, 813 (2004).
3. F. Masia *et al.*, Phys. Rev. B **73**, 073201 (2006).

July 24 (Friday)

9:00 – 10:30

Session M9

Nanophotonics

International Conference Room

MSS-EP2DS Parallel session

Kobe Chinese food town

Picosecond coherent control of dressed states in a single quantum dot

S. J. Boyle[1], A. J. Ramsay[1], A. P. Heberle[2,3], M. Hopkinson[4], A. M. Fox[1] and M. S. Skolnick[1]

[1] *Department of Physics and Astronomy, University of Sheffield, Sheffield, S3 7RH, UK*

[2] *Department of Physics and Astronomy, University of Pittsburgh, Pittsburgh, Pennsylvania 15260, USA*

[3] *Sullivan Park, R&D Center, Corning Incorporated, Corning, NY, 14831, USA*

[4] *EPSRC National Centre for III-V Technologies, University of Sheffield, Sheffield, S1 3JD, UK*

Keywords: Quantum dot, coherent control, dressed states, quantum information

Interest has recently been generated in exciton-photon dressed states in quantum dots (QD) due to possible quantum information (QI) applications. Several frequency-domain observations have been made, but for QI applications dynamic control is also required. Here, we observe the evolution of the Rabi splitting of an Autler-Townes doublet on a picosecond timescale, and coherent beating between dressed states, directly resolving a Rabi oscillation in the time domain. We show that dressed states may be gated on and off on picosecond timescales in a fully coherent process.

We excite a single self-assembled InGaAs QD with picosecond laser pulses. A photocurrent detection method is used. Fig. 1 (a) shows the exciton-biexciton (X-2X) system. The X and 2X states are coupled on-resonance by the control laser, mixing the basis-states to form a Rabi-split pair of dressed states α, β. The ground to dressed-state transitions (0-α, 0-β), known as an Autler-Townes doublet, are observed via resonant absorption of a probe laser.

Fig. 1 (b) shows a grayscale plot of photocurrent versus detuning of the probe laser, and time delay between control and probe pulses. The splitting is observed to follow the Gaussian envelope of the control pulse. Fig. 1 (c) shows a numerical simulation of the experiment. Off-resonant coupling is also investigated.

Beats between the dressed states are observed using slow control and fast probe pulses. The probe pulse creates an equal superposition of the α and β states, which acquire a relative phase shift due to the Rabi-splitting caused by the control pulse. This results in a beat between X and 2X states, measured as a change in photocurrent as the time delay is varied, as shown for various control pulse areas ($\Theta_{control}$) in fig. 2. Clear increase of the Rabi frequency with increasing pulse area is observed. At the largest pulse areas negative going signals are observed as the Autler-Townes splitting approaches the ~0.8meV width of the probe pulse. Taken together, these results constitute optically-gated measurements of Rabi oscillations, observed directly in the time domain.

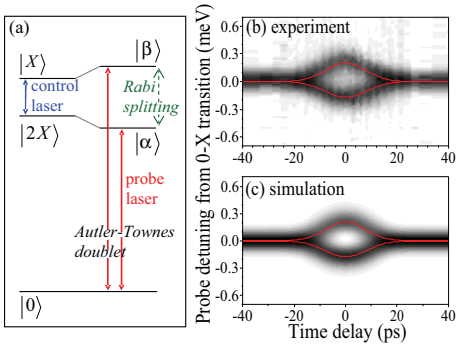

Fig.1 (a) Dressing of exciton and biexciton states. (b) Time-resolved measurement of the Autler-Townes splitting. (c) Numerical simulation of (b).

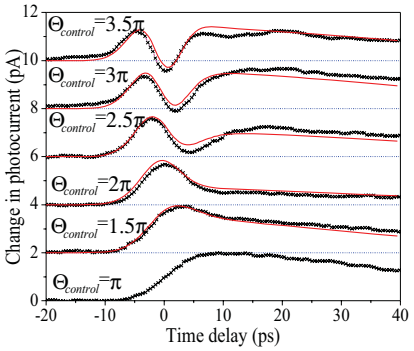

Fig.2 Beats between exciton-biexciton dressed states, or time-resolved Rabi oscillations. Red lines are fits from numerical simulations.

Tailoring optical modes in semiconductor microtube bottle resonators

Ch. Strelow, C. M. Schultz, H. Rehberg, A. Stemmann, H. Welsch, Ch. Heyn, D. Heitmann, and T. Kipp
Institute of Applied Physics, University of Hamburg, Germany

Keywords: microcavities, microtubes

We report on the realization of microtube bottle resonators formed by rolled-up semiconductor bilayers. The optical eigenmodes, which were probed by the photoluminescence of self-assembled InAs quantum dots embedded into the tube wall, show axial field distributions which resemble to the probability density of particles in one-dimensional potentials. We demonstrate that these modes can be tailored by a specific structuring of the tube geometry along the tube axis.

Our microtubes are fabricated by exploiting the self-rolling mechanism of thin strained GaAs/InGaAs bilayers grown in molecular beam epitaxy and using optical lithography and wet-etching processes. Recently we showed that multi-walled microtubes, which are raised from the substrate, can act as a ring resonator [1, 2, 3]. These microtubes have diameters of about 5 µm and overall wall thicknesses of 100-200 nm. Light is circularly confined by waveguiding inside the tube wall.

Here, we present a novel design that turns our microtubes into bottle resonators and allows one to realize a fully-controlled light confinement also along the tube axis . Figure 1(a) sketches a microtube with a parabolic lobe at the outside rolling edge. Micro photoluminescence measurements of such a microtube with spatial resolution along the tubes z axis are shown in figure 1(c). We observe groups of modes that are axially localized at the lobe which is depicted in figure 1(b). Within the groups the modes exhibit an increasing number of axial antinodes with increasing energy.

In order to model a microtube bottle resonator we made an adiabatic separation of circular and axial light propagation. This leads to a quasi-Schrödinger equation for the axial modes including a quasi potential that can be calculated from the specific shape of the lobe. Applying a waveguide model [2] we calculated that the shape of the lobe linearly transforms into the shape of the quasi potential and, thus, the parabolic lobe induces a harmonic quasi potential. Figure 1(d) shows solutions of the quasi-Schrödinger equation obtained by discretization of the space and subsequent diagonalization of the resulting algebraic equations. We observe a very nice agreement of measurements and calculations also for differently shaped lobes and quasi potentials. This demonstrates the ability of precisely tailor the axial eigenmodes.

We acknowledge financial support by the Deutsche Forschungsgemeinschaft via SFB 508 and GK 1286.

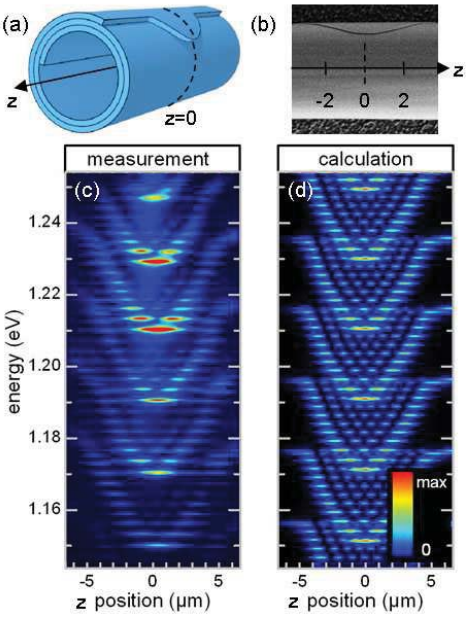

Figure 1: (a) Sketch of a microtube bottle resonator. (b) Scanning electron micrograph from the lobe position. (c) Spatially and energetically resolved photoluminescence. (d) Numerically calculated intensities and energies.

References

[1] T. Kipp et al., Phys. Rev. Lett. **96**, 077403 (2006).

[2] Ch. Strelow et al., Phys. Rev. B **76**, 045303 (2007).

[3] Ch. Strelow et al., Phys. Rev. Lett. **101**, 127403 (2008).

Observation of unique photon statistics of single artificial atom laser

M. Nomura, N. Kumagai, S. Iwamoto, Y. Ota, and Y. Arakawa

Institute for Nano Quantum Information Electronics, Research Center for Advanced Science and Technology, Institute of Industrial Science, University of Tokyo, Tokyo, Japan

Keywords: quantum dot, quantum optics, photonic crystal, nanocavity, semiconductor laser

Development of nanotechnology enables laser oscillation with a small number of emitters, such as a one-atom laser [1]. Such a laser is, in principle, implementable in also solid-state materials by using a semiconductor nanocavity and single quantum dot (SQD). We demonstrate an optically pumped InAs SQD laser with photonic crystal (PhC) nanocavity and its unique photon statistics including both single QD nature and positive photon correlation below and around the threshold, respectively.

The sample was grown on a semi-insulating(100)-oriented GaAs substrate by molecular beam epitaxy. A 160-nm-thick GaAs slab layer includes single self-assembled InAs QD layer. The areal QD density is ~1-2x10^8 cm^{-2}. The nanocavity, which consists of three missing air holes at the center of the PhC pattern, functions as an optical cavity. The detailed fabrication method has been reported in our previous paper [2].

Spectral tuning of the target exciton by temperature tuning method controls the gain of the cavity system. At zero detuning, the coupling of the single exciton distinctly increases the material gain of the system, resulting significant reduction in the threshold pump power. The light-in vs. light-out (L-L) plot at zero detuning is shown in Fig. 1(b). The estimated pump power is ~42nW, while sufficiently detuned cases show ~145 nW. To investigate the photon statistics of the laser, we measured photon correlation function at the exciton coupled condition at 39 K (Fig. 1(c-e)). The results show phase transition from single photon emission (c) to stimulated emission regime (e) with positive photon correlation around the threshold (d). This is a unique photon statistics for a laser with single emitter.

This research was supported by the Special Coordination Funds for Promoting Science and Technology and by KAKENHI 20760030, MEXT, Japan.

References

1. J. McKeever *et al*., Nature **425**, 268-271 (2003).
2. M. Nomura *et al*, Opt. Express **14**, 6308 (2006).

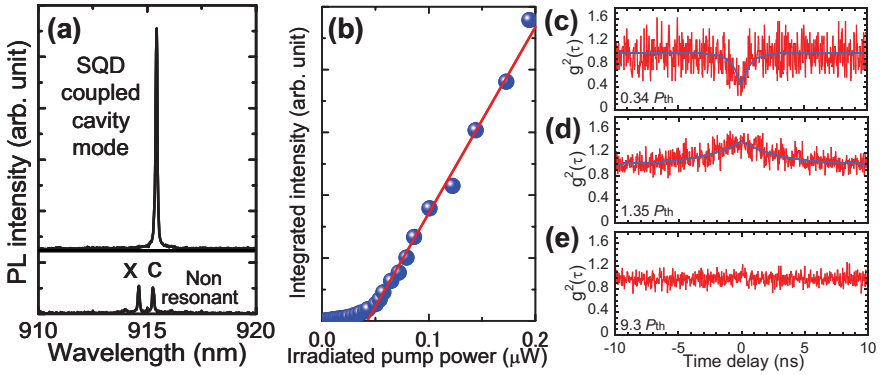

Fig1. (a) PL spectra taken at an exciton coupled and non-resonant conditions. (b) L-L plot of the SQD laser. (c)-(e) Photon correlation functions below (c), around (d), and above (e) the laser threshold of *P*th = 42 nW.

Pulsed injection of vortices in a polariton condensate

D. Sanvitto[*], L.Viña[*], A. Lemaître[**], J Bloch[**], E. Karimi[†§], B. Piccirillo[†], and L. Marrucci[†§]

[*] *SEMICUAM. Universidad Autónoma. E-28049 Madrid. Spain*

[**] *LPN/CNRS. LPN/CNRS, Route de Nozay, 91460, Marcoussis, France.*

[†] *Dip. Scienze Fisiche, Universita' di Napoli. 80126 Napoli, Italy*

[§] *CNR-INFM Coherentia, Compl. Univ. di Monte S.Angelo. 80126 Napoli, Italy*

Keywords: Polariton condensates, vortices, time-resolved spectroscopy

Observation of quantized vortices, suggesting parallelisms between non-equilibrium polariton condensates and conventional superfluids, have been reported either by spontaneous formation and pinning in the presence of disorder [1, 2] or by imprinting it onto the signal or idler of an optical parametric oscillator (OPO) [2]. Here we report the first observation of a polariton condensate receiving a quantised angular momentum by means of a short optical pulse and maintaining its rotation for a time much longer than both the pulse duration and the polariton lifetime. This observation shows a peculiar character of polariton condensates which strengthen its analogy with supercurrents in superconductors or persistent flow in condensates [3].

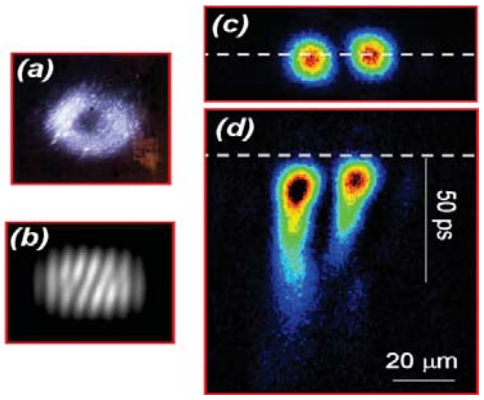

Fig.1 (a) Probe profile in space. (b) Interferogram of the probe with a shifted mirrored image. (c) Streak image of a cross section of the space (horizontal) *vs*. time (vertical) emission of the probe only. (d) Same as in (c) for the perturbed OPO signal after the probe (white, dashed lines mark the time origin, t=0).

We use a λ/2 AlAs microcavity with a 20 nm GaAs QW at its centre. At 10 K, the heavy-hole excitons of the QW are strongly coupled with the cavity mode (Rabi splitting ~4.4 meV). The wedge-shaped cavity allows for tuning of the resonance between the QW exciton and the cavity mode by changing the position of the excitation spot on the sample. We exploit an OPO configuration to create a polariton condensate at k=0, and at a slightly negative detuning, in a relatively large area (Ø ~ 50 μm). We perturb the OPO´s signal state with a, smaller in size, pulsed (2 *ps* long) probe carrying an orbital angular momentum *l*=1.

Figure 1 summarizes the most relevant findings of our experiments. The probe profile in real space is shown in panel (a) and the corresponding interferogram with a shifted mirrored image, by a retroreflector, in (b) evidencing the typical pair of fork-like dislocations. A cross section of the probe-only emission arriving at t=0 (dashed line) and its time evolution is depicted in (c) (space *vs*. time). The corresponding strikes in the perturbed OPO configuration are shown in (d), lasting now for several tens of picoseconds: the probe enhances the polariton-signal emission by a factor of ~5 with a delay of ~10 *ps* after the pulse arrival.

References

1. K.G. Lagoudakis, *et al.*, Nature Phys. **4**, 706 (2008).
2. D.N. Krizhanovskii, *et al.*, this conference.
3. A. Amo, *et al.*, Nature **459**, 291 (2009).

Dynamic control of polariton condensates using surface acoustic waves

E. Cerda-Méndez*, D. Krizhanovskii**, K. Biermann*, K. Guda**, R. Bradley**, P. V. Santos*, R. Hey* and M. S. Skolnick**

** Paul-Drude-Institut für Festkörperelektronik, Berlin, Germany*

*** Department of Physics and Astronomy, University of Sheffield, Sheffield, United Kingdom*

Keywords: microcavity polaritons, parametric scattering, surface acoustic waves

Macroscopically occupied polariton phases (condensates) arising from either Bose-Einstein condensation (BEC) or Optical Parametric Oscillation (OPO) in strongly coupled semiconductor microcavities have been shown to exhibit a number of interesting quantum phenomena, such as collective superfluid behaviour[1] (OPO), spatial and temporal coherence (OPO, BEC) and vortices (BEC). These polariton condensates are closely analogous to the BEC of atoms with one significant difference: the polariton condensate is an intrinsically out-of-equilibrium system, since it arises from a dynamical equilibrium between driving by the pump laser and dissipative effects due to losses.

Here, we report the dynamic control of the energy spectrum and spatial coherence of polariton condensates formed by polariton-polariton scattering from the pump in external periodic potentials created by a non-piezoelectric Surface Acoustic Waves (SAW) of ~400 MHz frequency and wavelength λ_{SAW}=8 µm. The use of a non-piezoelectric SAWs is essential to observe condensation effects, because conventional piezoelectric SAWs[2] ionise excitons and result in the collapse of polariton states. The periodic SAW potential induces a modulation of the polariton dispersion with the marked formation of Brillouin zones of period $k=\pi/\lambda_{SAW}$ and energy stop band widths of ~0.5 meV (Fig.1a).

In the absence of a SAW, the OPO "signal" condensed state is formed at k=0 above threshold with a coherence length of about 20 µm. As the height of the SAW potential is increased we observe dramatic reduction of the spatial coherence length along the SAW propagation direction (L_X) by a factor of 3-4 (Fig.1b) due to the suppressed tunnelling between the adjacent SAW minima. This observation is analogous to the superfluid to Mott insulator phase transition in a gas of ultracold atoms. A smaller decrease of the coherence length L_Y perpendicular to the SAW direction by a factor of 2 (Fig. 1b) is attributed to the 1D character of the non-equilibrium OPO.

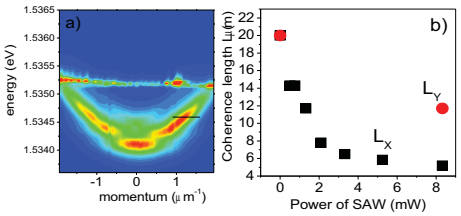

Fig.1 a) Dispersion of polaritons subject to a SAW potential. b) Spatial coherence length of OPO signal along (L_X) and perpendicular (L_Y) to the SAW.

The parametric scattering by a strongly detuned pump laser allows the observation of both zero- and π-like states[3], the energy between which can be actively tuned by changing the acoustic power. Finally, intensity correlation measurements of the emission originating from spatially separated regions demonstrate that the SAW potential acts as a "conveyor belt" transporting confined condensates over 10-15 µm distances.

Our work on polariton condensates in SAWs opens up new opportunities to investigate the coherent transport of condensates and the creation of entangled states.

References

1.A.Amo, et al, Nature **457**, 291 (2009)
2. M. M. de Lima Jr. *et al*, Phys. Rev. Lett. **97**, 045501 (2006)
3. Lai, C. W. *et al*. Nature **450**, 529-532 (2008)

July 24 (Friday)

11:00 – 12:30

Plenary Session 5, 6

Main Hall

EP2DS-MSS Joint session

Akashi bridge

Manipulation of Photons by Photonic Crystals

Susumu Noda
Department of Electronic Science and Engineering, Kyoto University, Kyoto 615-8510, Japan
Email: snoda@kuee.kyoto-u.ac.jp

Keywords: Photonic Crystals, Nanocavities and waveguides, Surface-photon physics, Photonic-crystal laser

Photonic crystals, in which the refractive index changes periodically, provide an exciting tool for the manipulation of photons and have made substantial progresses in recent years. In this presentation, I will discuss recent progresses in photonic-crystal researches including (i) two-dimensional photonic-crystal cavities and waveguides, (iii) three-dimensional photonic crystals, and (ii) two-dimensional photonic-crystal lasers.

(i) Two-dimensional photonic-crystal nanocavities and waveguides:

Remarkable progresses in nanocavities and waveguides based on two-dimensional (2D) photonic-crystals have been achieved recently. For example, nanocavity-Q over two millions [1,2] has been successfully achieved while maintaining ultrasmall modal volume based on the concept of Gaussian confinement [3, 4]. The combination of nanocavities and waveguides leads to the realization of photonic nano-devices [5, 6]. Here, if the properties of such photonic-crystal nanocavities and waveguides could be changed or controlled dynamically during their operations, the resulting functionalities would be greatly expanded. In the present talk, I at first discuss the dynamic control of photonic crystals [7,8], where the characteristics of nanocavities and waveguides are dynamically controlled within picosecond time scales, which will contribute to future applications including the stopping/slowing of light, quantum information systems, and next generation ultra-high capacity communications. Then, I will discuss the recent progress of photonic-crystal nanocavities combined with quantum dots, where the stress is on the importance of quantum anti-Zeno effects [9-11] as a third emission mechanism in addition to Purcell effect and vacuum Rabi-oscillation.

(ii) Three-dimensional photonic crystals:

3D photonic crystals with 3D periodic refractive-index distributions are expected to possess the capability of ultimate control of photons, and the manipulation of photons by 3D photonic crystals has so far been carried out by embedding artificial defects and light emitters 'inside' crystals [12-14], using 3D directional bandgap effects. In the present talk, I will describe that photons can be manipulated even at the 'surface' of 3D photonic crystals, where 3D periodicity is terminated [15]. This phenomenon is of interest because of its relevance to the surface plasmon-polariton effect of metals and the related surface photon physics. We first show that 3D photonic crystals possess surface states and that photons can be confined and propagate through them. Then I will demonstrate that 3D localization of photons at desired surface points is possible by forming a surface-

mode gap and introducing artificial surface-defect structures. Surprisingly, the obtained *Q* factors of the surface-defect mode are the largest reported for 3D photonic crystal nanocavities (up to ~9,000). This represents an important step towards realizing a new route for photon manipulation by 3D photonic crystals, and establishing the surface science of photonic crystals. Furthermore, the absorption-free nature of the 3D photonic-crystal surface could make possible new sensing applications and light-matter interactions.

(ii) Two-dimensional Photonic-Crystal Lasers:

Photonic-crystal surface-emitting lasers [16, 17] have recently attracted much attention because of their perfect, broad-area single-mode surface-emitting operation, their narrow beam divergence angles of < 1°, and the possibility of producing tailored beam patterns by controlling the electric field distribution inside the photonic crystal. These fascinating features arise from the photonic band-edge effect, where the group velocity of light becomes zero and a 2D cavity mode is formed. We will describe the recent progresses in such unique photonic-crystal lasers including the recent achievement in producing tailored beam patterns [18] and lasing oscillation in blue-violet wavelengths [19].

References:

[1] S.Noda, et al. *Nature Photonics*, 1 (2007) 449,
[2] Y. Takahashi, et al. *Optics Express*, 15 (2007) 17206.
[3] Y.Akahane, et al, *Nature*, 425 (2003) 944.
[4] B.S.Song, et al. *Nature Materials*, 4 (2005) 207.
[5] S. Noda, et al. *Nature*, 407 (2000) 608.
[6] B.S.Song, et al, *Science* 300 (2003) 1537.
[7] Y.Tanaka, et al, *Nature Materials*, 6 (2007) 862.
[8] U. Jeremy, et al. *Optics Express*, 16 (2008) 21721.
[9] M.Yamaguchi, et al, *Optics Express*,
[10] M. Yamaguichi, et al, arXiv: 0904.3697 (2009).
[11] S.Noda, *Science*,314 (2006) 260.
[12] S.Noda, et al. *Science*, 289 (2000) 608.
[13] S.Ogawa, et al. *Science*, 305 (2004) 227.
[14] K.Aoki, et al, Nature Photonics, 2 (2008) 688.
[15] Ishizaki and Noda, unpublished.
[16] M.Imada, et al, *Appl.Phys.Lett*., 75 (1999) 316.
[17] S.Noda, et al, *Science*, 293 (2001) 1123.
[18] E.Miyai, et al. *Nature*, 441 (2006) 946.
[19] H. Matsubara, et al, *Scienc*e, 319 (2008) 445.

Physics observed through shot noise measurements

Moty Heiblum

Braun Center for Sub Micron Research, Dept. of Condensed Matter Physic
Weizmann Institute of Science, Rehovot 76100, Israel

Shot noise measurements were proven to be a powerful tool to observe charge, interactions, statistics, and dephasing, as few examples. In this talk I will show new results of shot noise measurements in the fractional quantum Hall effect regime, which points at a more complicated interpretation of fractional charges. I will show results of measurements in a variety of filling factors, being the Laughlin's states (1/3, 2/5, 3/7, 2/3, 7/3) or the even denominator state (5/2), where the deduced charge is highly dependent on the range of measurements, such as the DC current, back-scattering probability of the quasiparticles, and the temperature. If one trusts shot noise measurements to be a good indicator of the charge, the theoretically expected charge seems to exist only under some specific conditions.

Author Index

C

D

E

F

G

H

L

M

N

O

P

R

S

T

U

V

W

X

Y

Z